

HILL GEOGRAPHER

ISSN 0970 - 5023



Vol. XXXXI: NOS 1 & 2
June & December 2025
Special Issue

**GEOGRAPHICAL SOCIETY OF THE
NORTH-EASTERN HILL REGION (INDIA)**

Department of Geography
North-Eastern Hill University, Shillong 793022
www.hillgeographer.in

HILL GEOGRAPHER

XXXXI: NOS 1 & 2
June & December 2025
Special Issue

ISSN 0970-5023

(A UGC-CARE enlisted journal)

This issue of Hill Geographer has been published with the generous financial assistance received from Indian Council of Social Science Research, New Delhi

Geographical Society of the North-Eastern Hill Region, India gratefully acknowledges the support received from the ICSSR



GEOGRAPHICAL SOCIETY OF NORTH-EASTERN HILL REGION
(INDIA)

Department of Geography
North-Eastern Hill University, Shillong 793022
www.hillgeographer.in

THE GEOGRAPHICAL SOCIETY OF NORTH-EASTERN HILL REGION (INDIA)

(Registered under Societies Act XXI, 1860)
Registration No. SR/TG SOT NEHR-299/82

CHIEF PATRON

Professor P. S. Shukla

Vice-Chancellor

North-Eastern Hill University
Shillong - 793022

EXECUTIVE COMMITTEE

(Office Bearers)

President: Prof Debendra Kumar Nayak

Vice-President: Prof. H. J. Syiemlieh

Secretary: Prof. P. K. Ryngha

Joint Secretary: Prof. Sunil Kumar De

Treasurer: Ms. Joyfully Pyngrope

EDITORIAL BOARD

Editor

Prof. H. J. Syiemlieh

Members

Prof. Debendra Kumar Nayak

Prof. A. C. Mohapatra

Prof. Surendra Singh

Prof. Niladri Ranjan Dash

Prof. A. K. Bora

Prof. Laxmi Sivaramakrishnan

Prof. Sunando Bandyopadhyay

Prof. Sachidanand Sinha

Prof. Ravindra G. Jaybhaye

Prof. Ashis Sarkar

Prof. A. K. Bhagabati

Dr. Subrata Purkayastha

Dr. Chandrakanta

Published by Prof. Prof. H. J. Syiemlieh, Editor, on behalf of the Geographical Society of North-Eastern Hill Region, Department of Geography, North-Eastern Hill University (NEHU), Shillong-793022 and Printed by Unique Phototype, 49 Guru Prosad Chowdhury Lane, Kolkata 700 006, India.

**The Editor is not responsible for opinions expressed by individual authors.*

HILL GEOGRAPHER

XXXXI: NOS 1 & 2
June & December 2025
Special Issue

ISSN 0970-5023

(A UGC-CARE enlisted journal)

Special Issue on
**Climate Change and Human Intervention
on Hydro-Geomorphological Hazards
in the Era of Sustainability**

Guest Editors

Jayanta Das¹, Asraful Alam¹, Sunil Kumar De²

¹Department of Geography, Rampurhat College, West Bengal

²Department of Geography, North-Eastern Hill University, Shillong, Meghalaya

GEOGRAPHICAL SOCIETY OF NORTH-EASTERN HILL REGION
(INDIA)

Department of Geography
North-Eastern Hill University, Shillong 793022
www.hillgeographer.in



Hill Geographer

XXXXXI: NOS 1 & 2 (2025)

Special Issue

ISSN 0970-5023

CONTENTS

Author/s	Title of the Article	Page No.
Research Paper/s		
Piu Saha, Deepak Kumar Mandal	Evaluation of Rainfall Pattern and Meteorological Drought Using Run Theory Approach in Rarh Region of West Bengal, India	1-15
Gargi Sarkar, Subhadip Gupta	Estimation of Water Quality through Machine Learning (ML): A Case Study of Chamta River, West Bengal	16-38
Khamnam Michael Meitei, Biswajit Das	Longitudinal Trends, Inter-River Variability and Water Quality Index Assessment of Major Rivers in Imphal Valley, Manipur	39-71
Rakshith C.M., Nirmala R., Pranith P.	Detection and Mapping of Geomorphic Changes: A Case Study of the Chandragiri Estuary, Kerala	72-84
Janardan Keshav Gavit, Rajaram Anna Jadhav	Climate Risks and Tribal Migration in the Girana–Godavari Basin of Maharashtra: A Hydro-Social Perspective	85-100
Nirmal Mondal, Sumaira Javaid, Dharmendra Kumar, Sumit Kar, Ilyass Hussain and Pervez Ahmed	Assessing the Impact of Fishing Nets and ‘Patas’ on Flood Dynamics in the Kaliaghai River, West Bengal	101-119
Ajit Kumar Singha, Ishwarjit Singh Elangbam	Anthropogenic Modification on Hydro-Dynamics of the Teesta River in Duars Region, West Bengal	120-137

Author/s	Title of the Article	Page No.
Manisha Pathak, Pranati Sarkar	A GIS-Based Evaluation of the Geomorphological Characteristics of Dikrong River Basin, Assam, India	138-154
Anu Tamang	Assessing the 2023 GLOF Impact on Teesta Bazar, Kalimpong District, West Bengal	155-168
Jayanta Das, Arijit Majumder, Sudarshana Sen, Pradip Chouhan, Namita Chakma, Md. Mofizul Hoque	Human Health Risk Exposure from Arsenic Pollution in the arsenic-affected areas of Malda district in the lower Gangetic plain	169-192
Dennis Lalhruaitluanga, K. Srinivasa Rao, Jimmy Lalnunmawia	Landslide Susceptibility Mapping of Mamit District, Mizoram: A Comparative Analysis of Bivariate Statistical Methods	193-214
Subha Roy, Souvik Das, Rajesh Hansda, Jaya Chatterjee, Md. Hasanur Jaman, Prakash Mistri, Somasis Sengupta	Coping with Soil Erosion: Present Status and Deep Learning-Based Future Projections in the Mayurakshi Basin, India	215-240
Imanuel Lawmchullova, Lalhnehsaki, Lalrinkimi	Assessing Rainfall Variability in Mizoram: Insights into the Tropical-Monsoon Dynamics of North-east India	241-255
Saidur Rahaman, Sujoy Kumar Malo, Mantu Das, Kunal Chakraborty, Snehasish Saha	GIS-Based Analysis of Site Suitability for Potential Agricultural Land Using MCDM Approach in Uttar Dinajpur District, West Bengal, India	256-292
Debapriya Poddar Sarbari Mukhopadhyay	Assessment of Prevalence of Arsenicosis using TOPSIS Model in Malda District, West Bengal	293-307
Asraful Alam, Md. Mofizul Hoque, Jayanta Das, Aznarul Islam	Rainfall Trend and its Variability Analysis of a sub-tropical Rainfall River Basin	308-324

About Guest Editors



Jayanta Das is Assistant Professor of Geography at Rampurhat College, West Bengal, India. He earned his PhD in Geography from the University of North Bengal, focusing on sustainable alternatives to tobacco cultivation in the Koch Behar district. His academic interests include climate change, applied geomorphology, hazard management, soil and agricultural geography, remote sensing, GIS, and environmental geography. He has published research in reputed international journals on flood risk assessment, groundwater recharge, land use analysis, and sustainable agriculture. Dr. Das has edited scholarly volumes and actively organizes conferences, seminars, and training programmes at national and international levels.

Email: jayanta.daas@gmail.com



Asraful Alam is Assistant Professor of Geography at Rampurhat College, affiliated to the University of Burdwan, West Bengal, India. He completed his postgraduate studies in Geography from Visva-Bharati University and obtained a Post Graduate Diploma in Geoinformatics from Jadavpur University, Kolkata. His research interests include environmental geography, hazard and disaster management, riverine processes, climate change studies, agricultural suitability analysis, and the application of remote sensing and GIS. He has published research articles in reputed peer-reviewed international journals and co-edited the book *Recent Advancement in Geographical Studies: A Multidimensional Outlook*.

Email: geoasraful@gmail.com



Sunil Kumar De is Professor and former Head of the Department of Geography at North-Eastern Hill University, Shillong, India. He is currently serving as President of the International Association of Geomorphologists (2022–2026) and has previously held several executive positions within the association. He completed his M.Sc. and PhD from the University of Calcutta. His research interests include geomorphological hazards, particularly landslides and soil erosion, fluvial dynamics, river health, and human–environment interactions. He has published extensively in national and international journals, edited books on geomorphology and environment, and supervised numerous doctoral and postgraduate research scholars.

Email: desunil@gmail.com

Climate Change and Human Intervention on Hydro-Geomorphological Hazards in the Era of Sustainability

Jayanta Das¹, Asraful Alam¹ and Sunil Kumar De²

¹*Department of Geography, Rampurhat College, Birbhum, West Bengal*

²*Department of Geography, North-Eastern Hill University, Shillong, Meghalaya*

Email: desunil@gmail.com

The eastern and northeastern regions of India are experiencing rapid environmental transitions shaped by climate variability, land-use change, and human interventions (Barman *et al.*, 2024; Nayak *et al.*, 2021; Roy *et al.*, 2022). These transformations have direct implications for water availability, soil stability, agricultural productivity, and hazard vulnerability (Nguyen *et al.*, 2023). Understanding these processes through scientific investigation is essential for sustainable regional planning and climate adaptation. To address the above-mentioned requirements, this SI entitled “Climate Change and Human Intervention on Hydro-Geomorphological Hazards in the Era of Sustainability” received 32 manuscripts between April 1, 2025 and June 30, 2025. Most of the submissions fell into the research topics of this SI. Finally, 16 manuscripts were accepted for publication in the Journal of Hill Geographer after providing the requested revisions by the authors where the average acceptance rate was 40.6%. This special issue brings together diverse research contributions focusing on rainfall dynamics, drought analysis, river morphology, soil erosion, water quality, and natural hazards. Using geospatial techniques, statistical models, and field-based observations, these studies explore how physical and human processes interact within fragile ecosystems. Collectively, they enrich our understanding of regional environmental challenges and highlight strategies for sustainable management. The collective findings presented in this Special Issue highlight the increasing sensitivity of hydro-geomorphological systems to both climatic variability and intensified human interventions. Across diverse physiographic settings, the studies consistently demonstrate that changes in rainfall patterns, land-use practices, and river regulation have significantly altered natural process-response mechanisms. Enhanced flood frequency, expanding drought-prone areas, accelerated soil erosion, and declining water quality emerge as common manifestations of

these interacting drivers, particularly in ecologically fragile and socio-economically vulnerable regions. Another key outcome of the Special Issue is the growing importance of geospatial and data-driven approaches in hazard assessment and environmental management. The application of remote sensing, GIS, statistical modeling, and machine-learning techniques has improved the accuracy of spatial prediction, risk mapping, and scenario analysis. These methodological advances not only strengthen scientific understanding of hydro-geomorphological hazards but also provide actionable insights for sustainable planning, disaster risk reduction, and climate adaptation strategies at local and regional scales.

References:

- Barman, S., Singh, W. R., Kalita, B., & Tyagi, J. (2024). A combined impact assessment of climate and land use/land cover change in an Eastern Himalayan watershed in northeast India. *Environmental Monitoring and Assessment*, 196(3), 294. <https://doi.org/10.1007/s10661-024-12433-4>
- Nayak, S., Maity, S., Singh, K. S., Nayak, H. P., & Dutta, S. (2021). Influence of the Changes in Land-Use and Land Cover on Temperature over Northern and North-Eastern India. *Land*, 10(1), 52. <https://doi.org/10.3390/land10010052>
- Nguyen, T. T., Grote, U., Neubacher, F., Rahut, D. B., Do, M. H., & Paudel, G. P. (2023). Security risks from climate change and environmental degradation: Implications for sustainable land use transformation in the Global South. *Current Opinion in Environmental Sustainability*, 63, 101322. <https://doi.org/10.1016/j.cosust.2023.101322>
- Roy, P. S., Ramachandran, R. M., Paul, O., Thakur, P. K., Ravan, S., Behera, M. D., Sarangi, C., & Kanawade, V. P. (2022). Anthropogenic Land Use and Land Cover Changes—A Review on Its Environmental Consequences and Climate Change. *Journal of the Indian Society of Remote Sensing*, 50(8), 1615–1640. <https://doi.org/10.1007/s12524-022-01569-w>



Evaluation of Rainfall Pattern and Meteorological Drought using Run Theory Approach in Rarh Region of West Bengal, India

Piu Saha^{1*} and Deepak Kumar Mandal¹

*¹Department of Geography and Applied Geography, University of North Bengal,
Darjeeling –734013, West Bengal*

**Corresponding author: piusaha.nbu@gmail.com*

Abstract: This study investigates the spatial variation of meteorological drought occurrences in the Rarh region of West Bengal, India, over the period from 1986 to 2020. Utilizing the Standardized Precipitation Index (SPI) across multiple time scales such as 3, 6, 12, and 24 months, this research provides a detailed analysis of drought severity, duration, and frequency. The findings reveal significant spatial variability in drought patterns, with the northern grids exhibiting higher coefficients of variation and kurtosis values, indicating a greater susceptibility to erratic rainfall and extreme weather events. The temporal analysis highlights notable drought frequency and severity trends, with certain periods experiencing prolonged and severe drought conditions. This study underscores the critical need for targeted drought mitigation strategies tailored to each sub-region's unique climatic and hydrological characteristics. This research provides valuable insights for regional planners, policymakers, and stakeholders through comprehensive statistical evaluation and mapping of drought indices. The results are crucial for developing adaptive strategies to enhance resilience against drought-induced challenges, ensuring sustainable water management and agricultural practices in the face of climate variability. The study's findings contribute to a broader understanding of drought dynamics and offer actionable recommendations for effective drought risk management in the Rarh region.

Keywords: Meteorological drought, Standardized precipitation index (SPI), Rainfall variability, Drought mitigation, Rarh region.

Introduction:

Drought represents a significant natural hazard, influencing agriculture, water resources, and human livelihoods on a global scale. It is recognized for its profound impacts across diverse ecological and socio-economic systems (Ghosh and Mistri, 2021). Among the various forms of drought, meteorological drought, characterized by prolonged periods of below-average precipitation, emerges as a prevalent challenge that necessitates comprehensive understanding and management (Guttman, 1999). The critical examination of the spatial distribution of meteorological drought occurrences becomes imperative for devising effective strategies aimed at mitigating drought impacts and enhancing resilience. This research centers on the Rarh region of West Bengal, India, identified as particularly susceptible to drought phenomena, thereby underscoring the region's need for detailed drought analysis (Heim, 2002). Through the analysis of historical precipitation data, this study endeavors to elucidate the spatial patterns of meteorological drought within the Rarh region. It seeks to evaluate the consequent effects on the local environment and population. Findings from this investigation are anticipated to furnish decision-makers and stakeholders with crucial insights, thereby facilitating the formulation of targeted drought mitigation approaches and bolstering regional adaptability to this enduring hazard.

The primary aim of this study is an exhaustive examination of spatio-temporal variances and characterization of rainfall-based drought indices, specifically targeting the Rarh region of West Bengal. It undertakes a thorough spatial evaluation to discern drought conditions across the varied landscape of the Rarh region, a pursuit to decode patterns and inconsistencies of drought occurrences within this distinct area (Ghosh and Mistri, 2021; McKee, *et al.*, 1993). Additionally, this investigation spans an extensive temporal frame, scrutinizing drought patterns from 1986 to 2020. This duration is pivotal for appreciating historical trends, cyclicity, and shifts in the frequency and intensity of drought, thus offering a longitudinal perspective on drought dynamics within the region (Guttman, 1999).

A cornerstone of this research is the application of the Standardized Precipitation Index (SPI) through IMD gridded rainfall data across diverse time scales—3, 6, 12, and 24 months. This computation is instrumental for a quantitative appraisal and juxtaposition of drought conditions over time, meticulously mirroring the climatic nuances of the Rarh region (Mishra and Singh, 2010; Nam *et al.*, 2015). By delving into SPI values, the study elucidates the severity and distinct characteristics of drought conditions in the Rarh region, aiming to furnish a detailed comprehension of how drought uniquely impacts this locale.

Moreover, the inquiry extends to assess the ramifications of identified drought patterns on water resources and agricultural modalities peculiar to the Rarh region. This exploration illuminates the socio-economic ramifications of drought conditions, rendering essential insights for regional stakeholders (Spinoni, *et al.*, 2014). By centering on the Rarh region of West Bengal, the study endeavors to deliver locale-specific insights into drought dynamics, indispensable for formulating localized drought risk management and mitigation strategies. The findings of this research are poised to assist regional planners, farmers, and policymakers in making enlightened decisions, thus enhancing resilience against drought-related challenges in the Rarh region.

Data Sources:

The rainfall, temperature, etc data has been collected from the IMD, Alipur, Kolkata and the Directorate of Agriculture, Agro-Meteorological Section, Government of West Bengal for about 35 years tentatively from 1986 to 2020. In case on insufficiency of data from those sources, the long-term daily rainfall data (spatial resolution 0.25 x 0.25 degree), maximum and minimum temperature data (spatial resolution 1 x 1 degree) of the study area has been downloaded from IMD, Pune website (https://imdpune.gov.in/Clim_Pred_LRF_New/Grided_Data_Download.html).

Methodology:

Standardized Precipitation Index (SPI)

The Standardized Precipitation Index (SPI) is a widely used drought index that provides a standardized measure of precipitation deficits or surpluses relative to the historical record for a specific region. The SPI is based on a probability distribution that describes the likelihood of a given amount of precipitation occurring in a given time period. The foundational methodology for SPI calculation follows the approach established by McKee, Doesken, and Kleist (1993) and the subsequent guidance provided by the World Meteorological Organization (WMO). The gamma distribution fitting and the normalization process are in accordance with established hydrological analysis techniques (Nam *et al.*, 2015; Tan, *et al.*, 2015).

Fitting the Probability Distribution:

For each grid, the monthly precipitation data were fitted to a probability distribution to model the observed precipitation frequency. Given that precipitation data are non-negative and can be highly skewed, a two-parameter gamma distribution was selected for this purpose. The gamma distribution is defined by the probability density function:

$$f(x; \alpha, \beta) = \frac{x^{\alpha-1} e^{-\frac{x}{\beta}}}{\beta^{\alpha} \Gamma(\alpha)} \quad (1)$$

where x represents the amount of precipitation, α is the shape parameter, β is the scale parameter, and $\Gamma(\alpha)$ denotes the gamma function.

Transformation to the Standard Normal Distribution:

The cumulative distribution function of the gamma distribution was employed to ascertain the cumulative probabilities associated with the observed precipitation amounts. These probabilities were subsequently normalized through a transformation to the standard normal distribution, yielding the SPI values. The transformation enables the representation of the precipitation anomalies as standardized deviations from the mean.

$$SPI = Z(P) \quad (2)$$

Where:

P is the cumulative probability,

Z is the z-score corresponding to P in the standard normal distribution.

Calculation of SPI Values for Multiple Time Scales:

SPI values were computed for four distinct time scales: 3, 6, 12, and 24 months. These multiple time scales allow the examination of different aspects of drought conditions, from short-term anomalies to longer-term trends. The SPI at a given time scale quantifies the precipitation deficit or surplus for the period relative to the long-term record, with the following general categorization:

Table 1. Classification used for SPI by McKee et al. (1993)

SPI Value	Class
> 2	Extremely wet conditions
$1.5 < \text{SPI} \leq 2$	Very wet conditions
$1 < \text{SPI} \leq 1.5$	Moderately wet conditions
$-1 \leq \text{SPI} \leq 1$	Near-normal conditions
$-1.5 \leq \text{SPI} < -1$	Moderate drought
$-2 \leq \text{SPI} < -1.5$	Severe drought
< -2	Extreme drought

The calculated SPI values enable a standardized approach to identify and monitor drought conditions, providing a valuable tool for water resource management and drought mitigation strategies.

Run theory:

The run theory was initially proposed by Yevjevich (Vicente-Serrano, *et al.*, 2010) employed in this research to identify and explore statistical properties associated with drought parameters. The primary focus is on run length (drought duration), sum sum (drought severity), and intensity. The crucial element in deriving these parameters is the threshold level, which can either remain constant or vary over time. For our analysis, we have set the threshold level at -1.0.

In the graphical representation, shaded areas in blue and red indicate positive and negative average monthly Standardized Precipitation Index (SPI) values, respectively. A drought event is defined as a continuous period during which the SPI remains below zero, reaching a value of -1.0 or lower and persisting for at least two consecutive months. The onset of a drought event is marked when the SPI consistently meets these conditions, and the event concludes when the SPI turns positive ($\text{SPI} > 0$).

Once drought events are identified, the run theory, as depicted in Figure 2, is applied to quantify four essential characteristics: duration (DD), intensity (DI), severity (DS), and

frequency. Drought duration (DD) refers to the period measured in the number of months between the initiation and termination of a drought event. Drought severity (DS) is determined by calculating the absolute sum of all drought index values throughout a drought event. Drought intensity (DI) is then computed as the ratio of severity to the duration of the drought. The relevant formulas are provided below, where “e” denotes a drought event, “j” represents a month, and “Index j” corresponds to the SPI value in a given month (Vicente-Serrano, *et al.*, 2010; Wilhite, 2000; WMO, 2012; Yevjevich, 1967).

$$D_s = \left| \sum_{j=1}^{D_d} \text{Index}_j \right| \quad (3)$$

$$D_i = \frac{D_s}{D_d} \quad (3)$$

Results and Discussion:

Descriptive statistics of annual rainfall:

The results revealed that mean annual rainfall of the study area ranging from 1,254.20 mm to 1,869.79 mm across the grids, indicating a spatially diverse pluviometric regime. The coefficient of variation (CV) across the grids ranged from 0.13 to 0.34, with higher CVs observed in the northern grids, indicating greater unpredictability of rainfall patterns. Kurtosis values varied, with several grids exhibiting high kurtosis, indicative of a propensity for extreme rainfall events. This was particularly observed in grids G37 and G44, where kurtosis exceeded 4.0. Skewness analysis suggested a mix of right-skewed (positive skewness) and left-skewed (negative skewness) distributions across the region, with notable right skewness in G37, implying a higher occurrence of extreme rainfall events in this grid. The spatial patterns observed from Figure 2 align with the descriptive statistics, showcasing distinct rainfall regimes within the Rarh region. The northern districts, represented by grids with higher CVs and kurtosis, may be more prone to erratic rainfall and extreme weather events. In contrast, the southern districts exhibit lower variability and a more symmetrical distribution of rainfall, as indicated by lower CVs and skewness values. The skewness in the data points to potential climatic asymmetries, where some areas might be at greater risk for drought conditions (negative skewness), while others could be more susceptible to floods (positive skewness). These findings are crucial for regional agricultural planning, particularly in determining crop types, irrigation requirements, and risk management strategies.

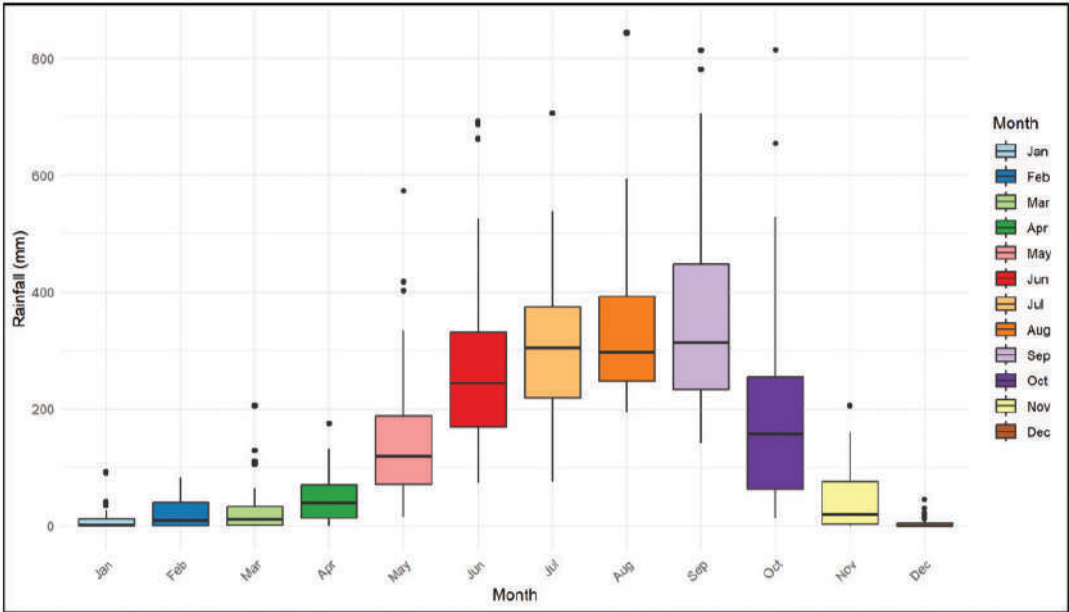
Drought frequency using SPI time scales:

The Figure 3 represents the spatial distribution of drought frequency using the Standardized Precipitation Index (SPI) in Rarh region of West Bengal during 1986 to 2020, indicating number of drought events occurred during this period. Based on short-term SPI value (SPI-3), the highest drought frequency (31–33 events) occurs in the south-eastern regionnamely Purba Medinipur, Pashim Medinipur and Hoara districts, indicating high susceptibility to short-term

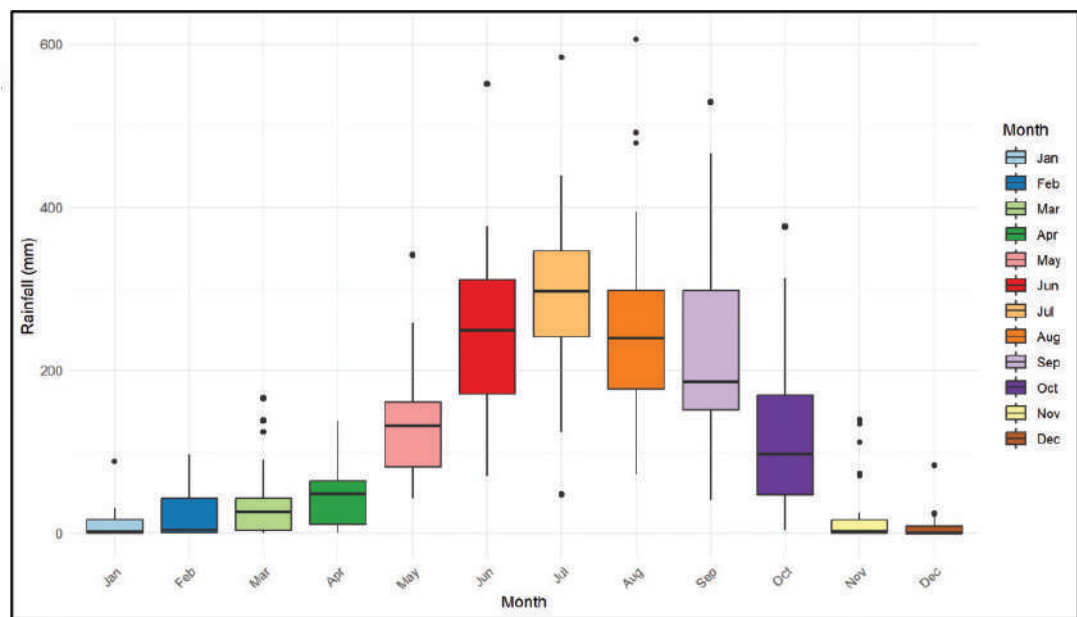
meteorological droughts, possibly due to erratic monsoon rainfall which affect crop failure. Northern and north-western areas (Murshidabad, Birbhum, Paschim Bardhaman) generally exhibit lower frequencies (19–22 events), indicating relatively stable short-term precipitation conditions. Spatial pattern shows localized hotspots of high frequency in the south-central belt (Figure 3a). Whereas 6-month SPI scale ranges between 9 to 25 (Figure 3b). A prominent high-frequency zone (23–25 events) is observed in the south-east (Purba Medinipur district), while much of the northern and eastern parts experience lower values (9–15 events). This scale captures seasonal drought, reflecting prolonged rainfall deficits beyond a single month but shorter than annual persistence.

The SPI-12 and SPI-24 indicates the spatial distribution of long-term drought events (Figure 3c and d). The SPI-12 showed that the central-western and south-western parts of the study area namely Purulia, Bankura and Jhargram districts have higher drought frequencies (9–12 events), possibly indicating recurring annual-scale water stress. The north-eastern belt shows the lowest values (2–4 events), suggesting relatively better annual precipitation stability (Figure 3 c). On the other hand, SPI-24 shows frequencies between 1 and 6 events during 1986-2020. South-eastern and central regions experience higher drought recurrence (5–6 events), indicating multi-year persistent dry spells. North-western and some eastern regions show the lowest frequency (1–2 events), indicating resilience to prolonged drought (Figure 3 c).

G1



G32



G56

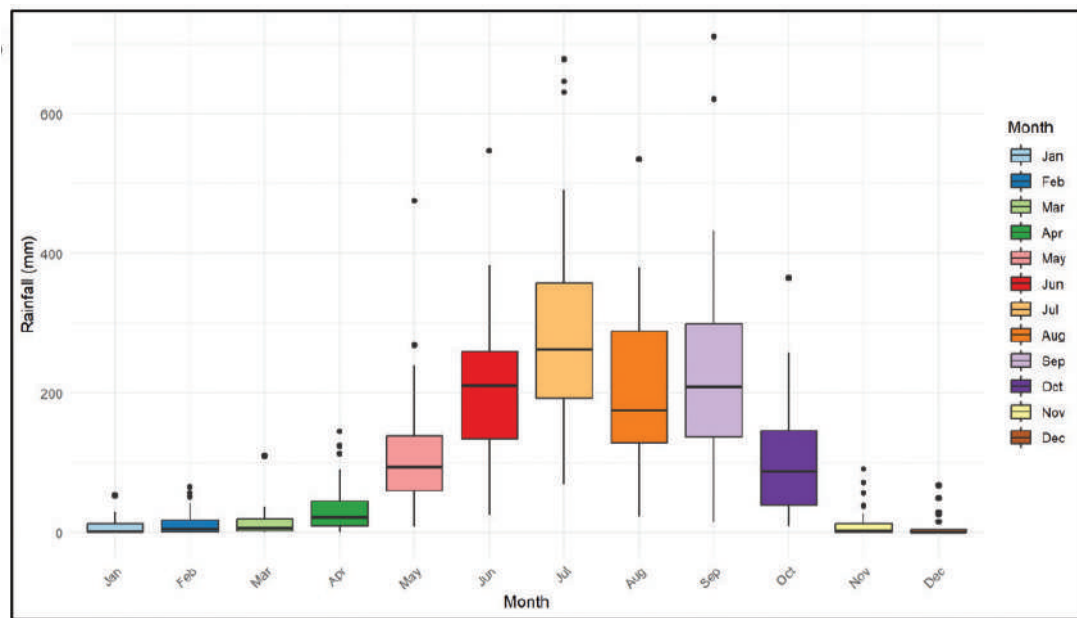


Figure 1. Boxplot selected Grids G1, G32 and G56

The south-eastern zone repeatedly emerges as a high drought frequency hotspot across all time scales, pointing to structural climatic vulnerability in that region. As the SPI timescale increases (from 3 to 24 months), the magnitude of drought frequency decreases, but spatial persistence of hotspots remains. Short-term droughts (SPI-3 and SPI-6) are more widespread

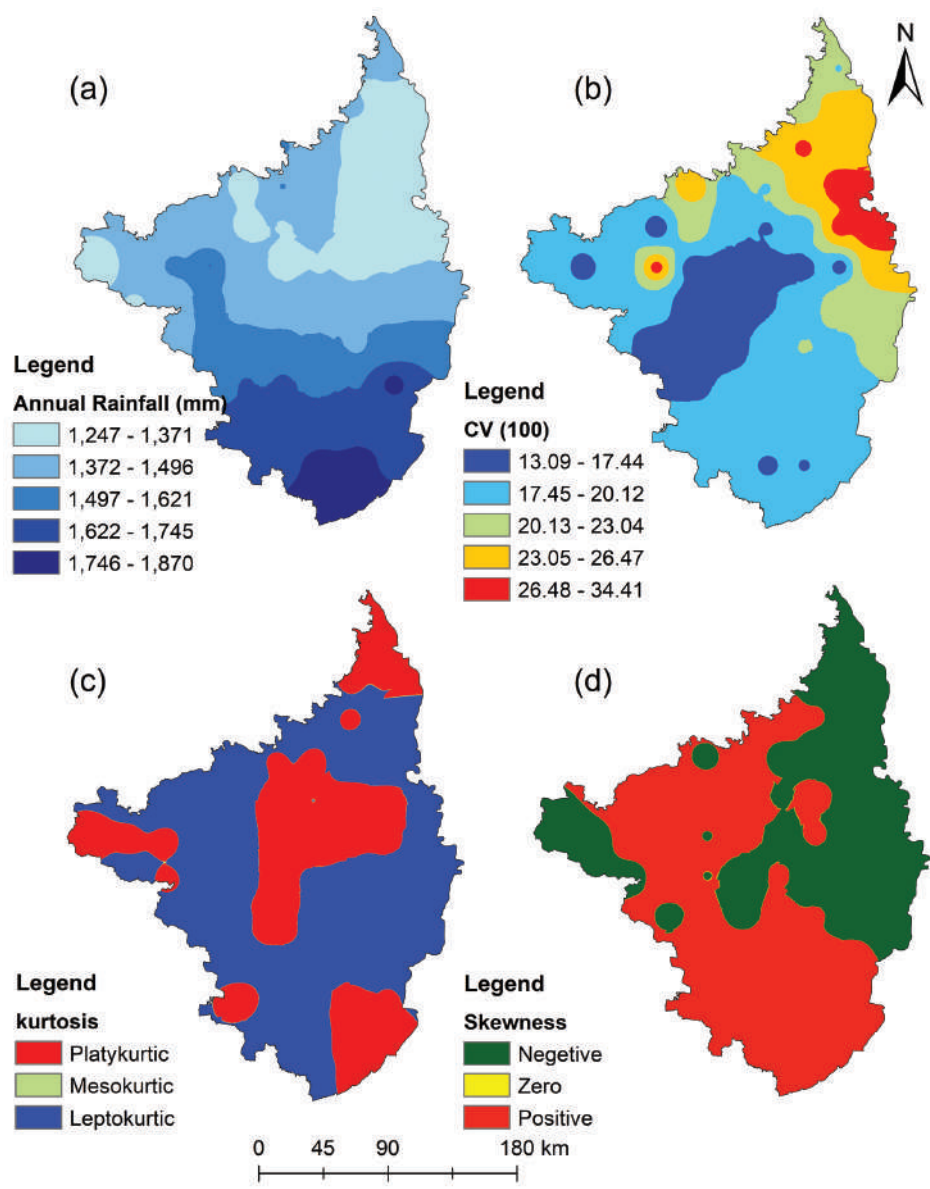


Figure 2. Descriptive Statistics of long-term annual rainfall (a) Mean (b) Coefficient of variation, (c) Kurtosis and (d) Skewness

and intense, whereas long-term droughts (SPI-12 and SPI-24) are more localized. These results highlight the need for targeted drought mitigation strategies, with seasonal and short-term measures in south-eastern areas, and long-term resilience building in south-western and central belts.

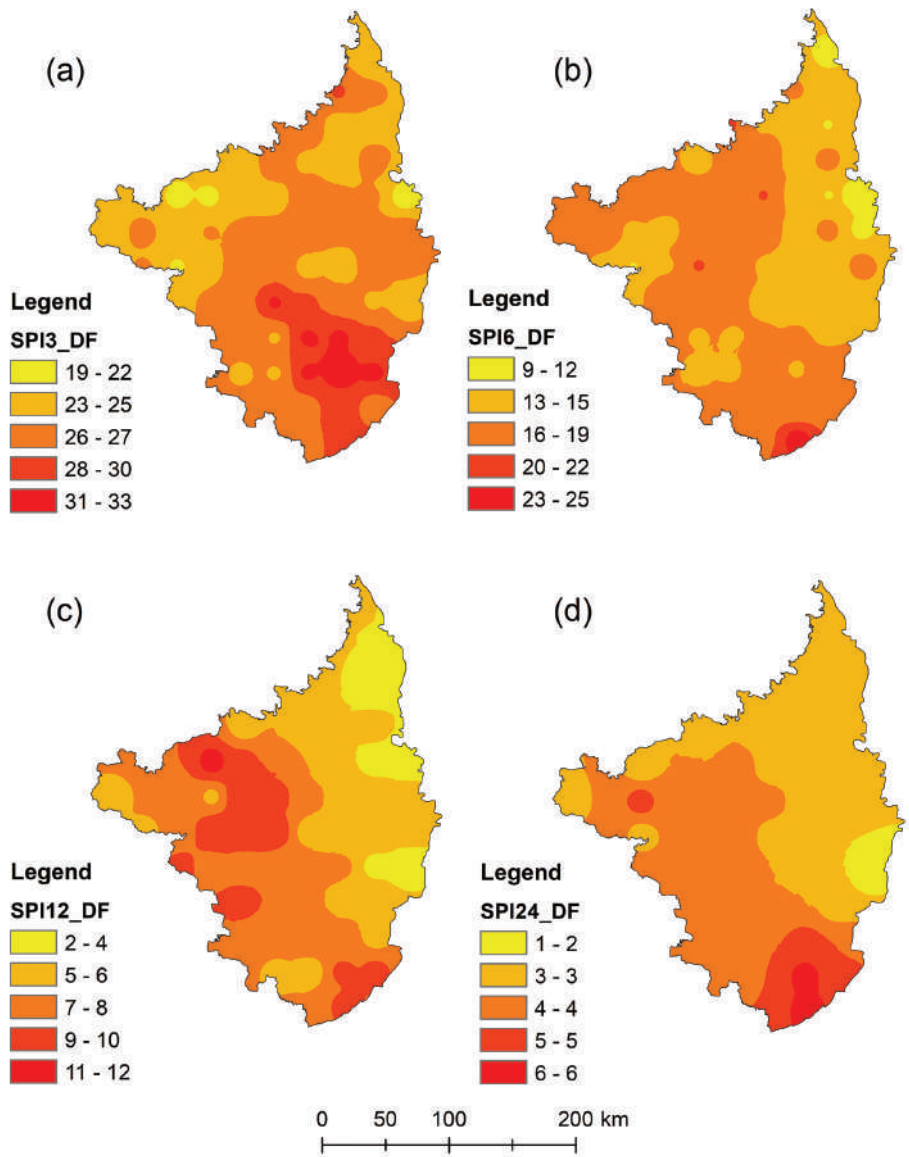


Figure 3. Drought frequency (DF) (a) SPI3 (b) SPI6, (c) SPI12 and (d) SPI24

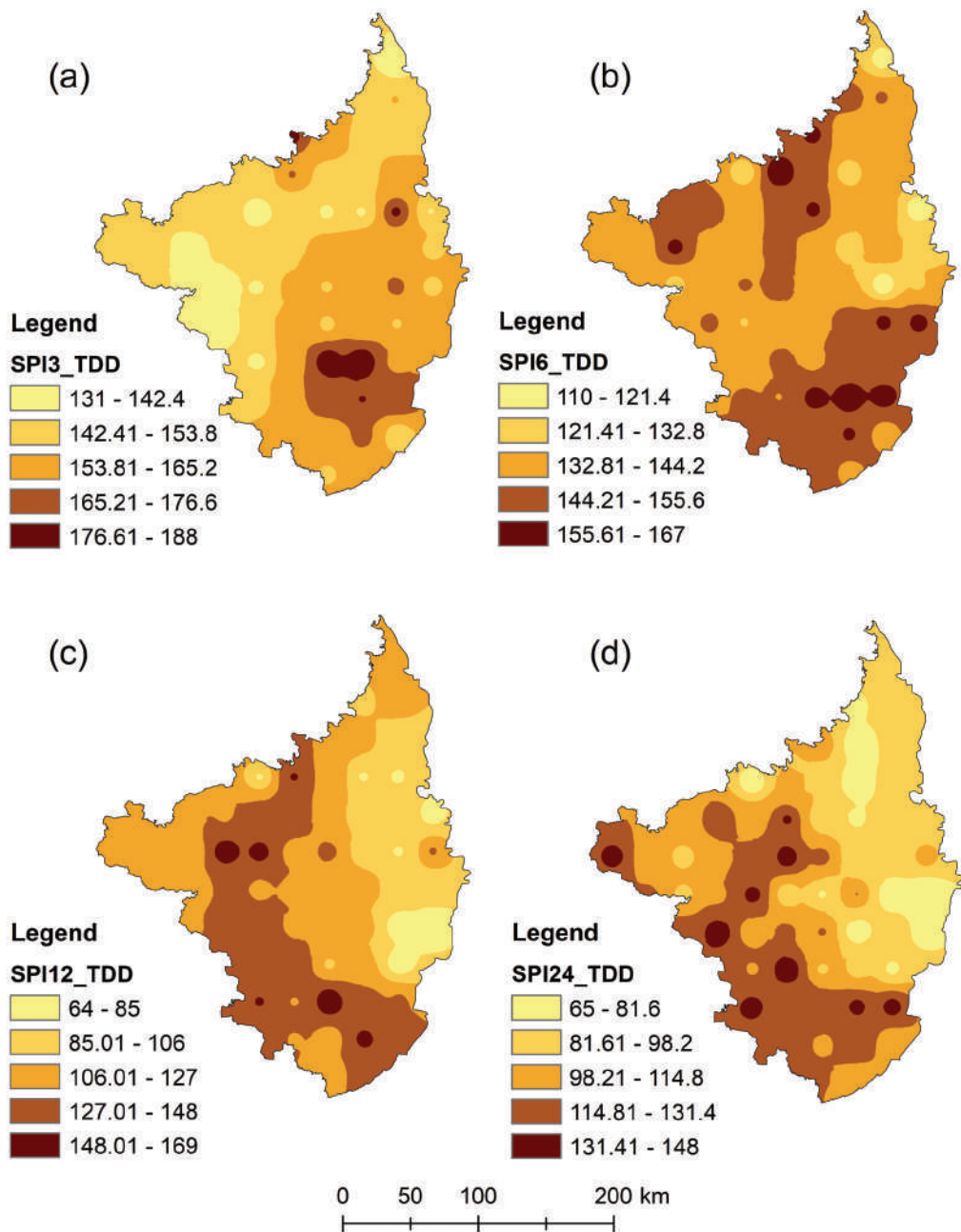


Figure 4. Total drought duration (TDD) (a) SPI3 (b) SPI6, (c) SPI12 and (d) SPI24

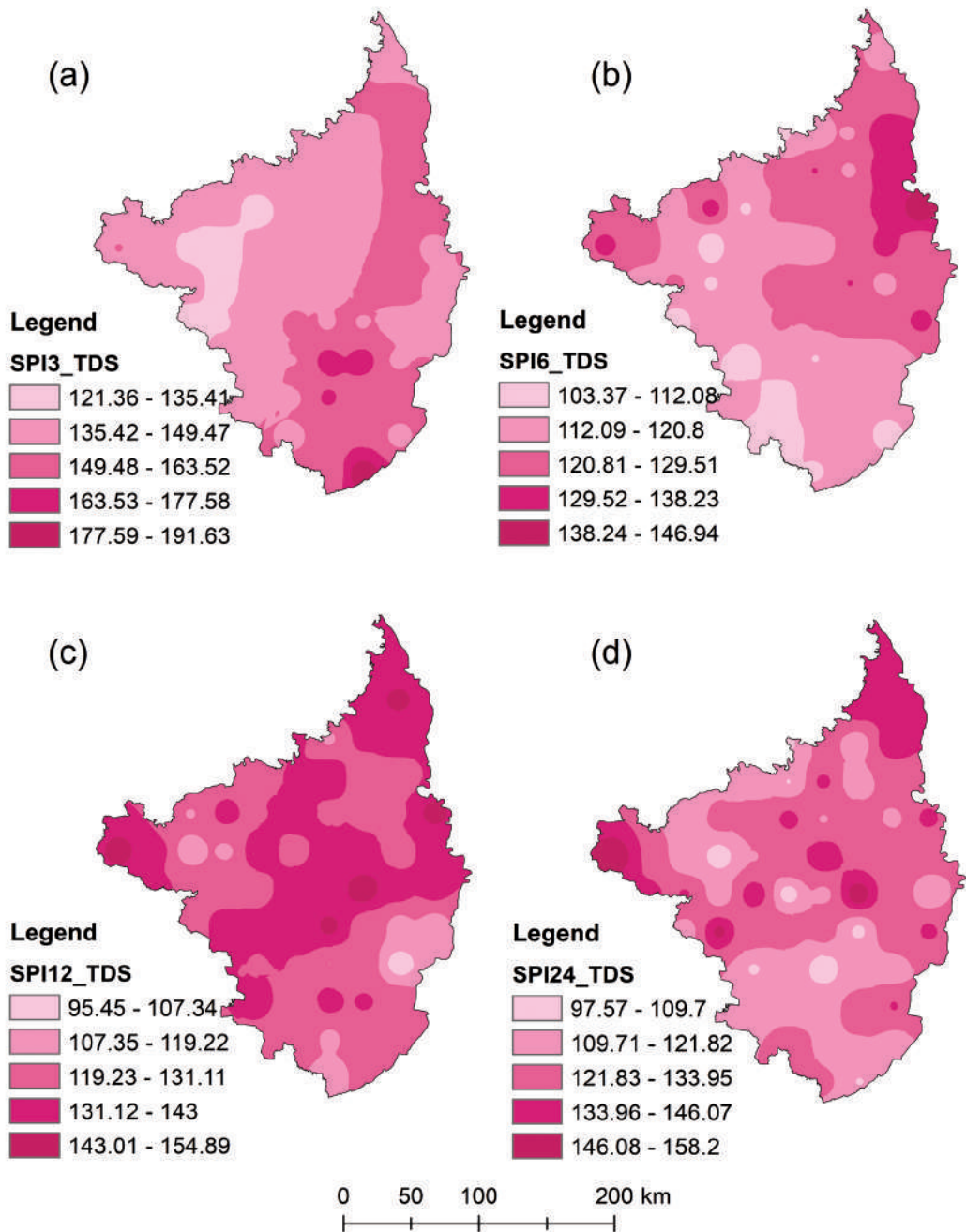


Figure 5. Total drought severity (TDS) (a) SPI3 (b) SPI6, (c) SPI12 and (d) SPI24

Total drought duration using SPI time scales:

The figure 4 illustrate the Total Drought Duration (TDD) in the Rarh region of West Bengal, India, using the Standardized Precipitation Index (SPI) over different time scales. TDD refers to the cumulative length of time during which drought conditions persist.

The short-term drought duration (SPI-3) ranges from 131 to 188 months across 63 grids. The highest TDD (176.61–188 months) is concentrated in the south-central zone namely Haora, Paschim Medinipur and Purba Medinipur districts, indicating persistent short-term drought episodes, which affected crops yield. On the other hand, the lowest TDD (131–142.4 months) is recorded in parts of the north-west and north-east, indicating fewer or shorter 3-month drought spells (Figure 4a). The mid-term drought duration (SPI-6) varies from 110 to 167 months (Figure 4b). The highest TDD (155.61–167 months) is observed in the south-east and isolated pockets in the north-east, pointing to areas prone to prolonged seasonal droughts. The shortest durations are mostly in the north-west and some central areas. The annual drought (SPI-12) duration varies between 64 and 169 months (Figure 4 c). The results showed that western, south-western, and parts of southern zones experienced the highest TDD (148.01–169 months), indicating recurrent and sustained annual drought conditions. Eastern zones, particularly in the north-east, experience lower durations (64–85 months), reflecting reduced annual-scale drought persistence. On the other hand, long-term drought (SPI-24) duration varies from 65 to 148 months (Figure 4d). The SPI-24 showed central, south-western, and south-eastern parts record the highest durations (131.41–148 months), highlighting regions vulnerable to multi-year drought persistence. The lowest values (65–81.6 months) are found in the north-west and some eastern sectors as per SPI-24.

South-central and south-eastern parts of Rarh region consistently exhibit high TDD values across short- to long-term SPI timescales, indicating chronic drought-prone conditions. TDD magnitude decreases as the SPI timescale increases, which is expected since longer timescales smooth short-term fluctuations, reducing the total number of identified drought months. The north-eastern and north-western parts of the study area generally exhibit shorter drought durations, indicating relative resilience to prolonged dryness. Spatial patterns of TDD largely align with drought frequency (DF) patterns, confirming that regions with higher drought recurrence also tend to experience longer drought spells.

Total drought severity using SPI time scales:

The short-term total drought severity (TDS) of the study area ranges from 121.36 to 191.63. The short-term (SPI-3) indicates the highest drought severity (177.59–191.63) is concentrated in the south-eastern region, indicating intense short-term drought conditions. Lower severity zones (121.36–135.41) are mostly in the north-west and parts of the north-east (Figure 5a). The mid-term total drought severity varies between 103.37 and 146.94 (Figure 5b). The results indicates that most severe seasonal droughts (138.24–146.94) appear in the north-east and south-east, consistent with seasonal drought hotspots, whereas the lowest severity is distributed mainly in north-western and central regions. The annual total drought duration

varies from 95.45 to 154.89. The high drought severity (143.01–154.89) is observed in the south-western, central, and localized southern zones (Figure 5c). The lowest values are found in parts of the north-east, indicating milder annual drought events there. The long-term total drought severity values range from 97.57 to 158.2 (Figure 5d). The SPI-24 showed that the highest drought severity (146.08–158.2) occurs in central and south-central zones, suggesting that when long-term droughts occur in these areas, they are intense and persistent. Lower severity (97.57–109.7) is concentrated in the north-west and isolated eastern pockets.

Across all timescales, south-eastern (Purba Medinipur, Paschim Medinipur, Hoara and Jhargram) and central belts (Bankura and Puruliya) appears as recurrent high-severity drought zones, aligning with the high drought duration (TDD) and frequency (DF) patterns from earlier figures. Short-term drought severity (SPI-3) shows the highest absolute values, which is expected since shorter timescales capture rapid and intense dry anomalies. Long-term severity patterns (SPI-12 and SPI-24) are more spatially homogeneous but still reveal persistent hotspots in the south-central belt. These results suggest that drought management strategies should prioritize south-east and central regions for both short-term drought relief and long-term resilience planning.

Conclusions:

This study applied the Standardized Precipitation Index (SPI) at multiple accumulation periods (3-, 6-, 12-, and 24-month) to quantify spatial drought characteristics in terms of frequency (DF), total duration (TDD), and total severity (TDS) using the run theory approach. The results revealed consistent spatial patterns across the three indicators, with the south-eastern and central regions emerging as persistent drought hotspots across both short- and long-term timescales. Short-term droughts (SPI-3 and SPI-6) were found to be more frequent and severe, whereas long-term droughts (SPI-12 and SPI-24) exhibited lower recurrence but higher persistence in certain zones.

The results indicate that northern grids of the Rarh region are more prone to erratic rainfall patterns and extreme weather events, as evidenced by higher coefficients of variation (CV) and kurtosis values. This spatial heterogeneity necessitates targeted drought mitigation strategies that consider the unique climatic and hydrological characteristics of each sub-region.

The strong spatial overlap between high DF, TDD, and TDS reveals the compounded drought vulnerability of specific sub-regions, demanding targeted interventions. These findings provide valuable inputs for drought early warning systems, agricultural planning, and water resource management, particularly in the identified hotspot areas. Future work should integrate climate projections and land-use dynamics to assess potential shifts in drought risk under changing climatic conditions.

Acknowledgements:

We acknowledge the support from Department of Geography and Applied Geography, University of North Bengal and Swami Vivekananda Merit-cum-Means Scholarship of West Bengal Government. We would like to express our heartfelt appreciation to all professionals,

and anyone who contributed to this research.

Funding:

Swami Vivekananda Merit-cum-Means Scholarship of West Bengal Government.

Data availability statement:

The data that support the findings of this study are not publicly available. However, anonymized data may be made available upon reasonable request to the corresponding author.

Author contribution statement:

Conceptualization, P.S., D.K.M.; methodology, P.S., D.K.M.; software, P.S., D.K.M.; validation, P.S., D.K.M.; formal analysis, P.S., D.K.M.; investigation, D.K.M., P.S.; resources, P.S., D.K.M.; data creation, P.S., D.K.M.; writing—original draft preparation, P.S., D.K.M.; writing—review and editing, P.S., D.K.M.; visualization, P.S., D.K.M.; supervision and revision, D.K.M., P.S.; All authors have read and agreed to the published version of the manuscript.

References:

- Ghosh, S., & Mistri, B. (2021). Assessing coastal vulnerability to environmental hazards of Indian Sundarban delta using multi-criteria decision-making approaches. *Ocean & Coastal Management*, 209, 105641.
- Guttman, N. B. (1999). Accepting the Standardized Precipitation Index: A calculation algorithm. *Journal of the American Water Resources Association*, 35(2), 311-322. <https://doi.org/10.1111/j.1752-1688.1999.tb03592.x>.
- Heim Jr., R. R. (2002). A Review of Twentieth-Century Drought Indices Used in the United States. *Bulletin of the American Meteorological Society*, 83(8), 1149-1165. [https://doi.org/10.1175/1520-0477\(2002\)083<1149:AROTCD>2.3.CO;2](https://doi.org/10.1175/1520-0477(2002)083<1149:AROTCD>2.3.CO;2).
- Mishra, A. K., & Singh, V. P. (2010). A review of drought concepts. *Journal of Hydrology*, 391(1-2), 202-216. <https://doi.org/10.1016/j.jhydrol.2010.07.012>.
- McKee, T. B., Doesken, N. J., & Kleist, J. (1993). The relationship of drought frequency and duration to time scales. In Proceedings of the 8th Conference on Applied Climatology (Vol. 17, No. 22, pp. 179-183). *American Meteorological Society*.
- Nam, W. H., Hayes, M. J., Svoboda, M. D., Tadesse, T., & Wilhite, D. A. (2015). Drought hazard assessment in the context of climate change for South Korea. *Agricultural Water Management*, 160, 106-117.
- Spinoni, J., Naumann, G., Carrao, H., Barbosa, P., & Vogt, J. (2014). World drought frequency, duration, and severity for 1951–2010. *International Journal of Climatology*, 34(8), 2792-2804.
- Tan, C., Yang, J., & Li, M. (2015). Temporal-spatial variation of drought indicated by SPI and SPEI in Ningxia Hui Autonomous Region, China. *Atmosphere*, 6(10), 1399-1421.

- Vicente-Serrano, S. M., Beguería, S., & López-Moreno, J. I. (2010). A Multiscalar Drought Index Sensitive to Global Warming: The Standardized Precipitation Evapotranspiration Index. *Journal of Climate*, 23(7), 1696-1718. <https://doi.org/10.1175/2009JCLI2909.1>
- Wilhite, D. A. (2000). Drought as a Natural Hazard: Concepts and Definitions. In D. A. Wilhite (Ed.), *Drought: A Global Assessment* (Vol. 1, pp. 3-18). Routledge.
- World Meteorological Organization (WMO), (2012). *Standardized Precipitation Index User Guide* (WMO-No. 1090), Geneva.
- Yevjevich, V. M. (1967). *Objective approach to definitions and investigations of continental hydrologic droughts*, An (Doctoral dissertation, Colorado State University. Libraries).



Estimation of Water Quality through Machine Learning (ML): A Case Study of Chamta River

Gargi Sarkar¹, Subhadip Gupta^{2*}

¹*Department of Geography, Sree Chaitanya College, Habra, West Bengal*

²*Department of Geography, Asutosh College, Kolkata, West Bengal*

**Corresponding author: subhadip.gupta@asutoshcollege.in*

Abstract: The current research is based on the water quality of a tiny river called Chamta, which is a part of Mahananda river system. The Chamta watershed is lying over the Darjeeling Himalayan foothills area. The quality of river water is determined by the water quality index (WQI), which is estimated on the basis of the selected water quality parameters. The data has been extracted from the set stations along the Chamta river by using field kits. The recorded data of water quality parameters are used to predict the water quality of this particular river for manage the riverine ecological health intact. Machine learning algorithms, like Linear regression, Random forests, K-Nearest Neighbors, SVM, LASSO regression, Extreme Gradient Boosting have been used to find the best fit model. The Linear Regression model and the Random Forest model has been detected as the best fit linear and non-linear machine learning model on the basis of the direction and magnitude of Mean Absolute Error (MAE), Mean Squared Error (MSE), R^2 , Akaike's Information Criterion (AIC), Schwarz's Bayesian Criterion (SBC) which can produce best predictive result of water quality of Chamta river with minimum possible error for managing the future water quality to keep intact the ecological services.

Keywords: Linear regression, Random forests, K-Nearest Neighbors, SVM, LASSO regression, Extreme Gradient Boosting, Parametric and non-parametric model, linear and non-linear model

Introduction:

Every waterbody has a chemical profile that shows how well it can support life or how dangerous it can be to ecosystems and human health (Uddin *et al.*, 2022; Kurwadkar *et al.*, 2022). Geochemical specification replicates the close correlations among the parameters of water chemistry and public health (Kanel *et al.*, 2023). Water quality of river water is crucial for sustainable management, ecological balance, and public health. Scientific assessment helps to make real understanding about the water quality and its function ability to preserve the aquatic ecosystem (Mishra *et al.*, 2025), which gives impact on native aquatic ecology as well as societal economy. Information regarding the presence of oxygen and toxic elements in water is very crucial for future use of that water resource (Zelenakova *et al.*, 2018; Huisman *et al.*, 2018). Quality of water acts as one of the indicators provides the mirror effect of environmental degradation which directly or indirectly affects the water resource mobilization by maintaining the ecosystem services (Walling & Webb, 1975). Water quality refers the physicochemical as well as biological which regulates the ecological and economic value of that particular waterbody (Meybeck *et al.*, 2006). Importance of water quality of river cannot be limited within its economic uses but the biodiversity, habitat function ability and ecological sustainability completely depended on the freshness of the available resources (Mishra *et al.*, 2025). Anh *et al.* (2023) gave caution over the entry of heavy metals in food chain as well as food web that may causes species declination. Existence of fresh water river favours nutrient cycling (Anh *et al.*, 2023). Fresh water acts as the source of drinking water, water for agriculture to ensure food security and industrial uses, whereas the contamination in water deteriorates public health (Das and Kumar, 2020, Zelenakova *et al.*, 2018). Field data recording on water quality and its scientific data analysis is very necessary for making the policy decisions of integrated management program to mitigate pollutants (Zelenakova *et al.*, 2018). True balance is needed between the developmental economy and environmental sustainability, while you go for use the existing water resource (Kumar, 2012), as most of the river water quality has been deteriorating by the name of so called 'development' of human being through their mechanized agricultural and industrial revolution and rapid urbanization (To, 2020). Human interference in form of agricultural, mining activity driven runoff can raise the salinity level in water body, which may modify the chemical profile as well as freshwater native biodiversity (Cañedo-Argüelles *et al.*, 2013). Addition of nutrient in form of phosphorus and nitrogen may increase the growth of algal blooms by enhancing the rate of eutrophication (Huisman *et al.*, 2018). Similar scenario has been sited at Jamuna River in Bangladesh (Rahman *et al.*, 2023), Iril and Sabarmati River (Bidyabati and Nath, 2023; Khatri *et al.*, 2020), Mahananda and Tapti rivers in India (Desai & Tank, 2017). Water quality indices are progressively used to study the health of ecosystem with any undisturbed regional references (Uddin *et al.*, 2021). Water quality has been assessed by using several water quality index (WQI) schemes like Indian Council of Medical Research (ICMR) and the Bureau of Indian Standards (BIS) (Dwivedi & Dubey, 2023), modified NSF, Weighted Arithmetic Water Quality Index (WAWQI) and the Canadian Council of Ministers of the Environment Water Quality Index (CCMEWQI) (Desai & Tank, 2017). Those schemes may produce different magnitude of WQI value as

they are associated with the regular reading of different water quality physiochemical and microbiological parameters like pH, turbidity, dissolved oxygen, biochemical oxygen demand, and total dissolved solids, calcium, magnesium, total alkalinity, total hardness as per regional suitability (Datchanamoorthy *et al.*, 2024; Dwivedi & Dubey, 2023; Bidyabati and Nath, 2023; Khatri *et al.*, 2020; Desai & Tank, 2017). Dissolved oxygen is an important sign because it is the “breath” of aquatic systems, which regulates the oxygen levels, existence of nutrient and passively controls the food webs (Jane *et al.*, 2021). pH, alkalinity, and hardness are one of the important controls of water quality as they work as silent determinant, which regulates how heavy metals or nutrients dissolve in water, how toxic certain ions are, and how well the water can handle the sudden change in chemical property by using the feedback mechanism. Fortin (2024) established that a neutralized acid-base normally refers that the diluted metals don’t twig to the present organisms as much and reduces the harmful impacts. Electrical conductivity (EC) and total dissolved solids (TDS) generate quick reactions about the ionic loads and hold non-linear complex relationship among them (Rusydi, 2018). Water chemistry affects by the presence of suspended solid in water which partially oppose the light from getting through (Adjovu *et al.*, 2023). In such cases, the WQI acts as a proxy indicator of environmental degradation, which may be considered as a effective tool for local administrative authority or concerned policy makers to take the remediation steps (Desai & Tank, 2017; Assessment of urban river water quality using modified NSF water quality index model at Siliguri city, West Bengal, India, 2022). Parametric (logistic regression, Support vector machine) models and non-parametric (K-Nearest Neighbors, SVM, XGBoost, LASSO) models are used for the analysis of WQI data. Parametric and non-parametric models are popular for the simplicity in computing and flexible adaptability in computing (Bellur *et al.*, 2023). Supervised non-parametric machine learning models are popular for predictive analysis regarding water quality on the basis of recorded data with greater accuracy (Tharun Kumar *et. al.*, 2023). Still inaccuracy may exist for WQI prediction until the ecosystem-specific supervised machine learning models are used (Datchanamoorthy *et al.*, 2024; Fernández del Castillo *et al.*, 2022). Case studies have been cited, where the Random Forest model considered as best fit model for the case study of Narmada (Gour & Gour, 2024) and a river reach at Rajasthan (Tolometti (2023), which shows minimum magnitude of error level as per MAE, RMSE and highest level of WQI predictive accuracy. K-Nearest Neighbours (KNN) model (Deosarkar *et. al.*, 2023), Extreme Gradient Boosting (XGBoost) (Elvin and Wibowo, 2024), XGBoost model (Zhao, 2024) and LASSO regression model (Hoque *et al.*, 2022; Am *et al.*, 2022; Nagalakshmi and Kumar, 2024), Support Vector Machine (SVM) model (Rogers and Ambili, 2024; Duan *et. al.*, 2023), have been used as the best fit water quality predictive model with highest magnitude of accuracy on the basis of MAE, RMSE and R^2 . Unpredictable character of environmental parameters might be responsible for the situational inaccuracy of the WQI through a particular recommended machine learning model (Datchanamoorthy *et. al.*, 2024). Success rate depends on the suitable parameter selection, intensive continuous data recording and proper statistical analysis, which determines the enhancement of fruitful watershed management plan (Alqahtani *et al.*, 2022; Swetha *et al.*, 2023; Rogers and Ambili, 2024).

Methodology:

Water pH (Figure 2), EC (Figure 3), TDS (Figure 8), DO (Figure 1), calcium (Figure 7), Magnesium (Figure 6), total hardness (Figure 5), total alkalinity (Figure 4) has been recorded (at the seven set stations along the Chamta river in the monsoon, pre-monsoon and post-monsoon months by using the field kits in the year of 2022. Water quality index has been estimated to represent the status of all associated water quality parameters in a holistic manner through the numerical value. The ICMR scheme (1975) has been used to estimate the WQI of Chamta river water. The biomedical and health data-based research of India is oriented and structured by the Indian Council of Medical Research institute (ICMR's National Ethical Guidelines, 2017), that is based on the international standards as well as suitable for the Indian scenario (Behera *et al.*, 2019). CIOMS guidelines (2016) gave significant global guidelines which was not region-specific for the local level community related environmental issues and water-based research (van Delden & van der Graaf, 2017; Mathur & Swaminathan, 2018). The 'Declaration of Helsinki' did not specifically concentrate on community scale impacts arising from the environmental degradation like-contamination of waterbody (Hrudey *et al.*, 2021; World Medical Association, 2013). Revised and modified U.S. Common Rule presented a few advantageous reforms; though it might not be familiar especially for the socio-economic scenario of India, where community health and hygiene has the foremost priority (Shrikhande *et al.*, 2023; LeCompte & Young, 2020; Walch-Patterson, 2020). ICMR guidelines of water quality analysis-based research is most relevant and dependable in comparison of CIOMS, Helsinki, and the U.S. Common Rule in India (LeCompte & Young, 2020; Saha *et al.*, 2020; World Medical Association, 2013). Calcium and EC have been deducted from the current data base before proceeding for the analysis of best-fit model to reduce the level of multicollinearity ($VIF < 10$). Distribution of each parameter is tested to find the best fitted model on the basis of 'p' value. Linear regression, Random forests, K Nearest Neighbors, SVM, LASSO regression machine models have been tested to determine the best fitted predictive model of WQI. Used data set was randomly divided into eighty percent (80%) as training data and twenty percent (20%) as test data for required validation, which could be used to evaluate efficacy of the introduced model (Gholamy, Kreinovich and Kosheleva, 2018). The training data set was used for finding the 'best' parameter values and the test set was used just for evaluating the results, avoiding overfitting and guaranteeing a fair best-possible evaluation of the expected accuracy (Joseph, 2022). An eighty-twenty (80-20) split has become a standard-thumb rule in machine learning and applied statistics for striking a happy medium between making the best use of your data to train the model, and having enough observations to test the model (Gholamy, Kreinovich and Kosheleva, 2018; Joseph, 2022). Further, experimental evaluations on multi-class classifiers show that the eighty-twenty (80-20) ratio can be yield reliably accurate performance of estimation (Rácz *et al.*, 2021). This twenty percent (20%) data of holdout validation is computationally efficient and perfectly acceptable procedurally (Joseph, 2022; Rácz *et al.*, 2021). Mean Absolute Error (MAE), Mean Squared Error (MSE), Coefficient of determination (R^2), Akaike's Information Criterion (AIC), Schwarz's Bayesian Criterion (SBC) are used as the performance indicators to select the best fit model. Attempt has been made to reflect the variable's importance under the introduced non-linear models.

Result and Discussion:

The best fitted distribution of the DO, pH, and TDS are Erlang, Generalized Extreme Value (GEV) and log-normally distributed respectively, whereas the EC, Total Alkalinity, Total Hardness and Magnesium follow the logistic distribution. It denotes that no one of the associated water quality parameters follow the normal distribution (Table 1). So, the non-parametric models might be suitable for the predictive analysis of the current data set. Linear association between the WQI and its regulatory variables might also be tested through the linear regression model. The data has been randomly split into two segments. 80% of the observations were used to train the model and remaining 20% is for validation. The following machine learning models are used to test the predictive accuracy of the WQI of Chamta river, like-Linear regression model, Random forests model, K Nearest Neighbors model, SVM model, LASSO regression model, Extreme Gradient Boosting model.

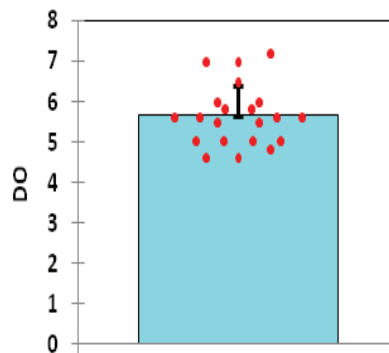


Figure 1. DO level along with mean at representative buffer villages along Chamta channel in April, July and October of surveyed year 2022.

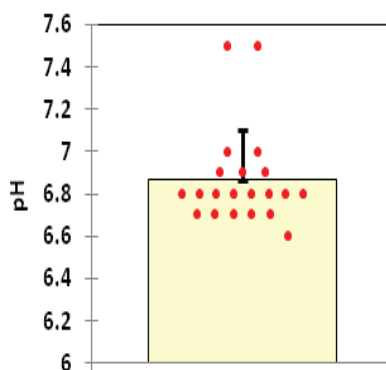


Figure 2. pH level at representative buffer villages along Chamta channel in April, July and October of surveyed year 2022

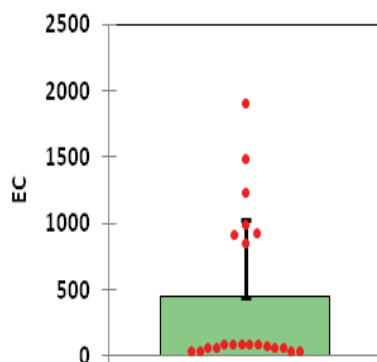


Figure 3. EC level at representative buffer villages along Chamta channel in April, July and October of surveyed year 2022

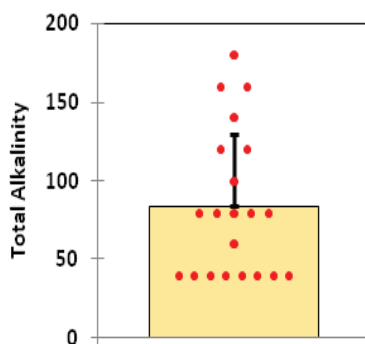


Figure 4. Total Alkalinity level at representative buffer villages along Chamta channel in April, July and October of surveyed year 2022

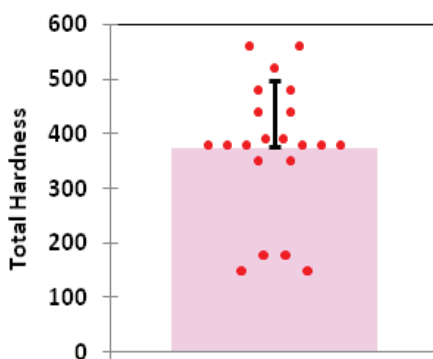


Figure 5. Total Hardness level at representative buffer villages along Chamta channel in April, July and October of surveyed year 2022

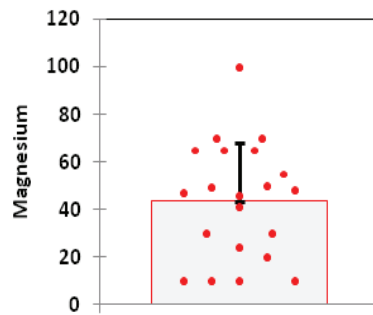


Figure 6. Magnesium level at representative buffer villages along Chamta channel in April, July and October of surveyed year 2022

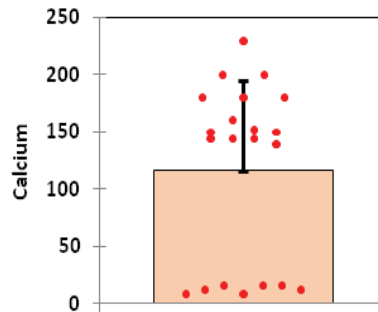


Figure 7. Calcium level at representative buffer villages along Chamta channel in April, July and October of surveyed year 2022

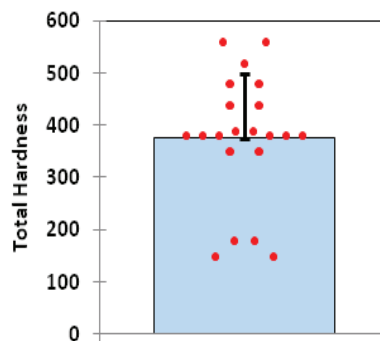


Figure 8. TDS level at representative buffer villages along Chamta channel in April, July and October of surveyed year 2022

Table 1. Best-fitted distribution model

Exploratory Parameters of water quality	Best fitted distribution	p Value
DO	Erlang	0.826
pH	GEV	0.338
EC	Logistic	0.379
Total Alkalinity	Logistic	0.359
TDS	Log-normal	0.018
Total Hardness	Logistic	0.379
Magnesium	Logistic	0.937

Linear Regression Model (LRM):

Linear regression models are essential statistical techniques for determining the connection between a dependent variable and one or more independent variables. Linear regression is widely used in a variety of sectors, including healthcare and social sciences, because to its simplicity and interpretability. Roustaei (2024) state that multiple linear regression allows for a more sophisticated study of correlations by expanding the model to incorporate numerous independent variables. Linear regression model is considered as such a method which is used for the estimation of the predictive magnitude of the dependent variable by using the independent variables under study. Linearity, independence, homoscedasticity, and normality of residuals are important requirements for valid inferences (Jacobs, 2023). A statistical technique for simulating the connection between a dependent variable and one or more independent variables is called linear regression. It makes the assumption that the variables have a linear relationship and estimates the coefficients for the explanatory variables (Das, 2019). ANOVA shows the LRM is extremely statistically significant for the prediction of WQI of Chamta river (Table 2). The highest magnitude of standardized coefficient is estimated against DO for the pred...iction of WQI through LRM (Table 3), that refers the dominant role of DO for the influence over the water quality of Chamta channel.

Table 2. Analysis of variance

Source	DF	Sum of squares	Mean squares	F	Pr > F
Model	6	4166.696	694.449	30.647	<0.0001
Error Corrected	10	226.600	22.660		
Total	16	4393.295			

Computed against model $Y=Mean(Y)$

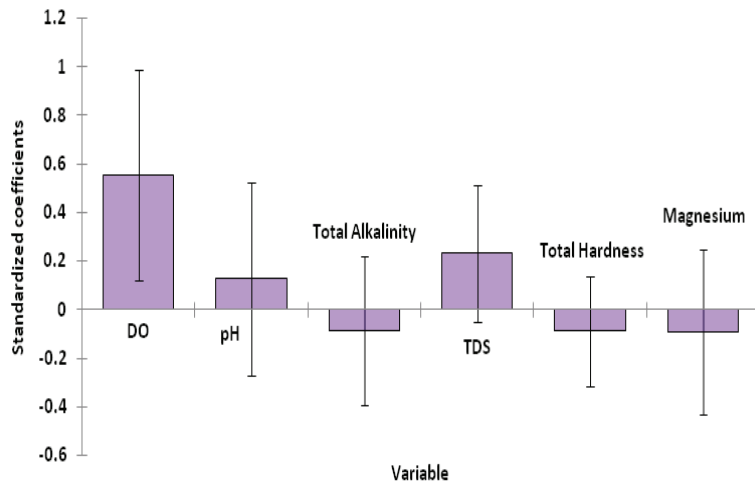


Figure 9. Standardized coefficients after LRM of the water quality parameters of Chamta river.

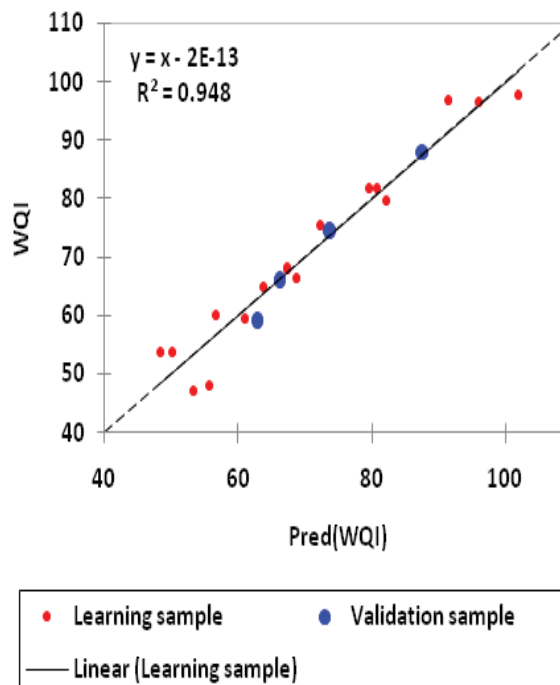


Figure 10. Relation between observed WQI and predicted WQI with learning samples and validation samples after LRM.

Random Forests Model (RFM):

Water quality prediction using the Random Forest model has emerged as a robust approach in various contexts, including groundwater, river ecosystems, and aquaculture (Fife & D’Onofrio, 2023; Couronné *et al.*, 2018). The robustness character of random forest model (RFM), as a consequence of its ensemble nature, is well accepted (Fife and D’Onofrio, 2023). This ensemble character consists of a number of independent decision trees which are built for using the bootstrap drawing and the to make easier the random feature selection process (Couronné *et al.*, 2018). This generates a higher resistance against the outliers or noises (Couronné *et al.*, 2018; Breiman, 2001). Since this model includes a larger number of decision trees to achieve the stability, the probability of the existence of generalization error is reduced under this particular model (Fife & D’Onofrio, 2023; Couronné *et al.*, 2018). The integrated diagnostic mechanism ranging from out-of-bag error of RFM emphasizes on the feature-importance metrics, which provide the information of the caliber and interpretability of an introduced model (Breiman, 2001; Couronné *et al.*, 2018; Fife & D’Onofrio, 2023). This machine learning technique excels in handling complex datasets and identifying significant water quality parameters, thereby facilitating informed decision-making for water management (Gour and Gour, 2024; Tolometti, 2023; Swetha *et al.*, 2023). DO, TDS and Magnesium have greater influence over WQI after RF model (Table 4) on the basis of mean increase error (Figure 12).

Table 3. Mean squared error:

OOB sample	29.6
Validation sample	10.5

Table 4. Variable importance:

Variables	Variable importance
DO	6.194
pH	3.483
Total Alkalinity	1.139
TDS	5.923
Total Hardness	3.917
Magnesium	4.730

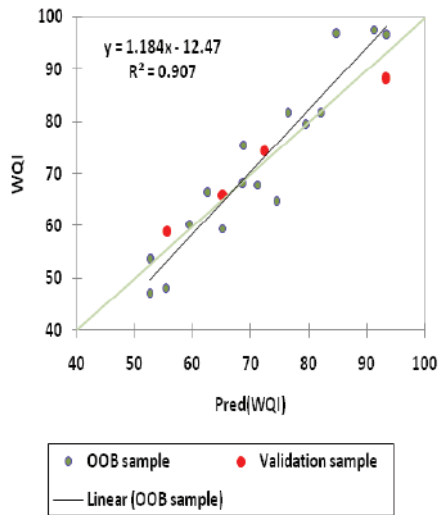


Figure 11. Relation between observed WQI and predicted WQI with observed samples and validation samples after RFM.



Figure 12. Variable importance of water quality parameters of Chamta river after RFM

Extreme Gradient Boosting Model (EGBM):

Extreme Gradient Boosting model is one of the popular water quality predictive models, which has wide use for environmental monitoring and management system (Elvin & Wibowo, 2024). Ensemble methods combining XGB with other algorithms like Random Forest and

K-Nearest Neighbor have also been explored, yielding better performance metrics compared to traditional models (Alabdeli *et al.*, 2024). The Gain component is nothing but the primary metric for controlling the complexities of the Extended Gradient Boosting Machine (EGBM) model (Chevalier and Côté, 2024). It is a measure of loss reduction, which statistically tests potential splits under the assumption of randomness and yield the greatest improvement in predictive accuracy of the introduced model (Chevalier and Côté, 2024; Boldini *et al.*, 2023). Gain support mechanism basically reduces the overfitting and biasness in split decisions (Chevalier and Côté, 2024; Zhang *et al.*, 2023). It combines the gain thresholds with unbiased estimators that would typically be calculated with out-of-bag samples (Zhang *et al.*, 2023). EGBMs can be enhanced the prediction effectiveness and have improved on interpretation and transparency (Chevalier and Côté, 2024). Gain is the most popular as well as cited control mechanism for executing the higher accuracy and generalized prediction through the bio-marker developmental indices (Boldini *et al.*, 2023; Zhang *et al.*, 2023). Result of mean squared error represents $MSE_{validation} > MSE_{learning}$ as expected (Table 5). Gain after EGBM measures the loss reduction or improvement in model accuracy. DO is found as most important control variable after EGBM on the basis of gain magnitude (Table 6 & Figure 14), which refer that the DO is more useful to improve the result accuracy of WQI. TDS ranks first on the basis of cover and frequency of EGB model for WQI of Chamta river. The predictive capacity of WQI of Chamta is controlled by the ‘Gain’ component of EGBM.

Table 5. Mean squared error:

Learning sample	0.000
Validation sample	29.552

Table 6. Variable importance

Variable	Gain	Cover	Frequency
DO	0.403	0.270	0.228
TDS	0.254	0.292	0.295
Total Hardness	0.190	0.106	0.149
Magnesium	0.124	0.054	0.065
Ph	0.028	0.181	0.153
Total Alkalinity	0.001	0.097	0.110

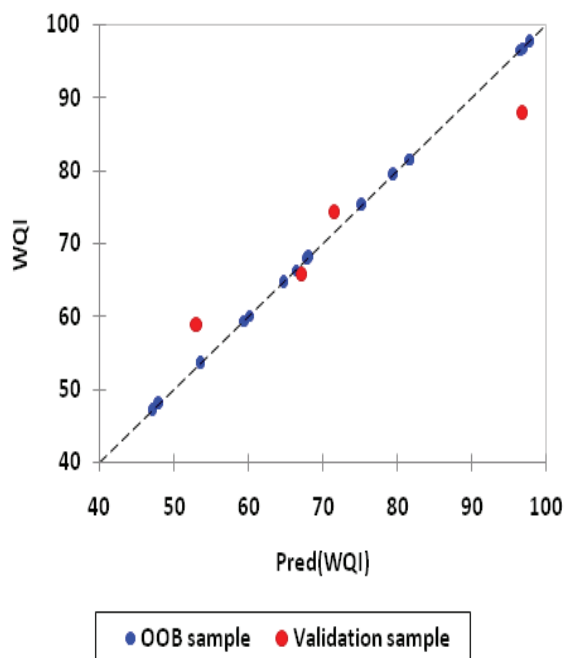


Figure 13. Relation between observed WQI and predicted WQI with observed samples and validation samples after EGBM

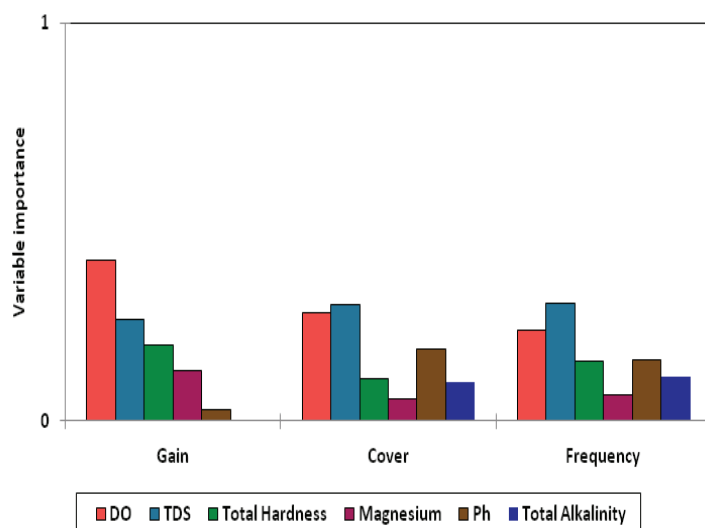


Figure 14. Variable importance of water quality parameters of Chamta river after EGBM

K Nearest Neighbors (KNN) Model:

The K-Nearest Neighbors (KNN) model has emerged as a significant tool for predicting water quality, leveraging historical data and various water quality parameters. K-Nearest Neighbors (KNN) model is very popular supervised learning technique, which is valued for being instance-based non-parametric character (Tahraoui *et al.*, 2023; Prasath *et al.*, 2017). Though ample experimental evidences have established that the correct choice of the metric significantly boosts the degree of performance, ease of understanding, adaptability, interpretability, and robust theory-make KNN a notable baseline and a useful tool for a range of machine learning tasks (Prasath *et al.*, 2017). KNN model’s effectiveness is underscored by its ability to handle missing data and optimize predictions through advanced techniques. KNN model has been used successfully to predict water quality with excellent accuracy, which facilitated the policymaker to take the necessary decisions (Deosarkar et. al., 2023, Tahraoui *et al.*, 2023). This particular non-linear model has unique ability to work with various water quality data set (Nadeem et. al., 2024). Four nearest neighbors target observations are listed along with their predicted magnitude of WQI of Chamta river (Table 7). The predictive WQI is the average of these predictive magnitudes.

Table 7. Predicted values

Observations	Prediction
Obs2	59.4
Obs3	53.6
Obs8	67.5
Obs18	90.4

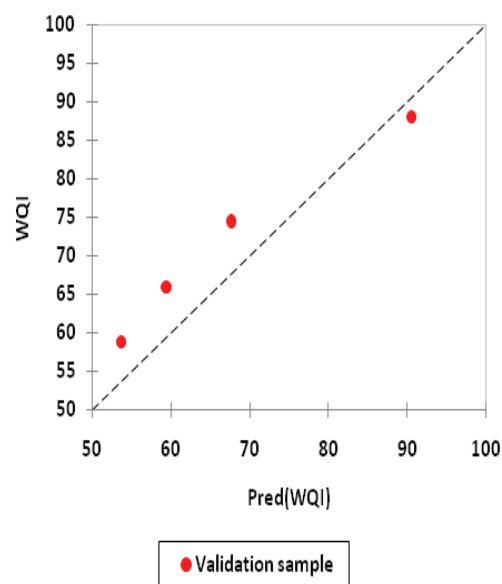


Figure 15. Relation between observed WQI and predicted WQI with validation samples after KNN mode.

Support Vector Machine (SVM):

SVM model plays a promising role in prediction of water quality analysis by using the complex datasets to facilitate the water resource management (Yahya *et al.*, 2019). This model predictivity of WQI can be further enhanced by adding up several advanced optimized tools with significant accuracy even with the existing problem of presence of missing numbers in parameter’s column (Mamat *et al.*, 2023; Duan *et al.*, 2023; Xi and Xue, 2023). This kind of model is more useful for those ungauged streams, which has only field-based recorded data base (Yahya *et al.*, 2019). Conversely, while SVM models offer significant advantages, they may require substantial computational resources and expertise for optimal implementation, which could limit their accessibility in some regions. Support Vector Machine (SVM) model demonstrates amazing predictive ability of water quality where no prior record is available. Support vector machine (SVM) is distinguished by the traditional regression methods, working with the principles of structural risk minimization, which allows the effective predictability even from a very limited dataset (Smola and Schölkopf, 2004). SVM achieved correlation coefficient magnitude of 0.97 with low margin of error while using a small dataset regarding water quality prediction in Langat river water (Yahya *et al.*, 2019). Support vector machine (SVM) model holds unique ability to efficiently tackle the multivariate data sets and nonlinearly associated variables under the study of water quality for its adaptability, robustness, identifying the outliers, kernel flexibility mechanism (Mamat *et al.*, 2023). As the $MSE_{validation} < MSE_{learning}$ samples refers the underfitted condition of the model with the present data set of the Chamta river (Table 8). Here the intercept is 31 (Bias), which means the WQI value will be considered as 31, when all the input features remain zero (Table 9). The prediction of WQI of Chamta river needs at least 17 support vector points after SVM, which can be treated as an effective SVR model (Table 9).

Table 8. Mean squared error:

Learning sample	87.466
Validation sample	38.845

Table 9. Estimation summary:

Response variable	WQI
Number of observations in the training set	17.000
Bias	31.534
Number of support vectors	17.000

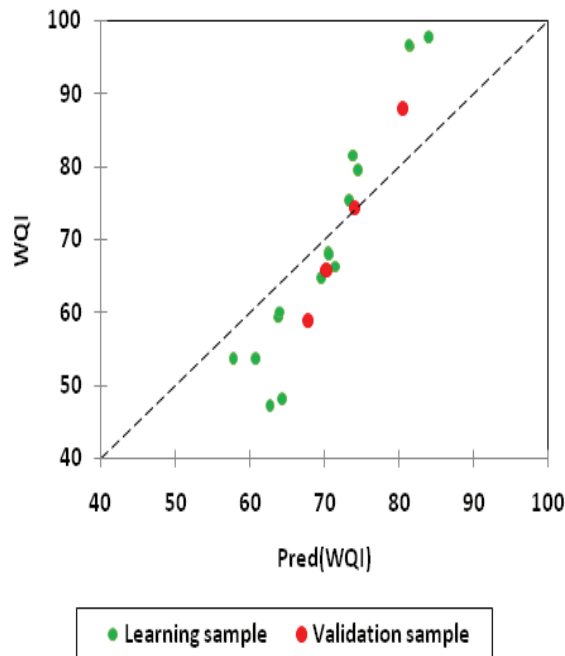


Figure 16. Relation between observed WQI and predicted WQI with learning samples and validation samples after SVM.

LASSO regression:

The LASSO regression model is a valuable tool for predicting water quality, offering a balance between model complexity and interpretability by performing variable selection and regularization. LASSO regression has its uniqueness to ignore the effect of multicollinearity among the n number of variables under study (Am *et al.*, 2022). It has the capability of selection effective variables which gives significant impact on water quality index, which enhances the capacity of predictability with greater accuracy (Saad *et al.*, 2023; Am *et al.*, 2022, Hoque *et al.*, 2022). LASSO regression model has the specialty of simultaneous component or variable selection under a single framework for water quality predictions, emphasizing on the strongest predictors, giving impact over the water quality (Tibshirani, 1996). LASSO regression model is particularly useful in water quality prediction which deals with many predictors. Saad *et al.* (2023) found LASSO regression as best fit model with more than 80% established association (R^2) for several studied water quality parameters for Tigris River. Temporal extensions of LASSO regression model were successfully implemented for the water quality prediction in the coastal zone with satisfaction (Zhang *et al.*, 2021). $MSE_{\text{learning sample}}$ is 22.9 (Table 10) and intercept is 7.549 (Table 11) after the LASSO regression model for the current dataset, where DO occurs highest coefficient as well as standard coefficient. It also justifies the immense significance of DO (Figure 18) for WQI prediction.

Table 10. Mean squared error:

Learning sample	22.9
-----------------	------

Table 11. Model parameters (WQI):

Variable	Coefficient	Std. coefficient
DO	11.642	0.578
Ph	0.000	0.000
Total Alkalinity	0.000	0.000
TDS	0.009	0.164
Total Hardness	0.000	0.000
Magnesium	-0.098	-0.151
Intercept	7.549	

The direction and magnitude of Mean Absolute Error (MAE), Mean Squared Error (MSE), R^2 , Akaike's Information Criterion (AIC), Schwarz's Bayesian Criterion (SBC) has been estimated in against of each performing machine learning model (Table 12). The lowest and the second lowest magnitude of MAE has been noticed for the model LRM and RF respectively. Similar trend has been followed in case of MSE. Maximum association has been found for the model of LR, where the second highest association is reflected by RF to predict the water quality of Chamta river. Again, the lowest and second lowest AIC is detected for LR and RF model, whereas the model X and Y show the same for SBC respectively.

Table 12. Performance metrics table

Performance metrics	Linear regression	Random forests	Extreme Gradient Boosting	K Nearest Neighbors	SVM	LASSO regression
MAE	1.314	2.818	4.632	5.211	5.314	15.246
MSE	4.055	10.557	29.552	30.212	38.845	416.302
R^2	0.966	0.911	0.750	0.744	0.671	-2.525
AIC	17.600	21.427	25.545	25.633	26.638	36.126
SBC	13.918	17.745	21.862	21.951	22.956	32.443

Graphical presentation represents the relationship between the observed WQI and predicted WQI, where the highest association has been seen in case of LRM with least margin of error among all the introduced machine learning models in this current research (Figure 10, 11, 13, 15, 16).

Conclusion:

The EGB, KNN, SVM and LASSO regression model has been established as relatively non-suitable for the prediction of water quality of the Chamta river, as the magnitude of MAE, MSE, AIC and SBC are higher than the RFM and LR model under this particular study. The regulatory water quality parameters are less associated with WQI in case of Chamta channel in case of the introduced EGB, KNN, SVM and LASSO regression model than the RF (non-linear) and LR (linear) model. The most accurate predictive parametric and non-parametric model of WQI Chamta are the Linear Regression Model (LRM) and Random Forest Model (RFM) respectively. Further analysis can be done on water quality by following other popular relevant schemes like Bureau of Indian Standards (BIS), Committee of the Canadian Council (CCME), National Sanitation Foundation (NSF) to test the predictive accuracy of the tested models under study. Accuracy of the prediction may also be improved by enhancing the number of representative water quality stations along Chamta river by enlarging the data size (N). Though, the Random Forest regression model is found as a popular scientific predictive model for the current case study with limited data-set, inclusion of the possibility of overfitting, complex computations, less interpretability than the simple mathematical model, sensitivity to class imbalance in presence of outliers should be avoided. Thorough, intensive refined preprocessing, suitable site and feature selections, assimilation of the hybrid ML models may enhance the model accuracy, which might be best fit with the natural on-field situation. MSE observed > MSE validated sample is normally documented, which has not been followed for this current study under RFM (Table 3). LRM is found best-fitted predictive model even with the non-parametric data base and smaller sample size. Caution should be raised against the issue of ignoring the actual occurring degradation of water quality due to the oversimplifying character of the WQI schemes, manual or instrumental errors taken place during data collection. The current water quality-based research can be considered as successful attempt of assemblage the ML techniques with primary field data to enhance the predictive accuracy of water quality especially for those ungauged streams like Chamta, which have no data. This scientific applicability of machine learning (ML) with field-data certainly encourages the regional researchers to go for the water quality related research on such ungauged but hydro-geomorphologically significant streams, which are never been tested yet due to data paucity.

References:

- Adjovu, G. E., Stephen, H., James, D., & Ahmad, S. (2023). Measurement of total dissolved solids and total suspended solids in water systems: A review of the issues, conventional, and remote sensing techniques. *Remote Sensing*, 15(14), 3534. <https://doi.org/10.3390/rs15143534>
- Alabdeli, H., Pareek, P. K., Shivaraj, S., Sihman Brahmatej Rupavath, R. V., & Das, A., 2024. Prediction of River Water Quality Index and Uncertainty Analysis using Machine Learning Techniques. 1–5. <https://doi.org/10.1109/ssitcon62437.2024.10796360>
- Am, D., V. A., Menon, V. K. K., Naushad, N. S., R, A., Thomas, G. M., & Jyothi, S. N., 2022. Prediction of Water Quality Parameters of River Periyar Using Regression Models. 2022 2nd International

Conference on Advance Computing and Innovative Technologies in Engineering (ICACITE), 53–57. <https://doi.org/10.1109/icacite53722.2022.9823774>

Assessment of urban river water quality using modified NSF water quality index model at Siliguri city, West Bengal, India., 2022. *Environmental and Sustainability Indicators*, 16, 100202. <https://doi.org/10.1016/j.indic.2022.100202>

Athanassopoulos, V., 2023. A meta heuristic optimization algorithm (Lion-BES-XGB) for water quality prediction. *Urban Water Journal*, 20(6), 751–762. <https://doi.org/10.1080/1573062x.2023.2209558>

Behera, S. K., Das, S., Xavier, A. S., Selvarajan, S., & Anandabaskar, N. (2019). Indian Council of Medical Research's National Ethical Guidelines... *Perspectives in Clinical Research*, 10(3), 108–114. https://doi.org/10.4103/picr.PICR_10_18

Bellur, A. P., VI, V., Choudary K, S., Kodipalli, A., Rao, T., & V, P., 2023. Water Quality Assessment Using Machine Learning: A Comparative Analysis. 320–325. <https://doi.org/10.1109/ciisca59740.2023.00068>

Bidyabati, S., & Nath, S., 2023. Monitoring and Assessment of Water Quality of Iril River, Manipur, India. *International Journal of Environment and Climate Change*. <https://doi.org/10.9734/ijecc/2023/v13i11316>

Boldini, D., et al. (2023). Practical guidelines for the use of gradient boosting for cheminformatics. *Journal of Cheminformatics*, 15, Article 101. <https://doi.org/10.1186/s13321-023-00743-7>

Breiman, L. (2001). Random forests. *Machine Learning*, 45(1), 5–32. <https://doi.org/10.1023/A:1010933404324>

Cañedo-Argüelles, M., Kefford, B. J., Schäfer, R. B., et al. (2013). Salinisation of rivers: An urgent ecological issue. *Environmental Pollution*, 173, 157–167. <https://doi.org/10.1016/j.envpol.2012.10.011>

Chevalier, D., & Côté, M.-P. (2024). From point to probabilistic gradient boosting for claim frequency and severity prediction, <https://doi.org/10.48550/arXiv.2412.14916>

Couronné, R., Probst, P., & Boulesteix, A.-L. (2018). Random forest versus logistic regression: A large-scale benchmark experiment. *BMC Bioinformatics*, 19, Article 270. <https://doi.org/10.1186/s12859-018-2264-5>

Das, P., & Kumar, M., 2020. Assessment of Water Quality Using Multivariate Analysis-A Case Study on the Brahmaputra River, Assam, India (pp. 179–194). Springer, Singapore. https://doi.org/10.1007/978-981-32-9771-5_10

Das, P., 2019. Linear Regression Model: Properties and Estimation (pp. 37–73). Springer, Singapore. https://doi.org/10.1007/978-981-32-9019-8_2

Datchanamoorthy, K., Padmavathi, B., Devaraj, D., Gayathri, T. R., & Hasitha, V., 2024. Hybrid Machine Learning Algorithms for Effective Prediction of Water Quality (pp. 469–480). Springer International Publishing. https://doi.org/10.1007/978-981-99-6906-7_40

Deosarkar, M., Tekawade, P., Themaskar, M., Uwais, R., Bhosale, V., & Thengre, M., 2023. Aqua Forecast: Machine Learning for Water Quality Prediction. 1352–1357. <https://doi.org/10.1109/icaiccit60255.2023.10465723>

- Desai, J., & Tank, S. K., 2017. Water Quality Index (WQI) of River Tapti-Surat, Gujarat, India. 390–399. <https://doi.org/10.15626/ECO-TECH.2010.041>
- Duan, Z.-M., Ji, W., Xue, Y., & Xi, Z., 2023. Spatio-Temporal Analysis of Water Quality Based on Gray Wolf Optimization and Support Vector Machines (GWO-SVM): A Case Study from Dongting Lake, China. 626–629. <https://doi.org/10.1109/ispds58840.2023.10235676>
- Dwivedi, R., & Dubey, A., 2023. A review of water quality index (WQI) assessment methods. International Journal of Chemical Research and Development. <https://doi.org/10.33545/26646552.2023.v5.i2a.51>
- Elvin, E., & Wibowo, A., 2024. Forecasting water quality through machine learning and hyperparameter optimization. Indonesian Journal of Electrical Engineering and Computer Science. <https://doi.org/10.11591/ijeecs.v33.i1.pp496-506>
- Fernández del Castillo, A., Yebra-Montes, C., Verduzco Garibay, M., de Anda, J., Garcia-Gonzalez, A., & Sebastián Gradilla-Hernández, M., 2022. Simple Prediction of an Ecosystem-Specific Water Quality Index and the Water Quality Classification of a Highly Polluted River through Supervised Machine Learning. Water, 14(8), 1235. <https://doi.org/10.3390/w14081235>
- Fife, D. A., & D'Onofrio, J. (2023). Common, uncommon, and novel applications of random forest in psychological research. Behavior Research Methods, 55, 2447–2466. <https://doi.org/10.3758/s13428-022-01901-9>
- Fortin, C. (2024). Metal bioavailability in aquatic systems—beyond complexation and competition. Frontiers in Environmental Chemistry, 5, 1345484. <https://doi.org/10.3389/fenvc.2024.1345484>
- Gholamy, A., Kreinovich, V., & Kosheleva, O. (2018, February). Why 70/30 or 80/20 relation between training and testing sets: A pedagogical explanation (Technical Report UTEP-CS-18-09). University of Texas at El Paso. https://scholarworks.utep.edu/cs_techrep/1209/
- Gour, M., & Gour, S., 2024. Chemical and Biological Profiling of Narmada River: A Random Forest Model-Based Water Quality Analysis. 14–26. <https://doi.org/10.9734/bpi/rdcbr/v9/3146>
- Hoque, J. M. Z., Ab Aziz, N. A., Alelyani, S., Mohana, M., & Hosain, M., 2022. Improving Water Quality Index Prediction Using Regression Learning Models. International Journal of Environmental Research and Public Health, 19(20), 13702. <https://doi.org/10.3390/ijerph192013702>
- Hrudey, S. E., Silva, D. S., Shelley, J., Pons, W., Isaac-Renton, J., Chik, A. H.-S., & Conant, B. (2021). Ethics guidance for environmental scientists engaged in surveillance of wastewater for SARS-CoV-2. Environmental Science & Technology, 55(13), 8484–8491. <https://doi.org/10.1021/acs.est.1c00308>
- Huisman, J., Codd, G. A., Paerl, H. W., Ibelings, B. W., Verspagen, J. M. H., & Visser, P. M. (2018). Cyanobacterial blooms. Nature Reviews Microbiology, 16(8), 471–483. <https://doi.org/10.1038/s41579-018-0040-1>
- Jacobs, J., 2023. Linear regression analysis (pp. 548–557). Elsevier eBooks. <https://doi.org/10.1016/b978-0-12-818630-5.10067-3>
- Jane, S. F., Hansen, G. J. A., Kraemer, B. M., et al. (2021). Widespread deoxygenation of temperate lakes. Nature, 594(7861), 66–70. <https://doi.org/10.1038/s41586-021-03550-y>
- Joseph, V. R. (2022). Optimal ratio for data splitting. Statistics in Medicine. Advance online publication.

<https://doi.org/10.1002/sam.11583>

- Juna, A., Umer, M., Sadiq, S., Karamti, H., Eshmawi, A., Mohamed, A. E., & Ashraf, I., 2022. Water Quality Prediction Using KNN Imputer and Multilayer Perceptron. *Water*, 14(17), 2592. <https://doi.org/10.3390/w14172592>
- Kanel, S. R., Majumder, S. D., Al-Abed, S. R., et al. (2023). Arsenic contamination in groundwater: Geochemical basis of mobilization and remediation. *ACS Environmental Au*, 3(2), 118–154. <https://doi.org/10.1021/acsenvironau.2c00053>
- Khatrri, N., Tyagi, S., Rawtani, D., & Tharmavaram, M. (2020). Assessment of river water quality through application of indices: a case study River Sabarmati, Gujarat, India. *Sustainable Water Resources Management*, 6(6), 1–11. <https://doi.org/10.1007/S40899-020-00459-8>
- Kumar, P. M. (2012). Physico-Chemical Parameters of River Water: A Review. *International Journal of Pharmaceutical & Biological Archive*, 3(6). <http://www.ijpba.info/ijpba/index.php/ijpba/article/viewFile/890/604>
- Kurwadkar, S., Dane, J., Kanel, S. R., Córdova de la Cruz, G., Ambade, B., & Nadagouda, M. N. (2022). Per- and polyfluoroalkyl substances in water and wastewater. *Science of the Total Environment*, 809, 151003. <https://doi.org/10.1016/j.scitotenv.2021.151003>
38. LeCompte, L. L., & Young, S. J. (2020). Revised Common Rule changes to the consent process and consent form. *Ochsner Journal*, 20(1), 62–75. <https://doi.org/10.31486/toj.19.0055>
- Mamat, N., Razali, S. F. M. and Hamzah, F. B. (2023). Enhancement of water quality index prediction using support vector machine with sensitivity analysis. *Frontiers in Environmental Science*, 10, 1061835. <https://doi.org/10.3389/fenvs.2022.1061835>
- Mathur, R. and Swaminathan, S. (2018). National ethical guidelines for biomedical & health research involving human participants, 2017: A commentary. *Indian Journal of Medical Research*, 148(3), 279–283. <https://doi.org/10.4103/0971-5916.245303>
- Meybeck, M., Peters, N. E., & Chapman, D. V. (2006). 91 Water Quality. <https://doi.org/10.1002/0470848944.HSA093>
- Mishra, S. K., Kumar, V., Kumar, J., Jha, D. N., Alam, A., Thakur, V. R., Verma, S. kumar, Singh, U., & Das, B. K. (2025). Water Quality Assessment of River Ganga, India Using Water Quality Index and Multivariate Statistical Techniques. <https://doi.org/10.1007/s10661-025-13669-4>
- Nadeem, I. A., Yahya, A., Rehman, A. U., Javaid, S., Ali, T. M., & Mir, A. (2024). An Intelligent Technique for Predicting Quality of Drinking Water. 1–5. <https://doi.org/10.1109/dasa63652.2024.10836500>
- Nagalakshmi, Er. P., & Kumar, D. (2024). Water quality prediction using machine learning technique. *Indian Scientific Journal Of Research In Engineering And Management*, 08(07), 1–11. <https://doi.org/10.55041/ijrsrem36721>
- Nguyen, T. A., Le, D. C., Nguyen, T. H. N., Schmalz, B., & Tran, L. L. (2023). Influences of key factors on river water quality in urban and rural areas: A review. *Case Studies in Chemical and Environmental Engineering*. <https://doi.org/10.1016/j.cscee.2023.100424>
- Prasath, V. B. S., Abu Alfeilat, H., Hassanat, A. B. A., Lasassmeh, O., Tarawneh, A. S., Alhasanat, M. B., & Salman, H. S. E. (2017). Distance and similarity measures effect on the performance of K-Nearest Neighbor classifier-a review. <https://doi.org/10.48550/arXiv.1708.04321>

- Rácz, A., et al. (2021). Effect of dataset size and train/test split ratios in QSAR/multiclass classification: A quantitative evaluation. *Molecules*, 26(4), Article 1111. <https://doi.org/10.3390/molecules26041111>
- Rahman, Md. H., Khan, B., Ahsan, A., Imteaz, M., & Al-Ansari, N. N. (2023). Evaluation of the surface water quality using global water quality index (WQI) models: perspective of river water pollution. *Dental Science Reports*, 13. <https://doi.org/10.1038/s41598-023-47137-1>
- Rogers, O. N., and Ambili P S. (2024). Water quality prediction with machine learning algorithms. *EPRA International Journal of Multidisciplinary Research*. <https://doi.org/10.36713/epra16318>
- Roustaei, N. (2024). Application and interpretation of linear-regression analysis. 13, 151–159. <https://doi.org/10.51329/mehdiophthal1506>
- Rusydi, A. F. (2018). Correlation between conductivity and total dissolved solid in various types of water: A review. *IOP Conference Series: Earth and Environmental Science*, 118, 012019. <https://doi.org/10.1088/1755-1315/118/1/012019>
- Saad, S., Elshazly, A., Senousi, A. M., Darwish, W., Baraka, M., & Ahmed, W. (2023). Water quality parameters prediction of tigris river using sentinel-2 data and lasso regression. *ISPRS Annals of the Photogrammetry, Remote Sensing and Spatial Information Sciences*. <https://doi.org/10.5194/isprs-annals-x-1-w1-2023-863-2023>
- Saha, A., Ghosh, S., Sinha, R. N., Thangiah, G., & John, O. (2020). Water quality, sanitation, and hygiene among the tribal community... *Journal of Family Medicine and Primary Care*, 9(11), 5711–5718. https://doi.org/10.4103/jfmpe.jfmpe_1519_20
- Smola, A. J., & Schölkopf, B. (2004). A tutorial on support vector regression. *Statistics and Computing*, 14(3), 199–222. <https://doi.org/10.1023/B:STCO.0000035301.49549.88>
- Swetha, P., Rasheed, A. H., & Harigovindan, V. P. (2023). Random Forest Regression based Water Quality Prediction for Smart Aquaculture. 1–5. <https://doi.org/10.1109/I3CS58314.2023.10127488>
- Tahraoui, H., Toumi, S., Hassein-Bey, A. H., Bousselma, A., Sid, A. N. E. H., Belhadj, A.-E., Triki, Z., Kebir, M., Amrane, A., Zhang, J., Assadi, A. A., Chebli, D., Bouguettoucha, A., & Mouni, L. (2023). Advancing Water Quality Research: K-Nearest Neighbor Coupled with the Improved Grey Wolf Optimizer Algorithm Model Unveils New Possibilities for Dry Residue Prediction. *Water*. <https://doi.org/10.3390/w15142631>
57. Tharun Kumar, D., Krishna, V., Venkata, D., & Prasad, V. (2023). Machine Learning and Ensemble Techniques for Water Quality Analysis of Korattur Lake. 1–9. <https://doi.org/10.1109/gcat59970.2023.1035331>
- Tibshirani, R. (1996). Regression shrinkage and selection via the lasso. *Journal of the Royal Statistical Society: Series B (Methodological)*, 58(1), 267–288. <https://doi.org/10.1111/j.2517-6161.1996.tb02080.x>
- To, T. C. (2020). Water quality assessment of saigon river for public water supply based on water quality index. *Vietnam Journal of Science and Technology*, 58, 85. <https://doi.org/10.15625/2525-2518/58/5A/15203>
- Tolometti, G. D. (2023). Ground Water Quality Index Prediction Using Random Forest Model (pp. 469–477). https://doi.org/10.1007/978-981-19-8825-7_40

61. Uddin, M. G., Nash, S., & Olbert, A. I. (2021). A review of water quality index models and their use for assessing surface water quality. *Ecological Indicators*, 122, 107218. <https://doi.org/10.1016/j.ecolind.2020.107218>
- Uddin, M. G., Nash, S., Rahman, A., & Olbert, A. I. (2022). A comprehensive method for improvement of WQI models for coastal water quality assessment. *Water Research*, 219, 118532. <https://doi.org/10.1016/j.watres.2022.118532>
- van Delden, J. J. M., & van der Graaf, R. (2017). Revised CIOMS international ethical guidelines... *JAMA*, 317(2), 135–136. <https://doi.org/10.1001/jama.2016.18977>
- Walch-Patterson, A. (2020). Exemptions and limited IRB review: A practical look at the 2018 Common Rule requirements. *Ochsner Journal*, 20(1), 87–94. <https://doi.org/10.31486/toj.19.0095>
- Walling, D. E., & Webb, B. W. (1975). Spatial Variation of River Water Quality: A Survey of the River Exe. *Transactions of the Institute of British Geographers*, 65, 155. <https://doi.org/10.2307/621615>
- World Medical Association. (2013). Declaration of Helsinki: Ethical principles for medical research involving human subjects. *JAMA*, 310(20), 2191–2194. <https://doi.org/10.1001/jama.2013.281053>
- Xi, Z., & Xue, Y. (2023). A Comparative Study of SVMs Model Optimized by Machine Learning Methods in Water Quality Assessment of Dongting Lake. 608–611. <https://doi.org/10.1109/ispds58840.2023.10235625>
- Yahya, A. S. A., Ahmed, A. N., Othman, F., Ibrahim, R. K., Afan, H. A., El-Shafie, A. H., Fai, C. M., Hossain, S., Ehteram, M., & El-Shafie, A. (2019). Water Quality Prediction Model Based Support Vector Machine Model for Ungauged River Catchment under Dual Scenarios. *Water*, 11(6), 1231. <https://doi.org/10.3390/W11061231>
- Zelenakova, M., Purcz, P., Pintilii, R. D., Blistan, P., Hlušík, P., Oravcová, A., & Hashim, M. A. (2018). Spatio-temporal Variations in Water Quality Parameter Trends in River Waters. *Revista De Chimie*, 69(10), 2940–2952. <https://doi.org/10.37358/RC.18.10.6659>
- Zhang, S., Wu, J., Jia, Y., Wang, Y.-G., Zhang, Y., & Duan, Q. (2021). A temporal LASSO regression model for the emergency forecasting of the suspended sediment concentrations in coastal oceans: Accuracy and interpretability. *Engineering Applications of Artificial Intelligence*, 100, 104206. <https://doi.org/10.1016/j.engappai.2021.104206>
- Zhang, Z., Zhang, T., & Li, J. (2023). Unbiased gradient boosting decision tree with unbiased feature importance, <https://doi.org/10.48550/arXiv.2305.10696>
- Zhao, J. (2024). Water quality prediction based on High-Dimensional Dataset Integration Prediction Model. *Pakistan Journal of Life and Social Sciences*, 22(2). <https://doi.org/10.57239/pjlss-2024-22.2.00726>



Longitudinal Trends, Inter-River Variability, and Water Quality Index Assessment of Major Rivers in Imphal Valley, Manipur

Khamnam Michael Meitei¹ and Biswajit Das^{1*}

¹*Department of Geography, Manipur University, Canchipur –795003*

**Corresponding author: bdas9800@manipuruniv.ac.in*

Abstract: Rivers play a vital role in sustaining ecological balance, supporting biodiversity, and meeting domestic and agricultural needs, especially in environmentally sensitive regions like Northeast India. In the Imphal valley of Manipur; Imphal, Iril, Thoubal, and Nambul rivers are essential hydrological lifelines. But they are increasingly threatened by urban expansion, untreated sewage discharge, and agricultural runoff. This study undertakes a comprehensive assessment of water quality across these rivers using secondary data from the Central Pollution Control Board (2022). It analyses 14 physicochemical and biological parameters through longitudinal trend analysis, inter-river comparisons, and Water Quality Index (WQI) computation. The findings shows significant spatial disparities, with the Nambul River showing the most degraded condition. This river has characterised by high biochemical oxygen demand, low dissolved oxygen, elevated electrical conductivity, and severe coliform contamination particularly at Hump Bridge. While the Thoubal River maintains comparatively better water quality mostly at upstream locations. Statistical tools such as Mann-Kendall trend test, Sen's slope estimator, ANOVA, and Tukey's HSD test reported longitudinal deterioration and inter-river variability. Water quality index classifies the Imphal, Iril, and Thoubal rivers as 'Good', while the Nambul River as 'Fair'. The microbial and organic contamination shows the urgent need for wastewater treatment and pollution control. By adopting longitudinal profiling and composite index-based approach, this study offers a robust scientific foundation for sustainable river management and supports regional policy interventions which is aligned with SGD 6 (Clean Water and Sanitation).

Keywords: Longitudinal Trend, Water Quality Index (WQI), Coliform Contamination, Sustainable River Management, Nambul River.

Introduction:

Rivers are freshwater ecosystems that function as the arteries of our planet. They sustain global biodiversity, regulate biogeochemical cycles, and support the development of human civilizations. Their protection is one of the central objectives of the Sustainable Development Goal 6 (Clean Water and Sanitation). This calls for the protection and restoration of water-related ecosystems (United Nations, 2015). This call is urgent in ecologically sensitive and biodiversity-rich regions like Northeast India. In Northeastern region of India, river are not merely water sources but are deeply interwoven with the regional economy, culture, and environmental stability (Bhattacharjee *et al.*, 2022; Ghosh *et al.*, 2020).

Within this regional context, the state of Manipur's Imphal valley presents a focused case study. The four major rivers of the Imphal Valley are the Imphal, Iril, Thoubal, and Nambul; and they serve as the hydrological lifelines of the state. They fulfils essential socio-economic functions and maintain the ecological balance (Singh and Gupta, 2020; Singh and Singh, 2020). However, the integrity of these rivers is increasingly compromised. They face severe pressure from anthropogenic factors of rapid and unregulated urban expansion, direct discharge of untreated domestic sewage, indiscriminate solid waste dumping, and extensive agricultural runoff with chemical fertilisers and pesticides. These stressors are known to profoundly degrade river ecosystems. They cause loss of aquatic biodiversity, and risks to public health, thereby jeopardizing the sustainability of water resources (Devi *et al.*, 2021; Sharma and Singh, 2022; Sharma *et al.*, 2021).

A review of the existing literature reveals that while the issue of water pollution in Manipur has received scholarly attention, the scope of inquiry has been largely fragmented. Numerous studies have documented pollution in the rivers of the valley. For instance, research has often focused on individual rivers, such as the Nambul, Thoubal, or Iril, but these investigations tend to concentrate on specific, often easily accessible river stretches (Kumar and Singh, 2018; Ningthoujam and Devi, 2018; Singh *et al.*, 2022). This approach is informative for localised assessments. But it offers limited insight into longitudinal dynamics. It also fails to capture how water quality evolves along a river's entire course.

Furthermore, a significant limitation of past work is the predominant single-river focus, resulting in absence of comparative inter-river evaluations (Meitei and Bhargava, 2019; Bora and Goswami, 2017). This gap restricts to assess differential environmental degradation among rivers. They are exposed to varying degrees of urbanisation and agricultural intensification. Without such comparisons, it is impossible to prioritise conservation efforts or allocate management resources effectively. Finally, assessment tools like the Water Quality Index (WQI) are known for translating complex data into simple metric (Uddin *et al.*, 2021), but their application within the valley is inconsistent. This tool is rarely combined with longitudinal framework, thus falling short of delivering a comparative river health across the valley.

The limitations in the existing work give rise to clear and significant research gaps. There is a pressing need for a more holistic and integrated assessment of the Imphal valley's river systems. Specifically, there is a dearth of studies that: (i) conduct a systematic longitudinal trend analysis along the complete courses of these rivers to detect pollution gradients and

identify contamination hotspots; (ii) perform a statistically rigorous comparative inter-river assessment to quantify and contrast the degradation levels across the four major rivers; and (iii) integrate these spatial and comparative analyses with the WQI to develop a comprehensive and easily communicable environmental diagnostic tool.

The main objectives of the study are: (1) To analyse the longitudinal trends of key water quality parameters across major rivers in the Imphal valley; (2) To examine inter-river variability and identify statistically significant differences in water quality parameters; and (3) To compute and interpret the Water Quality Index (WQI) to classify the overall water quality status of these rivers.

Study Area:

The study is focused on the Imphal valley. The valley comprises the districts of Imphal East, Imphal West, Bishnupur, Thoubal, and Kakching. It is the state's most densely populated and agriculturally productive part. It is drained by four principal rivers: Imphal, Iril, Thoubal, and Nambul (Figure 1); which serve as the primary water source for domestic, agricultural, and industrial needs, making them critical to the valley's sustainability.

The defining problem of this study area is the critical and accelerating degradation of its river systems, driven by intense and largely unregulated anthropogenic pressures. The unique geography concentrates Manipur's population and economic activities, transforming its rivers into sinks for pollutants. The main problem is unregulated urban discharge, where unplanned urbanization results in raw sewage and runoff flowing directly into the rivers. The Nambul River serves as pollution hotspot receiving direct sewage outfalls as it passes through Imphal city (Devi and Singh, 2021). Secondly, agricultural runoff supply high loads of fertilisers and pesticides into the rivers, which is contributing to eutrophication (Laishram *et al.*, 2022). Beyond that, the constant dumping of solid waste chokes the rivers, altering their natural flow. This combination of urban, agricultural, and solid waste has made the area into water quality crisis.

Materials and Methods:

Data Source and Water Quality Parameters

This study utilises secondary data on water quality collected under the National Water Monitoring Programme (NWMP), published by the Central Pollution Control Board (CPCB) in 2022. The dataset includes values recorded from multiple monitoring locations located along the selected rivers in the valley.

A total of 14 physicochemical and biological parameters were considered in the initial analysis, including Temperature, Dissolved Oxygen (DO), pH, Electrical Conductivity (EC), Biochemical Oxygen Demand (BOD), Fecal Coliform (FC), and Total Coliform (TC) in maximum and minimum values. These parameters are standard parameters used for assessing water quality of rivers (Kannel *et al.*, 2007; Tyagi *et al.*, 2013).

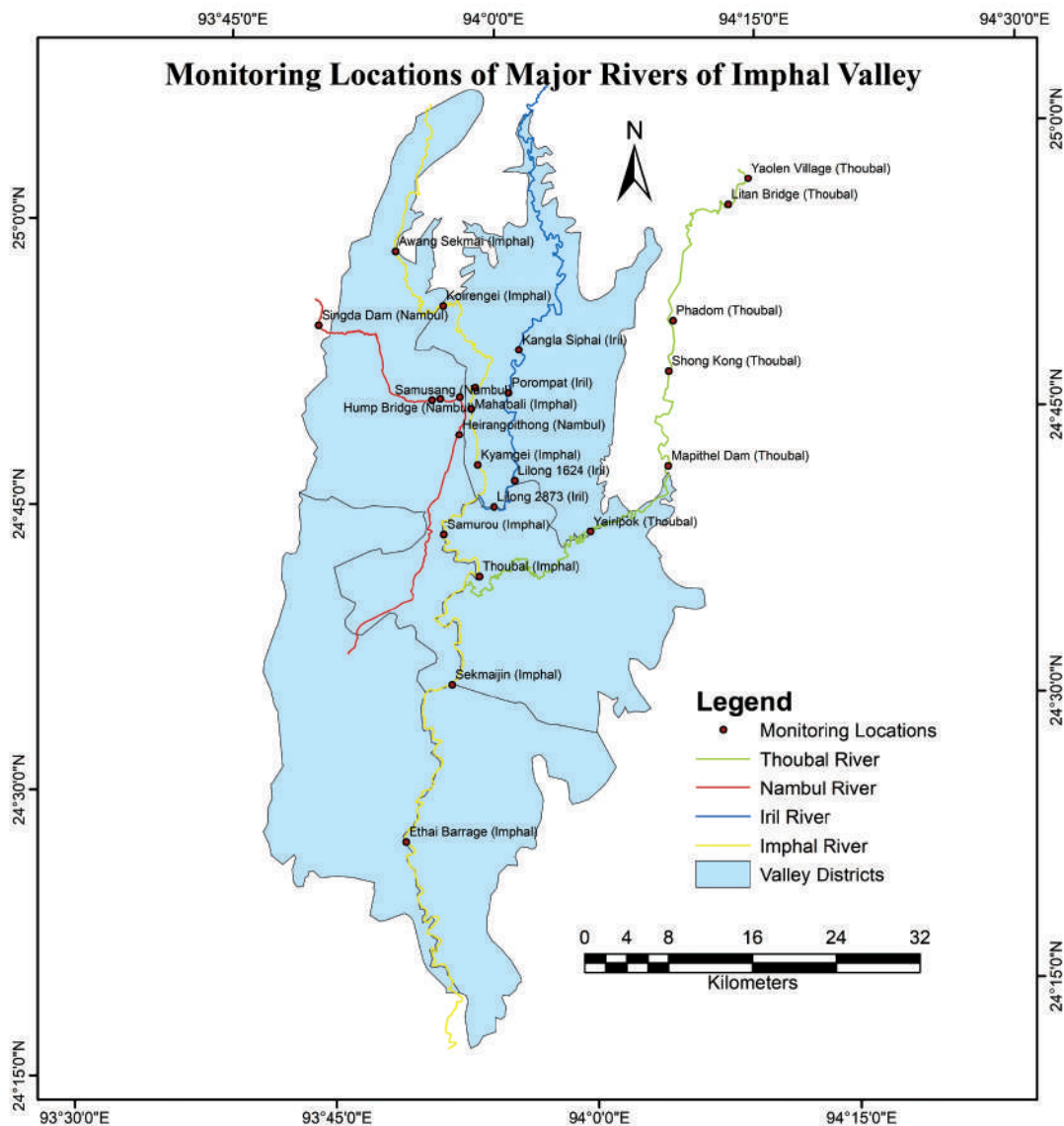


Figure 1. Monitoring Locations of Major Rivers of Imphal Valley.

Trend Analysis:

To assess longitudinal trends in water quality parameters along the river stretches, the non-parametric Mann-Kendall trend test is applied. It is a statistical tool to detect monotonic trends in longitudinal profiling (Helsel and Hirsch, 2002). Sen's slope estimator is also employed to quantify the rate of change of water quality parameter per monitoring location. The Mann-Kendall test statistic, S , is calculated as follows:

$$S = \sum_{k=1}^{n-1} \sum_{j=k+1}^n \operatorname{sgn}(x_j - x_k)$$

Where: n is the number of data points.

x_j and x_k are the data values at points j and k ($j > k$).

The sgn function is the signum function, defined as:

$$\operatorname{sgn}(x_j - x_k) = \begin{cases} +1, & \text{if } x_j - x_k > 0 \\ 0, & \text{if } x_j - x_k = 0 \\ -1, & \text{if } x_j - x_k < 0 \end{cases}$$

A positive value of S indicates an increasing trend, while a negative value indicates a decreasing trend.

The Sen's slope, β , is the median of all slopes calculated between each pair of points in the dataset:

$$\beta = \operatorname{Median} \left(\frac{x_j - x_k}{j - k} \right) \text{ for all } k < j$$

Statistical Analysis of Inter-River Variation

To examine whether the water quality parameter differs between rivers, a One-Way Analysis of Variance (ANOVA) was conducted. Tukey's Honestly Significant Difference (HSD) post-hoc test is applied to identify specific river pairs for significant parameters (Field, 2013). This pinpoints localised pollution issues within the Imphal valley river system. The core of ANOVA is the F-statistic, which is a ratio of the variance between the groups to the variance within the groups. The fundamental model for one-way ANOVA is:

$$Y_{ij} = \mu + \alpha_i + \varepsilon_{ij}$$

Where: Y_{ij} is the j^{th} observation in the i^{th} group.

μ is the overall grand mean of the data.

α_i is the effect of being in group i .

ε_{ij} is the random error for that observation.

The F-statistic is calculated as:

$$F = \frac{MSB}{MSW} = \frac{\sum_{i=1}^k n_i (\bar{Y}_i - \bar{Y})^2 / (K - 1)}{\sum_{i=1}^k \sum_{j=1}^{n_i} (Y_{ij} - \bar{Y}_i)^2 / (N - k)}$$

Where: MSB is the Mean Square Between groups.

MSW is the Mean Square Within groups.

k is the number of groups (rivers).

n_i is the number of observations in group i .

N is the total number of observations.

\bar{Y}_i is the sample mean for group i .

\bar{Y} is the grand mean of all observations.

Tukey's HSD calculates a q-statistic for each pair of means to determine if their difference is statistically significant.

$$q = \frac{|\bar{Y}_i - \bar{Y}_j|}{\sqrt{\frac{MSW}{n}}}$$

Where: \bar{Y}_i and \bar{Y}_j are the means of the two groups being compared.

MSW is the Mean Square Within groups from the ANOVA analysis.

n is the number of observations per group.

This calculated q value is then compared to a critical value from the studentised range distribution to determine significance.

Water Quality Index (WQI) Computation

To compute water quality for each point, the Weighted Arithmetic Index Method of Water Quality Index is used. This method synthesises multiple water quality parameters into a single numerical value, enabling simplified interpretation and classification of river quality and health (Pesce and Wunderlin, 2000; Tyagi *et al.*, 2013).

Parameter Selection: Twelve parameters are selected for WQI computation which is based on their environmental importance and data availability. They include maximum and minimum values of DO, pH, EC, BOD, and FC, and TC.

Quality Rating: Quality rating (qi) is calculated for each water quality parameter using the following formula:

$$qi = \left(\frac{\text{Actual Value} - \text{Ideal Value}}{\text{Standard Value} - \text{Ideal Value}} \right) \times 100$$

Where: Actual Value = Mean of maximum and minimum recorded values

Ideal Value = Most desirable value for that parameter

Standard Value = Maximum permissible value as per CPCB norms

Weight Assignment: Each parameter was assigned a relative weight (wi) based on its importance to overall water quality (Tyagi *et al.*, 2013). The assigned weights are 0.17 (DO), 0.11 (pH), 0.10 (EC), 0.11 (BOD), 0.16 (FC), and 0.15 (TC) and the total sum of assigned weights ($\sum wi$) is 0.80.

WQI Calculation: The WQI is computed as:

$$WQI = \frac{\sum (qi \times wi)}{\sum wi}$$

This provides a composite index to classify water quality into excellent, good, fair, poor or very poor.

Parameter Standards Used: The study adopts specific ideal and standard values for water quality parameters in line with CPCB guidelines. For DO, the ideal value was set at 7.5 mg/L, with a standard permissible limit of 4 mg/L. The ideal pH was considered to be 7.0, falling within the acceptable range of 6.5 to 8.5. EC had an ideal benchmark of 150 µmho/cm and a maximum standard value of 1000 µmho/cm. For BOD, the ideal level was 3 mg/L and the standard upper limit was 6 mg/L. Microbial parameters had both the ideal and standard values set at 0 MPN/100ml. TC had an ideal value of 100 MPN/100ml, with a maximum permissible standard of 500 MPN/100ml.

The primary novelty of this research lies in its integrated and synergistic framework. It moves beyond the limitations of previous localised or single-river studies by being the first to combine longitudinal, inter-river, and WQI-based analyses into a single, cohesive assessment for the entire Imphal valley river system. This approach provides a holistic and comparative understanding of river dynamics that has heretofore been absent. The implementation of this work is substantial. The finding will produce ‘water quality map’. It will provide environmentalists, policymakers, and urban planners with clear, evidence-based diagnostics. This study will enable the precise identification of pollution hotspots for targeted intervention. This will also support the strategic prioritization of river restoration projects. Ultimately, this research aims to provide the robust scientific foundation needed to support regional sustainable water resource management and advance efforts toward achieving SDG 6 in Manipur.

Results and Discussions:

Longitudinal Trends of Key Water Quality Parameters across Major Rivers in the Imphal Valley

To assess the qualitative status of the rivers in the valley, the study refers to the Designated Best Use Water Quality Criteria by CPCB, which classifies water sources into five distinct classes (A to E) based on their suitability for specific uses (CPCB, 2008). These classes are critical thresholds for evaluating river water quality across different monitoring locations. Table 1 provides criterial values for key water quality parameters under each designated class of water use.

Table 1. Designated Best Use Water Quality Criteria

Class of water	Class A	Class B	Class C	Class D	Class E
Designated-Best-Use	Drinking Water Source without conventional treatment but after disinfection	Outdoor bathing (Organised)	Drinking water source after conventional treatment and disinfection	Propagation of Wildlife and Fisheries	Irrigation, Industrial Cooling, Controlled Waste Disposal
Dissolved Oxygen (mg/L)	≥6	≥5	≥4	≥4	—
pH Range	6.5 – 8.5	6.5 – 8.5	6.0 – 9.0	6.5 – 8.5	6.0 – 8.5

Class of water	Class A	Class B	Class C	Class D	Class E
Designated-Best-Use	Drinking Water Source without conventional treatment but after disinfection	Outdoor bathing (Organised)	Drinking water source after conventional treatment and disinfection	Propagation of Wildlife and Fisheries	Irrigation, Industrial Cooling, Controlled Waste Disposal
Electrical Conductivity ($\mu\text{mhos/cm}$)	—	—	—	—	≤ 2250
Biochemical Oxygen Demand (mg/L)	≤ 2	≤ 3	≤ 3	—	—
Total Coliform (MPN/100ml)	≤ 50	≤ 500	≤ 5000	—	—

Source: CPCB, 2008

This framework was used in the study to compare observed values of DO, pH, BOD, EC, and TC across monitoring locations on the rivers. By comparing the actual values against these criteria, the study assess longitudinal variability and identify segments of the rivers that fail to meet the minimum requirements for specific uses. The DO and BOD values were important to evaluating the biological health and self-purifying capacity of the rivers. The pH and EC values assess the chemical environment of the river stretches. Coliform indicates fecal contamination and anthropogenic pollution.

Temperature:

The Imphal River has stable maximum temperature of 28°C across all its monitoring stations, except at Mahabali (Figure 2). The slight increase at Mahabali is due to the river's entry into the urban area of Imphal city. The Iril River has a constant maximum temperature of 28°C, with the exception of Kangla Siphai. But both these rivers have no significant trend in maximum temperature. While the Thoubal River shows a stable maximum temperature of 27°C across most locations, with exceptions at Phadom and Yairipok. A decreasing trend is observed at -0.20°C per monitoring location. The Nambul River shows an increasing trend, with +0.40°C per site, except at Heirangoithong. It records a slight cooling due to its increasing distance from Imphal city.

Regarding minimum temperature, the Imphal River remains at 16°C across most sites, with slight reductions at Koirengei, Sekmajin, and Ethai Barrage. These reductions are due to cooler environmental conditions farther from the urban centre. Statistically, there is no trend in minimum temperature for this river. The Iril River shows an increasing trend in minimum temperature, ranging from 16 to 17°C at +0.25°C per monitoring location. The Thoubal River shows alternating fluctuations between 16 and 17°C. The Nambul River shows an increasing trend in minimum temperature at around 16°C, with +0.30°C per monitoring site.

A slight increase in temperature is observed in the downstream sections of the Imphal River at Mahabali and Nambul River at Hump Bridge. The longitudinal increase in temperature can be attributed to several factors. Upstream courses are shaded by vegetation and thereby lowering temperature. The clearing of this vegetation for urban and agricultural expansion downstream increases solar radiation on the surface (Poole and Berman, 2001). Furthermore, urban areas create a 'heat island' effect, and the discharge of warmer domestic sewage and surface runoff from thermally retentive surfaces like asphalt and concrete can elevate the temperature of receiving water bodies (Kinouchi *et al.*, 2007).

This trend is consistent with findings from other urban river studies. A study on the Mithi River in Mumbai also reported higher temperatures in urbanised segments due to reduced riparian cover and thermal inputs from urban runoff (Pravin and Panneerselvam, 2021). The temperature change influences the metabolism of aquatic organisms and, reduces the solubility of DO. These exacerbates the stress on the aquatic ecosystem (Wetzel, 2001).

Dissolved Oxygen:

The Imphal River maintains a constant maximum DO of 7.4 mg/L (Figure 3). Some slightly elevated values are at Kiyamgi and Samurou, which are located in the middle reaches of the river. The Iril River shows a decreasing trend in DO maximum, declining from 7.6 to 7.4 mg/L along its course. Similarly, the Thoubal River maintains a consistent DO maximum of 7.4 mg/L at most sites, but except at Phadom and Shong Kong. However, statistics says the Imphal, Iril, and Thoubal Rivers have no significant trends in DO maximum. The Nambul River shows a decreasing trend in DO maximum, with an average concentration of around 7.0 mg/L, declining at a rate of -0.20 mg/L per monitoring location. Despite variations, all four rivers meet the minimum threshold DO maximum requirements: ≥ 6 for Class A, ≥ 5 for Class B, and ≥ 4 mg/L for Classes C and D.

The Imphal River shows fluctuations in minimum DO, ranging between 6.6 and 7.2 mg/L. Some lower values are recorded at Mahabali and Kiyamgi due to the discharge of pollutants from Imphal City. Statistically, the river has a slight increasing trend in DO minimum, at +0.10 mg/L per monitoring location. Conversely, the Iril River has a decreasing trend in DO minimum, falling from 7.2 to 6.8 mg/L at a rate of -0.15 mg/L per site. The Thoubal River maintains a stable DO minimum of 7.2 mg/L. But it shows a significant increasing trend of +0.30 mg/L per monitoring location. The Nambul River demonstrates a rapidly decreasing trend in DO minimum, declining at a rate of -0.50 mg/L per location, primarily due to the discharge of municipal waste. Yaolen Village, site on the Thoubal River, records a DO minimum of 5.5 mg/L, below the Class A threshold (≥ 6 mg/L), indicating that the water between Yaolen Village and Litan Bridge is not safe for drinking without conventional treatment. Except for Singda Dam, all monitoring sites on the Nambul River fail to meet the Class A threshold, and two marginal sites also fall short. The most polluted locations, Hump Bridge and Heirangoithong, record DO minimum below the Class B threshold (≥ 5 mg/L). This makes the river water between Naoremthong and Heirangoithong unfit even for outdoor bathing.

A declining trend in DO is observed. The lowest values are recorded in the Nambul River at urban monitoring stations like Hump Bridge. The depletion of DO, often referred to as DO sag, is a direct consequence of high organic loads entering the rivers. Untreated and partially treated sewage from residential areas, commercial establishments, and organic waste introduce a large amount of biodegradable matter. Aerobic microorganisms decompose this organic matter, and consume DO in an amount proportional to the organic load, leading to hypoxic ($\text{DO} < 2\text{--}3 \text{ mg/L}$) or even anoxic ($\text{DO} \text{ approx. } 0 \text{ mg/L}$) conditions (Chapra, 2008). The sluggish flow in certain urban stretches can further limit natural re-aeration from the atmosphere.

This sharp decline in DO is a hallmark of urban river pollution globally. Studies on the Ganga River at Kanpur and the Yamuna River at Delhi have shown drastic DO sags downstream of major urban wastewater outfalls (CPCB, 2018; Sharma and Singh, 2021). The DO likely observed in the Nambul River ($< 4 \text{ mg/L}$) are similar to those reported in these heavily polluted river stretches, indicating severe organic pollution and rendering the water unfit for supporting healthy aquatic life, as per CPCB (2019) guidelines which recommend a minimum of 5 mg/L for bathing purposes. This finding supports earlier study of Singh et al. (2013) on the Nambul River, which also identified organic pollution from the Imphal city area as the primary cause of oxygen depletion.

pH:

The Imphal River has a constant maximum pH of 7.5 with minor deviations (Figure 4). There is no significant trend in maximum pH. The Iril River has a slight decrease in pH maximum from 7.6 to 7.5. The Thoubal River shows fluctuations in pH maximum, averaged at 7.6, except at Yairipok. Despite the fluctuations, it demonstrates an increasing trend of $+0.05 \text{ pH}$ per monitoring location. While the Nambul River displays variable pH maximum values around 7.4. It has a drop to 7.0 at Hump Bridge, which is due to the heavy discharge of acidic municipal waste. Statistically, the Nambul River shows a decreasing trend in pH maximum at a rate of -0.15 pH per monitoring location. Nonetheless, all monitoring sites of the four rivers fall within the permissible pH maximum range for different water use classes: 6.5–8.5 for Classes A, B, and D; 6.0–8.5 for Class E; and 6.0–9.0 for Class C.

In pH minimum, the Imphal River fluctuates but with a sharp decline to 7.0 at Kiyamgi. This decline is due to its passage through Imphal city. But no significant trend is observed. The Iril River has a consistent minimum pH of 7.2 across all monitoring locations, with no trend. The Thoubal River fluctuates around 7.2 and shows no statistical trend in pH minimum. The Nambul River shows a decline, and it fluctuates at around 6.6. It has a sharp drop from 7.3 at Singda Dam to 6.5 at Hump Bridge. This sharp drop is due to municipal waste discharge. Statistically, the Nambul River shows a decreasing trend in minimum pH, with a rate of -0.25 pH per monitoring site. While all monitoring sites of the Imphal, Iril, and Thoubal rivers fall within the acceptable range of pH minimum values, the Hump Bridge site on the Nambul River falls below the 6.5 threshold. Naoremthong to Heirangoithong of the Nambul River doesn't meet the minimum pH ranges for Classes A, B, and D. This river segment is not

suitable for direct human consumption, outdoor bathing, and aquatic life propagation.

The pH values likely remain within a slightly alkaline range (e.g., 7.2-8.5) but might show minor fluctuations downstream. The natural pH of rivers is determined by the geology of the catchment area and its carbonate. The alkalinity in downstream urban areas is caused by the discharge of domestic wastewater containing alkaline soaps and phosphate-based detergents (Verma *et al.*, 2020). The river's natural buffering capacity prevents drastic pH changes unless there is a significant point source of industrial acidic or alkaline effluent, which does not appear to be the dominant issue here.

This observation of pH remaining relatively stable and slightly alkaline in sewage-impacted rivers is common. A study of Singh *et al.* (2017) on the Varuna River in Varanasi found similar trends, where pH remained in the alkaline range (7.5-8.4) despite heavy pollution loads. The river is polluted organically and microbially, it has not yet reached a state of chemical imbalance characteristic of industrial pollution, which could drastically alter pH.

Electrical Conductivity:

The Imphal River has fluctuations in maximum EC at around 285 $\mu\text{mho/cm}$ (Figure 5). Some elevated values are at some middle-course locations such as Kiyamgi and Thoubal. But the river shows a significant decreasing trend in maximum conductivity at a rate of -12.5 $\mu\text{mho/cm}$ per monitoring location. The Iril River experiences an increase in maximum conductivity from 285 to 380 $\mu\text{mho/cm}$ along its course and demonstrates a significant increasing trend of +25 $\mu\text{mho/cm}$ per monitoring location. The Thoubal River maintains fluctuations around 265 $\mu\text{mho/cm}$ for maximum conductivity but shows a significant decreasing trend of -15 $\mu\text{mho/cm}$ per location. The Nambul River shows a marked increase in maximum conductivity from 180 to 740 $\mu\text{mho/cm}$. It has a rapid rising trend of +150 $\mu\text{mho/cm}$ per monitoring location. This sharp increase, particularly from 340 to 790 $\mu\text{mho/cm}$ at Hump Bridge, is attributed to substantial municipal waste discharge into the river. Nonetheless, all monitoring locations across the four rivers remain well within the maximum permissible threshold of 2250 $\mu\text{mho/cm}$ for Class E (irrigation, industrial cooling, and controlled waste disposal).

Regarding minimum conductivity, the Imphal River fluctuates around 140 $\mu\text{mho/cm}$ and shows no significant trend. The Iril River has a stable minimum conductivity of 160 $\mu\text{mho/cm}$ along its course. The Thoubal River's minimum conductivity fluctuates near 180 $\mu\text{mho/cm}$. But it has a significant decreasing trend of -5 $\mu\text{mho/cm}$ per monitoring location. Conversely, the Nambul River experiences an increase in minimum conductivity from 97 to 310 $\mu\text{mho/cm}$, with a significant increasing trend of +50 $\mu\text{mho/cm}$ per monitoring location. All monitoring locations across the four rivers conform to the maximum permissible conductivity threshold of 2250 $\mu\text{mho/cm}$ for Class E.

EC shows a marked and significant increase along the longitudinal profile of the rivers, especially the Nambul. Conductivity is total dissolved solids (TDS) or the concentration of ionised substances. The downstream increase is due to receiving of dissolved salts from various anthropogenic sources. These include ions like chlorides (Cl_-), phosphates (PO_{43-}), and nitrates (NO_{3-}) from domestic sewage, detergents, and agricultural runoff (Kaushal *et al.*,

2005). Urban runoff also contributes by washing dissolved salts and ions from impervious surfaces into the river. Thus, high conductivity is an excellent indicator of pollution from catchment area runoff and wastewater discharge.

The increase in conductivity in response to urbanization is a well-documented phenomenon. Tali et al. (2021) studying rivers in Kashmir found a strong positive correlation between the degree of urbanization in the catchment and the river's EC. The findings for the Nambul River mirror the situation in other Indian urban rivers where conductivity values can increase several-fold as they pass through a city, signaling a heavy load of dissolved pollutants (Jain, 2002).

Biochemical Oxygen Demand:

The Imphal River maintains a constant maximum BOD of approximately 3.4 mg/L across most monitoring locations (Figure 6). But it shows a rapid increase from 3.4 at Kiyamgi to 4.6 mg/L at Thoubal. Statistically, the river has a significant increasing trend of +0.05 mg/L per monitoring location. The Iril River has a gradual rise in maximum BOD from 3.2 to 3.3 mg/L. It shows an increasing trend of +0.10 mg/L per monitoring location. The Thoubal River follows a pattern similar with the Imphal River. It maintains a stable BOD maximum near 3.4 mg/L. But it has a sharp increase from 3.3 at Phadom to 4.6 mg/L at Thoubal. It shows a decreasing trend of -0.25 mg/L per monitoring location. The Nambul River has a marked increase in BOD maximum from 3.3 to 5.6 mg/L, accompanied by a strong increasing trend of +0.60 mg/L per monitoring location. All monitoring locations across the four rivers exceed the maximum permissible BOD thresholds for Class A (≤ 2 mg/L), Class B, and Class C (≤ 3 mg/L), indicating that the river waters are not safe for drinking without treatment, organised outdoor bathing, or use as a drinking water source after conventional treatment.

For minimum BOD, the Imphal River fluctuates around 3.0 mg/L except at Koirengei and Kiyamgi, which levels are below the threshold, with no significant trend. The Iril River shows fluctuating minimum BOD, but with a significant increasing trend of +0.08 mg/L per monitoring location. The Thoubal River maintains a near-constant BOD minimum of about 3.0 mg/L, except at Litan Bridge and Yairipok, and shows a decreasing trend of -0.15 mg/L. The Nambul River has considerable fluctuations in minimum BOD but shows a significant increasing trend of +0.50 mg/L per monitoring site. Three monitoring stations on the Imphal River (Koirengei, Kiyamgi, and Samurou) record minimum BOD below the maximum threshold (≤ 3 mg/L) for Classes B and C, suggesting suitability for organised outdoor bathing and drinking water after conventional treatment at these sites. Similarly, except for Lilong₁₆₂₄ on the Iril River and Yairipok on the Thoubal River, all monitoring sites comply with these BOD minimum thresholds. However, for the Nambul River, with the exceptions of Singda Dam and Heirangoithong, all other locations exceed the maximum permissible BOD minimum, indicating unsuitability for outdoor bathing and drinking water use after treatment.

BOD increases dramatically in downstream sections, with the Nambul River exhibiting

the highest values, classifying it as polluted. BOD is the most direct measure of biodegradable organic pollution. The extremely high BOD values in the Nambul River, particularly at Hump Bridge, in the heart of Imphal city, are unequivocally caused by the massive and continuous influx of raw sewage and organic waste from households, markets (e.g., Khwairamband Keithel), and other commercial units. The high BOD load is the primary cause for the low DO levels discussed earlier; they share a strong inverse relationship (Chapra, 2008).

The BOD observed in the Nambul River (potentially much higher) are comparable to those found in critically polluted river stretches in India. The CPCB identifies river stretches with BOD > 6 mg/L as 'Priority II' or higher polluted stretches (CPCB, 2018). The results firmly place the urban stretch of the Nambul in this category. For comparison, studies by Bhardwaj et al. (2017) on the Hindon River reported similar high BOD levels caused by unabated discharge of municipal and industrial wastewater. This highlights a systemic failure of wastewater management common to many Indian cities.

Fecal Coliform:

The Imphal River has high variation of maximum FC, with average at 88.89 MPN/100mL (Figure 7). But it has no significant trend along its course. While the Iril River shows a gradual increase in maximum FC, rising from 45 to 95 MPN/100mL. It has a significant increasing trend of +12.5 MPN/100 mL per monitoring location. The Thoubal River shows a gradual decline in maximum FC, decreasing from 140 to 65 MPN/100mL. It has a significant decreasing trend of -12.5 MPN/100mL per location. The Nambul River experiences a sharp increase in maximum FC values from 35 to 260 MPN/100mL, with a pronounced significant increasing trend of +50.0 MPN/100mL per monitoring site.

Regarding minimum FC, the Imphal River fluctuates considerably with an average of 43.33 MPN/100mL. But it shows a significant increasing trend of +1.2 MPN/100mL per monitoring location. The Iril River's minimum FC gradually increase from 25 to 50 MPN/100mL. It has a significant upward trend of +8.3 MPN/100mL per site. The Thoubal River displays a general decrease in minimum FC, averaging 19.17 MPN/100mL. It has significant decreasing trend of -5.0 MPN/100mL per location. However, an exception occurs between Mapithel Dam and Yairipok, where levels rise sharply from 10 to 50 MPN/100mL, indicating significant fecal contamination discharge along this stretch. The Nambul River shows a rapid increase in minimum FC counts from 10 to 140 MPN/100mL. It has increasing trend of +35.0 MPN/100mL per monitoring location.

Total Coliform:

The Imphal River has a gradual increase in maximum TC, rising from 175 to 245 MPN/100mL (Figure 8). It has a significant increasing trend of +3.5 MPN/100mL per monitoring location. The Iril River shows a rapid increase in maximum TC, from 80 to 210 MPN/100mL. It has increasing trend of +35.0 MPN/100mL per location. Conversely, the Thoubal River's maximum TC fluctuate considerably, averaging 143.33 MPN/100mL. But it displays a significant decreasing trend of -25.0 MPN/100mL per monitoring site. The Nambul River

has a rapid and marked increase in maximum TC from 210 to 945 MPN/100mL, with a strong positive trend of +250.0 MPN/100mL per monitoring location. All four rivers exceed the maximum threshold for class A water quality (≤ 50 MPN/100mL), indicating they are unsafe for drinking water sources without conventional treatment. However, the Imphal, Iril, and Thoubal rivers remain within the class B threshold (≤ 500 MPN/100mL), making them suitable for organised outdoor bathing. While two monitoring sites along the Nambul River, at Hump Bridge and Heirangoithong, exceed this threshold, rendering these sections unsafe even for outdoor bathing. All monitoring locations across the four rivers fall within the class C limit (≤ 5000 MPN/100mL), but are unsuitable for drinking water even after conventional treatment.

Minimum TC vary across the rivers. The Imphal River fluctuates with an average of 115.56 MPN/100mL and shows a significant increasing trend of +2.1 MPN/100mL per location. The Iril River demonstrates a gradual increase from 50 to 130 MPN/100mL with a significant upward trend of +20.0 MPN/100mL per site. The Thoubal River maintains an average minimum TC count of 47 MPN/100mL but shows a sudden increase between Mapithel Dam and Yairipok from 45 to 105 MPN/100mL, despite a significant overall decreasing trend of -8.3 MPN/100mL per monitoring location. The Nambul River has a rapid increase in minimum TC levels from 30 to 730 MPN/100mL, with a strong increasing trend of +200.0 MPN/100mL per site. Notably, all monitoring points in the Imphal River exceed the Class A threshold for minimum TC counts, confirming unsuitability for drinking water without treatment. The upper monitoring locations in the Iril and Nambul rivers fall below this threshold, which are safe for use as drinking water sources. Similarly, most of the Thoubal River (except Phadom and Yairipok) complies with Class A standards. For class B criteria (≤ 500 MPN/100mL), the Imphal, Iril, and Thoubal Rivers meet standards, supporting safe use for outdoor bathing. The Nambul River sites at Hump Bridge and Heirangoithong exceed these limits, posing risks even for bathing purposes. Across all rivers, class C thresholds are met, but this still does not support drinking water use post conventional treatment.

Both coliform counts are exceptionally high in the downstream, urbanised sections, far exceeding permissible limits for any designated use. Coliform bacteria are indicators of fecal contamination. Their presence in staggeringly high numbers is direct and conclusive evidence of the discharge of untreated human and animal faeces into the river system. This is a severe public health hazard, as their presence implies the potential presence of other dangerous waterborne pathogens like *Vibrio cholerae*, *Salmonella typhi*, and *Giardia lamblia* (WHO, 2017). The source is clearly the lack of a centralised sewerage system and the direct channelling of domestic waste into the rivers.

This finding is tragically common across urban India. The National Green Tribunal has repeatedly highlighted the issue of direct sewage discharge into rivers. The World Health Organization (WHO, 2017) guideline for recreational water is <1000 E. coli /100mL. The findings show values orders of magnitude higher, similar to reports on the Yamuna in Delhi, where FC counts can reach millions of MPN/100mL (Sharma and Singh, 2021). This finding

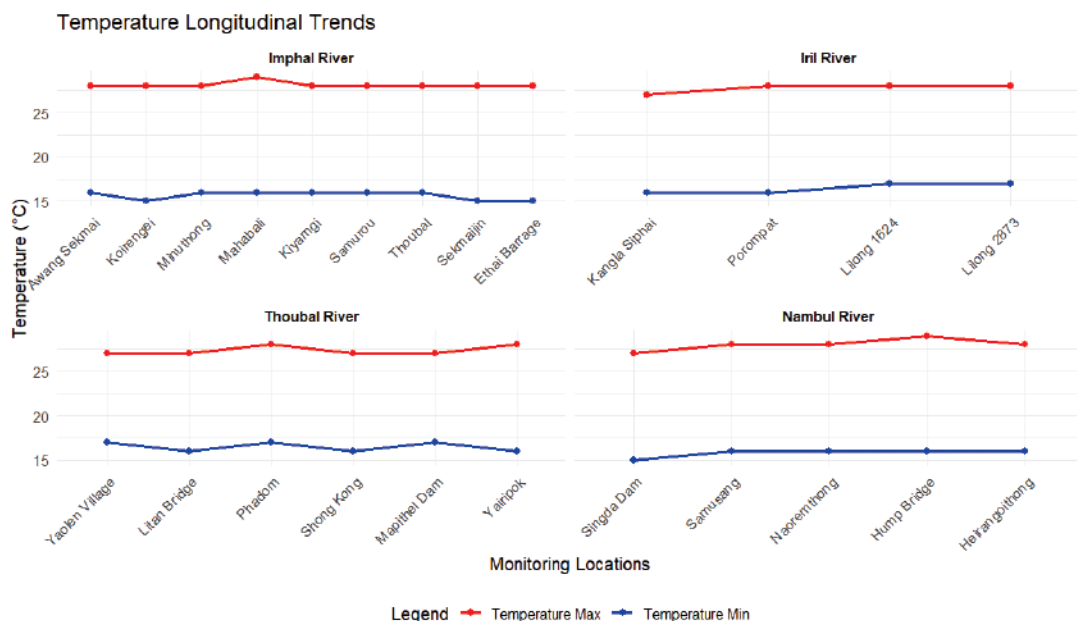


Figure 2. Longitudinal Trends of River Temperature.

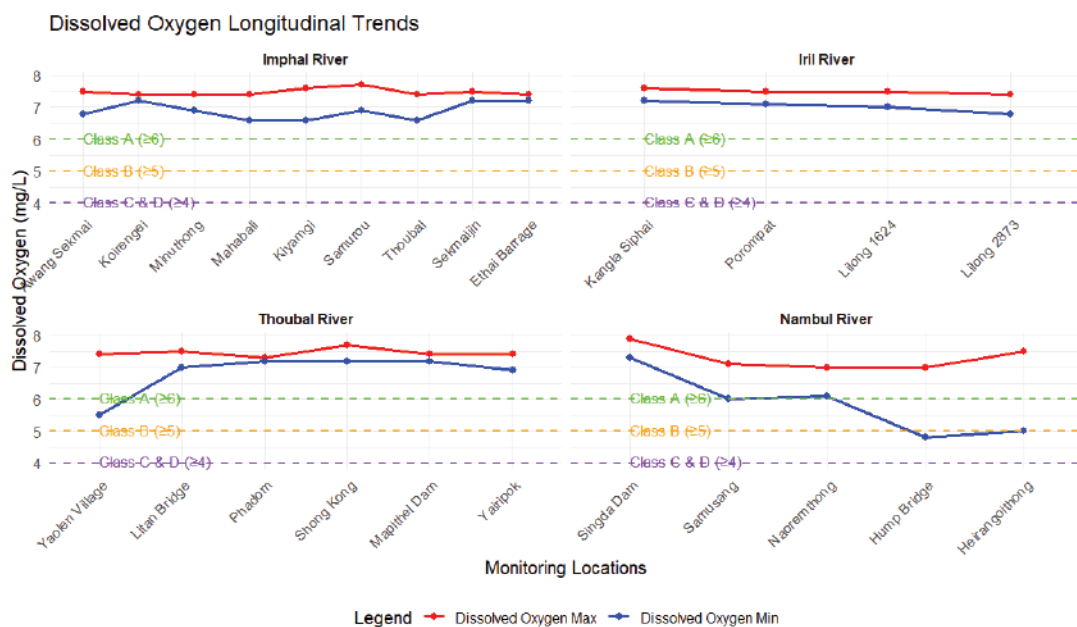


Figure 3. Longitudinal Trends of River Dissolved Oxygen

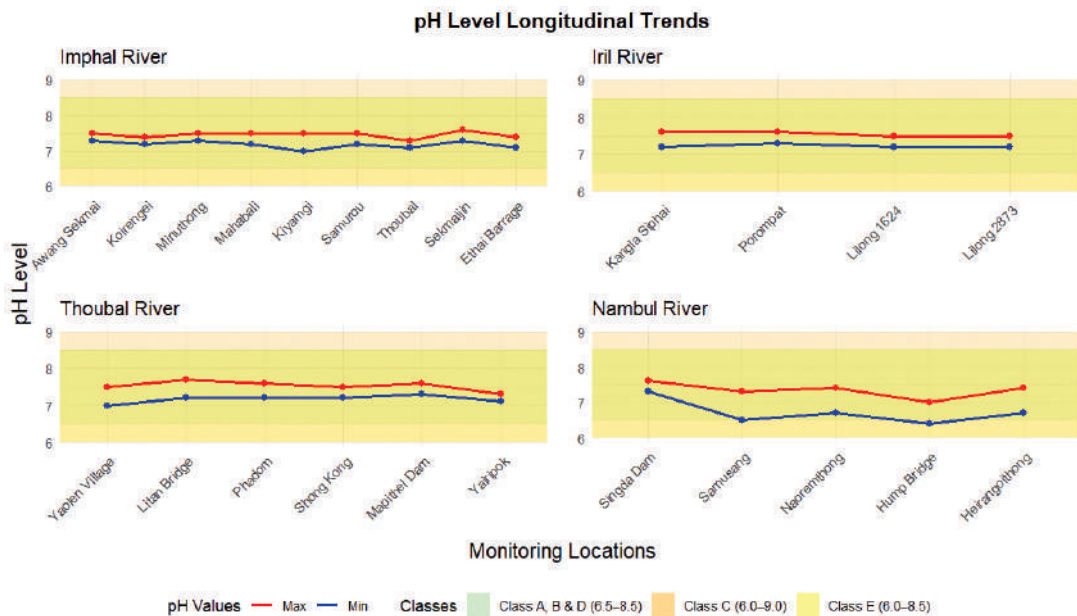


Figure 4. Longitudinal Trends of River pH Level



Figure 5. Longitudinal Trends of River Conductivity

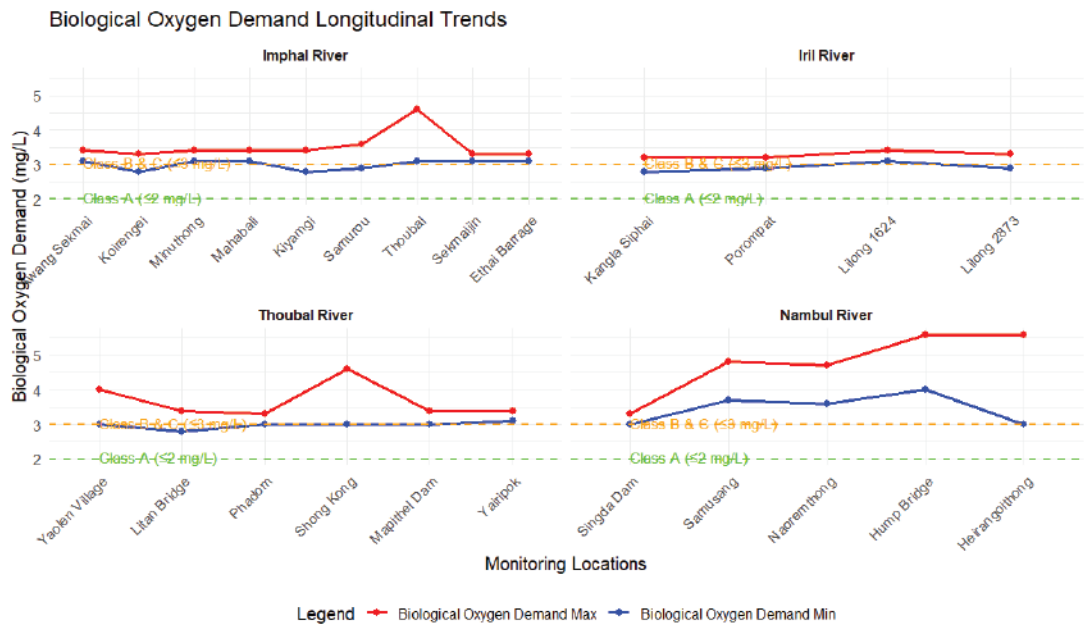


Figure 6. Longitudinal Trends of River Biochemical Oxygen Demand

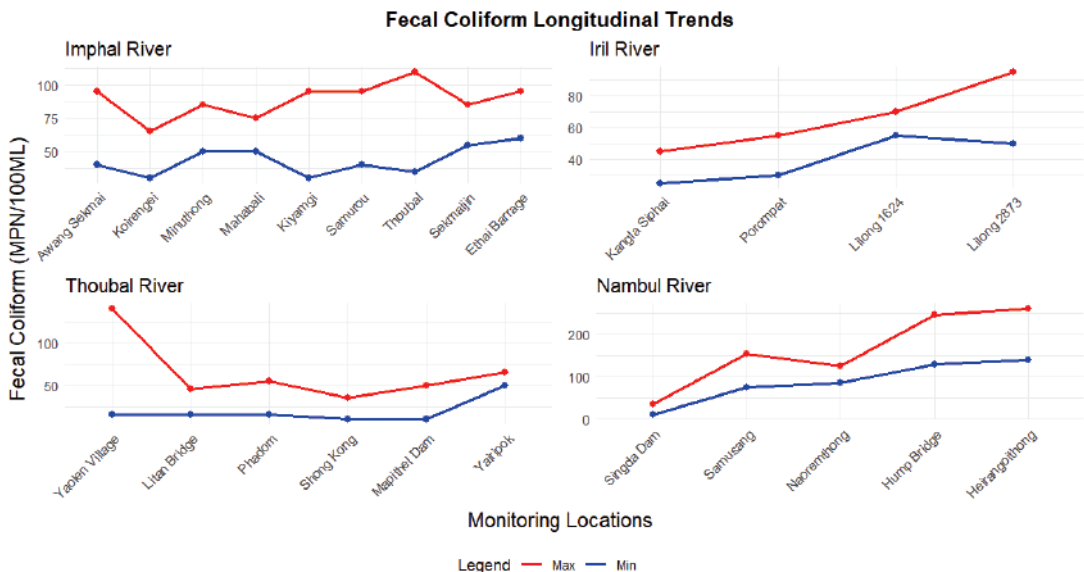


Figure 7. Longitudinal Trends of River Fecal Coliform

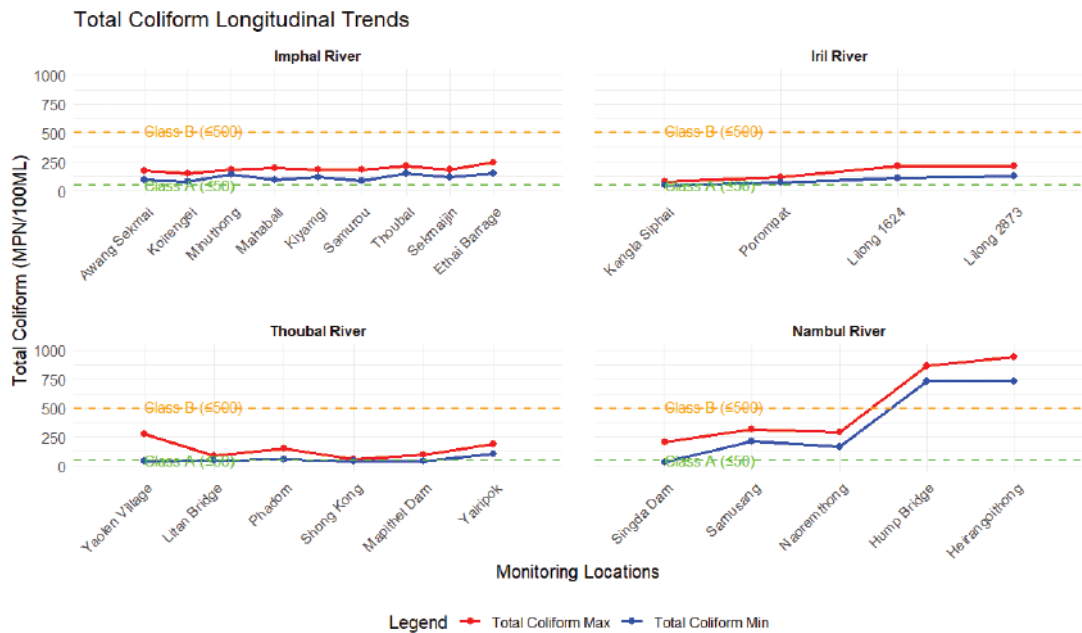


Figure 8. Longitudinal Trends of River Total Coliform

supports that the primary problem in the rivers is microbiological, stemming from inadequate sanitation infrastructure. Table 2 presents the longitudinal trends of 14 key water quality parameters across the four rivers, analysed using Mann-Kendall Test and Sen's Slope estimator. For the Imphal River, five parameters, DO (Min), BOD (Max), FC (Min), and TC (Max and Min), have increasing trends, with Sen's slopes ranging from +0.05 to +3.5 per monitoring location. EC Max is the only parameter showing a decreasing trend at -12.5 per location. All these trends are significant at 5 percent, except BOD Max, which is significant at 10 percent. In the Iril River, eight parameters, including Temperature Min, EC Max, BOD (Max and Min), FC (Max and Min), and TC (Max and Min), demonstrate increasing trends, with Sen's slopes ranging from +0.08 to +35.0 per monitoring location. DO Min is the only parameter showing a decreasing trend at -0.15 per location. All trends in this river are significant at 5 percent, while the fecal and TC parameters (Max and Min) are highly significant at 1 percent.

Table 2. Longitudinal Trend Results (Mann-Kendall Test and Sen's Slope)

Parameter		Imphal River (9 ML)	Iril River (4 ML)	Thoubal River (6 ML)	Nambul R (5 ML)
Temperature	Max	No trend (p=0.78)	No trend (p=0.85)	↓ -0.20/ML **	↑ +0.40/ML ***
	Min	No trend (p=0.45)	↑ +0.25/ML **	No trend (p=0.62)	↑ +0.30/ML ***

Parameter		Imphal River (9 ML)	Iiril River (4 ML)	Thoubal River (6 ML)	Nambul R (5 ML)
DO	Max	No trend (p=0.15)	No trend (p=0.91)	No trend (p=0.23)	↓ -0.20/ML **
	Min	↑ +0.10/ML **	↓ -0.15/ML **	↑ +0.30/ML ***	↓ -0.50/ML ***
pH	Max	No trend (p=0.32)	No trend (p=0.70)	↑ +0.05/ML *	↓ -0.15/ML **
	Min	No trend (p=0.67)	No trend (p=0.55)	No trend (p=0.41)	↓ -0.25/ML ***
EC	Max	↓ -12.5/ML **	↑ +25.0/ML **	↓ -15.0/ML ***	↑ +150.0/ML ***
	Min	No trend (p=0.88)	No trend (p=0.77)	↓ -5.0/ML **	↑ +50.0/ML ***
BOD	Max	↑ +0.05/ML *	↑ +0.10/ML **	↓ -0.25/ML ***	↑ +0.60/ML ***
	Min	No trend (p=0.12)	↑ +0.08/ML **	↓ -0.15/ML **	↑ +0.50/ML ***
FC	Max	No trend (p=0.18)	↑ +12.5/ML ***	↓ -12.5/ML ***	↑ +50.0/ML ***
	Min	↑ +1.2/ML **	↑ +8.3/ML ***	↓ -5.0/ML **	↑ +35.0/ML ***
TC	Max	↑ +3.5/ML **	↑ +35.0/ML ***	↓ -25.0/ML ***	↑ +250.0/ML ***
	Min	↑ +2.1/ML **	↑ +20.0/ML ***	↓ -8.3/ML **	↑ +200.0/ML ***

Note: ML = Monitoring Locations

↑ = Increasing trend, ↓ = Decreasing trend, No trend indicates $p \geq 0.10$.

Significance: * (10%), ** (5%), *** (1%)

The Thoubal River has decreasing trends for nine parameters, Temperature Max, EC (Max and Min), BOD (Max and Min), and FC and TC (Max and Min), with Sen's slopes ranging from -0.15 to -25.0 per monitoring location. Only DO Min and pH Max show increasing trends of +0.30 and +0.05 per location, respectively. All minimum parameter trends are significant at 5 percent, with DO Min significant at 1 percent. For the maximum parameters, statistical significance is at 1 percent except for Temperature and pH, at 5 percent and 10 percent, respectively. The Nambul River shows increasing trends in ten parameters, Temperature (Max and Min), Conductivity (Max and Min), BOD (Max and Min), and FC and TC (Max and Min), with Sen's slopes ranging from +0.30 to +250.0 per monitoring location. Conversely, both Max and Min of DO and pH display decreasing trends with slopes between -0.15 and -0.50. All parameters are significant at 1 percent, except for both Max values of DO and pH, which are significant at 5 percent. The analysis of longitudinal trends, moving from upstream to downstream locations, reveals a consistent pattern of water quality degradation, which is a classic symptom of anthropogenic pressures in a riverine ecosystem (Sener *et al.*, 2017).

This deterioration is particularly pronounced as the rivers flow through densely populated and commercially active urban centres of the Imphal Valley.

Figure 9 presents a Heatmap illustrating the longitudinal trends of 14 key water quality parameters across four rivers based on Mann-Kendall Test. The Imphal River shows five parameters with increasing trends and one with a decreasing trend. The Iril River has eight increasing and one decreasing trends, indicating overall rising values for most parameters. The Nambul River displays the most variability, with ten parameters increasing and four decreasing, where each parameter consistently follows either an increasing or decreasing pattern along its course. While the Thoubal River's trend differs from the others, showing only two parameters with increasing trends and nine with decreasing trends. This suggests a general improvement or reduction in many water quality parameters for Thoubal, contrasting with the mostly increasing trends observed in Imphal, Iril, and especially Nambul rivers. The Heatmap highlights the distinct longitudinal water quality dynamics across the four rivers. Figure 10 illustrates the Sen's Slope values for 14 key water quality parameters across the four rivers, divided into (a) steep slopes and (b) gentle slopes. In Figure 10(a), among six parameters with steeper slopes, the Imphal River shows the smallest slopes, while the Nambul River has the largest. Nambul is receiving substantial inputs of FC and TC along with dissolved substances reflected in high conductivity. This suggests a significant pollution load

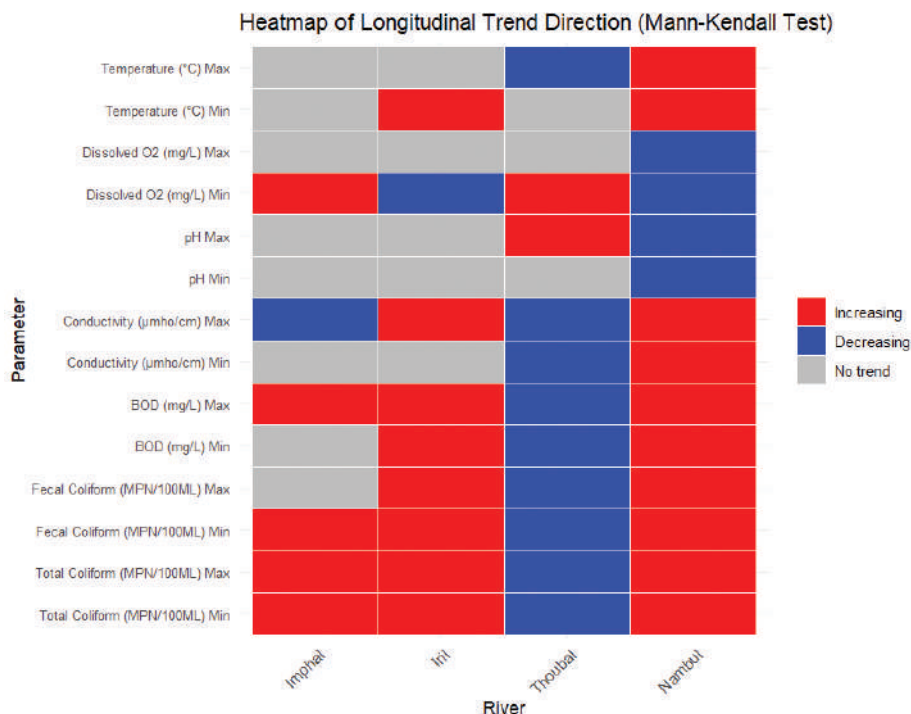


Figure 9. Heatmap of Longitudinal Trend Direction (Mann-Kendall Test)

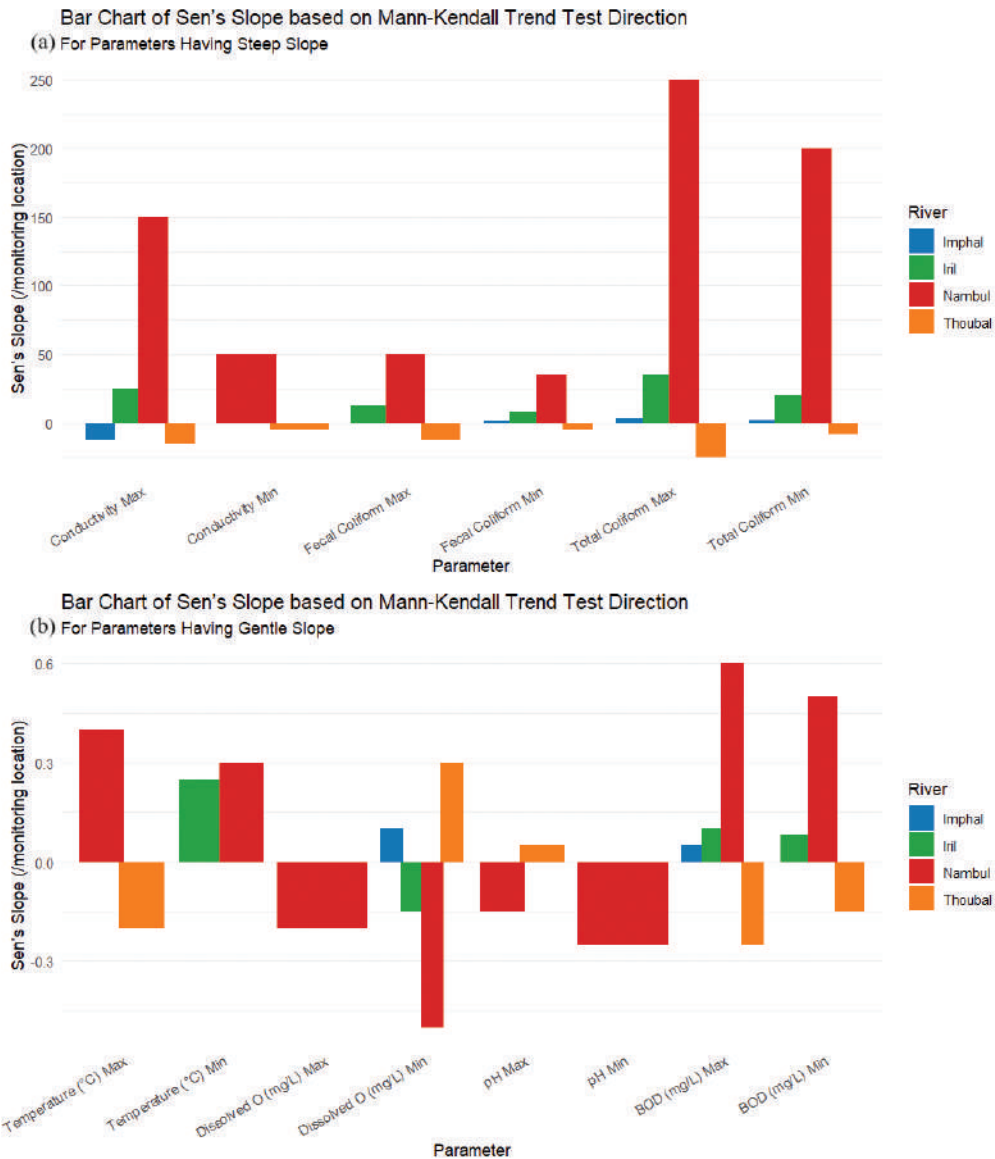


Figure 10. Bar Charts of Sen's Slope (a) Steep Slope and (b) Gentle Slope

in Nambal. The Iril and Thoubal rivers fall in between, with Imphal, Iril, and Nambal showing mostly increasing trends except for one parameter in Imphal. Conversely, the Thoubal River displays mainly decreasing trends, likely due to natural self-purification processes that reduce pollution as the river flows downstream.

In Figure 10(b), comparing eight parameters with gentler slopes, the pattern is similar:

Imphal has the smallest slopes, and Nambul the largest.

The Imphal River shows slight improvement with increased minimum DO. The Thoubal River has the best conditions, with higher DO and lower temperature and BOD. The Nambul River shows worrying signs with rising temperatures and BOD levels, while DO and pH are declining.

Inter-River Variability in Water Quality Parameters among Different Rivers within the Imphal Valley:

Table 3 provides the results of One-Way ANOVA (Omnibus Test) that include F-statistics, p-values, and significance levels for 14 water quality parameters across four major rivers in the Imphal Valley. Among these, five parameters, maximum conductivity, and both maximum and minimum values of FC and TC, are highly significant at 1 percent. Three parameters, minimum conductivity, and maximum and minimum values of DO, are significant at 5 and 10 percent. The remaining six parameters, both maximum and minimum values of temperature, pH, and BOD, are not significant. These findings indicate that microbial contamination (coliforms) and conductivity has the greatest variability among the rivers, while core physicochemical parameters such as temperature and pH remain relatively stable. The observed differences in DO suggest variations in organic pollution load or differences in aeration conditions across the rivers.

Table 3. One-Way ANOVA Results (Omnibus Test)

Parameter	F-Statistic	p-value	Significance	Interpretation ($\alpha = 0.05$)
Temperature (°C) Max	0.98	0.41		Not
Temperature (°C) Min	1.45	0.24		Not
DO (mg/L) Max	5.67	0.002	**	Very Significant
DO (mg/L) Min	3.12	0.03	*	Significant
pH Max	2.01	0.12		Not
pH Min	1.89	0.14		Not
EC Max	18.21	<0.001	***	Highly Significant
EC Min	4.33	0.008	**	Very Significant
BOD (mg/L) Max	2.56	0.06		Not
BOD (mg/L) Min	1.23	0.31		Not
FC Max	22.45	<0.001	***	Highly Significant
FC Min	9.87	<0.001	***	Highly Significant
TC Max	28.90	<0.001	***	Highly Significant

Parameter	F-Statistic	p-value	Significance	Interpretation ($\alpha = 0.05$)
TC Min	15.32	<0.001	***	Highly Significant

Significance Levels: *** $p < 0.01$ (Highly Significant), ** $p < 0.05$ (Very Significant), and * $p < 0.10$ (Significant)

Table 4 presents the pairwise post-hoc Tukey HSD test results for the eight water quality parameters found to be statistically significant. The Nambul River has significant differences in maximum DO when compared with the other three rivers, with the most pronounced variation observed between Nambul and Iril Rivers, significant at 1 percent. For minimum DO, Nambul also shows significant variation with all three rivers at 1 percent, with the greatest difference occurring between Nambul and Imphal Rivers. Significant variation is observed between Imphal and Thoubal Rivers. In terms of maximum conductivity, both the Thoubal and Nambul Rivers demonstrate significant differences from the other rivers at 1 percent, with the largest disparity found between Thoubal and Nambul. For minimum conductivity, a significant difference at 1 percent is observed between Nambul and Imphal Rivers.

Table 4. Pairwise Comparison Table of Post-Hoc Tukey HSD Results (for Significant Parameters)

Parameter	Comparison	Difference	p-value	Significance
DO (Max)	Nambul vs. Imphal	+0.34	0.007	**
	Nambul vs. Iril	+0.52	<0.001	***
	Nambul vs. Thoubal	+0.46	0.001	**
DO (Min)	Nambul vs. Imphal	-1.24	<0.001	***
	Nambul vs. Iril	-1.18	<0.001	***
	Nambul vs. Thoubal	-0.74	<0.001	***
	Thoubal vs. Imphal	-0.50	0.003	**
EC (Max)	Nambul vs. Imphal	+318.9	<0.001	***
	Nambul vs. Iril	+275.6	<0.001	***
	Nambul vs. Thoubal	+441.1	<0.001	***
	Thoubal vs. Imphal	-122.2	<0.001	***
	Thoubal vs. Iril	-165.6	<0.001	***
EC (Min)	Nambul vs. Imphal	+68.9	<0.001	***
	Nambul vs. Iril	+52.2	0.015	*

Parameter	Comparison	Difference	p-value	Significance
FC (Max)	Nambul vs. Imphal	+112.2	<0.001	***
	Nambul vs. Iril	+154.4	<0.001	***
	Nambul vs. Thoubal	+162.2	<0.001	***
	Imphal vs. Iril	+42.2	0.001	**
	Imphal vs. Thoubal	+50.0	<0.001	***
FC (Min)	Nambul vs. Imphal	+65.6	<0.001	***
	Nambul vs. Iril	+74.4	<0.001	***
	Nambul vs. Thoubal	+95.6	<0.001	***
	Thoubal vs. Imphal	-30.0	0.001	**
TC (Max)	Nambul vs. Imphal	+317.8	<0.001	***
	Nambul vs. Iril	+380.0	<0.001	***
	Nambul vs. Thoubal	+377.8	<0.001	***
	Imphal vs. Iril	+62.2	<0.001	***
	Imphal vs. Thoubal	+60.0	<0.001	***
TC (Min)	Nambul vs. Imphal	+337.8	<0.001	***
	Nambul vs. Iril	+361.1	<0.001	***
	Nambul vs. Thoubal	+403.3	<0.001	***
	Thoubal vs. Imphal	-65.6	<0.001	***

Significance Levels: *** $p < 0.01$ (Highly Significant), ** $p < 0.05$ (Very Significant), and * $p < 0.10$ (Significant)

Regarding microbial contamination, both Imphal and Nambul Rivers show significant differences in maximum FC levels when compared with the other rivers, nearly all at 1 percent significance. The highest variation is recorded between Imphal and Nambul. For minimum FC, Nambul River again differs significantly from the other three rivers at 1 percent, with the most substantial difference observed between Nambul and Thoubal. A similar trend is seen for TC counts: both Imphal and Nambul Rivers differ significantly from the others in terms of maximum values, with the highest variation between Iril and Nambul. For minimum TC, Nambul shows significant differences with all other rivers at 1 percent, with the largest gap between Nambul and Thoubal, and an additional significant difference noted between Imphal and Thoubal. Figure 12 visually represents the statistically significant inter-river differences for these key parameters.

Statistical analysis of ANOVA and Tukey's HSD shows significant differences of

parameters among the four rivers. The Nambul has been the most polluted and the Thoubal has been cleaner. This river variability is linked with the land use, population density, and hydrological characteristics within each river’s catchment area.

Nambul River’s catchment includes the most densely populated and commercial core of Imphal city. It has a relatively low flow rate and acts as the primary recipient of urban drainage, leading to a low assimilation capacity and its highly degraded state. Imphal and Iril rivers also flow through urban areas but have larger catchment areas and higher discharges compared to the Nambul, which likely aids in greater dilution and self-purification (Pandey and Singh, 2017). In Thoubal River, a significant portion of its upper catchment lies in hilly, forested, and less populated areas. Therefore, its upstream water quality is comparatively better due to a lower influx of pollutants, a pattern consistent with the established principle that forested headwaters yield higher quality water (Sliva and Williams, 2001).

This pattern, where water quality directly reflects catchment characteristics, is a universal principle. A study by Sener et al. (2017) on the Aksu River in Turkey showed a strong correlation between land use patterns and river water quality, and with urban and agricultural lands being the primary sources of pollution. The findings provide a clear case study of this principle within the micro-context of the Imphal Valley, emphasizing that river management cannot be separated from land use planning in the catchment.

Water Quality Index (WQI) For Assessing the Overall Water Quality Status of the Major Rivers in Imphal Valley:

Table 5 provides the classification reference of Water Quality Index (WQI), while Table 6 presents the computed WQI scores for each monitoring location across the four major rivers in the Imphal Valley. All monitoring stations along the Imphal River fall under the ‘Good’ category, with WQI scores ranging from 41.7 at Koirengei to 48.9 at Thoubal. And all monitoring locations along the Iril River are also classified as ‘Good,’ with scores ranging from 38.2 at Kangla Siphai to 45.1 at Lilong₂₈₇₃.

Table 5. WQI Classification Reference

WQI Range	Water Quality Rating	Description
0-25	Excellent	Very clean water, suitable for all purposes
26-50	Good	Safe for drinking with conventional treatment
51-75	Fair	Requires advanced treatment for drinking, suitable for irrigation
76-100	Poor	Not suitable for drinking without extensive treatment
>100	Very Poor	Highly polluted, only suitable for industrial cooling after treatment

Table 6. Water Quality Index Results with Key Issues

River	Monitoring Location	WQI Score	Water Quality Rating	Key Issues
Imphal	Awang Sekmai	42.3	Good	Slightly Elevated Coliform Levels
	Koirengei	41.7	Good	Moderate Coliform Presence
	Minuthong	43.1	Good	Elevated TC
	Mahabali	43.8	Good	Coliform Levels Near Upper Limits
	Kiyamgi	45.2	Good	Variable Conductivity, Coliform
	Samurou	44.6	Good	Coliform Levels Need Monitoring
	Thoubal	48.9	Good	Highest BOD In Imphal, Elevated Coliform
	Sekmai jin	42.9	Good	Moderate FC
	Ethai Barrage	47.5	Good	Elevated Coliform Counts
Iril	Kangla Siphai	38.2	Good	Minimal Issues
	Porompat	39.4	Good	Slight Conductivity Variation
	Lilong ₁₆₂₄	43.7	Good	Elevated Coliform Levels
	Lilong ₂₈₇₃	45.1	Good	High Conductivity, Coliform
Thoubal	Yaolen Village	52.3	Fair	Low DO Min, High Coliform Variation
	Litan Bridge	37.8	Good	Minimal Issues
	Phadom	39.2	Good	Slight Coliform Presence
	Shong Kong	35.6	Good	Minimal Issues
	Mapithel Dam	36.9	Good	Minimal Issues
	Yairipok	42.8	Good	Moderate Coliform Levels
Nambul	Singda Dam	41.5	Good	Coliform Variation
	Samusang	68.4	Fair	High BOD, Low pH Min, Very High Coliform
	Naoremthong	65.7	Fair	High BOD, Coliform, Conductivity
	Hump Bridge	89.2	Poor	Extremely High Coliform, BOD, Conductivity
	Heirangoithong	82.6	Poor	Very High Coliform, BOD, Conductivity

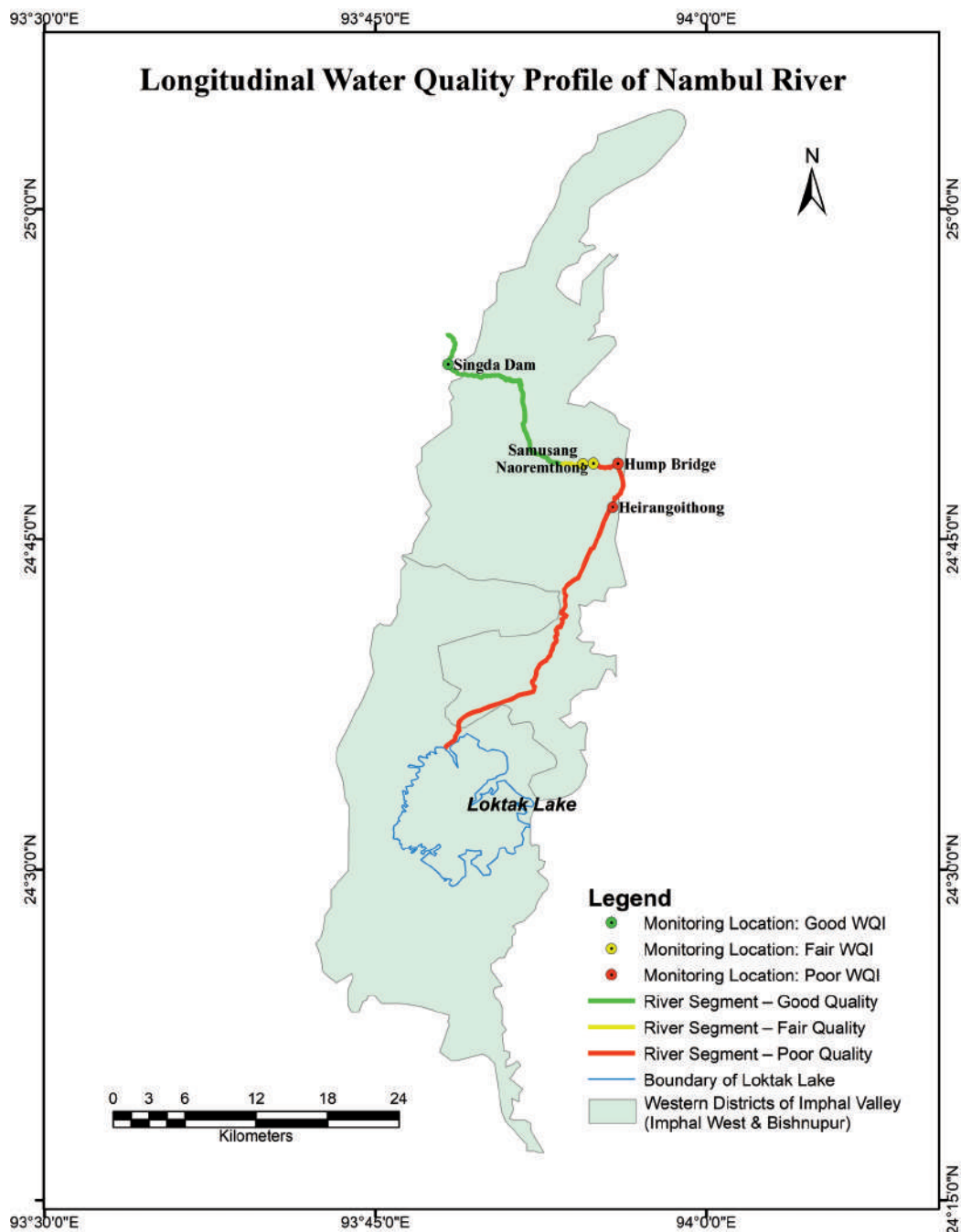


Figure 11. Longitudinal Water Quality Profile of Nambul River

For the Thoubal River, all locations are classified as ‘Good,’ except Yaolen village, which falls under the ‘Fair’ category with a WQI score of 52.3 which is due to Low DO Min, High Coliform. The WQI scores for Thoubal range from 35.6 at Shong Kong to 42.8 at Yairipok. While the Nambul River displays a wider range of water quality conditions. The first one is in ‘Good’ water quality, the next two upstream monitoring sites are categorised as ‘Fair,’ while the two downstream locations fall under the ‘Poor’ category. The lowest WQI score (65.7) is recorded at Naoremthong, and the highest (89.2) at Hump Bridge. These values indicate the poorest water quality among all rivers, particularly at Hump Bridge and Heirangoithong. The longitudinal water quality profile of Nambul River, which ultimately fall into the Loktak Lake degrading the water quality of the only floating lake in the world (Figure 11).

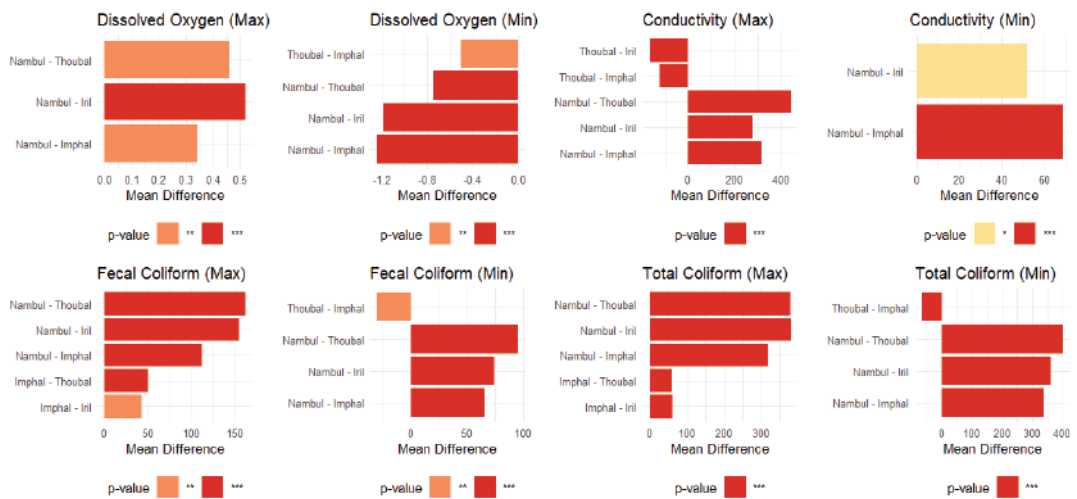


Figure 12. Row Chart of Inter-River Variation for Significant Parameters (Post-Hoc Tukey HSD Test)

Overall, 19 of the monitoring locations across the four rivers are classified as ‘Good,’ while three are categorised as ‘Fair’ (including locations on the Nambul and Thoubal rivers), and two are classified as ‘Poor,’ both situated along the Nambul River. This analysis highlights that water quality is good in the Imphal, Iril, and Thoubal Rivers, with the exception of Yaolen village on the Thoubal River. The Nambul River, however, has the most degraded water quality, especially at its lower reaches.

Table 7 presents the average Water Quality Index (WQI) scores for the four major rivers in the Imphal Valley. Based on the WQI classification, the Thoubal, Iril, and Imphal Rivers are categorised as having ‘Good’ water quality, while the Nambul River as the ‘Fair’ category. Among the rivers classified as ‘Good,’ the Thoubal River has the lowest average WQI score at 40.8. It indicates relatively better water quality within this category. The Imphal River has the highest WQI score with 44.4 among the ‘Good’ rivers. The Nambul River has the highest WQI score with 69.5 of all rivers. The Nambul River is in the ‘Fair’ category.

Table 7. River-wise Average WQI

River	Average WQI	Overall Water Quality Rating	Key Issues
Imphal	44.4	Good	Coliform levels need monitoring at several locations
Iril	41.6	Good	Good with some conductivity variations
Thoubal	40.8	Good	Yaolen Village requires attention
Nambul	69.5	Fair	Severe contamination at multiple locations

The Nambul River has been most polluted among the four rivers. Hump Bridge and Heirangoithong are the most impacted sites. These locations have high concentrations of both FC and TC, higher BOD, and increased EC. They are the indicators of microbial contamination and organic pollution.

Coliform contamination is the most widespread issue across four rivers. EC shows variability across sites. BOD levels remain within acceptable thresholds, except in the Nambul River. While the Thoubal River demonstrates the best water quality, particularly at Shong Kong, Litan Bridge, and Mapithel Dam, which have the lowest WQI scores, ranging from 35.6 to 37.8. Despite localised pollution hotspots, especially within the Nambul River, the overall water quality across the rivers is classified as ‘Good’ according to the WQI assessment.

WQI classifies the Imphal, Iril, and Thoubal rivers as ‘Good’, while the Nambul River falls as in ‘Fair’ category. The WQI synthesises complex data into a single score, making it a powerful tool for policy communication (Brown *et al.*, 1970). The ‘Fair’ classification for the Nambul River is the cumulative effect of the heavily weighted negative impacts of high BOD, low DO, high conductivity, and extremely high coliform counts. These parameters, indicative of severe organic and fecal pollution, drag the overall index score down. Conversely, the ‘Good’ status of the Thoubal River is a result of its lower levels of these key pollutants, reflecting a healthier upstream catchment.

The use of WQI for classifying Indian rivers is widespread. For example, WQI assessments of the Godavari River by Kulkarni *et al.* (2019) showed a clear gradient from ‘Excellent/Good’ in forested upstream areas to ‘Poor/Very Poor’ in urban and industrial downstream segments. WQI results for the Nambul are comparable to those reported for polluted urban rivers across the country, such as the Adyar River in Chennai (Sundar *et al.*, 2021). The health of other rivers serves as a stark reminder of what’s at stake. It shows the standard risk losing if urban growth continues uncontrolled. These findings provide clear evidence for a two-pronged approach: urgently prioritise cleaning up the Nambul River while actively protecting healthier rivers from suffering the same fate.

Conclusion:

This study shows the state of the Imphal Valley’s aquatic lifelines. It reveals a classic narrative of riverine degradation where the intensity of human activity dictates ecological health. The investigation, with longitudinal trend analysis, inter-river statistical comparisons, and Water

Quality Index (WQI), moves beyond routine monitoring to provide a definitive diagnosis of a system under immense stress. The principal conclusion is unambiguous: the significant spatial disparity in water quality across these four rivers is a direct and quantifiable consequence of unchecked urbanization and the systemic failure to manage wastewater, with the Nambul River serving as a tragic archetype of urban river decay.

The major findings of this research present a cascade of ecological and public health concerns. The Nambul River, in its journey through the heart of Imphal city, shows a classic urban stream syndrome. This has DO levels plummet to hypoxic conditions that are incapable of supporting healthy aquatic fauna, while the BOD soars, signaling a system overwhelmed by organic pollutants. Above all, the alarming levels of FC and TC has transformed the river into a dangerous pipeline for waterborne illnesses. In stark contrast, the Thoubal River, especially in its forested upper reaches, functions as an invaluable regional benchmark, demonstrating the water quality that is achievable in the absence of overwhelming anthropogenic pressure, yet its health remains precarious against advancing development.

This sharp dichotomy is not merely observational but is statistically validated. The Water quality assessment classifies the Imphal, Iril, and Thoubal rivers as 'Good,' but the Nambul River as 'Fair'. This quality rating shows that the Nambul is failing as a cohesive ecosystem. The widespread organic and microbial pollution highlights a critical gap in urban planning and environmental governance, a challenge of many rapidly growing urban centres in sensitive ecological regions. The findings, therefore, serve as a microcosm of a larger regional issue and affirm that achieving the United Nations' Sustainable Development Goal 6 (Clean Water and Sanitation) in Manipur is fundamentally contingent on addressing the direct discharge of municipal sewage.

This study serves as a critical call to action. This necessitates an immediate shift from passive monitoring to a targeted management strategy. One approach is an urgent remediation plan for the heavily polluted Nambul River through engineering solutions. Another approach is the proactive conservation strategy for the Thoubal, Imphal, and Iril rivers centered on catchment-level management to prevent their decline. The research acknowledges limitations of its reliance on secondary data and the absence of seasonal data. This show the need for future studies using high-resolution primary data and seasonal monitoring. The findings provide an undeniable, evidence-based mandate for action. It calls for a 'Nambul River Action Plan,' that will highlight a direct public health threat from alarming FC levels requiring immediate awareness campaigns, and stress that managing these rivers is the most critical strategy for preserving the ecological integrity of the downstream Loktak Lake. Ultimately, this research translates water quality data into a clear agenda. The agenda is to empower stakeholders to engineering solutions. This will secure the region's public health, ecological stability, and sustainable future.

References:

Bhardwaj, V., Singh, D. S., and Singh, A. K., 2017. Water quality of the Hindon river and its tributaries in Uttar Pradesh, India with reference to seasonal variation, Sustainable Water Resources

Management, 3: (2): 147–162. <https://doi.org/10.1007/s40899-017-0097-9>.

- Bhattacharjee, S., Chakraborty, S., and Das, P., 2022. River water quality assessment and pollution source identification using multivariate statistical techniques: A case study, *Environmental Science and Pollution Research*, 29: (12): 17845–17862.
- Bora, M., and Goswami, D. C., 2017. Water quality assessment in terms of water quality index (WQI): Case study of the Kolong River, Assam, India, *Applied Water Science*, 7: (6): 3125–3135.
- Brown, R. M., McClelland, N. I., Deininger, R. A., and Tozer, R. G., 1970. A water quality index-do we dare?, *Water and Sewage Works*, 117: (10): 339–343.
- CPCB., 2018. River stretches for restoration of water quality. Ministry of Environment, Forest and Climate Change, Government of India.
- CPCB., 2019. Water quality criteria. Ministry of Environment, Forest and Climate Change, Government of India.
- CPCB., 2022. *National Water Monitoring Programme (NWMP) – Water quality data*, Ministry of Environment, Forest and Climate Change, Government of India.
- Chapra, S. C., 2008. Surface water-quality modeling, Waveland Press.
- Devi, A., and Singh, R. K., 2021. Impact of urban sewage on the physicochemical characteristics of the Nambul River, Manipur, *Journal of Environmental Management and Planning*, 8: (2): 45–58.
- Devi, N.L., Yadav, I.C., and Shihua, Q., 2021. Water quality assessment of the Loktak Lake in Manipur, Northeast India using multivariate statistical techniques, *Environmental Monitoring and Assessment*, 193: (4): 1–18.
- Ewaid, S. H., Abed, S. A., and Al-Ansari, N., 2020. Water quality index for Al-Gharraf River, southern Iraq, *Water*, 12: (7): 2038. <https://doi.org/10.3390/w12072038>
- Field, A., 2013. *Discovering statistics using IBM SPSS statistics*, 4th ed., SAGE Publications.
- Ghosh, H., Roy, S., and Bhattacharya, A., 2020. Environmental degradation in the river systems of Northeast India: Causes and implications, *Journal of Environmental Geography*, 13: (1–2): 23–30.
- Helsel, D.R., and Hirsch, R. M., 2002. *Statistical methods in water resources*, Vol. 323, U.S. Geological Survey.
- Jain, C. K., 2002. Water quality of the Ganga river in the deltaic region, West Bengal, India, *Water-SA*, 28: (3): 335–342. <https://doi.org/10.4314/wsa.v28i3.4907>.
- Kannel, P.R., Lee, S., Lee, Y.S., Kanel, S. R., and Khan, S. P., 2007. Application of water quality indices and dissolved oxygen as indicators for river water classification and urban impact assessment, *Environmental Monitoring and Assessment*, 132: (1–3): 93–110.
- Kaushal, S. S., Groffman, P. M., Likens, G. E., Belt, K. T., Stack, W. P., Pace, M. L., and Fisher, G. T., 2005. Increased salinization of fresh water in the northeastern United States, *Proceedings of the National Academy of Sciences*, 102: (38): 13517–13520. <https://doi.org/10.1073/pnas.0506414102>.
- Khan, M. A., and Ahmad, S., 2011. Hydro-chemical characteristics of the surface water bodies in Imphal Valley, Manipur State, North-East India, *Journal of Applied Geochemistry*, 13: (1): 85–102.
- Kinouchi, T., Yagi, H., and Miyamoto, M., 2007. Increase in river water temperature in the suburbs of Tokyo and its effect on the thermal response of a paddy-dominated basin, *Hydrological Processes*, 21: (14): 1872–1884. <https://doi.org/10.1002/hyp.6414>.

- Kulkarni, V. R., Srinivas, B., and Kumar, R., 2019. Assessment of water quality of Godavari river using water quality index (WQI) and multivariate statistical analysis, *Environmental Monitoring and Assessment*, 191: (7): 425. <https://doi.org/10.1007/s10661-019-7561-2>.
- Kumar, A., and Singh, C.K., 2018. Assessment of surface water quality in Imphal River, Manipur, India, *International Journal of Environmental Sciences*, 9: (1): 45–56.
- Laishram, J., Devi, S. P., and Kumar, M., 2022. Assessment of non-point source pollution from agricultural catchments in the Thoubal River Basin, India, *Environmental Monitoring and Assessment*, 194: (3): 215. <https://doi.org/10.1007/s10661-022-09854-z>.
- Lalchand, P., 2019. Urbanization and river pollution in Northeast India: A case study of Nambul River in Imphal city, *Indian Journal of Environmental Protection*, 39: (8): 715–722.
- Meitei, N.S., and Bhargava, R., 2019. Water quality assessment of Nambul River in Imphal city, Manipur, *Journal of Environmental Science and Technology*, 12: (3): 112–120.
- Ningthoujam, R. K., and Devi, L. S., 2018. Assessment of water quality of the Imphal River, Manipur using WQI, *Pollution Research*, 37: (2): 356–361.
- Pandey, P. K., and Singh, P., 2017. Water quality assessment of the Ganga River at Varanasi, India, using a combination of multivariate statistical analysis and water quality indices, *Environmental Monitoring and Assessment*, 189: (8): 384. <https://doi.org/10.1007/s10661-017-6091-8>.
- Pesce, S.F., and Wunderlin, D. A., 2000. Use of water quality indices to verify the impact of Cordoba city (Argentina) on Suquia River, *Water Research*, 34: (11): 2915–2926.
- Poole, G. C., and Berman, C. H., 2001. An ecological perspective on in-stream temperature: Natural heat dynamics and mechanisms of human-caused thermal degradation, *Environmental Management*, 27: (6): 787–802. <https://doi.org/10.1007/s002670010188>.
- Pravin, R., and Panneerselvam, B., 2021. Spatiotemporal assessment of water quality of Mithi River, Mumbai, India using multivariate statistical techniques, *Arabian Journal of Geosciences*, 14: (3): 1–15. <https://doi.org/10.1007/s12517-021-06512-y>.
- Sener, S., Sener, E., and Davraz, A., 2017. Evaluation of water quality using water quality index (WQI) method and GIS in Aksu River (SW-Turkey), *Science of the Total Environment*, 584–585: 131–144. <https://doi.org/10.1016/j.scitotenv.2017.01.102>.
- Sharma, D., and Singh, S. K., 2021. Spatio-temporal assessment of water quality of the Yamuna River using geographical information system, *Applied Water Science*, 11: (2): 1–13. <https://doi.org/10.1007/s13201-020-01349-4>.
- Sharma, S., and Singh, P., 2022. Urbanization and its impact on river ecosystems: A review, *Applied Water Science*, 12: (5): 116. <https://doi.org/10.1007/s13201-022-01633-9>.
- Sharma, T., Singh, R. K., and Devi, C. H., 2021. Impact of anthropogenic activities on river systems in Imphal Valley, Manipur, *International Journal of Ecology and Environmental Sciences*, 47: (1): 25–32.
- Singh, A.K., Devi, S. M., and Sharma, P., 2022. Evaluation of surface water quality of Iril River using WQI and multivariate statistical techniques, *Environmental Science and Pollution Research*, 29: (13): 19284–19295.
- Singh, B. S., Romi, M. F., and Sharma, M. B., 2013. Water quality assessment of Nambul river, Imphal, Manipur with reference to WQI and NSF-WQI, *International Research Journal of Environment*

Sciences, 2: (4): 1-7.

- Singh, H.N., and Singh, T. B., 2020. Water quality assessment of Imphal River in Manipur using water quality index, *International Journal of Scientific Research in Environmental Sciences*, 8: (1): 34–43.
- Singh, M.S., and Singh, A. R., 2020. Hydrological and ecological significance of rivers in Imphal Valley, Manipur, *Manipur Geographical Journal*, 15: (2): 45–58.
- Singh, P., Singh, R., and Singh, R. L., 2017. Assessment of water quality of Varuna River at Varanasi, India with reference to metallic contents, *Journal of Environmental Protection*, 8: (12): 1435. <https://doi.org/10.4236/jep.2017.812088>.
- Singh, P. M., Laishram, R., and Lourembam, B., 2022. Spatial variation in surface water quality of urban rivers in Imphal Valley, Manipur, *Asian Journal of Water, Environment and Pollution*, 19: (3): 27–34.
- Singh, R., and Gupta, A., 2020. Impact of anthropogenic activities on water quality of major rivers in Manipur, *International Journal of River Basin Management*, 18: (2): 245–256.
- Singh, T. B., and Kumar, S., 2023. Anthropogenic stressors and water resource management challenges in the river systems of Manipur Valley, *Indian Journal of Water Resources*, 43: (1): 88-99.
- Sliva, L., and Williams, D. D., 2001. Buffer zone versus whole catchment approaches to studying land use impact on river water quality, *Water Research*, 35: (14): 3462-3472. [https://doi.org/10.1016/S0043-1354\(01\)00062-8](https://doi.org/10.1016/S0043-1354(01)00062-8).
- Sundar, S. R., Govindaradjane, S., and Raj, S. E., 2021. Assessment of water quality index of Adyar River, Tamil Nadu, India, *Materials Today: Proceedings*, 45: 6979-6983. <https://doi.org/10.1016/j.matpr.2021.01.442>.
- Tali, J. A., Lone, F. A., and Ganaie, J. A., 2021. Impact of urbanization on water quality parameters of river Jhelum, Kashmir Himalaya, *Environmental Monitoring and Assessment*, 193: (7): 1-16. <https://doi.org/10.1007/s10661-021-09199-5>.
- Tyagi, S., Sharma, B., Singh, P., and Dobhal, R. 2013. Water quality assessment in terms of Water Quality Index, *American Journal of Water Resources*, 1: (3): 34–38.
- Verma, S., Kumar, S., Gupta, A. K., and Kumar, R., 2020. Impact of anthropogenic activities on water quality of Ganga River at Rishikesh and Haridwar, Uttarakhand, India, *Environment and Ecology*, 38: (1): 108-115.
- Uddin, M. G., Nash, S., and Olbert, A. I., 2021. A review of water quality index models and their use for assessing surface water quality, *Ecological Indicators*, 122: 107218. <https://doi.org/10.1016/j.ecolind.2020.107218>.
- United Nations., 2015. *Sustainable Development Goals: 17 goals to transform our world*. Available at: <https://www.un.org/sustainabledevelopment/> [Accessed 24/03/25].
- Wetzel, R. G., 2001. *Limnology: Lake and river ecosystems* (3rd ed.), Academic Press.
- World Health Organization (WHO)., 2017. *Guidelines for drinking-water quality: fourth edition incorporating the first addendum*, World Health Organization.



Detection and Mapping of Geomorphic Changes: A Case Study of the Chandragiri Estuary, Kerala.

Rakshith C.M.¹, Nirmala R.^{1*} and Pranith P.¹

¹*Dept. of Marine Geology, Mangalore University, Karnataka –574199, India*

**Corresponding author: geonirmala19@gmail.com*

Abstract: Estuaries are incredibly productive ecosystems that play a vital role in supporting rich biodiversity. It maintains water purification and provides flood control, all of which contribute to the economic health of coastal communities. The Chandragiri River, which flows westward, originates in the Western Ghats of the Kodagu district in Karnataka and has a course length of 105 km. It meanders through steep laterite hills, forming a unique tropical estuarine system around the town of Kasaragod, where it supports mangrove wetlands before emptying into the Arabian Sea. This study aims to investigate the spatio-temporal changes in the Chandragiri River estuary from 2000 to 2022. The analysis of dynamic changes in river estuaries involved processing multi-date imagery in a GIS environment to identify changes over time. Notably, no vented dams or reservoirs have been constructed along this river, allowing its sediment load to remain unaffected; however, sand mining has emerged as one of the most significant activities in the area. Observations from 2003 to 2004 highlighted changes in river flow and increased silting due to a newly constructed breakwater. Human activities such as sand mining and development have significantly altered the estuary, underscoring the need for improved management and conservation efforts.

Keywords: Chandragiri River, Estuary change, Sand mining, Remote Sensing and GIS

Introduction:

River mouths along tropical coastlines are highly dynamic environments that are significantly influenced by various human activities, including navigation, fisheries, aquaculture, agriculture, transportation, and infrastructure development which drive local economic growth. Therefore,

maintaining stable conditions around these areas is essential (Kerkhofs, *et al.*, 2005; Mahoney and Bishop, 2017). Presently, river mouths are confronted with several critical challenges, such as sedimentation, bank erosion, shifting mouths, and saltwater intrusion.

Changes in the morphology of river estuaries significantly affect estuarine hydrodynamics, ecosystems, and navigation. The processes of geomorphic evolution are mainly caused by the erosion, transportation of sediments and deposition (Kunhimammu *et al.*, 2009; De Jonge *et al.*, 1983). Recent studies highlight ecological and morphological changes in estuaries that are crucial for protecting the land from storms and pollutants. However, anthropogenic activities such as sand mining, dam and breakwater construction and have had a significant impact on estuaries and their surrounding areas (Deepika *et al.*, 2014; Nirmala, *et al.*, 2020; Shalini *et al.*, 2013; Sheela *et al.*, 2011). The morphology and evolution of the estuary are shaped by tides, waves, and other marine forces, which interact with the coastline in various ways (Kumar, and Jayappa 2009; Mar Roca, *et al.*, 2022; Wu *et al.*, 2022; Costa *et al.*, 2023; Kunhimammu Paravath and Nasar Thuvanismail, 2023).

Sand mining is a major cause of changes in river deltas; it leads to changes in river channels, erosion of river banks, and subsequent subsidence (Nithu *et al.*, 2019; Maria Aranda *et al.*, 2020; Shaji *et al.*, 2021). The Gangolli estuary (Deepika *et al.*, 2014) and Mulki-Pavanje estuary (Shalini *et al.*, 2013) on the west coast of Karnataka, the Muthalapozhi inlet and the Ponnani estuary in Kerala (Girija *et al.*, 2015; Sheela *et al.*, 2011) are notable examples of estuarine changes. Geoinformatics, through the use of remote sensing and GIS technology, serves as a valuable tool for analyzing the causes and mechanisms of long-term geomorphological changes from 2000 to 2022. It facilitates the assessment of alterations in estuaries and the factors influencing these changes over the years (Yang, 2005; Vos *et al.*, 2019; Nirmala *et al.*, 2020). The present study focuses on the morphological changes of the Chandragiri River delta, analyzing the geometric change and cross-sectional area through multi-date image analysis. Addressing these issues is crucial for the health and sustainability of estuaries and coastal areas. Prioritizing sustainable practices is essential to maintain the functionality of these important natural resources.

Study Area:

The Chandragiri River, also known as Payaswini River, is a west-flowing river that begins in the Kodagu district of Karnataka, flows towards Kerala through Kasaragod district, and finally joins the Arabian Sea. The drainage basin covers an area of 1244 sq km and is situated between 12°27' and 12°34' N and 74°58' and 75°42' E (Figure 1). The river has a total length of ~106 km, with an average annual runoff of ~3,12,052 m³ (Subrahmanya Prasad and Agretious Thomas, 2021). The average maximum and minimum temperatures are 37° C and 17° C, respectively. The district receives an annual average rainfall of 3350 mm. The river winds around Kasaragod town, forming a typical tropical estuarine system, supporting mangrove wetlands before it enters the sea.

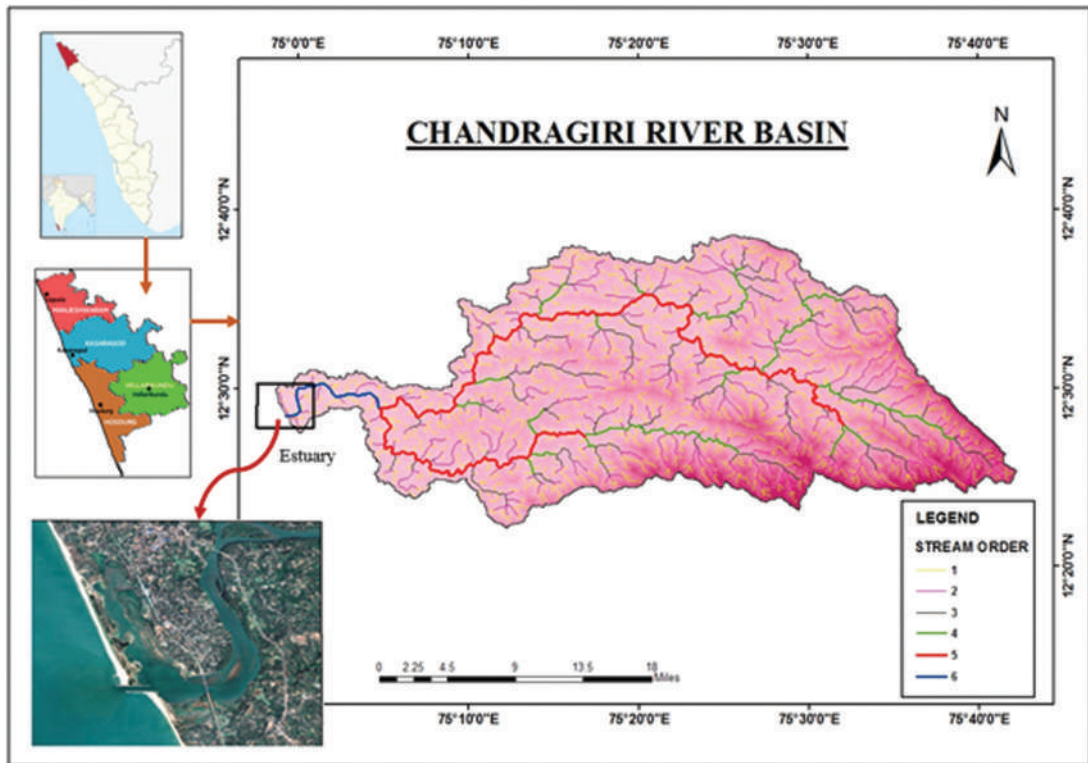


Figure 1. Location map of Chandragiri River estuary

Geologically, the drainage basin of the Chandragiri River is predominantly composed of Precambrian crystalline rocks, including Charnockites, hornblende-biotite gneiss, and high-grade schistose rocks, which are extensively lateritized in the lower reaches. The area is characterized by undulating topography and a short distance from the rivers to the sea, allowing rainwater to drain into the sea within hours, often transporting a significant amount of sediment. The upstream region of the river, located in Coorg, Karnataka, is highly prone to erosion and landslides (Rashma Jain *et al.*, 2019). This section is characterized by structurally fractured hills and substantial amounts of sediments, which contribute a significant amount of sediment to the river. Additionally, the lack of check dams along the river increases sand accumulation in the estuary, leading to sand mining (Diez *et al.*, 2014; Van Maren *et al.*, 2015; Iswana, *et al.*, 2019; Wu, *et al.*, 2022).

The coast of Chandragiri experiences two high and two low tides of approximately equal magnitude semi-diurnal tides on each lunar day. The tides in Kerala fall within the micro-tidal range of less than 2 meters and the average wind speed in Kasaragod is about 4 m/s. These interrelated factors create favorable tidal currents, which lead to accumulation on the Chandragiri coast.

Rainfall:

Kasaragod district experiences significant rainfall primarily from the Southwest Monsoon (June to September), with average annual precipitation ranging from 3000 mm to 3800 mm due to the orographic influence of the Western Ghats. The eastern hilly regions receive more than 4000 mm, while the coastal areas report around 3000–3200 mm (IMD, 2022; Sheela *et al.*, 2011).

Data and methodology:

Dynamic changes in river estuaries were analyzed through a comprehensive assessment of multi-date imagery. In this study, satellite imagery of Landsat 7 ETM (www.usgs.gov) and Google Earth images from 2000 to 2022 were used (Table 1). The images were processed using open-source software QGIS in a GIS environment and were projected from the Survey of India (SOI) toposheet. For each image, distinct layers were created and subsequently overlaid to facilitate comparison and detect changes over time (Dipson *et al.*, 2015). Furthermore, a land use and land cover change detection map was developed to identify the impacts of human activities in and around the estuary (Mar Roca, *et al.*, 2022; Vos, *et al.*, 2019).

Table 1. Data and data sources used in the study.

Data	Data source
Landsat 7 ETM satellite images (2000-2022)	earthexplorer.usgs.gov
Google Earth images (2000-2022)	Google Earth
SRTM DEM	earthexplorer.usgs.gov
Drainage, LULC	ArcGIS software
Rainfall data	IMD and KSNDMC

Results and Discussion:

The Chandragiri River discharges significant amounts of sediment, contributing to the dynamic nature of its estuary. Rainfall in Kasaragod is mainly driven by the Southwest Monsoon (June–September), contributing over 80% of annual precipitation, while the Northeast Monsoon adds 10–15%. These fluctuations impact river flow, groundwater recharge, and seasonal flooding, leading to higher sediment transport to estuarine mouths, resulting in sandbar breaches and mudflat expansion, particularly in the Chandragiri estuary (Sheela *et al.*, 2011; Roxy *et al.*, 2019).

Notably, there are no major dams/reservoirs constructed along the Kerala side of the Chandragiri River, allowing for an uninterrupted supply of sediment to the coastal area, which further facilitates the accumulation of sand at the estuary. Illegal sand mining is a prominent activity within this study area, occurring without oversight from the Harbor Engineering Department (Smits *et al.*, 2006; Stephan, *et al.*, 2022). The river sand extracted is highly

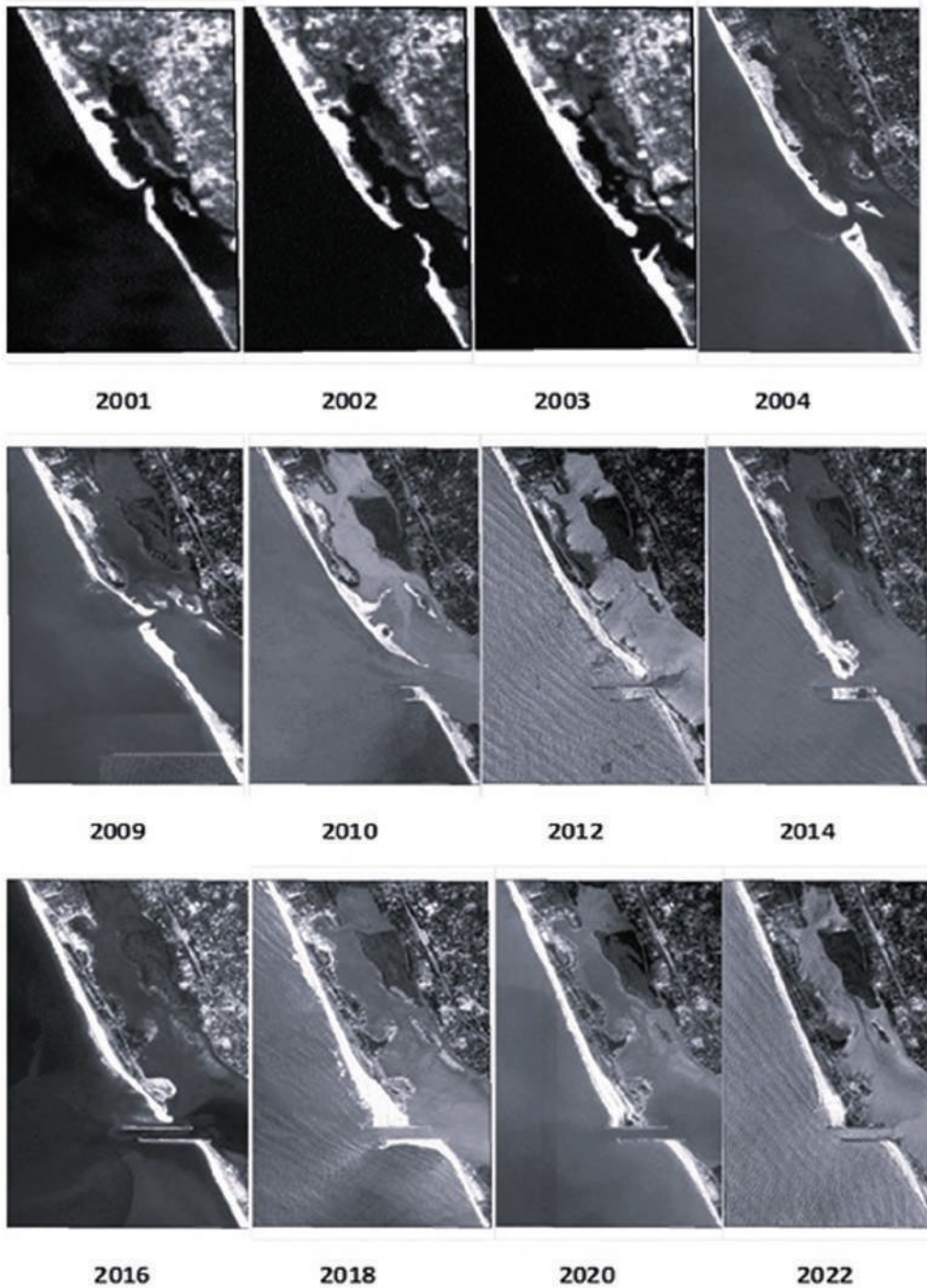


Figure 2. Multi-temporal images show changes over time.

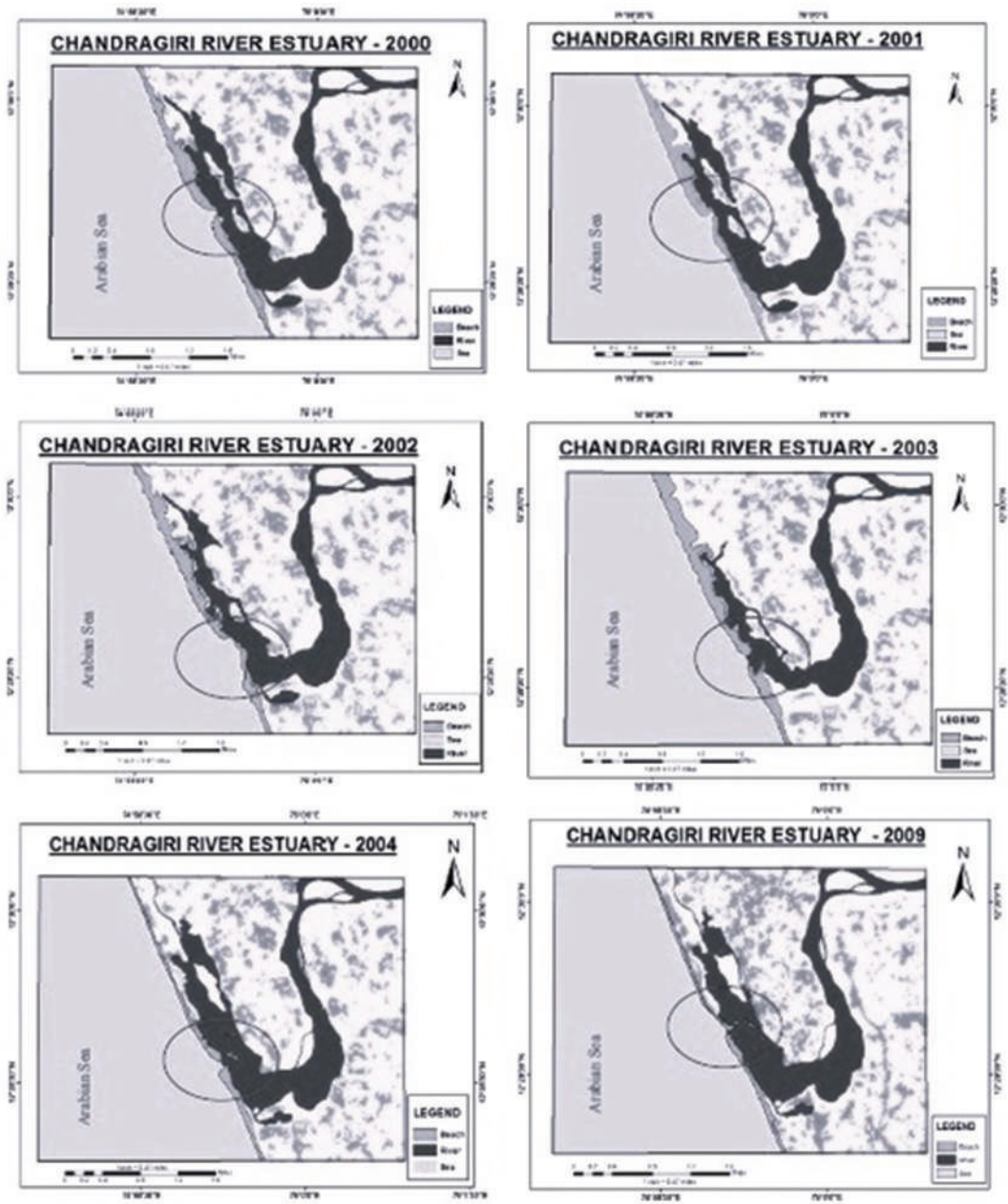


Figure 3. Geomorphological changes in the Chandragiri estuary from 2000 to 2009.

sought after for construction purposes due to its minimal processing requirements and superior quality compared to alternative sources.

Between 2000 and 2002, significant changes occurred in the river mouth and nearby coastline, with increased erosion noted at the southern spit in 2002 (Fig 3). By 2003, both sides of the river inlet showed structural changes, leading to a widening of the mouth compared to 2002. The inlet has also migrated southward due to ongoing sand mining activities, which have disrupted the coastline, altered the riverbed, eroded banks, and contributed to flooding (Dipson *et al.*, 2015; Nithu *et al.*, 2019). Excessive sand extraction, facilitated by the absence of dams or reservoirs, has altered the riverbed, forcing the river to change its course, eroding the banks, and contributing to flooding (Klemas, 2001; Levinson, 2005; Narayana *et al.*, 2005).

In 2004, observations noted asymmetrical morphological changes at the river mouth, particularly erosion on the northern coastline (Fig 3). A long, narrow sandbar was present to the right of the river mouth at that time. Initial hypotheses linked these changes to the tsunami of December 26, 2004, but it was determined that the coastline modifications had

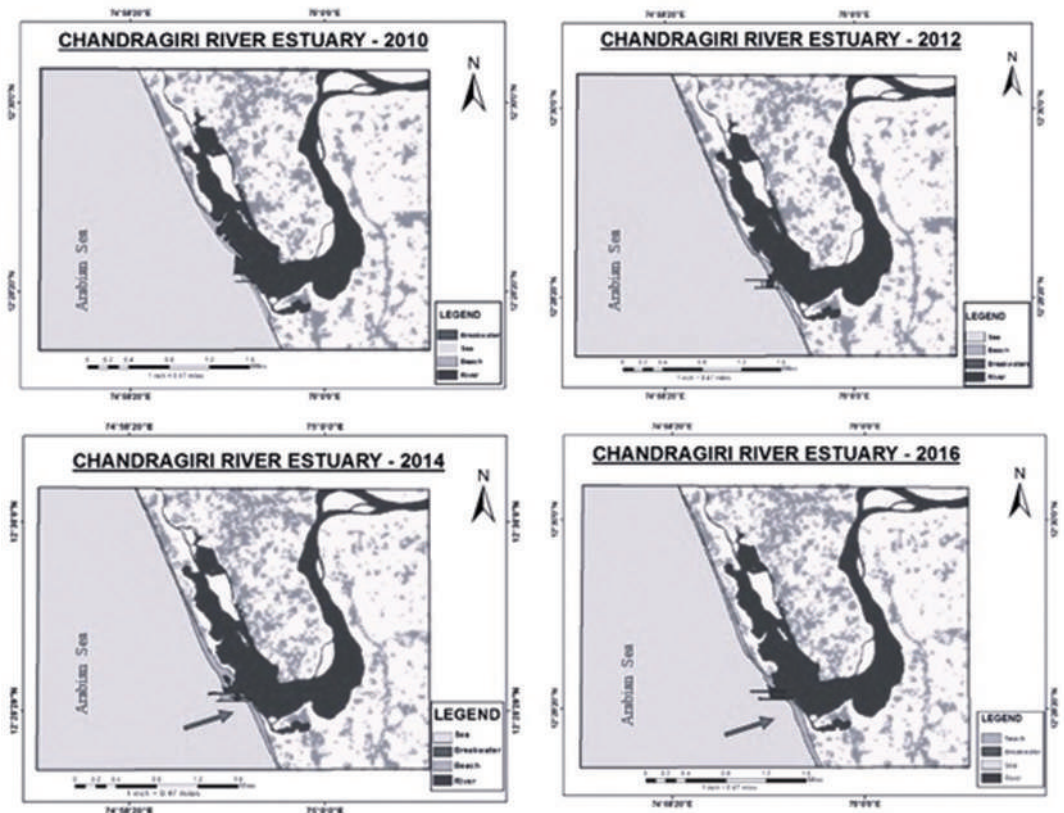


Figure 4. Geomorphological changes in the Chandragiri estuary 2010 and 2016.

already occurred before the tsunami, influenced by illegal sand mining (Iswana *et al.*, 2019; Narayana *et al.*, 2005; www.deccanherald.com; www.onmanorama.com). From 2004 to 2009, erosion continued, leading to significant changes, with the northern coastline elongating and shifting rightward due to increased sediment supply from flood events, even as the river mouth remained narrow.

In 2010, the seasonal closure of the inlet posed significant challenges for local fishermen. To address the issue of creating a perennial inlet, a proposal was made to construct two breakwaters intended to stabilize the river mouth (Fig 4). Construction commenced in the same year, with plans for a length of 495 meters for the southern breakwater and 490 meters for the northern breakwater. This construction flaw resulted in the formation of strong waves, complicating the process of launching boats into the sea. Following expert recommendations from the research station, a decision was made to extend both the southern and northern breakwaters seaward (Rao, *et al.*, 2015; Stephan, *et al.*, 2021).

Despite the completion of the breakwaters in 2010, silting at the river mouth persisted in subsequent years, particularly from 2012 onward, resulting in a shift of the river mouth from the northern side to the southern side. The entire estuarine geomorphology was altered due to excessive and unregulated illegal sand excavation activities. Field investigations and local interviews indicated that the estuary is highly dynamic, and sedimentation within the constructed breakwaters has rendered the boat channel completely obstructed. Fishermen continue to utilize the original estuary for access to the sea, as the newly formed boat channel between the breakwaters remains blocked by sedimentary deposits.

The transformation of the coastline was assessed at the land-water interface of the Chandragiri estuary during the year 2014 (Fig 4). The southern region experienced greater erosion, while the northern region witnessed substantial accretion. The dynamics of sediment loss and gain were influenced by the wave energy and littoral currents of the Arabian Sea, which are predominantly governed by longshore drift, wave action, sand mining practices, and artificial structures (Sheela, *et al.*, 2011; Little *et al.*, 2017).

In 2015, the Kerala government implemented a complete ban on sand mining in the Chandragiri estuary (source: www.onmanorama.com; Deccan Herald, June 14, 2015). During the accretion process of the beaches, the sediment accumulated within the breakwaters is entirely dredged by the harbor engineering department and subsequently sold to private contractors, who transport significant quantities of sand primarily from the sites where the breakwaters have been constructed (Munoz Perez, *et al.*, 2000; Girija, 2015; Lotze, *et al.*, 2006; Kunhimammu *et al.*, 2009; Van Maren *et al.*, 2015; Little *et al.*, 2017; Maria Aranda, *et al.*, 2020). In subsequent years, the increased flooding of the river during the monsoon season has led to substantial sand erosion along the riverbanks. Additionally, the construction of harbors near the shoreline has created adverse conditions for mangrove growth along the banks of the Chandragiri River.

In 2018, significant sand accretion occurred along the beaches, resulting in the obstruction of water flow through the breakwater regions, which had become saturated with silt and sand. The development of residential structures near the beach has inspired the construction of sea

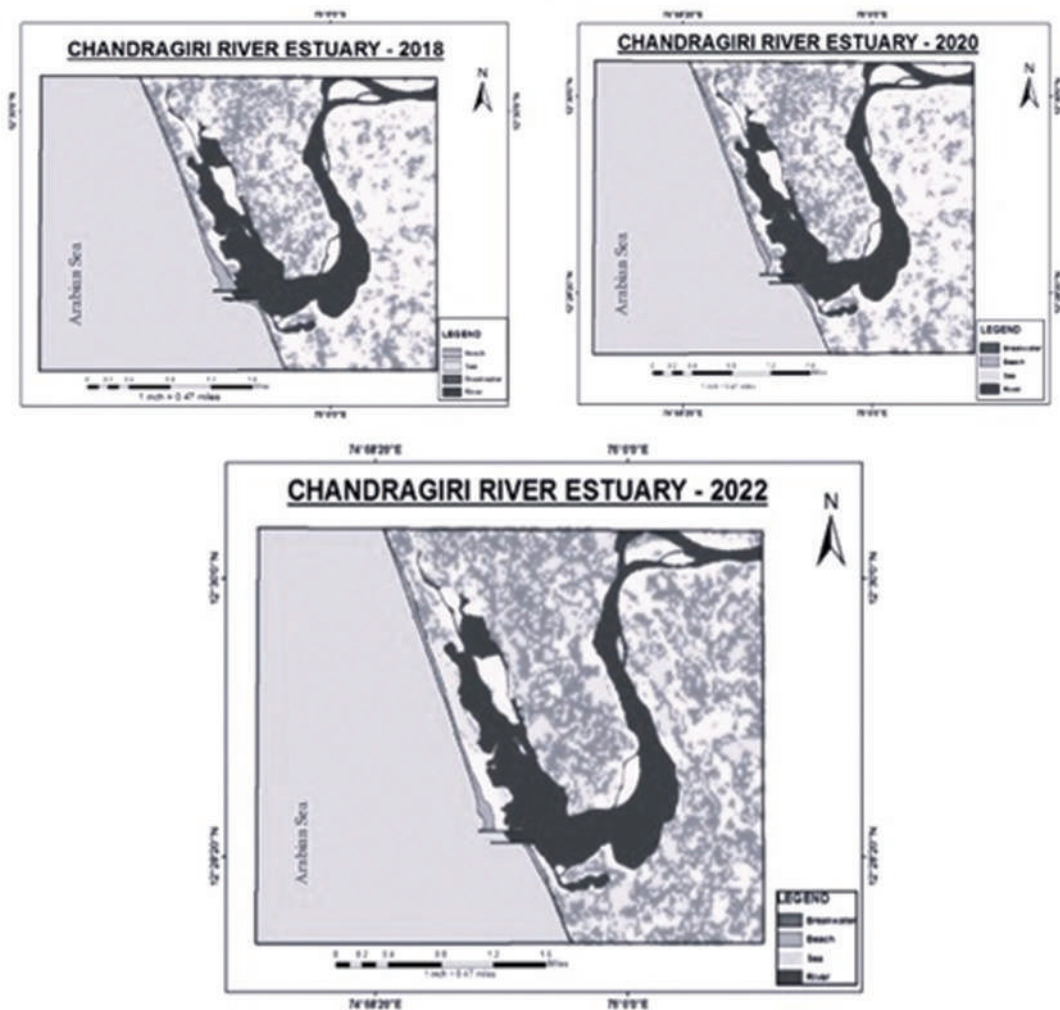


Figure 5. Geomorphological changes in the Chandragiri estuary 2010 and 2016.

walls (Fig 5). Significant changes have been recorded on the coast of the Chandragiri estuary, with clear evidence of sediment accumulation in the area. Compared to the period from 2000 to 2018, there was a significant transformation in the morphology of the river mouth and coastline in 2022, along with an increase in the number of settlements.

Recent studies have highlighted significant climatic changes in the Kasaragod district over the past few decades, including rising temperatures and variable rainfall patterns, which are attributed to climate change. From 2000 to 2022, El Niño events contributed to dry spells and salinity encroachment, while La Niña phases led to increased sediment transport and temporary flooding, although they pose long-term risks of erosion and ecological stress (Roxy

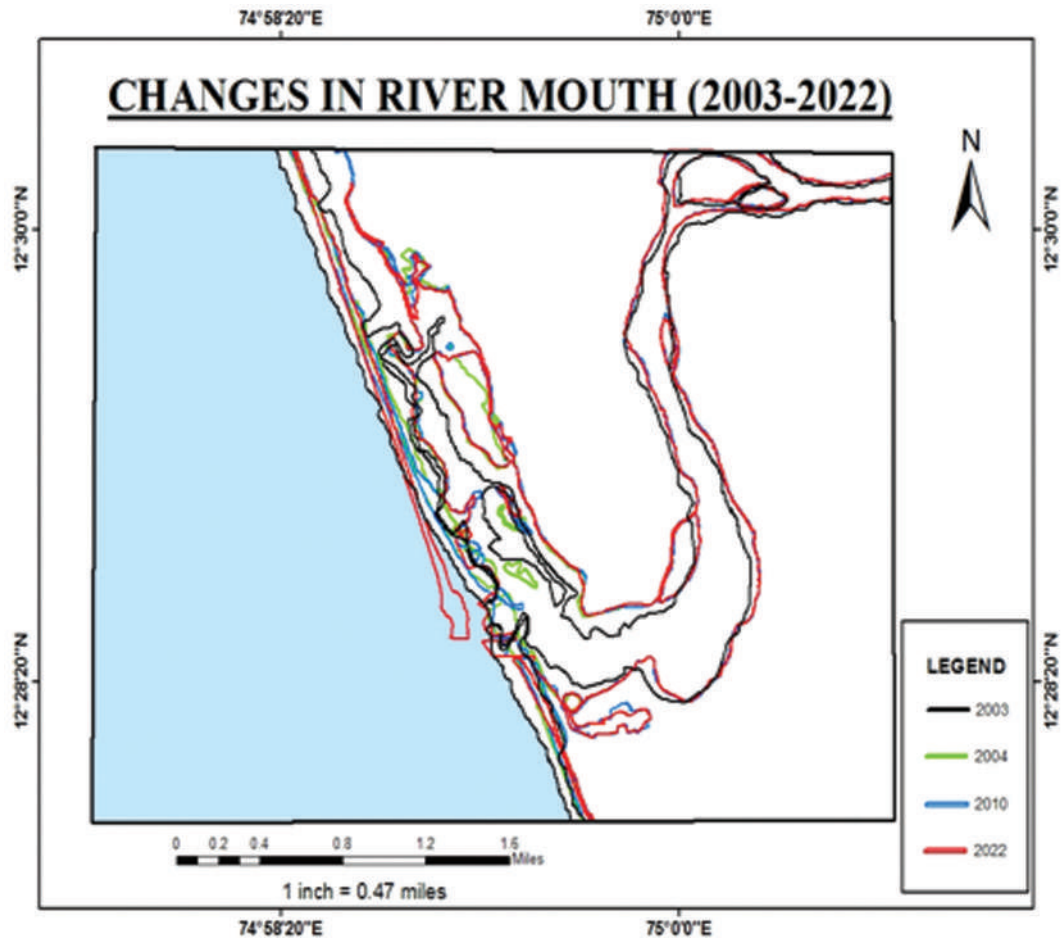


Figure 6. Morphological changes over time in the estuary of Chandragiri River.

et al., 2019; Shaji, 2021). The observations from the field study indicate that the physical and morphological changes in the Chandragiri estuary (Fig 6) contribute significantly to habitat degradation. Specifically, sand mining has led to increased saltwater intrusion in the estuary, which is adversely affecting local ecosystems. Moreover, erosion at the southern side is causing shorelines and landward areas to recede, leading to a permanent loss of coastal land. These factors collectively alter the physical landscape of the Chandragiri estuary and its surroundings, highlighting the need for sustainable management practices.

Conclusion:

Due to natural processes and human activities, the Chandragiri estuary has undergone major changes in its morphology. Notably, sand mining, the construction of breakwaters,

and land reclamation have played a major role as primary drivers of these transformations. These factors ultimately affect the Chandragiri estuarine environment, leading to disruptions in the ecosystem, habitat loss, saltwater intrusion, increased wave action, and shoreline recession. The construction of a breakwater at the mouth of the Chandragiri River established a safe navigable channel for fishing vessels. In the wake of these developments, the Kerala government completely banned sand mining from the Chandragiri River (www.deccanherald.com; www.onmanorama.com). Also, a seawall should be constructed to prevent coastal erosion from the southern breakwater. This study, conducted using geospatial tools, provides valuable insights for better management of the Chandragiri Estuary and other estuaries facing similar stressors.

References:

- A. J. M. Smits, Piet H. Nienhuis and H. L. F. Saeijs, 2006. Changing Estuaries, Changing Views. *Hydrobiologia*, 565(1):339-355. DOI: [10.1007/1-4020-5367-3_23](https://doi.org/10.1007/1-4020-5367-3_23).
- A. Kumar, and K. S. Jayappa, 2009. Long and Short- Term Shoreline Changes along Mangalore Coast, India. *International Journal of Environmental Research*, vol 3, 177–188.
- B. Deepika, Kumar Avinash and Katihalli Siddappa Jayappa, 2014. Impact of estuarine processes and hydro-meteorological forcing on landform changes: a remote sensing, GIS and statistical approach. *Arab J Geosci*. DOI [10.1007/s12517-014-1264-7](https://doi.org/10.1007/s12517-014-1264-7).
- Diez, J.J., Fernando, R., and Veiga, E.M., 2014. Coastal Impacts around Guadiaro River Mouth (Spain). In *Engineering Geology for Society and Territory*; Springer International Publishing: Cham, Switzerland, 2014; Volume 4.
- De Jonge, V. N., 1983. Relations between annual dredging activities, suspended matter concentrations, and the development of the tidal regime in the Ems estuary. *Canadian Journal of Fisheries and Aquatic Sciences* 40 (1), 289–300.
- D.S. Van Maren, T. Van Kessel, K. Cronin, and L. Sittoni, 2015. The impact of channel deepening and dredging on estuarine sediment concentration. *Continental Shelf Research*, volume 95, pp 1-14, <https://doi.org/10.1016/j.csr.2014.12.010>.
- Girija Ravi, 2015. Hydrodynamic Investigations on the Shoreline Changes Due to Construction of Breakwaters at the Muthalapozhi Inlet of Kerala Coast. *Conference Proceedings of International Journal of Engineering Research and Technology (IJERT)*. ISSN: 2278-0181. www.ijert.org NCRACE-2015.
- India Meteorological Department (IMD). (2022). Annual Rainfall Statistics of Kerala. IMD, Government of India.
- Iswana Adela, Gartika Setya Nugraha, Muhammad Irham, Saumi Syahreza, 2019. Spatial analysis of post tsunami 2004 coastline changes in Lampuuk, Aceh Besar. *IOP Conference Series Earth and Environmental Science*, 273(1):012046. DOI: [10.1088/1755-1315/273/1/012046](https://doi.org/10.1088/1755-1315/273/1/012046).
- J. SHAJI, 2021. Evaluating social vulnerability of people inhabiting a tropical coast in Kerala, south west coast of India. *International Journal of Disaster Risk Reduction*, vol 56, 102130, ISSN 2212-4209. [Doi.org/10.1016/j.ijdrr.2021.102130](https://doi.org/10.1016/j.ijdrr.2021.102130).

- Kerkhofs, M. J. J., T. Tiebosch, J. A. van der Velden & J. W. M. Kuijpers, 2005. Alternative management of the Haringvliet sluices: the first step towards major rehabilitation of the Rhine-Meuse estuary. *Archiv für Hydrobiologie Supplement* 155, Large Rivers 15: 569–578.
- Klemas, V.V., 2001. Remote sensing of landscape-level coastal environmental indicators. *Environmental Management*, 27, pp. 47–57.
- Kunhimammu Paravath, Nasar Thuvanismail, 2023. Shoreline Changes around Three Estuarine Harbours on Kerala Coast in India. *SSRG International Journal of Civil Engineering*, 10(7), 29–44, 2023. doi.org/10.14445/23488352/IJCE-V10I7P102.
- Kunhimammu Paravat, T. Jayadee, and P. I. Sheik Pareet, 2009. Influence of Estuarine Breakwater Constructions on Kerala Coast in India. *Advances in Water Resources and Hydraulic Engineering*, 836–843.
- Levinson, B., 2005. Remote sensing and the EPA Estuarine and Great Lakes Research Program. *International Journal of Remote Sensing*, 00, pp. 00–01.
- Little S., Spencer K. L., Schuttelaars H. M., Millward G. E., Elliott M., 2017. Unbounded boundaries and shifting baselines: Estuaries and coastal seas in a rapidly changing world. *Estuarine Coast. Shelf Sci.* 198, 311–319. doi: 10.1016/j.ecss.2017.10.010.
- Lotze, H.K., Lenihan, H.S., Bourque, B.J., Bradbury, R.H., Cooke, R.G., Kay, M.C., Kidwell, S.M.; Kirby, M.X., Peterson, C.H., and Jackson, J.B, 2006. Depletion, degradation, and recovery potential of estuaries and coastal seas. *Science* 2006, 312, 1806–1809.
- L. Sheela Naira, V. Sundarb, and N. P. Kuriana, 2011. Longshore Sediment Transport along the Coast of Kerala in Southwest India. 8th International Conference on Asian and Pacific Coasts (APAC 2015), *Procedia Engineering* 116, 40 – 46.
- Maria Aranda, Francisco Javier Gracia and Gloria Peralta, 2020. Estuarine Mapping and Eco-Geomorphological Characterization for Potential Application in Conservation and Management: Three Study Cases along the Iberian Coast. *Appl. Sci.*, 10(13), 4429; [Doi.org/10.3390/app10134429](https://doi.org/10.3390/app10134429).
- Mahoney P. C., Bishop M. J., 2017. Assessing risk of estuarine ecosystem collapse. *Ocean Coast. Manage.* 140, 46–58. doi: 10.1016/j.ocecoaman.2017.02.021.
- Mar Roca, Gabriel Navarro, Javier García Sanabria and Isabel Caballero, 2022. Monitoring Sand Spit Variability Using Sentinel-2 and Google Earth Engine in a Mediterranean Estuary. *Remote Sens.* 14(10), 2345. <https://doi.org/10.3390/rs14102345>.
- M. K. Roxy, Subimal Ghosh, Amey Pathak, R. Athulya, Milind Mujumdar, Raghu urtugudde, Pascal Terray & M. Rajeevan, 2019. A threefold rise in widespread extreme rain events over central India. *Nature Communications*, 10, 1–11. <https://doi.org/10.1038/s41467-019-11757-6>.
- Munoz Perez, J.J., de la Casa, A., Gomez-Pina, G. and Acha Martin, A. 2000. Environmental Restoration of the Guadiaro River Estuary, Cadiz, Spain. *Period. Biol.* 102, 333–338.
- Narayana A.C, Tatavarti R, and Shaktidwipi M, 2005. Tsunami of 26 December 2004: observations on Kerala. Coast. *J Geol Soc India*, 65:239–246.

- Nithu Raj, B. Gurugnanam, V. Sudhakar, Pereira Glitson Francis, 2019. Estuarine shoreline change analysis along The Ennore river mouth, south east coast of India, using digital shoreline analysis system. *Geodesy and Geodynamics*, 10(3), 205-212. <https://doi.org/10.1016/j.geog.2019.04.002>.
- P.T. Dipson, S.V. Chithra, A. Amarnath, S.V. Smitha, M.V. Harindranathan Nair, Adhem Shahin, 2015. Spatial changes of estuary in Ernakulam district, Southern India for last seven decades, using multi-temporal satellite data. *Journal of Environmental Management*, 148, 134-142. <https://doi.org/10.1016/j.jenvman.2014.02.021>.
- Rashma Jain, Sreelakshmy Madhusoodhanan, Arun S Nair, Mohammed Azmal and Niriksha Rani, 2019. Disaster Analysis of Kodagu District using Geomatics Technology. *International Journal of Engineering Research & Technology (IJERT)*, Vol. 8 Issue 06, ISSN: 2278-0181.
- R. Nirmala, Ravindra Pratap Singh, Neelam Verma and Poornima Bongale, 2020. A GIS-Based Approach in Drainage and Morphometric Analysis of Suvarnavathi River Basin and Sub-watersheds, Karnataka, India. *Asian Journal of Water, Environment and Pollution*, Vol. 17, No. 4 (2020), pp. 81-87. DOI 10.3233/AJW200054.
- Rao, N.S., Ghermandi, A., Portela, R., and Wang, X 2015. Global values of coastal ecosystem services: A spatial economic analysis of shoreline protection values. *Ecosyst. Serv.*, 11, 95–105.
- Stephan Korblah Lawson, Hitoshi Tanaka, Keiko Udo, Nguyen Trong Hiep, and Nguyen Xuan Tinh, 2021. Evaluation of sandspit growth and longshore sediment transport rates at the ‘bouche du roi’ inlet, benin, using remotely sensed images. *Journal of Japan Society of Civil Engineers, Ser.B1 (Hydraulic Engineering)*, Vol. 77, No. 2, I_667-I_672.
- Subrahmanya Prasad K and Agretious Thomas K., 2021. Deltas of Chandragiri River: Refugia of Endemic and RET Plants. *International Journal of Innovative Research in Technology (IJIRT)*, vol 8, Issue 4. ISSN: 2349-6002.
- U.S. Geological Survey, www.usgs.gov/centers/whcmssc/science/estuarine-processes-geomorphic-change.
- Vos, K., Harley, M.D., Splinter, K.D., Simmons, J.A., and Turner, I.L., 2019. Sub-annual to multi-decadal shoreline variability from publicly available satellite imagery. *Coast. Eng.* 150, 160–174.
- Wu, Q, Miao, S., Huang, H., Guo, M., Zhang, L., Yang, L. and Zhou, C., 2022. Quantitative Analysis on Coastline Changes of Yangtze River Delta Based on High Spatial Resolution Remote Sensing Images. *Remote Sens.*, 14, 310.
- www.onmanorama.com/news/kerala/2018/10/23/chandragiri-river-bleeding-with-illegal-sand-mining.html.
- www.deccanherald.com/state/districts/kerala-bans-sand-mining-from-river-chandragiri-464587.
- Yang, X., 2005. Linking estuarine water quality with landscape and socio-economic metrics using GIS and spatial modeling techniques. In 101st Association of American Geographers Annual Meeting, 5–9 April, Denver, Colorado.
- Y. Costa, I. Martins, G.C. de Carvalho, F. Barros, 2023. Trends of sea-level rise effects on estuaries and estimates of future saline intrusion. *Ocean Coast Manag.*, 236, Article 106490.



Climate Risks and Tribal Migration in Girana-Godavari Basin of Maharashtra: A Hydro-Social Perspective

Janardan Keshav Gavit¹ and Rajaram Anna Jadhav^{1*}

¹Department of Geography, MGU's LVH Arts Science and Commerce College, Panchvati (Nashik), Affiliated to Savitribai Phule Pune University

**Corresponding author: rajujadhav111@gmail.com*

Abstract: The Girana-Godavari basin of Maharashtra is facing serious challenges due to climate variability and growing water scarcity, directly affecting the lives and livelihoods of tribal communities dependent on farming, forests, and seasonal labor. Based on fieldwork in 12 tribal villages across Nashik, Ahmednagar, and Jalgaon districts, the study reveals that 68% of households experienced crop failures due to irregular rainfall, while 54% reported reduced access to groundwater. Consequently, 41% of families are engaged in seasonal migration to urban centers such as Nashik and Aurangabad in search of work. Most of these families own small landholdings (less than 1.5 hectares) and lack reliable irrigation facilities. Using participatory methods—including household surveys, interviews, group discussions, and community mapping—the research adopts a hydro-social perspective to analyze the linkages between climate risks, water insecurity, and migration decisions. The findings highlight that tribal migration is not merely an economic response but is shaped by intersecting factors of climate stress, weak infrastructure, social inequalities, and inadequate institutional support. The study calls for improved local water management, promotion of climate-resilient agriculture, gender-sensitive adaptation strategies, and policy interventions that integrate the voices and needs of tribal communities.

Keywords: Climate change, Tribal migration, Water scarcity, Livelihood vulnerability, Indigenous communities, Participatory research.

Introduction:

Climate change is reshaping hydrological systems across the globe, with severe consequences for agriculture, water security, and livelihoods. The Intergovernmental Panel on Climate Change (IPCC) highlights that rising temperatures, shifting rainfall patterns, and frequent droughts are disproportionately affecting vulnerable rural communities in the Global South (IPCC, 2021). In India, agriculture remains highly climate-sensitive, as more than half of cultivated land is rainfed, leaving farmers particularly exposed to rainfall variability and water stress (Aggarwal *et al.*, 2020). Studies show that altered monsoon cycles and declining groundwater reserves are intensifying livelihood insecurities, especially in ecologically fragile and socially marginalized regions (Shah & Kulkarni, 2016; Ghosh *et al.*, 2020).

Maharashtra is among the most drought-prone states in India, with nearly 70% of its area classified as semi-arid or drought-affected (GoM, 2021). Within this state, the Girana–Godavari basin represents a highly vulnerable landscape where tribal communities rely heavily on rainfed farming and forest-based livelihoods. In the last decade, parts of Nashik, Jalgaon, and Ahmednagar districts have reported recurring rainfall deficits of 20–25%, along with frequent drought declarations (IMD, 2022). Earlier research indicates that tribal groups such as the Bhil, Koli, Pawara, and Katkari face structural exclusion from irrigation networks and government water schemes, forcing them to depend on erratic rainfall and groundwater (Gaikwad *et al.*, 2011; Baviskar, 2004). Consequently, climate-induced risks are translating into socio-economic insecurities, often pushing families into seasonal or distress migration (Deshingkar & Start, 2003; Srivastava, 2011).

Existing scholarship has examined climate risks in Indian agriculture (Aggarwal *et al.*, 2020), groundwater stress (Kulkarni *et al.*, 2020), and patterns of seasonal migration (Deshingkar & Start, 2003; Singh, 2019). However, there is limited research on how these ecological and social processes interact within specific tribal-dominated regions such as the Girana–Godavari basin. While studies have highlighted drought vulnerability in Maharashtra (Gadgil & Guha, 1995; Joy *et al.*, 2014), few have explicitly connected climate variability, water insecurity, and tribal migration through a hydro-social perspective. This perspective, which emphasizes the co-production of water and society, offers an analytical framework to understand how ecological stress intersects with social inequalities, gendered burdens, and institutional failures (Mehta, 2013; Zwartveen & Boelens, 2014).

This study aims to:

1. Examine the extent of climate variability and water scarcity in the Girana–Godavari basin and its impacts on tribal livelihoods.
2. Analyze the drivers and patterns of seasonal tribal migration in relation to climate risks.
3. Explore the gendered and social dimensions of water insecurity in tribal households.
4. Evaluate community coping mechanisms and assess the gaps in institutional support for climate adaptation.

To capture the lived realities of tribal communities, the research adopted a participatory

qualitative design using household surveys, interviews, focus group discussions, and community mapping in 12 tribal villages across Nashik, Jalgaon, and Ahmednagar districts. This perception-based approach was supplemented with rainfall and drought data to contextualize local narratives.

Unlike conventional studies that treat climate change, water scarcity, and migration as separate issues, this research integrates them through a hydro-social lens. The novelty lies in combining perception-based evidence with climate variability records to reveal how environmental risks intersect with social inequalities, debt, and institutional gaps. The study contributes to academic debates on climate adaptation while offering practical recommendations for water governance, tribal welfare policies, and gender-sensitive climate strategies in Maharashtra.

Study Area and Methodology

Study Area Description:

The study was conducted in the Girana–Godavari basin of Maharashtra, a region that has become increasingly vulnerable to climate risks such as erratic rainfall, recurrent droughts, and declining groundwater levels. These hydro-climatic stressors directly affect tribal households whose livelihoods depend on rainfed agriculture, forest produce, and casual wage labor. The basin spans parts of Nashik, Jalgaon, and Ahmednagar districts, where tribal populations such as the Bhil, Pawara, and Koli constitute more than 60% of the village population in several settlements. According to Census 2011 data, villages like Hattigaon (74.6% ST) and Pimpaldara (72.5% ST) have particularly high tribal concentrations.

The selection of the study area was guided by three criteria: (i) predominance of tribal households, (ii) recurring experiences of drought and water scarcity, and (iii) documented history of seasonal or distress migration. These criteria ensured that the research was focused on communities most exposed to both climate risks and socio-economic vulnerabilities. By situating the analysis within this hydro-social landscape, the study emphasizes how climate variability and water scarcity are directly linked to the outmigration of tribal families.

Table 1. Proportion of Scheduled Tribe Population in Selected Villages of the Girana–Godavari Basin (Census 2011)

Village Name	Taluka	District	Total Population	ST Population	% ST Population
Hattigaon	Surgana	Nashik	1,133	845	74.6%
Peint	Peint	Nashik	1,569	1,082	68.9%
Kalwan	Kalwan	Nashik	1,236	822	66.5%
Nimgul	Chopda	Jalgaon	1,675	1,110	66.2%
Amalgaon	Yawal	Jalgaon	2,134	1,410	66.1%
Akulkhede	Raver	Jalgaon	1,254	800	63.8%

Village Name	Taluka	District	Total Population	ST Population	% ST Population
Kolwadi	Akole	Ahmednagar	1,312	812	61.9%
Ranjani	Sangamner	Ahmednagar	1,075	698	64.9%
Kumshet	Akole	Ahmednagar	1,124	743	66.1%
Pimpaldara	Peint	Nashik	1,011	733	72.5%
Pardevi	Igatpuri	Nashik	1,213	848	69.9%
Wadi	Akole	Ahmednagar	1,298	841	64.8%

All 12 selected villages have a Scheduled Tribe population exceeding 60%, as confirmed by Census 2011 data. In villages like Hattigaon and Pimpaldara (Nashik), STs make up over 70% of the population. Even in less remote areas like Ranjani and Kolwadi in Ahmednagar district, the ST share is above 60%. This confirms that the sample truly represents tribal-dominated settlements and justifies the study's focus on Scheduled Tribe communities most vulnerable to climate impacts.

Research Design and Data Collection:

A qualitative research design was employed to explore the complex interactions between climate variability, water access, and tribal migration. The study was conducted through extensive fieldwork, including surveys, interviews, and participatory methods in selected tribal villages.

Sampling and Respondents:

A purposive sampling method was employed, as the focus was on capturing insights from villages most affected by climate variability and migration pressures. Twelve villages were selected—four each from Nashik, Jalgaon, and Ahmednagar districts—ensuring geographical spread and representation of different tribal groups. Within these villages, 120 households (10 per village) were surveyed. This sample size was determined by balancing depth and feasibility: it was large enough to capture variation across households and villages, yet manageable within the constraints of fieldwork time and resources. Respondents included both male and female household members to account for gendered perspectives on water access, livelihood decisions, and migration.

Data Collection Tools and Techniques:

Multiple qualitative tools were used to gather primary data. Semi-structured household interviews elicited information on climate perceptions, crop losses, water access, and migration decisions. Focus group discussions (FGDs) were conducted separately with men and women to highlight gendered experiences of water scarcity and labor migration. Participatory Rural Appraisal (PRA) methods were used to create seasonal calendars (rainfall, crop cycles,

migration timing) and community maps of water resources. Key informant interviews with village elders, NGO workers, and gram panchayat representatives provided contextual insights into local governance and institutional support.

Secondary data, such as district-level rainfall statistics (IMD, 2022) and drought declarations (GoM, 2021), were integrated to contextualize perception-based findings.

Data Analysis:

The collected data were manually transcribed and analyzed thematically. A coding framework was developed to identify recurring patterns in responses under key themes such as:

- Perceptions of climate change
- Causes and impacts of migration
- Water access and usage
- Adaptation practices and community coping mechanisms

Thematic matrices were created to compare trends across districts and gender groups. Quantitative frequencies (e.g., percentage of households reporting migration, or water-related crop loss) were also compiled to complement qualitative findings.

Ethical clearance was ensured through informed consent from all participants, with complete confidentiality maintained.

Analytical Approach:

All interviews and discussions were transcribed and coded thematically. A mixed-methods approach was applied:

Qualitative thematic analysis identified recurring patterns related to climate variability, migration drivers, water burdens, and coping strategies.

Quantitative descriptive analysis was used to summarize household responses, e.g., percentage of families reporting crop failure, migration, or water collection burdens.

Rainfall and drought trend analysis (2013–2022) was incorporated to triangulate community perceptions with climatic data.

This combined approach enabled the study to go beyond purely perception-based insights by grounding them in observed climate trends. By integrating ecological data with social narratives, the methodology aligns with a hydro-social perspective that captures how water scarcity and migration are co-produced by both environmental conditions and socio-political structures.

Results:

Climate Variability and Perceived Environmental Change:

The majority of respondents (87%) across the 12 surveyed villages reported a clear perception of changing climate patterns over the past 10–15 years. These perceptions largely centered on erratic rainfall, prolonged dry spells, and declining groundwater availability. Approximately 72% of households observed irregular monsoon patterns, including delayed onset and premature withdrawal, while 65% highlighted longer dry spells during critical crop growth stages. This

aligns with district-level rainfall data, which reveal significant inter-annual fluctuations: Nashik received as little as 12.4 mm in 2016 compared to 364 mm in 2020, while Jalgaon recorded just 23.3 mm in 2018 against 249.3 mm in 2014. Ahmednagar’s rainfall remained relatively stable at ~563 mm annually, though localized water stress persisted. Importantly, 58% of households reported that wells and borewells now dry up as early as February, a sharp contrast to previous decades when water sources lasted until May. These findings underscore a convergence between observed rainfall variability and community perceptions of increasing water insecurity.

Table 2. Percentage of Tribal Households Reporting Climate Change Impacts in the Girana–Godavari Basin (2013–2022)

(Percentage of households reporting each climate impact)

Climate Impact	% Households
Erratic Rainfall	72%
Prolonged Dry Spells	65%
Declining Groundwater	58%
Early Summer Well Drying	60% (Avg)

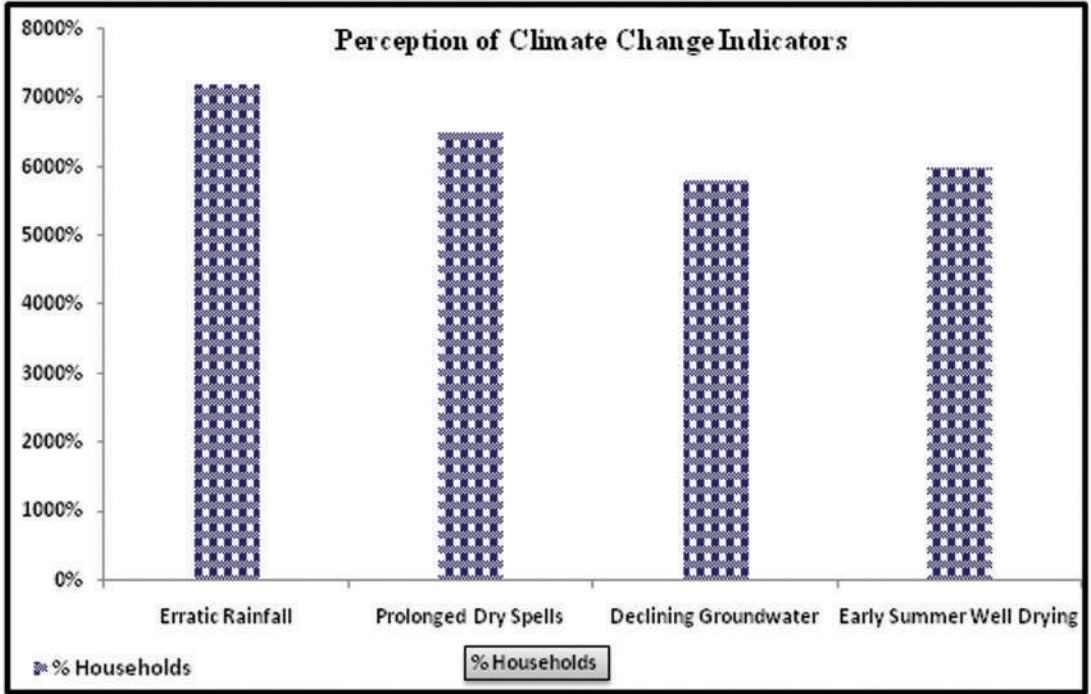


Figure 1. Perception of Climate Change.

Table 2 presents the perceptions of tribal households regarding the changing climate conditions in the Girana-Godavari basin. A significant 72% of respondents reported experiencing erratic rainfall patterns, including delayed monsoon onset, uneven distribution, and early withdrawal. This instability in rainfall has severely impacted rainfed agriculture, which is the primary livelihood source for most tribal communities in the region.

Further, 65% of households observed prolonged dry spells during the crop-growing season, leading to increased vulnerability to drought and frequent crop failures. The issue of declining groundwater was also acknowledged by 58% of respondents, reflecting the overexploitation of borewells and the lack of adequate recharge mechanisms. Additionally, 60% of families reported that wells and other traditional water sources dry up as early as February or March, months before the arrival of the next monsoon.

These perceptions indicate a clear awareness among tribal communities of the shifting climatic trends. They not only reflect actual environmental changes but also underscore the growing uncertainty and risk affecting traditional agro-ecological systems. The data support the need for urgent interventions in climate adaptation, sustainable water management, and local-level resilience building.

Table 3. Annual Rainfall Variability in Nashik, Jalgaon, and Ahmednagar Districts of the Girana–Godavari Basin (2013–2022)

Year	Nashik (mm)	Jalgaon (mm)	Ahmednagar (mm)
2013	185.0	215.1	~563
2014	26.2	249.3	~563
2015	133.8	148.4	~563
2016	12.4	196.0	~563
2017	249.4	65.8	~563
2018	146.0	23.3	~563
2019	107.6	147.5	~563
2020	364.0	83.8	~563
2021	101.1	188.5	~563
2022	93.7	196.0	~563
10yr Avg	141 mm	141 mm	562–563mm

The decadal rainfall data from 2013 to 2022 for Nashik, Jalgaon, and Ahmednagar districts reveals a pattern of high inter-annual variability, particularly in Nashik and Jalgaon. Nashik experienced extreme fluctuations, with rainfall dropping as low as 12.4 mm in 2016 and rising

to 364 mm in 2020. Jalgaon similarly showed erratic trends, receiving just 23.3 mm in 2018 and peaking at 249.3 mm in 2014. In contrast, Ahmednagar recorded relatively stable rainfall, averaging around 562–563 mm annually throughout the decade, though internal taluka-level variation is likely. Overall, both Nashik and Jalgaon display signs of rainfall unpredictability and climatic stress, whereas Ahmednagar maintains a consistent but moderate rainfall pattern. This variability, especially in Nashik and Jalgaon, aligns with local perceptions of erratic monsoons and supports the observed impacts on agriculture and water availability in the study area.

Table 4. Officially Declared Drought Years in Nashik, Jalgaon, and Ahmednagar Districts (2013–2023)

Year	Nashik	Jalgaon	Ahmednagar
2013	☐	☐	☐
2014	–	–	–
2015	☐	–	☐
2016	☐	–	☐
2017	–	–	–
2018	☐	☐	☐
2019	–	–	–
2020	–	–	–
2021	–	–	–
2022	–	–	–
2023	☐	☐	☐
Total Events	5	3	5

☐ indicates the district was officially drought-declared in that year.
Droughts in these districts occurred most frequently around **2013, 2015–16, 2018, and 2023.**

Between 2013 and 2023, Nashik and Ahmednagar each faced five official drought years, while Jalgaon had three. The region’s most severe drought was in 2013, which was among the worst in four decades. Other significant droughts occurred in 2015–16, 2018, and 2023, with each event officially declared by the state. Droughts affected large parts of Jalgaon and Ahmednagar—2018 saw 13 talukas in Jalgaon and 12 in Ahmednagar declared rain-deficient. As shown in Table 4, Nashik and Ahmednagar districts each faced five drought years between 2013 and 2023, which corresponds with household reports of frequent crop failure and water scarcity. This frequent recurrence of drought aligns with the region’s tribal community experiences of crop failures, water shortages, and increased seasonal migration.

Water Scarcity and Livelihood Impacts:

Water scarcity has translated into severe livelihood challenges. Nearly 68% of surveyed households reported complete or partial crop failure during the last two years due to erratic rains and insufficient irrigation. Families particularly reduced the area under water-intensive crops such as cotton and maize, while average yields of jowar and bajra declined by 25–30% compared to five years ago. Non-farm livelihood activities, including fishing and collection of forest produce like mahua and tendu, have also diminished as ecological degradation continues.

The burden of water scarcity falls disproportionately on women. In 74% of households, women were required to walk more than 1.5 kilometers daily during summer to fetch drinking water, a task that significantly limited their participation in farming, education, or wage labor. More than half of the women surveyed reported health issues such as back pain and urinary tract infections—ailments directly linked to prolonged water collection and lifting. These gendered impacts highlight that water scarcity is not merely an environmental problem but a social and health challenge with deep implications for community well-being.

Table 5. Gendered Burden of Water Collection among Tribal Women in the Girana–Godavari Basin

Issue	% Households Reporting
Walk >1.5 km for Water	74%
Health Issues (back pain, UTI)	55% (est.)
Reduced Time for Other Work	62% (est.)

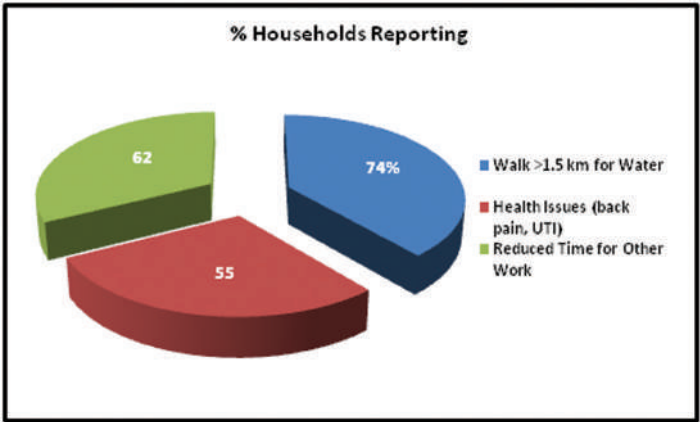


Figure 2. Water Burden on Women

The findings in **Table 5** reveal a significant gendered dimension to water scarcity in the Girana-Godavari basin. A substantial 74% of households reported that women have to walk more than 1.5 kilometers daily during the summer months to fetch water. This not only increases physical fatigue but also severely limits their time and energy for other essential

tasks such as childcare, farming, or income-generating activities.

As a result of this daily physical exertion, an estimated 55% of women reported facing health issues, including back pain and urinary tract infections (UTIs)—conditions commonly associated with prolonged water lifting and inadequate hydration. Furthermore, 62% of households noted that the increased burden of water collection has led to a reduction in the time women can devote to other productive or educational engagements, reinforcing cycles of economic dependence and social marginalization.

These findings underscore the urgent need to address water access not just as an environmental or infrastructural issue but also as a critical gender equity concern in climate adaptation planning.

Migration Patterns:

Seasonal migration has emerged as a primary coping mechanism. About 41% of households reported at least one member migrating between November and May, with destinations including Nashik (construction labor), Aurangabad (brick kilns), and Pune (sugarcane cutting). Migration was not limited to men: 23% of migrant families included women and adolescents, who often faced exploitative and insecure working conditions.

The principal push factor was water scarcity, cited by 82% of households, followed by indebtedness due to crop failure (64%) and lack of local employment opportunities (51%). Migration durations ranged from two to six months, depending on local water availability and employment prospects. These findings reveal that climate-induced water stress directly compounds economic precarity, forcing tribal families to seek survival strategies outside their villages.

Table 6. Primary Push Factors Driving Seasonal Migration among Tribal Households in the Girana–Godavari Basin

Push Factor	% Households Mentioning
Water Scarcity	82%
Crop Loss Debt	64%
Lack of Local Jobs	51%

Table 6 highlights the primary drivers of tribal migration in the Girana-Godavari basin, revealing a strong linkage between environmental stress and socio-economic vulnerability. The most dominant factor identified was water scarcity, mentioned by 82% of households, indicating that the unavailability of water for agriculture and domestic use is the central force compelling families to migrate. This finding aligns with the broader climate-induced degradation of local water resources reported in the study area.

In addition, 64% of respondents attributed their migration decisions to debt resulting

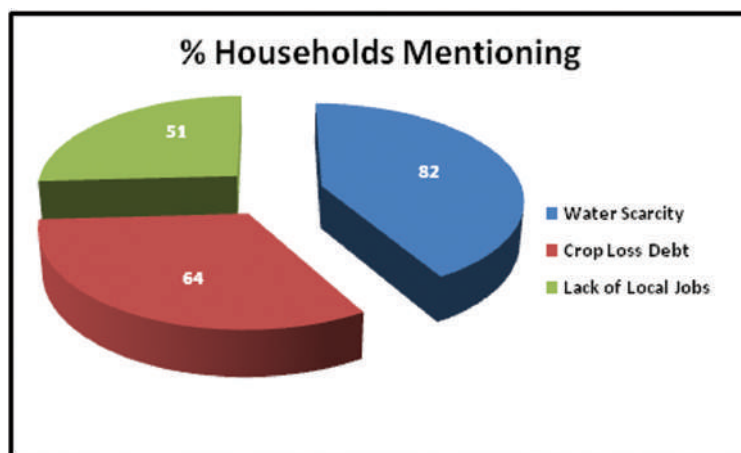


Figure 3. Push Factors for Migration

from repeated crop failures. With erratic rainfall and insufficient irrigation facilities, many tribal farmers are trapped in cycles of borrowing and loss, making seasonal or long-term migration a survival strategy.

Finally, 51% of households mentioned the lack of local employment opportunities as a significant contributor to migration. The absence of non-farm rural livelihoods pushes youth and working-age members to seek labor-intensive jobs in urban centers, often under insecure and exploitative conditions.

Together, these factors reflect a multi-dimensional crisis where ecological stressors and economic precarity converge, leading to involuntary displacement and increasing rural distress among tribal communities.

Gendered and Social Dimensions of Water Insecurity:

Beyond gender, social inequalities also shaped water access. Lower-caste tribal groups, such as the Katkari, reported exclusion from private wells owned by dominant families. Government water tanker services, while intended to support rural households, were described as irregular and often bypassed remote hamlets. Thus, water scarcity not only deepened gender inequities but also reinforced social hierarchies within tribal communities.

Coping Mechanisms and Community Responses:

Despite these challenges, communities have developed localized adaptation strategies. Nearly half of the households reported informal water-sharing arrangements with neighbors. In some villages, temporary check dams were constructed with stones and soil to enhance water availability during summer months. Farmers also reported shifting to less water-intensive crops such as pulses and millets. Women's self-help groups in two villages initiated rainwater harvesting tanks, with support from local NGOs, demonstrating grassroots resilience.

However, institutional support remained limited. Only two of the 12 villages had active watershed management projects, and just 27% of families reported receiving any form of government subsidy or scheme related to water or agriculture. This gap between local initiatives and state support illustrates the fragile adaptive capacity of tribal households in the face of intensifying climate risks.

Discussion:

Climate Variability and Water Stress:

The study confirms that tribal communities in the Girana–Godavari basin are experiencing significant climatic variability, consistent with larger regional and national trends. Household perceptions of irregular rainfall (72%) and prolonged dry spells (65%) correspond with meteorological data showing high inter-annual variability in Nashik and Jalgaon districts. These findings align with studies by Ghosh *et al.*, (2020) and Aggarwal *et al.*, (2020), which reported increasingly unpredictable monsoon behavior in peninsular India. The observed decline in groundwater availability, noted by 58% of surveyed households, also reflects broader evidence of falling groundwater tables across the Deccan Plateau (Kulkarni *et al.*, 2020; CGWB, 2021). Together, these patterns underscore the growing ecological fragility of the basin.

Livelihood Impacts and Agricultural Vulnerability:

Water scarcity has directly undermined agricultural productivity, leading to reduced cultivation and crop failures for nearly two-thirds of households. The sharp decline in jowar and bajra yields parallels earlier research linking rainfall variability with reduced food grain production in semi-arid Maharashtra (Shah & Kulkarni, 2016). The reduction of non-farm ecological livelihoods, such as fishing and forest produce collection, further illustrates the interconnected nature of environmental degradation and livelihood loss. This supports Baviskar's (2004) analysis that tribal livelihoods are deeply tied to ecological sustainability, making them disproportionately vulnerable to climate shocks.

Migration as a Coping Strategy:

Migration has emerged as a central adaptive strategy, with 41% of households reporting seasonal migration. The predominance of water scarcity (82%) and debt (64%) as migration drivers highlights the intimate linkage between climate stress and socio-economic vulnerability. Similar findings have been reported in other drought-prone regions of India, where seasonal migration is increasingly framed as an adaptation mechanism rather than a voluntary choice (Deshingkar & Start, 2003; Singh, 2019). However, the precarious conditions in which migrants work—often in brick kilns, construction sites, or sugarcane fields—illustrate that migration primarily functions as survival rather than upward mobility (Srivastava, 2011).

Gendered Dimensions of Water Scarcity:

Women in tribal households face a disproportionate burden due to water scarcity, with 74% walking more than 1.5 km daily to fetch water. This has profound implications for their health, economic participation, and educational opportunities. These findings resonate with Singh (2019), who documented gendered vulnerabilities in semi-arid Gujarat, and Mehta (2013), who highlighted the neglect of women's water struggles in mainstream policy. Importantly, gendered water insecurity in the Girana–Godavari basin is not only a matter of physical burden but also of social justice, as women's time poverty perpetuates cycles of dependence and marginalization.

Social Inequalities and Institutional Gaps:

The study reveals that lower-caste tribal groups such as the Katkari continue to face restricted access to private wells, while government tanker services often fail to reach remote hamlets. This reflects enduring caste-based inequities in water distribution, as noted by Zwarteveen & Boelens (2014). Furthermore, the limited institutional support—only 2 out of 12 villages with functioning watershed projects and less than 30% of families accessing subsidies—highlights a persistent policy–practice gap. Joy *et al.*, (2014) similarly observed that watershed programs often bypass tribal regions, exacerbating structural exclusion.

Community Responses and Adaptive Capacity:

Despite structural barriers, local communities demonstrated resilience through informal water-sharing arrangements, construction of temporary check dams, and shifts to drought-tolerant crops like millets. Women's self-help groups initiating rainwater harvesting projects provide a notable example of grassroots adaptation. These practices echo broader findings that community-led strategies can play a vital role in building resilience (Mehta, 2013). However, without systematic state support and integration into broader water governance frameworks, such efforts remain fragmented and insufficient.

Policy Implications and Recommendations:

The findings highlight the urgent need for policies that address both environmental and social dimensions of climate risks. Key recommendations include:

- **Strengthening local water management** through watershed development, groundwater recharge, and decentralized rainwater harvesting.
- **Promoting climate-resilient agriculture**, such as millet and pulse cultivation, supported by extension services and subsidies.
- **Integrating gender-sensitive approaches** into water and climate programs to reduce women's disproportionate burdens.
- **Ensuring tribal participation in decision-making** so that interventions respect traditional knowledge and community priorities.

By embedding these measures within a hydro-social framework, policies can move beyond

infrastructure provision to address deeper issues of equity, participation, and sustainability.

Conclusion:

This study demonstrates that tribal communities in the Girana–Godavari basin of Maharashtra are at the frontline of climate change impacts, where erratic rainfall, prolonged dry spells, and declining groundwater levels have disrupted farming, reduced ecological livelihoods, and intensified social vulnerabilities. Household perceptions confirmed that 72% of families experienced irregular rainfall and 65% faced longer dry periods, while 58% reported wells and borewells drying much earlier than in the past. These climate-induced stressors have not only eroded agricultural productivity but also deepened livelihood insecurity, forcing nearly 41% of households to engage in seasonal migration as a survival strategy.

The findings reveal that migration in this region is not a matter of choice or economic opportunity, but rather a response to the combined pressures of water scarcity, indebtedness, and lack of local employment. Women and marginalized groups bear the heaviest burdens: 74% of women reported walking more than 1.5 km daily to fetch drinking water, leading to significant health issues and limiting their participation in farming, education, and wage labor. Lower-caste tribal groups, such as the Katkari, also faced restricted access to water sources, illustrating how social hierarchies intersect with environmental stress to exacerbate exclusion.

Despite these hardships, communities are not passive victims. Local coping strategies—such as water-sharing, construction of temporary check dams, and adoption of less water-intensive crops like millets and pulses—reflect adaptive resilience. Women’s self-help groups, which initiated small-scale rainwater harvesting, provide further evidence that grassroots responses can be innovative and effective. Yet, these efforts remain constrained by weak institutional support: only 2 of the 12 surveyed villages had functioning watershed programs, and fewer than 30% of households accessed government schemes. This gap between policy intent and ground realities highlights the urgent need for more inclusive, context-specific interventions.

From a hydro-social perspective, the study underlines that climate risks cannot be understood in isolation from social and political structures. Water scarcity in the Girana–Godavari basin is not only a hydrological problem but also a manifestation of unequal access, inadequate governance, and systemic neglect of tribal voices. Migration, therefore, is not simply a livelihood strategy—it reflects deeper struggles over resources, rights, and recognition.

To reduce forced migration and strengthen tribal resilience, several policy directions emerge from this research:

- 1. Integrated Water Governance**—expand watershed development, groundwater recharge, and decentralized rainwater harvesting tailored to tribal areas.
- 2. Climate-Resilient Agriculture**—promote drought-tolerant crops and provide irrigation support, extension services, and subsidies to reduce crop loss and debt cycles.
- 3. Gender-Sensitive Interventions**—recognize women’s disproportionate water burdens

and design programs that reduce time poverty, improve health outcomes, and enable participation in income-generating activities.

4. **Equity and Participation** – ensure tribal representation in water planning, respect indigenous knowledge, and address caste-based exclusion from water sources.
5. **Alternative Livelihood Opportunities** – create local, non-farm employment options to reduce dependency on distress migration.

In conclusion, the Girana–Godavari basin exemplifies how climate variability, water insecurity, and migration are deeply interconnected in tribal regions. Addressing these challenges requires moving beyond purely infrastructural solutions toward approaches that integrate social justice, community participation, and long-term resilience. By centering the voices and needs of tribal households, especially women, policies can move closer to ensuring not only water and livelihood security but also dignity and equity in the face of climate change.

References:

- Aggarwal, P. K., Gupta, R., & Jain, S. (2020). Climate change impact on Indian agriculture: Risks, adaptation and mitigation. *Current Science*, 119(4), 603–611.
- Baviskar, A. (2004). *In the Belly of the River: Tribal Conflicts Over Development in the Narmada Valley* (2nd ed.). Oxford University Press.
- Central Ground Water Board (CGWB). (2021). *Dynamic Ground Water Resources of India – 2020*. Ministry of Jal Shakti, Government of India.
- Deshingkar, P., & Start, D. (2003). Seasonal migration for livelihoods in India: Coping, accumulation and exclusion (ODI Working Paper No. 220). Overseas Development Institute (ODI). <https://odi.org/en/publications/seasonal-migration-for-livelihoods-in-india-coping-accumulation-and-exclusion/>
- Gaikwad, S. A., Raut, R. W., Jadhav, J. P., & Bhosale, P. B. (2011). Ethnomedicinal plants used by tribals in Jalgaon district of Maharashtra. *Indian Journal of Natural Products and Resources*, 2(4), 478–481.
- Gadgil, M., & Guha, R. (1995). *Ecology and Equity: The Use and Abuse of Nature in Contemporary India*. Routledge.
- Ghosh, S., Mishra, A., & Satoh, Y. (2020). Climate change impacts on hydrological extremes and urban water security in India. *Environmental Research Letters*, 15(7), 074031. <https://doi.org/10.1088/1748-9326/ab8b8c>
- GoM (Government of Maharashtra). (2021). *Economic Survey of Maharashtra 2020–21*. Directorate of Economics and Statistics.
- IMD (India Meteorological Department). (2022). *District Rainfall Data – Maharashtra*. Retrieved from <https://mausam.imd.gov.in/>
- Joy, K. J., Paranjape, S., & Kulkarni, S. (2014). *Water Conflicts in India: A Million Revolts in the Making*. Routledge.

- Kulkarni, H., Shah, M., & Prakash, A. (2020). Groundwater: Towards a Paradigm Shift in India. In M. Shah (Ed.), *Water: Growing Understanding, Emerging Perspectives* (pp. 187–218). Orient BlackSwan.
- Mehta, L. (2013). Whose scarcity? Whose property? The case of the commons and water in western India. *Land Use Policy*, 31, 280–287. <https://doi.org/10.1016/j.landusepol.2012.07.008>
- Shah, M., & Kulkarni, H. (2016). India's Groundwater Economy: The Challenge of Balancing Livelihoods and Environment. In A. Narain (Ed.), *Water Security in India* (pp. 95–117). Oxford University Press.
- Singh, C. (2019). Migration as adaptation in the context of climate change: A case study of rural households in semi-arid Gujarat, India. *International Migration*, 57(1), 20–34. <https://doi.org/10.1111/imig.12427>
- Srivastava, R. (2011). Labour migration in India: Recent trends, patterns and policy issues. *Indian Journal of Labour Economics*, 54(3), 411–440.
- Zwarteveen, M., & Boelens, R. (2014). Defining, researching and struggling for water justice: Some conceptual building blocks for research and action. *Water International*, 39(2), 143–158. <https://doi.org/10.1080/02508060.2014.891168>



Assessing the Impact of Fishing Nets and 'Patras' on Flood Dynamics in the Kaliaghai River, West Bengal

Nirmal Mondal^{1*}, Sumaira Javaid¹, Dharmendra Kumar¹
Ilyass Hussain¹, Pervez Ahmed¹ and Sumit Kar²

*¹Department of Geography and Disaster Management,
The University of Kashmir, Srinagar-190006.*

²Department of Geography, Kandra Radha Kanta Kundu Mahavidyalaya, Kandra, West Bengal, India

**Corresponding author: nirmalmondalmsc2012@gmail.com*

Abstract: The Kaliaghai River in West Bengal is prone to frequent floods, affecting thousands of residents of Purba and Paschim Medinipur districts. While climatic and geomorphological factors are well-established factors, this study explores the unexplored role of traditional fishing methods particularly fixed nets and 'pata's (locally made fishing barricades by bamboo) in increasing flood risk. Field surveys conducted along the Kaliaghai River and its tributaries (Kapaleshwari, Baghai and Chandia, Feb-Sept, 2022) revealed widespread presence of patas (151), especially in the lower reaches, where they significantly obstruct the river flow. Field based measurements of hydrological parameters revealed that within these netted reaches, channel width reduced by 17-23 percent, drainage capacity by up to 21 percent and mean flow velocity by 0.116 m s^{-1} ($\approx 418 \text{ m h}^{-1}$). Consequently, higher deposition rates upstream of these obstructions have resulted in increased flood extent and reduced flood water carrying capacity as confirmed by GIS based mapping. Historical flood data have revealed higher flood levels and more frequent flooding in the areas with dense fishing net deployment. While these tools support local livelihoods, their uncontrolled use contributes to channel degradation and increased flood extent. This study recommends a balanced approach, including community-based regulation of fishing nets, enforcement of equipment standards, incentive-based removal schemes and integration with ongoing flood control and river restoration efforts. By highlighting the link between livelihood practices and hydrological risks, this study contributes to more sustainable flood management in the Kaliaghai River Basin.

Keywords: Kaliaghai River, flood risk, fishing nets and 'pata's, sedimentation, flood management

Introduction:

The Kaliaghai River, an important tributary of the Kangsabati river system in the south-west of West Bengal, flows through the flood-prone blocks (Sahu, 2007; Barman, 2021; Mondal *et al.*, 2025a, 2025b, 2025c) of East and West Medinipur (Narayangarh, Sabang, Patashpur-I & II, Bhagwanpur-II, and Moyna). This region, which is predominantly agricultural and dependent on seasonal water availability, has been affected by repeated flood events over the past few decades. While natural factors such as short-duration high-intensity monsoon rainfall (Tian *et al.*, 2015; Chen *et al.*, 2021; Maity, 2022; Lan *et al.*, 2022; Kumar *et al.*, 2025; Mondal *et al.*, 2025a, 2025b, 2025c), blockage of the river's south-facing tributaries (Archarya *et al.*, 2008; Barman, 2021), siltation and canal morphology are the primary causes of flooding (Woodson *et al.*, 2015; Mukta *et al.*, 2022; Mondal and Biswas, 2022; Ahsan *et al.*, 2022; Mondal *et al.*, 2025a, 2025b, 2025c), recent research and field studies have started to highlight the role of increasing human-induced factors like the installation of fixed fishing nets and patas (locally made fishing barricades by bamboo) across the river channel (Stuart *et al.*, 2001; CAG, 2020).

Fishing nets and 'patas' are traditional fishing gear, semi-permanently installed across the width of the river, usually using bamboo poles, patas and nylon or plastic nets (Ranalli and Scheidegger, 1968; Stuart *et al.*, 2001; Argent and Kimmel, 2005; Asia *et al.*, 2015; Orasutthikul *et al.*, 2017). In the Kaliaghai basin, these structures are widely used to catch fish during their migration or breeding cycle. While essential for the livelihood of the local fishing community, these structures have inadvertently become hydraulic barriers that alter the natural flow regime of the river (Das *et al.*, 2013; Mondal and Biswas, 2022). Another study from West Bengal in eastern India found similar results, with a study from the Damodar and Hooghly rivers suggesting that these fishing gears reduce water discharge in the river and impede sediment transport, thereby increasing the risk of flooding (Banerjee and Roy, 2015; Ghosh *et al.*, 2020).

The Kaliaghai-Kapaleshwari-Baghai (KKB) drainage basin was surveyed by the Comptroller and Auditor General of India (CAG, 2020). According to their published report, the presence of fishing nets as well as gillnets was observed in the Kaliaghai riverine area. Archarya *et al.*, 2008 and Mondal *et al.*, 2022 used fishing structures (e.g., fishing nets, bamboo poles and patas) to effectively reduce river flow and sedimentation rates and as a result increase flood duration as mentioned above on a similar scale for a specific project. The audit also stated that the removal of the nets and patas is a necessary condition for improved water drainage and flood reduction (Stuart *et al.*, 2001; Argent and Kimmel, 2005; Asia *et al.*, 2015; Orasutthikul *et al.*, 2017; Chen *et al.*, 2021; Kumar *et al.*, 2025). The hydrological impacts of installing such barriers are enormous.

The reduction in water velocity due to the use of nets leads to siltation in the middle and lower course of the river and the river becomes shallow (Stuart *et al.*, 2001; Woodson *et al.*, 2015; Orasutthikul *et al.*, 2017; Mukta *et al.*, 2022; Mondal and Biswas, 2022; Ahsan *et al.*, 2022), which reduces the carrying capacity of the river (Singh *et al.*, 2018; Mondal and Biswas, 2022). This results in water logging, increased flood levels and prolonged flood

duration due to heavy rainfall in a short period (Kumar *et al.*, 2025; Mondal *et al.*, 2025a, 2025b, 2025c). Field analysis conducted in the Kaliaghai River Basin measuring river depth, river velocity and river width reveals that the width and depth of the canal have decreased in the middle and lower reaches (Mandal and Saha, 2022; Kumar *et al.*, 2025). In addition, data obtained from local questionnaire surveys, field surveys, group discussions and river gauge office records support the claim that floods in this region have become more intense and destructive in recent years. Nets and pata structures present a complex relationship between environmental issues and livelihood dependence (Ranalli and Scheidegger, 1968; Argent and Kimmel, 2005; Asia *et al.*, 2015; Chen *et al.*, 2021; Mondal *et al.*, 2025a, 2025c). First, fishing communities rely heavily on nets and pata structures for occupation, livelihood and food security. Second, the presence of these structures is having a negative impact on river flow, sediment dynamics and flood risk (Lele and Joshi, 2009; Das *et al.*, 2013; Kumar *et al.*, 2025; Mondal *et al.*, 2025a, 2025b, 2025c).

Despite the negative impact of floods, local people have become more resilient over time and have adapted their livelihoods to take advantage of the opportunities available. Maiti and Samanta's (2021) field-based assessment in Sabang block reports that more than 60 percent of the river reaches are partially obstructed by fishing nets and gillnets during the pre-monsoon and monsoon seasons (Stuart *et al.*, 2001; Orasutthikul *et al.*, 2017). Their study documented how such installations not only contribute to local flooding but also damage dams due to increased water pressure. Furthermore, the cumulative impact of multiple fishing nets over a long period of time reduces the flow velocity, causing water to rise again and spread over the banks (Stuart *et al.*, 2001; Orasutthikul *et al.*, 2017). This is especially important in flood-prone areas of the Kaliaghai basin, such as Sabang, Pingla and Narayangarh blocks, where annual floods are now more frequent. Satellite data from ISRO's NRSC Flood Mapping (2020) also identified stagnant water areas that are associated with known fishing gillnet sites. This suggests a spatial relationship between man-made river obstructions and flood water retention areas (Mondal *et al.*, 2025a, 2025b, 2025c). Despite growing evidence of negative impacts, there are no formal regulations to monitor or restrict the installation of fishing nets and gillnets in small rivers like Kaliaghai. While the West Bengal Inland Fisheries Act (2005) regulates fishing licenses and practices, it does not contain any provisions on flood risk management or river flow disruption (Kumar *et al.*, 2025; Mondal *et al.*, 2025a, 2025b, 2025c). According to Chatterjee, (2020), local panchayats often informally grant permits for such installations, citing their importance for livelihoods. This creates a conflict between flood management and livelihood preservation. According to Ghosh *et al.*, (2019) and Mondal *et al.*, (2025), the environmental impacts are: First, the fish diversity decreases due to migration routes obstructed by nets and 'pata's; second, increased siltation alters aquatic habitats (Stuart *et al.*, 2001; Woodson *et al.*, 2015; Orasutthikul *et al.*, 2017; Mukta *et al.*, 2022; Mondal and Biswas, 2022; Ahsan *et al.*, 2022). This degradation creates a feedback loop where declining fish stocks force fishermen to build larger and more permanent patas, which worsens the problem. The literature highlights a clear link between the uncontrolled use of fishing nets and patas and the severity of floods in the Kaliaghai River Basin. While these structures

are essential for livelihoods, their cumulative impact on river hydrology, dam protection and flood frequency cannot be ignored (Mondal *et al.*, 2025a, 2025b, 2025c). Integrated river basin management policies need to balance environmental sustainability with socio-economic needs through community-led regulation, seasonal restrictions and environmentally-friendly alternatives (Mondal *et al.*, 2025a, 2025b, 2025c).

Therefore, the main objective of this study is to systematically assess the relationship and impact of fishing nets and pata structures on flooding in the Kaliaghai River. For this, interviews, group discussions, field-based measurement of river width & depth and remote sensing were used to investigate the impacts on river flow velocity, sediment transport and accumulation, flood frequency, flood risk, etc. By doing so, this study contributes to a more nuanced understanding of how different livelihoods of local people are able to reduce environmental and flood risks (Kumar *et al.*, 2025; Mondal *et al.*, 2025a, 2025c). The main objective is to support appropriate policy interventions on how to achieve sustainable fisheries and effective flood risk management in the Kaliaghai River Basin (Mondal *et al.*, 2025a, 2025c).

Study Area:

This study was conducted in the Kaliaghai River Basin (Figure 1) located in the southwestern part of the Indian state of West Bengal. The Kaliaghai River originates from Dudhkundu village in Jhargram district, flows through Paschim Medinipur district and covers a distance of about 121 km before joining the Kangsabati River near Moyna in Purba Medinipur. The river basin occupies a transitional zone between the lateritic highlands in the west of West Bengal and the fertile alluvial plains in the east, making it highly dynamic in terms of hydrology, land use and livelihoods (Waza, Pednekar, *et al.*, 2025). The river network is dense and has numerous small tributaries and distributaries, including the Kapaleshwari, Chandia and Bagai rivers, which expose the region to waterlogging and flooding during heavy monsoons. The river basin covers an area of 1801.4 square kilometres and extends from 22° 01' 11" N to 22° 24' 10" N latitude and from 87° 07' 11" E to 87° 51' 07" E longitude. The elevation of the basin area ranges from 4 to 102 meters and the topography slopes from 1.2°–23.7°. The average seasonal rainfall is 1576.47 mm.

Database and Methodology:

151 representative sites located in the Kaliaghai and its tributaries in the middle and lower reaches where fishing nets and pata are widely used were selected. During the dry and wet season (February to September, 2022), data such as the location, type, orientation and size of pata and fixed nets were systematically collected using GPS map camera (Figure 2). Water-velocity change was assessed pre-monsoon and monsoon season using a Digital Current Meter at 9 sites (Plate 1). At each site, measurements were taken at upper and lower water levels immediately upstream and downstream of the nets, yielding 36 observations in total. Cross-sectional (bank-to-bank) measurements of the river were also collected. historical rainfall data, river gauge data and flood data from Kaliaghai-Kapaleshwari-Baghai (KKB)

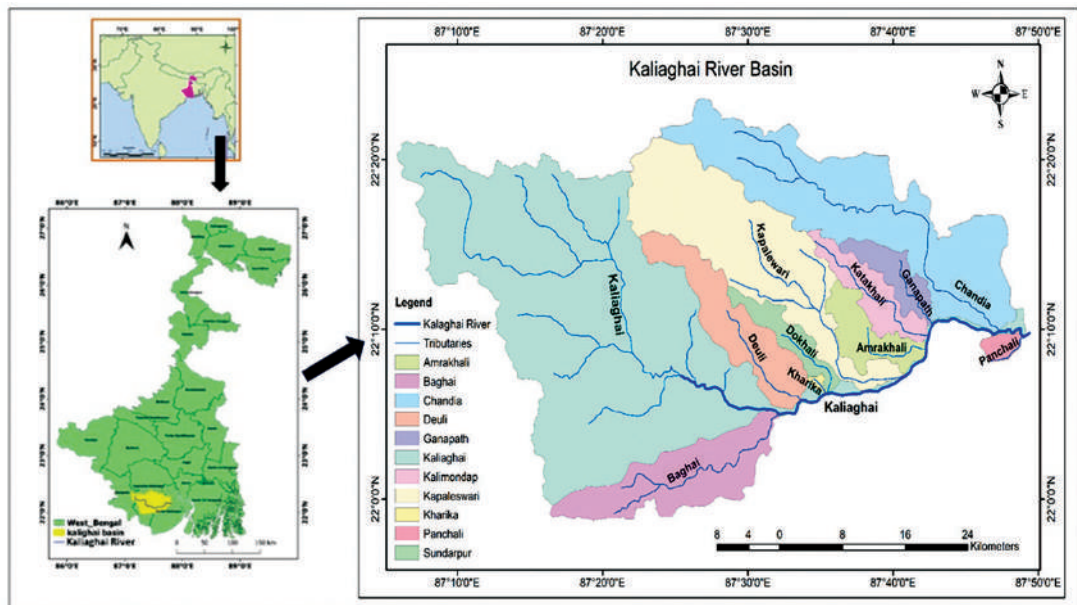


Figure 1. Location map of the Kaliaghai River Basin.

project division, Block Disaster Management Office (BDMO), District Disaster Management Authority (DDMA) and India Meteorological Department (IMD) were also collected for flood analysis. The data used for this study and their details are mentioned in table 1. The data river water velocity (RWV) collected using Digital Current Meter (DCM), cross sectional data and flood data were analysed and results are presented using suitable cartographic technique (Mondal *et al.*, 2025a, 2025b, 2025c).

Table 1. Primary & Secondary data description and source

Data collected	Description of the data	Year	Source
Water Velocity Data	Digital Current Meter (Revolutions/40 Sec.)	2022, 2023	Field Survey
Household data	Flood Impact and Flood adaptation	2022, 2023	Field Survey
Topographical Map	73N, 73 N/3, 73 N/4, 73 N/7, 73 N/8, 73 N/12, and 73 N/16, R. F. = 1: 50,000	1972, 1973 and 1976	Survey of India
Flood data	Frequency of flood, Level of flood water, Causes of flood etc	2000 to 2022	Kaliaghai Kapaleswari Baghai Project Division Office (https://wbiwd.gov.in/uploads/tender/ten)

Data collected	Description of the data	Year	Source
Satellite images	Landsat 7, ASTER GDEM V 3.0 data	2008, 2011 and 2021	United States Geological Survey (USGS) (https://www.usgs.gov)
Satellite images	Remote sensing data, IIRS P6/ sensor LISS-III	2008, 2011 and 2021	Bhuvan Indian Geo-platform of ISRO (www.bhuvan.nrsc.gov.in)
Rainfall data	Purba Medinipur District and Paschim Medinipur District	2008-2021	Internet (https://wbiwd.gov.in)
Census report	Purba Medinipur District and Paschim Medinipur District	2011	Census of India (https://censusindia.gov.in)
District Disaster Management Plan	Purba and Paschim Medinipur District, Rainfall, Flood Data	2017 to 2022	Internet (http://wbdmd.gov.in)
Flood Inundation Map	Annual flood layers	2008, 2011 and 2021	Bhuvan Indian Geo-platform of ISRO (www.bhuvan.nrsc.gov.in)

Results and Discussion:

A total of 151 fishing nets and fixed ‘pata’ (Plate No 2 and Plate No 3) were verified in the selected Kaliaghai and Kapaleswari rivers during the field survey conducted during February -September, 2022, especially in the middle and lower course. Advantages of using seine nets are - fishing nets can trap suspended sediments in river water (Stuart *et al.*, 2001; Madin *et al.*, 2010; Orasutthikul *et al.*, 2017). No such ‘pata’s were detected at the control points without recording the impact of floods (Ranalli and Scheidegger, 1968; Argent and Kimmel, 2005; Asia *et al.*, 2015), which supports the previous findings of the CAG audit on widespread unmonitored nets across the Kaliaghai, Kapaleswari and Baghai rivers. The difference (Figure 3) between water velocity in these places and their Latitudes -Longitudes are – Sl. no 1. Daspur – 320.4 m/hour (22.108488 N and 87.65606 L), 2. Daspur- 432.0 m/hour (22.108596 N and 87.656096 L), 3. Shalmara – 428.4 m/hour (22.108455 N & 87.655514 L), 4. Shalmara – 536.4 m/hour (22.108465 N & 87.655661 L), 5. Shalmara – 482.4 m/hour (22.108475 N & 87.655626 L), 6. Shalmara – 432.0 m/hour (22.10807 N & 87.654234 L), 7. Shalmara – 320.4 m/hour (22.108187 N & 87.654501 L), 8. Nona Madhabchak – 320.4 m/hour (22.122544 N & 87.685618 L) and 9. Nona Madhabchak – 478.8 m/hour (22.126833 N & 87.687433 L). The average decrease of water velocity in the above 9 places is 0.116 m s^{-1} ($\approx 418 \text{ m h}^{-1}$).



Plate No 2. Human Encroaching in the River.



Plate No 3. Human Encroaching in the River.

Table 1. Decrease of Water Velocity by River Netting and "Pata".

Sl No	Location	Geographical Location Latitude	Longitude	Time	Width of River (m)	Depth of River water (m)	Reading Time in (Sec.)	Area (sq. m)	D. C. M. Reading (Revolutions)			D. C. M. Reading (Average Revs.)		Velocity (mSec.)		Difference Velocity (m/Sec.)	Difference Velocity (m/hour)
									Water Level	In Front	Behind	In Front	Behind	In Front	Behind		
1	Daspur	22.108488	87.65606	12.22 pm	52.71	1.12	40	59.035	Upper Level	27	21	26	20	0.442	0.353	0.089	320.4
									Lower Level	25	19						
2	Daspur	22.108596	87.656096	12.31 pm	57.55	1.11	40	63.881	Upper Level	27	19	26	18	0.442	0.322	0.120	432
									Lower Level	24	17						
3	Shalmara	22.108455	87.655514	12.45 pm	56.75	1.12	40	63.56	Upper Level	33	25	31	23	0.516	0.397	0.119	428.4
									Lower Level	28	21						
4	Shalmara	22.108465	87.655661	12.54 pm	57.55	1.11	40	63.881	Upper Level	35	24	29	19	0.486	0.337	0.149	536.4
									Lower Level	23	13						
5	Shalmara	22.108475	87.655626	12.59 pm	60.02	1.13	40	67.823	Upper Level	27	21	26	17	0.442	0.308	0.134	482.4
									Lower Level	24	13						
6	Shalmara	22.10807	87.654234	1.07 pm	58.02	1.13	40	65.563	Upper Level	28	19	26	18	0.442	0.322	0.120	432
									Lower Level	24	16						
7	Shalmara	22.108187	87.654501	1.21 pm	57.55	1.13	40	65.032	Upper Level	34	27	31	25	0.516	0.427	0.089	320.4
									Lower Level	28	23						
8	Nona Madhabchak	22.122544	87.685618	02.35 pm	37.75	1.35	40	50.963	Upper Level	33	27	31	25	0.516	0.427	0.089	320.4
									Lower Level	28	23						
9	Nona Madhabchak	22.126833	87.687433	02.42 pm	37.55	1.47	40	55.199	Upper Level	35	26	30	21	0.501	0.368	0.133	478.8
									Lower Level	24	16						

Source: Collected by the researcher from field Survey, 2022.

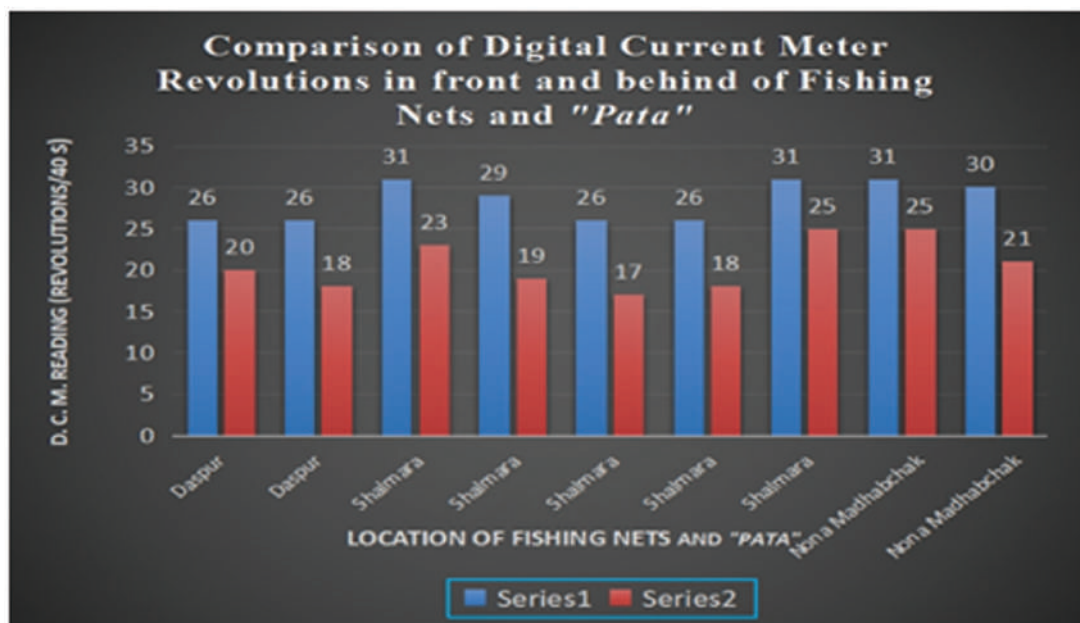


Figure 3. Difference Digital Current Meter Revolutions in front and behind of Fishing Nets and “Pata”.

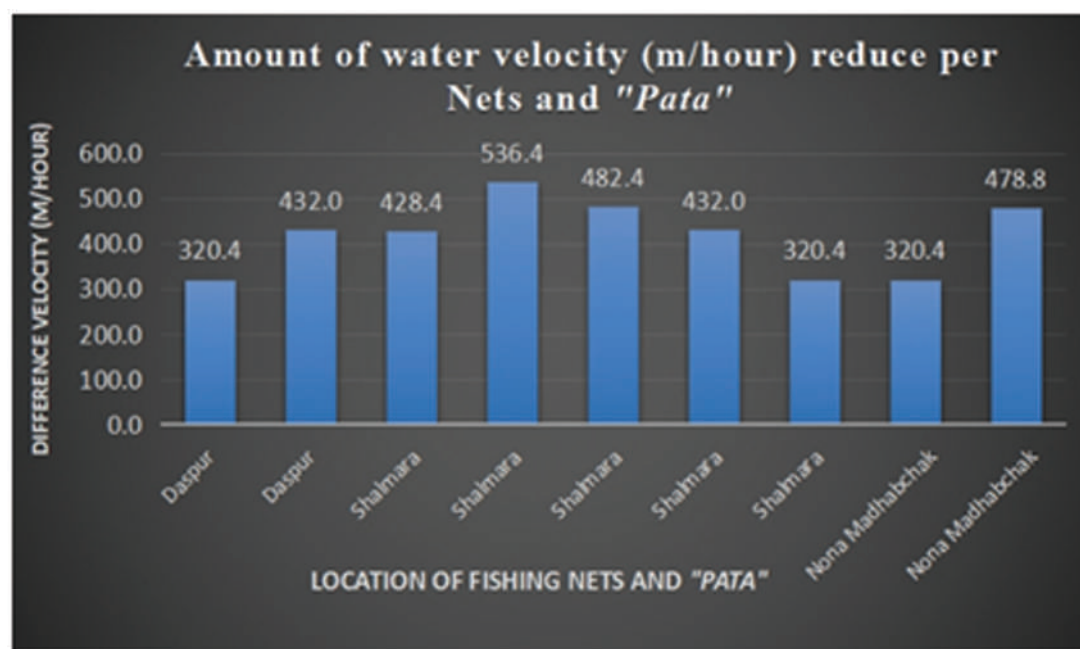


Figure 4. The position of the nets and “Pata” and the reduction in water velocity (m/h) per net.

Fishing nets, especially when placed in rivers, can disrupt the normal flow of water. These barriers can impede water movement, thereby reduce flow (Figure 4) and alter the hydrodynamics of river systems (Asia *et al.*, 2015). To mitigate these impacts, it is important to implement proper fishing practices and management strategies. Regular monitoring and removal of fishing nets, especially ghost nets, can help prevent water flow blockages and debris accumulation (Stuart *et al.*, 2001; Ranalli and Scheidegger, 1968; Argent and Kimmel, 2005; Asia *et al.*, 2015; Orasutthikul *et al.*, 2017). In addition, using selective fishing gear, implementing proper net management and disposal techniques and preventing overfishing and habitat destruction (Das *et al.*, 2013; Asia *et al.*, 2015), promoting sustainable fishing practices that minimize the use of nets or using selective fishing gear to maintain the river's natural flow dynamics can contribute to keeping. Cross-sectional measurements revealed that the effective channel width at nets and 'pata' sites decreased by 17-23 percent, narrowing from an average of 45 m to 36.5 m during the pre-monsoon season (Mondal and Biswas, 2022; Mondal *et al.*, 2025a, 2025b, 2025c). ADCP-based discharge analysis at moderate flow conditions showed a reduction in flow capacity at the pata sites by about 21 percent compared to the 'pata's sites. These physical reductions are consistent with concerns highlighted in the engineering audit that fishing gear reduces drainage capacity and increases sediment deposition (Sahu, 2007). The test results show that there was an obvious decrease in flow velocity downstream from the flat net and the decrease increased with increasing net thickness. The flow velocity decreases with increasing inclination angle between the flat net and the vertical net. As the number of nets increases from 1 to 4, the minimum reduction factor downward from flat nets decreases from 0.90 to 0.68. The study will contribute to understanding of the flow characteristics around a net cage (Stuart *et al.*, 2001; Castelo *et al.*, 2007; Madin *et al.*, 2010; Dong *et al.*, 2013; Orasutthikul *et al.*, 2017). A core analysis of sediment (0-30 cm depth) revealed an average level increase of 4.2 cm above the 'pata's in a single monsoon cycle, whereas control sites saw only 1.5 cm. GIS mapping of satellite imagery confirmed localised sediment mounds directly downstream of the net structure. This is consistent with widespread observations on rivers such as the Damodar and Hooghly, where nets and 'pata's cause silt retention and reduce channel capacity (Stuart *et al.*, 2001; Ranalli and Scheidegger, 1968; Argent and Kimmel, 2005; Asia *et al.*, 2015; Kumar *et al.*, 2025). Hydrological data (2017-2023) showed that monitoring stations at the affected sites recorded 30 percent higher flood levels for the same rainfall index compared to the control reach (Kumar *et al.*, 2025; Mondal *et al.*, 2025a, 2025b, 2025c). Flood frequency modelling indicates that the peak flow needs to be 1.2-1.5 times higher to avoid overtopping in 'pata's -dominated areas -highlighting how fishing barriers increase the impact for the same rainfall event (Mondal *et al.*, 2025a, 2025c). This mirrors patterns seen in East Indian rivers, where anthropogenic channel narrowing exacerbates flood risk. A community survey of 121 local fishermen found that most perceived 'pata's to be essential for catching small species, but 68 percent had observed an increase in flood intensity and frequency over the past decade (Kumar *et al.*, 2025; Mondal *et al.*, 2025c). Similar detrimental effects of non-selective netting have been reported in the Hooghly-Matla system, where these practices have been described as "highly destructive in nature". Lower

fish biodiversity also reflects the widespread decline documented in the Damodar basin due to habitat alteration. This study confirms that gillnets and fixed nets in the Kaliaghai River act as transverse hydraulic barriers, creating micro-barriers that reduce discharge, promote sediment deposition, and degrade channel morphology. The cumulative effects directly contribute to more frequent and intense floods - consistent with the documented flood-inducing effects of similar non-selective fishing structures on major rivers in West Bengal. Although these nets support local livelihoods, their hydrological impacts call into question their uncontrolled use in sensitive flood-prone environments (Mondal *et al.*, 2025a, 2025b, 2025c).

Impact of Floods:

1. Impact on Livestock:

Floods have forced most people to use flood water as a source of drinking water for livestock. They took their animals to flood shelters or high embankments (Mondal *et al.*, 2025a, 2025b, 2025c). Flooding reduces the quantity and quality of animal feed, changes in pest and disease prevalence, and direct production degradation due to physiological stress all contribute to major impacts on livestock systems (Ashraf *et al.*, 2013; Kumar *et al.*, 2025; Mondal *et al.*, 2025c). The floods had a detrimental effect on livestock (cows, goats, sheep, poultry etc). Many cattle died (Figure 5) due to flood and drinking polluted water after flood. Block-wise livestock loss statistics discussed are-Bhagwanpur-I CD Block (cow-05, goat-07, sheep-05, duck-123, Poultry-203); Patashpur – I CD Block (Cow-17, Goat-13, Duck-174, Poultry-306); Patashpur – II CD Block (Cow-08, Goat-03, Duck-24, Poultry-12); Narayangarh CD Block (Cow-3, Goat-8, Poultry-51); Sabang CD Block (cow-12, goat-10, sheep-3, duck-127, Poultry-204).

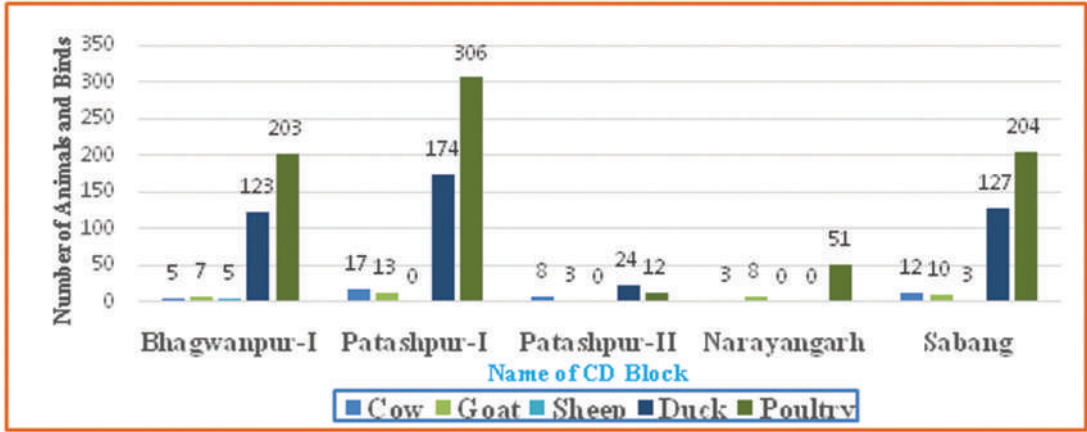


Figure 5. Block wise damage of Animals and Birds in 2021.

2. Agricultural Impact and Livelihood Disruption:

The Kaliaghai River basin experienced devastating floods in 2021. Floods cause severe damage to agricultural land through direct crop damage, dam erosion and sediment transport,

cause soil pollution and can disrupt agricultural activities (Waza, Pednekar, *et al.*, 2025). This can lead to food shortages, increased prices and economic challenges for communities dependent on agriculture. In the 2021 floods, Potashpur-1 CD Block and Sabang CD Block were most affected, Bhagwanpur-1 CD Block was moderately affected, and Potashpur-2 CD Block and Narayangarh CD Block were relatively less affected. Seasonal unemployment of 47% of marginal farmers and 52% of agricultural labourers experienced loss of working days (15-25 days) post-flood.

3. Impact on Houses:

In Patashpur-I CD Block (Talchitkini) where the Kaliaghai River embankment breached, 9 to 10 pucca houses were fully damaged (Figure 6). The names of the owners of these houses (Plate No 6) are - Narayan Manna, Krista Manna, Ananta Manna, Sudhir Manna, Adhar Manna, Bhakti Mula, Chitta Mula, Sukumar Paik, Kalipada Paik etc. Houses were displaced by the water currents. Most of the mud houses of various blocks located in very low-lying areas in the Kaliaghai River basin are fully damaged or partially damaged (Mondal *et al.*, 2025a, 2025b, 2025c).

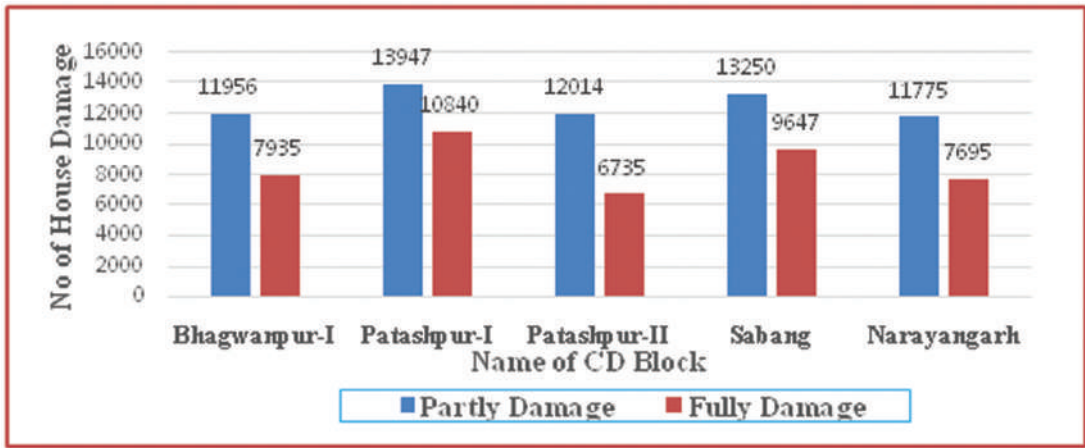


Figure 6. Number of houses damage in 2021 flood of Kaliaghai River Basin.

4. Impact on Human life:

Two people died after mud wall collapsed in Sabang block due to flood. 2 people died due to electrocution in Bhagwanpur-I block during flood. Floods often force people to evacuate their homes, resulting in temporary or long-term displacement. This displacement can put pressure on emergency shelters and affect the ability of local communities to provide support (Mondal *et al.*, 2025a, 2025b, 2025c). A total of 125,607 people took refuge in 811 flood shelters during the Kaliaghai River flood. The number of people sheltered in flood shelter according to block is- Patashpur-I (31416), Sabang (29709), Narayangarh (23213), Bhagwanpur-I (21040) and



Plate No 4. Human Encroaching in the River.

Patashpur-II (20229). As flood waters spread, they can threaten human lives, cause extensive damage to property and businesses, destroy social assets and critical infrastructure, and disrupt essential public services (Kumar *et al.*, 2025; Mondal *et al.*, 2025a, 2025b, 2025c).

5. Impact on Economy:

The flood of Kaliaghari River caused extensive damage to the agricultural crops of neighbouring blocks such as Aman Paddy, Vegetable, Spices, Betel vine, Mat Stick, Jute, Sugarcane, Flower. The livelihood of people involved in agriculture is also damaged (Mondal *et al.*, 2025a, 2025b, 2025c). Due to Mat Stick damage, Sabang's famous mat making cottage industry is completely damaged. The resulting disruption to business and transportation can have a significant economic impact. Damage to infrastructure, including roads and bridges, can disrupt the movement of goods and people, affecting local and regional economies. Often the effects of flooding are long-term and extremely costly, catastrophic and distressing for the communities involved. On average, households reported losses of 9,000-12,000 rupees per flood, mainly due to agricultural losses and wage losses.

Findings:

1. Field visits have found the presence of numerous fixed nets and patas (151) in the Kaliaghari, Kapaleshwari and Baghai rivers and their numbers are gradually increasing, but no formal monitoring or removal of these has been done by the government or the Kaliaghari-Kapaleshwari-Baghari (KKB) Project Division.
2. These fishing nets and patas structures restrict the cross-sectional flow of the river,

thereby reducing the drainage capacity and increasing sediment deposition, which directly exacerbates the risk of floods.

3. Lack of management in the government planning-flood control programme under the KKB project, which reflects a gap between strategic design and ground implementation.
4. It has been observed that if floods occur due to heavy rainfall during September-October, they are extremely destructive (Kumar *et al.*, 2025; Mondal *et al.*, 2025a, 2025b, 2025c). During floods, people in low-lying areas are shifted to high embankments, flood shelters, schools, colleges etc. for safe shelter (Mondal *et al.*, 2025c).
5. Every year during the rainy season, the residents of the lower reaches of the basin experience flood water levels reaching close to 3 to 4 meters. This causes severe damage to the mud houses. Therefore, the local people of the area have modified their houses (Flood-Resistant Construction-FRC). Now they are raising the platform below their houses 3 to 4 meters ES (Elevated Structures) above the local foundation level to cope with the floods.

Remedial measures:

1. Community-driven monitoring and incentive framework Form local flood-control committees-including fisheries, gram panchayats, NGOs, and government officials-to regularly monitor river width.
2. Policy reform and adaptive enforcement Strengthen enforcement under the West Bengal Inland Fisheries Act (amendments of 1984, 1993, and 2008), with a particular focus on gear control and habitat restoration. Initiate awareness campaigns to guide fishermen towards eco-friendly nets and seasonal fishing practices.
3. Complementary channel restoration Resume river revitalization works to achieve the design bed width target. Combine mechanical dredging with bio-engineering techniques – such as geo-felt dams -to prevent reinfestation at bottleneck hotspots.
4. Channelization of the canals Channelization is a general term for a variety of modifications to channels that are usually intended to increase water flow rates, channel volume, or both. A close network of canals mitigates the flood problem to a great extent as the flood water flowing into the river can be distributed into different canals (Rudra, 2002; Mondal *et al.*, 2025a, 2025c; Kumar *et al.*, 2025). Channel changes increase the discharge and rate of currents and hence excess water is carried away. The channel may be widened and deepened, especially where soil erosion and subsequent sedimentation have partially filled the channel (Stuart *et al.*, 2001; Mondal and Biswas, 2022; Mondal *et al.*, 2025a, 2025b, 2025c; Kumar *et al.*, 2025).
5. Improving carrying capacity of water of the river Deepening of Kaliaghai River has been done in 2011-2013. Rehabilitating and widening, straightening and clearing of vegetation and debris from the river bed of major and minor channels associated with this river. This increases the flood water carrying capacity of the river. Channel improvement is complemented by bank stabilization by planting deep-rooted trees on embankments (Acharya *et al.* 2010; Mondal *et al.*, 2025; Mondal *et al.*, 2025a, 2025b, 2025c). River meandering takes a long time to drain flood water.

6. Construction of high embankments and installation of multiple Lock Gates Construction of high and strong dams and installation of multiple Lock Gates in the original course of the river can be planned. First, three kilometres of original river channel should be revived from Amgachia Sluice-gate to Mangalamaro Canal or four kilometres of new river channel should be dug from Balabhadrapur to the original river channel near Mangalamaro Bazar (Mondal *et al.*, 2025a, 2025c). By constructing a high embankment with the excavated soil, the water should be released into the Itaberia Canal (Rasulpur River) at a controlled level through the lock gate. As a result, the excess rainfall of Kaliaghai River can easily drain into the Bay of Bengal through Rasulpur River (Barman, 2021; Kumar *et al.*, 2025; Mondal *et al.*, 2025a, 2025c).
7. Bypass and channel diversion A bypass and diversion channel (Figure 7) needs to be constructed from Kaliaghai River to Chandia River. It will be possible to build the debikhali canal by deepening and widening it. It starts from north side halishahar of Kaliaghai River and extends to big pool, small pool and Dobandi and joins Chandia River. As a result, it will be possible to divert the excess flood water of Kaliaghai River to Chandia River. Again, when there is a possibility of flood in Chandia River, the excess flood water will have to be diverted to Kaliaghai River. That is, a lock gate system will be introduced in the debikhali canal. According to the local people, the construction of this canal (bypass) will reduce the intensity and level of floods in Kaliaghai and Chandia rivers (Mondal *et al.*, 2025a, 2025b, 2025c).

Conclusion:

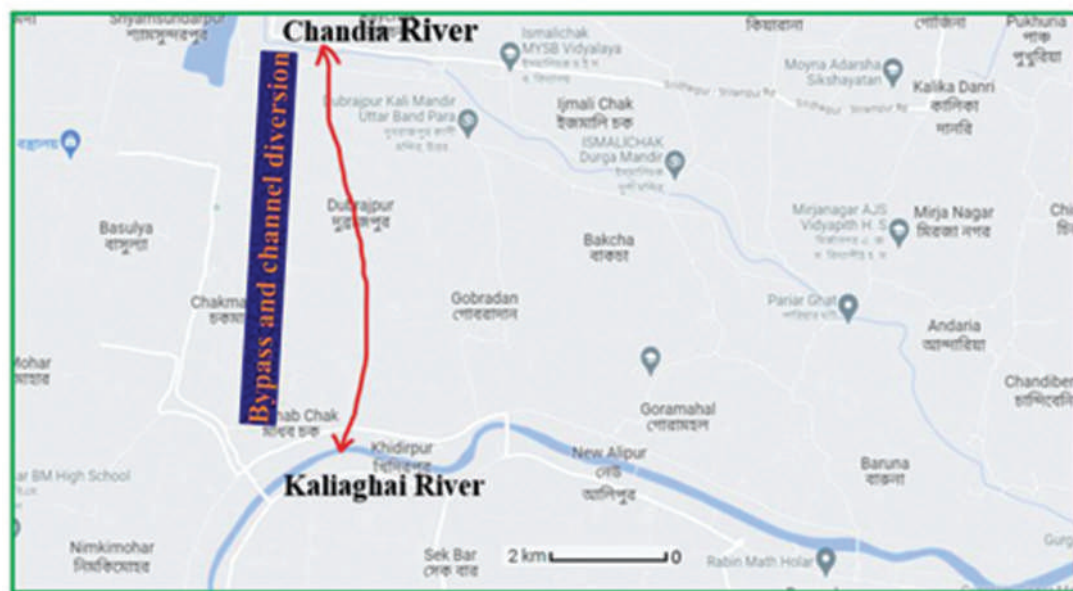


Figure 7. Red line indicates the path of Bypass and channel diversion.

The present study critically examines the impact of traditional fishing structures, fixed fishing nets and 'pata's on flood in the Kaliaghai River in West Bengal. Although these fishing practices are deeply embedded in the local socio-economic structure and support the livelihoods of thousands of rural households, their unintended hydrological consequences pose significant challenges for sustainable flood management in the region (Kumar *et al.*, 2025; Mondal *et al.*, 2025a, 2025b, 2025c). Field investigations conducted along different stretches of the Kaliaghai River revealed a consistent pattern-significant reduction in channel width 17-23 percent and reduction in drainage capacity up to 21 percent and decrease of water velocity 0.116 m s^{-1} ($\approx 418 \text{ m h}^{-1}$) in areas with dense 'pata's. These man-made barricades restrict the natural flow of the river, especially during the pre-monsoon and monsoon seasons, which increases the risk of waterlogging in the lower catchment. Furthermore, it has been observed that these fishing structures act as sediment traps, leading to localized waterlogging of the riverbed. As a result, the river's flood-carrying capacity is further reduced, making it vulnerable to flooding during heavy rainfall (Mondal *et al.*, 2025a, 2025b, 2025c). However, without any government control, the use of various fishing equipment, firstly, reduces the number of aquatic organisms and severely damages the aquatic ecosystem. Second, it causes serious problems in the wealth, lives and livelihoods of people living in flood-prone areas. Therefore, a comprehensive integrated approach is required to address these challenges of livelihood dependence, flood risk and resource loss (Kumar *et al.*, 2025; Mondal *et al.*, 2025a, 2025b, 2025c). In conclusion, we can say that fishing nets, various fishing tools (Stuart *et al.*, 2001; Orasutthikul *et al.*, 2017) and traditional fishing methods like 'patas' are very important and profitable economically, unscientific farming of the local people on the banks of these rivers, illegal encroachment, uncontrolled use, narrowing of the river width etc. contribute a lot to the accumulation of sediment in the river, water flow and increase the risk of floods (Mondal *et al.*, 2025a, 2025b, 2025c). Therefore, it is very important to maintain a balance between preserving the livelihood of the people and maintaining the water holding capacity of the river. These can only be achieved through inclusive studies, science-based and participatory monitoring and management strategies of local people and government, which can be properly implemented to improve the social status of the people living in the Kaliaghai River Basin, environmental sustainability and flood resilience (Kumar *et al.*, 2025; Mondal *et al.*, 2025a, 2025b, 2025c).

Suggestions:

The key appropriate suggestions are proper and systematic removal of 'patas', reduction of the number of family-based nets, increase in the size of nets, use of alternative fishing methods, community-based monitoring of fishermen, reduction of river meandering, river restoration, sediment management and increase in the water holding capacity of the river, etc.

References:

Acharyya, N., Maiti, S., & Bandyopadhyay, J. Modeling Flood of Patashpur-I Block, In Purba Medinipur, West Bengal Using Geoinformatics.

- Ahsan, K., Rashid, M. B., & Talukder, S. (2022). Tidal River siltation and its impact in the coastal parts of Bangladesh. *International Journal of Economic and Environmental Geology (IJEEG)*, 13(2), 35-41.
- Argent, D. G., & Kimmel, W. G. (2005). Efficiency and selectivity of gill nets for assessing fish community composition of large rivers. *North American Journal of Fisheries Management*, 25(4), 1315-1320.
- Asia, F. B., Pascual, P. C. V., & Asia, N. S. (2015). Traditional fishing gears and fishing methods of Ilocos Norte, Philippines. *Journal of Applied and Physical Sciences*, 1(1), 19-28.
- Bandyopadhyay, S., Das, S., & Ghosh, A. (2015). Human Interventions and River Flow Obstruction in Lower Bengal. *Journal of River Studies*, 12(3), 112-120.
- Banerjee, A., & Roy, N. (2015). Impact of anthropogenic obstructions on floodplain hydrology in South Bengal. *Indian Journal of Geography and Environment*, 35, 88-97.
- CAG (2020). Performance Audit Report on Drainage and Irrigation Projects in West Bengal. Comptroller and Auditor General of India.
- Chatterjee, R. (2020). Community Fishing and Governance Dilemmas in Rural Bengal. *Journal of Rural Studies*, 44(1), 77-89.
- Chen, Y., Wang, X., Huang, L., & Luo, Y. (2021). Spatial and temporal characteristics of abrupt heavy rainfall events over Southwest China during 1981–2017. *International Journal of Climatology*, 41(5), 3286-3299.
- Dutta, R., & Sarkar, P. (2018). Influence of Anthropogenic Activities on River Morphology in West Bengal. *Geographical Review of India*, 80(1), 45–56.
- F. B. Asia and R. R. Garcia, "Catching efficiency of multiple handlines operated in payaw areas," *Asian Fisheries Science*, vol. 22, no. 1, pp. 309-317, 2009.
- Ghosh, D., Chakraborty, R., & Sanyal, P. (2020). Human interventions and their impact on flood regimes in eastern Indian rivers. *Water Resources Management*, 34(2), 465-480.
- Ghosh, S., Nandi, A., & Roy, B. (2019). Impacts of Fishing Structures on River Ecology: A Case from Bengal Delta. *Aquatic Environment Journal*, 7(1), 33–41.
- Government of West Bengal. (2005). West Bengal Inland Fisheries Act.
- Kumar, P. K., Madhnure, P., & Lamsoge, B. R. (2025). Long-term monsoon rainfall variability (1998–2023) and its impact on groundwater level dynamics in Maharashtra state. *Theoretical and Applied Climatology*, 156(6), 335.
- Lan, M., Huo, F., Zhou, L., Jiang, S., Cai, R., & Chen, J. (2022). Mechanisms of short-duration heavy rainfall in the western Pacific subtropical high area: An analysis of two rainstorms of 2018 in Hunan Province, China. *Atmosphere-Ocean*, 60(1), 1-12.
- Lele, S., & Joshi, A. (2009). Adapting traditional resource use in the context of environmental change. *Ecology and Society*, 14(2): 16.
- Maiti, S., & Samanta, A. (2021). Anthropogenic Pressure and Flood Vulnerability in the Lower Kaliaghai Basin. *Environmental Studies Report*, 16(2), 93–104.
- Maity, S. S., & Maity, R. (2022). Changing pattern of intensity–duration–frequency relationship of precipitation due to climate change. *Water Resources Management*, 36(14), 5371-5399.
- Mondal, N., & Biswas, B., (2022). "Human Adjustments to Flood Hazards in The Kaliaghai River

Basin, West Bengal, India” Thesis submitted for the degree of Master of philosophy in science (Geography) of the University of Burdwan, West Bengal. 15-12-2022.

- Mondal, N., & Saha, S. (2022). Traditional fishing practices and flood vulnerability: A case study of Kaliaghai River Basin, West Bengal. *International Journal of Rural and Regional Studies*, 8(1), 55–67.
- Mondal, N., Kar, S., Hussain, I., Farooq, A., & Ahmed, P. (2025c). The Impact of Kaliaghai River Flood (2021): A Detailed Study of Socio-Economic and Environmental Consequences in West Bengal.
- Mondal, N., Kumar, D., & Nazir, O. (2025b) Spatial Assessment of Rural Socio-Economic Development: A Study of Purba Medinipur District, West Bengal.
- Mondal, N., Kumar, D., & Wasit, M. (2025a). Assessing the Socio-economic and Environmental Consequences of the 2021 Floods in the Kaliaghai River Basin, West Bengal.
- Mukta, A. Y., Haque, M. E., Islam, A. R. M. T., Fattah, M. A., Gustave, W., Almohamad, H.,... & Ghassan Abdo, H. (2022). Impact of canal encroachment on flood and economic vulnerability in Northern Bangladesh. *Sustainability*, 14(14), 8341.
- Orasutthikul, S., Unno, D., & Yokota, H. (2017). Effectiveness of recycled nylon fiber from waste fishing net with respect to fiber reinforced mortar. *Construction and building materials*, 146, 594-602.
- Ranalli, G., & Scheidegger, A. E. (1968). A test of the topological structure of river nets. *Hydrological Sciences Journal*, 13(2), 142-153.
- Sahu, A.S. (2014): A study on Moyna basin water-logged areas (India) using remote sensing and GIS methods and their contemporary economic significance. *Geography Journal*, [Internet]. [cited 2015 April 16], Vol. 2014:1-9. Available from: <http://www.hindawi.com/journals/geography/2014/401324/>.
- Singh, R. B., Mal, S., & Sinha, R. (2018). *River Systems of India: Issues and Concerns*. Springer India.
- Stuart, J. N., Watson, M. L., Brown, T. L., & Eustice, C. (2001). Plastic netting: an entanglement hazard to snakes and other wildlife. *Herpetological review*, 32(3), 162-163.
- Tian, F., Zheng, Y., Zhang, T., Zhang, X., Mao, D., Sun, J., & Zhao, S. (2015). Statistical characteristics of environmental parameters for warm season short-duration heavy rainfall over central and eastern China. *Journal of Meteorological Research*, 29(3), 370-384.
- Waza, A. U. D., Pednekar, S., Gadhe, U. G., Kumar, K., & Tomar, S. (2025). Dynamics of Land Use / Land Cover Transformation: A Geospatial Study of Lidder Watershed of Kashmir Valley, India Area. In R. Sema (Ed.), *Land and Water Nexus in South Asia* (p. 437). Springer Nature Switzerland. <https://www.barnesandnoble.com/w/land-and-water-nexus-in-south-asia seemarani/1146974684>
- Woodson, M. K. (2015). The impact of flooding on Hohokam canal irrigation agriculture. *Traditional arid lands agriculture: Understanding the past for the future*, 180-216.



Anthropogenic Modification on Hydro-dynamics of the Teesta River in Duars Region, West Bengal

Ajit Kumar Singha¹ and Ishwarjit Singh Elangbam^{1*}

¹Department of Geography, Sikkim University, Sikkim, India

**Corresponding author: eisingh@cus.ac.in*

Abstract: Teesta river is one of the highly engineered river in India. It drains across the Chicken Neck corridor which connects main India with entire North East region. Siliguri city is located on the right bank of the river in Duars which is fastest growing city in West Bengal next to Kolkata. The river has got immense anthropogenic imprints which modify its natural hydro morpho dynamics. In this paper, three anthropogenic interventions which have different intensity and nature of modification in the river have been studied. Three anthropogenic interventions are firstly the construction of barrage, bridges across the river; secondly the construction of embankment and spur along river banks and thirdly, sand and stone quarrying in river bed. In addition, land use and land cover changes around the river for 42 years in Duars has also been studied which may directly and indirectly influenced in river ecosystem. For the study, LANDSAT imageries from 1978-2020 and Survey of India toposheet 1943 were used to analyze bank line shifting, erosion- accretion with help of indices like NDWI and MNDWI. The river in the study area in Duars region, West Bengal was divided into three Reaches on basis of different hydro morphic dynamics. Reach 2 is the most engineered reach which affects substantially hydro morpho dynamic of the section but also both the reaches. 60.36% of entire river of both right and left banks in the study has got embankment. But it varies in bank-wise, embankment on right and the left bank with 73.19% and 47.26% respectively. The right bank most engineered and urbanized than the left bank by which left bank becomes more erosive recently. Among the three Reaches, 2nd Reach has got maximum embankment with 91% and its right bank with 99% embankment. Stone and sand quarrying is most concentrated in Reach 1 with 97% and it is from two tributaries, Ghish and Chel with 78%.

Key Word: Engineered river, Urbanization, Embankment, Sand quarrying and Hydro morpho dynamics.

Introduction:

Rivers have been heavily engineered for power generation, to protect the land against floods, irrigation, transportation, to meet demand of freshwater both urban and rural (Best, 2019; Downs, Gergory, 2004; Marsh, 1864; Thomas, 1956). Measures such as dam construction, embankment, spur, channelization, sand and stone quarrying have transformed natural channel of meandering, braiding and anabranching into narrower, straighter and shorter rivers (Alexander *et al.*, 2012; Hohensinner *et al.*, 2011; Uehlinger *et al.*, 2009). Due to its fixed channel and width, an engineered river can only respond to such human intervention by changing its geomorphic thresholds in order to maintain its equilibrium which influence channel slope, velocity through erosion or aggradation (Habersack *et al.*, 2016; Harmar *et al.*, 2005; Quick *et al.*, 2020; Surian, Rinaldi, 2003; Blom *et al.*, 2016; De Vriend, 2015; Blom *et al.*, 2016, 2017; Mackin, 1948). Channel bed incision and erosion may enhance flood risk due to weakening of river structures (Buijse *et al.*, 2002; Habersack *et al.*, 2013; Hiemstra *et al.*, 2020). The distribution of bed sediment texture along the longitudinal profile in engineered river is also modified. The bigger sediments which confined in upper riparian has extended to lower riparian.

Duars is located around the chicken neck corridor, 22 km wide which connect entire north east India with rest of India (Ghising, 2024). All trains and road transportation need to cross Duars area. Duars region is extended longitudinally from the piedmont of Himalaya where rivers which are coming from Himalayan forms braided due to sudden change of gradient and deposition of eroded sediments from mountains followed by flood plain. The rivers channels are frequently shifted extensively and loss many properties and settlements along the river. In 1929, there was market in Mekhleganj on the left bank of Teesta which was completely washed out (Survey of India, 1929). In order to control, tame and utilize river, it is a challenging task for engineers. They concretized maximum extend of the river and tamed which advertently affect natural flow dynamics of a river. The construction of infrastructure and concretization in Teesta in Duars region started during colonial period. Massive land use land cover of the region also changed during colonial time due to extensive deforestation for tea plantation, timber business, mineral extraction etc. in the region as well as in entire north east region. Railway line laid down and road construction speeded up that enabled to transport mineral and resources from the north east region to mainstream India. But during colonial period, there was less control over river except construction of rail line and bridges in Duars region. Recently, human intervention and modification in the river has repeatedly increased. The land use and land cover along the river in the study area has also been drastically changed as it becomes hub of business centers, manufacturing center, settlement, tourism and rapid urbanization with infrastructural development in the area. The multiple barrages, bridges, railway lines, concretization etc. have been constructed over main channel and tributaries which modify flow and channels morphology. This creates downstream water scarcity, creates char lands, river bed siltation by upstream sediment load, water logging, floods etc. During dry season, it is found that the river bed has been filled up with boulders and sands downward which shows the river has lost its natural motion in upstream and downstream.

Among the main rivers in the region are the Teesta, the Jaldhaka, the Torsha and the Sankosh river and their tributaries on the east. The Teesta river, is the western most river of the region (Das, 1998 and Debnath, 2010). The Teesta river is originated from extreme north of Sikkim in mountainous area as Chhombo Chhu fed by many sources including Tso Lhamo lake, Khangse glacier, Pahunri glacier in North Sikkim at an elevation above 5000m. It is a right bank tributary of the Brahmaputra (CISMHE, 2006 and Meetei *et al.* 2007). Total length of the river before joining the Brahmaputra in Bangladesh is 414 km in which 94 km (Sevoke, West Bengal to Border of Bangladesh) in Duar region of West Bengal in the district of Jalpaiguri (Singha and Elangbam, 2025). The total catchment area of the river is about 10,155 Km² in India out of which 8051 Km² in hill areas and 2104 Km² in Duar region of West Bengal (CISMHE, 2006). The longitude and latitudinal extension of the river in the Duar region, West Bengal (Sevoke to Bangladesh border) 88.30 -89.00 E and 26.10 -26.50 N (Figure no 1). The present study has made an attempt to study nature, type of anthropogenic intervention affects the river hydro morpho dynamics. There are two objectives in this study as given below:

1. To study different anthropogenic interventions in the Teesta river in study area
2. To analyze nature of modification of Teesta river under anthropogenic factors.

Materials and Methods:

The study is entirely based on secondary data and primary survey on quarrying sites with GPS device. Table 1 shows the data used for the present paper.

Table 1. Secondary Sources of data

SL. No.	Types of data	Spatial Resolution	Source	Year
1	Landsat 2 MSS	68 meter	https://earthexplorer.usgs.gov/	1978
2	Landsat-5 TM	30 meter	https://earthexplorer.usgs.gov/	1990
3	Landsat-7 ETM+	30 meter	https://earthexplorer.usgs.gov/	2000
4	Landsat -8 OLI/TIRS	30 meter	https://earthexplorer.usgs.gov/	2010
5	Landsat-8-OLI/TIRS	30 meter	https://earthexplorer.usgs.gov/	2020
6	Survey of India topographical (78F)	1inch to 4mile	https://maps.lib.utexas.edu/maps/topo/india_253k/	1943

For the extraction of bank line, the following indices in the equation 1, 2 and 3 were used. Green and NIR bands in NDWI based on McFeeter (1996) for segregation of land from water, where pixel for water features as 1 and for land as 0 to achieve a binary image. The MIR band of Landsat 7 and SWIR band of Landsat 5 and 8 along the green band were used for calculating MNDWI based on Xu (2006).

NDWI= Green – NIR/Green + NIR ----- (1)

MNDWI= Green – MIR/ Green + MIR ----- (2)

MNDWI= Green – SWIR/ Green + SWIR -----(3)

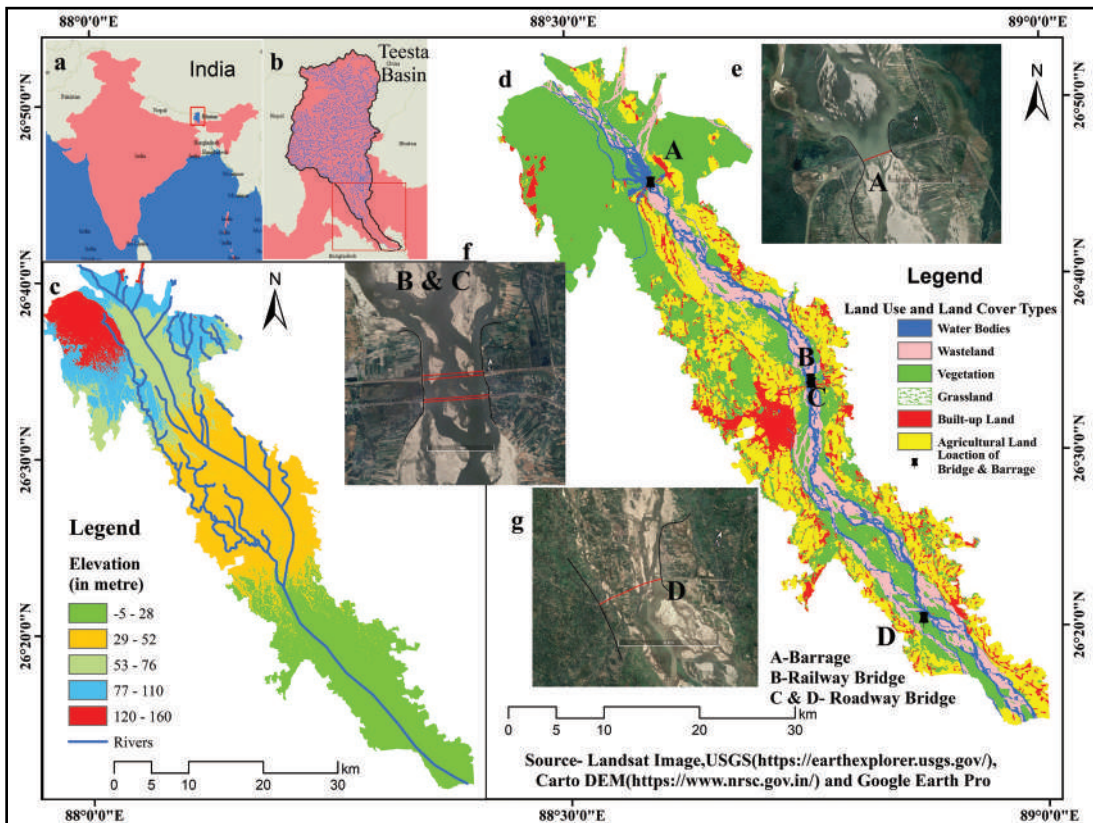


Figure 1. Location Map of the Study Area (a- India; b- Teesta basin in Sikkim and West Bengal; c- elevation of sub basin of study area in Duars; d- LULC of sub basin in 2020; A- Gajoldoba Barrage; B, C- Rail and Road Bridge at Domahani and; D- road bridge at Mekhliganj)

Finally, MNDWI images were used for digitizing the bank line position of right and left bank through ArcGIS 10.2.2 version. Different position of bank lines in different period (1978, 1990, 2000, 2010 and 2020) were superimposed and subsequently measured extend and direction of shifting, erosion and deposition at 15 cross sections along the river. Land Use and Land cover had also been studied for 42 years around the river in the region. The time period has been divided interval has been chosen because of episodic rate of human intervention and availability of quality satellite imagery. 15 cross sections have been prepared in the river on basis of different morpho dynamics of the river. From Sevoke to Gajoldoba is about 17 km in which 7 cross sections were prepared and in the remaining 77 km downward of the river till Bangladesh border, only 8 cross sections were made. This study area has been divided into three Reaches broadly based on morpho dynamics of the river. First Reach comes under the Megafan Teesta from Sevoke to Gajoldoba near piedmont followed by 2nd Reach which is transition part of braided extended from first Reach and meander and 3rd Reach is lower part characterized by meander.

Anthropogenic Interventions:

Since civilization, humans have been continuously intervening river in different ways that directly or indirectly affected river ecosystem. Recently the Duars area, a riverine plain has been transforming very fast through urbanization, infrastructural development, land use land cover changes. The large rivers in the world are heavily engineered (Arbos *et al.*, 2020). Some of the important anthropogenic intervention take place on any river channel that influence channel morphology are bridge, barrage, embankment, hydro power reservoir, diversification of channel as canal irrigation etc. There is a spatio-temporal dimension of anthropogenic intervention on river accordingly responded by the river to maintain an equilibrium in the study area. The anthropogenic interventions in Teesta river can be classified in two broadly in the way of nature of engineering activities that the upper riparian of Teesta which passes in mountainous area where nature of engineering activities are related to construction hydro power dam and in the lower riparian area of Teesta in Duars is related to control of flood, channel instability and harnessing sediment etc.. Bridges and barrage are common in both upper and lower but dimensions are different.

1. Bridge and Barrage:

The bridge piers play a significantly role in the river environment and river morphological features. River water flow, sediment distribution and wave regulation largely rely on bridge piers in the river which modify current, whirling, velocity and direction of normal flow of river. Pier scouring occurs when velocity of river is suddenly increased and it washes away big amounts of sediments adjacent to bridge piers (Ashmore and Parker, 1983; Heidarnejad *et al.*, 2010). Most of the soil particles surrounding the bridge piers are removed by turbidity currents (Pasiok and Szydło, 2010), and they are deposited as bars at the immediate downstream of the bridge.

The barrage over Teesta river at Gajoldoba was started construction since 1975 and completed in 1981 which located in the Reach 1, upper most part of the river in the study area. This barrage was built for diverting water from Teesta to Mahananda river where Fulbari barrage regulates water for agriculture purpose as well as fresh water supply for Silliguri town (Govt. of West Bengal, 1998). Teesta river before barrage, there were many channels two different streams with extensive sand bars (Figure 2). But after the completion of barrage, the main channel was tamed and reduced to one main channel narrowed by barrage which modified the nature and flow of channel completely. Before the commission of barrage, river channel was broad and extensive with channel islands in upper riparian but after the commission of barrage the channel became broaden and extensive with channel island in lower riparian below the barrage (Figure 2). The channel width at barrage point construction was 4655.8 m in 1978 while after construction, it reduced to 941 m in 1990. There was an extensive channel bar along right bank and channel island on left side till 1978 before the construction around the barrage site. After construction since 1990, these channel bar and island started decreasing and completely disappeared in 2010 and left them as a small dissected channel islands (Figure

2) (Singha and Elangbam, 2025). The channel gradient has also changed as the channel slope became steeper just before barrage and after barrage downward more elevated (Figure 5). It shows that flow and velocity increase by which materials are being removed from upper the barrage and deposited downward after crossing barrage. This deposition of sediment forms extensive bar and island which seen in 2000 (Figure 2)

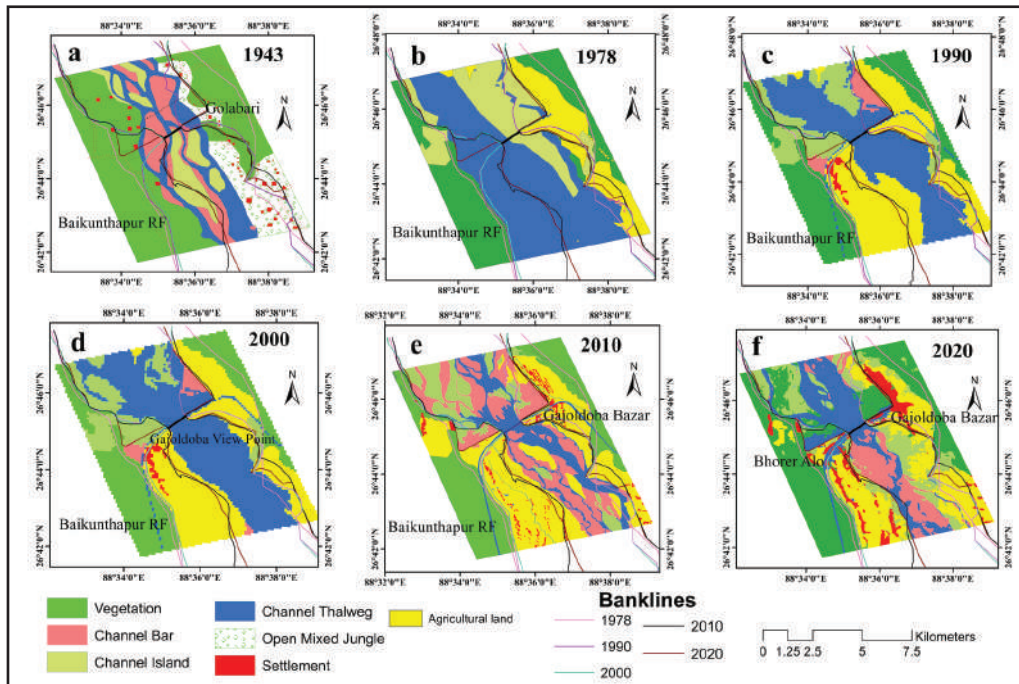


Figure 2. (a) and (b) Channel morphology before construction of Gajoldoba Barrage(1943 and 1978) and (c), (d), (e) and (f) Channel morphology after construction of barrage(1990, 2000, 2010 and 2020 respectively).

The railway line and bridge over the Teesta river at Domohami had been laid down parallel to each other in a short distance (Figure 3). The channel width before construction at bridge site was 2005.4 m in 1943 and after construction, it reduced to 1024m in 1978 (Singha and Elangbam, 2025). The channel had been narrowed down by embankment with more than one km length for the railway line and bridge. The main channel tends to move from south west to south east after crossing the bridge downward and formed extensive sand bar on right side and about 20 Km² sand island on left side which seen in 1978 image above the railway line disappeared in 2000. From 1990 onward, the channel below the bridge tends to move from south east to south west and became broader than channel above the railway (Figure 3). This may happen because of narrowing down of channel along railway line and bridge and increase velocity of flow subsequently increase erosion which deepening the valley above the railway line. After the bridge, velocity decrease and sediments start deposited and form an elevated channel bed associated with extensive channel bar on the right bank and island on the

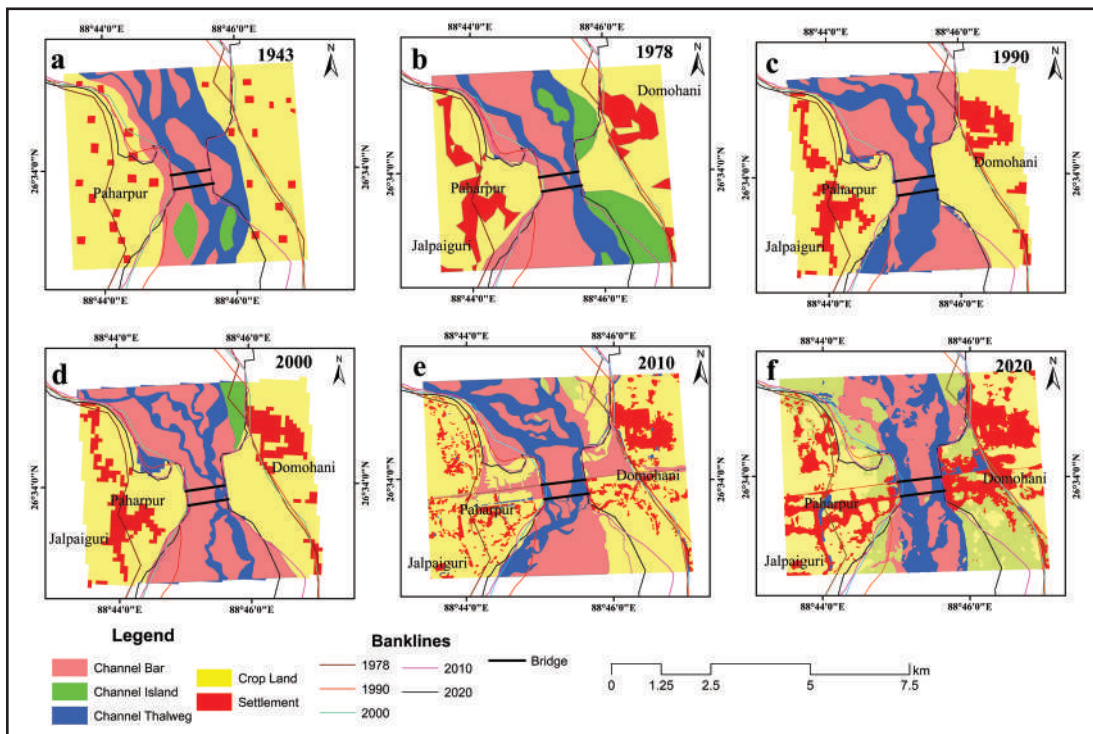


Figure 3. (a) channel morphology before construction of Rail and Road way bridge at Domohani two dark lines shows the location of railway and bridge; (b), (c), (d), (e) and (f) Channel morphology after construction of bridge and railway line.

left bank downward which are seen in 1978 image (Figure no 3 and 5).

The influence of bridge across the Teesta at Mekhliganj on morphology of the river in reach 3 was found very profound. Among all constructions across the Teesta in Duars area, the bridge in Mekhliganj is a recent. The red line drawn over the river is the position of the bridge. Before the construction, the channel width at bridge point was 4382.7 m in 2010 after construction, it reduced to 2759.3m in 2020. The bridge was constructed after more than 5 km embankment on the left bank which seen in 2020 imagery as a dark line (Figure no 4-f). The upper channel and lower channel near the bridge shows intensive erosion from increasing velocity due to drastically narrowed down of channel by embankment (Figure no 4 and 5).

2. Embankment:

Each river has natural mechanism to build its own elevated bank which checks channel water from being spilled. This is known as natural levees. This is formed by continuous deposition of fine sediment on bank during bank full water flow. Naturally, the channel always tries to maintain an equilibrium in levees between continuous deposition on bed of the river channel which shallowing river and increasing height of natural levees (Hudson, 2007). Subsequently, natural levees are higher than settlements. Some time such natural levees are broken during

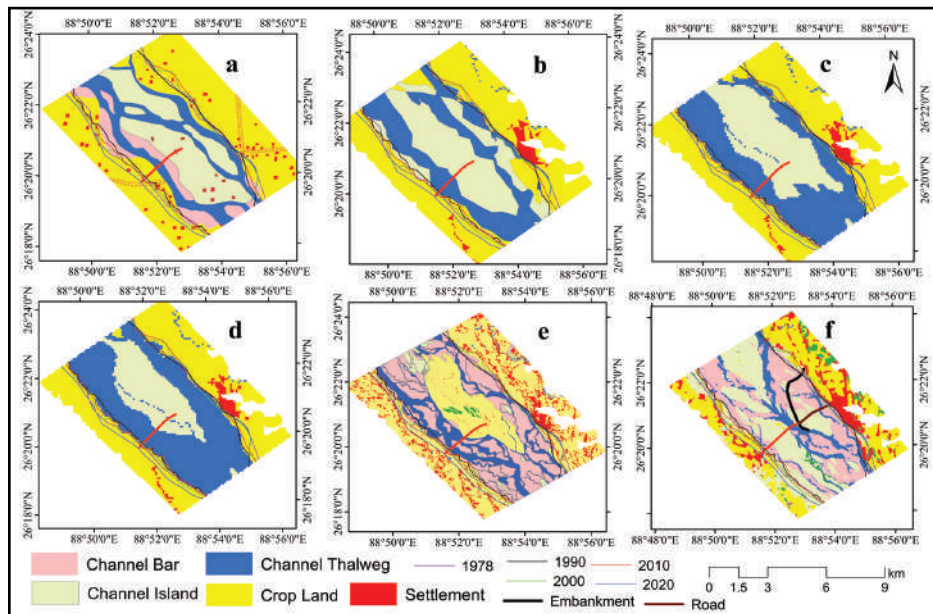


Figure 4. Channel Morphology at Mekhligang (a,b,c,d and e) before bridge construction and f after bridge construction.

bankful flow of river which lead to catastrophe and wash away entire villages, like Kosi river embankment incident in 2008 (Kafle *et al.*, 2017). In order to control bank instability, artificial embankment is made along the channel or concretization of channel in lacustrine plain.

The Teesta river in the study area, Duars region has different length of man made embankment on both side of bank lines due to different length of meander loops. The right bank has 97.34 km while left bank has 101.48 km in the study area. The total length bank line of both left and right is 198.82 km in which 119.52 km (60.36%) has got embankment. The length of embankment on right bank is about 71.26 km (73.19%) while on left bank with 48.26km (47.26%) (Table 2). The left bank line is longer but got lesser embankment whereas right bank line is lesser but got more embankment. It depends on settlement and infrastructural development on the bank. Rapid urbanization in and around Siliguri and infrastructural development is observed more on right bank than left bank of the river. Among three Reaches, the Reach 1 has got least embankment only 43.7% due to piedmont location where active distributaries and less settlement. Even the embankment is not continuous and there are many portions left without embankment. But in Reach 2, both left and right bank lines are getting embankment continuously and completely with 91% except few point on left bank without being embankment. The right bank of reach 2 has got 99% embankment. In Reach 3, embankment on right bank line is done regularly while on the left bank line has some break areas with 60.69% embankment (Table 2). Both the bank lines in lower riparian are left without embankment where there is less settlement.

Generally, embankment on the right bank is continuous with many break point in all three Reaches. The portion on the upper and lower of the channel are not getting embankment

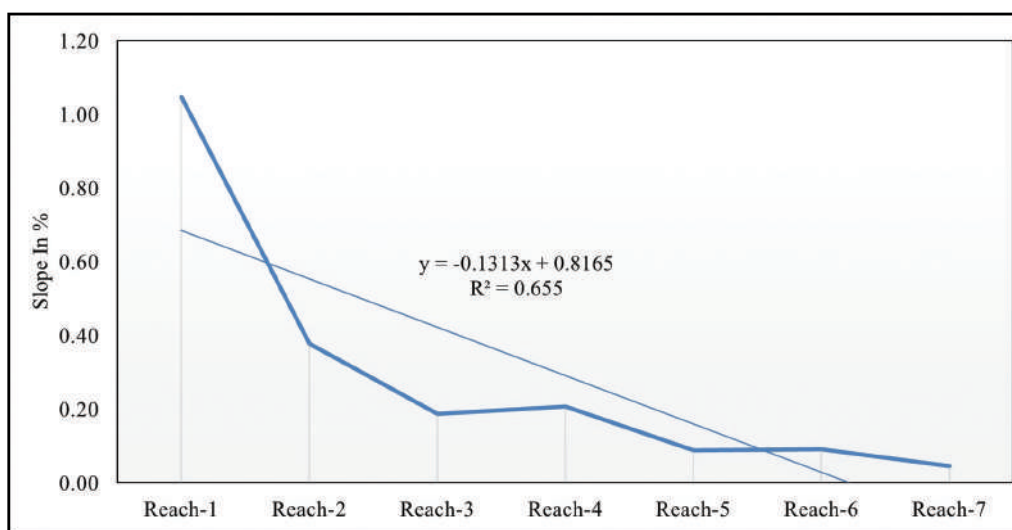


Figure 5. Channel Gradient of Teesta River from Sevok to Bangladesh Boarder.

where the river characterized by active braided and meandering channel. The embankment on the left bank is more haphazard and many break points which shows active lateral erosion.

There are many spurs along the river. Spurs are protruding and striking toward water movement or transverse structure. It reduces flow of water in channel near bank so that bank will be protected from erosion. The channel line where spurs are concentrated are used for agriculture purposed. Spur reduces erosion and enhance deposition of fine sediments which are very fertile. There are 103 spurs in the longitudinal profile of the channel in the study area. Out of total spur in the channel, 55.3% of spurs are on right bank and 44.7% on the left bank. This shows the right bank is more regulated due to urbanization and agricultural land. In Reach wise, maximum number of spurs are found in Reach 2 with 44.6% followed by Reach 3 with 42.7% and least in Reach 1 with 14.5% (Figure 6).

Table 2. Embankment of Teesta river in Duars region in 2020.

Reach	Length of Bank (In Km)			Length of Embankment (In Km)		
	Right Bank	Left Bank	Total (%)	Right Bank (%)	Left Bank (%)	Total (%)
1	35.52	43.66	79.18(39.8%)	18.41 (51%)	15.40 (35.2%)	33.81 (42.7%)
2	29.86	28.90	58.79(29.5%)	29.59(99%)	19.65 (67.9%)	49.24(83.7%)
3	31.96	28.93	60.89(30.62%)	23.25 (72.7%)	13.71(47%)	36.96(60.69%)
Total	97.34	101.48	198.82	71.26(73.2%)	48.26(47%)	119.52(60.36%)

3. Sand Quarry:

There are four main tributaries the river in Reach 1, Mal, Chel, Ghish and Lish from where sands and stones are extracted. The total number of sites of extraction is 40 and cover about 937.31 acres. Maximum quarrying sites are located in the Ghish with 54.1% in terms of area followed by Chel with 24.5%. From main channel Teesta only 16%. These two tributaries have 78% of quarrying site (District Survey Report, 2020). All stone quarrying sites are located along Ghish and Chel but one from main channel Teesta and Lish in Reach 1. Almost all quarrying sites are located in Reach 1 with more than 97% (Table 3). Its shows that sand

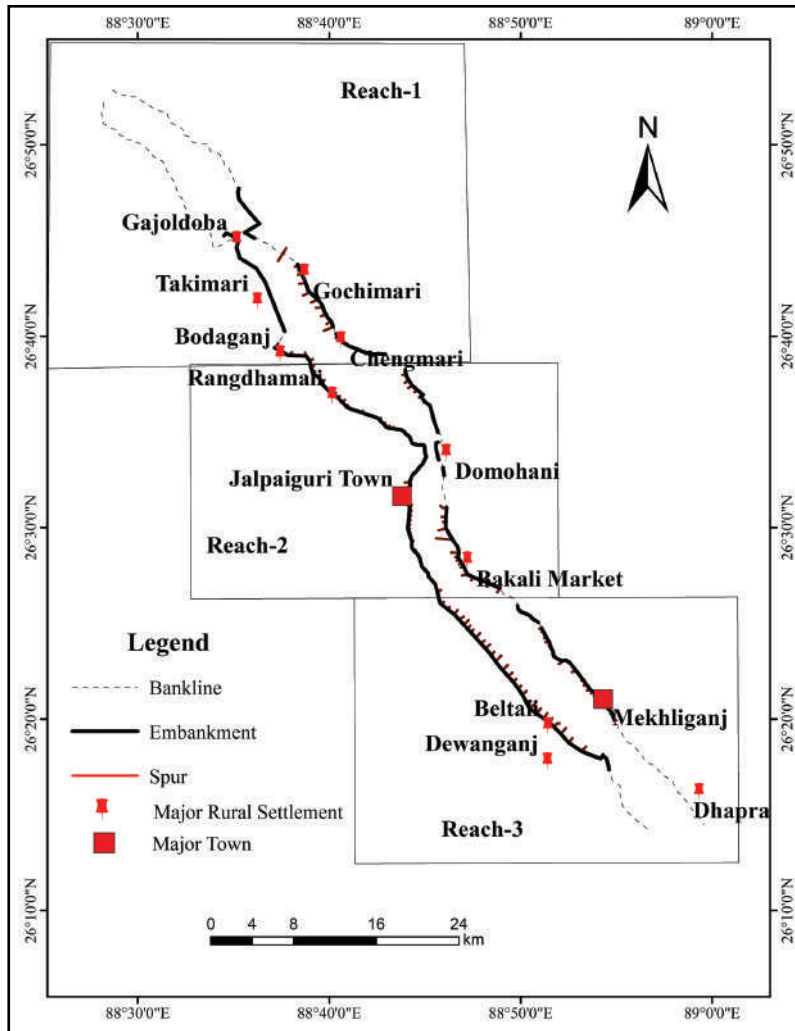


Figure 6. Embankment and Spurs along the Teesta River (a) at Gajoldoba, (b) at Rangdhamali, (c) at Domohani and (d) at Dhapra (Mekhliganj).

and stone are collected near foothill. There are four quarrying sites in Reach 2, main sites are at Gopalganj and Randhami and one quarrying site, Helapakuri in Reach 3, all sites are located along the main channel (Figure 7). There are few quarrying sites located along main channel because of deeper channel and most of the time with water available in main channel. Most of the quarrying sites are located small tributaries at foothills where torrential flow in channel brought large volume of sand and stone and soon after channels become dry and shallow also which make easier to extract. There are well established chip factories near the Ghish and Chel tributaries.

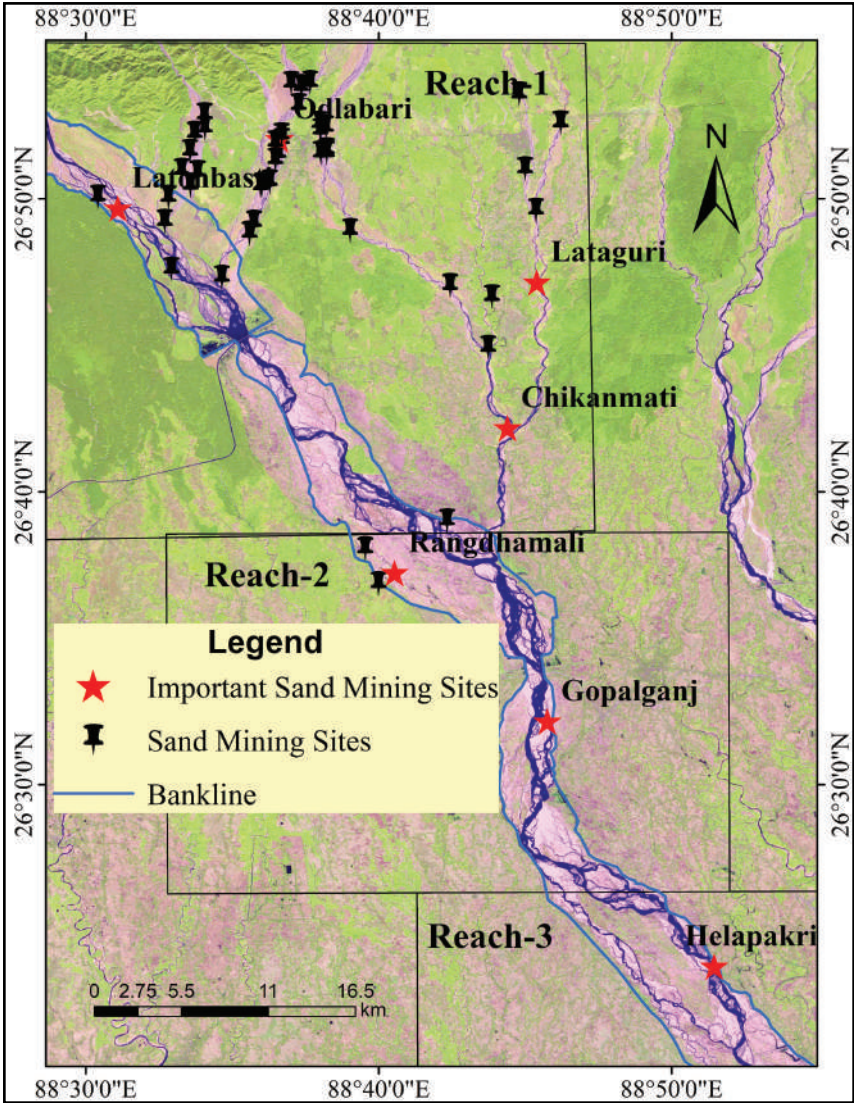


Figure 7. Quarrying Sites of the Teesta river and its Tributaries a. Odlabari mining in Reach 1..

Table 3. Location of Sand Quarrying Along Teesta in Duars region 2020.

SL. No.	Block	Mouza	J.L. No.	Plot No.	Area (in acres)	River	Material
1	Jalpaiguri	Barapetia natun bus	1	10(P)	4.98	Teesta	Sand
2	Matiali	Neora Majhiali	20	430(P), 437(P)	3.25	Neora	Sand
3	Mal	Songachhi Tea Garden	4	1	8	Mal	Sand
4	Mal	Neora Maj hiali-Mal	20	43, 41, LR	4	Mal	Sand
5	Mal	Neora Maj hiali-Mal	44	17,48,590	4	Mal	Sand
6	Mal	Paschim Damdim and Odelabari	39	1434(P),	4	Chel	Sand
7	Mal	Odelabari	20	205 4(P)	99	Chel	Sand
8	Mal	Uttar Phulbari	12	103(P)	23.2	Ghish	Sand
9	Mal	Odlabari	20	3, 84,85,264,265,266	101	Ghish	Sand
10	Mal	Manabari TG	22	1, 2, 3, 9	45	Ghish	Sand
11	Mal	Manabari TG	22	503, 506, 507,508	103	Ghish	Sand
12	Mal	Uttar Phulbari	12	103(P)	91	Ghish	Sand
13	Mal	Odlabari	20	86, 87	103	Ghish	Sand
14	Mal	Odlabari	20	1, 2, 3, 4, 5, 8	4.97	Ghish	Sand & stone
15	Mal	Dakshin phulbari	13	15(P), 20(P),21p	5	Ghish	Sand & stone
16	Mal	Manabari TG	22	428, 431, 433,435, 450, 451, 452	4.6	Ghish	Sand & stone
17	Mal	Dakshin phulbari	13	17(P), 21(P)	5	Ghish	Sand & stone
18	Mal	Dakshin phulbari	13	141(P)	5	Ghish	Sand & stone
19	Mal	Odlabari	20	87, 149, 150,152, 267, 268	4.97	Ghish	Sand & stone
20	Mal	Odlabari		894(P), 897(P),,895p. 619p, 624p, 625p, 626, 854p, 622p, 623, 621p	4.8	Chel	Sand & stone
21	Mal	Uttar phulbari	12	29	4.87	Ghish	Sand & stone
22	Mal	Odlabari	20,39	1183(P), 851(P)	2.68	Chel	Sand &stone
23	Mal	Turibari	23	500, 563, 564,565p	4.48	Chel	Sand
24	Mal	Odlabari, Panchhim Damdim	20,39	(Rs) 1183(P),13,16,17p	4.8	Chel	Sand & stone
25	Mal	Dakshin phulbari	13	(RS) 141	4.87	Ghish	Sand

SL. No.	Block	Mouza	J.L. No.	Plot No.	Area (in acres)	River	Material
26	Mal	Odlabari	20	1183(P), 1189p, 1190p, 1191p, 1992p	4.8	Chel	Sand
27	Mal	Dakshin phulbari	13	RS 141(P)	5	Ghish	Sand
28	Mal	Odlabari	20	RS1192(P), 1193p, 1194p, 1201p, 1202p, 1203p,1204p,	2.6	Chel	Sand
29	Mal	Odlabari Uttar Phulbari	20,12	1, 2, 3, 4, 79,80,103	4.74	Ghish	Sand & stone
30	Mal	Turibari	23	RS 564(P), 565p	4.48	Chel	Sand & stone
31	Mal	Uttam Phulbari	12	6(P)	4.89	Ghish	Sand & stone
32	Mal	Dakshin Phulbari	13	97	4.8	Ghish	Sand & stone
33	Mal	Manabari TG	21	1(P), 2(P), 3(P),9p	4.41	Ghish	Sand
34	Mal	Kalagaity	6	LR 301(P), 302p,304	7.7	Lish	Sand & stone
35	Mal	Paschim Damdim	39	201(P), 202(P)	4	Chel	Sand
36	Mal	Odlabari	20	1434(P), 2054(P)	99	Chel	Sand
37	Jalpaiguri	Patkata	05	LR 03	80	Teesta	Sand
38	Maynaguri	Gopalganj	25	LR032	3.5	Teesta	Sand
39	Maynaguri	Baikur (Gourgram Helapakuri)	90	LR 053	3	Teesta	Sand
40	Rajganj	Junglee mahal (Lantonbasti)	1	LR 001	60	Teesta	Sand & stone

4. Land Use Land Cover Changes around the Teesta River in Duars:

Land use and land cover of Teesta river basin in Duars region had been studied from 1978 to 2020. Six (6) categories of land use have been classified such as agriculture, built up, grass land, vegetation, waste land and water body. In this 42 years of LULC analysis of the sub basin, it was found that areas under agriculture and water body have been drastically reduced. In 1978, areas under agriculture and water bodies were 454.10 Km² which was 44.15% of the sub basin and 202.70 Km² (19.71%) respectively but in 2020, areas under agriculture and water bodies had reduced to 286.40 Km² (28.01) and 68.39 Km² (6.69%) respectively. Every year agricultural area has got affected by hydro dynamics of the channel because of its low lying areas. Whereas maximum area increased in 2020 from 1978 were found in waste land with 9.64%, grass land(16.81%), built up area (9.78%) and vegetation (29.07%) which were only 0.07%, 9.56%, 4.86% and 21.66% respectively in 1978. Increase in waste land is the area where new sands are deposited in agricultural areas. Water body areas are found turned into grass land because area has been used by community for grazing side (Singha and Elangbam,

2025). Built up area was almost negligible in Reach 1 but in 2020 large areas came under built up as well as in Reach 2 and 3 too (Table 4 and Figure 8). The Siliguri town located on the right bank of the river is fastest growing city in West Bengal after Kolkata. The dynamic land use and land cover of study area might get influenced to hydro morpho dynamics of the river due to change in surface run off and loose sediments.

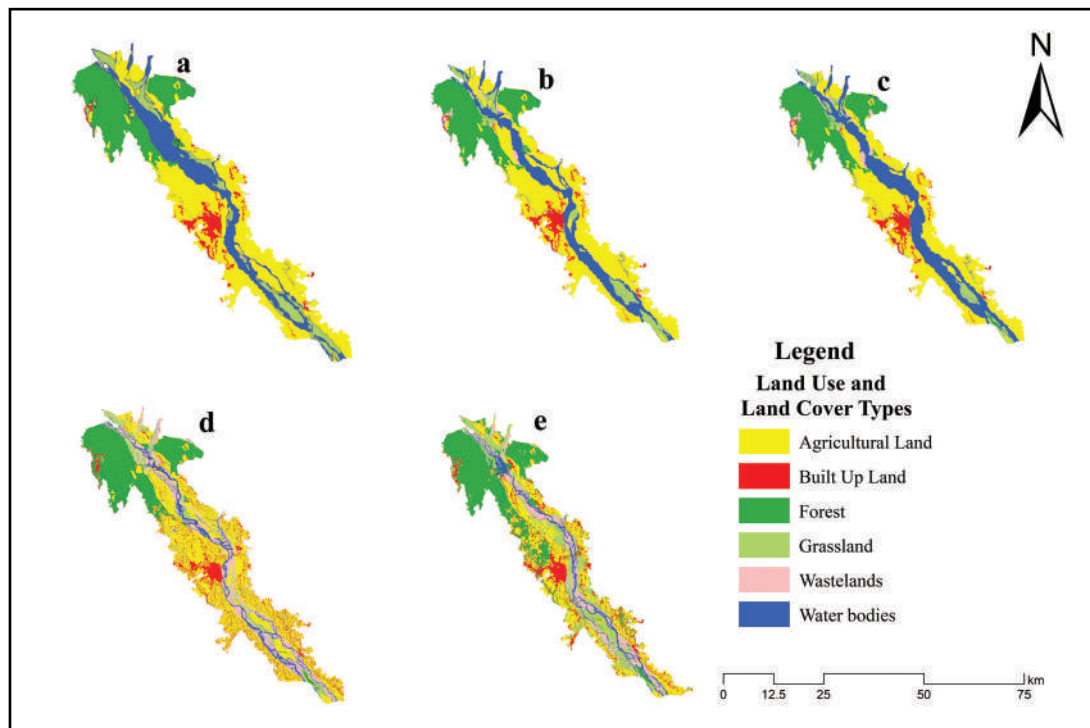


Figure 8. Showing Land use land cover change of Teesta River riparian in from Sevoke to Bangladesh boarder, (a) 1978, (b) 1990, (c) 2000, (d) 2010 and (e) 2020...

5. Hydro morpho Dynamics of the Teesta River:

In 42 years, changes in hydro morpho dynamics of Teesta river in four periods in reference to deposition and erosion (Table 5). In 1978-1990, in all three Reaches, the right bank had highest erosion and least depositional in 42 years whereas the left bank had highest depositional activities in 42 years and subsequent less erosion. In 1990-2000, some differences had been observed from previous period that deposition on the left bank and erosion on the right bank with less extensive in all three reaches. In 2000- 2010, the right bank had the least erosion and highest deposition in 42 years whereas left bank had highest erosion in 42 years and less depositional activities. In 2010-2020, both left and right bank erosional and depositional activities were less that show river has got maximum embankment and controlled.

Table 4. Temporal Change of Erosion and Deposition of Teesta River

Year	Erosion (km ²)		Deposition (km ²)	
	Right Bank	Left Bank	Right	Left
1978-1990	17.67	9.95	3.02	38.58
1990-2000	3.21	13.66	5.64	6.64
2000-2010	2.45	19.93	20.93	8.86
2010-2020	9.59	8.93	5.50	7.87
1978-2020	9.31	19.69	32.25	28.83

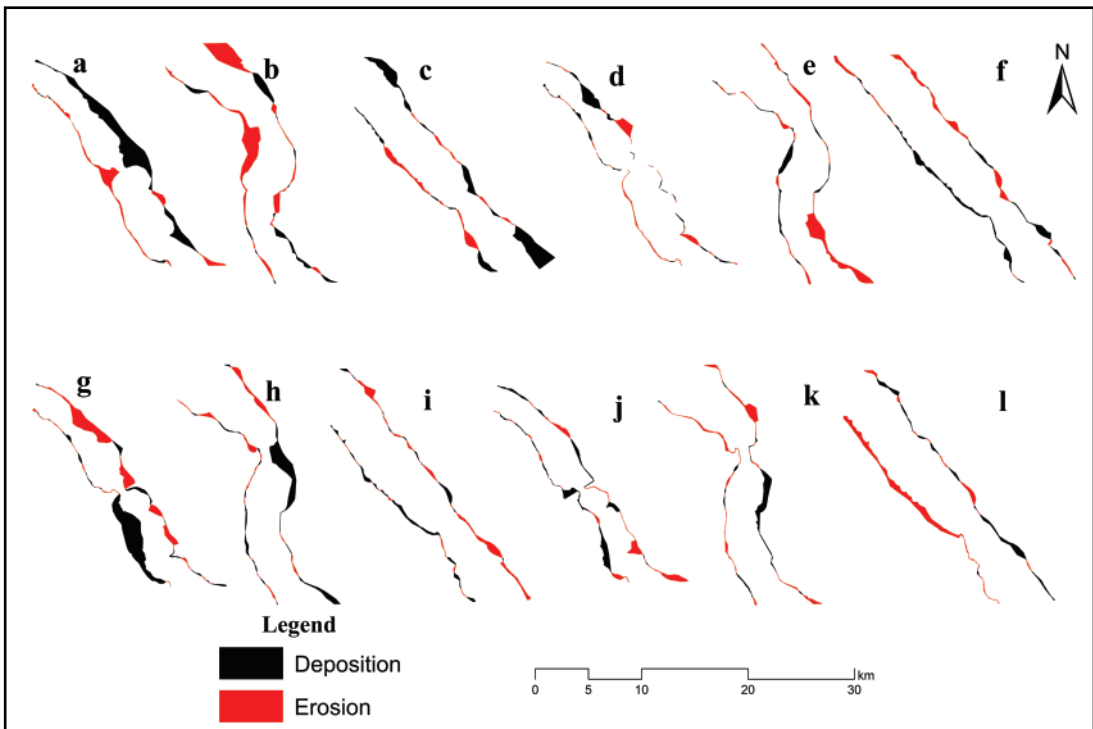


Figure 9. Showing Reach wise erosion and deposition activities in four temporal period- 1978 to 1990, 1990 to 2000, 2000 to 2010 and 2010 to 2020 respectively with alphabetical order subsequently. Reach 1 (a, d, g and j); Reach 2 (b, e, h and k) and Reach 3 (c, f, i and l).

Conclusion:

The Teesta river originated from the north eastern tip of Sikkim and joins the mighty Brahmaputra in Bangladesh. The present study in Daur's region of West Bengal is from the Sevoke to Bangladesh border. Daur's region is one of the most geopolitically sensitive and has also undergone drastic land use changes in recent years. The river's hydro dynamic in

the region has been transformed by anthropogenic activities. The longitudinal profile of the river in the study area has been divided into three Reaches in order to understand properly. The Reach 1 which located at piedmont of Himalaya is the least anthropogenic intervention among three reaches in term settlement, embankment and spurs whereas 97% of sand and stones quarrying are taken place. In this reaches one barrage is located at Gajoldoba. Before the barrage, the width of river at point of barrage was 4.6km and after the completion of barrage, the river width reduced to less than one km and due to reduce in width increase velocity of flow which affected gradient of the channel, deposition and erosion. Near the barrage, gradient is found deeper and elevated downward. In the upper part of barrage, there was huge sand island before construction but after construction, upper sand bar and island has disappeared due high velocity and deposited to lower part of the barrage. The Reach 2 is highly engineered section of the river in term of embankment, spur, bridges and railway line across the river, rapid urbanization as Siliguri city is the fastest growing city in West Bengal and intensive agricultural areas etc. It is also found that most substantial transformation in hydro morpho dynamic in the river which affect not only in the reach itself but also in upper and lower reaches. Because of embankment, spur and bridges across the river, the channel becomes more straighten, narrowed that increase velocity of discharge, erosion subsequently influence to channel gradient, size of sediment deposition etc. A bridge and railway line across the river at Domohain reduced width of the river from about 2km to 1 km. This reduction in channel width increases velocity and shifting of sand bar and sand island from upper to lower of the bridge and channel become steeper gradient near the barrage. The Reach has got maximum embankment with 83.7% and 99% embankment on right bank. The Reach has maximum spurs also with 44.6%. The reach 3 has also lesser engineered than reach 2 but more than reach 1. The behavior of the both banks of the channel are different. The left bank was less erosive but recently it becomes highly erosive because right bank has got maximum embankment and spurs due to rapid urbanization and properties. Major hydro morphic changes of the rivers due to anthropogenic activities can summarized in term of erosion and deposition that till 1990 erosion and deposition were haphazard on both banks and right bank had been affected by huge erosion and on left bank had huge deposition. After 1990, it becomes vice versa, erosion on left bank and deposition on right bank due embankment and erosion on left bank. After 2010 onward, erosion and deposition on both banks become more stable and less because both the banks have got massive embankment. This shows river becomes more stable due to heavy engineering works.

References:

- Alexander, J. S., Wilson, R. C., & Green, W. R. (2012). A brief history and summary of the effects of river engineering and dams on the Mississippi river system and delta. Department of the Interior, US Geological Survey.
- Ashmore, P., & Parker, G. (1983). Confluence scour in coarse braided streams. *Water Resources Research*, 19(2), 392-402.

- Best, J. (2019). Anthropogenic stresses on the world's big rivers. *Nature Geoscience*, 12, 7–21. <https://doi.org/10.1038/s41561-018-0262-x>
- Blom, A., Arkesteijn, L., Chavarrias, V., & Viparelli, E. (2017a). The equilibrium alluvial river under variable flow and its channel-forming discharge. *Journal of Geophysical Research: Earth Surface*, 122, 1924–1948. <https://doi.org/10.1002/2017JF004213>
- Blom, A., Chavarrias, V., Ferguson, R. I., & Viparelli, E. (2017b). Advance, retreat, and halt of abrupt gravel-sand transitions in alluvial rivers. *Geophysical Research Letters*, 44, 9751–9760. <https://doi.org/10.1002/2017GL074231>
- Blom, A., Viparelli, E., & Chavarrias, V. (2016). The graded alluvial river: Profile concavity and downstream fining. *Geophysical Research Letters*, Vol. 43. <https://doi.org/10.1002/2016GL068898>
- Buijse, A. D., Coops, H., Staras, M., Jans, L. H., van Geest, G. J., Grift, R. E., et al. (2002). Restoration strategies for river floodplains along large lowland rivers in Europe. *Freshwater Biology*, Vol. 47(4), 889–907. <https://doi.org/10.1046/j.1365-2427.2002.00915>
- Downs, P. W., & Gergory, K. J. (2004). *River channel management: Toward sustainable catchment hydrosystems*. London.
- Ghising, A.K. (2024). The Siliguri Corridor: A Historical Analysis of Geo- Political Vulnerability in Eastern India. *International Journal of Social Science Research And Review*, Vol 7 (4). Pp 217-228.
- Government of West Bengal, (2020). *Survey District Report of Jaipauri (For Mining of Minor Minerals)*
- Habersack, H., Jger, E., & Hauer, C. (2016). The status of the Danube river sediment regime and morphology as a basis for future basin management. *International Journal of River Basin Management*, Vol. 11. <https://doi.org/10.1080/15715124.2013.815191>
- Harmar, O. P., Clifford, N. J., Thorne, C. R., & Biedenharn, D. S. (2005). Morphological changes of the Lower Mississippi River: Geomorphological response to engineering intervention. *River Research and Applications*, Vol. 21. <https://doi.org/10.1002/rra.887>
- Hiemstra, K. S., van Vuren, S., Vinke, F. S. R., Jorissen, R. E., & Kok, M. (2020). Assessment of the functional performance of lowland river systems subjected to climate change and large-scale morphological trends. *International Journal of River Basin Management*. <https://doi.org/10.1080/15715124.2020.1790580>
- Hohensinner, S., Jungwirth, M., Muhar, S., & Schmutz, S. (2011). Spatio-temporal habitat dynamics in a changing Danube River landscape 1812–2006. *River Research and Applications*, Vol. 27. <https://doi.org/10.1002/rra.1407>
- Mackin, J. H. (1948). Concept of the graded river. *GSA Bulletin*, Vol. 59. [https://doi.org/10.1130/0016-7606\(1948\)59](https://doi.org/10.1130/0016-7606(1948)59)
- Marsh, G. (1864). *Man and nature*. New York, Charles Scribner.
- McFeeters, S.K. (1996) The Use of the Normalized Difference Water Index (NDWI) in the Delineation of Open Water Features. *International Journal of Remote Sensing*, 17. <http://dx.doi.org/10.1080/01431169608948714>

- Meetei L. I., Pattanayak, S. K., Bhaskar, A., Pandit, M. K. & Tandon, S. K. (2007). Climatic imprints in Quaternary valley fill deposits of the middle Teesta valley, Sikkim Himalaya. *Quaternary International*. Vol. 159(1). Pp. 32–46. doi:10.1016/j.quaint.2006. 08.018
- Ministry of Environment and Forest, Govt. of India (2005). Carrying Capacity Study of Teesta Basin In Sikkim. Vol-IV, Water Environment. Centre for Interdisciplinary Studies of Mountain and Hill Environment, University of Delhi.
- Pasiok, R., & Stilger-Szydło, E. (2010). Sediment particles and turbulent flow simulation around bridge piers. *Archives of Civil and Mechanical Engineering*, Vol. 10(2), 67-79.
- Quick, I., König, F., Baulig, Y., Schriever, S., & Vollmer, S. (2020). Evaluation of depth erosion as a major issue along regulated rivers using the classification tool Valmorph for the case study of the Lower Rhine. *International Journal of River Basin Management*, Vol. 18(2).<https://doi.org/10.1080/15715124.2019.1672699>
- Singha, A.K. and Elangbam, I.S. (2025). Hydro-dynamics of the Teesta River and its Implication on Riparian villages in Duars Region, West Bengal. *Spixiana*, Vol. 9 (3) <https://doi.org/14.4016.spixiana.2025.9.3.018>.
- Surian, N., & Rinaldi, M. (2003). Morphological response to river engineering and management in alluvial channels in Italy. *Geomorphology*, 50(4), 307–326. [https://doi.org/10.1016/S0169-555X\(02\)00219-2](https://doi.org/10.1016/S0169-555X(02)00219-2)
- Thomas, W. L. (1956). *Man's role in changing the face of the earth*. Chicago, University of Chicago Press.
- Uehlinger, U. F., Wantzen, K. M., Leuven, R. S., & Arndt, H. (2009). The rhine river basin. In K. Tockner (Ed.), *Rivers of Europe*. London, UK: Academic Press.
- Xu, H. (2006) Modification of Normalized Difference Water Index (NDWI) to Enhance Open Water Features in Remotely Sensed Imagery. *International Journal of Remote Sensing*, Vol. 27.<http://dx.doi.org/10.1080/01431160600589179-1>



A GIS Based Evaluation of the Geomorphological Characteristics of Dikrong River Basin, Assam, India

Manisha Pathak^{1*}, Pranati Sarkar¹

¹*Department of Geography, School of Earth Sciences,
Assam University Diphu Campus, Diphu, Karbi Anglong, Assam –782462*

**Corresponding author: pathakmanisha708@gmail.com*

Abstract: The quantitative analysis is essential to determine the geomorphic features of a drainage basin which will help to understand the different hydrological behavior as well as to determine the geomorphic hazard of a river basin. In the present study, a quantitative analysis has been carried out by applying the remote sensing and GIS tools to evaluate the geomorphic behavior of the Dikrong River basin. The morphometric parameters were evaluated from the CARTOSAT DEM by examining three aspects namely linear, areal and relief aspects respectively. The output of the analysis found that the upper catchment areas and the central part of the Dikrong River basin covered by high relief with a steep slope and the elevation gradually decreased towards the lower part of the basin. The high runoff and sufficient flow of water with low infiltration rate indicate the high flood risk in the low-lying areas of the basin. The finding of the present study will help to understand morphological characteristics of the River that helps to the planner for the sustainable management of the watershed.

Keywords: Quantitative analysis, GIS & Remote sensing, CARTOSAT DEM, Dikrong River

Introduction:

The natural resources like land and water etc. are limited on the earth and uses of these resources increasing in present days as a result, the expansion of the developmental activities. Therefore, a sustainable development and conservation of the resources are essential for the future development and for that management of the watershed is required to conserve the

resources and attaining the sustainable development of the resources (Choudhari, P.P., et al., 2018). The drainage basin is the primary geomorphic unit and its detail analysis helps to measure the hydrological, evolutionary and geological processes of the watershed which is significant for the management of a watershed (Saha, S., et al., 2022). The hydrological, topographical features and the geology of an area are interrelated with each other and the quantitative study can be used to determine the link between form and the size of an area. The runoff characteristics, form of a basin, development of a basin area, sediment deposition all are result of the processes of hydrological activity of a River which are understood and assessed through the measurement of statistical analysis. Therefore, the quantitative technique is necessary to identify the geomorphic features such as sites of water storage, the potential of ground water and runoff behavior etc. Morphometric techniques are a statistical investigation of the different features and dimensions of the earth's surface (Horton, 1945; Strahler, 1952). Horton in 1945 first proposed statistical techniques to determine the drainage network of a river, and Strahler explained in the year of 1957. The traditional method of the quantitative study of River basin is time consuming and requires resources as well as the human effort, since the researchers need to conduct the field surveys to collect data and also extracting the hydrological analysis by using toposheet is also time consuming.

The development of remote sensing and GIS in the field of geomorphological studies makes the process more specific and cost efficient and GIS tools can easily process high resolution DEM to conduct the hydrological investigation (Chowdhury, Md. S., 2024). The combination of GIS and remote sensing is suitable for the study of large scale area and the high resolution spatial data can provide the accurate results and help to solve the complicated problem in the quantitative study of the different aspect of a River (Shekar, P.R., & Mathew, A., 2024). The combined use of GIS and remote sensing data makes it possible to access the details of runoff rate, infiltration and the ground water potentiality of a drainage basin. GIS technology can manage large area investigations of stream pattern, anomaly analysis, land use changes, and can handle large sized databases of a watershed (Vinothkumar, R., et al., 2016). Thus, the application of Geospatial technology, along with remote sensing data, is an efficient and necessary method for detailed geomorphic evaluation of a watershed (Singh, M.C., et al., 2023).

In recent decades, the remote sensing and GIS technology have been used for management of watershed and sub watershed prioritization, as well as to detect the susceptibility of fluvial hazard such as flash flood, river bank erosion etc., within a River basin (Obeidat, M., et al., 2021). The measurement of different sub morphometric parameters, such as linear, areal and relief aspects provide the geological and hydro-geomorphological details of a watershed. Morphometric features are simple approach that can be applied for the assessment and protection of natural resources and determine the intensity of flash flood of a watershed (Charizopoulos, N., et al., 2019).

There are different aspects under the analysis of the morphometrical study of a river basin, and each parameter can describe the different hydrological features such as the probability of flood and erosion, sediment flow etc., of a particular drainage basin. Thus, the result of

the statistical analysis is not only essential for the management of a watershed and resource conservation but also useful for discipline such as the management of agriculture. It also helps to understand the ecosystem of a River. The Dikrong River basin is a one of the Dynamic North bank tributaries of Brahmaputra, originated in the high Arunachal Himalayan Mountains and covers two states of India with large catchment areas. The Dikrong River, like other alluvial river has experienced several geomorphological hazards such as bank erosion and annual flooding during every monsoon season. A quantitative measurement is essential in the river basin to identify the influencing parameters of the occurrence of fluvial hazard as well for sustainable watershed management, to mitigate the hazard in the future. The present study has to evaluated the geomorphological characteristics of the Dikrong river in Assam, and its result will be helpful for the policy makers and the planners to understand the morphology and determine the scientific conservation policy for the resources of the river basin.

Study Area:

The Dikrong River covers two states of India viz. Assam and Arunachal Pradesh and it is the

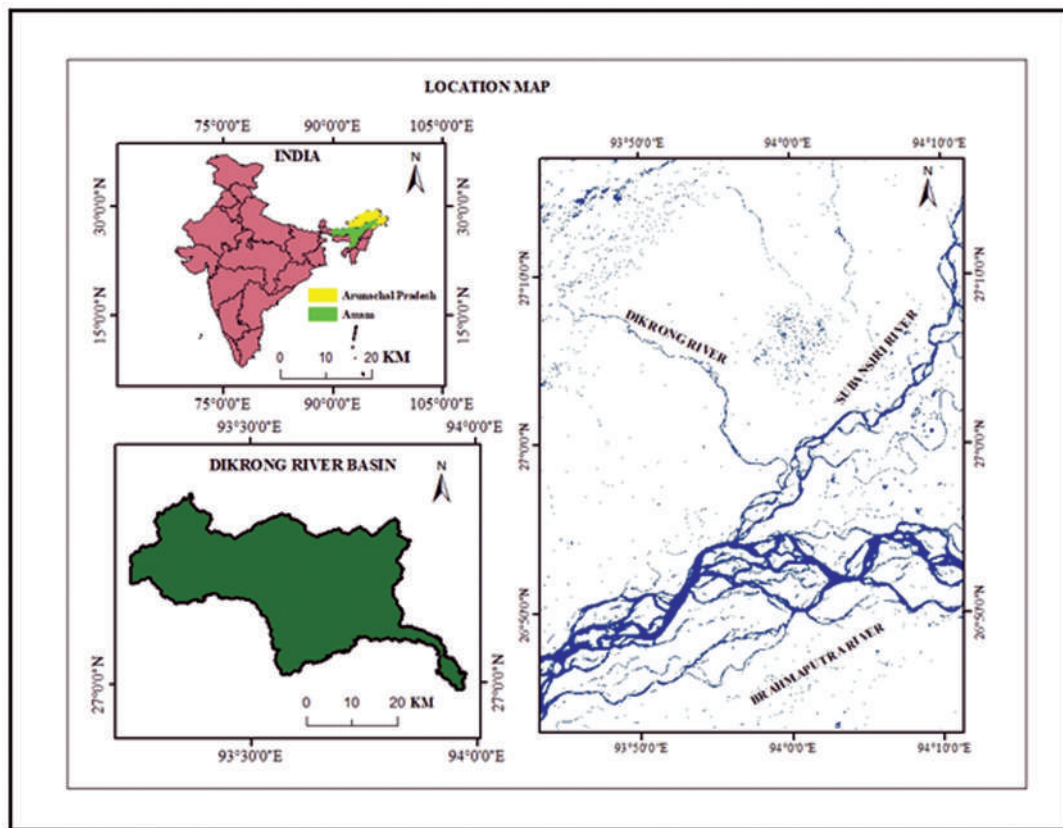


Figure 1. Location of the Dikrong River basin.

sub tributary of the Subansiri River which is a tributary of the mighty Brahmaputra River. (Figure 1 shows the location map of study area). The river flows from the hilly areas of the Papumpare district of Arunachal Pradesh towards the plain areas of the Lakhimpur district of Assam and finally joins the Subansiri River. The basin area of the Dikrong River is located between the 26°56'33" N to 27°43'66" N latitude and 93°48'37" E to 93°48'35" E, respectively. The upper section of the basin experience severe cold climate during winter with a high rainfall in summer season, while a humid type of climate is found in the lower parts of the basin area. During the monsoon season, the basin area experience more than 1500 mm annual rainfall and an average temperature 37°C in summer and 10°C winter. The Dikrong river basin can be classified into two topographic regions; one is piedmont hills and lower alluvial plains of the Brahmaputra River. The upper catchment areas of the basin have an uneven topography with a steep slope while the lower catchment areas consist of low-relief areas. The watershed which frequently experiences flash flood during the monsoon season.

Data:

A detail quantitative evaluation was performed in the Dikrong River basin to examine the geomorphic features of the River. In the study, the CARTOSAT DEM was used to extract the contours, drainage network and the analysis of the geomorphic parameters performed in the GIS (Geographic Information System) tools. The Survey of India (SOI) toposheets with a scale of 1:50,000 were also applied in the present study along with the digital elevation model to determine the drainage characteristics of the River.

Methodology:

Drainage network extraction:

In the study, both the SOI toposheet and the CARTOSAT DEM were used to conduct the detail evaluation of the drainage network (table1 shows details of data applied in the present study). The watershed of the River basin delineated from the DEM and base map of the basin prepared from the SOI Toposheet. The drainage network of the Dikrong River basin extracted from the CARTOSAT DEM by using the geoprocessing tools of the GIS software and Strahler method applied for determine the stream ordering of the drainage basin. The geomorphic study is classified into three section which are linear, areal and relief and each sub parameters of the river were measured by using the standard formula and analyzed the impact of each parameter on the geomorphology of the river basin. The methodology applied to measure the quantitative evaluation and it results are mention in the flow charts in Fig 2.

Table 1. Details of data applied in the present study.

Data Type	Scale/Resolution	Source
Toposheet	1:50,000 scale	Survey of India
CARTOSAT DEM	30 meter	Bhuvan

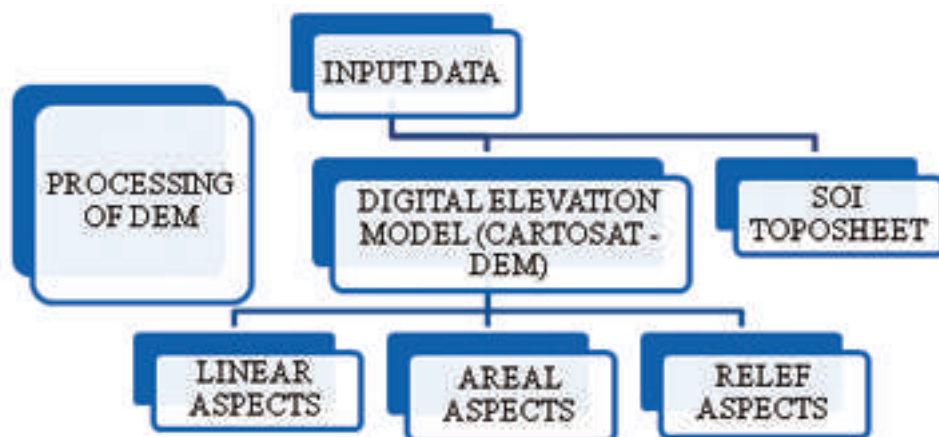


Figure 2. Flow chart of methodology.

Result and Discussion:

The geomorphic aspect are categorized into linear, areal and relief aspects and analyzed the relation between the results of each parameters with the hydrological processes of the River.

Linear parameters of the Dikrong River:

The linear parameters used to determine the development of drainage pattern and the features drainage network that useful to identify the geological and topographical structure of a River basin.

Stream order:

The primary step of the quantitative study is the analysis of the stream ordering. In the present study, the Strahler's method (1952) of stream ordering is applied and it is observed from the analysis that the Dikrong River is a sixth order River basin with the highest frequency of the basin is first order stream. The number of stream order decreases with the increasing order of stream (Figure 5A, shows the stream order map of Dikrong river basin) and the presence of maximum stream order in the basin indicate the possibility of maximum surface water in the basin and it also revealed the potentiality of the occurrence of flood in the river basin. The distribution of stream order and number of a River basin influenced by the topography and the physiographical properties of the area.

Stream number (Nu):

The number of stream one of the essential morphometric features of a River basin which used to determine the flow characteristics of water. As per the Horton (1945), the maximum number order stream recorded the first order stream. The presence of maximum number of stream indicate the minimum infiltration rate and more flow of water. The calculation of the present

study has shown that the stream number of 1st, 2nd, 3rd, 4th, 5th and 6th order are 1123, 256, 61, 15, 4 and 1 respectively. Thus it has shown a decreasing number of streams according to the increasing order and the study revealed that the Dikrong River has sufficient flow of water.

Bifurcation Ratio (Rb):

The value of Rb varies due to the changing topography and geological features of a River basin. The value of Rb used to determine the surface water flow characteristics of a river basin and indicates the potentiality of the occurrence of flood hazard of a basin. Horton proposed the average value bifurcation ratio in 1945. The high value of Rb found in the highly dissected areas and minimum value observed in the low relief areas. In the study, order wise Rb value has calculated and it is found that the high Rb value observed in the lower order stream and it gradually decreases with increasing order except in 4th order stream. The Rb value of 4th stream order has shown a lower value which indicates the distortion due to the geological component. The Rb value of the Dikrong River basin is 4.08 which indicate the high probability of the occurrence of flood in the basin (Table 2, Figure 3 shows the bifurcation ratio of Dikrong river basin) and the calculated value of Rb also represent that the drainage basin is highly dissected with high runoff.

Table 2. Bifurcation Ratio.

Stream Order	Stream Number	Bifurcation Ratio	Rb
1	1123	4.39	4.08
2	256	4.20	
3	61	4.07	
4	15	3.75	
5	4	4.00	
6	1		

Weighted Mean Bifurcation Ratio (Rbw):

The Rbw is measured to determine the form and the identify the impact of lithological features on the drainage pattern of a River basin and the Strahler in 1952 first applied in the measurement of Rbw in the study of River morphology. The Rbw of the Dikrong River is 4.33 and it represents the elongated form of the basin with high possibility of erosion activity.

Stream length (Lu):

The measurement of order wise the stream length of a river basin helps to measure the topographical, hydrological characteristics of a River basin. The presence of minimum elevation of a Basin generally showing the maximum stream length whereas the high gradient area with fine texture showing the minimum length of stream. Graphically, it represents in a

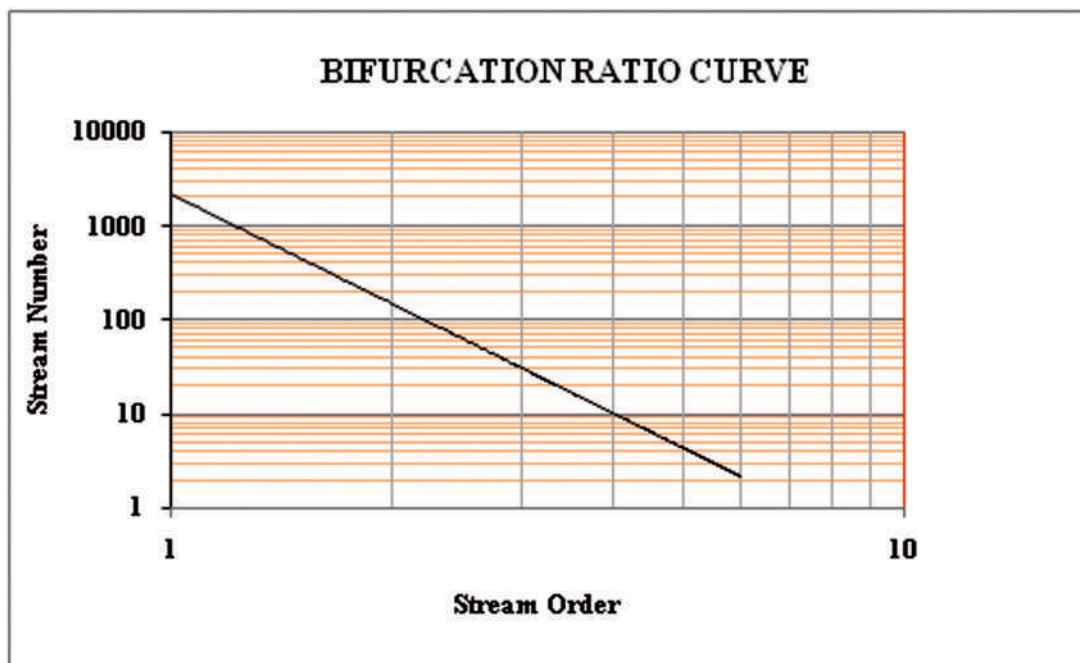


Figure 3. Bifurcation ratio curve.

logarithm graph where stream length plotted against the stream order and the pattern of the graph helps to determine topographical features of the basin (Table 3 & Figure 4 represent the stream length of the basin).

Table 3. Order wise stream length ratio.

Stream Order	Stream length (km)	Mean stream length (km)	Cumulative mean stream length (km)	Stream Length ratio
1	653.64	3.26	3.26	1.54
2	344.54	1.77	5.03	1.21
3	145	1.04	6.07	1.02
4	58.4	0.14	6.21	1.02
5	103.76	0.11	6.32	
6	35.43	35.43		

Sinuosity Index (SI):

The sinuosity index is used to measure the variability of the River channel pattern of River basin. The sinuosity calculated by dividing the length of the River channel by the length of the valley. Generally the River channel having value more than 1.5 is known as meandering river

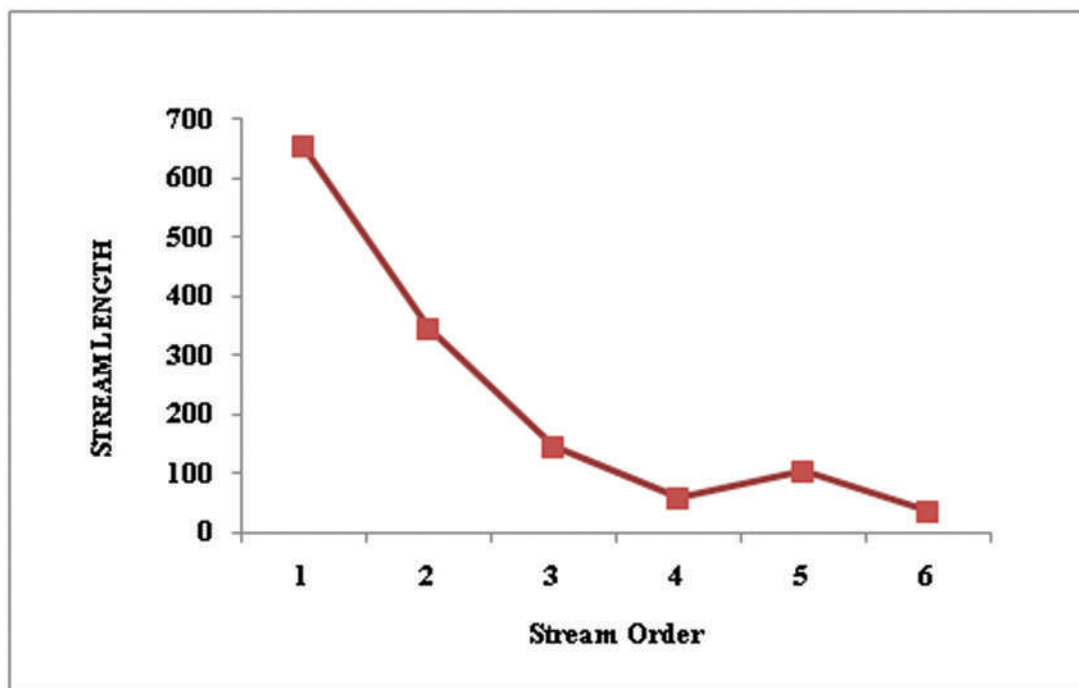


Figure 4. Law of stream length.

and below 1.5 is called sinuous. The SI value of the Dikrong River basin is 1.77 which is more than 1.5 and thus the Dikrong River is a meandering River. Muller in 1968 applied two types of method used to determine the sinuosity which is hydraulic sinuosity index and topographic sinuosity index (Table 4 indicates Hydraulic & Topographic Sinuosity Index). The value of the Hydraulic Sinuosity Index of the River basin revealed that 45.64% has impact the sinuosity of the River by the different hydraulic properties of the River such as water runoff, discharge etc. The value of TSI indicate that 55.67% topographic properties influenced the sinuosity of the Dikrong River basin such as soil texture, seismic activities etc.

Table 4. Hydraulic and Topographic Sinuosity Index.

Parameters	Result
Hydraulic Sinuosity Index (HSI)	45.64
Topographic Sinuosity Index (TSI)	55.67

Areal Parameters of the Dikrong River:

Evaluation of the different areal parameters of a River is essential to determine the geometric properties of a River such as the drainage form, drainage pattern, stream frequency and infiltration capacity etc.

Basin Area (A) and Basin Perimeter (P):

The basin area of a drainage basin is essential component to understand the hydrological characteristics and the lithological features of a River basin. The perimeter of drainage is another important component of geomorphological studies that represent the boundary of a watershed. The minimum length of perimeter represent the circular form of a basin and maximum length indicating the elongated structure of a drainage basin. The total basin area and the perimeter of the Dikrong River basin are 1331.54 Km² and 288.18 Km.

Length of the basin (Lb):

The basin length is the measurement of maximum length of a drainage basin parallel to the main channel of the basin (Schumm, 1956). The basin length of the Dikrong River is 74.60 Km.

Stream Frequency (F):

The number of stream per unit area is known as stream frequency (Horton, 1945) and it measures to identify the hydrological features of a River basin such as the water flow, availability of surface and ground water etc in a drainage basin. The value of the properties of stream frequency influenced by the drainage texture and the rock properties of a basin area. The high flood frequency value will observe in a River basin where low infiltration rate and hard rock materials are presence. The stream frequency of the Dikrong River basin is 1.09 that represents the low infiltration rate with steep gradient and high runoff rate.

Form Factor (Ff):

The value of form factor measured from the basin area and the square of the length of the drainage basin (Horton, 1932). The Ff determine the duration of water flow within a River basin and the shape of the basin. The low Ff value indicate the elongated shape with a minimum peak flow of maximum duration of time, whereas maximum Ff value represent the circular form of the basin and high peak flow with shorter duration of time. The Ff value of the Dikrong River basin is 0.23 which represent the elongated form of the basin with a longer duration of water flow.

Infiltration Number (If):

The product of drainage density and frequency is infiltration number (Df). The maximum value of infiltration number represents the high runoff with a low rate of infiltration and that type of basin, more prone to the occurrence of flood. On the other hand minimum value indicates the low runoff and high rate of infiltration where as the low value represent the minimum infiltration rate with high runoff. The infiltration rate of the Dikrong River basin is 1.09 and it represents the minimum infiltration rate with maximum runoff rate.

Circulatory ratio (Rc):

The circulatory ratio of a drainage basin used to measure the shape of a basin and it value

varies from 0 to 1 (Miller, A.A., 1953). The value of R_c near 1 represent the circular form of a basin whereas the R_c value near 0 indicating the elongated form of a basin. The River which are originated in the mountainous region and flow towards the plateau and hilly region are more in elongated in shape. The R_c value of the Dikrong River basin is 0.2 which represent the elongated form of the drainage basin and also indicate the presence of structural disturbances.

Texture Ratio (Dt):

The texture ratio of a River basin calculated by dividing the number of first order stream to the perimeter of the drainage basin (Adhikary, P.P., & Dash, J., 2018). The value of the R_t depends upon the number factors such as the relief properties of the landscape, rate of water permeability etc. The texture ratio of the Dikrong River is 3.89, representing the minimum potentiality of the occurrence of soil erosion.

Shape Factor (Bs):

The shape factor of a River basin calculates to measure the erosion rate. The minimum value of B_s indicates the rate of erosion is low in the basin whereas high B_s value represents the high rate of erosion rate. The B_s value of the Dikrong River basin is 4.17, it indicate the rate of erosion is maximum in the basin.

Constant of channel maintenance (C):

The inverse of drainage density is the constant channel of maintenance and the value of it depend on the geological and climatic properties of a region. The high value of C indicates the maximum permeability with resistant type of rock with vegetation covered area. Whereas low value of C represents the low resistant of rock type with absence of vegetation cover and minimum permeability. The constant of channel maintenance of the Dikrong River is 1 indicates the good coverage of vegetation with resistant rock type presence in the watershed.

Length of overland flow (Lo):

The length of overland flow is used to determine the information of the water flow path and it value depends on the relief properties of the terrain. The length of overland flow is an important component affecting hydrological and physiographical properties of River basin. The relief properties of drainage basin is an important controlling component of the value of Length of overland flow. The high value of L_o found in the River basin slope of the basin is steep and minimum L_o observed in the areas of gentle slope. The L_o value of the Dikrong River basin is 0.5 which indicate the long flow path of the basin with a gentle slope and it also revealed that the surface water will take maximum time to reach the stream channel in the basin.

Drainage density:

The drainage density of a drainage basin denotes the total stream length within a particular area (Shekar, P.R., & Mathew, A., 2024). The analysis of drainage density determines the

spacing of stream which influence the surface runoff as well as the permeability rate of a drainage basin and it represent in km/Km^2 or m/m^2 . The drainage density of a River basin measures by applying the different geomorphometric factors, elevation, seismicity, rock properties, climate, forest and vegetation type (Zavoianu, I., 1985). As per the calculated value of Dd, the Dikrong River basin is classified into five classes of drainage density from very low to very high. (Table 5 shows the categories of Dd). The low drainage density observed in the areas where dense vegetation, low relief with permeable rocks is found whereas high drainage density area indicating the presence of sparse vegetation covers impermeable rocks material with high relief (Figure 5B, represent Drainage density map). The maximum drainage density of the river basin represents the maximum runoff and sufficient surface water flow.

Table 5. Different Categories of drainage density.

Drainage density (per km^2)	Classes
< 1.50	Very low
1.51 – 3.00	Low
3.01 – 4.00	Moderate
4.01 – 5.00	High
> 5.00	Very High

Drainage pattern:

The arrangement of the stream network is known as drainage pattern that developed by the rivers, streams and lakes in a River basin (Tufu, F.G., & Feyissa, T.A., 2018). The topography, geological structure, slope etc are responsible for the drainage pattern of a particular River basin. The dendritic pattern of drainage found in the Dikrong River basin that indicates the presence of homogenous rock materials in the watershed.

Relief Parameters:

The measurement of relief of an area used to identify the topographical features that also help to determine the risk zone of soil erosion of a watershed. In the present study, the relative relief, dissection index and slope parameters have analyzed to understand the relief properties and its influence on the fluvial processes of the river basin.

Relative Relief:

The difference between the highest and lowest relief of the River basin is known as relative relief. The relative relief maps provide the topographical variability and it influences on the runoff properties as well as the erosion and depositional activities of a River basin. The Dikrong River basin is classified into five numbers of classes as per the value of relative relief of the basin viz., very low, low, medium, high and very high respectively (Table 6 shows categories of relative relief). The resulted relative relief map of the Dikrong River basin

represent that presence of high elevation in the upper section of the North Western part of the basin influence the maximum flow of water with high erosion processes and it carries the eroded material towards the southern part of the watershed. The elevation gradually decreases towards the southern part of the watershed and very low relief observed in that areas which represent the drainage basin experience high-rate deposition in the low-lying areas of the basin and the areas frequently affected by the heavy flood during the monsoon period of time (Figure 5C shows relative relief map of Dikrong river basin.)

Table 6. Categories of Relative relief.

Relative Relief in meter	Category
< 370	Very Low
371 – 700	Low
701 – 1030	Medium
1031 – 1361	High
> 1361	Very High

Dissection Index (DI):

The intensity and the nature of the properties of soil erosional activities in a particular area are identify by the dissection index. The dissection index also determines the stage of erosional cycle of an area or a drainage basin as well as it can identify the surface material properties of the area based on the DI value. The minimum DI value indicate the mature stage of the erosion with low erosional activities and the less number of stream network. On the other hand the maximum DI value represents the availability of hard rock with maximum number of streams. The Dikrong River is classified into five categories as per the calculated value of DI from very low to very high (Table 7 represent categorization of Dissection Index). The dissection map of the Dikrong River has shown that the upper catchment areas of the basin experiences low rate of erosion and it gradually increases with decreasing altitude and the high rate of erosion found in the southern part of the middle section of the basin (Figure 5D, represent the Dissection Index map of Dikrong river).

Table 7. Categories of Dissection Index.

Dissection Index	Category
< 0.50	Very low
0.51 – 0.60	Low
0.61 – 0.70	Moderate
0.71 – 0.80	High
> 0.80	Very high

Slope:

The slope map helps to determine the topographical variability and its impact on the direction of water flow and the velocity of water. It also helps to identify the properties of infiltration and erosional processes in a drainage basin. The gentle or level slope has a reverse relation with the soil erodibility and steep slope has shown the direct relation with it. The low rate of infiltration will be found in the steep slope areas and gentle slope indicate the maximum infiltration capacity of a particular area. As per the calculated value of slope in the present study, the Dikrong River basin is classified into five different classes from level slope to very steep slope (Table 8 E, indicates categories of slope). The slope map of the Dikrong River has shown that the level and gentle slope observes in the southern section of the plain areas of the basin and the moderate slope found more or less all over the area of the watershed except the plain areas of the basin. The steep slope and very steep occupied the high elevation areas of the upper section of the basin (Figure 5E) represent slope map of Dikrong River basin).

Table 8. Categories of Slope

Slope (in degree)	Category
< 8.00	Level
8.01 – 16.00	Gentle
16.01 – 24.00	Moderate
24.01 – 32.00	Steep
> 32.00	Very Steep

Discussion:

The geomorphic analysis of a River basin is essential to determine its lithological and hydraulic properties, as well as their impact on the geomorphic behavior of the basin. It also helps identify the fluvial originated disaster and helps to determine the mitigation measures. The geomorphic analysis of the all-important parameters of the Dikrong River basin was conducted and the results provide information on the hydrological parameters along with their influence on the dynamic geomorphic processes of the river basin. The present analysis revealed that the application of high-resolution DEM with use of GIS tools make it easy to measure the geomorphic parameters with high accuracy. The analysis of the linear features of the river basin indicates that the maximum probability of the sufficient flow of surface water flow associate with the possibility of the flooding and erosion activities within the watershed. The meandering nature of the Dikrong River channel revealed that both the topographic and hydraulic factor plays a prominent role in the meandering nature of the river channel. The maximum number of the distribution of 1st order stream in a basin represent the sufficient flow of water within the watershed and water accumulation in the lower catchment areas of

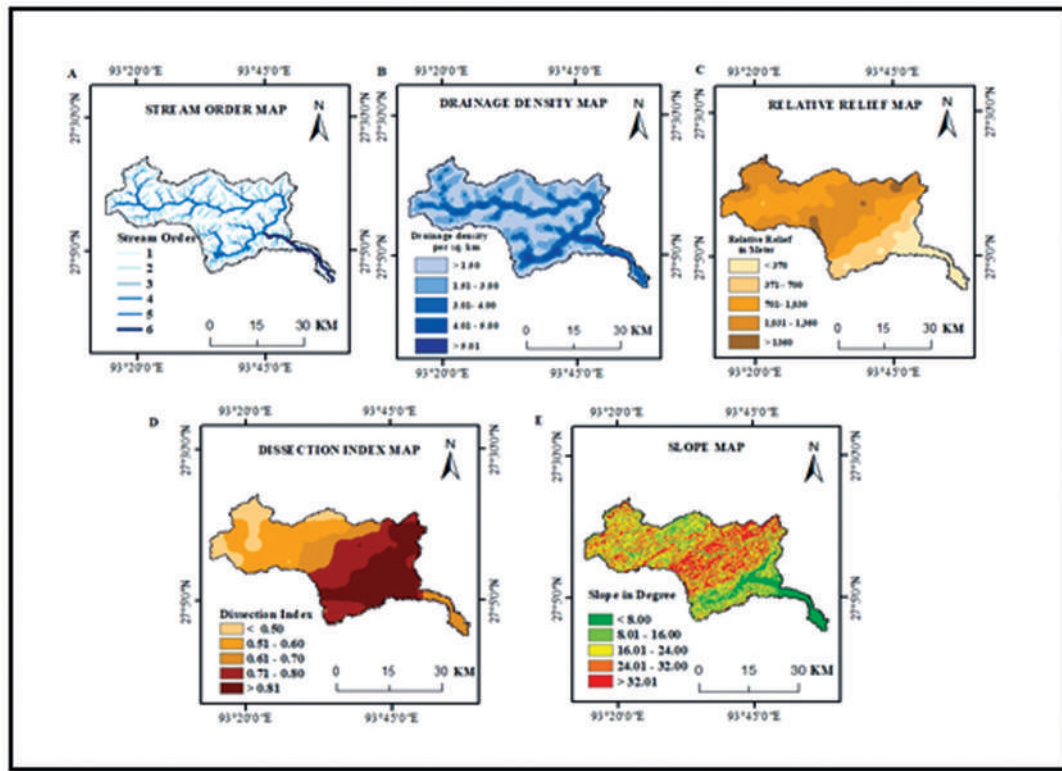


Figure 5. Law of stream length.

the basin (Kumari, P., *et al.*, 2021). In Dikrong River basin, the number of 1st order streams is highest and they are distributed across the maximum portion of the basin. This indicates that river basin experiences maximum flow of water and possibility of flash flood in the lower section of the Brahmaputra plain areas of the watershed. The decreasing number of stream length ratio from lower to higher order represents the youthful stage of fluvial system. The region falls under an active tectonic zone, which affects the stream pattern of the drainage basin (Subrahmanyam, K., *et al.*, 2005).

The areal parameters of a River basin provide the essential information about the structure, form, texture along with the hydrological properties of the watershed. The Dikrong River occupies an area of 1331.54 Km² indicating that the basin carries sufficient volume of surface water, allowing flow through the basin for a long duration of time. This also represent a possibility of high flood risk in the basin area. The maximum infiltration value of a River basin indicate the minimum rate of infiltration with high rate of runoff in the catchment (Bhatt, S., & Ahmed, S.A., 2014). The results of the value of Infiltration of the drainage basin revealed that the River basin experienced low rate of infiltration with high runoff rate. The

Dikrong River basin has long flow path with a value of 0.5 that represent the possibility of flood occurrence in the basin. The dendritic stream pattern mostly found in the areas with homogenous rocks is found without an impact on the structure of geological features of a basin (Pareta, K., & Pareta, U., 2011). The dendritic pattern of drainage indicates the presence of homogenous rock materials in the watershed.

The relief aspects of the river basin indicate that the high relief presence in the northwestern part of the upper and central part of the basin while low relief found in the southwestern part of the basin. The dissection map of the Dikrong River basin illustrates the erosional processes of the basin, values near 0 represent absence of erosional processes whereas value near to 100 indicates maximum erosion rate (Mishra, A.K., & Rai, S.C., 2020). The maximum erosion activities occur the southern part of the middle section of the basin. The slope map of the river basin not only provides the gradient features of the basin but also indicates the water flow direction and erosion activities in relation to the infiltration rate. The maximum steep slope presence in a basin represents the greater erodibility of the area (Rai, P.K., *et al.*, 2018). The Gentle slope is found in the lower part of the basin and steep slope mostly observe in the middle section and some section of the upper part of the basin.

The study is conducted on Dikrong River of Lakhimpur district, which is also well known for its flood disaster, the village dwellers of the district suffer numerous problems due to bank erosion and flood, as these disasters have devastated many infrastructures, agricultural land. Therefore, it is necessary to study the geomorphological characteristics of the basin so that it will be convenient to implement the remedial measures in the highly effected region. Furthermore, it is also significant for further studies of planners to manage and conserve the water resources. Although, the study has some constrains such as, very minimum study has been conducted on Dikrong River, therefore, there has been very limited literature survey on this river basin.

Conclusion:

It is observed from the result of the analysis that the Dikrong River basin has sufficient flow water and the longer flow path indicate the possibility of the occurrence of flood in the surrounding Riverine areas of the basin. The high relief with steep slope covered the middle and upper section of the basin that influence the erosion rate, runoff and infiltration rate of the basin. The Dikrong River basin has high runoff rate with low infiltration rate and the high rate of erosion activities found in the middle section of the basin which indicate that the deposition of the sediments occurs in the lower part of the basin and high flood risk found in the south eastern part of the Dikrong River basin. The detail evaluation of the geomorphic parameters of the Dikrong River may help the planner and geomorphologist to understand the geomorphic features of the basin for the management of the watershed as well as the construction of different development project.

References:

- Adhikari., & Dash, J., (2018). Morphometric Analysis of Katra Watershed of Eastern Ghats: A GIS Approach, *International Journal of Current Microbiology and Applied Sciences*,7(3), Pp 1651-65.
- Bhatt S, Ahmed SA (2014) Morphometric analysis to determine floods in the Upper Krishna basin using Cartosat DEM, *Geocarto Int* 29(8),Pp 878–894, <http://doi.org/10.1080/10106049.2013.868042>.
- Choudharia, P.P., Nigamb, G.K., Singh, S.K., & Thakur, S., (2018). Morphometric based prioritization of watershed for groundwater potential of Mula river basin, Maharashtra, India, *Geology, ecology and landscape*, 2(4), Pp 256–267.
- Chowdhury, Md. S., (2024). Morphometric analysis of Halda River basin, Bangladesh, using GIS and remote sensing techniques, *Heliyon*, 10.
- Charizopoulos, N., Mourtziou, P., Psilovikos, T., Psilovikos, A., & Karamotsou, L. (2019). Morphometric analysis of the drainage network of Samos Island (northern Aegean Sea): Insights into tectonic control and flood hazards, *Comptes Rendus-Geoscience*, 351, 375–383.
- Horton, R.E., (1945). Erosion development in stream and their drainage basins, *Geol Soc Am Bull*, 56, Pp 275–370, [https://doi.org/10.1130/0016-7606\(1945\)56](https://doi.org/10.1130/0016-7606(1945)56).
- Kumari, P., Kumari, R., & Kumar, D., (2021). Geospatial approach to evaluate the morphometry of Sabarmati River Basin, India, *Arabian Journal of Geosciences*, 14(206), <https://doi.org/10.1007/s12517-021-06577-7>.
- Mishra, A.K., & Rai, S.C., (2020). Geo-hydrological inferences through morphometric aspects of the Himalayan glacial-fed river: a case study of the Madhyamaheshwar River basin, *Arabian Journal of Geosciences*, 13(533), <https://doi.org/10.1007/s12517-020-05571-9>.
- Obeidat, M., Awawdeh, M., Hantouli, F.A., (2021). Morphometric analysis and prioritization of watersheds for flood risk management in Wadi Easal Basin (WEB), Jordan, using geospatial technologies, *Journal Flood Risk Management*, DOI:10.1111/jfr3.12711.
- Pareta K, Pareta U (2011) Quantitative morphometric analysis of a watershed of Yamuna Basin, India using ASTER (DEM) data and GIS, *Int J Geomat Geosci* 2(1),Pp 248–269.
- Rai, P.K., Chandel, R.S., Mishra, V.N., & Singh, P., (2018). Hydrological inferences through morphometric analysis of lower Kosi river basin of India for water resource management based on remote sensing data, *Applied water science*,8(15).
- Saha, S., Das, J., & Mandal, T., (2022). Investigation of the watershed hydro-morphologic characteristics through the morphometric analysis: A study on Rayeng basin in Darjeeling Himalaya, *Environmental Challenges*, 7.
- Shekar, P.R., & Mathew, A., (2024). Morphometric analysis of watersheds: A comprehensive review of data sources, quality, and geospatial techniques, *Watershed Ecology and the Environment*, 6, Pp 13 – 25.
- Shekar, P.R., & Mathew, A., (2024). Morphometric analysis of watersheds: A comprehensive review of data sources, quality, and geospatial techniques, *Watershed Ecology and the Environment*, 6, Pp 13 – 25.

- Strahler AN (1952a) Geological Society of America Bulletin Dynamic basis of geomorphology. [https://doi.org/10.1130/0016-7606\(1952\)63](https://doi.org/10.1130/0016-7606(1952)63)
- Singh, M.C., Satpute, S., & Prasad, V., (2023). Remote sensing and GIS-based watershed prioritization for land and water conservation planning and management, *Water Science & Technology*, 1(233), doi: 10.2166/wst.2023.207.
- Sreedevi PD, Subrahmanyam K, Ahmed S (2005) The significance of morphometric analysis for obtaining groundwater potential zones in a structurally controlled terrain, *Environ Geol* 47, Pp 412–420. <https://doi.org/10.1007/s00254-004-1166-1>.
- Tufu, F.G., & Feyissa, T.A., (2018). Morphometric Analysis of Kito and Awetu Sub Basins Jimma, Ethiopia, *American Journal of Water Science and Engineering*, 4(3), Pp 80-90, doi: 10.11648/j.ajwse.20180403.14.
- Vinothkumar, R., Arunvenkatesh, S., Janapriya, S., Rajasekar, M. & Muthuchamy, I. 2016 Morphometric analysis and prioritization of Palathodi watershed in Parambikulam-Aliyar basin, Tamil Nadu using RS and GIS, *Asian J. Environ. Sci.* 11 (1), 51–58. <https://doi.org/10.15740/HAS/AJES/11.1/51-58>.
- Zăvoianu I., (1985). *Morphometry of drainage basins*, Elsevier, Amsterdam.



Assessing the 2023 GLOF Impact on Teesta Bazar, Kalimpong District, West Bengal

Anu Tamang

Department of Geography and Applied Geography, University of North Bengal
rs_anu@nbu.ac.in

Abstract: On October 4, 2023, Teesta Bazar, located in the Kalimpong district of West Bengal, experienced severe devastation due to the Glacial Lake Outburst Flood (GLOF) that occurred from the South Lhonak Glacier. This study uses mixed approach combining household surveys, satellite data and secondary sources, to evaluate the extent of damage to houses, infrastructure and livelihoods. The results show that vulnerable groups such as women, children and older people, face greater challenges. The flood caused land subsidence, a change in the River course and debris deposition of up to 2 meters. The event highlighted critical gaps in early warning systems, disaster preparedness and government response. Although relief aid provided some financial assistance, it was insufficient for recovery. To minimise future risks and enhance community resilience, the study highlights the urgent need for an efficient early warning system, mental health support, disaster preparedness and effective relocation strategies.

Keywords: Glacial Lake Outburst Flood (GLOF), land subsidence, disaster preparedness, vulnerability assessment.

Introduction:

The Himalayan region of Sikkim is home to glaciers, glacial lakes and snow-capped summits. Over 80 glaciers cover an area of 436 km² (Banerjee, P., et al 2023). According to ICIMOD (International Centre for Integrated Mountain Development), there are 266 glacial lakes in the Sikkim Himalayas, spanning 20.2 km² (Banerjee, P., et al., 2023). Of all these lakes, 18 to 21 have high GLOF potential (Aggarwal, et al., 2016; Banerjee, P., et al., 2023).

A Glacial Lake Outburst Flood (GLOF) is a glacial-related hazard. ICIMOD defines “Glacial Lake Outburst Flood or GLOF, as a sudden release of water from a lake fed by glacier melt that has formed at the side, in front, within, beneath or on the surface of a glacier”

(2018). It is often triggered by either an earthquake, the displacement wave from an avalanche of rock or ice, overtopping erosion, the collapse of moraine dams when ice buried within them melts, an abrupt inflow of water into a glacial lake such as from heavy rains or drainage from lakes further up-glacier, seepage or piping in the dam or rise in water level (Shrestha, B. B., *et al.*, 2010; Kumar, B., *et al.*, 2015; Gao, J., *et al.*, 2024; Saha, S., *et al.*, 2025). Often, these factors lead to disastrous downstream floods, posing a significant risk to the surrounding residents and the environment.

The size and number of these glacial lakes are constantly changing, due to the retreat of glaciers and temperature rises brought on by climate change (Gao, J., 2024; Upadhyaya, H., 2021). In the Sikkim Himalayas, the South Lhonak glacier is a rapidly retreating glacier and the lake it forms is one of the largest and fastest-growing lakes (Sattar, A., 2021; Saha, S., *et al.* 2025). The glacier receded 2 km in 46 years from 1962 to 2008 (Raj *et al.*, 2013). It further retreated by ~400 m from 2008 to 2019 (Sattar, A., 2021). The catastrophic GLOF incident that occurred in the early hours of 4th October, 2023, from the South Lhonak glacier in North Sikkim is one of the worst incidents the area has ever witnessed. Massive flow destroyed the Chungthang Dam (Teesta Stage III Dam) that is situated 62 km downstream (Sattar, A., 2021) and these together have caused a severe flood in the Teesta Rivervalley, where the flood washed out multiple bridges; NH10 was damaged and many towns lying along the Teesta River belt of both Sikkim and West Bengal, namely Chungthang, Munshithang, Dikchu, Singtam, Tar Khola, Rangpo, Melli, Teesta Bazar, Gel Khola and Bangay Bazar, were severely affected.

Among the worst-affected areas was the populated Teesta Bazar, located along the Teesta River in the Kalimpong district of West Bengal, which experienced significant devastation. The incident caused tremendous damage to 45 houses, roads and infrastructure, including the deposition of 120 to 180 inches of debris (Rao, P., 2023). In addition to seriously damaging the local infrastructure, including roads, residential areas and agricultural land, the flood has also altered the River course, widening the river's flow, causing land subsidence and further displacing the communities.

Although numerous preliminary assessments have documented the extent of damage (Rao, 2023) limited research has been performed on comprehensive vulnerability assessment at the community level. This paper fills this gap by examining the demographic, socio-economic and physical impacts of the 2023 GLOF on Teesta Bazar, as well as linking findings to resilience and policy recommendations.

Study Area:

Teesta Bazar village is located along the left bank of the Teesta River in the Kalimpong CD Block I of the Kalimpong district of West Bengal. It extends from 27°4'0.89"N-27°3'19.23"N latitude and 88°25'31.69"E-88°25'34.47"E longitude. Located at the valley bottom, Teesta Bazar is an important commercial centre for the villages on the hilltops, such as Pesoke, Magwa and Takling. It serves as a hub for essential goods, transportation and trade, especially in selling agricultural products and plays an important part in the local economy. However, its proximity to the River, makes it highly vulnerable to floods. GLOF event, which occurred

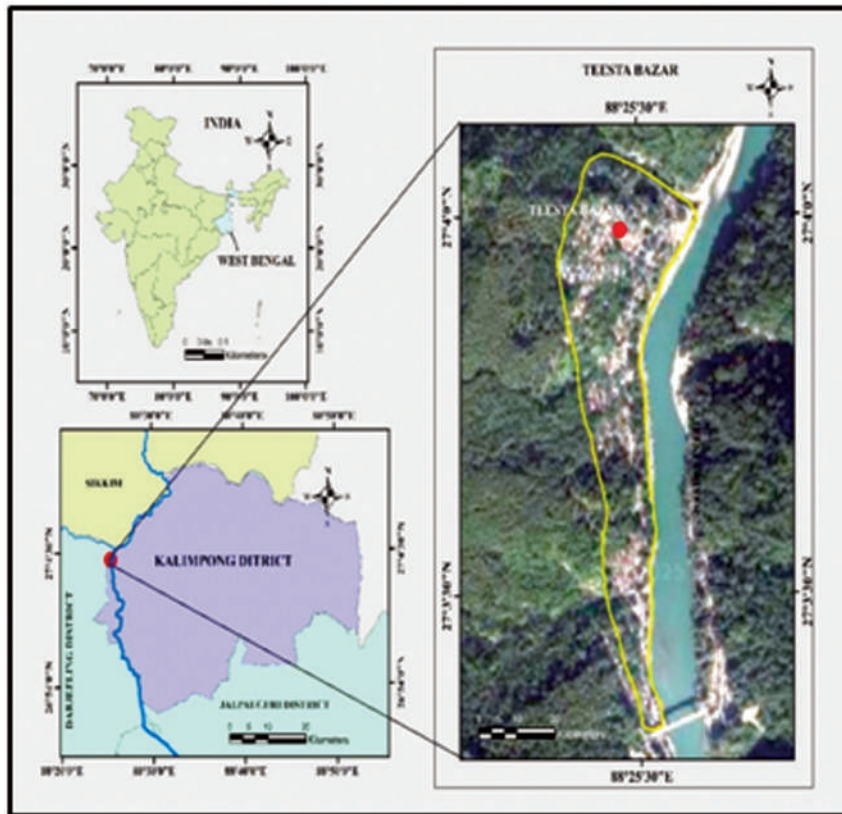


Figure 1. Location Map of Teesta Bazar in Kalimpong District.

on 4th October 2023, was one such event that disrupted the well-being and livelihood of the community living in the Teesta Bazar area, causing widespread destruction. According to the 2011 Census, Teesta Bazar D.I.F has a total population of 2953, of which 1530 are males and 1423 are females.

Methodology:

A mixed-methods is used in this study combining, primary data (household survey), secondary data (reports and literature) and geospatial analysis (satellite imagery).

Data Collection:

Primary Data:

A primary survey was carried out to gather the data on the demographic conditions, the GLOF impact and the residents' experiences and perceptions regarding the event.

Secondary Data:

Secondary data were collected from journals, articles and the Assessment Report by Sikkim and Save The Hills (NGO) of Kalimpong district.

Geospatial Analysis:

Satellite imagery was utilized to analyse changes in River dynamics and infrastructure damage. Landsat 8 (OLI-TIRS) (<https://earthexplorer.usgs.gov/>) images were used to visualise the area before and after the event using different time frames. Arc GIS Software was used to determine the differences in River width before and after the event using the shape file of the outlined River. The NDWI (normalized difference water index) delineated Teesta River areas using satellite images based on the green and NIR band.

Sample Strategy:

According to the Census of India 2011, there are 633 total households in the Teesta Bazar D.I.F. Since, flood-affected households are the target sample in the study area, 45 households were severely affected by the 2023 GLOF. Therefore, 10% of the total households, i.e., 66 households were, surveyed using the Simple Random Sampling Without Replacement Technique. This 10% sample size was chosen because it gives a manageable and representative picture of the people who are directly affected. In other words, it represented both severely and moderately affected households while remaining representative of the entire population.

Results and discussion:

Demographic vulnerability:

Teesta Bazar was the worst-affected area by GLOF in West Bengal. Of the 269 people in 66 households surveyed, the majority were in the working-age group (16–64 years old) 75% of the women and 70% of the men. This group was significant, especially during the evacuation, when young people moved older and younger people to safer locations as water level rose. However, the survey results show that certain groups faced disproportionate challenges during the disaster.

According to 67% of households, the elderly (those over 65, comprising 10% of males

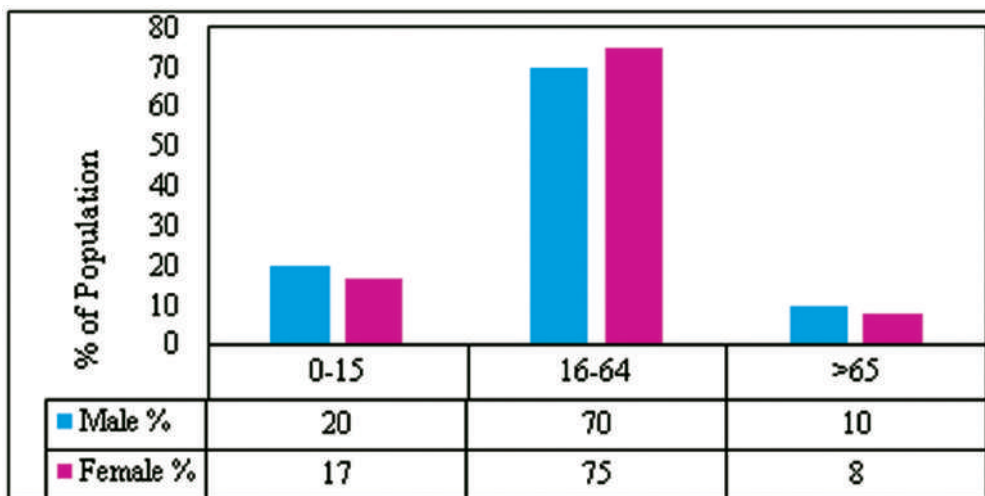


Figure 2. Age Structure of the surveyed household showing a dominance of the working-age group (16-64).

and 8% of females), women, and children (0–15 years, comprising 20% of males and 17% of females) were more impacted because of their specific vulnerabilities.

Vulnerability of Women:

Women are especially vulnerable because they have fewer resources and less control over their lives (Gokhale. V, 2008). Women are more vulnerable to disasters due to traditional gender roles, unequal power and status, low wages and additional responsibilities like child care (Donner. W and Rodríguez. H, 2011). Despite being the most active and resourceful responders in the aftermath, reconstructing homes and livelihoods, women struggle more to provide a stable life for their families. The survey found that there is still gender inequality in Teesta bazar area. Women are still not allowed to make decisions and are still dominated by males, even in community's committee that were set up after a disaster.

Religious and Community Resilience:

Residents of Teesta Bazar come from diverse religious and cultural backgrounds, having resided there for generations. Of the 66 sample households, 65 percent are Hindu, 20 percent are Christian, 11 percent are Buddhist and 5 percent are Muslim. It is worth mentioning that, regardless of religion or caste, people experienced events together. However, in terms of recovery, there is a variation among these households.

It is observed that Christian households recovered more quickly than the other households. This is because, during the disaster relief recovery phase, churches come forward with several initiatives to provide care, such as emergency food, assistance with sanitation, counselling, and basic care for those affected at disaster sites. In other words, Christian families received extra assistance from the government in addition to government help, unlike families in other communities.

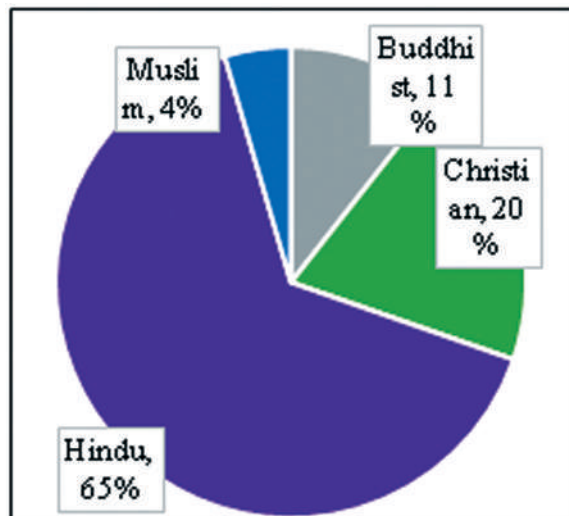


Figure 3. Religion composition of surveyed household in Teesta Bazar.

House Location:

During the survey, it was seen that 70 percent of households were located in a highly vulnerable area, 25 percent in a moderately vulnerable area and only 5 percent in a safe area. The vulnerability of these households is measured based on the proximity of their houses to the River water, mud splash and cracks. Additionally, 54 percent of the households were located at a distance of 0-5 m, close to each other. A large proportion of households, 43 percent have been living in the area for more than 50 years and 21 percent of households for more than 100 years, reflecting a deep-rooted settlement despite recurring floods.

Physical and Environmental Impact:

On the night of October 4, 2023, people became homeless and displaced in hours. The intensity of the flood was so severe that it washed away 14 houses at once from the Gaffer busty of Teesta Bazar and many others were damaged due to the deposition of thick sediments. The GLOF caused a lot of damage to buildings and the environment around them.

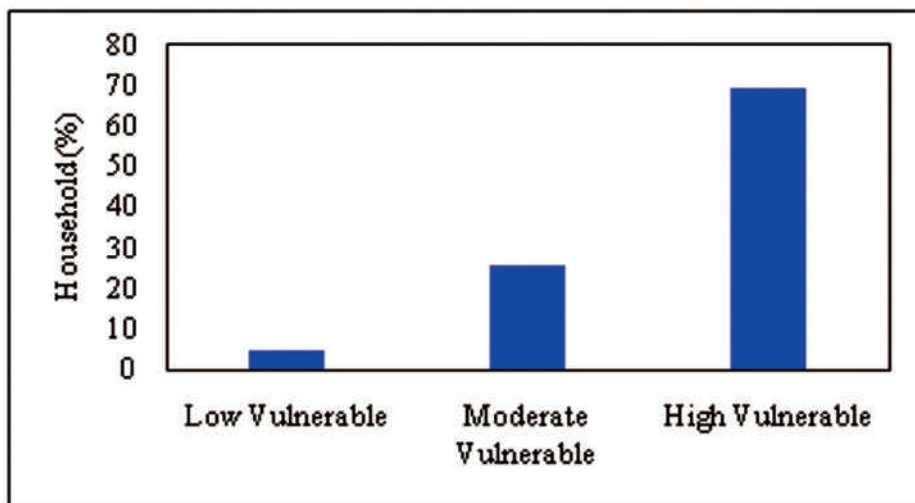


Figure 4. Spatial distribution of the surveyed households based on vulnerability level (low, high, moderate) in relation to the Teesta river.

• Debris Deposition:

The flood deposited a thick layer of sediments and debris. The roads were blocked by sediment and debris deposition ranging from 120 to 180 inches (Rao, P., 2023). 41 percent of the surveyed households were covered by the sediment deposition of more than 2 meters. As per the records, Mr Lalitendu Tripathi, Executive Director of NHPC (North Bengal and Sikkim), stated in an interview with Himal World, that the debris deposits had raised the level of the entire Teesta Basin by 3–4 meters (Rao, P., 2023). It took at least two weeks for local government bodies, community groups, NGOs and local individuals to clear the debris of 25 percent of the affected households.

However, 18 percent of the households have not yet removed the debris or sediment deposition from their houses because they are either fully buried under the sediment or are unfit for habitation. These people reside either in the evacuation camp at the Community Hall of Teesta Haat Bazar or in the rented house, depending on their financial condition. Six families were still residing in the evacuation camp centre of Teesta Haat Bazar at the time of the survey.

River Dynamics and Land Subsidence:

The massive deposition and resulting change in the riverbed caused the Teesta river to flow close to the mountain leading to erosion at its base. Thus, it accelerated the rate of land subsidence, especially in Krishnagram, previously known as Bhasuwa(subsidence), where the



Plate No. 1: A vehicle buried under a thick debris in Teesta bazar after GLOF, showing how much sediment was deposited.

(Source: Save The Hills Blog,2023)



Plate No.2: Community volunteers clearing debris in Teesta bazar, reflecting local participation in disaster response.

(Source: Save The Hills Blog,2023)

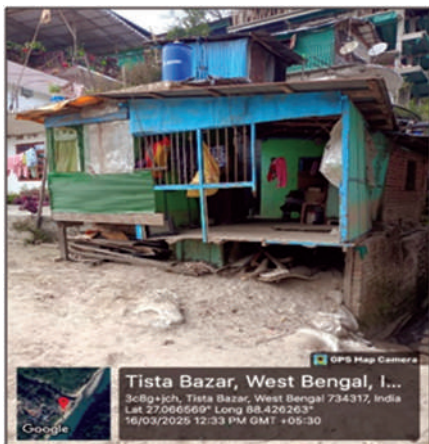


Plate No.3: A household in Teesta bazar still occupied despite its ground flood being covered by debris, showing resilience and limited relocation option.

(Source: Field Survey, 2025)

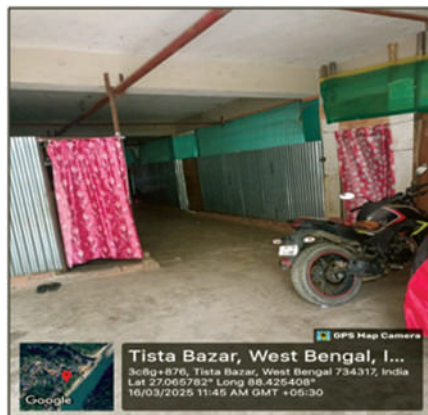


Plate No.4: Evacuation center set up at Teesta Haat Bazar Community hall, providing temporary shelter for displaced families.

(Source: Field Survey, 2025)

river water now flows near its toe. Fifty-nine percent of surveyed households stated that the subsidence activity had intensified, with a rate of 20-25 inches/year. The consequences include house tilting, cracking and wide fractures in the ground.

Socio-Economic and Livelihood Impact:

The incident of a flood which occurred on 4th October 2023, at 4 am, was one of the tragic events for the residents of Teesta Bazar. The incident has caused significant disruption in their daily life and routines. They lost their houses, land, cars, personal belongings, including

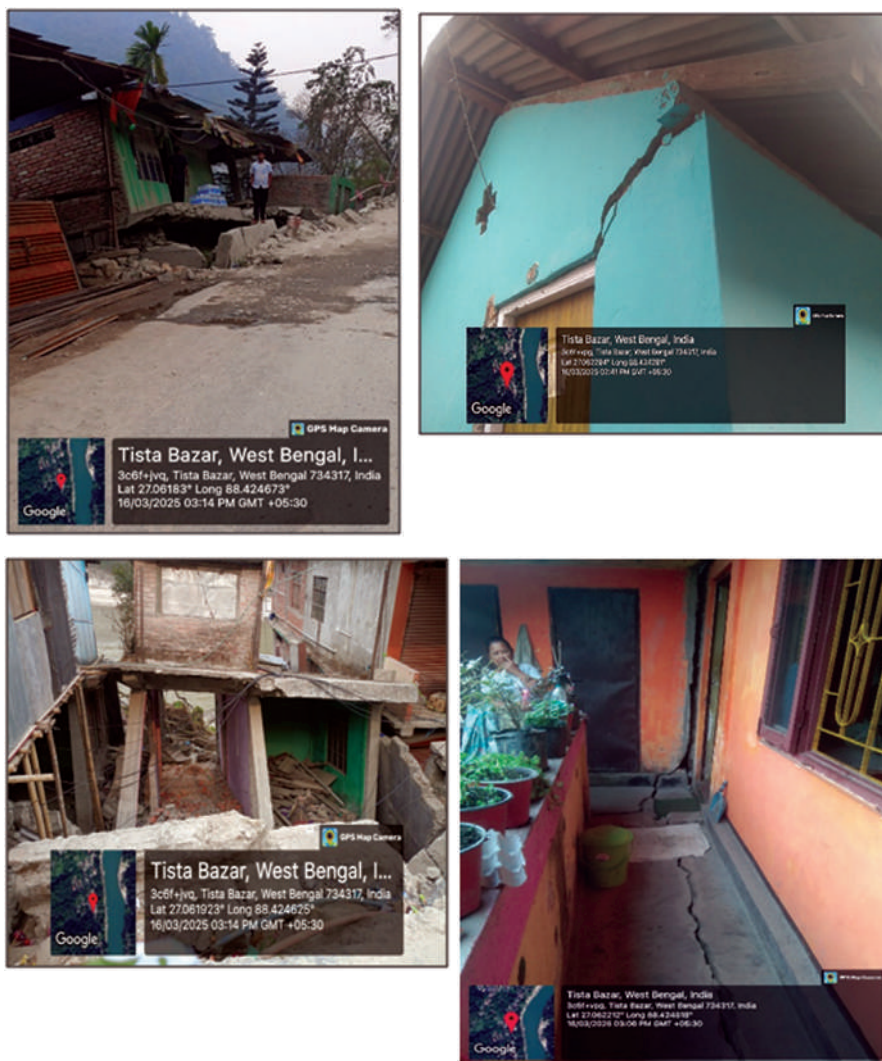


Plate No: 5-8: Subsidence-affected household in Krishnagram, Teesta Bazar, where tilting and widening ground fractures indicate accelerated land sinking after the flood.
(Source: Field Survey, 2025)

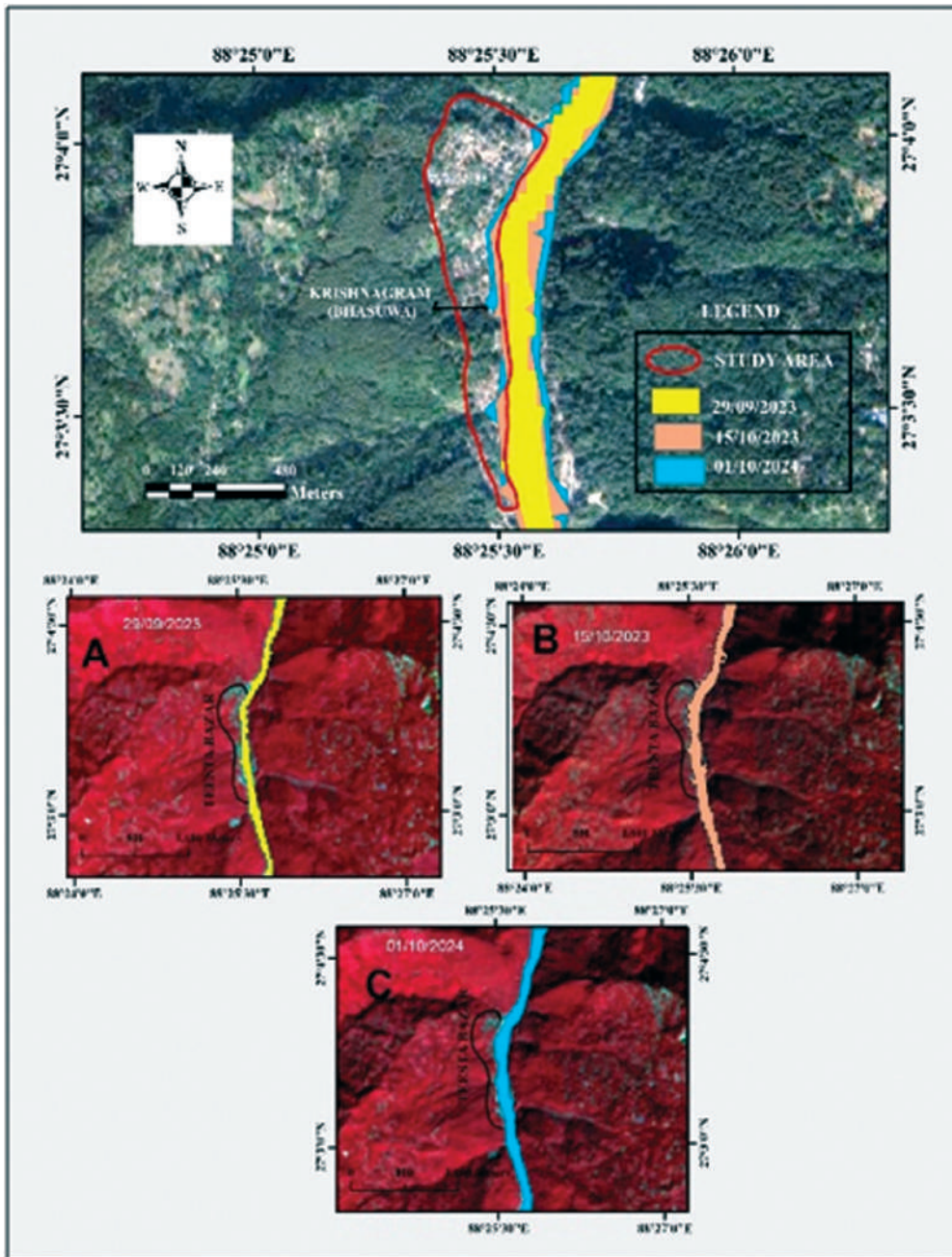


Figure 5. Satellite imagery of Teesta bazar before and after the October 2023 flood, showing river widening, course changes and significant silt deposition contributing to land subsidence.

Satellite images before the event of GLOF b) and c) satellite images after the event of GLOF.

(Source: USGS.)

money, ornaments and documents. Not only this, the flood also damaged the business sector, as it washed away the shops, which are the only means of livelihood for many households. Thus, the GLOF event caused extensive socio-economic damage and severely disrupted livelihood.

Income Loss:

The community's income is generally low. The income level shows that 42 percent of households have a monthly income of less than Rs10,000/month. They are mainly working as drivers, labourers, shopkeepers, carpenters and rafting guides. Numerous stores and tourism-related enterprises were lost as a result of the disaster. Significantly, 12 percent of the surveyed population, primarily the youths working at the Triveni campsite, were unemployed after the flood. However, based on skill and qualification, 3 percent have worked as a driver and cook at the Sevoke-Rangpo rail line project in the ICRON International Company.

Financial Assistance;

Following the disaster, the Government of West Bengal has provided financial assistance of Rs.75000/- to the households that had completely lost their property and Rs.5000/- to those whose houses were destroyed by sediment deposition. Although, 61 percent households have received Rs.75000/- and 39 percent households have received Rs.5000/- from the state government, the affected households are not satisfied with the grants as the amount is insufficient to reconstruct their house or restart their lives.

Psychological Trauma:

The event left the inhabitants traumatized. 30 percent of the surveyed households' family members experience emotional and psychological problems after the flood. Problems like depression, anxiety, high blood pressure and sleep disorders were some of the health-related issues that people have faced due to the incident. Despite all these traumas, only 14 percent of the households stated that mental health services, such as counselling or trauma support, were available to them through the NGOs. Mental health services are important not only to support the individual mentally but also helps them to build up the coping mechanisms within themselves to deal with their current problems and prepare for the future.

Institutional Response And Preparedness Gaps:

The GLOF highlighted significant weaknesses in the institutional response and preparedness gaps.

Early Warning system failure:

Sixty-eight percent of the surveyed households reported that they did not receive any warning before the event, which tragically occurred at 4 am. Early warning systems are essential for disaster risk reduction, as they provide timely alerts about impending hazards (Roy, K., 2024).

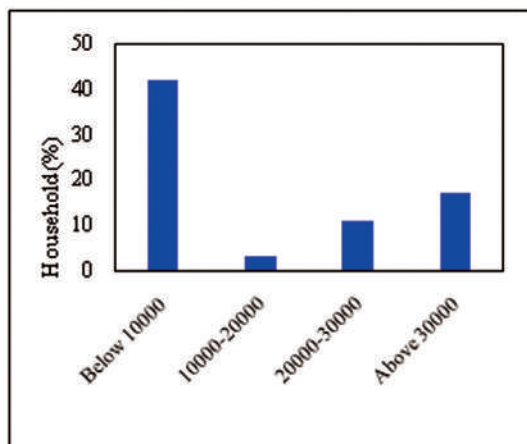


Figure 6. Monthly household income level of surveyed families. The majority earns less than Rs.10000/month, which limits their capacity for recovery.

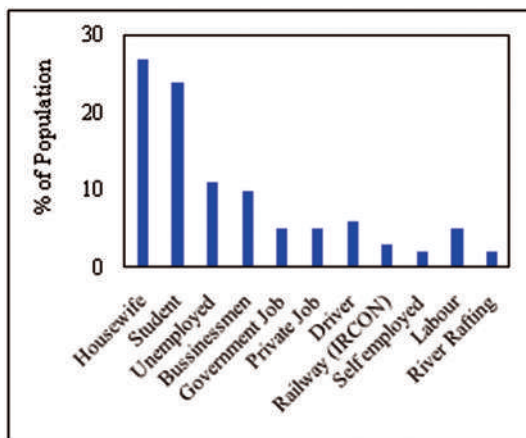


Figure 7. Occupation structure of surveyed households. A significant proportion are engaged in trade, driving and daily wage labour, all of which are severely disrupted by the flood.

The early warning system which was installed in Sikkim for GLOF failed to provide timely alerts to the downstream community such as Teesta bazar. As a result, there were more hurried evacuations and greater loss of movable items.

Government Response Perception:

Regarding the preparedness of local government and authorities for the GLOF event, 83 percent of surveyed households felt that the authorities were unprepared for the disaster due to

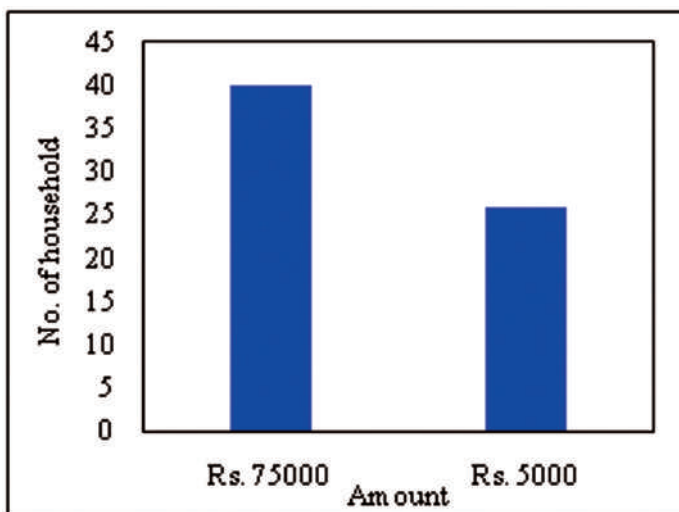


Figure 8. Financial assistance received by the surveyed household from the government of West Bengal, after the GLOF event.

slow responses, poor communication and weak infrastructure. In addition, around 68 percent of households believe that the government's response to flood during and after the event was ineffective as their needs were not adequately met during the disaster.

Community Preparedness:

As a result of these gaps, 58 percent of households feel that the community is not sufficiently trained to respond to future disastrous events. The primary needs expressed by the community are the installation of proper early warning system (61 percent household), evacuation plans, weather updates, emergency contact information and safety protocols.

Perception and Awareness:

Perceptions and awareness of the GLOF event vary significantly among the Teesta bazaar's affected households. Many residents have different perspectives about the GLOF event, its causes and the effectiveness of response measures.

GLOF Awareness:

A significant majority, 70 percent of the surveyed households, were unaware about the Glacial Lake Outburst Flood (GLOF) risk in their region before the October 2023 event. While 30 percent of the households were aware about the risk of the GLOF, they had not prepared for the severity of the flood.

Climate Change Perception:

Regarding climate change and awareness, 52 percent households strongly believe that climate change played a role in the severity of the GLOF event and 35 percent have somewhat agree. However, a contrasting view exists regarding local environmental change, with 74 percent of households not agreeing that local changes contributed to the GLOF.

This contrasting opinion about global and local climate change is stem from people having heard and learned about the rising temperature and its effect on the global environment through educational institutions, news and other sources. However, they have not noticed such changes at the local level as they consider the variation in temperature and flooding as part of the natural cycle rather than the result of climate change. Nevertheless, all households expressed their support and willingness to participate in local programs focusing on raising awareness about climate change and disaster preparedness in the future.

Conclusion and Recommendation:

On 4th October 2023, the Glacial Lake Outburst Flood (GLOF) event, devastated the Teesta Bazar area. It destroyed houses, roads, dams, bridges and other infrastructure as well as the livelihoods of the people who lived along the River valley. The failure of the early warning system and the community's general lack of knowledge about GLOF made the situation even worse. Even though the financial aid was not sufficient and psychological trauma was bad,

the families that were affected showed strength and a desire to participate in future disaster preparedness measures. To transition from temporary relief to effective long-term and community-oriented disaster management, following policy-relevant recommendations are crucial:

Policy Recommendations:

Establish an effective Early Warning System: Develop a reliable and efficient system that provides all communities downstream with previous information on weather conditions, water levels, flood forecasts and evacuation plans.

Mandatory GLOF awareness plan: Since a significant 70% proportion of households were unaware of the possibility of GLOF in the Teesta River valley before the 2023 flood, awareness about climate change, GLOF hazards and preparedness such as, what to do before and after the disaster is necessary. Such awareness programs should be held regularly by NGOs and local authorities, so that, they can prepare themselves for future such events.

Prioritized mental health services: Many people are struggling with the mental/psychological trauma of losing their houses and livelihoods. For this, counselling and mental health services should be made available to them to cope with the impact of the flood. NGOs and government agencies should collaborate to provide continuous psychological support to the affected households.

Revise financial compensation policy: The state must re-evaluate and increase the financial aid, potentially by providing loan or insurance, as the current compensation of Rs.5000 and Rs 75000 is grossly insufficient to cover the cost of rebuilding and livelihood restoration.

Relocation and protective infrastructure: The government authority should consider relocating highly vulnerable households lying close to the river to a safer area, or alternatively, employ better construction techniques and materials. Furthermore, the community's strong recommendation for the construction of a protective wall along the riverside of Teesta bazar is a critical protective measure that must be completed promptly.

By implementing these comprehensive strategies, involving sustained collaboration of government bodies, NGOs and local governments, the resilience of Teesta bazar to future GLOF events can be significantly enhanced.

Acknowledgements:

I would like to express my sincere gratitude to my supervisor, Dr. Indira Lepcha Nee Lama for her continuous guidance and support. I am also thankful to Awaz Gurung, Sawart Rai M.A students from Department of Geography and Applied Geography, and Kamal Rai M.A student from the Department of Central for Himalayan Studies, for their assistance during the field survey. Special thanks to my friend Sneha Dahal, sister Smriti Dahal, nephew Salon Tamang and Awaz Rai, for their dedication and support, without whom my field survey would not have been possible. I am also grateful to the local residents for their cooperation throughout the survey.

References:

- Azad, J., and Pritchard, B., (2023). The importance of women's roles in adaptive capacity and resilience to flooding in rural Bangladesh. *International Journal of Disaster Risk Reduction*. Volume 90, ISSN 2212-4209.
- Aggarwal, S., Rai, S.C., Thakur, P.K., and Emmer, A., (2017). Inventory and recently increasing GLOF susceptibility of glacial lakes in Sikkim, Eastern Himalaya, *Geomorphology*, Volume 295, Page no:39-54
- Banerjee, P. and Bhuiyan, C., (2023). Glacial lakes of Sikkim Himalaya: their dynamics, trends, and likely fate—a timeseries analysis through cloud-based recomputing, and machine learning, *Geomatics, Natural Hazards and Risk*, 14:1, 2286903, DOI: 10.1080/19475705.2023.2286903
- Donner. W and Rodríguez. H. (2011). *Disaster Risk and Vulnerability: The Role and Impact of Population and Society*. Population Reference Bureau. Washington, D.C. <https://www.prb.org/resources/disaster-risk/>
- Gao, J., Du, J., Bai, Y., Chen, T., Zhuoma, Y., (2024). The Impact of Climate Change on Glacial Lake Outburst Floods. *Water*, 16, 1742.
- Gokhale. V. (2008). Role of Women in Disaster Management: An Analytical Study with Reference to Indian Society. The 14th World Conference on Earthquake Engineering. Beijing, China. (pg. no-1-2,6-7)
- ICIMOD- International Centre for Integrated Mountain Development
<https://www.icimod.org/mountain/glacial-lake-outburst-flood/>
- Preliminary Assessment Report Flash Flood in Sikkim and North West Bengal
- Raj, K.B.G., Kumar, V.K., SN, R., (2013). Remote sensing-based inventory of glacial lakes in Sikkim Himalaya: semi-automated approach using satellite data. *Geomatics, Natural Hazards and Risk* 4 (3), 241–253.
- Rao, P., 2023. Save The Hills Blog (Vision of Hell)<http://savethehills.blogspot.com/2023/10/photo-essay-on-glacial-lake-outburst.html>
- Rao, P., 2023. Save The Hills Blog (Vision of Hell)
<http://savethehills.blogspot.com/2023/11/report-and-recommendations-on-glof.html>
- Roy, K., (2024). Glacial Lake Outburst Threats and Management: Insight from Sikkim's Flood Event. *Journal of Arts, Humanities and Social Sciences*. Volume - 7, Issue – 01
- Saha, S., Bera, B., Sengupta, D., Mukhopadhyay, U., Ghosh, D., Tamang, L., Bhattacharjee, S. and Sengupta, N., (2025). Multiple dRivers of the recent South Lhonak glacial lake outburst flood in Sikkim Himalaya and its aftermath on Teesta River Valley, *Geosystems and Geo environment*.
- Sattar, A., Goswami, *et al.*, (2021). Future glacial lake outburst flood (GLOF) hazard of the South Lhonak Lake, Sikkim Himalaya. *Geomorphology*, 388:107783. <https://doi.org/10.1016/j.geomorph.2021.107783>
- Shrestha, B., Nakagawa, H., Kawaike, K., Baba, Y., and Zhang, H., (2010). Glacial Lake Outburst due to Moraine Dam Failure by Seepage and Overtopping with Impact of Climate Change, *Annals of Disaster Prevention Research Institute., Kyoto Univ.*, No. 53
- Upadhyaya, H., (2021). Assessing the impact of Climate Change on GLOF: A study of Sikkim in Eastern Himalayas. *International Journal of Geology, Earth & Environmental Sciences* ISSN: 2277-2081, Vol. 11, pp. 142-148



Human Health Risk Exposure from Arsenic Pollution in the Arsenic-affected Areas of Malda district in the Lower Gangetic Plain

Jayanta Das^{1*}, Md. Mofizul Hoque¹, Arijit Majumder²,
Sudarshana Sen³, Pradip Chouhan³, Namita Chakma⁴

¹*Department of Geography, Rampurhat College, Rampurhat, Birbhum –731224*

²*Department of Geography, Jadavpur University, Kolkata –700032*

³*Department of Sociology, University of Gour Banga, Malda –732103*

⁴*Department of Geography, The University of Burdwan, Bardhaman –713104*

**Corresponding author: Jayanta.daas@gmail.com*

Abstract: Water is one of the most essential natural resources, and safe water is a vital element on Earth as human health relies on it. In this context, the human health risk (both carcinogenic and non-carcinogenic) from arsenic exposure has been assessed through health risk indices for different age and sex groups in this investigation. Besides, the level of arsenic pollution has been evaluated using the Contamination Factor (CF) index. The study detected elevated arsenic concentrations in groundwater within the analysed blocks of Malda and found that 83.2% of water samples exceeded the permissible limit for drinking. CF indicates that 81.6% of samples are highly polluted, rendering them unsuitable for drinking and other human uses. The hazard quotient (HQ) shows that 83.2% of samples pose a non-carcinogenic risk from oral arsenic exposure across all groups. For dermal exposure, 28.8% of samples for adults (men and women) and 8% for children present risks. The total hazard index (THI) reveals that 83.2% of samples carry a non-carcinogenic risk for all groups. The carcinogenic risk index suggests that 83.2% of samples pose a carcinogenic risk through oral exposure, while only 8% pose a risk to adults via dermal exposure. The cancer index (CI) confirms that 83.2% of samples present a significant carcinogenic risk from both oral and skin exposure. Furthermore, ANOVA indicates a notable variation in health risks among different groups. This study aids in ensuring access to safe drinking water, promotes health awareness among stakeholders and regional planners, supports sustainable water resource management, and contributes to the achievement of Sustainable Development Goal 6 (SDG 6): clean water, sanitation, and hygiene.

Keywords: Arsenic pollution; Contamination factor; Carcinogenic and non-carcinogenic risk; Dermal and oral exposure; Human health.

Introduction:

Arsenic is a chemical component, a metalloid and notoriously toxic (Ahmed *et al.*, 2022). It is toxic to humans as it leads to human health and environmental hazards (Rae, 2020). It is also termed as the 'King of Poisons', used as a weapon of murder (El-Ghiaty and El-Kadi, 2021). It is a trace element and a poison in high amounts, but ultra-trace amounts are recommended because it can be an essential food ingredient or beneficial for hamsters, rats, chickens, and goats (VAN PAEMEL *et al.*, 2010). It and its compounds are largely used in agriculture, medicine, animal feed, electronics, chemical warfare agents, metallurgy, etc. (Shaji *et al.*, 2021). However, it is stated that any form of arsenic has a serious risk to human health (Genchi *et al.*, 2022). Arsenic pollution of groundwater is one type of groundwater contamination (Santra, 2017). It is a well-known problem that affects millions of people worldwide (Prakash and Verma, 2021). Concentrations of arsenic in groundwater and its contamination are found in more than 70 countries in the world (Shankar *et al.*, 2014). Arsenic concentration in groundwater is a naturally occurring process, but higher concentrations lead to arsenic contamination in groundwater (Kanel *et al.*, 2023). Arsenic sources in groundwater are both natural and anthropogenic (Raju, 2022). The natural sources of arsenic in groundwater include arsenic-bearing minerals dissolution in rocks and soils affected through geological processes (Palma-Lara *et al.*, 2020). Whereas, anthropogenic sources such as mining, industrial activities and the use of arsenic-containing pesticides (Palma-Lara *et al.*, 2020). Moreover, the construction of wells in areas having high arsenic concentration in soil and rock (Erickson *et al.*, 2019), dewatering and the burning of fossil fuels may also contaminate groundwater (Watson *et al.*, 2022; Abanyie *et al.*, 2023). It is generally distributed in the environment, found in water, soil and air (Nriagu *et al.*, 2007). Its exposure occurs through polluted drinking water, food or industrial procedures (Fatoki and Badmus, 2022). Its exposure leads to a variety of serious health problems, including gastrointestinal problems, cardiovascular and nervous system damage, and the risk of various cancers (Ozturk *et al.*, 2022). Arsenic exposure through drinking water is a global health concern as rising awareness (Monteiro De Oliveira *et al.*, 2021). Hence, human health risk assessment from arsenic is the utmost priority globally.

The widespread presence of toxic arsenic in groundwater and its associated problems remains a critical issue across India (Afreen *et al.*, 2025). In India, groundwater arsenic contamination has been reported across 4 union territories and 20 states, putting more than 100 million people at risk (Kumar and Shekhar, 2025). Moreover, an elevated concentration of arsenic is found along the Ganges River (Shaji *et al.*, 2021), specifically in West Bengal and Uttar Pradesh, where its concentration lies from 10 to 3200 mg/l (Shankar *et al.*, 2014). The Ganga River basin faces groundwater-related issues, particularly the concentration of arsenic in several parts of the basin (Poddar *et al.*, 2023). The lower Gangetic River Basin, precisely the Malda district in West Bengal, is considered to be the area most seriously affected by arsenic pollution in groundwater, leading to considerable human health and socio-economic challenges (Chakraborti *et al.*, 2009; Sarkar and Pal, 2021; Das *et al.*, 2015).

As it leads to several health-related problems and socio-economic challenges, human health risk assessment from it has also become of utmost importance in recent decades

worldwide (Li *et al.*, 2025). Human health risks from arsenic largely depend on the arsenic concentration in drinking water, the amount of water consumed, and the duration of exposure. In this regard, the assessment of non-carcinogenic and carcinogenic risks associated with arsenic exposure is the most vital measure globally (Dhamija and Joshi, 2025). Several studies have been conducted worldwide on arsenic contamination and its impacts on human health (Afreem *et al.*, 2025; Prasath, 2025; Saxena, 2025; Sridhar and Parimalarenganayaki, 2025; Nayeem *et al.*, 2025; Mahar *et al.*, 2024). However, human health impact assessments, particularly of non-carcinogenic and carcinogenic risks from arsenic exposure, remain scarce in the study area. Moreover, the studied blocks of Malda are severely affected by arsenic pollution, with high arsenic levels observed in groundwater (Mazumder *et al.*, 2020). Therefore, the present study examines the concentration of arsenic in groundwater and evaluates the potential human health risks associated with arsenic contact. The main objectives of this investigation are: 1) to measure arsenic levels in groundwater, and 2) to estimate potential human health risks, both non-carcinogenic and carcinogenic, from arsenic exposure via oral and dermal ingestion across different age and gender groups in the study area. This research will assist stakeholders and regional planners in sustainable water resource management and in raising health awareness.

Materials and methods:

Study area:

The current study emphasises the severely arsenic concentration areas of the lower Gangetic River Basin, precisely the Malda district in West Bengal (Figure 1). Malda district, located in the northern part of West Bengal, spans approximately 3,733 km² and is bordered by Bangladesh to the east and the Ganges River to the south. The district's geographical position within the fertile alluvial plains of the lower Gangetic basin makes it particularly vulnerable to groundwater contamination (Chakraborti *et al.*, 2009). The reliance on hand-pumped tubewells, many of which are contaminated with arsenic, exacerbates the public health crisis in the region (Mazumder *et al.*, 2020; Sarkar and Pal, 2021). Five arsenic-contaminated blocks such as Manikchak, Kaliachak I, II, and III and English Bazar of Malda district, have been selected for the present investigation (Figure 1). In Malda, the Manikchak block is known for its high levels of arsenic contamination, with groundwater arsenic concentrations often exceeding 50 µg/L (Mukherjee *et al.*, 2006). Besides, Kaliachak I, II, and III blocks are severely affected, with arsenic levels frequently surpassing safe drinking water limits, posing a serious risk to the local population (Rahman *et al.*, 2003). Although the English Bazar is less affected than other blocks, but still presents significant challenges due to its reliance on contaminated groundwater (Das *et al.*, 2015). The study area is selected based on existing review research and focuses on the severely arsenic-affected or concentrated areas of the district.

Database:

The present study is based on primary data collected from a field survey. A total of 250 water samples were gathered from five Community Development (CD) blocks, i.e. Manikchak,

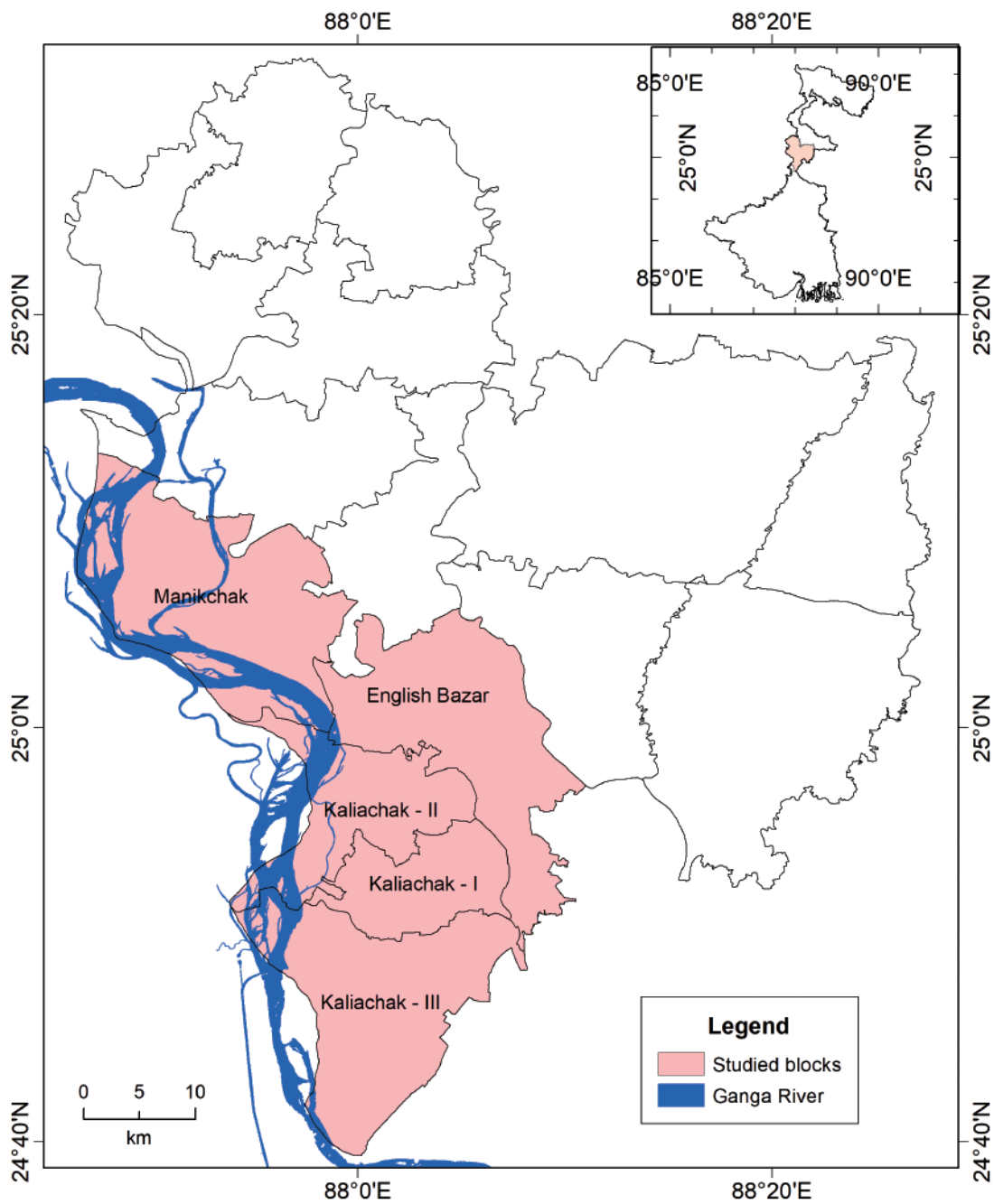


Figure 1. Location of the study area.

Kaliachak I, II, and III and English Bazar of Malda district. Specifically, 50 water samples were collected from each CD block in Malda and tested for arsenic concentration in groundwater for drinking purposes, as well as analysed for human health risk assessment. These samples were tested using the Arsenic Test Kit (Aquasol) to measure arsenic levels in groundwater. Water samples were collected purposively from locations spatially distributed across districts and blocks.

Methodology:

In the investigation, the arsenic pollution level has been assessed through the contamination factor (CF). Besides, the human health risk from arsenic contamination has been measured through health risk assessment indices (Carcinogenic and non-carcinogenic). The mathematical calculations of the present investigation are described below. A detailed systematic approach to human health risk assessment is presented in Figure 2.

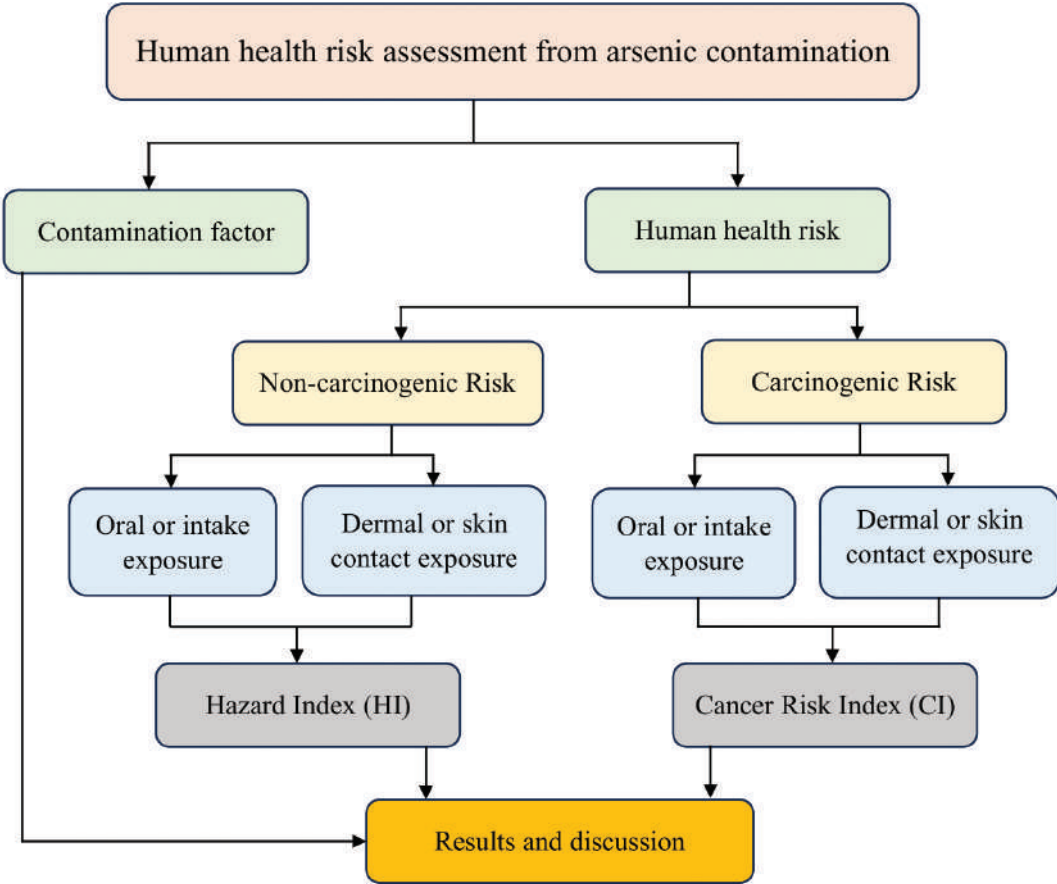


Figure 2. Methodological flow chart of human health risk assessment.

2.3.1 Contamination factor (CF) analysis:

The contamination factor is used to describe the quality of water by determining the severity of water pollution. In the present investigation, the CF has been computed by using the arsenic standard value set by the Bureau of Indian Standards (BIS, 2012) and the World Health Organization (WHO, 2011). It is calculated by using Eq. 1 (Mohan *et al.*, 2024).

$$CF = \frac{C_i}{C_o} \quad \dots (1)$$

Where CF stands for the contamination factor, C_i denotes the arsenic concentration, and C_o denotes the standard, background or reference value of arsenic prescribed by BIS (2012) and WHO (2011). Water is considered polluted when the CF value is >1 . Besides, the degree of contamination factor is categorised into four classes: safe (<1), moderate (1-3), high (3-6), and very high (>6) based on the CF values (Hoque *et al.*, 2023).

2.3.2 Human health risk analysis:

Human health risks are identified as a threat that leads to daily intake of toxic elements such as arsenic, fluoride and nitrates through oral and dermal exposure. Thus, assessing the future threat of these toxic elements to human health is crucial as they lead to various diseases. In the present investigation, human health risk, i.e. non-carcinogenic risk or hazard quotient (HQ) and carcinogenic risk (CR), is assessed through oral and dermal exposure to arsenic present in water.

2.3.2.1 Exposure analysis:

(a) Oral or intake exposure:

The oral exposure is assessed for individuals ingesting arsenic (As) from drinking water. The average daily dose (ADD) of arsenic via drinking water has been calculated to determine the health risk using Eq. 2 (Nemati *et al.*, 2025; Sunitha *et al.*, 2022).

$$ADD = \frac{CW \times IR \times ED \times EF}{ABW \times AET} \quad \dots (2)$$

Where ADD denotes the average daily dose of arsenic (mg/kg/day). CW denotes arsenic (As) concentration in drinking water (mg/l). IR is an ingestion rate (l/day). ED denotes exposure duration (years). EF denotes exposure frequency (days/year). ABW denotes average body weight (kg) while AET denotes average exposure time (days), ($AET = ED$). The values of these indicators are represented in Table 1.

Table 1. Oral and dermal exposure values of selected indicators for human health risk assessment from arsenic

Indicators	unit	Value for			Exposure type
		Children	Men	Women	
IR	l/day	0.64	2	2	Oral
ED	years	12	68	70	Oral/Dermal
EF	days/year	365	365	365	Oral
	days/year	350	350	350	Dermal
ABW	kg	30	65	60	Oral/Dermal
AET	days	12 x 365	65 x 365	60 x 365	Oral
	days	18 x 200	60 x 200	60 x 200	Dermal
SA	cm ²	6600	18000	16000	Dermal
EV	-	1	1	1	Dermal
Kp	cm/h	10-3	10-3	10-3	Dermal
tevent	h/event	0.54	0.71	0.71	Dermal

Source: Based on Kumar *et al.* (2025)

(b) Dermal or skin exposure:

Arsenic can also enter the human body through skin contact with water during bathing, swimming and other domestic activities. The dermal absorbed dose (DAD) of arsenic through skin contact with water has been calculated to quantify the health risk using Eq. 3 and 4 (Kumar *et al.*, 2025).

$$DAD = \frac{DA_{event} \times EV \times ED \times EF \times SA}{ABW \times AET} \quad \dots (3)$$

Where, $DA_{event} = Kp \times C_w \times tevent \dots (4)$

DAD denotes the dermal absorbed dose of arsenic (mg/kg/day). DA_{event} denotes absorbed dose at each exposure event (mg/cm²). EV denotes the event frequency of daily exposure. SA denote the total surface area of skin available for contact (cm²). Kp denotes the dermal permeability coefficient of arsenic in water (cm/h). tevent denotes the duration of a single contact event (h). CF is the unit conversion factor (0.001 l/cm³). Other parameters are described in the oral or intake exposure section.

2.3.2.2 Health risk assessment:

Human health risk has been analysed through non-carcinogenic (hazard quotient) and carcinogenic risk (CR).

(a) Non-carcinogenic risk (hazard quotient):

In this study, non-carcinogenic risk has been measured through oral consumption and skin

absorption of arsenic. It has been assessed through the hazard quotient, i.e. oral (HQ_{oral}) and dermal (HQ_{dermal}) exposure and calculated using Eqs. 5 and 6 (Nayeem *et al.*, 2025).

$$HQ_{oral} = \frac{ADD}{RfD} \quad \dots (5)$$

$$HQ_{Dermal} = \frac{DAD}{RfD} \quad \dots(6)$$

Where HQ_{oral} and HQ_{dermal} stand for hazard quotient for oral and dermal exposure respectively. ADD and DAD stand for the average daily dose and dermal absorbed dose, respectively. RfD is oral (0.0003 mg/kg/day) and dermal (0.000123 mg/kg/day) reference dose for arsenic (Demissie *et al.*, 2024).

(b) Total Hazard Index (THI):

The total hazard index has been calculated from combined (oral and dermal) exposure using Eq. 7 following Demissie *et al.* (2024).

$$THI = HQ_{oral} + HQ_{Dermal} \quad \dots (7)$$

According to the USEPA's health risk assessment standard, the threshold value for non-carcinogenic is 1 (USEPA, 2014). The HQ and THI are >1, indicating a health risk for the human body and <1, indicating no potential health risk (Moultoucomarassamy *et al.*, 2024). Moreover, a higher HQ value denotes a greater human health risk. Further, the THI values are categorised into four classes such as negligible (<0.1), low significant health effect (0.1-1), medium significant health effect (1-4), and very high risk (>4) (Moultoucomarassamy *et al.*, 2024).

(c) Carcinogenic Risk (CR):

The carcinogenic risk for arsenic has been calculated by using Eqs. 8 and 9 following Kumar *et al.* (2025).

$$C_{roral} = \frac{ADD}{CSF} \quad \dots \quad (8)$$

$$CR_{Dermat} = \frac{DAD}{CSF} \quad \dots(9)$$

Where CSF denotes carcinogenic slope factor for oral and dermal exposure to arsenic. The recommended doses are 1.5 mg/kg/day for oral exposure and 3.66 mg/kg/day for dermal exposure of arsenic (Mahar *et al.*, 2024; Chen *et al.*, 2023).

Further, the total cancer risk (TCR) or cancer index (CI) has been computed by combining oral and dermal cancer risks using Eq. 10 (Bashir *et al.*, 2025; Patel *et al.*, 2021).

$$CI = CI_{oral} + CI_{Dermal} \quad \dots(10)$$

The acceptable limit of cancer risk from arsenic is. If the CI value is greater than 10^{-4} consider a high cancer risk (Moultoucomarassamy *et al.*, 2024).

3. Results:

3.1 Groundwater arsenic contamination:

Groundwater arsenic pollution is a form of groundwater contamination. Arsenic is a toxic compound that enters the human body through oral and dermal exposure. Long-term exposure to this toxic element leads to numerous health problems and even cancer. In the present study, it ranges from 0.001 (BDL) to 2 mg/l with an average concentration of 0.29 mg/l. This (average concentration) is much higher than the permissible limit (0.01 mg/l) of arsenic concentration in drinking water prescribed by the WHO and BIS. Specifically, it varies from 0.001 to 1.8 mg/l with a mean value of 0.31 and 0.36 mg/l in Kaliachak-I and II respectively, 0.001 to 1.5 mg/l with a mean value of 0.25 and 0.18 mg/l in Kaliachak-III and English Bazar correspondingly, and 0.001 to 2 mg/l with a mean value of 0.35 mg/l in Manikchak. It is also found that the arsenic concentration is comparatively high in the Kaliachak-II block, followed by the Manikchak, according to the mean value (Figure 3). Moreover, 83.2% of water samples from Malda exceed the permissible limit of the arsenic concentration. Besides, 88%, 94%, 78%, 84% and 72% of samples for Kaliachak I, II, and III, Manikchak, and English Bazar respectively, lie above the permissible limits. These results show that water is unsuitable for human use.

3.2 Contamination factor assessment:

The contamination factor has been used to evaluate the quality of water to assess its suitability for drinking and other purposes. In the study, it ranges from 0.1 to 200 with a mean value of 29.06. Besides, 83.2% of water samples exceed the accepted value of CF, i.e. 1, signifying polluted water. Furthermore, it has been classified and found that 16.8% of samples are safe, 1.6% are highly, and 81.6% are very highly polluted based on its categorical classification. Hence, these results reveal that 16.8% of water samples have their suitability for drinking and other purposes use while the rest (83.2%) are unsuitable for human use (Figure 4)

3.3 Human health risk assessment:

In the present study, human health risk (both carcinogenic and non-carcinogenic) has been measured through the average daily and dermal absorbed dose for different age and sex groups. It is found that it (ADD) ranges from 3.08×10^{-5} to 6.15×10^{-2} mg/kg/day with a mean value of 8.94×10^{-3} mg/kg/day for men, 3.33×10^{-5} to 6.67×10^{-2} mg/kg/day with a mean value of 9.69×10^{-3} mg/kg/day for women and 2.13×10^{-5} to 4.27×10^{-2} mg/kg/day with a mean value of 6.20×10^{-3} mg/kg/day for children (Table 2). It is comparatively high for women followed by men and children, according to mean values. However, the DAD varies from 3.90×10^{-7} to 7.80×10^{-4} mg/kg/day with a mean value of 1.13×10^{-4} mg/kg/day for men, 3.87×10^{-7} to 7.73×10^{-4} mg/kg/day with a mean value of 1.12×10^{-4} mg/kg/day for women and 1.39×10^{-7} to 2.77×10^{-4} mg/kg/day with a mean value of 4.03×10^{-5} mg/kg/day for children. The DAD is comparatively higher

for men followed by women and children based on the mean values. These results portray that ADDoral for women and DAD for men is high compared to other age and sex groups. A higher ADDoral for women is due to higher exposure duration and DAD for men is due to a higher surface area of skin available for contact than the other age and sex groups.

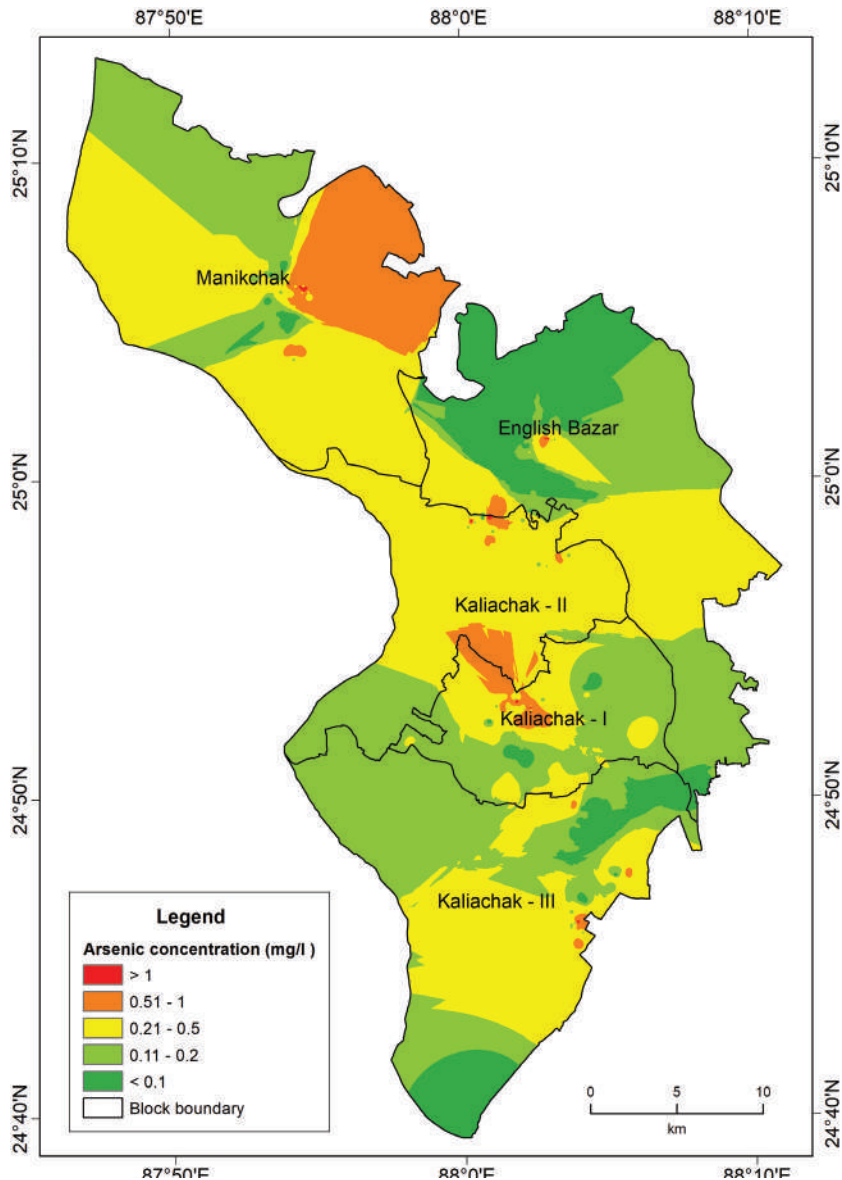


Figure 3. Concentration of arsenic in water samples.

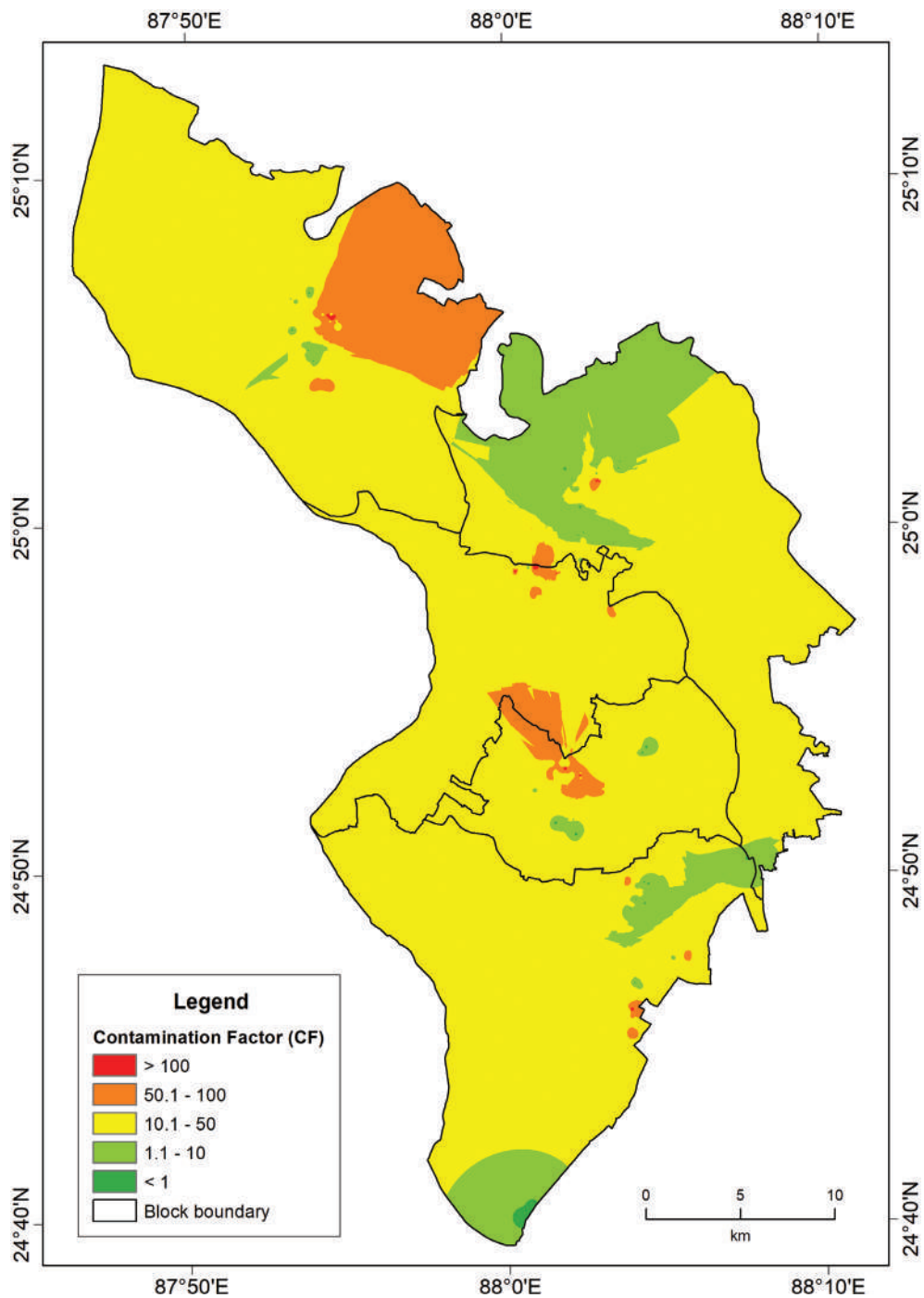


Figure 4. Contamination factor and water suitability.

Table 2. Average values of ADD, HQ, THI, CR, and CI for both oral and dermal exposure

Age group	ADD		HQ		THI	CR		CI
	Oral	Dermal	Oral	Dermal		Oral	Dermal	
Men	10-3 × 8.94	10-4 × 1.13	29.80	0.92	30.72	10-3 × 5.96	10-5 × 3.10	10-3 × 5.99
Children	10-3 × 6.20	10-5 × 4.03	20.66	0.33	20.99	10-3 × 4.13	10-5 × 1.10	10-3 × 4.14
Women	10-3 × 9.69	10-4 × 1.12	32.29	0.91	33.20	10-3 × 6.46	10-5 × 3.07	10-3 × 6.49

3.3.1 Non-carcinogenic risk assessment:

Non-carcinogenic risk has been measured through oral and dermal exposure to arsenic which is mentioned below.

3.3.1.1 Non-carcinogenic risk from oral exposure:

In the study, the non-carcinogenic risk from oral exposure to arsenic has been assessed through the hazard quotient (HQ). It is found to be 0.10 to 205.13 with a mean value of 29.80 for men, 0.11 to 222.22 with a mean of 32.29 for women, and 0.07 to 142.22 with a mean of 20.66 for children (Table 2). The oral HQ is comparatively high for women followed by men and children, based on the mean HQ. Moreover, it is also found that 83.2% of water samples exceeded the HQ value of 1 for all the respective groups of people, indicating non-carcinogenic risk from oral exposure to arsenic. Besides, spatial variation maps show that a significant portion of the study area, the HQ values range from 10.1 – 100, indicating a higher non-carcinogenic risk from oral exposure to arsenic for the respective group of people (Figure 5a-c).

3.3.1.2 Non-carcinogenic risk from dermal exposure:

The non-carcinogenic risk from dermal exposure has also been assessed through the HQ. In this study, it varies from 0.0032 to 6.34 with a mean value of 0.921 for men and from 0.0031 to 6.29 with a mean of 0.913 for women. However, it ranges from 0.0011 to 2.25 with a mean of 0.327 for children (Table 2). The dermal HQ is comparatively high for men followed by women and children as per the mean HQ values. Moreover, 28.8% of water samples for adults and 8% for children exceeded the HQ value 1, indicating non-carcinogenic risk from dermal exposure to arsenic. Besides, spatial variation maps represent a major portion, except that in some parts of the study area, the HQ value lies <1, indicating no non-carcinogenic risk from dermal exposure to arsenic for the respective group of people and it is low for children (Figure 5d-f).

3.3.1.3 Total hazard index from oral and dermal exposure:

In this study, the total hazard index (THI) or cumulative hazard quotients varies from 0.11 to 211.47 with a mean value of 30.72 for men and 0.11 to 228.51 with a mean of 33.20 for women. It also varies from 0.07 to 144.48 with a mean of 20.99 for children (Table 2). The THI is comparatively higher for women, followed by men and children, as per mean THI values (Figure 6). Moreover, 83.2% of water samples for all the respective groups of people

lie above the HQ value of 1, indicating non-carcinogenic risk from combined oral and dermal exposure to arsenic. Besides, from the categorical classification, 16.8% of the samples for children have a negligible non-carcinogenic health risk. However, 16.8% of the samples for adults have a low significant non-carcinogenic health risk. Whereas 83.2% of samples for adults and 81.6% children lie in the very high risk (>4). Furthermore, the spatial variation map for THI shows similar results as for oral exposure to arsenic (Figure 5g-i).

3.3.2 Carcinogenic risk assessment:

Carcinogenic risk refers to the prediction of cancer risk from exposure to toxic elements. In the study, the carcinogenic risk has been measured from both oral and dermal exposure

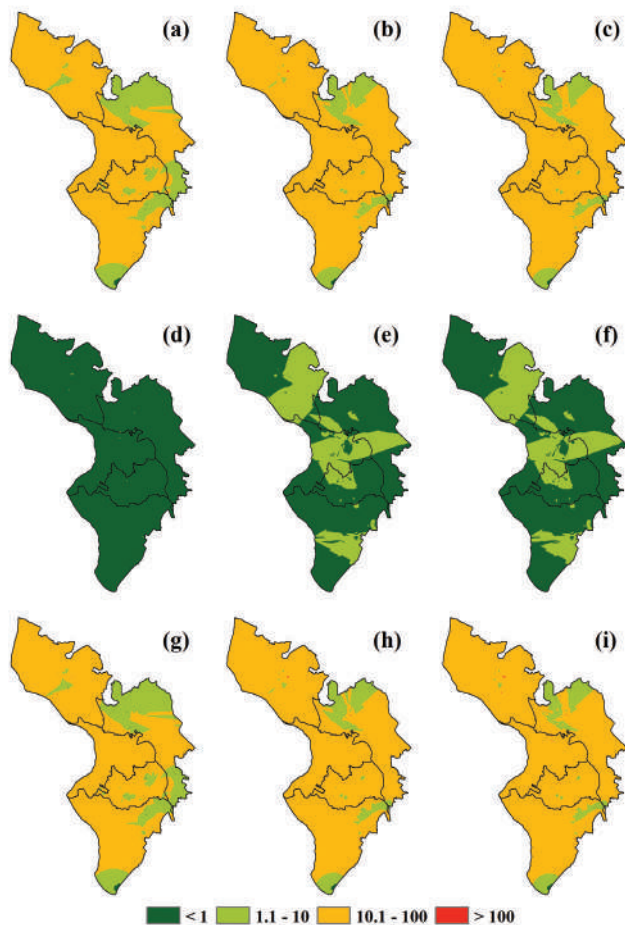


Figure 5. Non-carcinogenic risk (hazard quotient) assessment; (a-c) oral, (d-f) dermal and (g-i) total hazard index (Note: a, d and g for children; b, e and h for men; c, f and i for women).

to arsenic for different age and sex groups. The tolerable range and the risk appears to be significant if the value is $> 10^{-4}$.

3.3.2.1 Carcinogenic risk from oral:

The carcinogenic risk from oral exposure ranges from 2.05×10^{-5} to 4.10×10^{-2} with a mean value of 5.96×10^{-3} for men, 2.22×10^{-5} to 4.44×10^{-2} with a mean value of 6.46×10^{-3} for women and 1.42×10^{-5} to 2.84×10^{-2} with a mean value of 4.13×10^{-3} for children (Table 2). It is high for women compared to other age and sex groups based on the mean values. Besides, 83.2% of samples exceeded the acceptable limit for all the groups of people, indicating a significant carcinogenic risk from the oral exposure to arsenic. Moreover, the spatial variation map indicates that major portions of the study area have a significant carcinogenic risk from oral arsenic exposure and values range from 0.0011 to 0.01 (10^{-3} to 10^{-2}) (Figure 6a-c).

3.3.2.2 Carcinogenic risk from dermal:

The carcinogenic risk from dermal exposure is found to be 1.07×10^{-7} to 2.13×10^{-4} with a mean value of 3.10×10^{-5} for men and 1.06×10^{-7} to 2.11×10^{-4} with a mean value of 3.07×10^{-5} for women. However, for children, it is found to be 3.79×10^{-8} to 7.57×10^{-5} with a mean value of 1.10×10^{-5} (Table 2). It is high for men compared to other groups of people based on the mean value. Besides, only 8% of samples exceeded the acceptable limit for adults, indicating carcinogenic risk from dermal exposure to arsenic. Furthermore, the values < 0.0001 (10^{-4}) lie in almost all portions of the study area, indicating no cancer risk from dermal arsenic exposure (Figure 6d-f).

3.3.2.3 Cancer index (CI) from oral and dermal:

The cancer index or total potential cancer risk values from cumulative oral and dermal exposure range from 2.06×10^{-5} to 4.12×10^{-2} with a mean value of 5.99×10^{-3} for men. For women, it ranges from 2.23×10^{-5} to 4.47×10^{-2} with a mean value of 6.49×10^{-3} . While it varies from 1.43×10^{-5} to 2.85×10^{-2} with a mean value of 4.14×10^{-3} for children (Table 2). It is high for women compared to other groups of people based on the mean values. Besides, 83.2% of samples exceeded the acceptable limit for all the groups of people, indicating a significant carcinogenic risk from combined oral and dermal exposure to arsenic. Further, a similar result is observed for the CI as oral exposure to arsenic in the spatial variation map (Figure 6g-i).

3.4 ANOVA:

In the present investigation, one-way ANOVA has been applied to observe significant variation in health risk between the studied gender and age groups. It is found that all health risk indicators have a significant difference in the study area, demonstrating a significant difference in the health risk among the groups of people (Table 3).

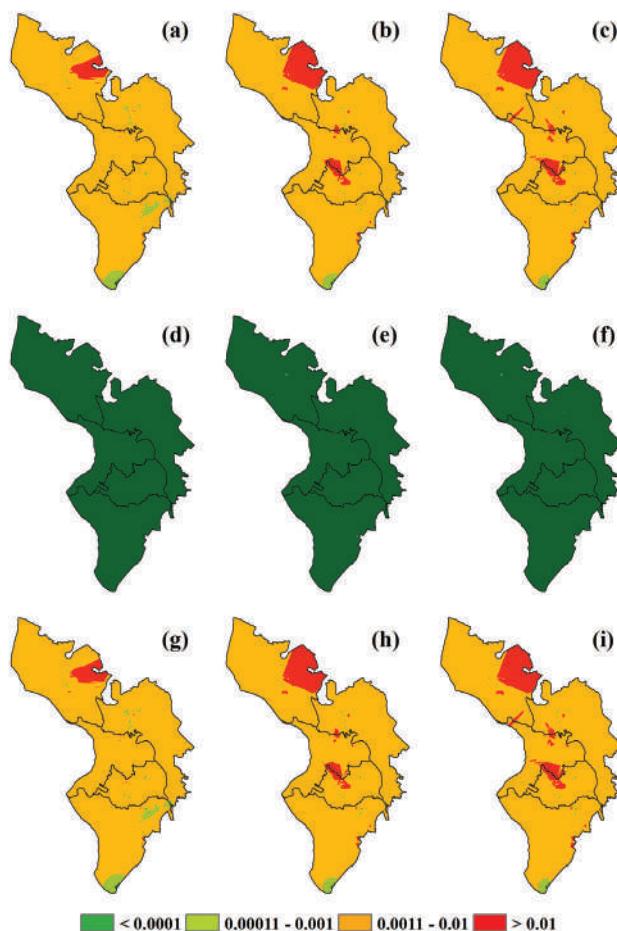


Figure 6. Carcinogenic risk assessment; (a-c) oral, (d-f) dermal and (g-i) total hazard index (Note: a, d and g for children; b, e and h for men; c, f and i for women).

Table 3. One-way ANOVA representing the health risk variation among the different age groups of people (Children, men and women)

Indicators	F	P-value	F-critical	Remarks
OHQ	7.608487	0.000535651	3.007778	Alternative
DHQ	31.02065	1.14353E-13		
THI	8.019464	0.000358141		
CRO	7.608487	0.000535651		
CRD	31.02065	1.14353E-13		
CI	7.67821	0.000500275		

Degree of freedom: 2 and significance level: 0.05

3.5 HCA:

In the present study, Hierarchical cluster analysis (HCA) was used to assemble water samples into clusters based on their similarity. A total of 250 water samples were clustered into two broad groups. The location Ids. of 1, 3, 8, 19, 42, 51, 55, 59, 68, 74, 80, 102, 121, 123, 125, 135, 144, 151-154, 158, 159, 189, 201 and 202 were clustered into the 1st broad group though the rest were clustered into the 2nd broad group (Figure 7). Besides, the 1st broad group were further divided into two sub-groups. In this group, the locations of 1, 3, 51, 55, 59, 123, 152-154, 201, and 202 were clustered into 1st sub-group, while the rest were in the 2nd sub-group. Moreover, the 2nd broad group were also divided into two sub-groups. In this group, the locations of 9, 11, 13, 14, 17, 18, 28, 31, 35, 39, 41, 43-45, 48, 54, 58, 60, 61, 63, 66, 67, 69, 71, 73, 75, 76, 79, 81, 82, 84, 86, 91, 98, 103, 106, 112, 116, 119, 120, 122, 124, 134, 143, 160, 163, 165, 167-169, 179, 181, 187, 190-193, 195, 206, 212, 213, 215, 220 and 230 were clustered into one sub-group and rest were clustered into other sub-clustered.

4 Discussion:

Arsenic is a toxic element, and chronic exposure to it can lead to several long-term diseases, including cancer (Singh *et al.*, 2025). Its pollution and effects on human health are major concerns worldwide (Bhat *et al.*, 2024). Elevated levels of arsenic in surface and ground water which are used for drinking, domestic activities (such as bathing, cooking, cleaning), and irrigation pose serious health risks (Kumar and Nayak, 2025; Hoque *et al.*, 2022). As a public health concern, this study examined arsenic contamination levels and their impact on individuals of different ages and genders within the study area. In the examined blocks of Malda district, high arsenic concentrations were detected in groundwater, with 83.2% of water samples exceeding the permissible limit of 0.01 mg/l as per the WHO (2011) and BIS (2012) standards. The highest arsenic level, of 2 mg/l, was found at Sekhpura village in the Manikchak community development block, significantly surpassing safe levels for drinking water. Similarly, in Adami Tulu Jido Kombolicha District, East Shoa Zone, Oromia Region, Ethiopia, 48.8% of samples exceeded permissible limits, with a maximum concentration of 0.4 mg/l reported by Demissie *et al.* (2024). The contamination factor (CF) also indicates a high degree of arsenic pollution in the study regions, as 83.2% of water samples are deemed unsuitable for human consumption whether for drinking or other uses. Conversely, Kumar *et al.* (2025) found only 23.53% of samples in the Bidupur block of Vaishali district, Bihar (India), to be unsuitable. Moreover, health risk assessments based on average daily and dermal absorbed doses reveal that oral exposure is higher among women due to longer exposure durations, while dermal exposure is greater in men because of the larger skin surface area available for contact. The non-carcinogenic risk assessment shows a substantial health threat from arsenic exposure (both oral and dermal), with 83.2% of water samples posing a non-carcinogenic risk across all groups. Patel *et al.* (2021) identified a higher non-carcinogenic risk from oral exposure among children. Additionally, comparable to non-carcinogenic risks, 83.2% of samples also carry a carcinogenic risk for all demographic groups, indicating a

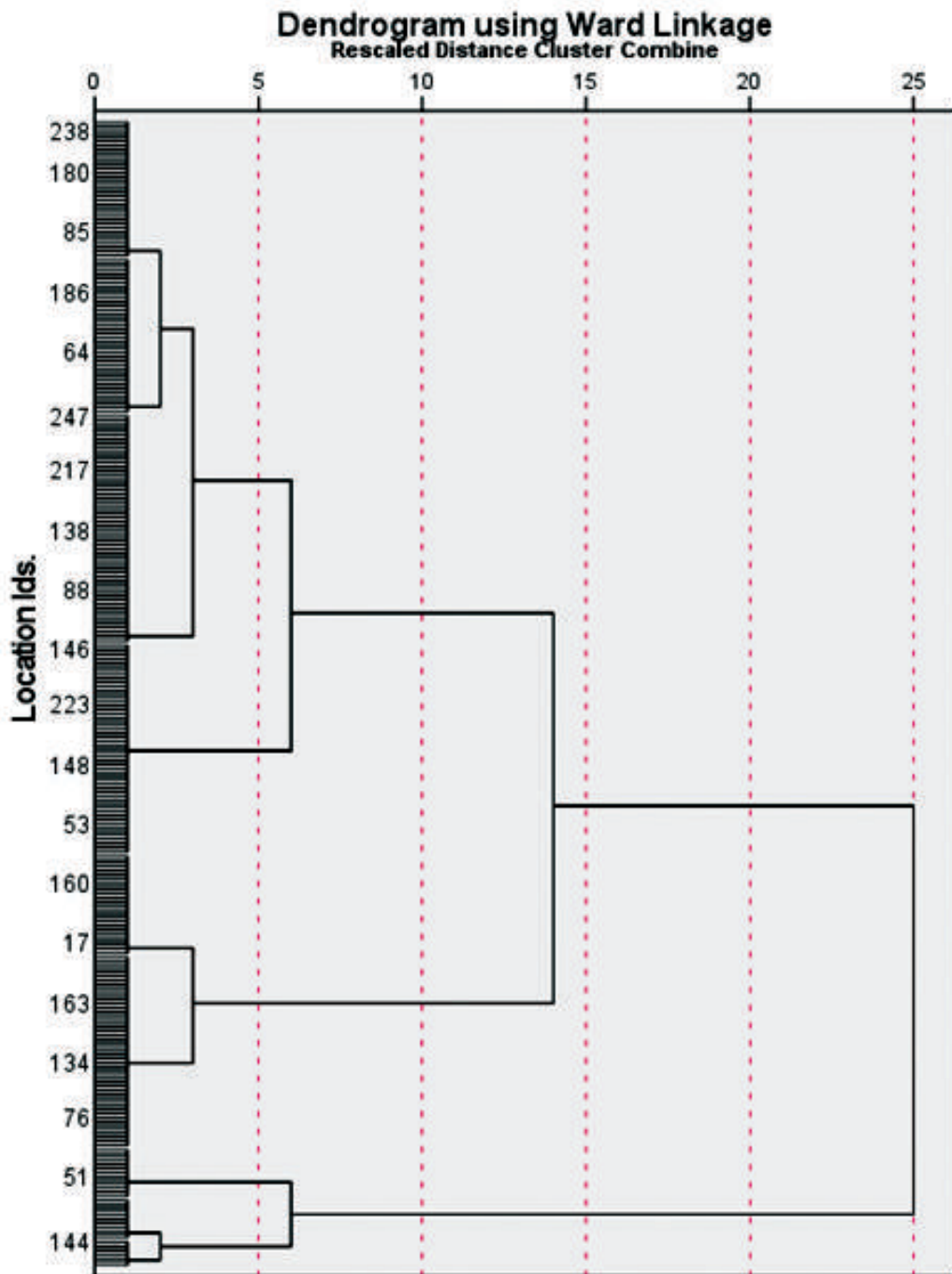


Figure 7. Dendrogram using HCA of arsenic health risk for the section.

significant threat from combined oral and dermal arsenic exposure. Overall, the evaluation of human health risks (both non-carcinogenic and carcinogenic) points to a greater health hazard from arsenic, particularly affecting women more than other groups within the study area. The findings largely align with those of Kumar *et al.* (2025). Furthermore, ANOVA analysis reveals significant differences in health risks among various population groups.

Furthermore, as elevated arsenic concentrations are found in the study area, long-term exposure to arsenic leads to severe health impacts, such as arsenic poisoning (arsenicosis). The effects of arsenic exposure on human health have been observed, and arsenic poisoning cases have been identified in the study area (Figure 8a-d). As the study findings indicate a health risk (both carcinogenic and non-carcinogenic) from arsenic exposure during the field investigation, these effects are also evident in the area. People are suffering from arsenic poisoning, which can lead to cancer, and some individuals have even died due to cancer caused by arsenic poisoning, according to local residents. The major reasons behind the higher concentration of arsenic in these locations are the geological processes involving lithological and pedological factors and the impact of the river Ganga. Arsenic is mainly deposited in the groundwater through the leaching process in the region.

5. Signification, limitations of the study and policy recommendations:

This study is pioneering work that attempts to evaluate arsenic contamination and assess the impact of its exposure on human health risks (carcinogenic and non-carcinogenic) based on field investigations. However, there are some limitations in this study, such as the lack of secondary data regarding water quality, especially arsenic levels in the spatio-temporal dimension. Additionally, this study focuses solely on arsenic contamination and its effects on human health; it does not address the impact of other trace elements (toxic metals). Nevertheless, the findings of the current study are important for formulating policy recommendations. For example, initiatives like the provision of safe drinking water through the Jal Jeevan Mission (JJM) and projects similar to Sajal Dhara, as well as human health risk assessments, could be pursued for future development. The present study indicates that 83.2% of water samples from the sites are unsuitable for human use and pose health risks. Therefore, the water quality at these locations should be monitored regularly across different seasons and avoided for future use. Furthermore, groundwater should be purified before drinking and other uses within the study area. In many countries worldwide, strict regulations are in place for arsenic concentrations in drinking water, with a maximum contaminant level (MCL) of less than 0.01 mg/l to protect health. Thus, this study may be useful for various stakeholders and regional planners, helping to devise better plans for ensuring safe drinking water and raising health awareness. This approach could help reduce groundwater reliance and promote sustainable surface water management.

6. Conclusions:

In this study, a high concentration of arsenic in groundwater is observed in the studied blocks of Malda, which is significantly above the acceptable limit for drinking water. It is also found that



Figure 8. Field photo regarding the impact of arsenic exposure on human health, arsenic poisoning, or arsenicosis, (a-d) arsenic patient.

83.2% of water samples exceed the permissible limit. Specifically, the arsenic concentration in groundwater is higher in the Kaliachak-II block compared to other blocks in Malda, with 94% of water samples surpassing the permissible limit and an average arsenic concentration of 0.36 mg/l. Moreover, CF reveals that 81.6% of the samples are highly contaminated, and overall, 83.2% are unfit for drinking and human consumption in the study area. Additionally, human health risk assessment shows that the average daily dose (ADD) of arsenic via oral intake is higher for women, while dermal exposure is higher in men than in other age and gender groups. The non-carcinogenic risk assessment, based on the hazard quotient (HQ), indicates that 83.2% of the samples pose a non-carcinogenic risk from oral exposure across all relevant groups. However, 28.8% of samples for adults and 8% for children pose a non-carcinogenic risk from dermal exposure. The total hazard index (THI) confirms that 83.2% of the samples present a non-carcinogenic risk for all groups. The carcinogenic risk from oral arsenic exposure shows that 83.2% of samples have a carcinogenic risk across all groups, whereas only 8% of samples pose a carcinogenic risk to adults through dermal exposure. The cancer index (CI) also indicates that 83.2% of the samples carry a significant carcinogenic risk from both oral and skin exposure to arsenic. Furthermore, ANOVA reveals a significant difference in health risks among different groups. Consequently, this research aims to support safe drinking water practices and promote health awareness among stakeholders and regional planners, thereby contributing to sustainable water resource management and the achievement of Sustainable Development Goal 6 (SDG 6).

The Acknowledgements:

We would acknowledge the Indian Council of Social Science Research (ICSSR).

Funding:

This study was funded by the Indian Council of Social Science Research (ICSSR), F.N. 49/2024-25/JJM/SC/RP/ICSSR.

Data availability statement:

Data will be made available on request.

Author contribution statement:

All authors were involved in the conception and design of the study and reviewed the final manuscript version. J.D. is the principal investigator responsible for conception, investigation, project administration, visualization, and writing of the original manuscript. A.M., S.S., P.C., and N.C. participated in conceptualisation, data curation, formal analysis, and investigation. M.M.H. contributed to conceptualisation, data curation, formal analysis, investigation, methodology, software, visualisation, writing – original draft, and review & editing.

Conflict of Interest:

The authors declare that they have no known competing financial interests or personal relationships that could have appeared to influence the work reported in this paper.

Clinical trial number: not applicable

References:

- Abanyie, S. K., Apea, O. B., Abagale, S. A., Amuah, E. E. Y., & Sunkari, E. D. (2023). Sources and factors influencing groundwater quality and associated health implications: A review. *Emerging Contaminants*, 9(2), 100207. <https://doi.org/10.1016/j.emcon.2023.100207>
- Afreen S, Kumari P, Sulaiman MA, Zafar MM, Divya, Ranjan S et al (2025) Comparative health risk assessment of arsenic and fluoride toxicity in the rural area groundwater in the middle Gangetic plain at Muzaffarpur, India. *Bull Natl Res Cent* 49(1): 56. <https://doi.org/10.1186/s42269-025-01344-0>
- Ahmed SF, Kumar PS, Rozbu MR, Chowdhury AT, Nuzhat S, Rafa N et al (2022) Heavy metal toxicity, sources, and remediation techniques for contaminated water and soil. *Environ Technol Innov* 25: 102114. <https://doi.org/10.1016/j.eti.2021.102114>
- Bashir MH, Asif A, Ahmad HR, Abbas A, Shehzad MT (2025) Spatio-temporal assessment of heavy metal contamination in groundwater along Madhuana drain, Faisalabad: source apportionment and health risk analysis. *Environ Geochem Health* 47(7): 251. <https://doi.org/10.1007/s10653-025-02563-0>
- Bhat, A., Ravi, K., Tian, F., & Singh, B. (2024). Arsenic contamination needs serious attention: an opinion and global scenario. *Pollutants*, 4(2), 196-211. <https://doi.org/10.3390/pollutants4020013>

BIS (2012) DRINKING WATER – SPECIFICATION. https://cpcb.nic.in/wqm/BIS_Drinking_Water_Specification.pdf

Chakraborti D, Das B, Rahman MM, Chowdhury UK, Biswas B, Goswami AB et al (2009) Status of groundwater arsenic contamination in the state of West Bengal, India: A 20 year study report. *Mol Nutr Food Res* 53(5): 542-551. <https://doi.org/10.1002/mnfr.200700517>

Chen X, Liu S, Luo Y (2023) Spatiotemporal distribution and probabilistic health risk assessment of arsenic in drinking water and wheat in Northwest China. *Ecotoxicol Environ Saf* 256: 114880. <https://doi.org/10.1016/j.ecoenv.2023.114880>

Das, N., Patel, A. K., Deka, G., Das, A., Sarma, K. P., & Kumar, M. (2015). Geochemical controls and future perspective of arsenic mobilization for sustainable groundwater management: a study from Northeast India. *Groundwater for Sustainable Development*, 1(1-2), 92-104. <https://doi.org/10.1016/j.gsd.2015.12.002>

Demissie S, Mekonen S, Awoke T, Teshome B, Mengistie B (2024) Examining carcinogenic and noncarcinogenic health risks related to arsenic exposure in Ethiopia: A longitudinal study. *Toxicol Rep* 12: 100-110. <https://doi.org/10.1016/j.toxrep.2024.01.001>

Dhamija S, Joshi H (2025) Human Health Risk Assessment from Arsenic Pollution in a Groundwater–Soil–Crop System. *J Hazard Toxic Radioact Waste* 30(1): 04025029. <https://doi.org/10.1061/JHTRBP.HZENG-1493>

El-Ghiaty MA, El-Kadi AO (2021) Arsenic: Various species with different effects on cytochrome P450 regulation in humans. *EXCLI J* 20: 1184. DOI: 10.17179/excli2021-3890

Erickson, M. L., Malenda, H. F., Berquist, E. C., & Ayotte, J. D. (2019). Arsenic concentrations after drinking water well installation: Time-varying effects on arsenic mobilization. *Science of the Total Environment*, 678, 681-691. <https://doi.org/10.1016/j.scitotenv.2019.04.362>

Fatoki, J. O., & Badmus, J. A. (2022). Arsenic as an environmental and human health antagonist: A review of its toxicity and disease initiation. *Journal of Hazardous Materials Advances*, 5, 100052. <https://doi.org/10.1016/j.hazadv.2022.100052>

Genchi, G., Lauria, G., Catalano, A., Carocci, A., & Sinicropi, M. S. (2022). Arsenic: a review on a great health issue worldwide. *Applied Sciences*, 12(12), 6184. <https://doi.org/10.3390/app12126184>

Hoque MM, Islam A, Islam ARMT, Pal SC, Mahammad S, Alam E (2023) Assessment of soil heavy metal pollution and associated ecological risk of agriculture dominated mid-channel bars in a subtropical river basin. *Sci Rep* 13(1): 11104. <https://doi.org/10.1038/s41598-023-38058-0>

Hoque MM, Islam A, Mahammad S (2022) Assessing the surface and bottom river water quality for drinking purpose and human health risk analysis: a study of Damodar River, India. *Arab J Geosci* 15(23): 1734. <https://doi.org/10.1007/s12517-022-10987-6>

Kanel, S. R., Das, T. K., Varma, R. S., Kurwadkar, S., Chakraborty, S., Joshi, T. P.,... & Nadagouda, M. N. (2023). Arsenic contamination in groundwater: Geochemical basis of treatment technologies. *ACS Environmental Au*, 3(3), 135-152. <https://doi.org/10.1021/acsenvironau.2c00053>

Kumar M, Panday DP, Goswami R, Neog N, Bahukhandi KD, Zhang J, Bhattacharya P (2025) Dynamics of Arsenic Co-contamination in the Groundwater of the Eastern Himalayas: The Biogeochemical

Drivers and GRACE-Based Evidence. *ACS ES T Water* 5(6): 2833-2847. <https://doi.org/10.1021/acsestwater.4c00106>

- Kumar P, Khan PK, Kumar A (2025) Health risk assessment upon exposure to groundwater arsenic among individuals of different sex and age groups of Vaishali district, Bihar (India). *Toxicol Rep* 14: 102024. <https://doi.org/10.1016/j.toxrep.2025.102024>
- Kumar V, Shekhar S (2025) Insights into the arsenic contamination status and hydrogeochemical characteristics of major river basins in Bihar, India, after two decades of investigations. *H2Open J* 8(3): 115-138. <https://doi.org/10.2166/h2oj.2025.055>
- Kumar, S., & Nayak, D. (2025). Assessing the health costs of arsenic-contaminated drinking water in Bihar, India: A bivariate probit analysis. *Groundwater for Sustainable Development*, 29, 101429. <https://doi.org/10.1016/j.gsd.2025.101429>
- Li J, Guo C, Liu Y, Han B, Lv Z, Jiang H et al (2025) Chronic arsenic exposure-provoked biotoxicity involved in liver-microbiota-gut axis disruption in chickens based on multi-omics technologies. *J Adv Res* 67: 373-386. <https://doi.org/10.1016/j.jare.2024.01.019>
- Mahar H, Memon AR, Ishfaq A, Soomro SA (2024) The surveillance of arsenic levels in the drinking water of primary schools and the assessment of the potential cancer-related health risks of children in Multan, Pakistan. *Emerg Contam* 10(1): 100252. <https://doi.org/10.1016/j.emcon.2023.100252>
- Mazumder, D. N. G., Ghosh, A. K., Majumdar, K. K., Mukherjee, S., & Majumder, P. K. (2020). Ground water arsenic contamination in Malda, West Bengal, India: epidemiology and efficacy of mitigation measures. DOI: 10.5530/ijmedph.2020.1.7
- Mohan I, Jasrotia R, Dhar S, Bhau BS, Pathania D, Khargotra R (2024) Pollution indices and correlation of heavy metals contamination in the groundwater around brick kilns in Jammu and Kashmir, India. *Heliyon* 10(6). <https://doi.org/10.1016/j.heliyon.2024.e27869>
- Monteiro De Oliveira EC, Caixeta ES, Santos VSV, Pereira BB (2021) Arsenic exposure from groundwater: environmental contamination, human health effects, and sustainable solutions. *J Toxicol Environ Health - B* 24(3): 119-135. <https://doi.org/10.1080/10937404.2021.1898504>
- Mouttoucomarassamy S, Virk HS, Dharmalingam SN (2024) Evaluation and health risk assessment of arsenic and potentially toxic elements pollution in groundwater of Majha Belt, Punjab, India. *Environ Geochem Health* 46(6): 208. <https://doi.org/10.1007/s10653-024-02002-6>
- Mukherjee A, Sengupta MK, Hossain MA, Ahamed S, Das B, Nayak B et al (2006) Arsenic contamination in groundwater: a global perspective with emphasis on the Asian scenario. *J Health Popul Nutr* 24(2): 142-163
- Nayeem SMMR, Zakir HM, Sharmin S, Rashid MH, Sarker A, Rahman A et al (2025) Elevated levels of Pb, Mn and Cd in deep aquifers of Gazipur, Bangladesh: A threat to drinking water safety and public health. *J Hazard Mater Adv* 18: 100698. <https://doi.org/10.1016/j.hazadv.2025.100698>
- Nemati B, Fallahizadeh S, Mostafaei G, Miranzadeh MB (2025) Health risk assessment of toxic elements in Kashan drinking water reservoirs using Monte Carlo simulation and sensitivity analysis. *Sci Rep* 15(1): 17806. <https://doi.org/10.1038/s41598-025-01847-w>
- Nriagu, J. O., Bhattacharya, P., Mukherjee, A. B., Bundschuh, J., Zevenhoven, R., & Loeppert, R. H.

- (2007). Arsenic in soil and groundwater: an overview. *Trace Metals and other Contaminants in the Environment*, 9, 3-60. [https://doi.org/10.1016/S1875-1121\(06\)09001-8](https://doi.org/10.1016/S1875-1121(06)09001-8)
- Ozturk M, Metin M, Altay V, Bhat RA, Ejaz M, Gul A et al (2022) Arsenic and human health: genotoxicity, epigenomic effects, and cancer signaling. *Biol Trace Elem Res* 200(3): 988-1001. <https://doi.org/10.1007/s12011-021-02719-w>
- Palma-Lara I, Martínez-Castillo M, Quintana-Pérez JC, Arellano-Mendoza MG, Tamay-Cach F, Valenzuela-Limón OL et al (2020) Arsenic exposure: A public health problem leading to several cancers. *Regul Toxicol Pharmacol* 110: 104539. <https://doi.org/10.1016/j.yrtph.2019.104539>
- Patel AK, Singh A, Das N, Kumar M (2021) Health risk associated with consumption of arsenic contaminated groundwater in the Ganga and the Brahmaputra floodplain of India. *Case Stud Chem Environ Eng* 3: 100103. <https://doi.org/10.1016/j.csee.2021.100103>
- Poddar D, Mukhopadhyay S, Das J (2023) Assessment of the Social Impact of Arsenicosis Through Groundwater Arsenic Poisoning in Malda District. In: *Monitoring and Managing Multi-hazards*. Springer, Cham, pp 221-235. https://doi.org/10.1007/978-3-031-15377-8_15
- Prakash S, Verma AK (2021) Arsenic: it's toxicity and impact on human health. *Int. J. Biol. Innov* 3(1): 38-47. <https://doi.org/10.46505/IJBI.2021.3102>
- Prasath BB (2025) Heavy Metal Pollution in Groundwater: Environmental and Health Concerns in Gujarat, India. In: *Groundwater Resource Management Planning Strategies: A Geospatial Approach: Volume 1*. Cham, Springer Nature Switzerland, pp 155-172. https://doi.org/10.1007/978-3-031-88870-0_6
- Rae ID (2020) Arsenic: its chemistry, its occurrence in the earth and its release into industry and the environment. *Chem Texts* 6(4): 25. <https://doi.org/10.3389/fphar.2021.643972>
- Rahman MM, Mandal BK, Chowdhury TR, Sengupta MK, Chowdhury UK, Lodh D et al (2003) Arsenic groundwater contamination and sufferings of people in North 24-Parganas, one of the nine arsenic affected districts of West Bengal, India. *J Environ Sci Health - A* 38(1): 25-59. <https://doi.org/10.1081/ESE-120016658>
- Raju, N. J. (2022). Arsenic in the geo-environment: A review of sources, geochemical processes, toxicity and removal technologies. *Environmental research*, 203, 111782. <https://doi.org/10.1016/j.envres.2021.111782>
- Santra, B. K. (2017). Arsenic contamination of groundwater in West Bengal: awareness for health and social problems. *International Journal of Applied Science and Engineering*, 5(1), 43-46. DOI: 10.5958/2322-0465.2017.00005.3
- Sarkar, M., & Pal, S. C. (2021). Human health hazard assessment for high groundwater arsenic and fluoride intact in Malda district, Eastern India. *Groundwater for Sustainable Development*, 13, 100565. <https://doi.org/10.1016/j.gsd.2021.100565>
- Saxena V (2025) Water quality, air pollution, and climate change: investigating the environmental impacts of industrialization and urbanization. *Water Air Soil Pollut* 236(2): 73. <https://doi.org/10.1007/s11270-024-07702-4>
- Shaji E, Santosh M, Sarath KV, Prakash P, Deepchand V, Divya BV (2021) Arsenic contamination of

groundwater: A global synopsis with focus on the Indian Peninsula. *Geosci Front* 12(3): 101079. <https://doi.org/10.1016/j.gsf.2020.08.015>

- Shankar, S., Shanker, U., & Shikha. (2014). Arsenic contamination of groundwater: a review of sources, prevalence, health risks, and strategies for mitigation. *The scientific world journal*, 2014(1), 304524. <https://doi.org/10.1155/2014/304524>
- Singh, S., Singh, N., Chauhan, A., Koshta, K., Baby, S., Tiwari, R.,... & Srivastava, V. (2025). Prenatal arsenic exposure alters EZH2/H3K27me3 to induce RKIP/NF-kB/ERK1/2-mediated early-onset kidney disease in mouse offspring. *Environmental Science and Pollution Research*, 1-20. <https://doi.org/10.1007/s11356-025-36229-2>
- Sridhar D, Parimalarenganayaki S (2025) Groundwater quality assessment in urban parts of Vellore city, India: Focusing on Nitrogen Species contamination and its health risk analysis. *Clean Eng Technol* 26: 100945. <https://doi.org/10.1016/j.clet.2025.100945>
- Sunitha V, Reddy YS, Suvarna B, Reddy BM (2022) Human health risk assessment (HHRA) of fluoride and nitrate using pollution index of groundwater (PIG) in and around hard rock terrain of Cuddapah, AP South India. *Environ Chem Ecotoxicol* 4: 113-123. <https://doi.org/10.1016/j.enceco.2021.12.002>
- USEPA (2014) Human Health Evaluation Manual, Supplemental Guidance: Update of Standard Default Exposure Factors, OSWER Directive 9200. United States Environmental Protection Agency, Washington, DC, pp 1–120
- VAN PAEMEL, M., DIERICK, N., JANSSENS, G., FIEVEZ, V., & DE SMET, S. (2010). Selected trace and ultratrace elements: Biological role, content in feed and requirements in animal nutrition—Elements for risk assessment. *EFSA Supporting Publications*, 7(7), 68E. <https://doi.org/10.2903/sp.efsa.2010.EN-68>
- Watson, J., Thomas, S., & Goodfellow, T. (2022). Groundwater resource management during construction dewatering. *Sustainable Water Resources Management*, 8(4), 91. <https://doi.org/10.1007/s40899-022-00678-1>
- WHO (2011) Guidelines for Drinking-water Quality. https://iris.who.int/bitstream/handle/10665/44584/9789241548151_eng.pdf



Landslide Susceptibility Mapping of Mamit District, Mizoram: A Comparative Analysis of Bivariate Statistical Methods

Dennis Lalhruaitluanga^{1*}, K. Srinivasa Rao¹ and Jimmy Lalnunmawia¹

¹*Department of Geology, Mizoram University, Aizawl – 796001, India*
Corresponding author: dennisfanai08@gmail.com

Abstract: This research work conducted landslide susceptibility mapping within the Mamit District of Mizoram, India. It seeks to present the necessity for risk assessment in landslide prone areas, especially during the monsoon seasons. This study also comparatively analyses the efficiency of four distinct bivariate statistical approaches like the Frequency Ratio (FR), Information Value (IV), Shannon Entropy (SE) and Weight of Evidence (WofE) to develop landslide susceptibility maps. The analysis utilised 318 past landslide points and 13 landslide causative factors generated within ArcGIS 10.8. The resulting susceptibility maps produced were assigned five susceptibility classes: “very low”, “low”, “moderate”, “high”, and “very high”. The findings revealed that the SE method was the best effective approach among the methods utilised because of its superior prediction ability. The SE method achieved AUC scores of 84.2 and 84.6 per cent for success and prediction correspondingly. Also, the findings suggest that vital factors that contribute to landslide susceptibility include slope degrees ranging from 37° to 78°, elevations between 739 and 1420 m, barren land, built-up areas, low vegetation regions, lithology characterised by grey sandy splintery shale, siltstone and mudstone, proximity to roads within 100 to 300 m and long-term annual rainfall levels between 23,884 and 24,514 mm (2013 to 2022). Susceptibility classes varied among the different methods, with ‘Moderate’ and ‘Low’ classes covering most areas.

Keywords: Landslide Susceptibility Mapping, Geographic Information System, Bivariate Statistical Methods, Mamit District, Mizoram.

1. Introduction:

Landslides are one of the most destructive natural catastrophes at a global scale [1,2]. India is a country with high number of landslides occurrences, where about 12.6 per cent of the

total landmass (0.42 million km²) of the country is at risk of landslides [3,4]. As stated by the National Disaster Management Authority (NDMA) [5], in India, the number of casualties due to landslides ranged between hundreds and more than a thousand each year, depending on the severity of monsoon seasons and events that result in landslides [4,6]. The Landslide Atlas of India stated that Mizoram has the highest number of landslide incidences recorded throughout the country in 1998-2022 [7]. In Mizoram alone, landslide events have been very devastating with some notable ones being the 1992 South Hlimen landslide which took around 100 lives and the Laipuitlang rockslide in 2013 which claimed 17 lives [1,7]. Melthum, Aizawl landslide on 28th of May 2024, resulted to 34 fatalities, and evacuation of 54 houses affecting 72 families [8]. The 2010 landslide and subsidence that occurred at Bazar Veng locality in Mamit town led to the evacuation of 50 families and demolition of 43 houses [9].

This work discussed the need of risk assessment in landslide prone regions, especially during the monsoon seasons, and is the first comparative validation of four separate bivariate statistical methodologies in Mamit district, Mizoram using a cross-validation methodology. Although the four bivariate models (FR, SE, WofE and IV), have been widely used in other global contexts and other regions of India [10–12], few studies have tested these techniques in the unique geological and climatic setting of Mamit district Mizoram, and none have conducted systematic model cross-validation in the region. The primary research in Mizoram has mainly been on the individual landslide studies or hazards zonation of the site by various methodologies. For example, [9] have applied “landslide hazard zonation of Mamit town using Remote Sensing and GIS techniques” [5], with a weightage rating system, and [7] have applied three bivariate statistical models (IV, FR, and WofE) to Aizawl Municipal area with success rates of 83.7-83.9 per cent.

Recent studies show that bivariate statistical methods like Frequency Ratio, Evidential Belief Function (EBF) and Index of Entropy (IOE) are effective in landslide susceptibility mapping in Mizoram [13,14]. These models and especially EBF and IOE have demonstrated high levels of predictive accuracy and are confirmed as powerful models of integrating high susceptible zones to aid disaster mitigation and informed land-use development [13]. Nevertheless, these studies were also geographically constrained and have not used thorough comparative validation of several bivariate methods with cross-validation to have a wider regional scope. Earlier research in Northeast India has centred on individual states such as Meghalaya [15] or specific highway corridors within Manipur [10], whereas no literature-based comprehensive comparative bivariate validation of Mizoram has been carried out [7]. The study addresses a serious deficiency in landslides susceptibility mapping in Northeast India, namely the first comprehensive comparative study of these four bivariate models with stringent validation in the geologically weak terrain of the Middle and Upper Bhuban formations of the Surma Group of Mizoram [9].

This paper fills that gap as it offers the first valid comparative study of FR, IV, SE and WofE techniques in the weak geologic terrain of the Middle and upper Bhuban formations of the Surma Group of the Mizoram. The results will be useful in the scientific knowledge and practical decision making in disaster risk management and planning in high landslide risk regions of Mamit district.

Study area:

The study region, Mamit District is situated in the northeast state of Mizoram, India. It covers an area of 3025.75 Km²s and geographically lies on the coordinates of 23.94°N latitude and 92.48°E longitude. It is also bounded by Kolasib district on the east, Aizawl district on the south, North Tripura district on the north and shares its boundary in the west with Bangladesh. It is also covered by Survey of India toposheets 83D/8, 84A/5, 84A/9 and 84A/10.

Geomorphologically, the district is dominated by the mountainous and parallel to sub-parallel trend of hill ranges oriented in north-south. The entire landscape is characterised

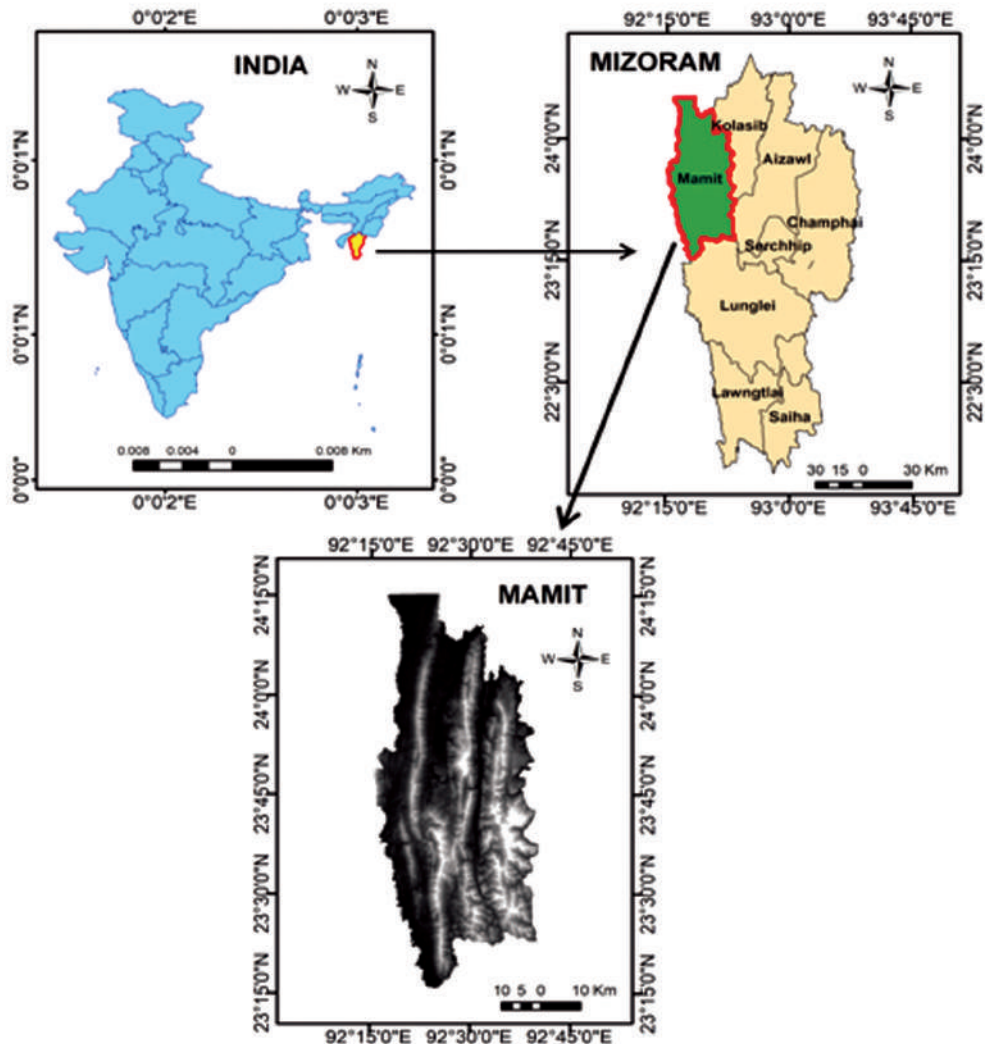


Figure 1. Map of the study area, Mamit District.

by steep-sided hills separated by narrow synclinal valleys which is characteristic for denudostructural hills and valleys [16]. Lithologically the region is largely dominated by argillaceous rocks such as shale, siltstone and mudstone and fine-grained compact sandstone [16]. The major geologic formation is Barail formation (Oligocene age) and Surma formation (Miocene age), of which Bhuban formation of Surma Group occupies about 90% of the district. This formation is characterised by alternating beds of hard sandstone, shale and siltstone [16]. The Surma Group represents sedimentary sequences deposited in deltaic to shallow marine environments, which add to the inherent instability of the slope, which is further affected by coastal stability [7].

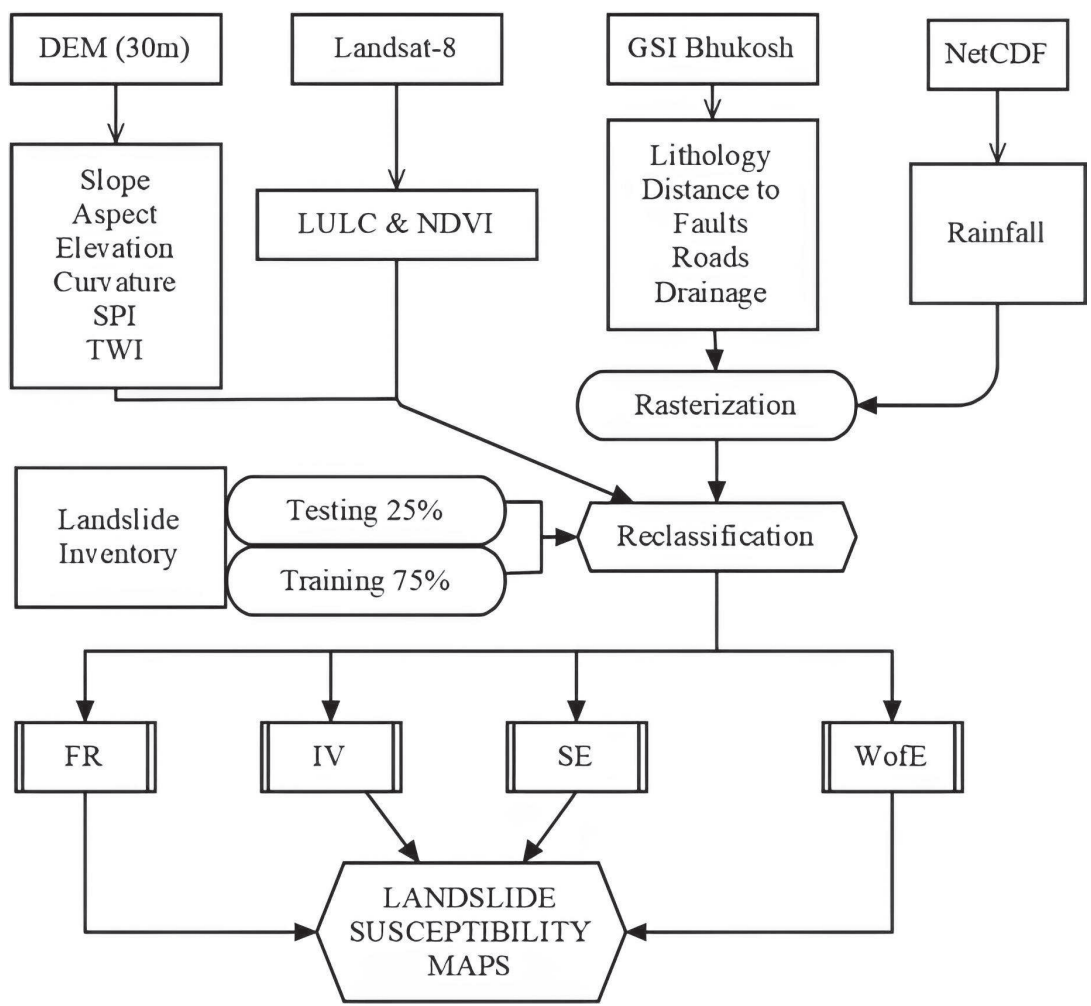


Figure 2. Flow diagram of the process..

Mamit district is highly vulnerable to landslides, which reoccurs with high degree of severity during monsoon season. Few significant landslide events have essentially caused large socio-economic consequences such as the demolition of 43 houses, and the evacuation of 50 families in the locality of Bazar Veng, Mamit in 2010 [9]. Other landslide events have also occurred during the past few years which led to the closure of national highways NH-44 and NH-108, leading to major disruptions in regional mobility and trade. Frequency and magnitude of incidence of such landslides are the evidence of importance of systematic landslide susceptibility analysis, determining mitigation approaches and land use planning [13,17].

2. Materials and Methods:

The procedure used to prepare the landslide susceptibility map of Mamit District include gathering of data, preprocessing of landslide causing factors within ArcGIS environment, acquiring of the previous landslide points, and the usage of the bivariate statistical approaches. A graphic illustration of the process carried out is shown in Figure 2.

2.1 Data Collection:

Reputable sources of data have been used to carry out the current analysis using satellite imagery, meteorologic records, and geological databases, as outlined in Table 1. All datasets were standardised to 30m resolution using ArcGIS 10.8, to ensure consistency in subsequent analyses.

Table 1. Data utilised for the study with their sources

Sl. No.	Data Type	Particulars	Resolution/ Format	Data Source
1	Satellite Data	DEM and Landsat-8	30 m	https://earthexplorer.usgs.gov/
2	Rainfall Data	NetCDF Gridded Data	0.25° × 0.25°	https://www.imdpune.gov.in/
3	Geological Data	Lithology, Faults	Vector	https://bhukosh.gsi.gov.in/
4	Landslide Data	Points and Polygons	Vector	Fieldwork + https://bhukosh.gsi.gov.in/

2.2 Landslide Inducing Factors Generation and Classification:

Thirteen factors that influence landslide occurrence were identified for the study region. These factors were chosen according to the accessibility of data and their proven significance in similar geological and climatic environments.

2.2.1 Topographic Factors:

- a. **Slope:** Generated from DEM using Horn’s algorithm (Spatial Analyst Tools > Surface > Slope) in ArcGIS 10.8 with a Z-factor of 1.0. Continuous slope data were classified into

five categories (0°–15°, 15°–25°, 25°–35°, 35°–45°, >45°) using the Natural Breaks (Jenks) method, optimising variance between classes while minimising within-class variance to reflect natural topographic groupings in the Mamit District.

- b. **Aspect:** Derived via the compass direction method (spatial analysis tools > surface > aspect). It was categorised into ten divisions: Flat, N, NE, E, SE, S, SW, W, NW and N, following standard directional conventions.
- c. **Curvature:** Calculated with a Z-factor of 1.0 (Spatial Analyst Tools > Surface > Curvature). Categorised into three classes (flat, concave and convex) using thresholds of -0.05 and 0.05, consistent with prior topographic studies.
- d. **Elevation:** DEM was utilised to generate the elevation which was categorized into five categories using natural breaks (Jenks) to ensure distinct elevation representation within the study region.

2.2.2 Hydrological Factors:

- a. **Rainfall:** Obtained as average monthly precipitation in NetCDF format (0.25° × 0.25°) from the India Meteorological Department, interpolated to 30 m resolution using bilinear interpolation. Long term annual averages (2013–2022) were classified into five categories via the Natural Breaks method to capture regional precipitation patterns.
- b. **Stream Power Index (SPI):** As shown in equation 1, it is calculated as,

$$TWI = \ln \frac{As}{\tan(\beta)} \quad \dots (1)$$

where As is the flow accumulation derived using the D8 algorithm (Spatial Analyst > Hydrology > Flow Direction, Flow Accumulation). The SPI was categorized into five quantile groups to maintain balanced terrain representation.

- c. **Topographic Wetness Index (TWI):** As shown in equation 2, TWI is calculated as

$$TWI = \ln \frac{As}{\tan(\beta)} \quad (2)$$

where As is the specific catchment area and β is the local slope angle in radians [18,19].

The TWI was classed into five categories using the Natural Breaks (Jenks) method in ArcGIS 10.8 to delineate variations in soil moisture conditions.

- d. **Distance from Drainage:** Determined by applying the Strahler method with a 500-cell threshold to generate a stream network, followed by Euclidean distance computation. Categorised into five classes using Natural Breaks to identify significant proximity zones.

2.2.3 Other Environmental Factors:

- a. **Distance to Roads:** Determined using the Euclidean Distance tool in ArcGIS 10.8 [20], after converting shapefiles from GSI Bhukosh into a 30 m raster. It was reclassified into five categories.

- b. **Land Use and Land Cover (LULC):** Landsat-8 imagery was used to generate LULC by using supervised classification in ArcGIS. Five major LULC types were identified: forests, water bodies, agriculture land, barren land, and built-up areas.
- c. **Normalised Difference Vegetation Index (NDVI):** Using Landsat-8 imagery, NDVI was calculated as shown in equation 3.

$$NDVI = \frac{(NIR - Red)}{(NIR + Red)} \quad \dots (3)$$

Where **NIR** is the Near-Infrared band of the electromagnetic spectrum. It is classified into five categories via Natural Breaks to indicate vegetation density variations.

2.2.4 Geological factors:

- a. **Distance to faults:** Faults are weakness or fractures within the strata or bed of the rocks that can influence landslide. Distance to faults is classed into five distinct classes in metres.
- b. **Lithology:** Lithology means the types of rocks or sediments associated to form the topography or landscape. The different classes of lithological groups within the study area were attained from the GSI portal which was converted into raster format to ensure the layer compatibility for mathematical modelling. All factors were standardised to a 30 m resolution and aligned to the same spatial extent in ArcGIS 10.8 to facilitate compatibility with bivariate statistical analyses. The generated thematic maps of the landslide-inducing factors are shown in Figure 3.

2.2.5 Landslide Inventory:

A high-quality landslide inventory was created that included a large amount of field work that led to the recording of 318 events which were mapped, and the location data of the events was recorded at high accuracy using handheld GPS units. Geological databases and historical records were then combined to maximise the level of dataset completeness [21,22]. The data was randomly divided to calibration and validation sets 75 and 25 percent as training and testing set respectively (238 and 80 points) as shown in Figure 4.

2.4 Statistical Methods:

Four bivariate statistics methods were utilised to conduct the spatial related investigation between landslide influencing factors and occurrences: Frequency Ratio (FR), Shannon Entropy (SE), Weight of Evidence (WofE), Information Value (IV). These methods have been chosen because they were effectively used in landslide susceptibility studies [23–26].

- a. **Frequency Ratio (FR):** This procedure is to divide the frequency of the number of landslides inside a factor class by the frequency of all landslides signifying relatively importance [27–30]. It is expressed in equation 4 as

$$FR_i = \frac{N_{pix}(S_i) / \sum N_{pix}(S)}{N_{pix}(N_i) / \sum N_{pix}(N)} \quad \dots (4)$$

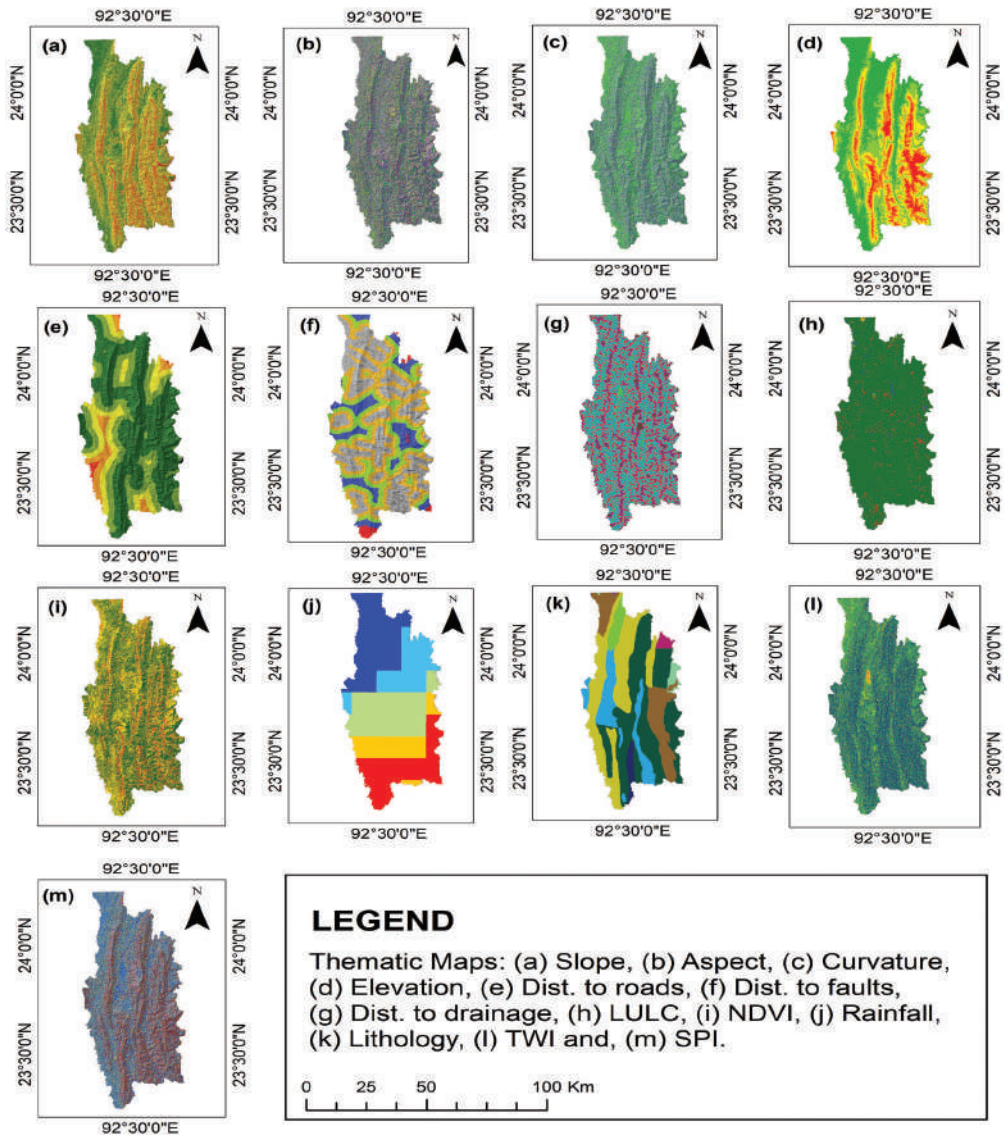


Figure 3. Thematic maps of different landslide inducing factors.

where FR_i = Frequency ratio of the class i , $N_{pix}(S_i)$ is the total number of landslide pixels in class i , the total number of landslide pixels in all classes = $\sum N_{pix}(S)$, $N_{pix}(N_i)$ is the number of pixels in class i (landslide + non-landslide), and $\sum N_{pix}(N)$ is the total number of pixels in the study area [28,31,32]. $FR_i > 1$ implies higher susceptibility to landslides in that particular class and $FR_i < 1$ implies lower susceptibility to landslides. Once the frequency ratio FR_i of each conditioning factor is computed then LSI of a location (pixel) is calculated

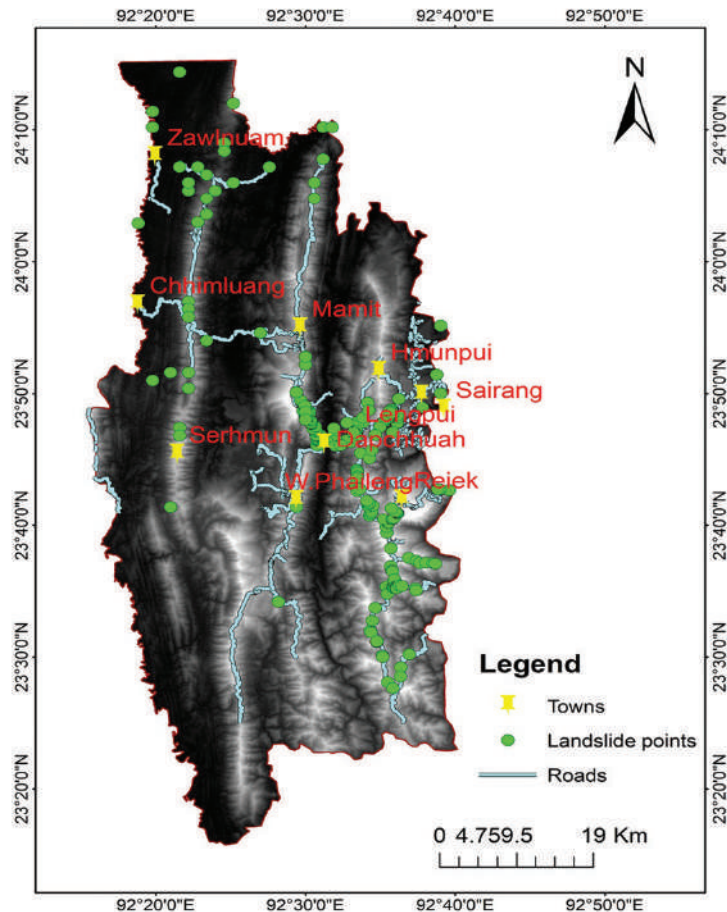


Figure 4. Landslide inventory of the study area.

by summing over frequency ratios of the classes to which the pixel belongs to in all the conditioning factors.

$$LSI = \sum_{j=1}^n FR_{ij} = \dots (5)$$

where FR_{ij} is Frequency Ratio of class ' i ' of factor ' j ' which is used to condition the given pixel and n is the number of conditioning factors.

- b. **Shannon Entropy (SE):** The Shannon Entropy (SE) method offers an objective means of allocating weights to landslide conditioning factors by quantifying the uncertainty of landslide occurrences among factor classes and helps reduce subjectivity in susceptibility mapping [33–37]. The class probabilities for factor j with m_j classes are calculated as:

$$P_{ij} = \frac{FR_{ij}}{\sum_{i=1}^{m_j} FR_{ij}} \quad \dots (6)$$

The entropy for factor j is computed as:

$$E_j = (\ln m_j)^{-1} \sum_{i=1}^{m_j} P_{ij} \ln P_{ij} \quad \dots (7)$$

The information (divergence) of factor j is given by:

$$V_j = 1 - E_j \quad \dots (8)$$

The normalized weights across all n factors are computed as:

$$W_j = \frac{V_j}{\sum_{k=1}^n V_k} \quad \dots (9)$$

where n denotes the total number of criteria.

The final Landslide Susceptibility Index (LSI) was generated by summing the weights for each factor class:

$$LSI = \sum_{i=1}^n W_j \quad \dots (10)$$

where, W_j implies the weight of the j^{th} factor.

- c. **Weight of Evidence (WofE):** It is a statistical, a bivariate process used in landslide susceptibility mapping to identify probability of landslides occurrence with respect to spatial interaction between historical landslides, and other conditioning factors [29,38,39]. WofE is defined as follows:

$$W^+ = \ln \frac{P\{F|L\}}{P\{F|\bar{L}\}} \quad \dots (11)$$

$$\text{and } W^- = \ln \frac{P\{\bar{F}|L\}}{P\{\bar{F}|\bar{L}\}} \quad \dots (12)$$

where F indicates existence of the desirable type of the landslide conditioning factor, \bar{F} represents its absence, L and \bar{L} denotes the presence and absence of landslides, respectively, and P is the probability ratio and ln is the natural logarithm [40]. The following equation will give the weight of the contrast value (C) in terms of positive and negative weights:

$$C = W^+ - W^- \quad \dots (13)$$

Each factor classes were summed together with the weights of value of contrast (C) to create a Landslide Susceptibility Index (LSI).

$$LSI = \sum_{i=1}^n C \quad \dots (14)$$

where 'i' is the class of factors whose values differ from 1 to n.

- d. **Information Value (IV):** This method is a statistic based procedure that determines the extent to which occurrence of a particular kind of a conditioning factor will either increase or decrease the possibility of landslide occurrences relative toward random spatial distributions [41, 42]. The weight for each factor class (W_i) is calculated as

$$W_i = \ln \frac{N_{pix}(Si) / N_{pix}(Ni)}{\sum N_{pix}(Si) / N_{pix}(Ni)} \quad \dots (15)$$

where $N_{pix}(Si)$ is the number of landslide pixels in class 'i', $N_{pix}(Ni)$ is the total number of pixels in class 'i', $\sum N_{pix}(Si)$ is the total number of landslide pixels in the study area, and $\sum N_{pix}(Ni)$ is the total number of pixels in the study area [43,44].

A positive value of W_i indicates that the number of landslides in that respective group is above average showing a better relationship with landslides, whereas a negative W_i means there is a weaker relationship.

The Landslide Susceptibility Index (LSI) map was then formulated by totalling the weights from all factor classes [45]:

$$LSI = \sum_{i=1}^n W_i \quad \dots (16)$$

where 'n' is the number of factor classes.

The spatial relationships amongst the inducing factors and landslides derived from different methods are shown in Table 2. The resulting weighting factors were utilised to create landslide susceptibility maps, delineating zones of varying risks. The spatial relationships are given in Table 2.

Table 2. Spatial relationships of landslide conditioning factors.

Factors	Class	No. of pixel in class	LS pixel in class	% of pixel in class	% of LS pixel in class	IV	FR	W+	W-	C
Aspect	North	186684	13500	5.5	7.39	0.29	1.34	0.31	-0.001	0.31
	NE	407627	25200	12.02	13.79	0.14	1.15	0.14	-0.001	0.14
	East	525125	28800	15.48	15.76	0.02	1.02	0.01	0	0.01
	SE	423367	34200	12.48	18.72	0.41	1.5	0.43	-0.003	0.43
	South	321958	18000	9.49	9.85	0.04	1.04	0.03	0	0.03
	SW	437317	17100	12.89	9.36	-0.32	0.73	-0.34	0.001	-0.35
	West	520052	20700	15.33	11.33	-0.3	0.74	-0.33	0.002	-0.33
	NW	399623	23400	11.78	12.81	0.09	1.09	0.08	0	0.08
Curvature	North	170237	1800	5.02	0.99	-1.61	0.2	-1.68	0.002	-1.68
	Concave	764314	46800	22.51	25.62	0.13	1.14	0.13	-0.001	0.13
	Flat	1966961	101700	57.94	55.67	-0.04	0.96	-0.05	0.001	-0.05
	Convex	663790	34200	19.55	18.72	-0.04	0.96	-0.06	0	-0.06
Dist. to Drain- age	100-300	58223	5400	1.72	2.96	0.54	1.72	0.58	0	0.58
	301-500	467770	52200	13.78	28.57	0.73	2.07	0.78	-0.006	0.79
	501-700	1171597	73800	34.52	40.39	0.16	1.17	0.16	-0.002	0.16
	701-900	1696471	51300	49.98	28.08	-0.58	0.56	-0.61	0.009	-0.62
Elevation	0-155	1149720	27000	33.89	14.78	-0.82	0.44	-0.87	0.008	-0.88
	156-331	812923	19800	23.96	10.84	-0.8	0.45	-0.83	0.005	-0.84
	332-518	671973	33300	19.81	18.23	-0.08	0.92	-0.1	0.001	-0.1
	519-738	541782	43200	15.97	23.65	0.39	1.48	0.41	-0.003	0.42
	739-1420	216172	59400	6.37	32.51	1.63	5.1	1.89	-0.011	1.9
Dist. to Faults	100-300	2037463	99900	60.26	54.68	-0.09	0.91	-0.11	0.002	-0.11
	301-500	1018548	51300	30.12	28.08	-0.07	0.93	-0.08	0.001	-0.08
	501-700	296503	30600	8.77	16.75	0.65	1.91	0.7	-0.003	0.7
	701-900	28738	900	0.85	0.49	-0.55	0.58	-0.57	0	-0.57

Factors	Class	No. of pixel in class	LS pixel in class	% of pixel in class	% of LS pixel in class	IV	FR	W+	W-	C
Lithology	Ferruginous sst with siltstone and clay	156997	5400	4.95	2.96	-0.51	0.6	-0.48	0.001	-0.48
	Grey sandy splintery shale, siltstone and mud- stone	296831	82800	9.36	45.32	1.58	4.84	1.91	-0.015	1.92
	Shale-siltstone se- quence with sst	107825	8100	3.4	4.43	0.26	1.3	0.35	-0.001	0.35
	Shale, siltstone and fossiliferous sst	421486	27000	13.29	14.78	0.1	1.11	0.18	-0.001	0.18
	Shale, siltstone with coal and sst.	51692	4500	1.63	2.46	0.41	1.51	0.51	0	0.51
	Shale, siltstone, mudstone, sst	903191	8100	28.48	4.43	-1.83	0.16	-1.85	0.009	-1.86
	Sst with subordinate siltstone, mudstone, shale	1233275	46800	38.89	25.62	-0.42	0.66	-0.38	0.005	-0.38
LULC	Forest	3300552	145800	97.64	79.8	-0.2	0.82	-0.22	0.008	-0.22
	Barren Land	59083	29700	1.75	16.26	2.23	9.3	2.87	-0.006	2.87
	Built-up	20663	7200	0.61	3.94	1.86	6.45	2.23	-0.001	2.23
NDVI	High Vegetation	1545149	41400	44.56	22.66	-0.67	0.51	-0.74	0.01	-0.74
	Low Vegetation	1434333	79200	41.36	43.35	0.05	1.05	0.02	0	0.02
	No Vegetation	488062	62100	14.08	33.99	0.88	2.42	0.93	-0.008	0.94
Rainfall (mm)	22,203 - 23,043	689635	19800	20.31	10.84	-0.64	0.53	-0.66	0.004	-0.67
	23,044 - 23,883	438134	18000	12.9	9.85	-0.27	0.76	-0.29	0.001	-0.29
	23,884 - 24,514	826032	86400	24.33	47.29	0.66	1.94	0.71	-0.009	0.72
	24,515 - 25,099	559110	31500	16.47	17.24	0.05	1.05	0.04	0	0.04
	25,100 - 26,029	882524	27000	25.99	14.78	-0.56	0.57	-0.6	0.005	-0.6
Dist. to Roads (m)	100-300	1830505	173700	54.35	95.07	0.56	1.75	0.6	-0.017	0.62
	301-500	859165	5400	25.51	2.96	-2.12	0.12	-2.21	0.009	-2.22

Factors	Class	No. of pixel in class	LS pixel in class	% of pixel in class	% of LS pixel in class	IV	FR	W+	W-	C
Slope	501-700	477255	900	14.17	0.49	-3.22	0.04	-3.41	0.006	-3.42
	701-900	201357	2700	5.98	1.48	-1.39	0.25	-1.44	0.002	-1.44
	11°-19°	215726	4500	6.52	2.46	-0.97	0.38	-0.99	0.002	-0.99
	20°-27°	496906	19800	15.03	10.84	-0.33	0.72	-0.32	0.002	-0.33
	28°-36°	1363043	72900	41.22	39.9	-0.03	0.97	-0.02	0	-0.02
	37°-78°	1230985	85500	37.23	46.8	0.23	1.26	0.26	-0.004	0.27
SPI	-14.51	493073	16200	14.58	8.87	-0.49	0.61	-0.52	0.002	-0.53
	-1.85	1686545	74700	49.86	40.89	-0.2	0.82	-0.21	0.004	-0.22
	-1.5	307318	23400	9.09	12.81	0.34	1.41	0.36	-0.002	0.36
	-1.26	812833	63000	24.03	34.48	0.37	1.44	0.38	-0.004	0.39
TWI	0.64 - 11.1	82915	5400	2.45	2.96	0.19	1.21	0.19	0	0.19
	2.4 - 5.4	196434	2700	5.9	1.48	-1.39	0.25	-1.42	0.002	-1.42
	5.5 - 7.3	393617	10800	11.81	5.91	-0.69	0.5	-0.71	0.002	-0.71
	7.4 - 10	1239713	65700	37.21	35.96	-0.03	0.97	-0.03	0	-0.03
	15-24	1501995	103500	45.08	56.65	0.23	1.26	0.25	-0.005	0.26

3. Results and Discussion:

3.1 Spatial Distribution of Landslide Susceptibility:

The landslide susceptibility maps of Mamit District were developed based on four bivariate statistical methodologies viz. Frequency Ratio, Information Value, Weight of Evidence and Shannon Entropy. Each generated Landslide Susceptibility Map (LSM) were categorised into five susceptibility classes: “very low”, “low”, “moderate”, “high” and “very high” [5] (Figure 4). These maps show the different spatial distributions of landslide susceptible area within the district, as highlighted in (Table 3).

The “high” and “very high” susceptibility zones are mostly observed along slopes with higher angles and high elevated lands with weak topsoil, and those that lie on lithological units that are very weak, especially grey sandy splintery shale, siltstone and mudstone. Also, areas that are closer to the major roads and drainages are more prone, because of large number of anthropogenic interferences, improper drainage system and high amount of rainfall during the monsoon seasons.

Table 3. Area occupied by susceptibility classes in each model

Susceptibility Class	FR Area		SE Area		WofE Area		IV Area	
	Km ²	%	Km ²	%	Km ²	%	Km ²	%
Very Low	782.6	26.9	679.5	23.3	416.6	14.3	416.6	14.3
Low	868.5	29.8	703.3	24.1	757.1	26.0	757.1	26.0
Moderate	735.5	25.2	742.7	25.5	931.0	32.0	931.0	32.0
High	363.0	12.5	538.7	18.5	594.1	20.4	594.1	20.4
Very High	163.6	5.6	249.0	8.5	214.2	7.4	214.2	7.4

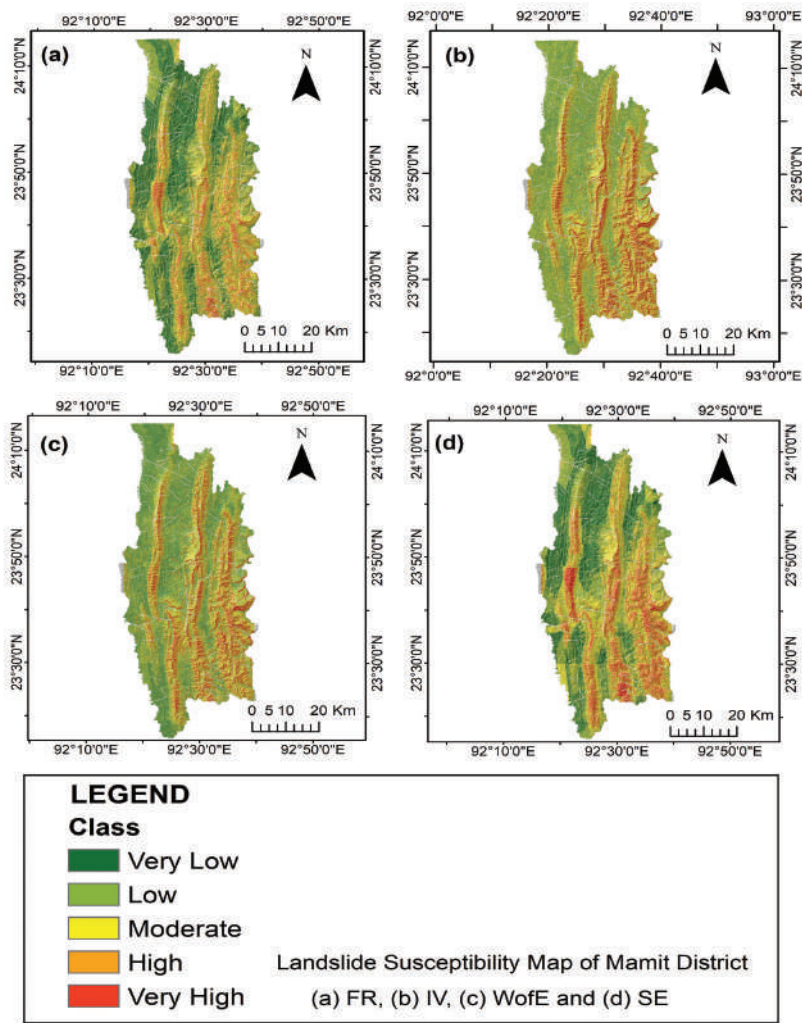


Figure 4. Landslide Susceptibility Maps of Mamit District.

3.2.2 Model Performance Assessment:

The performance of every model was assessed with the Area Under the Receiver Operating Characteristic Curve (AUC) [20], which is a standard practice for assessing landslide susceptibility models. The success rate based on the training dataset (238 landslide points) indicated that SE achieved the highest performance (AUC = 84.2%), followed by FR (83.5%), WofE (80.7%), and IV (80.0%). The prediction rate, derived from the testing dataset (80 landslide points), further confirmed SE's superior predictive capability of SE (AUC = 84.6%), followed by FR (83.6%), WofE (81.8%), and IV (79.1%). The success and prediction AUC diagrams are given in Figure 5.

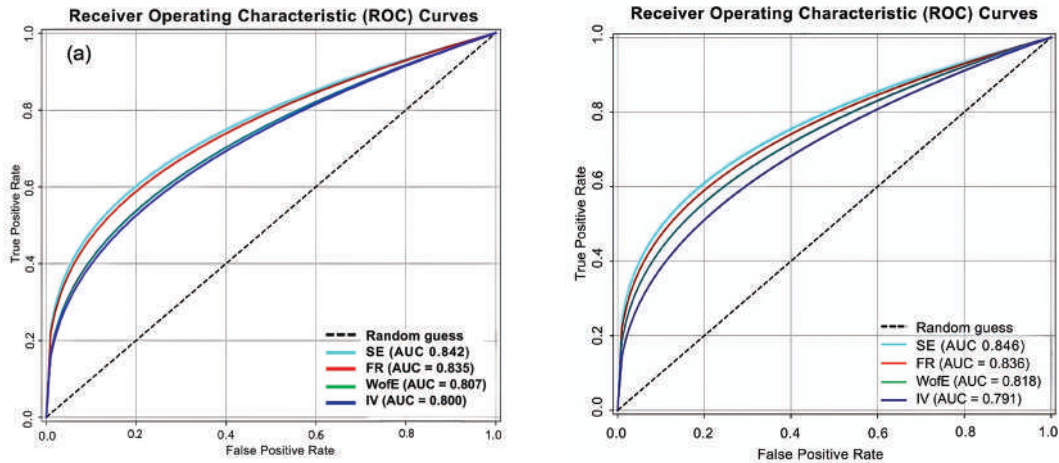


Figure 5. Success and prediction rate AUC diagrams for each model.

To further validate the robustness and generalizability of the models, a 5-fold cross-validation was performed. This process partitions the entire landslide inventory into five subsets, iteratively training the model on four folds and validating on the remaining one. The results, as shown in Table 5, confirm the consistent superiority of the SE model, which achieved the highest mean AUC value of 0.869 (± 0.035). The cross-validation AUC curves for all methods are presented in Figure 6, with the SE model's curve demonstrating not only a higher mean but also stable performance across all folds, as indicated by the narrower standard deviation band. This rigorous testing protocol mitigates the risk of overfitting and provides greater confidence in the model's predictive capability when applied to new, unseen data.

3.3 Influence of Conditioning Factors:

Among the thirteen factors, the primary inducing factors controlling landslide susceptibility in Mamit District were identified by their associated weights and classes in all four models (Table 5):

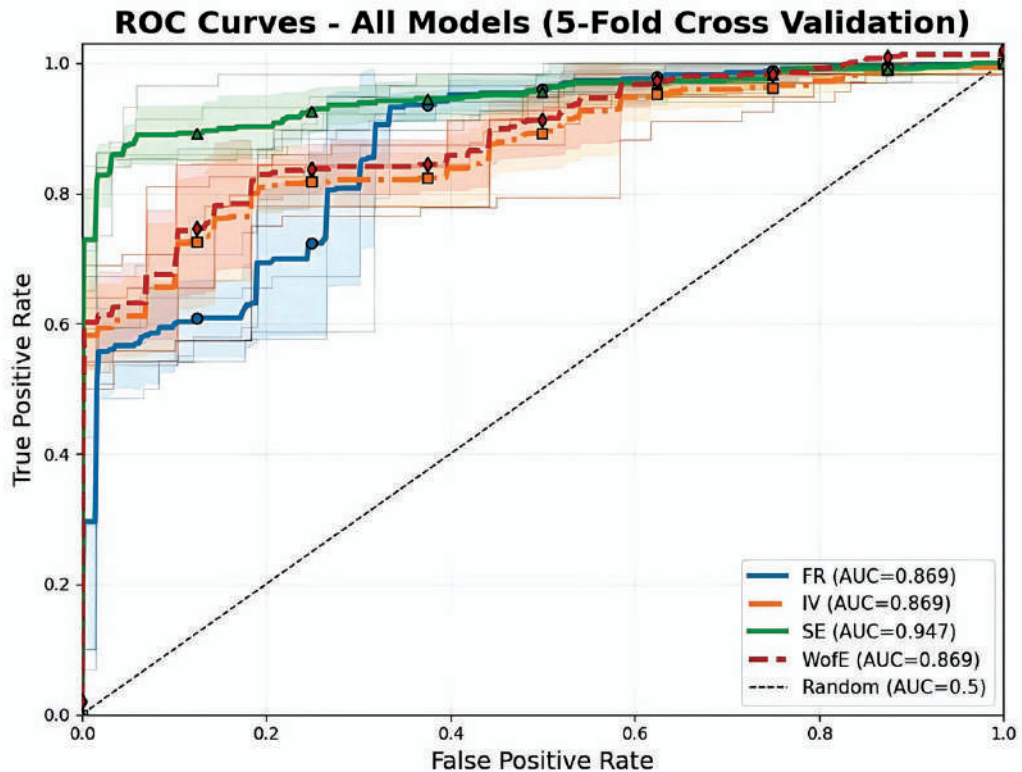


Figure 6. Cross Validation ROC-AUC of all models.

Table 5. Primary landslide conditioning factors of the study area.

Conditioning Factor	Class	Physical Interpretation
Slope	37°-78°	Steep slopes increase instability
Elevation	739-1420 m	Higher zones with intensified rainfall
Lithology	Grey sandy splintery shale, siltstone and mudstone	Weak sedimentary rocks highly prone to weathering
LULC (Land Use/Land Cover)	Barren land, Built-up	Lack of vegetation and human disturbance
Long term Annual Rainfall (2013-2022)	23,884-24,514 mm	Intense precipitation saturates slopes
Distance to Roads	100-300 m	Slope cutting and anthropogenic impact
Distance to Drainage	301-700 m	Toe erosion and water saturation near streams

Zones exhibiting combinations of these characteristics showed higher susceptibility and corresponded with known landslide events. This shows that both geophysical and human-related activities trigger slope instability within the region.

3.4 Zoning and Regional Patterns:

The foothills, roadsides and northwest valleys were a major hazard area as identified by all the four models. The susceptibility maps (Figure 4) have much in common when compared with each other particularly in the high and very high susceptible regions. The specificity of spatial overlay between models confirms that the concentrations of the highest risks coincide with the settlements, carrier roads and with the areas with steep topography and weakly consolidated sedimentary strata.

3.5 Implications for Disaster Risk Reduction:

The vulnerability maps produced in this research can provide a sound foundation on a specific land-use, infrastructure strengthening and emergency preparedness. The risky areas in the highways and in the highly populated valleys should receive priority. Retaining walls and drainage management should be implemented as engineering interventions voiding landslide threat in the monsoon season.

The comparative analysis proves the efficiency of Shannon Entropy to determine susceptibility in complex topography and climatic conditions. This approach and process can be used and modified to other such parts of Northeast India and surrounding regions in the Himalayas.

3.6 Limitations of the study:

Lack of time series data on landslides could be a constraint when carrying out dynamic hazard estimation; future studies should consider use of multi-year inventories, and weather data. It excluded some influential factors like the type of soil and the level of ground waters because of the shortage of data. It is suggested to extend the modelling strategy to machine learning methods to increase the precision. Findings of integrated disaster risk analysis must consider community-level factors of vulnerability and resilience.

4. Conclusion:

To develop the Landslide Susceptibility Map (LSM) for Mamit District, four distinct bivariate statistical techniques were utilised: Frequency Ratio (FR), Information Value (IV), Weight of Evidence (WofE), and Shannon Entropy (SE). Among these four methods, the SE method achieved the best result in producing the highest predictive accuracy, i.e. 84 per cent. The comparative analysis between these methods also shows that the SE method achieved the highest success and predictive power (84.2 and 84.6 per cent respectively).

The final susceptibility maps generated using all these methods collectively indicates that steep slopes (37°-78°), grey sandy splintery shale, siltstone and mudstone lithological units, heavy monsoon rainfall, absence of vegetation and certain anthropogenic activities like road constructions and improper drainage systems greatly increases the district's vulnerability to landslides.

The outcome of this research highlights that SE method can provide a reliable result in

preparing susceptibility maps in complex geological settings and landforms like Mamit district. The susceptibility maps developed using these methods can aid in land-use planning and policymaking. The generated maps also identify that “High” and “Very High” susceptibility zones are areas close to major roads, and near settlements which indicates the need for extensive geotechnical investigations. Such areas falling under these zones must be closely invigilated and a well-engineered infrastructure, proper drainage systems and reinforced retaining walls must be taken into considerations to mitigate and minimize landslide and its possible damages during heavy monsoon seasons.

Acknowledgements: The authors appreciate the Department of Geology at Mizoram University, Aizawl, Mizoram, India, for their resources and support, which were crucial for this research.

References:

- Akinci H, Zeybek M. Comparing classical statistic and machine learning models in landslide susceptibility mapping in Ardanuc (Artvin), Turkey. *Natural Hazards*. 2021;108(2): 1515–1543. <https://doi.org/10.1007/s11069-021-04743-4>.
- Aziz K, Sarkar S, Sahu P. Comparative analysis of frequency ratio, information value, and analytical hierarchy process statistical models for landslide susceptibility mapping in Kashmir Himalayas. *Arabian Journal of Geosciences*. 2024;17(1): 36. <https://doi.org/10.1007/s12517-023-11842-y>.
- Agrawal N, Dixit J. GIS-based landslide susceptibility mapping of the Meghalaya-Shillong Plateau region using machine learning algorithms. *Bulletin of Engineering Geology and the Environment*. 2023;82(5): 170. <https://doi.org/10.1007/s10064-023-03188-2>.
- Addis A. GIS-Based Landslide Susceptibility Mapping Using Frequency Ratio and Shannon Entropy Models in Dejen District, Northwestern Ethiopia. Ariyur K (ed.) *Journal of Engineering*. 2023;2023: 1–14. <https://doi.org/10.1155/2023/1062388>.
- Anbazzhagan S, Ramesh V. Landslide hazard zonation mapping in ghat road section of Kolli hills, India. *Journal of Mountain Science*. 2014;11(5): 1308–1325. <https://doi.org/10.1007/s11629-012-2618-9>.
- Barman J, Das J. Comprehensive landslide prediction mapping using bivariate statistical models of Mizoram state of Northeast India. *Journal of Spatial Science*. 2024;69(3): 963–993. <https://doi.org/10.1080/14498596.2024.2335262>.
- Barman J, Ali SS, Biswas B, Das J. Application of index of entropy and Geospatial techniques for landslide prediction in Lunglei district, Mizoram, India. *Natural Hazards Research*. 2023;3(3): 508–521. <https://doi.org/10.1016/j.nhres.2023.06.006>.
- Balamurugan G, Ramesh V, Touthang M. Landslide susceptibility zonation mapping using frequency ratio and fuzzy gamma operator models in part of NH-39, Manipur, India. *Natural Hazards*. 2016;84(1): 465–488. <https://doi.org/10.1007/s11069-016-2434-6>.
- Chatterjee U, Lalmalsawmzaauva KC, Biswas B, Pal SC, [eds]. *Landslides in the Himalayan Region: Risk Assessment and Mitigation Strategy for Sustainable Management*. Singapore: Springer Nature Singapore; 2024. <https://doi.org/10.1007/978-981-97-4680-4>.

- Chanu ML, Bakimchandra O. Landslide susceptibility assessment using AHP model and multi resolution DEMs along a highway in Manipur, India. *Environmental Earth Sciences*. 2022;81(5): 156. <https://doi.org/10.1007/s12665-022-10281-4>.
- Central Ground Water Board. Ground Water Information Booklet: Mamit District, Mizoram. 2013.
- Conforti M, Aucelli PPC, Robustelli G, Scarciglia F. Geomorphology and GIS analysis for mapping gully erosion susceptibility in the Turbolo stream catchment (Northern Calabria, Italy). *Natural Hazards*. 2011;56(3): 881–898. <https://doi.org/10.1007/s11069-010-9598-2>.
- Chen W, Pourghasemi HR, Zhao Z. A GIS-based comparative study of Dempster-Shafer, logistic regression and artificial neural network models for landslide susceptibility mapping. *Geocarto International*. 2016;32(4): 367–385. <https://doi.org/10.1080/10106049.2016.1140824>.
- Conforti M, Ietto F. Modeling Shallow Landslide Susceptibility and Assessment of the Relative Importance of Predisposing Factors, through a GIS-Based Statistical Analysis. *Geosciences*. 2021;11(8): 333. <https://doi.org/10.3390/geosciences11080333>.
- Cao Y, Zhang S, Nan Y, Wei X, Xiong W, Fan W. Landslide susceptibility assessment using the Weight of Evidence method: A case study in Xunyang area, China. *PLOS ONE*. 2021;16(1): e0245668. <https://doi.org/10.1371/journal.pone.0245668>.
- Dikshit A, Sarkar R, Pradhan B, Segoni S, Alamri AM. Rainfall Induced Landslide Studies in Indian Himalayan Region: A Critical Review. *Applied Sciences*. 2020;10(7): 2466. <https://doi.org/10.3390/app10072466>.
- Das S, Sarkar S, Kanungo DP. A critical review on landslide susceptibility zonation: recent trends, techniques, and practices in Indian Himalaya. *Natural Hazards*. 2023;115(1): 23–72. <https://doi.org/10.1007/s11069-022-05554-x>.
- Das S, Sarkar S, Kanungo DP. An ensemble approach of bi-variate statistical models with soft-computing techniques for GIS-based landslide susceptibility zonation in the Kalimpong region of Darjeeling Himalaya, India. *Environment, Development and Sustainability*. 2024;27(7): 16841–16882. <https://doi.org/10.1007/s10668-024-04592-8>.
- Es-smairi A, Elmoutchou B, Mir RA, Ouazani Touhami AE, Namous M. Delineation of landslide susceptible zones using Frequency Ratio (FR) and Shannon Entropy (SE) models in northern Rif, Morocco. *Geosystems and Geoenvironment*. 2023;2(4): 100195. <https://doi.org/10.1016/j.geogeo.2023.100195>.
- Ghosh T, Kumar D, Bhowmik S, Ghosh S, Jaiswal P. Generating Substantially Complete Landslide Inventory using Multiple Data Sources: A Case Study in Northwest Himalayas, India. *Journal of the Geological Society of India*. 2020;95(1): 45–58. <https://doi.org/10.1007/s12594-020-1385-4>.
- Hong H, Liu J, Bui DT, Pradhan B, Acharya TD, Pham BT, et al. Landslide susceptibility mapping using J48 Decision Tree with AdaBoost, Bagging and Rotation Forest ensembles in the Guangchang area (China). *CATENA*. 2018;163: 399–413. <https://doi.org/10.1016/j.catena.2018.01.005>.
- Jain N, Roy P, Martha TR, Jalan P, Nanda A. Landslide atlas of India (Mapping, monitoring and R&D studies using remote sensing data). Report number: NRSC-RSA-GSG-GMED-FEB 2023-TR-0002167-V1.0, 2023.

- Kutlug Sahin E, Ipbuker C, Kavzoglu T. Investigation of automatic feature weighting methods (Fisher, Chi-square and Relief-F) for landslide susceptibility mapping. *Geocarto International*. 2017;32(9): 956–977. <https://doi.org/10.1080/10106049.2016.1170892>.
- Kavzoglu T, Sahin EK, Colkesen I. An assessment of multivariate and bivariate approaches in landslide susceptibility mapping: a case study of Duzkoy district. *Natural Hazards*. 2015;76: 471–496. <https://doi.org/10.1007/s11069-014-1506-8>.
- Kouamou Njifen SR, Enyegue A Nyam FM, Bikoro MBA, Ngouokouo AT, Tabod CT. Modeling groundwater potential zones in the Kribi-Campo region, South Cameroon using geospatial techniques and statistical models. *Modeling Earth Systems and Environment*. 2023;9(1): 913–935. <https://doi.org/10.1007/s40808-022-01544-x>.
- Kayastha P, Dhital MR, De Smedt F. Landslide susceptibility mapping using the weight of evidence method in the Tinau watershed, Nepal. *Natural Hazards*. 2012;63(2): 479–498. <https://doi.org/10.1007/s11069-012-0163-z>.
- Kritikos T, Davies T. Assessment of rainfall-generated shallow landslide/debris-flow susceptibility and runout using a GIS-based approach: application to western Southern Alps of New Zealand. *Landslides*. 2015;12(6): 1051–1075. <https://doi.org/10.1007/s10346-014-0533-6>.
- Laltanpuia ZD, Martha T, Koduri S, Khanna K. Bivariate statistical models for Landslide susceptibility mapping at local scale in the Aizawl municipal area, Mizoram, India. *Himalayan Geology*. 2024;45: 39–57.
- Lallianthanga RK, Lalbiakmawia F, Lalramchuana F. Landslide Hazard Zonation Of Mamit Town, Mizoram, India Using Remote Sensing And GIS Techniques. *International Journal of Geology*. 2013;3.
- Langping Li, Li L, Hengxing Lan, Lan H, Changbao Guo, Guo C, et al. A modified frequency ratio method for landslide susceptibility assessment. *Landslides*. 2017;14(2): 727–741. <https://doi.org/10.1007/s10346-016-0771-x>.
- Mandal S, Mondal S. *Geoinformatics and Modelling of Landslide Susceptibility and Risk: An RS & GIS-based Model Building Approach in the Eastern Himalaya*. Cham: Springer International Publishing; 2019. <https://doi.org/10.1007/978-3-030-10495-5>.
- Manchar N, Benabbas C, Hadji R, Bouaicha F, Grecu F. Landslide Susceptibility Assessment in Constantine Region (NE Algeria) By Means of Statistical Models. *Studia Geotechnica et Mechanica*. 2018;40(3): 208–219. <https://doi.org/10.2478/sgem-2018-0024>.
- NDMA. National Landslide Risk Mitigation Programme (NLRMP) Phase-1. 2025.
- NDMA. Annual Report 2020-21. 2021.
- Nguyen TTN, Liu CC. A New Approach Using AHP to Generate Landslide Susceptibility Maps in the Chen-Yu-Lan Watershed, Taiwan. *Sensors*. 2019;19(3): 505. <https://doi.org/10.3390/s19030505>.
- Nohani E, Moharrami M, Sharafi S, Khosravi K, Pradhan B, Pham BT, et al. Landslide Susceptibility Mapping Using Different GIS-Based Bivariate Models. *Water*. 2019;11(7): 1402. <https://doi.org/10.3390/w11071402>.

- Pellicani R, Spilotro G. Evaluating the quality of landslide inventory maps: comparison between archive and surveyed inventories for the Daunian region (Apulia, Southern Italy). *Bulletin of Engineering Geology and the Environment*. 2014;74(2): 357–367. <https://doi.org/10.1007/s10064-014-0639-z>.
- Rahaman A, Venkatesan MS, Ayyamperumal R. GIS-based landslide susceptibility mapping method and Shannon entropy model: a case study on Sakaleshapur Taluk, Western Ghats, Karnataka, India. *Arabian Journal of Geosciences*. 2021;14(20): 2154. <https://doi.org/10.1007/s12517-021-08422-3>.
- Sangi L, Ralte Z, Roluahpuia B, Dinpuia L, Lalnunmawia J, Tlau L, et al. Preliminary investigation on Cyclone Remal-induced landslides in Aizawl, Mizoram, Northeast India, on the 28th of May 2024. *Landslides*. 2025;22(5): 1563–1575. <https://doi.org/10.1007/s10346-025-02477-z>.
- Sengupta A, Nath SK. GIS-Based Landslide Susceptibility Mapping in Eastern Boundary Zone of Northeast India in Compliance with Indo-Burmese Subduction Tectonics. In: Shit PK, Pourghasemi HR, Bhunia GS, Das P, Narsimha A (eds) *Geospatial Technology for Environmental Hazards*. Cham: Springer International Publishing; 2022. p. 19–37. https://doi.org/10.1007/978-3-030-75197-5_2.
- Sestraş P, Vereş I, Cîmpeanu SM, Sălăgean T, Bilaşco Ştefan, Bondrea MV, et al. Landslides Susceptibility Assessment Based on GIS Statistical Bivariate Analysis in the Hills Surrounding a Metropolitan Area. *Sustainability*. 2019;11(5): 1362. <https://doi.org/10.3390/su11051362>.
- Senthilkumar H, Selvaraj EN. GIS-based frequency ratio and Shannon entropy modeling for landslide susceptibility mapping: A case study in Kundah Taluk, Nilgiris District, India. *Open Geosciences*. 2025;17(1): 20220757. <https://doi.org/10.1515/geo-2022-0757>.
- Saranaathan SE, Mani S, Ramesh V, Prasanna Venkatesh S. Landslide Susceptibility Zonation Mapping Using Bivariate Statistical Frequency Ratio method and GIS: A Case Study in Part of SH 37 Ghat Road, Nadugani, Panthalur Taluk, The Nilgiris. *Journal of the Indian Society of Remote Sensing*. 2021;49(2): 275–291. <https://doi.org/10.1007/s12524-020-01207-3>.
- Suman Sarkar, Sarkar S, Archana Roy, Roy AK, Tapas R. Martha, Martha TR. Landslide susceptibility assessment using Information Value Method in parts of the Darjeeling Himalayas. *Journal of The Geological Society of India*. 2013;82(4): 351–362. <https://doi.org/10.1007/s12594-013-0162-z>.
- Zhang YX, Li LP, Wu YM, Lan HX, Tian NM, Chen JH. Optimizing the frequency ratio method for landslide susceptibility assessment: A case study of the Caiyuan Basin in the southeast mountainous area of China. *Journal of Mountain Science*. 2020;17(2): 340–357. <https://doi.org/10.1007/s11629-019-5702-6>.



Coping with Soil Erosion: Present Status and Deep Learning-Based Future Projections in the Mayurakshi Basin, India

Subha Roy¹, Souvik Das¹, Rajesh Hansda¹, Jaya Chatterjee¹,
Md. Hasanur Jaman², Prakash Mistri³ and Somasis Sengupta^{1*}

¹*Department of Geography, The University of Burdwan*

²*Department of Social Sciences, Dankuni S. Sr. Madrasah, Dankuni CC, Hooghly –712310*

³*Department of Geography, Kishore Bharati Bhagini Nivedita College, Kolkata –700060*

**Corresponding author: ssengupta@geo.buruniv.ac.in*

Abstract: Measurement of actual soil loss being undergone in an areal unit is unfeasible. Therefore, prediction-based models (such as the Revised Universal Soil Loss Equation, RUSLE) are extremely popular at the basin-scale. The RUSLE Model which takes into account the dynamic factors such as rainfall and landuse landcover alongwith the static ones such as soil and slope characteristics, is endowed with the ability of assessing the temporal changes in soil erosion categories. This paper is an attempt to understand the temporal dimension of soil erosion wherein the RUSLE-based soil loss was estimated for the years 2011 and 2021. Between 2011 and 2021, the soil loss has increased by about 6%. This adds to the growing concern for soil resources in this region. This paper has also integrated the deep learning methodology (Artificial Neural Network, ANN) taking the years of 2011 and 2021 as input rasters. Using the above-mentioned algorithm, the predicted soil loss in the next five decades was assessed (2021 – 2071). It is observed that the patches may increase in extent by about 50% in the next five decades if the current rate of erosion is intact. Finally, it is recognized that due to the lower clay content (< 30%) in the upper and middle domains of the basin, the study suggests the use of plot-scale mulching technique as an efficient measure to combat soil erosion in the region.

Keywords: RUSLE, Landscape ecological metrics, Artificial Neural Network (ANN), Deep Learning, Mulching

1. Introduction:

One of the greatest problems associated with agriculture and consequent sustainable development is the topsoil loss due to a host of sub-aerial processes. According to estimates, about 1094 Mha of land is getting eroded by running water (Dutta *et al.*, 2017). This huge loss of arable soil is reflected by the fact that about 15-30 billion tons of sediments are being transported annually to the oceans by various rivers across the world (Milliman and Syvitski, 1992; Walling and Webb, 1996). This has disastrous implications in many of the developing nations of the world where agriculture constitutes the primary economic activity of a major chunk of the population. A myriad of factors interplay to determine the nature and magnitude of the process of sub-aerial soil erosion (Wischmeier and Smith, 1978; Renard *et al.*, 1997; Mutua *et al.*, 2006; Oliveira *et al.*, 2019). Soil erosion is predominantly a quasi-natural hazard influenced by a host of natural factors such as surface runoff, slope and soil characteristics (Civeira *et al.*, 2016; Dutta *et al.*, 2017; Oliveira *et al.*, 2019) as well as the anthropogenic ones which include landuse changes, deforestation, construction activities and agricultural practices (Setegn *et al.*, 2010; Gebremicael *et al.*, 2013; Kim *et al.*, 2013). Almost 91% of the areas worldwide are facing potential soil loss ranging from <5 to 40 tons/ha/yr (Sharda *et al.*, 2013). This reiterates the need for appropriate regional plans for encountering this problem so as to prevent further loss of this valuable natural resource. Policy makers across the globe need to understand the importance of soil for sustainable agriculture and hence decision support systems and priority areas need to be devised as soon as possible (Mutua *et al.*, 2006, Dutta *et al.*, 2017).

Probably, the prerequisite for formulating an appropriate erosion management policy is measurement and monitoring of erosion. However, the exact quantification of erosion is practically impossible and unviable. Therefore, under data scarce scenarios, prediction-based models based on stochastic analysis of various conditioning factors are available in literature (Lorup and Styczen, 1996). Predominantly index-based, such models take into consideration a multitude of factors controlling erosion. The choice and selection of such parameters may vary as per the study area, depending on the availability of data and significance of each parameter (Morgan *et al.*, 1998; Hoyos, 2005; Lim *et al.*, 2005; Yuksel *et al.*, 2008; Ranzi, 2012). Although a number of prediction-based models are available in the academic domain, the Universal Soil Loss Equation (USLE) and the Revised Universal Soil Loss Equation (RUSLE) are reasonably popular. The model has been globally used successfully for prediction of the catchment-scale soil erosion, the catchment size spatially varying (Pandey *et al.*, 2009; Kumar and Gupta, 2016). Five major factors are taken for the operation of the RUSLE Model namely rainfall (R), soil erodibility (K), slope length and steepness (LS), crop management (C) and conservation support practice (P). The five parameters encompass both the physical (slope, precipitation and soil characteristics) and anthropogenic (landuse, conservation practices, etc.) dimensions of soil erosion (Farhan *et al.*, 2013). In recent decades, remote sensing and geographical information systems have emerged as powerful tools to overlay multiple parameters and spatially analyse them at a larger areal extent. This has made the process of estimating catchment-scale erosion easier and viable (Jasrotia and Singh, 2006; Krishna

Bahadur, 2009; Chou, 2010). Another significant advantage of these modern techniques is the ability to analyse multi-temporal data. Therefore, systematic understanding of the process of erosion becomes possible in a temporal framework. In the last few years, advanced data-driven machine learning and deep learning technologies have emerged which has helped in predicting the future scenario based on the temporal dynamics (Krishna Bahadur, 2009; Chou, 2010). Therefore, management practices can be spatially prioritized, which helps a lot in policy-making (Krishna Bahadur, 2009). This becomes extremely important in the tropical regions of eastern where agriculture is the primary occupation of a major chunk of population.

The present paper is, therefore, an endeavour to understand the process of soil erosion and its temporal change in the alluvial soils of the Mayurakshi River Basin of Eastern India. We amalgamate field studies, laboratory analysis of soil samples and remote sensing data before applying the RUSLE Model for predicting soil erosion. This analysis involved collection of 50 (fifty) soil samples at 2 * 2 km intervals and then analysing them in the laboratory for extracting the information about soil texture and soil organic matter (by Walkley & Black Method). Soil pH was measured in the field by a pH meter. These soil parameters are recorded as input parameters for deriving the Soil Erodibility Factor (K Factor). In order to get an idea about the temporal dimension of soil erosion, we carried out the decadal analysis for the years 2021 and 2011. One of the primary objectives of this paper is to suggest suitable management policies for soil conservation. For this purpose, the Z-Scores of soil loss values were taken and the areas displaying high Z values ($z > 3$) were identified as erosion hotspots. Also, the soil erosion scenarios (Rasters for 2021 and 2011) were modelled using the data-driven deep learning technique of Cellular-Automata based Artificial Neural Network (CA-ANN) for predicting the possible erosion scenarios and hotspots for the next fifty years (at 10-year interval). Deep Learning-based future prediction of scenarios is primarily observed in landuse studies wherein the researchers attempt to predict the condition in the future. Such an application in soil erosion studies may help in the better understanding and management of degraded soils throughout the world.

Based on the results of RUSLE, hotspot analysis and CA-ANN based future prediction, this paper analyses the hotspots of high erosion with respect to their orientations and decadal changes. It was also seen how the extent, location and configuration of these patches of high soil erosion have changed in the last 10 years (2011-21). Finally, some possible soil conservation measures are suggested considering their feasibility in the Mayurakshi River Basin of eastern India.

2. The Study Area:

The river basin selected for this study is the Mayurakshi Basin in eastern India (Figure 1). The river is an important river for the Indian states of West Bengal and Jharkhand. The importance becomes greater for the state of West Bengal because of the presence of fertile land rich in agriculture. The area encompassed by the basin is about 9596km² enclosed between 24°29' N to 23°54' N latitudes and 86°49' E to 88°12' E longitudes (Islam and Deb Barman, 2020). A number of tributary basins contribute to the waters of the Mayurakshi Basin,

the most prominent being the Kopai, the Dwarka and the Brahmani. The river originates from the Trikut Hills of the Chhotanagpur Plateau (CP) in the state of Jharkhand in India. The Mayurakshi River flows for about 250km before debouching into the Bhagirathi-Hugli River near Kalyanpur, West Bengal. The course of this river is predominantly irregular with different topographic characteristics. In the upper reach (Figure 1a) which includes the eastern fringes of the CP, the elevation is high but the gradient is low. So, the flow of this river is generally sluggish with no major anomaly. Similar to the upper domain, the lower domain of the basin is characterized by absence of any major relief features. The flat alluvial tract of West Bengal is encompassed in this domain. This area is rich in agriculture due to fertile soil (Roy *et al.*, 2025). In between the above-mentioned domains is the middle domain where the Mayurakshi River has cut across a series of low-lying hills of the CP. In this domain, lies Massanjore, where a dam has been built to cater to the irrigation needs in the downstream sections. In this part, igneous and metamorphic rock exposures are seen along the course of the Mayurakshi River. The region is generally humid with an average rainfall of 1060 to 1100 mm annually. However, the discharge varies throughout the year with the highest amount of water carried by the river in the Indian monsoon season (June – September). This basin is a part of the Ganga Basin or the Lower Ganga Basin to be more specific. Since the Ganga is an international river, long term discharge data of all the gauging sites in the Ganga Basin, including the Mayurakshi Basin, is classified. So, the data is not readily available in this basin. The soils of this region are predominantly alluvial in the middle and lower domains of the basin. So, this contributes to increased fertility of the soils. In fact, the state of West Bengal through which the river flows in its middle and lower domains, is rich in agriculture. In the upper domain of the basin over the CP, the red and lateritic soils are found.

3. Method and Materials:

The Revised Universal Soil Loss Equation (RUSLE) given by Renard *et al.*, (1997) is a modified version of the original Universal Soil Loss Equation (USLE) proposed by Wischmeier and Smith (1978) in the United States Department of Agriculture (USDA) Handbook Number 537.

3.1 The RUSLE Model:

One of the most popular empirical (RUSLE) model to use estimate the amount of actual soil loss in an areal unit. Eq. 1 describes the empirical form of the RUSLE (Renard *et al.*, 1997)

$$A = R \times K \times LS \times C \times P \dots\dots\dots \text{Eq.1}$$

where, A is the average annual soil loss in an areal unit (tons/ha/yr), R is the average annual rainfall erosivity factor (Mjmmha-1h-1yr-1), K is the soil erodibility factor (t hMJ-1mm-1), LS is a dimensionless factor associated with slope-length and slope-steepness, respectively, C is the vegetation cover factor and P is the conservation support practice factor.

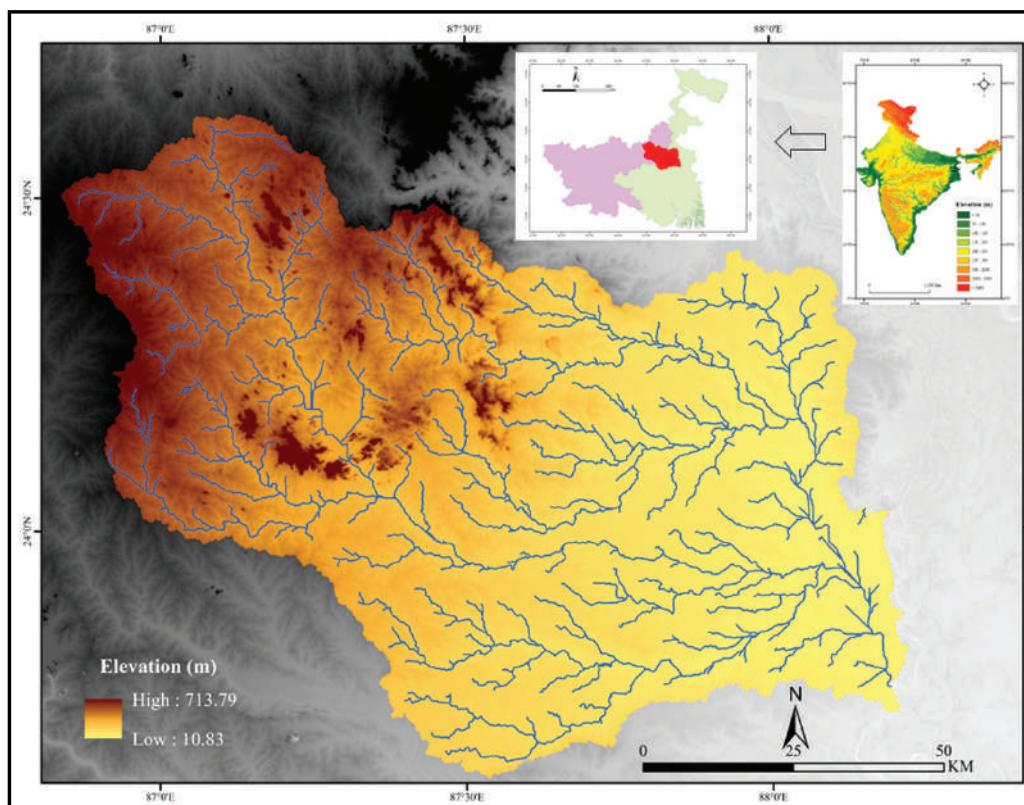


Figure 1. Location of the studied basin.

3.1.1. Rainfall Erosivity Factor (R):

It has been well recognized that surface runoff contributes the most towards soil erosion.

The RUSLE Model recognizes the same and therefore, estimation of soil erosion considers the rainfall and its intensity. Primarily runoff is dependent upon the amount of rainfall, but the intensity, terminal velocity and size of raindrop and distribution (secondary factors) are also significant (Singh, 2006, Blanco-Canqui and Lal, 2008). The total rainfall energy (E) and intensity of rainfall (I_{30}) (maximum 30 min) and its long-term average to determine the R factor. The amount of runoff associated with the rainfall quantifies the numerical value of R (Wischmeier and Smith, 1978; Lorup and Styczen, 1996; Renard *et al.*, 1997; Singh, 2006, Lee and Heo, 2011).

However, most of the areas in the world lack the 30min rainfall duration data. So, estimating the erosion at the catchment-scale is extremely unviable. Therefore, in the present time researchers have often used monthly rainfall and its relation to the annual rainfall as a proxy for a particular place to identify the intensity of rainfall.

Arnoldus (1980) proposed the Modified Fournier Index (MFI), this equation has been

used the present study is represented in Eq. 2.

$$R = 1.735 \times 10^{[1.5 \log_{10}(\text{MFI}) - 0.8188]} \dots\dots\dots \text{Eq. 2}$$

The MFI represents the ratio between average monthly precipitation and the average annual precipitation. The MFI-based rainfall erosivity factor has been widely used in India in numerous studies on estimating the soil erosion (Raj *et al.*, 2022). Therefore, the soil erosion in this study has been estimated using the MFI. Rainfall data viz., monthly and annual, were obtained on the well-tested Tyndall Climatic Data for the years 2021 and 2011 in raster formats (Mitchell et al. 2003) which provides the monthly rainfall data from the years 1901 to 2021. These were then analysed and processed in order to get the spatial variation in R Factor for the years 2021 and 2011.

3.1.2 Soil Erodibility Factor (K):

The pedological character of the soil was carried out through fieldwork and laboratory analysis of the soil samples. In the Mayurakshi Drainage Basin divide dimension 2km * 2km grids and the sites falling at the grid intersections were visited and 50 soil samples collected. After that drying the collected soil sample were taken in the laboratory and carried out by the Walkley and Black method and sieving to determine the organic matter and textural characteristics of soil, respectively. In the field an electrode-based pH meter was used for getting the soil pH. Then the ArcGIS environment spatially plotted the data and selected points and the separated raster of soil texture (silt, sand and clay percentage) and extracted organic matter and soil pH by the Inverse Distance Weighting (IDW) Module of ArcGIS. The K Factor was obtained following the equation 3:

$$K = (0.043 \times \text{pH}) + (0.62 \div \text{OM}) + (0.0082 \times S) - (0.0062 \times C) \times \text{Si} \dots\dots\dots \text{Eq.3}$$

where, K = soil erodibility (t hMJ-1mm-1), pH is the acidity/alkalinity of the soil, OM is Organic matter (%), S is Sand content (%), Si is silt content (%) C is clay ratio = % Clay/ (% Sand + % silt)

3.1.3 Slope Length and Steepness Factor (LS):

To compute the LS Factor for the study area the equations developed by Wischmeier and Smith (1978) and Moore and Burch (1986b) were used. In this study, the 12.5m resolution ALOS-PALSAR DEM (Scene 1: ALPSRS117443100, Path-154, Frame-3100; Scene 2: ALPSRS117443150, Path-154, Frame-3150; acquisition date of the DEMs: 8 April 2008) using in ArcGIS platform to identified LS factor (Eq. 4).

$$LS = \left(\frac{As}{22.13} \right)^{0.6} \times 1.4 \left(\frac{\sin^1 B}{0.0894} \right)^{1.3} \dots\dots\dots \text{Eq. 4}$$

where, LS = LS Factor, As = Flow Accumulation Raster and B = Slope in radians
This freely-available DEM generates the ellipsoidal height, i.e. the elevation above the local ellipsoidal surface. So, the raw DEM was corrected by the Earth's Gravity Model 2008 (EGM

2008), defined on a 5 arc-minute square grid (Pavlis et al. 2012) as per Eq. 5.

$$H_o = H_e - h \dots \dots \dots \text{Eq.5}$$

where, ‘Ho’ is the orthometric height of a point on the earth’s surface, ‘He’ is the ellipsoidal height of the same point on the surface of the earth, and ‘h’ is the correction factor or the EGM2008 geoidal elevation (data available across the globe at 5 arc-second resolution at https://earthinfo.nga.mil/GandG/wgs84/gravitymod/egm2008/egm08_wgs84.html).

3.1.4 Crop Management factor (C):

The C-factor is defined as the ratio of soil loss from the land covered by the crop patterns under specific conditions to the corresponding loss from uncovered area such as clean-tilled, water body and fallow land (Wischmeier and Smith, 1978; Renard *et al.*, 1997; Singh, 2006; Kolli *et al.*, 2021). The range of C factor is from 0 to 1, where higher values depict the highly erosion prone areas. On the other side, lower values indicated less erosion which means dense vegetation cover effect (Erencin, 2000).

$$C = \frac{NBIL}{NDVI} \dots \dots \dots \text{Eq. 6}$$

where, C is the Crop Management Factor, NDVI = Normalised Differenced Vegetation Index

given as $\frac{NIR - RED}{NIR + RED}$, NBIL = Normalised Bare Soil Index given as $\frac{NIR - SWIR}{NIR + SWIR}$.

NIR (Near Infra-Red), SWIR (Short Wave Infra-Red) and RED represent the different bands of multi-spectral imagery.

Landsat 8 OLI (2011, December) and ETM+ (2011, December) data were downloaded from United States Geological Survey (USGS) to estimate the C factor in this study area.

3.1.5 Support Practices (P):

Table.1. Values of P factor respected Land use/ Land cover type.

Type	Value
Dense Vegetation	0.8
Light Vegetation	0.8
Built up area	1
Agricultural land	0.5
Water Body	1
Fallow Land	0.9

It is known that the conservation practices designed for preventing soil erosion may control the degree of erosion to some extent. This is easy to achieve by observation at the plot-scale but at the catchment scale, which is characterized by different kinds of conservation

practices based on individual land type, such unique definition and indexing of P Factor may not be possible. Therefore, in the catchment scale analysis, the United States Department of Agriculture (USDA) assumed that landuse landcover types may be treated as an indicator for the P-Factor. Accordingly, various landuse landcover classes were assigned unique values of P Factor which have been displayed in Table 1 (USDA, 1981). Therefore, cloud free Landsat OLI 8 and Landsat ETM+ data to used different classes of Land Use Land Cover (LULC). Supervised image classification with the Maximum Likelihood Classifier were undergone on image to identified LULC and verified the field investigation (2021) and 2011 LULC map verified Goggle Earth Satellite imageries. However, Kappa Coefficient used the validated LULC 2021 and 2011 the overall value come out to be 89% and 81%, respectively for the teras 2021 and 2011. On the basis of the USDA Handbook No.282 (1981) (Wischmeier and Smith, 1978; Renard *et al.*, 1997; Thomas *et al.*, 2018), the P Values (Table.1) were assigned and the classified image was reclassified in ArcGIS to get the continuous raster for the P Factor in the Mayurakshi River Basin.

After estimating all the quantitative parameters in RUSLE equation, in Map Algebra of ArcGIS environment the individual rasters of each factor were multiplied with each other and the estimate of the annual soil loss for the Mayurakshi River Basin was obtained.

The same procedure was repeated for the decadal consecutive years of 2011 but the LS and K factors are constant because those two factors not major change within 10 years.

3.2 Hotspot Analysis:

The term ‘hotspot’ is often used in the field of ecology which represent areas with outstanding biodiversity or a high concentration of biological values. Although the broad expansion of the term hotspot in the field of hazard studies especially erosion is a reasonably a recent phenomenon. In simple words, erosion hotspots are referred to those patches/areas in a larger areal unit where the erosion undergone is significantly higher than other regions. Although there are no significant scales for identifying an area as an erosion hotspot, the statistical analysis of the erosion results may help in detection of the erosion hotspots in a region. For the detection of the erosion hotspots, we have applied the Z-Score normalization as per the Equation 7.

$$E_{zi} = \frac{e_i - \bar{e_i}}{e_i \sigma} \dots\dots\dots \text{Eq.7}$$

where, E_{zi} = Z-Score Normalization of the erosion magnitudes of pixel, = Erosion value of pixel i (as per the RUSLE 2021), = Average value of the RUSLE based soil loss for the studied river basin and = Standard Deviation of the RUSLE based soil loss for the studied basin system.

3.3 Temporal Change in soil loss and future prediction:

In the last few years, machine learning technologies have emerged in the domain of environmental sciences for predicting various aspects of the environment. Based on the

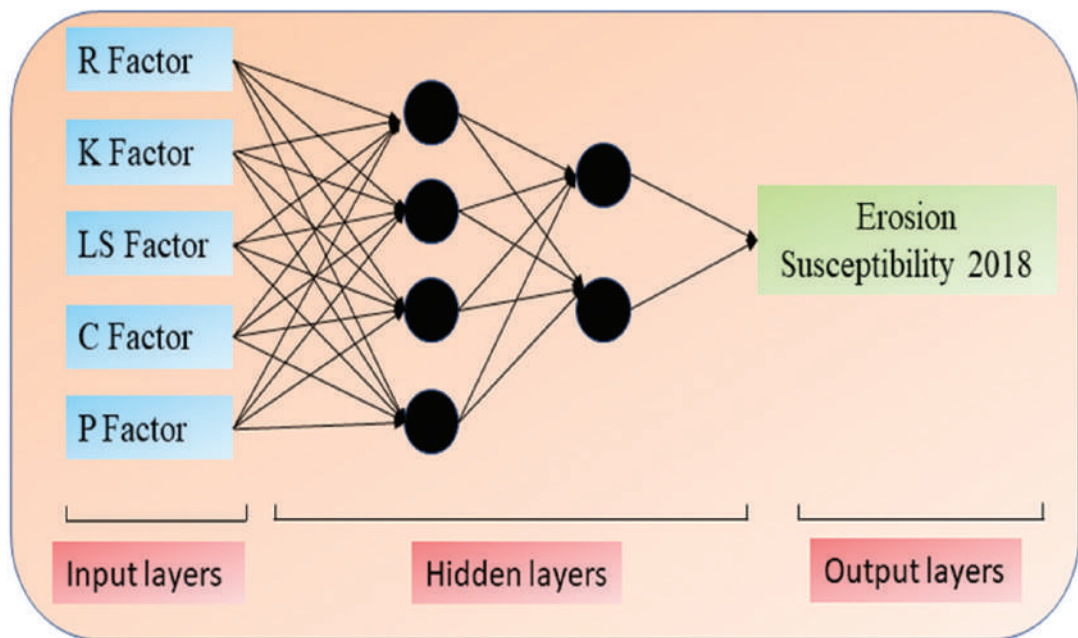


Figure 2. Mechanism of hidden layer in Artificial.

analysis of big datasets, genetic algorithms in machine learning technologies have the inherent capacity of building models that can iteratively learn and process hidden insights (Figure2) and possible non-linearity from large quantities of data (Kim and Gilley, 2008; Olaweyin and Chen, 2018). The Artificial Neural Network (ANN) (Olaweyin and Chen, 2018) is one such kind of supervised machine learning which has been borrowed from the realm of biological sciences and has the inherent ability to detect patterns and trends that are extremely complex for human brains and statistical techniques to analyse (Kura and Beyene, 2020). One of the most popular ANN approaches is the Cellular Automata (CA) which estimates the future pixel state in accordance with the initial state of the pixel alongwith considerations on the neighbourhood and some transitional probability rules (Liu *et al.*, 2017). The advantage of this technique lies in the fact that the nonlinear stochastic land category transition processes can be represented efficiently (Batty *et al.*, 1997; Liu *et al.*, 2017). CA-based ANN models have been widely used in the urban landuse simulations (Clarke and Gaydos, 1998; Li *et al.*, 2011; Liu *et al.*, 2017). Some studies have also focussed on simulating deforestation induced by human activities (Kok and Winograd, 2002; Kura and Beyene, 2020). However, although the process of soil erosion is temporally dynamic and prone to human alterations of the landscape, the application of ANN models is limited (Gholami *et al.*, 2021). In this paper, the RUSLE-based erosion scenario for the year 2011 has been used as the input layer. The Future Landuse Simulation (FLUS) model proposed by Liu *et al.*, (2017) has been used in this paper. The FLUS model is argued to be an improvement over the traditional top-down CA models

because the FLUS integrates the bottom-up approach in the CA models by incorporating the background effects of dynamic climate change, which is very significant in soil erosion considering that R factor is of temporal dimension. The model has been found to be highly applicable in predicting the future of urban heat islands (Yang *et al.*, 2022), carbon biomass (Zeng *et al.*, 2022), etc.

This CA simulation involves two steps. First an ANN is used for training and estimation of the probability of occurrence of each landuse type (erosion category type in this paper). This ANN consists of three layers viz., an input layer, a hidden layer and an output layer.

The input layers taken for this analysis include the spatially independent variables of R, K, C and P factors (detailed description given earlier). This can be mathematically expressed as Eq.8.

$$X = [x_1, x_2, \dots, x_n]^T \dots \dots \dots \text{Eq. 8}$$

where, x_i represents the i th input layer input.

All the input neurons act on the neuron j of the hidden layer on pixel p_1 . The signal received at time t is estimated by Eq. 9.

$$\text{net}_j(p_1, t) = \sum_i w_{ij} * x_i(p_1, t) \dots \dots \dots \text{Eq. 9}$$

where $\text{net}_j(p_1, t)$ represents the signal received by the hidden layer neuron, $x_i(p_1, t)$ is the i th variable associated with the input neuron i on the pixel p_1 time t ; and w_{ij} are the weights assigned to the hidden layer, calibrated by an activation function which is characteristically sigmoid (Eq. 10).

$$\sigma = \frac{1}{(1 + e^{-\text{net}_j(p_1, t)})} \dots \dots \dots \text{Eq. 10}$$

The output of the hidden layer is given as

$$H = f(\sigma(I)) = f(\sigma(f(x))) = f(\sigma(\sum_{i=1}^n (x_i * w_i))) \dots \dots \dots \text{Eq. 11}$$

where, f is the Sigmoid Activation Function and H is the probability of occurrence of for each erosion category type. A higher value of H means that the particular pixel has a higher probability of falling in that category. However, the weights of the hidden layer need to be continuously adjusted in order to reduce the errors in the output layer. This is called iteration and was done by a backpropagation algorithm given as

$$\Delta w = w - w_{\text{old}} = -\eta \frac{\partial E(w)}{\partial w} = \eta \dots \dots \dots \text{Eq. 12}$$

where, w = weights, $E(w)$ is the cost function that measures how far the current network's output is from the desired one, $\frac{\partial E(w)}{\partial w}$ is the partial derivative of the cost function E that specifies the direction of the weight adjustment to reduce the error, η is the learning rate which is measured as the number steps for each iteration of the weight update equation.

The next step involved the self-adaptive inertia and competitive mechanism. This is basically the formulation of a relationship between the probability of occurrence surface for a specific erosion category type and the given spatial factors (in this case R, K, LS, C, P). Apart from the probability of occurrence, other factors such as neighbourhood condition

and competition among different erosion category types also play a part in determining the land category transformation. Hence, the combined probability of each pixel must address these aspects. The neighbourhood statistics were computed by establishing a neighbourhood development density effect which has been given in Eq. 13.

where, TGC is the total number of pixels occupied by the erosion category type k at the last iteration time (t - 1) in the N * N window. This is given as $TGC = \sum_{N \times N} \text{con}(c_p^{t-1} = k)$. The different erosion categories give variable neighbourhood effects and these effects are weighted as wk for the kth category of erosion.

Therefore, the final probability for each iteration time for a pixel was computed after combining the probability-of-occurrence of land use type k on grid cell (based on ANN), neighbourhood effect and conversion cost. This work of future prediction was carried out using the GeoSOS-FLUS software downloaded from <http://www.geosimulation.cn/flus.html>) (Li *et al.*, 2011; Liu *et al.*, 2017).

4. Results:

Figure 3 displays the annual soil loss in the studied basin for the year 2021. It is evident that the basin loses about 14.2 tons per hectare annually on an average. The annual soil loss (2021) for the Mayurakshi Basin has been shown in Figure 3. The average annual soil loss in the studied basin is 15 tons/ha/year, ranging from < 5 to > 30 tons/ha/year. On the basis of Natural Breaks

Method, the Mayurakshi Basin on the basis of the RUSLE based soil loss, was divided into five major classes which has been outlined in Table 2. The map showing the spatial variation in the soil loss of the studied basin implies that the annual soil loss decreases from upper to the lower domain of the basin. This is interesting because the upper domain predominantly constitutes a hard rock terrain and the lower domain is over a flat, featureless plainland which is rich in alluvium. So, this finding gives an impression that probably the topography plays a significant role in the spatial distribution of soil loss in the Mayurakshi Basin.

4.2. Soil Erosion Risk: Temporal Variations (2011-2021):

The quasi-natural process of soil erosion is an extremely dynamic phenomenon. This means that the extent and intensity of soil loss has been changing throughout time. This is becoming extremely important in the recent times, when the increasing role of anthropogenic processes contribute to increasing the intensity and amount of soil loss in a region. Therefore, the primary requisite of any management initiative on soil erosion is to monitor the temporal change in the process of erosion in a region. In the Mayurakshi Basin, an attempt has been made to assess the temporal change with respect to the years 2021 (Figure3) and 2011(Figure4) on

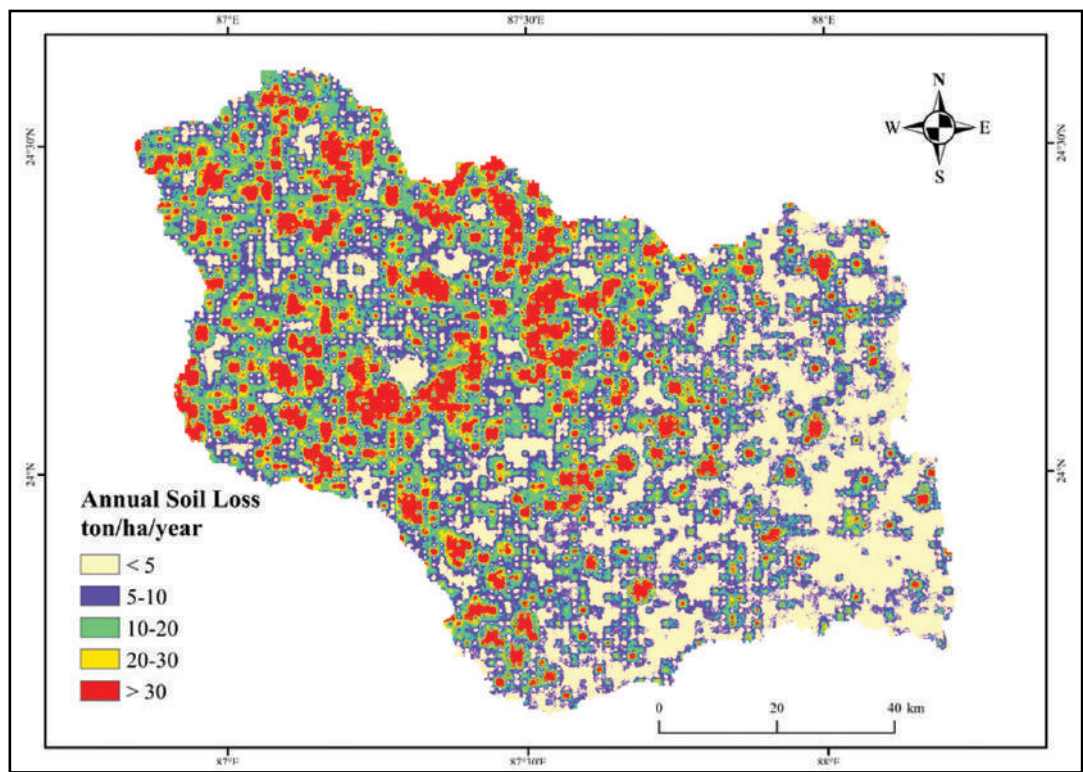


Figure 3. Spatial variation in the RUSLE-derived annual soil loss 2021of Mayurakshi River Basin.

the basis of the RUSLE Model. It is necessary to point out that in the context of the causal factors of erosion, those which are expected to alter significantly with respect to time include climate, vegetation and landuse landcover. Slope and soil characteristics are less likely to change within a short span of time. Therefore, with respect to the RUSLE Model, the R Factor which is affected by the changing climatic conditions, the C Factor which is sensitive to clearing of natural vegetation and deforestation and the landuse landcover induced P Factor are subject to temporal variations within a short time frame. So, the Tyndall Climatic data for the year 2011 was downloaded from the designated website and the R Factor was generated by employing Eq. 2. Similarly, the landuse landcover map was generated by the exercise of Supervised Image Classification

Table 2. Area and Percentage of various soil loss categories in the Mayurakshi River Basin.

Index	Erosion classes	Soil loss (t h ⁻¹ y ⁻¹)	Percentage
<5	Very Low	< 5	23.663
5-10	Low	5-10	31.330
10-20	Moderate	10-20	23.248
20-30	High	20-30	9.543
>30	Very High	>30	12.535

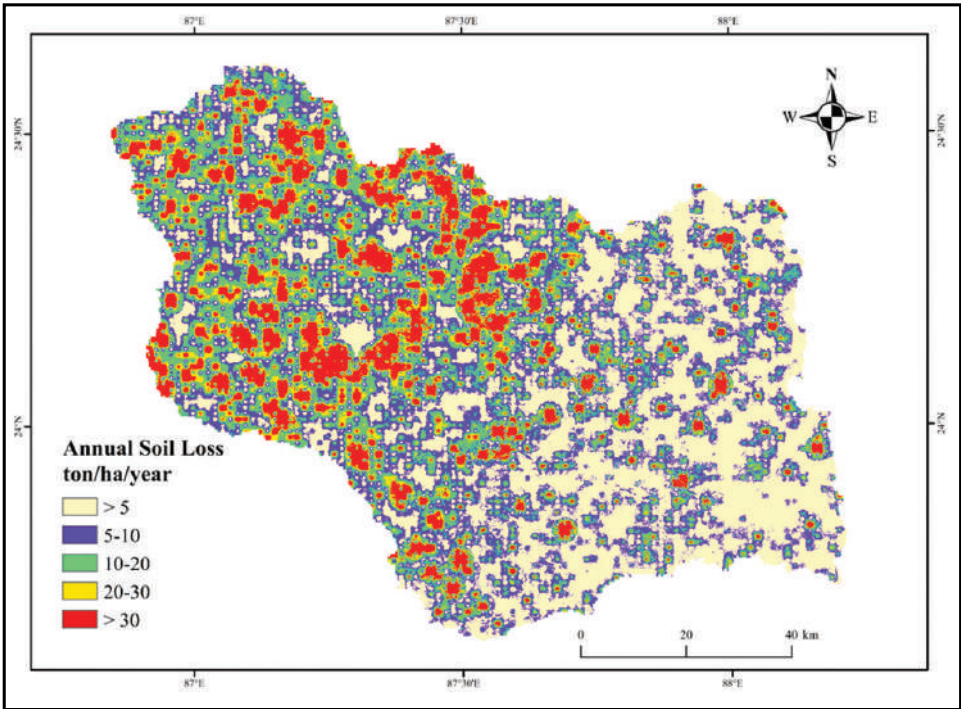


Figure 4. Spatial variation in the RUSLE-derived annual soil loss 2011of Mayurakshi River Basin.

Maximum Likelihood Classifier Algorithm) from the LANDSAT imageries procured from the USGS website. This LULC map was then reclassified as per USDA to get the values of the P Factor. The C Factor was obtained from the same images of 2011 by band ratioing as per Eq. 6. The final RUSLE map was obtained by the Raster Calculator module in ArcGIS and displayed in Figure 3.

The range of values in each class has been kept the same as Figure 3 for easy comparison.

In 2011, the average soil loss in the Mayurakshi Basin had been 13.87 tons/ha/year. Earlier it was seen that in 2021, the corresponding soil loss was 14.90 tons/ha/year, a rise by over 7%. However, not all the areas in the basin have witnessed similar change in erosion. So, the intra-basin spatial change in soil loss was quantified by subtracting the soil loss raster of 2011 from the soil loss raster of 2021. This was done by the Raster Calculator Module in ArcGIS and mapped accordingly (Figure 5). Positive values in the resultant raster represent an increase in soil loss and vice versa. The concerning fact is that in the river basin under investigation, most of the areas have experienced an augmentation of the soil loss. This holds true especially in the north-western corner of the map (upper domain) as well as in the middle domain immediately downstream of the Massanjore Dam.

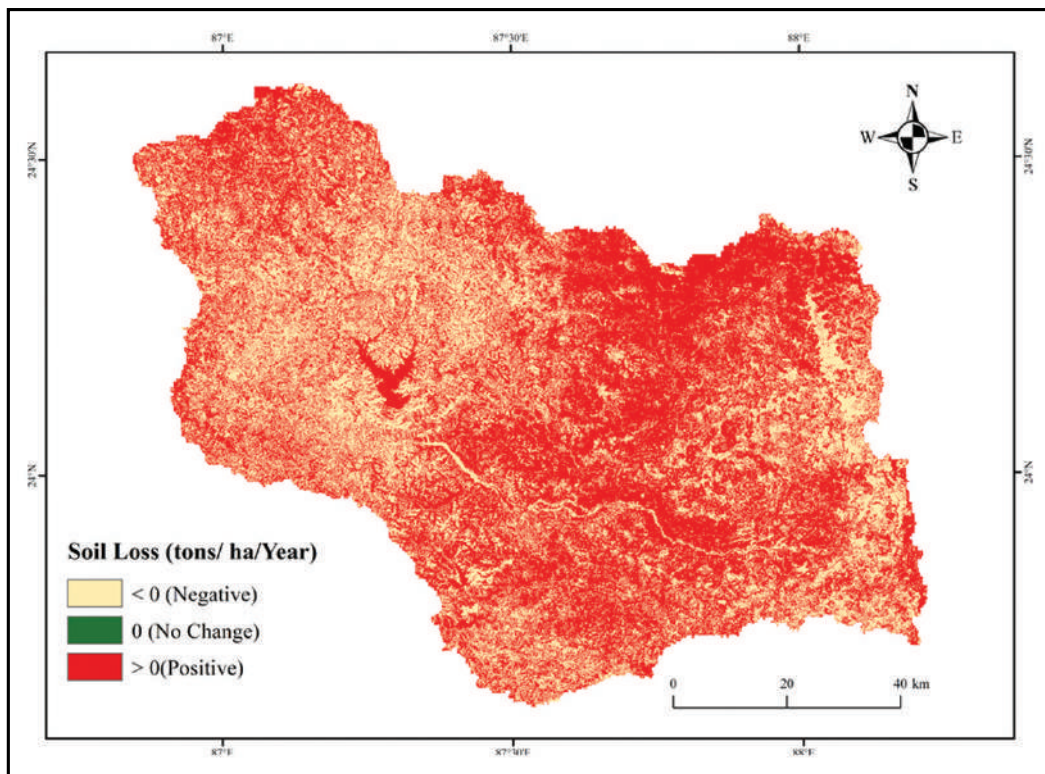


Figure 5. Difference between (2021 and 2011) annual soil loss of Mayurakshi River Basin.

4.3 Erosion Hotspot in Mayurakshi River Basin:

The Z-Score normalization maps of the erosion susceptibility and soil loss by RUSLE are displayed in Figs.6. Z Score ratings greater than 0 represent the areas where the erosion is less than the average. And the Z-Scores greater than 0 represent regions where the erosion incurred is greater than the average. The Ezi values of each pixel in the RUSLE-based (2021) soil loss for the Mayurakshi Drainage System were then analysed and as per the Normal Probability Distribution Rule, Ezi values > 3 were identified as erosion hotspots. It is a well-established fact that in case of a normal distribution, more than 99% of all observations lie between mean and three times of the standard deviation ($\text{Mean} + 3 \text{ SD}$). Therefore, any observation with value of Z greater than $+3$ is regarded to be an outlier. Therefore, any pixel (area) with Ezi > 3 will be an outlier and an erosion hotspot. Figure 5 reveals that the erosion hotspots obtained after Z-Score normalization of the RUSLE-based erosion potential are well pronounced. This is particularly observed in the middle domain of the Mayurakshi Basin, in the vicinity of the Massanjore Dam. Similarly, the upper reach of the Dwarka River display a well-pronounced zone of erosion hotspot. Also, a pronounced portion of erosion hotspot is observed in the upper domain. In all other regions (which comprises about 90% of the area), the erosion hotspots are absent. This implies that erosion is low.

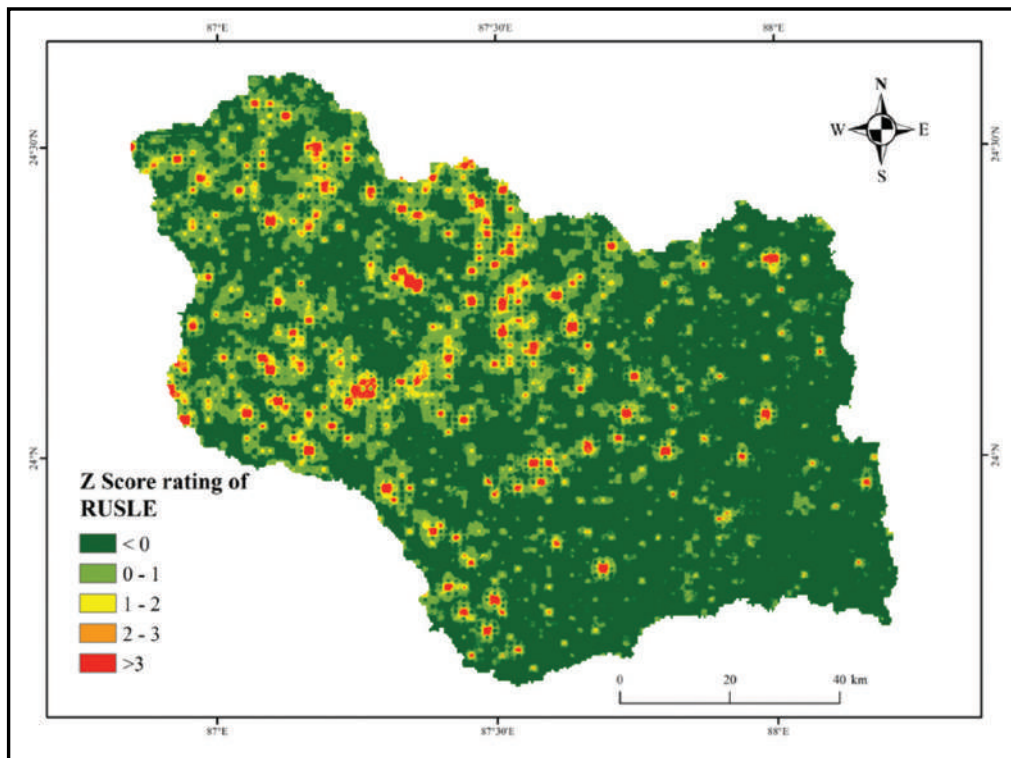


Figure 6. Difference between (2021 and 2011) annual soil loss of Mayurakshi River Basin.

4.4 Future Projections of Soil Loss in the Mayurakshi Basin using Artificial Neural Network:

The success of any hazard management strategy is based on future considerations. Since soil erosion is an important quasi-natural hazard, it is imperative that any erosion management protocol must include the future considerations. This means that the future scenario of erosion/soil loss needs to be suitably predicted and appropriate conservation techniques need to be spatially prioritized. This study has, therefore, attempted to predict the future scenario of soil loss in the next fifty years. For this purpose, the RUSLE based soil loss (for 2011) (Figure 4) was processed in FLUS 2.1 to obtain the ANN-based future soil loss of 2021. were used and the Artificial Neural Network (ANN) Model was applied for predicting the soil losses for the years 2031, 2041, 2051, 2061 and 2071 for the Mayurakshi Basin. The spatial variations in the soil loss for the years 2031 – 2071 at an interval of 10 years were analysed. It is pertinent to mention here that we have ensured that the same dataset is used for the years 2011 and 2021. For example, for estimating the R Factor, the Tyndall Climatic data has been used and also the LANDSAT data of 30m resolution has been used for LULC types. This is imperative so as to remove the possible bias that may be arisen due to differing resolutions among the datasets.

This study has applied the multi-classifier backward propagation algorithm in the FLUS 2.1 software to predict the future scenario of the RUSLE-based soil loss for the Mayurakshi Basin. The change detection from 2011 to 2021 (Table 3) was carried out with the help of the Markov Chain Model. Then this ANN Model was applied in FLUS 2.1 to get the future scenario of 2031 – 2071 at an interval of 10 years.

Table 3. Conversion Metrics 2011 to 2021 soil erosion risk.

Erosion Type (ton/ha/year)	<5	5-10	10-20	20-30	>30
< 5	57645	12782	9432	7852	2211
5-10	1249	5172	551	75	15
10-20	13	446	923	167	76
20-30	3	42	153	291	133
>30	0	4	39	95	681
Total	58910	18446	11098	8480	3116

The same categories of soil erosion were kept intact for the ANN-derived soil loss maps for the all the future years. This was done so as to avoid confusion that may be encountered due to differing class limits. The maps for the years 2031, 2041, 2051, 2061 and 2071 are displayed in (Figure7a-e), respectively. A general scrutiny of these maps reveal that the pattern and orientation of the future maps of soil loss are, more or less, similar to the soil loss map of 2021(Figure3). That is, the locations of the areas/patches of high, moderate and low erosion have not changed much, only the extent of these patches have increased significantly. This is well illustrated in Table 4 where the number of pixels in each erosion category for the successive years is given.

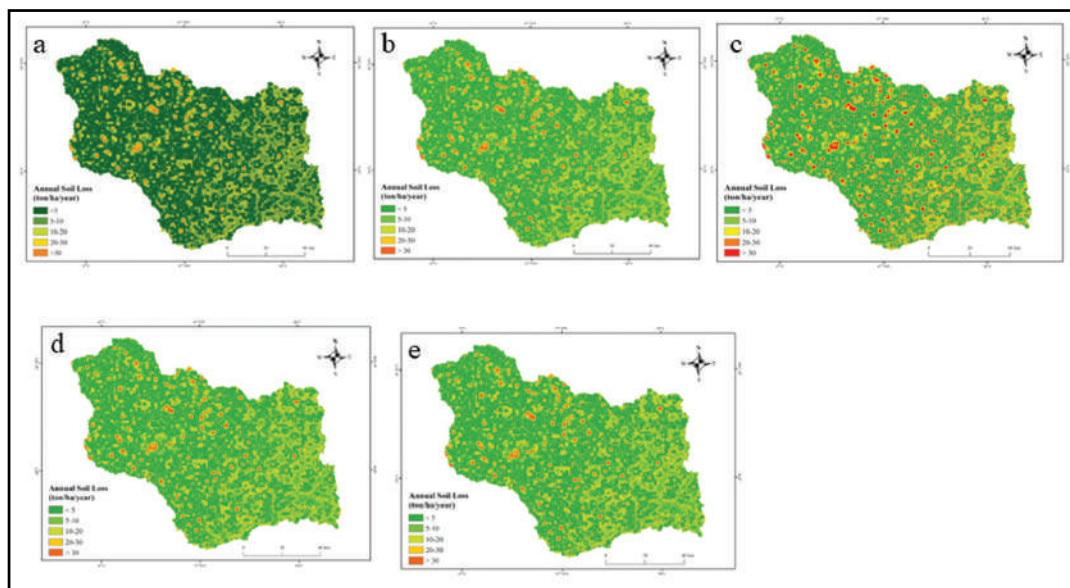


Figure 7. Predicted annual soil loss with the help of ANN in the Mayurakshi Drainage in the year (a)2031, (b)2041,(c)2051,(d)2061,(e)2071.

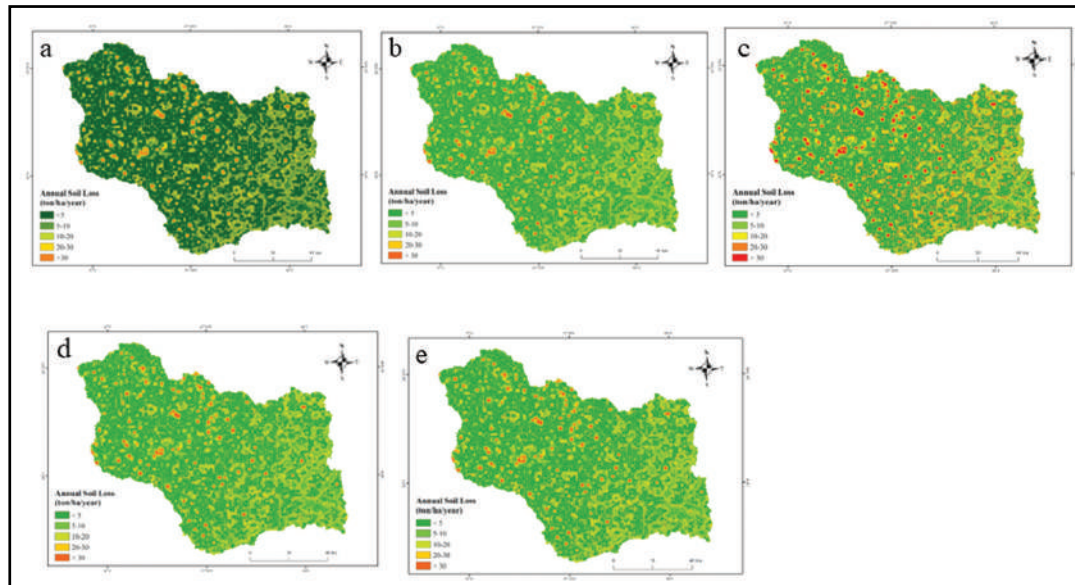


Figure 8. Percentage of pixels in different erosion categories from 2021 to 2071.

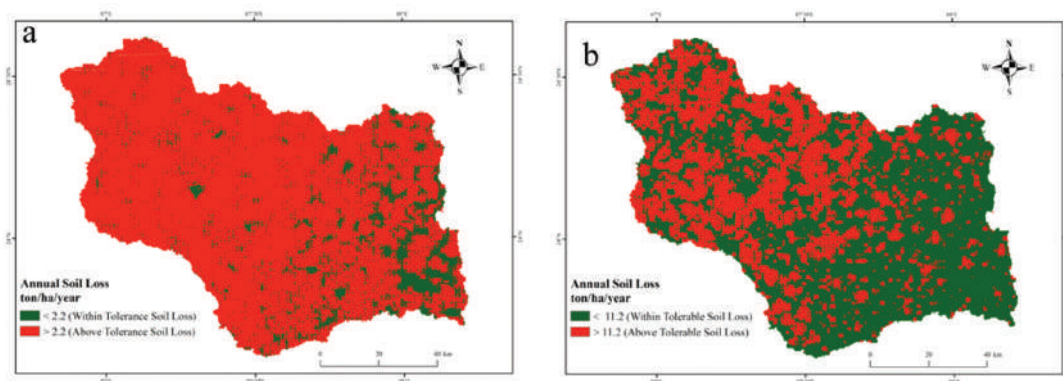


Figure 9. Spatial mapping of soil loss and its tolerance limit in the Mayurakshi Basin with (a) respect to the rate of new soil formation (2.2 tolerance), (b) agricultural sustainability (11.2 tolerance).

The graphical representation of the number of pixels in different erosion categories for the years 2021– 2071 is represented in Figure 8. The line graph reveals that the number of pixels for the very low erosion class (< 5 tons/ha/year) decreases considerably from 2021 to 2071. The number of pixels in this category decreases from 5.9 million in 2021 to 2.1 million in 2071, the percentage decreasing from 58.9% to 21.5%, which is about 38% decrease. In the moderate erosion category (10 – 20 tons/ha/year), the corresponding positive increase of 11 to 20% has occurred between 2021 to 2071. Similarly, the percentage of erosion pixels in the high (20 – 30 tons/ha/year) and the very high category (> 30 tons/ha/year) have increased from 8.50% to 12.08% and 3.09% to 14.06%, respectively. Therefore, this is ample prediction that the degree of soil erosion hazard in the studied basin has increased considerably from 2021 to 2071.

This is because the proportion of pixels of very low erosion has decreased significantly and in the high erosion category, this percentage has increased. Hence, it may be assumed that in the next 50 years, a considerable portion of the studied basin will have greater erosion potential.

5. Conclusion:

It has been stated earlier that soil erosion is a major problem in the environmental management globally. In the Mayurakshi Drainage Basin, it has been observed that the percentage/proportion of high and very high erosion categories has been increasing from 2011. Also, it is expected that such areas/patches of high erosion are to increase in the next fifty years (2021 – 2071).

This calls for site-specific conservation measures in the region. Under such circumstances, it is needless to state that appropriate management strategies need to be undertaken so as to prevent the patches of high erosion to expand further. The utility of applying the landscape ecological metrics in the field of soil erosion is exemplified by the fact that in resource scarce scenario, the conservation measures can be prioritized in areas of high and moderate erosion patches.

In this connection, it may be mentioned that FAO (2019) has suggested establishing a threshold between acceptable and non-acceptable levels of erosion in an areal unit. The Revised World Soil Charter proposes that proper soil management strategy should ensure that the ecosystem services derived from the soil are adequately maintained or even enhanced. It should no way significantly impair the soil capacity to agriculture and biodiversity (FAO, 2019). Therefore, an acceptable or tolerable level of soil erosion is required to be proposed which has been defined by Verheijen *et al.*, (2019) as the cumulative (all agents combined) soil erosion rate above which the soil functions and ecosystem services provided by the soil deteriorate significantly. FAO (2019) has proposed two major approaches in specifying the tolerance level of soil loss (Tsl). These are as follows: a) Tolerance value maintaining the dynamic equilibrium of the soil at a particular areal unit b) Tolerance value which takes into consideration and manages the function of the soil to maintain the production of biomass (Duan *et al.*, 2016; Verheijen *et al.*, 2019).

The first approach to propose a value of Tsl is based on the comparison of the rate of soil loss to the rate of new soil formation. Montgomery (2007) proposes an average value of 2.2 tons/ha/year after his systematic review of more than 180 research papers in this domain. Although there are lower threshold values of Tsl, such as 0.2 – 1.4 tons/ha/year (Bui *et al.*, 2011; Verheijen *et al.*, 2019). The second approach to calculate Tsl has been popularized by the United States Department of Agriculture (USDA). This is important with respect to agricultural sustainability because USDA-based Tsl as the maximum level of soil loss, will permit optimum productivity of agriculture (Wischmeier and Smith, 1978). Based on different literatures, the optimum level of Tsl have been ascertained as ranging from 4.5 to 11.2 tons/ha/year. The RUSLE-based soil erosion map of 2021 has been reclassified twice for class limits 2.2 and 11.2 tons/ha/year in the ArcGIS environment. The maps of tolerable soil loss delineate the regions associated with a soil erosion greater than the limit of tolerance. These maps are depicted in Figs 9(a-b).

Even a cursory examination of the above maps reveals that a major portion of the studied basin is characterized by soil loss greater than the tolerance level. In fact, more than 95% of the areas in the Mayurakshi Basin (Figure 9a) reveal soil loss greater than 2 tons/ha/year, the tolerance limit with respect to the formation of new layer of soil. A close look at the Figure9b reveals that about 60% of the areas experience soil loss greater than 11.2 tons/ha/year. Since this is the tolerance level for agricultural sustainability, this figure draws more attention as a greater proportion of the region is associated with agricultural activities. Such areas of greater than tolerance are, more or less, concentrated in the upper and middle domains of the basin, especially upstream of the Massanjore Dam and the gorge formed by the Mayurakshi River in the middle domain. So, such areas need to be prioritised for erosion management.

One of the principal components of sustainable soil management is controlling the quasi-natural process of soil erosion. This is important because sustainable management of soil erosion is necessary to prevent degradation of the soil and the consequent losses in crop productivity and sedimentation of rivers and reservoirs. The Voluntary Guidelines for Sustainable Soil Management (VGSSM), as proposed by FAO (2019) has listed four major groups of erosion-control measures.

The first group of remedies involve minimizing the landuse changes (such as deforestation) which make the soil loose and vulnerable for removal by erosion agents. It been estimated that such major landuse changes result in enhancing the rate of soil erosion by about 10 – 20%, the percentage increasing with respect to the amount of land that has been converted (Guo and Gifford, 2002; Poeplau *et al.*, 2011).

The second and third approaches deal with protecting the soil surface from erosion. This requires minimizing the depth of runoff and flow velocity on the hillslopes. This can be achieved through reduced tillage, preferably absence of tillage. Other measures such as construction of terraces try to reduce the runoff. Terraces are extremely popular in the field of oil erosion control but measures such as strip cropping, contour planting, agro-forestry, grassed waterways and vegetative buffer strips may also help in reducing the menace of erosion (FAO, 2019).

The fourth set of arrangements is aimed at minimizing the export of soil particles, nutrients and pollutants from the soil. These measures are associated with sediment trapping, thereby reducing the input of sediments in the rivers and reservoirs. Some of such measures include riparian buffers, check dams and sediment ponds (Mekonnen et al. 2015).

In the Mayurakshi Basin, such measures are immediately required to control the hazard of soil erosion. An immediate need of the hour is to first concentrate the patches of high erosion (> 30 tons/ha/year). Such high-erosion patches are, predominantly concentrated in the upper and middle domain of the Mayurakshi Drainage Basin as well as the upper reach of the Dwarka River. In the lower domain, these patches are conspicuously absent. This fact is well established by the tolerance limit maps of the studied basin (Figs.9a, b), wherein it was evident that the lower domain of the studied drainage displays below-tolerance levels of soil erosion. Therefore, effective erosion control measures are the need of the hour in the upper and middle domains of the basin. The first group of measures as suggested by the FAO (2019) include minimizing landuse changes and promoting greenery and afforestation. However, considering the fact that the basin belongs to the densely populated Indian states of West Bengal and Jharkhand, such steps may not be feasible. Secondly, a major part of the upper and middle domain is covered by fallow lands and vegetation as revealed by the landuse landcover map of the studied basin. In the vicinity of the Massanjore Dam in the middle domain dense vegetation cover is found. These are the areas of steep slopes, the outcome of the Chhotanagpur Plateau outliers. It is possible that the presence of dense vegetation in this region has led to an overall decrease in the soil loss. So, proper steps in the form of legislation and implementation need to be taken so as to prevent any form of deforestation in this region. The vast proportion of fallow lands situated in the upper domain, need to be addressed with suitable afforestation techniques so as to prevent future land encroachment. The next popular approach is the no till or reduction in tillage. This process has been found to be extremely suitable in temperate regions, but has found very little success in tropical and sub-tropical areas (Mhazo et al. 2016) of which the studied basin is a part. However, it has beenfound that tillage reduction technique can work efficiently in soils with low clay content (< 30%). Figure10 reveals that in the upper and middle domains, the clay % is reasonably lower (18

– 22%). Considering this, it appears that irrespective of the climate being tropical, tillage reduction can be an efficient tool in reducing the surface runoff and hence erosion, especially in the patches of high erosion of the upper and middle domains of the Mayurakshi Basin. However, Pittelkow et al. (2015) are of the opinion that reduction or no tillage has a drastic effect on the crop yields. This is particularly true for the tropical areas where the crop yields have reduced by about 15.1%. The corresponding value for temperate regions is only 3.4%. These societal implications, once again, discourage the farmers from adopting no tillage or tillage reduction as a technique to reduce soil erosion, especially in the studied basin.

Another popular technique widely used in the domain of soil erosion mitigation and management is mulching. Mulching is defined as any material with the exception of soil or vegetation that acts as a permanent/semi-permanent cover over the soil surface. This technique has always caused a reduction in soil erosion and sedimentation and is extremely suitable at the plot-scale (Prosdocimi et al. 2016). The suitability of the mulching technique is well illustrated by the fact that neither does it reduce the crop yields, nor does it require broader administrative decisions. Even a farmer, in charge of an agricultural plot, can use this technique to preserve the fertile soil in the period when the harvest is over and the land is barren. In the upper and middle domains of the studied basin, considering the fact that the patches of high erosion are not very extensive as of now, it is suggested that mulching can be one of the most successful techniques in the effective management of patches of high soil erosion. The suitability of this technique is enhanced by the fact that a major part of the upper and middle domain of the studied basin is covered by barren fallow land.

Sediment trapping with the help of bunds and terraces are also effective in reducing the process of erosion and sedimentation. This can be accomplished by local shrub and grass species, with no requirement of crop-specific management (Wei et al. 2010). Terraces physically break the continuous slope into a series of horizontal steps. However, such a technique may not be feasible for the studied basin because the patches of high erosion are not very extensive.

The success of any management strategy to combat the problem of soil erosion is predominantly dependent on the societal implication and participation. This brings into question the concept of soil governance. Soil governance is defined as the sum of all formal and informal institutions that determine the decision-making process of soil management. This decision-making concerns the government as well as the non-governmental institutions at each level. The formal and informal institutions described above include legislations, regulations, norms, perceptions, habits and attitudes of the stakeholders (Juerger and Hansjurgens, 2018). The local farmer or the pastoralist is the primary user of the local soil in a region. Therefore, it is obvious that the onus on the decision to adopt any soil conservation practice lies with the farmer. It is expected that a farmer in a developing country such as India will invest his/her time and resources on that option which will provide the highest return at the lowest risk. Possibly the first step in any soil management strategy is to identify where exactly is the erosion happening, i.e., the erosion hotspots (Boardman 2006). Finally, it is humbly submitted that although this study may be affected by the inherent limitations of possible minute errors

in the available datasets and absence of a suitable perception survey on the soil conservation techniques in this region, analysis has successfully identified the erosion-vulnerable patches/hotspots in the Mayurakshi River basin by integrating RUSLE, landscape ecology and deep learning technology in a single platform.

Acknowledgements:

Acknowledgements are due to the Editor and an anonymous reviewer for their constructive comments which helped in improving the clarity of an earlier version of the paper.

Funding:

No Funding was received for conducting this research work.

Data availability:

All data collected from Primary and Secondary based.

References:

- Batty M, Couclelis H, Eichen, M (1997) Urban systems as cellular automata. *Environ. and Plan : Plan. and Des.* 24:159–164. [10.1080/0965431042000312424](https://doi.org/10.1080/0965431042000312424).
- Blanco-Canqui H, Lal R (2008) *Principles of soil conservation and management*. Springer, Netherlands.
- Boardman J, Poesen J (2006) Soil erosion in Europe: major processes, causes and consequences. in *Soil Erosion in Europe* (eds J. Boardman and J. Poesen), John Wiley & Sons, Ltd, Chichester, UK. <https://doi.org/10.1002/0470859202.ch36>.
- Bui NB, Hancock JG, Wilkinson NS (2011) ‘Tolerable’ hillslope soil erosion rates in Australia: Linking science and policy. *Agri., Ecosys. & Environ.* 144: 136-149. <https://doi.org/10.1016/j.agee.2011.07.022>.
- Chou WC (2010) Modelling watershed scale soil loss prediction and sediment yield estimation. *Wat. Resour. Manag.* 24(10):2075–2090. <https://doi.org/10.1007/s11269-009-9539-6>.
- Civeira M, Oliveira M, Hower J, Agudelo-Castañeda D, Taffarel S, Ramos C, Kautzmann R, Silva LF (2016) Modification, adsorption, and geochemistry processes on altered minerals and amorphous phases on the nanometer scale: examples from copper mining refuse, touro, Spain. *Environ. Sci. Pollut. Res. Int.* 23:6535–6554.
- Clarke KC, Gaydos LJ (1998) Loose-coupling a cellular automaton model and GIS: Long-term urban growth prediction for San Francisco and Washington/Baltimore. *Inter. J. of Geogra. Infor. Sci.* 12:699–714. <https://doi.org/10.1080/136588198241617..>
- Duan, X., Xie, Y., Liu, B., Liu, G., Feng, Y., Gao, X., 2012. Soil loss tolerance in the black soil region of northeast China. *J. of Geogra. Sci.* 22(4), 737–751. <https://doi.org/10.1007/s11442-012-0959-5>.
- Dutta M, Saikia J, Taffarel SR, Waanders FB, de Medeiros D, Cutruneo CM, Saikia BK (2017) Environmental assessment and nano-mineralogical characterization of coal, overburden, and sediment from Indian coal mining acid drainage. *Geosci. Front.* 8:1285–1297. <http://doi.org/10.1111/j.1600-0587.2012.07348.x>.

- Erencia Z (2000) C-factor mapping using remote sensing and GIS. A case study of Lom Sak/Lom Kao, Thailand. Intern. Inst. for Aeros. Sur. and Ear. Sci. (ITC), Enschede/Holland.
- FAO (2019) Soil erosion: the greatest challenge to sustainable soil management. Rome. 100. Licence: CC BY-NC-SA 3.0 IGO.
- Farhan Y, Zregat D, Farhan I (2013) Spatial estimation of soil erosion risk using RUSLE approach, RS, and GIS techniques: a case study of Kufranja Watershed, Northern Jordan. J. Wat. Resour. Prot. 2013(5):1247–1261.[10.4236/jwarp.2013.512134](https://doi.org/10.4236/jwarp.2013.512134).
- Gebremicael TG, Mohamed YA, Betrie GD, Zaag P, Teferi E (2013) Trend analysis of runoff and sediment fluxes in the Upper Blue Nile basin: a combined analysis of statistical tests, physically based models and land-use maps. J. Hydrol. 482:57–68.
[10.1016/j.jhydrol.2012.12.023](https://doi.org/10.1016/j.jhydrol.2012.12.023)
- Gholami V, Sahour H, Amri AAH (2021) Soil erosion modelling using erosion pins and artificial neural networks. Catena, 196:(2021), 104902.
- Guo BL, Gifford MR (2002) Soil carbon stocks and land use change: a meta-analysis. Glo. Cha. Bio. <https://doi.org/10.1046/j.1354-1013.2002.00486>.
- Hoyos N (2005) Spatial modelling of soil erosion potential in a tropical watershed of the Colombian Andes. Catena. 63:85–108.<https://doi.org/10.1016/j.catena.2005.05.012>.
- Islam A, Deb Barman S (2020) Drainage basin morphometry and evaluating its role on flood-inducing capacity of tributary basins of Mayurakshi River, India, SN App. Sci.2,1087 (2020). <https://doi.org/10.1007/s42452-020-2839-4>.
- Jasrotia AS, Singh R (2006) Modeling runoff and soil erosion in a catchment area, using GIS, in the Himalayan region, India. Environ. Geology. 51: 29–37.[10.1007/s00254-006-0301-6](https://doi.org/10.1007/s00254-006-0301-6)
- Juerges N, Hansjürgens B (2018) Soil governance in the transition towards a sustainable bioeconomy – A review. J. of Cle. Produc. 170:1628-1639.<https://doi.org/10.1016/j.jclepro.2016.10.143>.
- Kim J, Choi J, Choi C, Park S (2013) Impacts of changes in climate and land use/land cover under IPCC RCP scenarios on streamflow in the Hoeya River Basin, Korea. Sci Tot. Environ. 452–453,[10.1016/j.scitotenv.2013.02.005](https://doi.org/10.1016/j.scitotenv.2013.02.005).
- Kim M, Gilley EJ (2008) Artificial Neural Network estimation of soil erosion and nutrient concentrations in runoff from land application areas. Compu. and elect. in agricul.64(2008):268-275. doi:10.1016/j.compag.2008.05.021.
- Kok K, Winograd M (2002) Modelling land-use change for Central America: With special reference to the impact of hurricane Mitch. Ecolo. Model. 149: 53–69. [10.1016/S0304-3800\(01\)00514-2](https://doi.org/10.1016/S0304-3800(01)00514-2).
- Kolli MK, Opp C, Groll M (2021) Estimation of soil erosion and sediment yield concentration across the Kolleru Lake catchment using GIS. Environ. Ear. Sci. 80:161. <https://doi.org/10.1007/s12665-021-09443-7>.
- Krishna Bahadur KC (2009) Mapping soil erosion susceptibility using remote sensing and GIS: a case of the Upper Nam Wa Watershed, Nan Province, Thailand. Environ. Geol. 57: 695–705.[10.1007/s00254-008-1348-3](https://doi.org/10.1007/s00254-008-1348-3).

- Kumar S, Gupta S (2016) Geospatial approach in mapping soil erodibility using CartoDEM – A case study in hilly watershed of Lower Himalayan Range. *J. of Ear. Sys. Sci.* 125 (7): 1463 – 1472. 10.1007/s12040-016-0738-2.
- Kura AL, Beyene DL (2020) Cellular automata Markov chain model based deforestation modelling in the pastoral and agro-pastoral areas of southern Ethiopia. *Remot. Sen. Appli.: Soci. and Environ.* 18: 100321. <https://doi.org/10.1016/j.rsase.2020.100321>
- Lee JH, Heo JH (2011) Evaluation of estimation methods for rainfall erosivity based on annual precipitation in Korea. *J. of Hydro.* 409(1-2): 30–48. <http://dx.doi.org/10.1016/j.jhydrol.2011.07.031>.
- Li X, Chen Y, Liu X, Li D, He J (2011) Concepts, methodologies: And tools of an integrated geographical simulation and optimization system. *Inter. J. of Geogra. Inform. Sci.*, 25:633–655. 10.1080/13658816.2010.496370.
- Lim KJ, Myung Sagong M, Engel BA, Tang Z, Choi J, Kim KM (2005) GIS-based sediment assessment tool. *Catena.* 64:61–80. 10.1016/j.catena.2005.06.013.
- Liu X, Hu G, Ai B, Li X, Tian G, Chen Y, Li S (2017) Simulating urban dynamics in China using a gradient cellular automata model based on S-shaped curve evolution characteristics. *Inter. J. of Geo. Infor. Sci.* 20:1–29. 10.1080/13658816.2017.1376065.
- Lorup JK, Styczen M (1996) Soil erosion modelling, in: Abbott, M.B., Refsgaard JC (Eds.) *Distributed hydrological modeling*. Water Science and Technology Library, Kluwer, Dordrecht, 93-120.
- Mekonnen M, Keesstra SD, Baartman JE, Ritsema CJ, Melesse AM (2015) Evaluating sediment storage dams: structural off-site sediment trapping measures in northwest Ethiopia, *Cuad. de Invest. Geo.* 41: 7–22.
- Milliman JD, Syvitski JPM (1992) Geomorphic/tectonic control of sediment discharge to the ocean: the importance of small mountainous rivers. *The J. of Geo.* 100: 525–544.
- Mitchell TD, Hulme M, New M (2002) Climate data for political areas. *Area.* 34: 109 – 112.
- Moore ID, Burch GJ (1986b) The physical basis of the slope factor in the universal soil loss equation. *Soil Sci. Soc. Am. J.* 50:1294–1298. <https://doi.org/10.2136/sssaj1986.03615995005000050042x>.
- Morgan RPC, Duzant JH (2008) Modified MMF (Morgan–Morgan–Finney) model for evaluating effects of crops and vegetation cover on soil erosion. *Ear. Sur. Pro. and Land.* 33:90 – 106. <https://doi.org/10.1002/esp.1530>.
- Mutua BM, Klik A, Loiskandl W (2006) Modelling soil erosion and sediment yield at a catchment scale: the case of Masinga Catchment, Kenya. *Land Degra. & Develop.* 17:557–570. <https://doi.org/10.1002/ldr.753>
- Mhazo N, Pauline CN, Vincent C (2016) Tillage impact on soil erosion by water: Discrepancies due to climate and soil characteristics. *Agri. Ecos. & Environ.* 230:231-243. 10.1016/j.agee.2016.04.033.
- Olawayin A, Chen Y (2018) Predicting the Future with Artificial Neural Network. *Pro. Com. Sci.* 140(2018): 383-392. 10.1016/j.procs.2018.10.300.
- Oliveira MLS, Saikia BK, Da Boit K, Pinto D, Tutikian BF, Silva LFO (2019) River dynamics and nanoparticle formation: a comprehensive study on the nanoparticle geochemistry of suspended sediments in the Magdalena River, Caribbean Industrial Area. *J. Clean. Prod.* 213:819–824.

- Pandey, A., Mathur, A., Mishra, S.K., Mal, B.C., 2009. Soil erosion modelling of a Himalayan Watershed using RS and GIS, *Environ. Ear. Sci.* 59, 399–410.[10.1007/s12665-009-0038-0](https://doi.org/10.1007/s12665-009-0038-0).
- Pavlis NK, Holmes SA, Kenyon SC, Factor JK (2012) The development and evaluation of the Earth Gravitational Model 2008 (EGM 2008). *J. of Geophy. Res.* 117: B04406. <https://doi.org/10.1029/2011JB008916>.
- Pittelkow C, Liang X, Linquist B (2015) Productivity limits and potentials of the principles of conservation agriculture. *Nature*. 517:365–368.<https://doi.org/10.1038/nature13809>.
- Poeplau C, Don A, Vesterdal L, Leifeld J, Wesemael VB, Schumacher J, Gensior A (2011) Temporal dynamics of soil organic carbon after land-use change in the temperate zone – carbon response functions as a model approach. <https://doi.org/10.1111/j.1365-2486.2011.02408.x>.
- Prosdociimi M, Jordán A, Tarolli P, Cerda A (2016) The effects of mulching on soil erosion by water. A review based on published data. Conference: European Geosciences Union General Assembly 2016, 18.
- Raj R, Saharia M, Chakma S, Rafieinasab A (2022) Mapping rainfall erosivity over India using multiple precipitation datasets. *Catena*, 214: 106256. <https://doi.org/10.1016/j.catena.2022.106256>
- Ranzi R, Le TH, Rulli MC (2012) A RUSLE approach to model suspended sediment load in the Loriver (Vietnam): effects of reservoirs and land use changes. *J. of Hydro.* 422-423: 17-29. <http://dx.doi.org/10.1016/j.jhydrol.2011.12.009>.
- Renard KG, Foster GR, Weesies GA, McCool DK, Yoder DC (1997) Predicting soil erosion by water: a guide to conservation planning with the revised universal soil loss equation (RUSLE). *Agricul. Handbook No. 703*, USDA, Washington DC.
- Roy S, Das S, Chatterjee J, Jaman MH, Sengupta S (2025) Interlinking erosion susceptibility, channel geometry and stream power: a case study of the Mayurakshi River, eastern India. *Environ Dev Sustain* 27, 17719–17740. <https://doi.org/10.1007/s10668-024-04634-1>
- Setegn SG, Dargahi B, Srinivasan R, Melesse AM (2010) Modeling of sediment yield from Anjeni-Gauged Watershed, Ethiopia using SWAT model. *J. Am. Water. Resour. Assoc.* 46(3):514–526.[10.1111/j.1752-1688.2010.00431.x](https://doi.org/10.1111/j.1752-1688.2010.00431.x).
- Sharda VN, Mandal D, Ojasvi PR (2013) Identification of soil erosion risk areas for conservation planning in different states of India. *J. of Envi. Bio.* 34: 219-226. <https://doi.org/10.1007/s11442-018-1466-0>.
- Thomas J, Joseph S, Thirvikramji KP (2018) Assessment of soil erosion in a tropical mountain river basin of the southern western ghat, India using RUSLE and GIS. *Geosci. Fron.* 9:893 – 906. <https://doi.org/10.1016/j.gsf.2017.05.011>.
- Walling DE, Webb BW (1996) Erosion and sediment yield: a global overview, In: Walling, D.E. and Webb, B.W. (Eds.), *Erosion and sediment yield: global and regional perspectives (Proceedings of the Exeter Symposium, July 1996)*. IAHS Publication No. 236: 3 – 19.
- Wei W, Chen DL, Fu JB, Chen J (2010) Water erosion response to rainfall and land use in different drought-level years in a loess hilly area of China. *Catena*.81: 24-31.

- Wischmeier WH, Smith DD (1978) Predicting rainfall erosion losses: a guide to conservation planning. Agriculture Handbook No. 537, USDA, Washington, DC.
- Yang Y, Guangrong S, Chen Z, Hao S, Zhouyiling Z, Shan Y (2022) Quantitative analysis and prediction of urban heat island intensity on urban-rural gradient: A case study of Shanghai. *Sci. of The Tot. Environ.* 829:154264.
- Yuksel A, Gundogan R, Akay AE (2008) Using the remote sensing and GIS technology for erosion risk Mapping of Kartalkaya Dam Watershed in Kahramanmaras, Turkey. *Sensors.* 8:4851–4865. <https://doi.org/10.3390/s8084851>.
- Zeng L, Liu X, Li W, Ou J, Cai Y, Chen G, Li M, Li G, Zhang H, Xu X (2022) Global simulation of fine resolution land use/cover change and estimation of aboveground biomass carbon under the shared socioeconomic pathways. *J. of Environ. Manag.* 312.
- Zhang H, Yang Q, Li R, Liu Q, Moore D, He P, Geissen V (2013) Extension of a GIS procedure for calculating the RUSLE equation LS factor. *Comput. Geosci.* 52: 177-188. <https://doi.org/10.1016/j.cageo.2012.09.027>.



Assessing Rainfall Variability in Mizoram: Insights into the Tropical-Monsoon Dynamics of Northeast India

Imanuel Lawmchullova^{1*}, Lalhnehsaki¹ and Lalrinkimi¹

¹*Department of Geography and Resource Management,
Mizoram University, Tanhril, Aizawl – 796004*

**Corresponding author: lawmchullova@gmail.com*

Abstract: This study investigates the time-series variability of rainfall in Mizoram, India, over the period 1986–2024 using descriptive statistical indices and trend analysis. Annual rainfall exhibited significant variation, ranging from 1739.18 mm to 2490.87 mm, with a mean of 2261.05 mm. Monthly precipitation patterns revealed a pronounced seasonal cycle, with June recording the maximum mean precipitation (448.36 mm) and minimum by January (6.5 mm). Spatial analysis indicated substantial station-wise disparities, with average annual rainfall ranging from 790.80 mm at Champhai to 3836.90 mm at Kolasib. Decadal shifts in rainfall distribution revealed a northward migration of high-rainfall zones and increasing spatial fragmentation in recent years. Trend analysis indicated mostly insignificant trends across months, seasons, and years, except for significant changes in specific months and stations—such as increasing trends in August and Lawngtlai, and decreasing trends in Champhai, Kolasib, and Mamit during recent decades. These findings underscore the region's complex rainfall dynamics driven by topographic and climatic influences, including orographic effects, monsoonal variability, and localized atmospheric conditions. The findings have direct policy relevance for sustainable water management, agricultural planning, and disaster risk reduction. Declining monsoonal rainfall and increasing irregularity highlight the need to strengthen rain-fed agricultural systems, promote soil and water conservation measures, and improve watershed-based planning.

Keywords: Time series, rainfall variability, non-parametric test, trend, Mizoram.

1. Introduction:

Climate change denotes sustained changes in average weather conditions over extended periods, significantly influencing precipitation patterns across the globe. As a critical element of the hydrological cycle, rainfall is especially vulnerable to these climatic changes. The north-eastern region of India, rainfall patterns are highly diverse and intricate. As noted by Singh *et al.* (2022), understanding climate changes pattern is significant for effective water resource management. Southwest monsoon mainly influences local precipitation pattern, mostly occur during May to September, and experiencing the average yearly precipitation ranging between 2,000 mm and 3,500 mm. Examine the spatio-temporal dissemination of precipitation, particularly climate variability is essential in the regions reliant on rain-fed cultivation. For instance, Lalchhandama *et al.* (2021), mentioned, the variations in climate variables can significantly affect a wide range of socio-economic activities in the region. In case of Mizoram, unpredictable rainfall patterns have frequently led to adverse outcomes, and recent study also observed unpredictable climatic behavior (Pandey *et al.* 2023). Mizoram holds particular importance for rainfall trend analysis due to its unique geographic and climatic setting within the Indo-Burma biodiversity hotspot, one of the world's most ecologically sensitive and rainfall-dependent regions. The state's rugged topography, dominated by steep hills and valleys, exerts strong orographic influences on precipitation patterns, leading to high spatial variability that is poorly captured in large-scale studies. Furthermore, Mizoram lies in the transition zone between the South Asian summer monsoon and the Southeast Asian monsoon systems, making it highly susceptible to shifts in monsoonal dynamics and climate variability. Despite this significance, long-term rainfall trend studies specific to Mizoram remain scarce, leaving critical gaps in understanding localized hydrological responses, water resource sustainability, agricultural productivity, and climate resilience in the region. Addressing this gap is essential for developing evidence-based adaptation and management strategies in the context of climate change.

Several studies have conducted on precipitation trends and patterns by robust and reliable test of parametric and non-parametric statistical techniques, such as the Mann-Kendall (MK) test, Modified Mann-Kendall (MMK) (Mann 1945) test, Sen's slope estimator (Q) (Sen 1968), Linear Regression Analysis (LRA), and the Innovative Trend Analysis (ITA) method. At the international scale, AlSubhi *et al.* (2021) reported a statistically significant decline in rainfall over the semi-arid Aseer region of Saudi Arabia during the period 1970–2017. However, the study did not account for the degree of slope or spatial distribution of precipitation variability. In a similar context, a time series analysis conducted in Iraq examined rainfall trends at 38 rain gauge stations spanning the period 1980–2021. The findings indicated no significant trends in 16 stations, with a few stations showing slight increases; however, the overall pattern revealed a general declining trend, despite the region's relatively uniform climatic conditions (Allami *et al.* 2024). In South Africa's eastern escarpment region, precipitation trends during 1961–2021 showed a statistically significant increase. The study further identified a shift in rainfall characteristics: while total yearly precipitation, the count of successive wet days, and moderate precipitation events (>10 mm/day) have become less frequent, the incidence

of intense rainfall events has increased. Similarly, Obot *et al.* (2025) identified a declining rainfall trend over a 51-year period (1960–2010) in Nigeria, particularly emphasizing that both statistically significant trends and notable shifts were more prevalent in the country's arid northern regions. In southern Africa, a study conducted in the Metuge District of Mozambique reported a statistically significant decline in both annual and monsoonal rainfall based on time series data from 1989 to 2022 (Comia *et al.* 2025). In South Asia, Sri Lanka, India's neighboring country exhibited comparable trends. A 60-year rainfall time series (1960–2020) revealed a general decline in precipitation (Iresh *et al.* 2025). The study highlighted pronounced regional and seasonal variability, with a mild decline in rainfall observed in the central highlands, while regions such as Maha Oya and Deduru Oya river basins observed increasing trends, underscoring the heterogeneous climatic behavior across the island. At the international scale, rainfall trend studies consistently reveal heterogeneous patterns, while some semi-arid and tropical regions show declining rainfall trends, others indicate increasing trends or a shift toward more intense rainfall events. These findings highlight the global variability of precipitation behavior, influenced by regional climatic systems and topographical differences.

As the national background, Kumar *et al.* (2010) conducted a rainfall trends over a 135-year period (1871–2005) at 30 sub-regions in India. The study observed that insignificant trends in annually, seasonal, and month-wise precipitation in all the regions. However, Gajbhiye *et al.* (2016) investigated a 101-year rainfall time series (1901–2002) for the Sindh River Basin and reported a statistically significant increase in both seasonal and annual rainfall throughout the basin. Bera (2017) investigated precipitation trends over a century (1901–2001) in 236 districts within the Ganga Basin. The study observed that the 50 per cent of the districts exhibit a decline in yearly precipitation, and 39 districts are notable decreases. Similarly, Rana *et al.* (2022) evaluated rainfall trends in the state of Uttarakhand, and reported significant declining trends in annual rainfall. Soren *et al.* (2023) reported temporal variations in rainfall patterns in the Mayurakshi Basin of eastern India, but declining trend is insignificant. Similarly, Laxmi *et al.* (2024) conducted rainfall trend in Kantamal watershed and observed non-significant decline in annual and monsoonal rainfall, while pre-monsoon season shows that consistently decrease in precipitation. Therefore, the national level long-term analyses similarly indicate mixed and regionally variable rainfall trends. Multi-decadal studies reveal that while some river basins and sub-regions experience declining or insignificant rainfall trends, others show localized increases, reflecting India's complex monsoon dynamics. This demonstrates that national-scale assessments often mask finer regional variations due to the country's diverse physiography and climatic gradients.

In the northeast India, Laskar *et al.* (2014) reported there is no statistically significant positive or negative trend from the study of a 100-year (1913–2012) rainfall time series. However, the post-monsoon season in Guwahati exhibited a notable upward trend. In contrary, within the same state of Assam, Gogi *et al.* (2022) reported a seasonal variation in rainfall trends, with significant declines trend observed for the months of September, December, January, and February, while statistically significant upward trend observed in May, June, and August. Furthermore, from the 150 years (1857–2006) analysis of entire northeastern region

of India highlighted a noteworthy decline in monsoon rainfall, but post-monsoon precipitation exhibited upward trend (Singh *et al.* 2022). Similarly, a recent study by Lawmchullova *et al.* (2024), reported an increasing of rainfall at Tlawng watershed form the analysis of 40-year historical time series, but statistically insignificant. Thus, at the regional scale, particularly in northeastern India, studies reveal spatial and seasonal inconsistencies in rainfall patterns. While long-term records suggest a general decline in monsoonal rainfall, some areas and seasons exhibit increasing or statistically insignificant trends.

2. Material and methods:

2.1 Study Area:

Mizoram, located in the northeastern region of India, is primarily a hilly state lying between 21°06'N - 24°31'N and 92°16'E - 93°26'E (Figure 1). Located in the extreme eastern region of the nation, it is bordered internationally by Myanmar on the east and south, and by Bangladesh on the west. Domestically, it adjoins the Indian states of Tripura to the northwest, Assam to the northeast, and Manipur to the north. Due to its topography, Mizoram experiences a moderate climate, ranging from subtropical to temperate depending on elevation, with an average annual temperature of approximately 26.27°C. The state experiences significant rainfall, primarily due to the Southwest Monsoon, which generally occurs between May and September. Annual precipitation ranges from 1739.18 mm to 2490.87 mm.

2.2 Data Acquisition:

Historical daily precipitation dataset during 1986–2023 was acquired from twenty-six rain gauge stations through the Department of Agriculture, Government of Mizoram. The rainfall data for the year of 2024 is acquired from the State Meteorological Centre, Directorate of Science and Technology, Government of Mizoram (MINECO), encompassing all districts within the state. The acquired dataset, comprising daily rainfall records, was systematically organized into standardized formats such as monthly, station-wise, decadal, and annual aggregates for subsequent analysis. Microsoft Excel was employed for preliminary data structuring, facilitating compatibility with the R programming environment for advanced statistical processing.

2.3 Mann- Kendall:

The MK test, in conjunction with Q estimator, constitutes a robust methodological framework for identification and calculating trends in historical datasets. Rainfall variability, even within homogeneous climatic zones or intra-basin regions, is a commonly observed phenomenon. Accordingly, a comprehensive analysis of precipitation at several time-based measures annual, seasonal, month-wise, and decadal is essential for understanding long-term patterns and trends. The present study investigates temporal variations of precipitation patterns in Mizoram, with comparative analyses conducted at the district level to enhance understanding for informed decision-making and future planning. Trend test is performed by MK and Q estimator. In addition, Inverse Distance Weighting (IDW) interpolation was applied to decadal

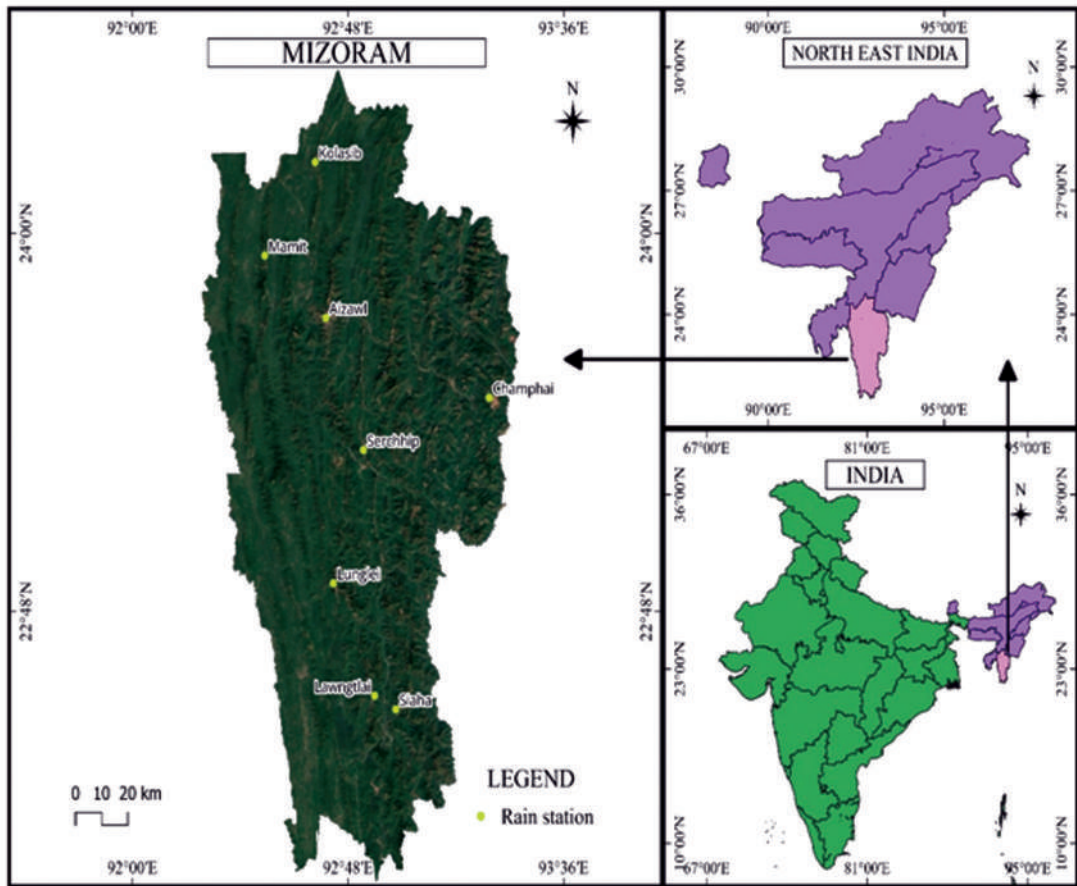


Figure 1. The geographical location of Mizoram, north-eastern corner of India.

rainfall data spanning 1986 to 2024, revealing a spatial shift in rainfall concentration across the state from southern regions to central areas, subsequently to the north, and most recently towards the western part of Mizoram.

The value of the statistic (S) is determined using the equation 1 – 2.

$$S = \sum_{k=1}^{n-1} \sum_{j=k+1}^n \text{sign} (x_j - x_k) \quad \dots \text{Equation 1}$$

Let n denote total count of datasets, x_j and x_k signify individual data points from series j and k , respectively. The *sign* is expressed as below:

$$\text{sign} (x_j - x_k) = \begin{cases} 1 & \text{if } x_j - x_k > 0 \\ 0 & \text{if } x_j - x_k = 0 \\ -1 & \text{if } x_j - x_k < 0 \end{cases} \quad \dots \text{Equation 2}$$

The formula for computing the variance of S is using equation 3 – 4.

$$VAR(S) = \frac{1}{18} \left\{ n(n-1)(2n+5) - \sum_{p=1}^g t_p(t_p-1)(2t_p+5) \right\} \dots \text{Equation 3}$$

where n is count datasets, g is tied group in a series and t_p signify tied series extent p
The statistic S is calculated with Kendall's as given by:

$$\tau = \frac{S}{D} \dots \text{Equation 4}$$

Where D is estimated as (Equation 5 - 6)

$$D = \sqrt{\frac{1}{2}n(n-1) - \frac{1}{2} \sum_{p=1}^g t_p(t_p-1)} \sqrt{\frac{1}{2}n(n-1)} \dots \text{Equation 5}$$

The S and $VAR(S)$ are calculated to standardized Z statistic if the $n > 10$,

$$z = \begin{cases} \frac{S-1}{[VAR(S)]^{\frac{1}{2}}} & \text{if } S > 0 \\ 0 & \text{if } S = 0 \\ \frac{S+1}{[VAR(S)]^{\frac{1}{2}}} & \text{if } S < 0 \end{cases} \dots \text{Equation 6}$$

The affirmative Z -statistic reflects a rising pattern, while a negative Z -statistic suggests a declining tendency. When the null hypothesis (H_0) is accepted, it implies there is no statistically meaningful trend present; in contrast, accepting the alternative hypothesis (H_a) confirms that a trend exists within the time series. Similarly, a positive Q_i value indicates a rise in rainfall, whereas a negative Q_i value points to a decline. The symbol α denotes the significance threshold (e.g., 0.05 or 0.01), which aligns with the predetermined confidence level.

2.4 Sen's Slope:

The degree of slope $Q(i)$ was computed using equation 7 - 8.

$$Q_{(i)} = \frac{x_k - x_j}{k - j}, \text{ for } j, k = 1, 2, 3, \dots, N \dots \text{Equation 7}$$

where x_j and x_k denotes data series values at times j and k , respectively. The median of slope is $Q_{(i)}$.

If N is even or odd, then Sen's estimator is expressed as;

$$Q_{med} = \begin{cases} Q_{\left(\frac{N+1}{2}\right)} & \text{If } N \text{ is even} \\ \frac{1}{2} \left(Q_{\frac{N}{2}} + Q_{\frac{N+2}{2}} \right) & \text{If } N \text{ is odd} \end{cases} \quad \dots \text{Equation 8}$$

2.5 Interpolation Technique:

The present study, the Inverse Distance Weighting (IDW) interpolation method was employed to generate spatial rainfall distribution maps. IDW was selected primarily for its computational simplicity, ease of implementation, and effectiveness in regions with limited and irregularly distributed rain gauge networks, such as Mizoram. The method assumes that nearby points exert a greater influence on the interpolated value than those farther away, which is suitable when the spatial autocorrelation structure of rainfall is not sufficiently strong or when the number of observation points is relatively small to model a reliable variogram. Although geostatistical approaches such as Ordinary Kriging or Universal Kriging can potentially provide more statistically optimal estimates by incorporating spatial autocorrelation, they require a large, evenly distributed dataset and a well-defined variogram model to ensure accuracy. In the case of this study, the density of rainfall stations and temporal consistency of data were not adequate to support robust variogram modelling. Therefore, IDW provided a more stable and transparent interpolation framework for the available dataset and is mathematically represented as equation 9 -10.

$$W_i = \frac{\frac{1}{d_i^p}}{\sum_{i=1}^n \frac{1}{d_i^p}} \dots \quad \text{Equation 9}$$

Point value is calculated using the formula (Purnomo, 2018):

$$\hat{Z}_0 = \sum_{i=1}^n W_i \cdot Z_i \dots \quad \text{Equation 10}$$

Where, \hat{Z}_0 = estimated point coordinate
 W_i = spatial weight at coordinate i
 Z_i = calculated point value at i
 d_i = separation between point i and the predicted location
 p = exponentially weighted factor

3. Results and Discussion:

3.1 The descriptive variability indices of rainfall:

The descriptive statistical analysis of precipitation in Mizoram from 1986 – 2024 reveals substantial spatio-temporal fluctuations in precipitation. The annual rainfall during this period ranged from 1739.18 mm to 2490.87 mm, with having an average of 2261.05 mm/

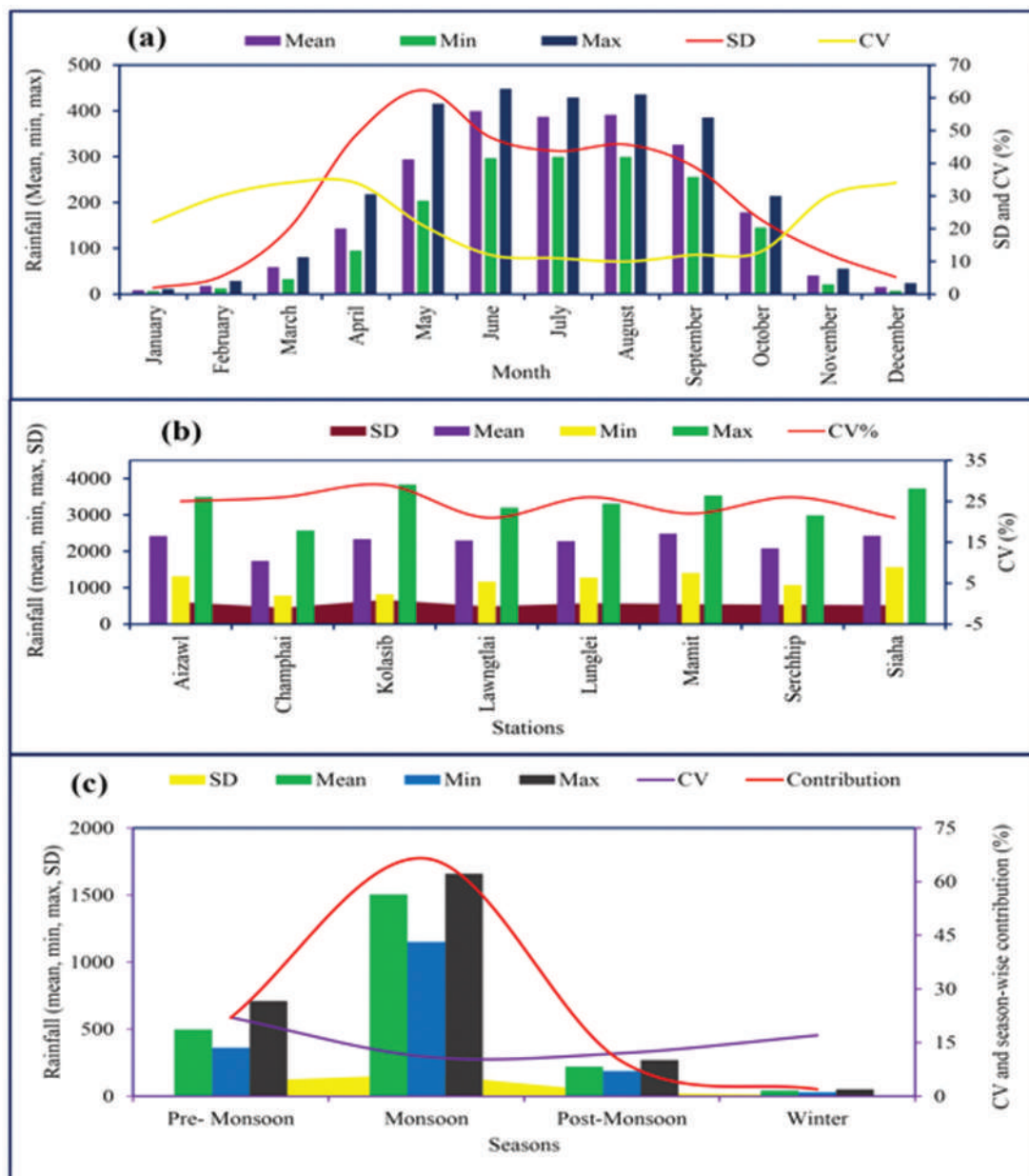


Figure 2. Showing the plot of descriptive statistic of rainfall in Mizoram (1986 - 2024); (a) monthly, (b) station-wise, (c) season-wise..

yr⁻¹. Figure 2(a) illustrates the monthly variability in rainfall across the studied years, with an average monthly precipitation of 188.58 mm/month. The highest average monthly rainfall was recorded in June (448.36 mm), whereas the lowermost was detected in January (6.5 mm).

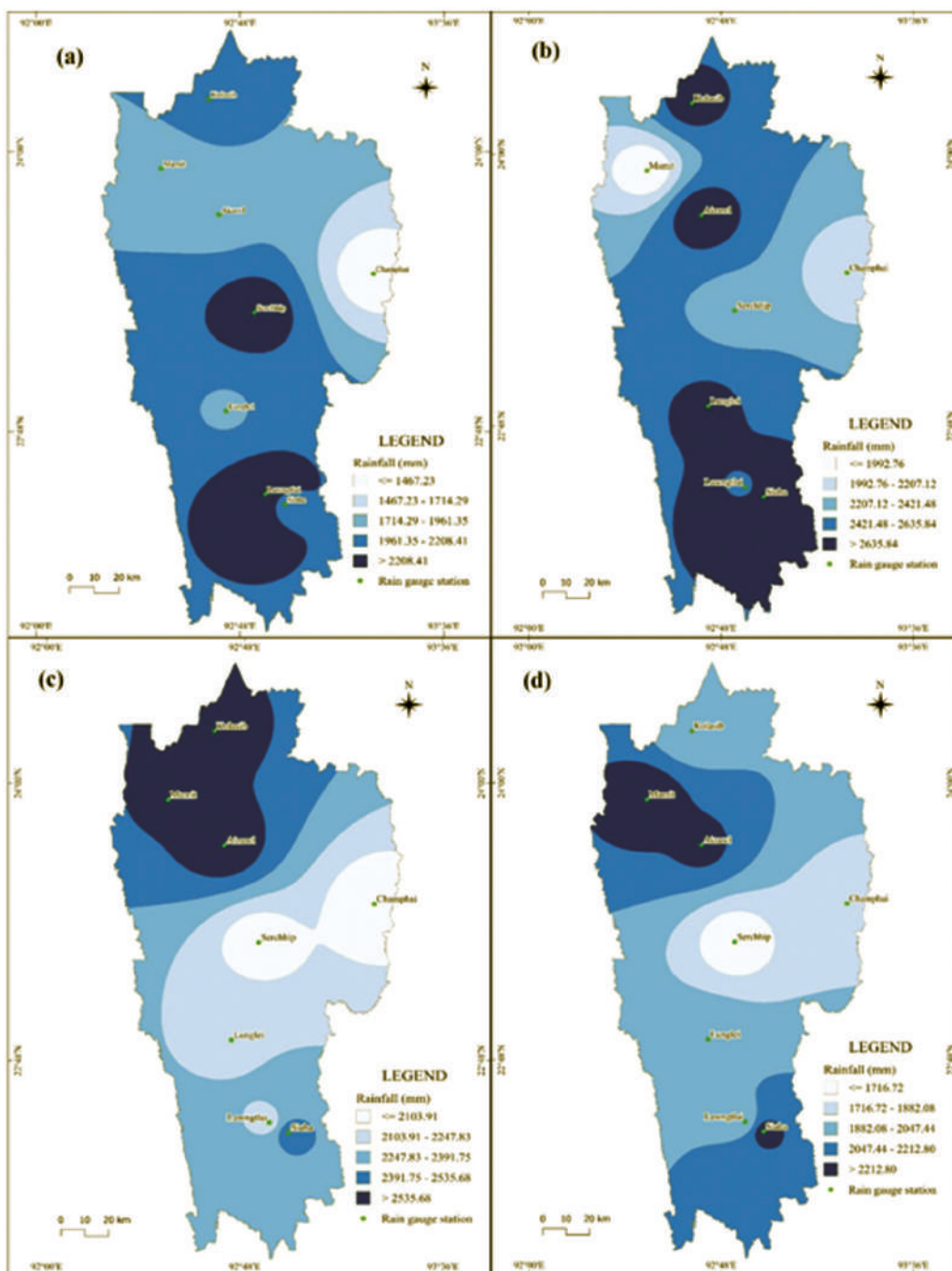


Figure 3. Spatial distribution pattern and intra-state variation of rainfall in Mizoram by decade-wise; (a) 1986 – 1995, (b) 1996 – 2005, (c) 2006 – 2015, and (d) 2016 – 2024.

The corresponding average standard deviation and coefficient of variation (CV) were 29.56 mm and 21.91 per cent, respectively. Figure 2(b) exhibit the spatial (station-wise) distribution of annual rainfall across various meteorological stations in Mizoram during the same period. The lowest and highest average annual rainfall amounts were recorded at Champhai (790.80 mm/yr⁻¹) and Kolasib (3836.90 mm/yr⁻¹), respectively. The associated standard deviation and CV were 549.59 mm and 24.50 per cent, indicating moderate variability among stations. Figure 2(c) depicts the season-wise distribution of precipitation during 1986–2024. The mean seasonal rainfall was 565.74 mm/season. Among the four seasons, winter contributed the least to the annual total with an average of 29.51 mm (1.88%), while the monsoon season recorded the highest contribution, averaging 1659.70 mm (66.45%). The average standard deviation and CV for seasonal rainfall were 76.37 mm and 15.5 per cent, respectively, highlighting relatively consistent seasonal patterns with some variability.

3.2 Intra-state variation of rainfall by decadal wise:

The decadal spatial distribution and intra-state variability of rainfall in Mizoram are depicted in Figure 3. During the decade 1986–1995 (Figure 3a), a higher concentration of precipitation was predominantly detected in the south to southern-central regions in the state, whereas the central-eastern areas experienced relatively lower precipitation. In the subsequent decade (1996–2005), the spatial pattern exhibited a noticeable shift, with zones of higher rainfall concentration extending from the southern to northern parts of central Mizoram. Concurrently, the central-eastern and northwestern regions recorded comparatively lower rainfall (Figure 3b). A continued spatial transition was evident in the decade 2006–2015, wherein the zone of maximum rainfall shifted further northward, while the central-eastern region remained consistently deficient in rainfall (Figure 3c). In the most recent decade (2016–2024), the rainfall distribution pattern became more spatially fragmented. The previously dominant high-rainfall zones diminished in extent, and the area of highest precipitation concentration shifted from the northern to the northwestern region of the state. In contrast, the central region experienced persistently low rainfall during this period (Figure 3d).

3.3 Rainfall trend; monthly, season-wise and annual:

Table 1 presents the test statistics—Z, Kendall's tau (τ), and Sen's slope (Q)—for mean monthly, seasonal, and annual precipitation in Mizoram during 1986–2024. The results indicate a negative but statistically insignificant trend during January–April and October–November. Conversely, the months from May to September and December exhibit positive, though statistically insignificant, trends. A significant upward trend was detected only in August, with a Z-value of 1.74, significant at the 90% confidence level and an estimated increase rate of 2.51 mm yr⁻¹. The monthly distribution of rainfall trends is evenly split, with 50% of months showing positive and 50% showing negative trends. The annual average Z-value of -0.9 suggests a non-significant declining trend. Similarly, seasonal trend analysis indicates no statistically significant changes, although monsoon and winter seasons show declining tendencies, while pre- and post-monsoon periods display positive trends.

Table 1. Test statistic of mean monthly, season-wise and annual rainfall of Mizoram (1986 - 2024)

Month	Z	Tau	Q
January	-0.13	-0.01	0
February	-1.28	-0.14	-0.23
March	-1.13	-0.12	-0.56
April	-0.6	-0.06	-0.64
May	0.45	5.26	1.24
June	1.5	0.16	1.88
July	0.67	7.69	1.12
August	1.74	0.19	2.51
September	0.12	0.01	0.19
October	-0.41	-0.04	-0.36
November	-1.51	-0.17	-0.72
December	0.13	1.74	0
Annual	-0.94	-0.1	-6.09
Pre- Monsoon	0	-1.34	-0.05
Monsoon	0.99	0.11	1.16
Post-Monsoon	-0.5	-0.05	-0.34
Winter	0.16	2.02	0.03
Z statistic significant at 90% level of confidence			

Table 2 summarizes the station-wise decadal rainfall trends in Mizoram for 1986–2024. During 1986–1995, stations such as Aizawl, Champhai, and Kolasib recorded increasing rainfall, whereas Lawngtlai, Lunglei, Serchhip, and Mamit exhibited decreasing trends, none of which were statistically significant. These findings are consistent with previous studies reporting high inter-annual variability in rainfall patterns across northeast India (Laskar *et al.* 2014; Singh *et al.*, 2022), largely attributed to the region’s heterogeneous terrain and strong orographic influences that modulate monsoonal precipitation. During 1996–2005, Kolasib, Lunglei, Champhai, and Serchhip exhibited negative trends, with Champhai showing a significant decline at the 90% confidence level (−36.67 mm yr^{−1}). In contrast, Mamit, Lawngtlai, and Saiha experienced positive but insignificant trends. This spatial inconsistency may be linked to the differential influence of monsoon onset and weakening wind circulation along the northern and eastern hill ranges (Pandey *et al.*, 2023). In the decade 2006–2015, most stations exhibited negative rainfall trends, except Lunglei, which maintained a weakly positive tendency. Mamit showed a statistically significant decrease ($Z = -2.28$, $p < 0.01$; −124.67 mm yr^{−1}), consistent with findings from other agro-climatic zones of eastern India, where a decline in monsoonal rainfall and an intensification of extreme events have been

documented (Soren *et al.* 2023; Bera, 2017). The alteration in the onset and duration of monsoon periods may partly explain this downward trend (Kumar *et al.* 2010).

Table 2. Decade-wise test statistic of Mizoram (1986 - 2024)

S no.	Station	Decadal							
		1986-1995		1996-2005		2006-2015		2016-2024	
		Z	Q	Z	Q	Z	Q	Z	Q
1	Aizawl	0.18	13.91	0.00	1.45	-0.54	-37.10	-1.56	-136.5
2	Champhai	0.00	0.70	-1.79	-36.67	-0.89	-39.55	-1.98	-87.63
3	Kolasib	0.72	43.58	-0.36	-30.55	-0.36	-17.38	-1.98	-181
4	Lawngtlai	-0.36	-25.67	0.18	6.67	-1.43	-122.55	2.19	142.77
5	Lunglei	-0.18	-4.88	-1.61	-86.40	0.18	29.18	-1.77	-131
6	Mamit	-0.18	-2.98	0.18	1.41	-2.68	-124.67	-1.15	-224.2
7	Serchhip	-0.54	-29.33	-1.61	-51.00	-0.72	-38.78	-0.52	-7.40
8	Siaha	0.00	5.00	0.18	32.81	-0.36	-45.17	-1.36	-29.29
	Z statistic significant at 90% level of confidence								
	Z statistic significant at 95% level of confidence								
	Z statistic significant at 99% level of confidence								

In the most recent decade (2016–2024), significant decreasing trends were detected at Champhai and Kolasib ($Z = -1.98$, $p < 0.05$), with corresponding slopes of $-87.63 \text{ mm yr}^{-1}$ and -181 mm yr^{-1} , respectively. Lunglei also displayed a declining trend ($Z = -1.77$, $p < 0.10$). Conversely, Lawngtlai exhibited a statistically significant positive trend ($Z = 2.19$, $p < 0.05$; $142.77 \text{ mm yr}^{-1}$). These observations corroborate recent assessments of rainfall patterns in northeast India that document declining monsoonal rainfall and increasing rainfall irregularity (Iresh *et al.* 2025; Singh *et al.*, 2022). The downward trend may be associated with influenced by micro-climatic condition or regional topography that modulate rainfall at finer scales (Rana *et al.* 2022; Comia *et al.* 2025)

The observed temporal and spatial variability in rainfall across Mizoram can be attributed to multiple interacting climatic and physiographic factors. On a large scale, ocean atmosphere phenomena such as the El Niño–Southern Oscillation (ENSO) and Indian Ocean Dipole (IOD) are known to influence the strength, onset, and withdrawal of the Indian monsoon, thereby modulating rainfall distribution over the northeast region. Positive ENSO and IOD phases often weaken monsoon circulation, leading to suppressed rainfall, whereas negative phases may enhance moisture convergence. Additionally, orographic effects and the region’s complex physiography, characterized by steep elevation gradients and varying slope orientations, play a

critical role in local rainfall distribution by altering moisture advection and convective activity. Moreover, land-use and land-cover changes, such as shifting cultivation, deforestation, and urban expansion, may further modify local microclimates by influencing evapotranspiration rates and surface roughness.

Thus, these interacting factors contribute to the observed heterogeneity in rainfall trends across Mizoram, suggesting that the detected temporal variations are not solely statistical artifacts but reflect the region's sensitivity to both large-scale climatic oscillations and localized environmental changes. The findings of this study hold significant implications for agriculture, water resources, and disaster management in Mizoram. The observed spatial and temporal variability in rainfall, including declining monsoonal precipitation and increasing irregularity, may directly affect rain fed agricultural systems that dominate the region. Reduced and erratic rainfall could lead to soil moisture deficits, delayed sowing, and lower crop yields, particularly for paddy and shifting cultivation systems that depend heavily on monsoon rains. In contrast, intensified rainfall events in certain months increase the risk of soil erosion and crop damage. From a water resource perspective, declining rainfall trends may impact streamflow regimes, groundwater recharge, and the sustainability of small-scale reservoirs. Furthermore, the uneven distribution of rainfall heightens the risk of both drought and flooding, complicating local water management strategies. The Mizoram topography steep terrain and fragile slopes, increased surface-off could also exacerbate landslides and flash floods, posing significant challenges for disaster preparedness and infrastructure resilience. Integrating rainfall trend information into agricultural planning, watershed management, and early warning systems will therefore be crucial for enhancing climate adaptation and sustainable resource management in the region.

Conclusion:

This study provides the comprehensive, long-term (1986–2024) spatio-temporal assessment of rainfall variability and trends across Mizoram using robust non-parametric methods, including the Mann–Kendall test, Sen's slope estimator. The findings reveal the distinct intra-decadal and spatial heterogeneity, with alternating zones of increasing and decreasing rainfall intensity that shift northward and westward over time. The analysis further demonstrates that rainfall variability in Mizoram is influenced by large-scale climatic oscillations (ENSO, IOD), combined with local orographic, physiographic, and land-use factors that modulate moisture dynamics and monsoon circulation. Moreover, the present study highlight the integration of multi-decadal, multi-scale statistical trend analysis revealed fine-scale rainfall dynamics in one of India's least-studied but hydrologically sensitive regions. By bridging gaps between national and regional assessments, this research advances understanding of how global and mesoscale climatic processes translate into localized hydro-climatic variability in the complex terrain of Northeast India. The study recommends the policy maker urgent need to integrate rainfall trend information into regional planning frameworks. Strengthening climate-resilient agricultural practices, such as crop diversification and soil-water conservation, will be vital to mitigate the impacts of declining and erratic rainfall on Mizoram's rain fed farming systems.

Similarly, adaptive water resource management including improved watershed management, reservoir capacity optimization, and rainwater harvesting should be prioritized to ensure long-term water security. Furthermore, the increased irregularity in precipitation and concentration of extreme rainfall events necessitate enhanced disaster preparedness strategies, including early warning systems and slope stabilization programs to reduce landslide and flood risks

Acknowledgement:

The authors gratefully acknowledge Department of Agriculture, and Directorate of Science and Technology, Government of Mizoram, for providing us rain gauge recorded historical rainfall data sets during a year of 1986 – 2024.

References:

- Allami, A., Kadhim, Y., & Al-Salihi, A. (2024). Innovative trend analysis of annual rainfall in Iraq during 1980-2021. *Journal of Agrometeorology*, 26(2), 196-203.
- Alsubih, M., Kumari, M., Mallick, J., & Ramakrishnan, R. (2021). Time series trend analysis of rainfall in last five decades and its quantification in Aseer Region of Saudi Arabia. *Arabian Journal of Geosciences*, 14(6).
- Bello, A. H., Scholes, M., & Francois, E. A. (2025). Spatio-temporal trends in daily precipitation extremes over the Enkangala escarpment of South Africa: 1961–2021. *Theoretical and Applied Climatology*, 156(3).
- Bera, S. (2017). Trend analysis of rainfall in Ganga Basin, India during 1901-2000. *American Journal of Climate Change*, 6(1), 116-131.
- Comia, H. R., Kenée, F. B., Nelson, F. C., Americano, J. M., & Mucova, S. A. R. (2025). Trend analysis of rainfall and temperature in Metuge district, northern Mozambique. *Discover Atmosphere*, 3(1), 8.
- Dore MHI. (2005). Climate change and changes in global precipitation patterns: what do we know? *Environ Int.* 31, 1167-1181.
- Gogoi, K., & Rao, K. N. (2022). Analysis of rainfall trends over Assam, North East India. *Current World Environment*, 17(2), 435-446.
- Gajbhiye, S., Meshram, C., Mirabbasi, R., & Sharma, S. K. (2016). Trend analysis of rainfall time series for Sindh river basin in India. *Theoretical and applied climatology*, 125, 593-608.
- Iresh, A. D. S., Athapattu, B. C. L., Fernando, W. C. D. K., & Obeysekera, J. (2025). Analysis of Long-Term Seasonal Rainfall Trends in Sri Lanka after Eliminating the Serial Correlation Effect. *Engineer: Journal of the Institution of Engineers, Sri Lanka*, 58(1).
- Kumar, V., Jain, S. K., & Singh, Y. (2010). Analysis of long-term rainfall trends in India. *Hydrological Sciences Journal–Journal des Sciences Hydrologiques*, 55(4), 484-496.
- Lalchhandama, G., Saitluanga, B. L., Rinawma, P., & Sellate, I. L. (2021). Long term annual and seasonal temperature and rainfall trend analysis in Aizawl District, Mizoram. *Research and Publication Cell, Govt. Hnahthial College*.

- Laskar, S. I., Kotal, S. D., & Bhowmik, S. (2014). Analysis of rainfall and temperature trends of selected stations over North East India during last century. *MAUSAM*, 65(4), 497-508.
- Lawmchullova, I., Rinkimi, L., & Bhaskara Rao, C. U. (2024). Trend analysis of rainfall (1984-2023) of Tlawng River basin of Mizoram, India using Man-Kendall test. *Journal of Agrometeorology*, 26(3), 391-394.
- Laxmi, S., Sahu, A. P., Paul, J. C., & Das, D. M. (2024). Application of innovative trend analysis for rainfall variability in the middle catchment of Mahanadi River basin, India. *Journal of Agrometeorology*, 26(2), 264-267.
- Mann, H. B. (1945). Nonparametric tests against trend. *Econometrica: Journal of the econometric society*, 245-259.
- Obot, N. I., Humphrey, I., & Jolayemi, O. R. (2024). Significant trends and structural shifts in rainfall patterns in Nigeria. *Acta hydrotechnica*, 37(67), 103-125.
- Pandey, V., Pandey, P. K., Chakma, B., & Ranjan, P. (2023). Influence of short- and long-term persistence on identification of rainfall temporal trends using different versions of the Mann-Kendall test in Mizoram, Northeast India. *Environmental Science and Pollution Research*, 31(7), 1–20.
- Purnomo, H. (2018). Aplikasi metode interpolasi inverse distance weighting dalam penaksiran sumberdaya laterit nikel (Studi kasus di Blok R, Kabupaten Konawe–Sulawesi Tenggara). *Jurnal Ilmiah Bidang Teknologi, ANGKASA*, x(1), 49–60.
- Rana, S., Deoli, V., & Chavan, S. (2022). Detection of abrupt change in trends of rainfall and rainy day's pattern of Uttarakhand. *Arabian Journal of Geosciences*, 15(7), 1-17.
- Sen, P. K. (1968). Estimates of the Regression Coefficient Based on Kendall's Tau. *Journal of the American Journal of the American Statistical Association*, 6363(324), 1379–1389.
- Singh, P., Kumar, N., & Mausam, I. M. D. (2022). Analysis of trend and temporal variability in rainfall over Northeast India. *MAUSAM*, 73(2), 307-314.
- Soren, D. D. L., Barman, J., & Biswas, B. (2023). A geo-spatial approach to rainfall variability and time series trend analysis in the Mayurakshi basin, Eastern India. *The Indian Geographical Journal*, 98(2), 150-169



GIS-Based Analysis of Site Suitability for Potential Agricultural Land Using MCDM Approach in the District of Uttar Dinajpur, West Bengal, India

Saidur Rahaman¹, Sujoy Kumar Malo¹, Mantu Das¹,
Kunal Chakraborty¹ & Snehasish Saha^{1*}

*¹Department of Geography & Applied Geography, University of North Bengal,
Raja Rammohunpur, Darjeeling –734013, West Bengal, India*

**Corresponding author: snehonbugeo09@nbu.ac.in*

Abstract: Analysing the appropriateness of agricultural sites at the provincial level is essential to developing the most sustainable management strategy. The main objective of the present research was to delineate suitability of agricultural fields in Uttar Dinajpur district, West Bengal using MCDM approach (Fuzzy AHP and Weighted Sum methods) in GIS platform. Twelve most influencing parameters like physical, hydrological, climatic, land use land cover etc. were taken into consideration and local knowledge based opinions were considered to find out an inference on weighting the parameters and sub-parameters. In this case, standard rules were followed (CR -0.07; CI -0.05) which was a valid pair-wise comparison matrix. The results identified that LULC (0.12), soil texture (0.11), and soil pH (0.10) had the highest specific weighting for the delineation of agriculturally suitable sites. Two MCDM methods were incorporated here but, notably Fuzzy AHP had better accuracy. The map of land-suitability (Fuzzy AHP) concluded that 43.62% of the studied area was for highly suitable, 33.09% was moderately suitable, and 20.94% was marginally suitable. Finally, a promising approach to site-specific policies for the management of soil, and planning for better land-use, and necessary protection for environment was attained involving and combining AHP, Fuzzy, and GIS based assessments.

Keywords: Agriculture, MCDM, Fuzzy AHP, Weighted Sum, GIS, Sustainable management.

Introduction:

The sustainable and responsible utilisation of natural resources, like land, that cannot be produced again is widely seen as one of the most significant markers of economic expansion. Natural and agricultural resources are under additional strain due to population growth, particularly in developing countries (Akpoti *et al.*, 2019). In order to supply the nutritional needs of the world's ever expanding growth of population, the food supply must increase. In general, agricultural resources are under stress due to both population growth and urbanization (Orhan *et al.*, 2003). Now, it is commonly understood that one of the most significant measures of economic progress is the logical and sustainable use of irreplaceable natural resources such as land (Ananda and Herath, 2009). Land suitability is closely associated with sustainable development, which, according to the WCED, involves meeting present demands without compromising the ability of future generations to meet their own (Planko and Silvius, 2017; Maddahi *et al.*, 2014). Land suitability analysis can help and create strategies to increase agricultural productivity by determining the arising and potential strength of land for future goals (Otgonbayar *et al.*, 2017; Shaw *et al.*, 2025). The land evaluation approach involves systematically evaluating the potential of land to determine the best location for growing a certain crop. In theory, the assessment of the climate, soil, water resources, topography, and environmental elements according to the specified criteria, as well as knowledge of the regional biophysical constraints, determines the potential of land suitable for agricultural use. Land suitability is evaluated using a rational agriculture system to optimise the usage of an area of land for a certain usage (Mustafa *et al.*, 2011; FAO, 1976). Global agricultural output and food security are seriously threatened by factors like improper land management, global climate change, and pressure to fulfil the rising food and fibre demand (IPCC, 2013; Kilic and Gunal, 2021). The agricultural sector has intensified and expanded throughout the last ten years because of rising population and correspondingly raising demand for food and other agricultural goods (Hemathilake and Gunathilake, 2022; Rudel *et al.*, 2009; Kopittke *et al.*, 2019; Tscharrntke *et al.*, 2012). Because of this, it is crucial to create land use plans that allow natural resources to be passed down to future generations and that allow for their sustainable and planned usage in a way that maximises their potential. Contrarily, increased opposition to the use of genetically modified plants, increasing pesticide and fertiliser dosages, and environmental concerns are being voiced on a global scale. The later, however, are modern technologies that could increase the production of food (Ustaoglu *et al.*, 2021; Khan *et al.*, 2022). Adaptability has an impact on crop demands and characteristics of soil, by comparing the land characteristics to the needs of the cultivated crops based on that the land suitability is determined (Feizizadeh *et al.*, 2014). The appropriateness of the land or land suitability is a method of measurements of various parameters of land, soil characteristics and infrastructural factors to make out how much they are suitable for crop production (Park *et al.*, 2011).

Several studies, such as those by Zolekar and Bhagat (2015), Pramanik (2016), Hassan *et al.* (2020), Tiwari and Ajmera (2020), Roy *et al.* (2022), Sengupta *et al.* (2022), and Anusha *et al.* (2023) have applied GIS-based Multi-Criteria Decision-Making (MCDM) approaches to assess agricultural land suitability across various regions in India. For instance, Pramanik

(2016) utilized AHP and GIS for land suitability analysis in Darjeeling; however, the study relied heavily on expert opinions, potentially introducing subjective bias in parameter weighting. It also failed to consider dynamic environmental changes and excluded critical socio-economic factors such as market access and infrastructure. Similarly, Zolekar and Bhagat (2015) assessed agricultural land suitability in the hilly regions of the Mula and Pravara basins in the Western Ghats, while Tiwari and Ajmera (2020) also depended primarily on static datasets and expert judgment without incorporating ground-truth validation or stakeholder engagement. Roy *et al.* (2022) focused on land suitability for rain-fed cultivation, and Anusha *et al.* (2023) examined semi-arid regions in Andhra Pradesh; however, both studies lacked consideration of future climate change scenarios and temporal variability in drought patterns. These limitations highlight a clear research gap, that in future approaches like land use dynamics, data-driven, and empirically validated studies for agricultural land suitability analysis may be taken-up and in view of this, our work is framed on dynamics of land use variations based on data-driven attempts associated with empirically validated field investigations to find out the agricultural suitability sites in future.

In this research, analysis of the appropriateness of agricultural land has been conducted using the Analytical Hierarchy process (AHP) (Saaty, 1980) approach combined with GIS application settings. The AHP method was utilized in multiple case studies worldwide to evaluate the appropriateness of agricultural land (Bozdağ *et al.* 2016; Pramanik, 2016; Yalew *et al.*, 2016; Hassan *et al.*, 2020). In the present study, the agricultural potential of Uttar Dinajpur District has been evaluated using a weighted overlay method, grounded in the Multi-Influencing Factor (MIF) framework. This approach effectively identifies and integrates the key factors influencing agricultural suitability (Roy *et al.*, 2022).

To carry out the land suitability analysis, a MCDM technique was employed. This model incorporates multiple parameters, including soil characteristics (i.e. pH, texture, moisture content, and organic carbon), climatic elements (i.e. temperature and precipitation), topographical features (i.e. elevation and slope), LULC, and accessibility factors i.e. proximity to rivers, roads, and markets (Ahmed *et al.*, 2016). The primary goal of this study was to delineate areas suitable for agriculture to ensure that future generations can meet their basic needs. Given that a significant proportion of the rural population in the study region relies heavily on agriculture as their principal livelihood, the study also aims to propose strategies to enhance economic conditions and promote sustainable agricultural development in Uttar Dinajpur District.

Geographical account of the study area:

The district spans across a land area of 3142 km² and it is situated between the latitudes of 25°17'10" N to 26°35'15" N and longitudes of 87°48'37" E to 88°33'10" E, bounded on the east by Bangladesh, the west by Bihar, the north by Darjeeling & Jalpaiguri districts, and the south by Malda District (Figure 1). The study area in general is flat and sloping slightly gentle towards the South. The area has been divided into two smaller sub-micro regions: (a) Islampur-Goalpokhar Plain and (b) Sudhani-Mahananda-Gamari Plain (Bose *et al.*, 2020).

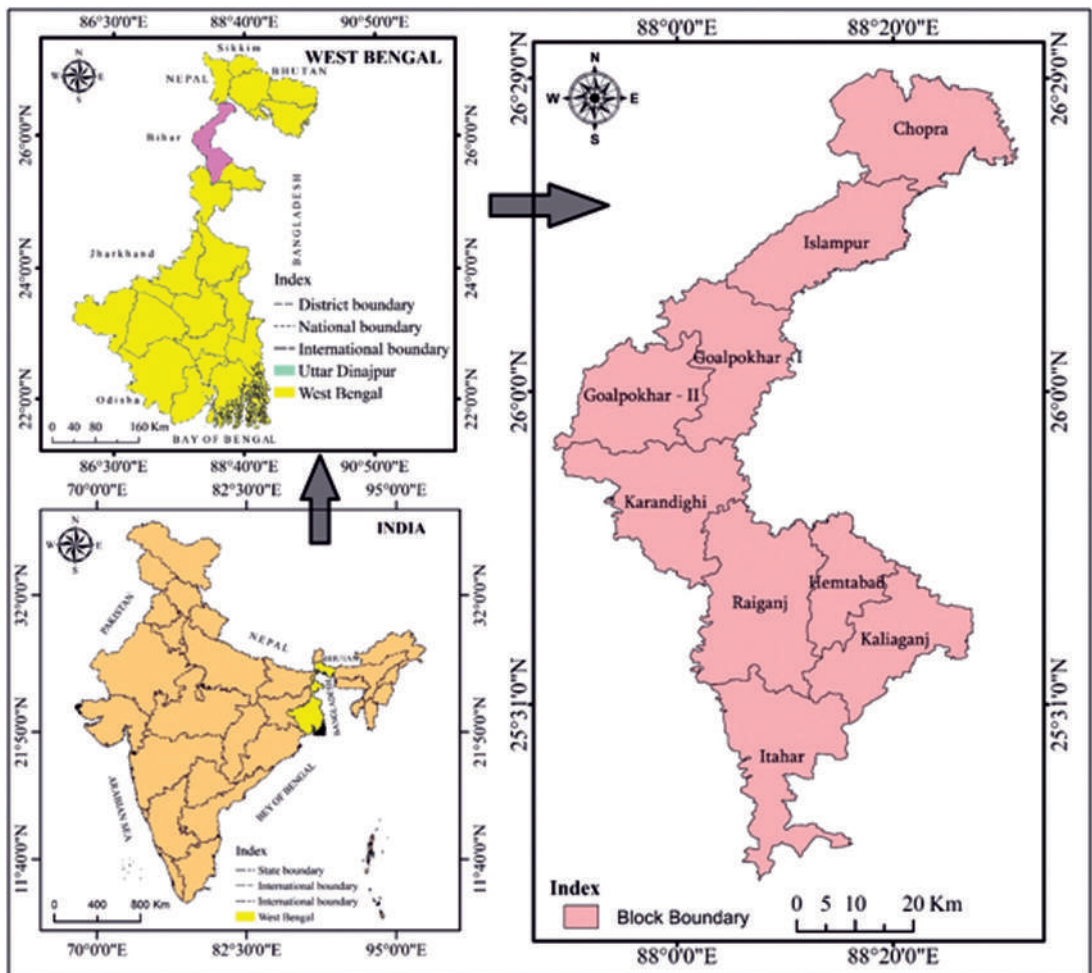


Figure 1. Locational identity of Uttar Dinajpur District in West Bengal.

Older and newer alluvium is the two categories into which the district's soil falls. Old alluvium can have a clay loam or stiff clay texture. Deep, neutral to slightly acidic soil characterizes the area (Sarkar, 2021). Rivers typically flow through direction because the district is generally flat along with a slightly gentle slope from north to south. The predominant rivers of the study area are Kulik, Nagar, Mahananda, Gamari, and Tangan. Despite being located north of the Tropic of Cancer, it is not as hot and humid. The Himalayan range keeps the area comfortable and cool.

In Uttar Dinajpur district, forest is primarily covered with mixed tropical northern deciduous vegetation. Forests are scattered erratically and primarily in small areas. With the exception of a small patch in Rajabhum-mouza in Chopra C.D. Block, most of the natural forests in the area are association of sal trees and are either seedlings or natural forests. Near

the Raiganj Bird Sanctuary, a significant portion of the forest is grown up around the bank of the river Kulik. The Raiganj (Kulik) Bird Sanctuary covers an area of approximately 1.5 km². Currently, 16 of these woods cover a total of about 600 hectares in the district. The Barind tract, a southern extension of an ancient alluvium geological formation, covers the region. The soils are recently formed, shallow, gravel- and sand-loam-rich alluvial soils that are black and brown in colour (Sarkar, 2021). Jute and paddy are commonly cultivated in lowland areas (Ghosh, 2024). A substantial tea plantation and numerous small and large tea gardens are found in the areas of Chopra, Islampur, and Goalpokhar-I C.D. blocks (Ghosh, 2024). The majority of Uttar Dinajpur's landscapes are plain. The monsoon has a significant impact on crop production. This region is susceptible to floods, which occurs nearly every year. On the other hand, when a drought occurs, the farmers start to squeal uncontrollably for water. Paddy, jute, pulses, and mustard are the primary crops grown on this land (Ghosh, 2024). The district's primary cash crop is jute. In the last few years, there has been a declining trend in the use of land for crop production (Sarkar, 2021; Ghosh, 2024). Furthermore, it has been observed that the district's tea plantations are expanding quickly, which may have a significant impact on future agricultural fields.

Database and Methodology:

Data sources:

The Uttar Dinajpur district's prospective agricultural site suitability was established using a variety of factors in order to find likely and appropriate locations for crop production. Different constraints and criteria were selected considering significance of them and their value in agricultural production. These elements were chosen based on extensive literature review and expert opinions. Twelve parameters were chosen that influence the agricultural site suitability analysis. These are soil properties namely soil reaction (i.e. pH), texture, moisture content, organic carbon; topographic factors i.e. locational elevation and slope; Climatic factors i.e. temperature conditions and rainfall occurrences; LULC, and few accessibility factors which includes proximity from river, proximity from road, and proximity from market in a distance dimension. Details about the required data sources were amalgamated in table 1.

Preparation of thematic layers:

To identify the agricultural land suitability sites in Uttar Dinajpur district, twelve thematic layers were selected of some soil physico-chemical characteristics (i.e. texture, reaction or pH, organic carbon, NDWI, site elevation, surface slope, LULC, Rainfall, temperature, proximity from river, proximity from road, and proximity from market. For the purpose of determining the final agricultural land suitability output, each of these layers has undergone preparation and processing under the GIS and Remote Sensing (RS) environments with their analytics (ArcMap 10.8 and Q-GIS 2.18), based on the knowledge from detailed literature review, field investigations and by sharing knowledge from local farmers. The selected theme layers were rasterized and then projected onto the UTM Projection, WGS 84 Datum, and 45-N zone. The

SRTM-DEM acquired from the USGS Earth Explorer was processed to create average slope and elevation data. The DEM was pre-processed using sink-filling in GIS (ArcMap 10.8). Finally, a grid of 1 km² was developed to deliver a map of the average slope (Figure 2).

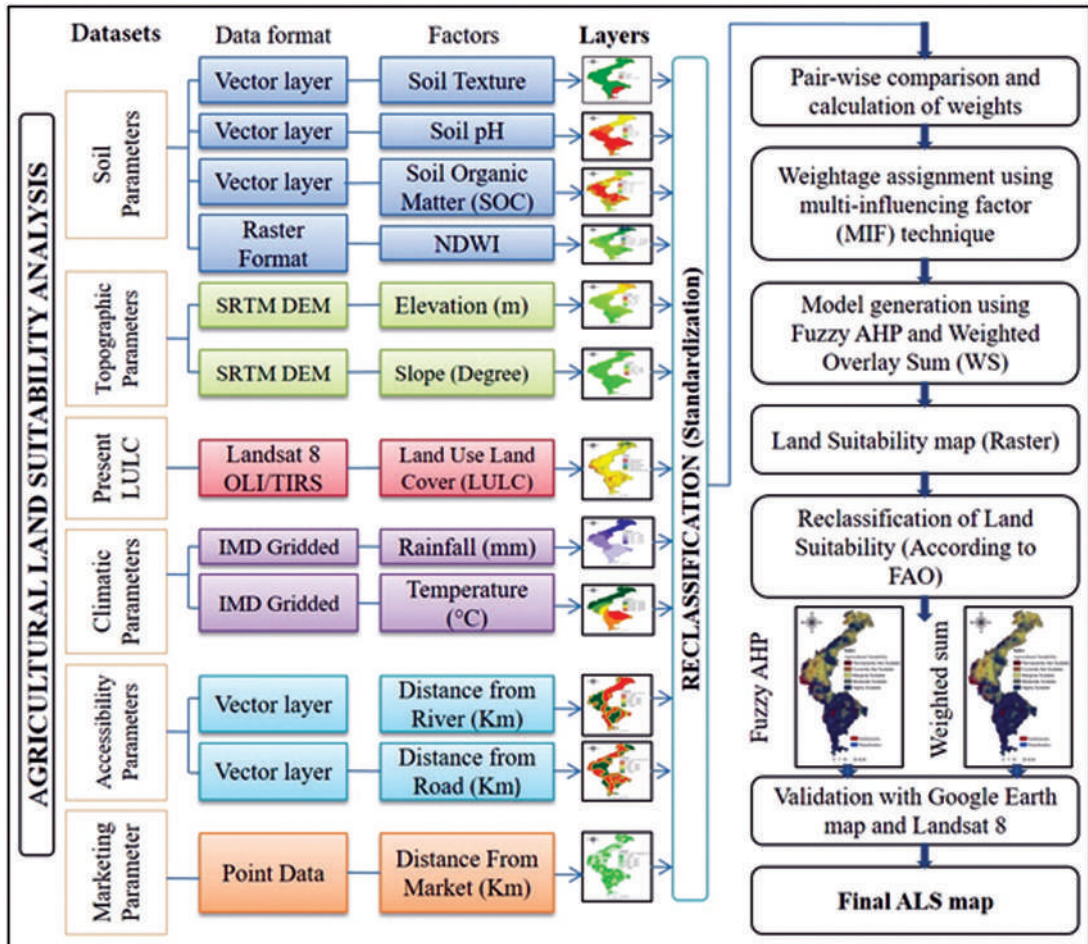


Figure 2. Methodological flowchart for determining the appropriateness of agricultural land use.

For the construction of LULC layers, the Landsat 8 OLI satellite imageries (30×30 m) were incorporated. The Landsat images (Row-42 and Path-139), which were initially a mosaic, underwent pre-processing i.e. atmospheric correction, spectral radiance scaling to convert each band's DN's value to the ToA radiance, and then techniques for band composition, edge enhancement, and ToA reflectance. Using supervised classification and a maximum likelihood technique, the final LULC map has been generated. It had five classes: settlements, sandbars, vegetation cover, water bodies, and agricultural land. NDWI was also created using the Landsat 8 dataset. In this case, modified NDWI technique was incorporated.

Table 1. Details about required data set using in agriculture land suitability assessment

Sl. No.	Major Factors	Sub-Factors	Data types	Details information	Sources
1	Soil parameters	Soil texture	Vector layer	FAO, UN, Version 3.6	https://www.fao.org/soils-portal
2		Soil pH	Vector layer		https://www.fao.org/soils-portal
3		Soil organic carbon	Vector layer	Satellite data - LISS-II sensors aboard IRS-1A / 1B/ 1C R.F. of soil maps - 1:250,000 and 1:50,000	https://bhuvan-app3.nrsc.gov.in/data/download
4		NDWI	Landsat 8 OLI/TIRS	USGS, Resolution-30 m × 30-m, Path-139, Row-042, date of Acquisition- 2022/10/20	https://earthexplorer.usgs.gov
5	Topographic parameters	Elevation	SRTM DEM	Resolution-1-ARC, date of publication-2014-09-23, SRTM1N25E088V3, SRTM1N26E088V3, SRTM1N25E087V3, SRTM1N26E087V3	https://earthexplorer.usgs.gov
6		Slope	SRTM DEM	Resolution-1-ARC, date of publication-2014-09-23, SRTM1N25E088V3, SRTM1N26E088V3, SRTM1N25E087V3, SRTM1N26E087V3	https://earthexplorer.usgs.gov
7	Present LULC	LULC	Landsat 8 OLI/TIRS	USGS, Resolution - 30 × 30 m, Path-139, Row-042, date of Acquisition- 2022/10/20	https://earthexplorer.usgs.gov
8	Climatic parameters	Rainfall	Point data	IMD (0.25° × 0.25°)	https://www.imdpune.gov.in/cmpg/Griddata/Rainfall_25_NetCDF.html
9		Temperature	Gridded data, 0.5° × 0.5°	CRU TS v. 4.04, 2011–19	https://crudata.uea.ac.uk/cru/data/hrg/cru_ts_4.04/
10	Accessibility parameters	Distance from River (DRi)	Vector layer	GSI, 2024	https://bhukosh.gsi.gov.in/Bhukosh/Public
11		Distance from Road (DRo)	Vector layer		
12	Marketing parameter	Distance from Market (DMa)	Point data	Google Earth, 2022 (The Directorate of Agricultural Marketing GoWB)	http://wbagrmarketingboard.gov.in

From the website of the GSI, information regarding DRi and DRo has been collected, while the data for distance from market (DMa) was obtained from the Geocoded version of

the Google Earth Pro application (2022). The layer is visible in the vector format; it underwent initial pre-processing in the GIS platform before being transformed into a raster data structure (dimension: 30×30 m.).

Soil maps including soil pH, texture, and organic carbon were obtained from the FAO and processed using a GIS platform (ArcMap 10.8 v.). Rainfall and temperature are the two important influencing factors in agriculture. Information about these two parameters was collected from IMD Pune gridded data sets which is available as a binary format. According to various studies (Kumar *et al.*, 2020; Ly *et al.*, 2013), the Kriging interpolation method is considered as a dependable and precise for spatial mapping of rainfall, temperature, soil pH, texture, and organic carbon. Once all selected thematic layers were digitized and redesigned into a raster data structure, reclassification was performed. However, the information was obtained from the Bhukosh website operated by the GSI in order to create a map illustrating the distance to the river. This specific layer was gathered in a vector format within a GIS system and later transformed into a raster layer. In the next step, the distance to major roads was determined by obtaining data from the OSM server. The distance from the market was obtained from the Market Survey report, specifically the Agricultural market directory, and processed as a thematic layer using ArcGIS software with Euclidean distance calculations, resulting in a raster format.

MCDM model building:

Fuzzy AHP:

Assessing agriculture land suitability entails employing a multi-criterion decision-making (MCDM) approach with a hierarchical construct or structure utilizing the AHP algorithm. This process involves categorizing land suitability, selecting the most significant variables, determining their weights, and developing a GIS-based Fuzzy model to generate a map illustrating land suitability (Zadeh's 1965). To simulate human knowledge and experience, fuzzy logic is employed (Cengiz and Akbulak, 2009). Fuzzy AHP uses fuzzy numbers, and that are more suitable when judgments are imprecise. It allows decision-makers to express uncertainty more effectively than traditional crisp values. By accounting for imprecision, Fuzzy AHP produces more robust results. These results are also less sensitive to small inconsistencies in the judgment matrix. Therefore, in this study, Fuzzy logic-based AHP has been applied. This method is particularly useful in agricultural land suitability analysis. It effectively manages the uncertainty and imprecision present in soil, climate, and expert judgment data. Unlike traditional AHP or crisp MCDM methods, Fuzzy AHP handles both qualitative and quantitative criteria. This leads to more realistic and flexible decision-making outcomes. Its hierarchical structure supports the systematic evaluation of complex land factors. As a result, it is well-suited for spatial and multi-criteria agricultural assessments. Overall, Fuzzy AHP improves the reliability and accuracy of land suitability classification when compared to non-fuzzy approaches i.e. traditional AHP, TOPSIS, VIKOR, simple additive weighting (SAW) etc.

Here, the opinions of experience local resident's and literature were contemplated for defining the weight of variables for determining the appropriateness of the land. The weights of the components selected to create multi-criteria decision-making analysis data ranged

from 0 to 1 (Malczewski, 1999). Using Saaty's critical scale ((1980), the agro-ecological and environmental factors were rated 1 to 9 for pair-wise comparison. During this step, a square pair-wise comparison matrix with all of its entries compared to each other was created (Saaty, 1994). The n-factor pair-wise comparison matrix A is defined as follows:

$$A = [a_{ij}] = \begin{bmatrix} a_{11} & a_{12} & \dots & \dots & a_{1n} \\ a_{21} & a_{22} & \dots & \dots & a_{2n} \\ \vdots & \vdots & \dots & \dots & \vdots \\ \vdots & \vdots & \dots & \dots & \vdots \\ a_{n1} & a_{n2} & \dots & \dots & a_{nn} \end{bmatrix} \quad (1)$$

If A is the matrix with a_{ij} elements, i and j are environmental factors and agro-ecological aspects, respectively. Formally, this matrix may be expressed likewise:

$$a_{ij} = 1/a_{ji} \quad (2)$$

Subsequently, creating pairwise factor comparison matrices, the vector of weights, $w = [w_1, w_2, w_3 \dots w_n]$, was produced by applying Saaty's eigenvector method.

Eq. (3) may be used to represent the land suitability evaluation performed making use of the GIS based Fuzzy-AHP. Additionally, determined were the classes of the weighted linear additive combination technique and the LS evaluation.

$$s = \sum_{i=1}^n W_i X_i \quad (3)$$

S stands for the LS classes, which are highly suitable, moderately suitable, marginal suitable, and not suitable. It also stands for the assessment index with a valuable element for the suitability class and the decision rule (Zhang *et al.* 2013). The W_i , X_i , and n represent the weight of factors (such as topography, climate, and soil data), the sub-factor score of i components, and the total number of contributing elements.

Finally, the MCDM analysis combined with the Fuzzy AHP method was utilized to generate an agricultural ALS map (refer to Tables 2, 3, 4, and 5). The GIS model builder incorporated the LS evaluation by applying the respective weights of different factors (Table 6). To develop the agricultural suitability map for Uttar Dinajpur District, the ArcGIS platform integrated the suitability levels of multiple thematic layers, governed by twelve key parameters.

Weighted Sum (WS):

The WS method (Mateo, 2012) is a simple method that is commonly employed in single-dimensional situations. Here also, one popular method known as weighted sum method was employed to assess the status of agricultural land suitability (Table 6). This method provides a simple yet effective way to integrate multiple criteria (i.e. soil properties namely soil reaction (i.e. pH), texture, moisture content, organic carbon; topographic factors i.e. locational elevation and slope; Climatic factors i.e. temperature conditions and rainfall occurrences; LULC, and few accessibility factors which includes proximity from river, proximity from road, and proximity from market in a distance dimension) into a single suitability score. WS

method allows combining multiple heterogeneous criteria into one composite index, making it easier to evaluate and compare different land parcels which suits to our study most because we had twelve numbers of criteria which was big in size. Each criterion is assigned a weight based on its importance and field based realistic information to eliminate judgemental bias. The weighted values are summed to calculate the final suitability score. Hence accepting the WS method was inevitable under such circumstances. Here, MCDM-weighted sum was calculated using the following equation (Eq. 4).

$$A_{*wsm} = \text{Max } k \sum_i^j a_{ij} w_j \quad (4)$$

In the case where $i = 1, 2, m$ and A_{*wsm} is the WS method score of the best alternative, n is the number of choice criteria, a_{ij} is the actual value of the i th alternative in terms of the j th criteria, and w_j is the weight of importance of the j th criteria... The sum of goods equals the entire value of each choice. When applied for the multi-dimensional decision-making issues, this method's difficulties also merged out.

Table 2. Pair-wise framework of Comparison Matrix for explaining Fuzzy AHP

Factors	LULC	Soil Texture	Soil pH	SOC	NDWI	Slope	Rainfall (mm)	Distance from River	Distance from Road	Distance from Market	Temperature	Elevation
LULC	1	1	2	2	2	2	1	1	1	2	2	2
Soil Texture	1	1	1	1	2	2	2	1	1	2	2	2
Soil pH	1/2	1	1	2	1	2	1	2	3	1	2	2
SOC	1/2	1	1/2	1	1	2	2	2	1	1	2	2
NDWI	1/2	1/2	1	1	1	1	2	1	1	2	2	2
Slope	1/2	1/2	1/2	1/2	1	1	1	2	2	2	2	2
Rainfall (mm)	1	1/2	1	1/2	1/2	1	1	1	2	2	1	2
DRi	1	1	1/2	1/2	1	1/2	1	1	2	2	1	1
DRo	1	1	1/3	1	1	1/2	1/2	1	1	1	2	2
DMA	1/2	1/2	1	1	1/2	1/2	1/2	1/2	1	1	1	2
Temperature	1/2	1/2	1/2	1/2	1/2	1/2	1	1	1/2	1	1	1
Elevation	1/2	1/2	1/2	1/2	1/2	1/2	1/2	1	1/2	1/2	1	1
Sum	9.00	10.00	10.83	13.50	13.00	15.50	14.50	16.00	19.00	18.50	21.00	23.00

Table 3. Calculating Consistency for Fuzzy AHP

Factors	LULC	Soil Texture	Soil pH	SOC	NDWI	Slope	Rainfall (mm)	Distance from River	Distance from Road	Distance from Market	Temperature	Elevation	Weighted sum value	Criteria Weight	MSV/CW
LULC	0.1205	0.1117	0.2069	0.1784	0.1762	0.1672	0.0770	0.0804	0.0749	0.1192	0.1034	0.0922	1.5081	0.1205	12.51
Soil Texture	0.1205	0.1117	0.1035	0.0892	0.1762	0.1672	0.1540	0.0804	0.0749	0.1192	0.1034	0.0922	1.3924	0.1117	12.47
Soil pH	0.0603	0.1117	0.1035	0.1784	0.0881	0.1672	0.0770	0.1607	0.2248	0.0596	0.1034	0.0922	1.4269	0.1035	13.79
SOC	0.0603	0.1117	0.0517	0.0892	0.0881	0.1672	0.1540	0.1607	0.0749	0.0596	0.1034	0.0922	1.2131	0.0892	13.60
NDWI	0.0603	0.0558	0.1035	0.0892	0.0881	0.0836	0.1540	0.0804	0.0749	0.1192	0.1034	0.0922	1.1046	0.0881	12.54
Slope	0.0603	0.0558	0.0517	0.0446	0.0881	0.0836	0.0770	0.1607	0.1499	0.1192	0.1034	0.0922	1.0866	0.0836	13.00
Rainfall (mm)	0.1205	0.0558	0.1035	0.0446	0.0441	0.0836	0.0770	0.0804	0.1499	0.1192	0.0517	0.0922	1.0225	0.0770	13.28
DRi	0.1205	0.1117	0.0517	0.0446	0.0881	0.0418	0.0770	0.0804	0.1499	0.1192	0.0517	0.0461	0.9828	0.0804	12.23
DRo	0.1205	0.1117	0.0345	0.0892	0.0881	0.0418	0.0385	0.0402	0.0749	0.0596	0.1034	0.0922	0.8947	0.0749	11.94
DMa	0.0603	0.0558	0.1035	0.0892	0.0441	0.0418	0.0385	0.0402	0.0749	0.0596	0.0517	0.0922	0.7518	0.0596	12.61
Temperature	0.0603	0.0558	0.0517	0.0446	0.0441	0.0418	0.0770	0.0804	0.0375	0.0596	0.0517	0.0461	0.6505	0.0517	12.59
Elevation	0.0603	0.0558	0.0517	0.0446	0.0441	0.0418	0.0385	0.0804	0.0375	0.0298	0.0517	0.0461	0.5822	0.0461	12.63
														$\frac{L_{max}}{n}$	12.76

Table 4. Pair-wise Normalized Comparison Matrix for preparation of Fuzzy AHP

Fac-tors	LULC	Soil Texture	Soil pH	SOC	NDWI	Slope	Rainfall (mm)	Distance from River	Distance from Road	Distance from Market	Temperature	Elevation	Sum	Criteria Weights	Criteria weight (%)
LULC	0.1111	0.1000	0.1846	0.1481	0.1538	0.1538	0.0690	0.0625	0.0526	0.1081	0.0952	0.0870	1.3260	0.12	12.054
Soil Texture	0.1111	0.1000	0.0923	0.0741	0.1538	0.1538	0.1379	0.0625	0.0526	0.1081	0.0952	0.0870	1.2286	0.11	11.169
Soil pH	0.0556	0.1000	0.0923	0.1481	0.0769	0.0769	0.0690	0.1250	0.1579	0.0541	0.0952	0.0870	1.1380	0.10	10.345
SOC	0.0556	0.1000	0.0462	0.0741	0.0769	0.0769	0.1379	0.1250	0.0526	0.0541	0.0952	0.0870	0.9814	0.09	8.922
NDWI	0.0556	0.0500	0.0923	0.0741	0.0769	0.0769	0.1379	0.0625	0.0526	0.1081	0.0952	0.0870	0.9691	0.09	8.810
Slope	0.0556	0.0500	0.0462	0.0370	0.0769	0.0645	0.0690	0.1250	0.1053	0.1081	0.0952	0.0870	0.9197	0.08	8.361
Rainfall (mm)	0.1111	0.0500	0.0923	0.0370	0.0385	0.0385	0.0690	0.0625	0.1053	0.1081	0.0476	0.0870	0.8468	0.08	7.698

Fac-tors	LULC	Soil Texture	Soil pH	SOC	NDWI	Slope	Rainfall (mm)	Distance from River	Distance from Road	Distance from Market	Temperature	Elevation	Sum	Criteria Weights	Criteria weight (%)
DRi	0.1111	0.1000	0.0462	0.0370	0.0769	0.0769	0.0690	0.0625	0.1053	0.1081	0.0476	0.0435	0.8841	0.08	8.037
DRo	0.1111	0.1000	0.0308	0.0741	0.0769	0.0769	0.0345	0.0313	0.0526	0.0541	0.0952	0.0870	0.8244	0.07	7.495
DMa	0.0556	0.0500	0.0923	0.0741	0.0385	0.0385	0.0345	0.0313	0.0526	0.0541	0.0476	0.0870	0.6559	0.06	5.962
Tem-pera-ture	0.0556	0.0500	0.0462	0.0370	0.0385	0.0385	0.0690	0.0625	0.0263	0.0541	0.0476	0.0435	0.5686	0.05	5.169
Eleva-tion	0.0556	0.0500	0.0462	0.0370	0.0385	0.0385	0.0345	0.0625	0.0263	0.0270	0.0476	0.0435	0.5071	0.05	4.610
													11	0.99	98.6330

Table 5. Calculated CI and CR value for accepting the weightage for MCDM modeling

L.max (λ_{max} .)	12.76
Total number of parameters (n)	12
Consistency Index (CI) = $(\lambda_{max} - n)/(n - 1)$	0.07
Random Index (RI)	1.48
Consistency ratio (CR) = CI/RI	0.05 (Valid pair-wise comparison matrix; according to Saaty 0.10 indicates maximum limit of acceptance)

Table 6. Multi criteria weighted factor for agricultural suitability identification for Fuzzy AHP

Criterion	Sub-criteria	Weight*	Influence of criteria (%)
LULC	Agriculture land	10	12
	Vegetation	8	
	settlements	6	
	sand bars	4	
	water bodies	0	
Soil texture	Loam	10	11
	sandy loam	5	
Soil pH	<4	3	10
	4 – 5	5	
	5 – 6	7	
	6 – 7	9	

Criterion	Sub-criteria	Weight*	Influence of criteria (%)
SOC (g/kg)	43 – 67	9	9
	37 – 43	7	
	30 – 37	5	
	23 – 30	3	
NDWI	– 0.4621 – –0.2757	9	9
	– 0.2757 – – 0.2274	7	
	–0.2274 – –0.1511	5	
	–0.1511 – 0.0000	3	
	0.0000 – 0.0671	1	
Slope (degree)	0 – 2.0	10	8
	2.01 – 3.59	8	
	3.59 – 5.32	6	
	5.31 – 7.76	4	
	>7.76	2	
Rainfall (mm)	2774 – 3193	9	8
	2357 – 2774	7	
	1939 – 2356	5	
	1521 – 1938	4	
	1101 – 1520	2	
DRi (m)	<1000	9	8
	1000 – 2000	7	
	2000 – 3000	5	
	3000 – 4000	4	
	> 4000	3	
DRo (m)	<1000	9	7
	1000 – 2000	7	
	2000 – 3000	5	
	3000 – 4000	4	
	> 4000	2	
DMa (m)	<1000	9	6
	1000 – 2000	8	
	2000 – 3000	7	
	3000 – 4000	6	
	> 4000	5	

Criterion	Sub-criteria	Weight*	Influence of criteria (%)
Temperature (°C)	24.64 – 24.94	8	5
	24.95 – 25.25	7	
	25.25 – 25.55	6	
	25.56 – 25.86	5	
	25.86 – 26.17	4	
Elevation (m)	< 20	10	5
	20 – 40	9	
	40 – 60	8	
	60 – 80	7	
	80 – 100	6	
	> 100	5	

* For Weighted Overlay Sum (WOS) # For Fuzzy AHP

Result & Discussion:

Factors affecting the land suitability:

Soil texture:

Soil texture is determined by the relative proportions of three primary particles: sand, silt, and clay, reflecting its complex composition (FAO, 1976). The texture of the soil has a direct impact on factors such as nutrient availability, particularly N, P, and K, as well as on soil thickness, water retention capacity, and moisture content (Mojid *et al.*, 2009; Roy *et al.*, 2022). In addition, soil texture influences a number of other variables, including agricultural inputs, cropping pattern, irrigation strategies, proper management of soil, and manure use (Dar *et al.*, 2012). In this pursuing study two textural classes have been found: Loamy soil (91.1%) and sandy loam soil (8.99%) (Figure 3a). Noteworthy, the loam textural type of soil has a greater influence in determining the agricultural land suitability sites (W-10). For instance, Loam soil is made up of a healthy mix of minerals, rock, sand, silt water, and organic materials. Microorganisms, insects, and worms in the soil replenish soil fertility. It is the healthiest form of soil due to its excellent composition that's why loam soils are ideal for plant growth.

Soil pH:

The pH of the soil is essential for microbial activity, nutrient availability, and overall crop growth (Mustafa *et al.*, 2011; Yalew *et al.*, 2016). Because of this, it is often known as the 'master soil variable,' as it affects numerous physico-chemical characteristics of the soil that are essential for plant development and agricultural productivity (Zhang *et al.*, 2019). A pH value below 7 indicates an acidic condition, whereas a value above 7 denotes alkalinity. However, for the majority of crops, pH levels between 5.5 and 7.0 are appropriate (Halder, 2013; Slessarev *et al.*, 2016). Within the current field of research, the pH of soil ranges from

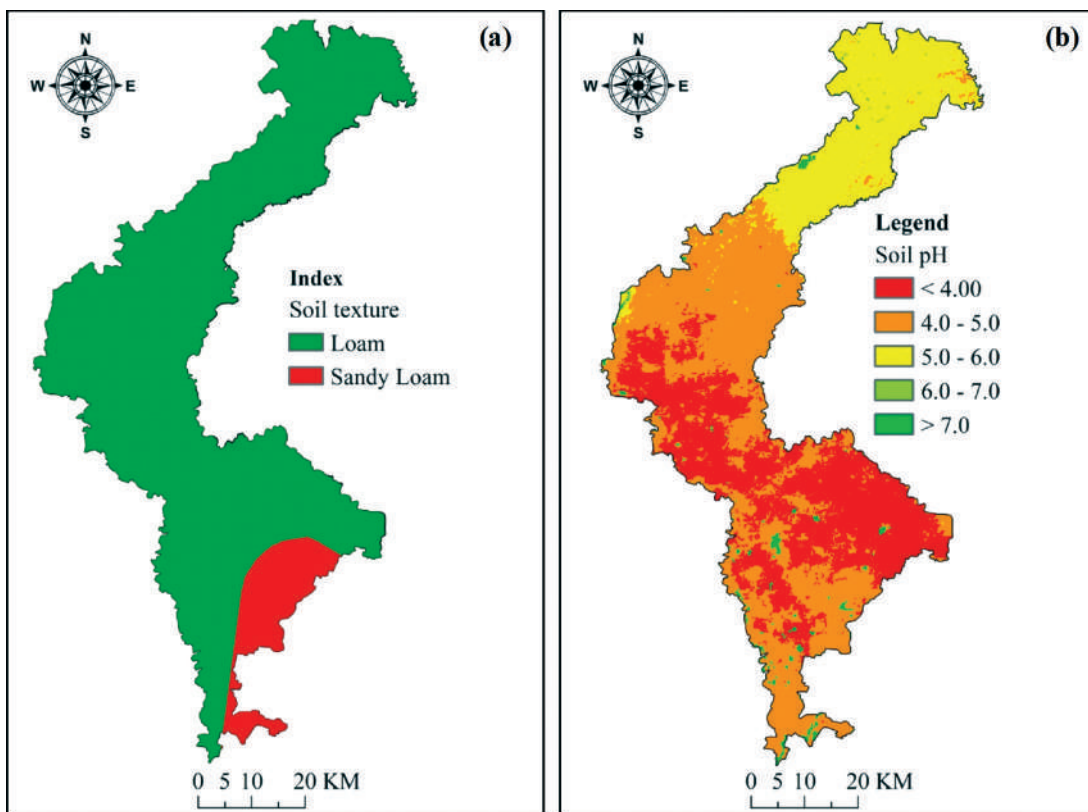


Figure 3. Potential agricultural land suitability indicators (a) Soil texture (b) Soil pH.

4 to 7 (Figure 3b). The spatial variation of pH value is showing that 31.68% of total land demarcated by pH range 4 (strongly acidic), 43.90% of land area demarcated by pH range 4-5 (moderately acidic), and 22.70% of land area demarcated by pH range 5-6 (Acidic). Noteworthy, highest weightage was assigned for the 6 to 7 pH class because bacterial activity is particularly best affected by this soil pH class which releases huge amounts of nitrogen and this can produce a more fertile field for agricultural production.

Organic Carbon (OC):

OC serves as a vital nutrient source and plays a key role in enhancing soil fertility, improving water retention, and supporting effective nutrient management essential for plant growth (Bandyopadhyay *et al.*, 2009). The decline of OC has a considerable impact on agricultural productivity and vegetation, particularly in lowland regions where soil erosion is a major contributing factor (Bhagat, 2013; Orhan, 2021). Soil organic carbon fosters a variety of soil activities that influence the physicochemical and biological quality of soil (Barah, 2010; Zolekar and Bhagat, 2015).

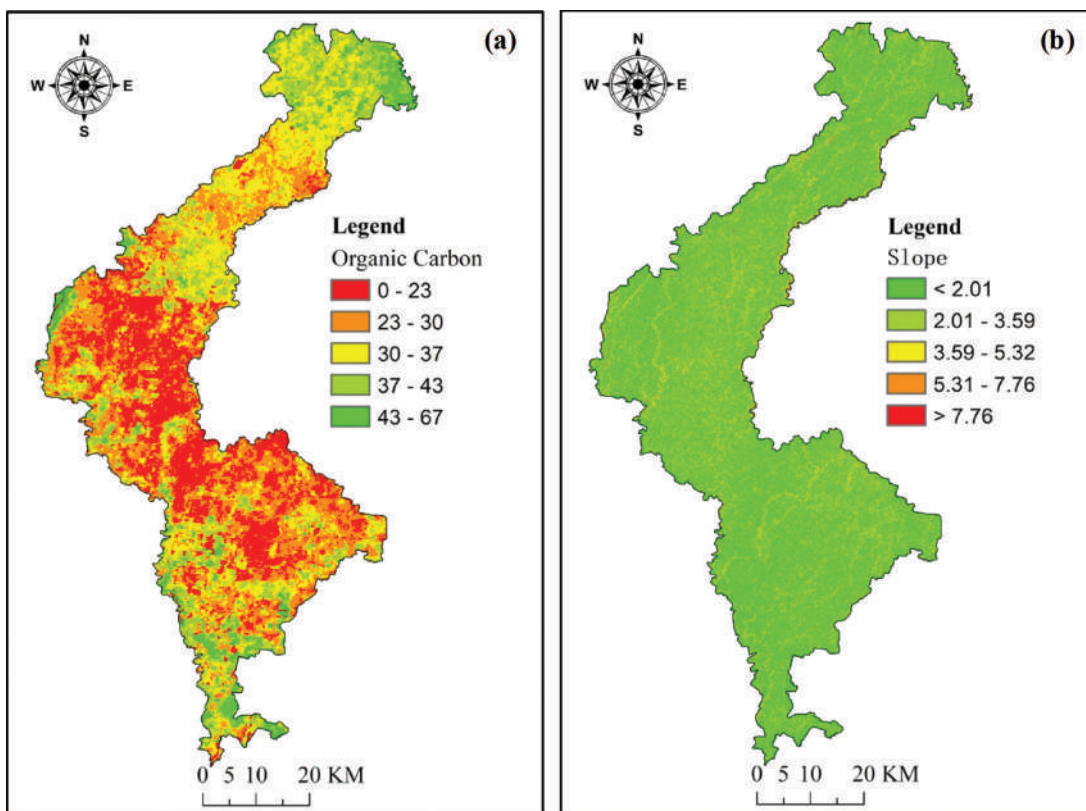


Figure 4. Potential agricultural land suitability indicators (a) Soil Organic carbon (b) Surface Slope.

In this study the concentration of organic carbon has been categorised into five classes (Figure 4a). However, 55.63% of land area having 0-3% of organic carbon concentration which are found most of the part of the study area, 39.19% of lands are having 3-3.4% of organic carbon and only 5.17% of land contains 4.3-6.7% of organic carbon. Highest amount of OC has been found in the northern most part of the Uttar Dinajpur District bounding areal coverage of the Chopra block and southernmost partial areas of the Itahar block because of the presence of clay content which is more in these regions. Best on priority, from standard practical point of view the 43-67 category of SOC class has a higher value of weightage ($W = 9$) in determining the agricultural site suitability zones. The spatial distribution of SOC in Uttar Dinajpur district has shown in Figure 4a.

Average Slope:

The study of surface slope is beneficial in determining ideal sites for a wide range of activities, like flood mitigation, forest conservation, and agricultural production (Bandyopadhyay *et al.*, 2009; Bhagat, 2009). The distribution of soil properties, including soil depth, moisture content,

texture, and nutrient availability, is influenced by slope conditions (Zolekar *et al.*, 2015). In areas characterized by gentle slopes at the base of hills and foothills, deep soils tend to be present. However, steep slopes are associated with thin soils and higher levels of degradation. Both the variety of soils and environmental elements has a high influence on the soil nutrients and available minerals present in the soil. The research area is categorized into five slope classes, with the maximum area of the lands in the District of Uttar Dinajpur showing slope dominantly with a value of $<2.1^\circ$ though very few areas with more than 7.76° (Figure 4b). Conversely, 50.98% of land area having the gentle slope ($<2.1^\circ$), and 39.74% of land having the slope of 2.1° - 3.59° while, 7.67% of land areas are having the slope of 3.59° - 5.32° . 1.19% of lands are having the slope of 5.32° - 7.76° and rest 0.42% of land areas are having the slope of $>7.76^\circ$ which falls in the northern part of Chopra block in the District. Consequently, regional variations in the depth and slope of the soil strongly affect nutrients, minerals, and agricultural practices (Mandal *et al.*, 2021). The Interesting fact is that average slope vs. agricultural site suitability status which is having an inverse relationship and that's why lower the surface slope class had assigned higher weightage and vice-a-versa (Table 6).

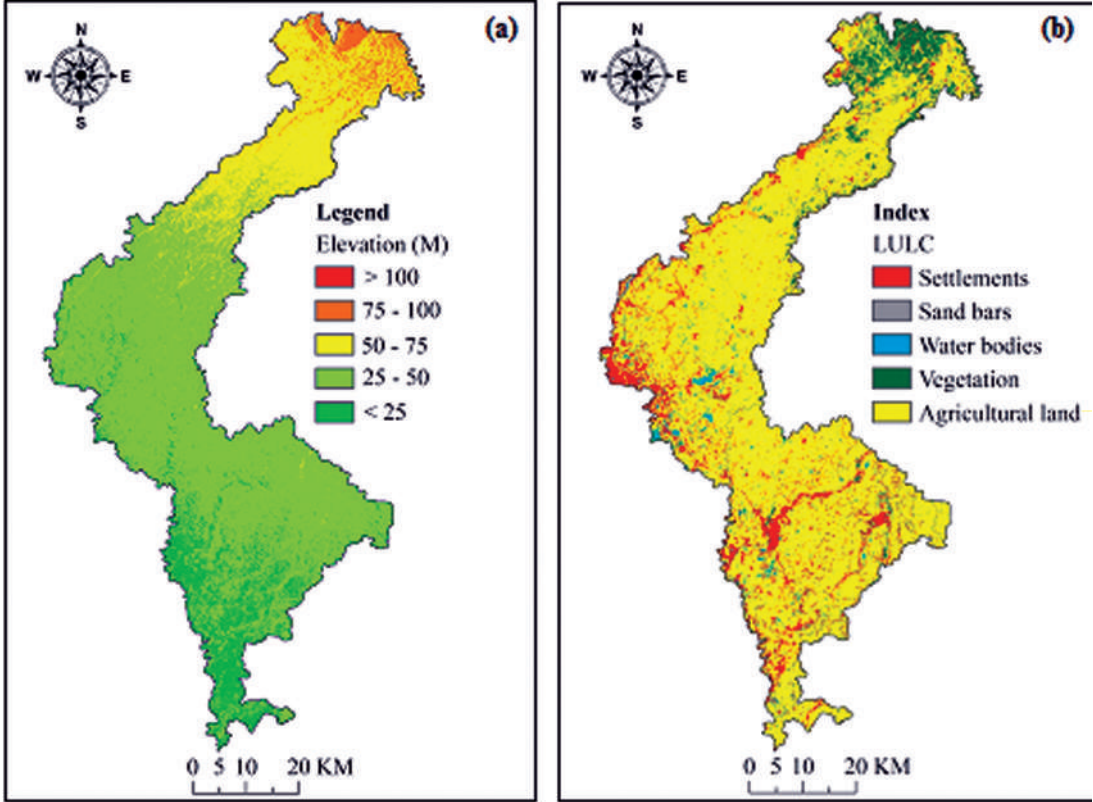


Figure 5. Potential agricultural land suitability indicators (a) Elevation (b) LULC.

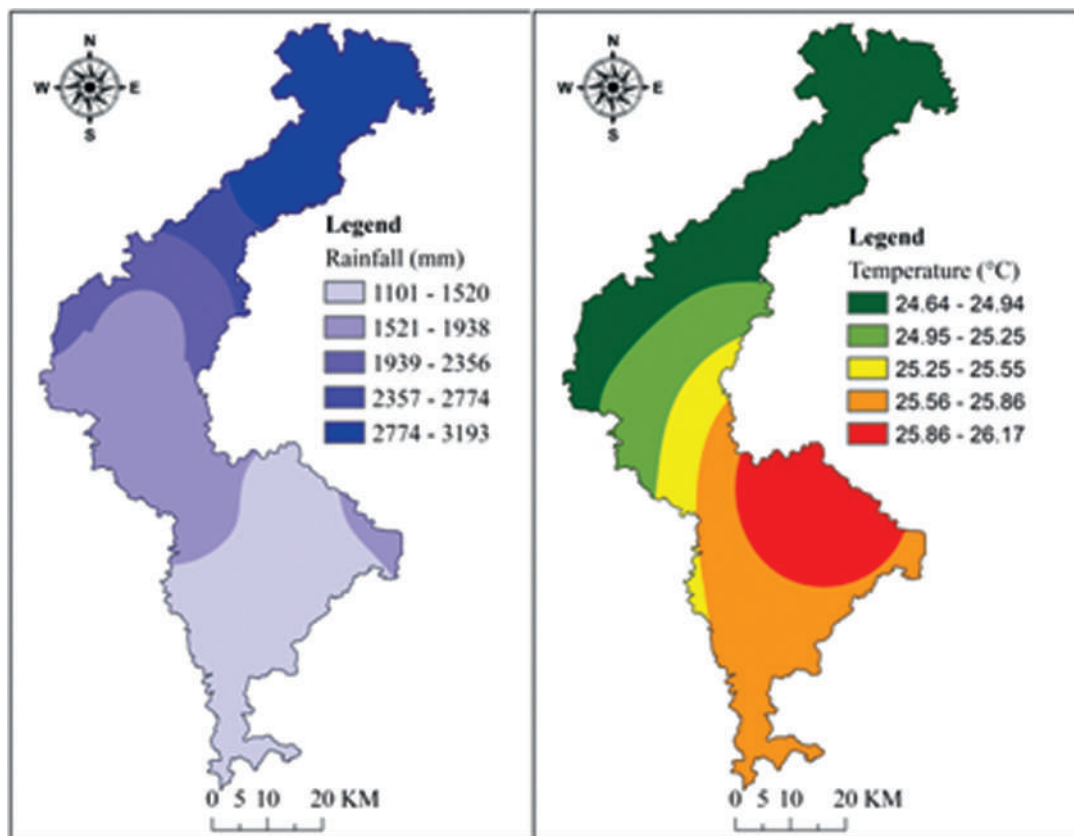


Figure 6. Potential agricultural land suitability indicators (a) Rainfall (b) Temperature.

Elevation:

Elevation plays a major role in agricultural output and variability (Koulouri and Giourga, 2007). Elevation rises from the sea level to the inland, affecting the climatic conditions in addition the morphological and physical changes within the same agronomic traits that influence the crop production (Akinci *et al.*, 2013). However, elevation of Uttar Dinajpur district ranges from averagely minimum of 25 to maximum of 100 m or slightly higher (Figure 5a). Moreover, 3.91% of land area having the elevation of 75-100m., whereas 18.28% land areas are having the elevation of 50-75m., and 69.34% land areas are having the elevation of 25-50m which is found most dominant over the study region. In comparison to the southern regions, the northernmost part of the research area has a higher topography. This region mostly consists of tea gardens because of its undulating topography in the north, whereas its gentle plains in the south offer good opportunities for agricultural development (DCHB, 2011). Here also inverse relationship between topographic elevation and level of suitability of crop lands (Table 6).

Rainfall and Temperature:

Climate factors, such as temperature and rainfall, have a considerable effect on a region's potential to produce agricultural production (Jain *et al.*, 2005). Additionally, these climatic factors have a favourable influence on all areas of land productivity and its outcome, such as crop production, cropping intensity, and growth rate of crops (Iizumi and Ramankutty, 2015). However, among these climatic factors, rainfall and temperature have the greatest effects on the suitability of the land (Jafari and Zeredar, 2010; Rhebergen *et al.*, 2016). The area is not receiving oppressive heat along the foothills of Sub-Himalayas of North Bengal. Close proximity to the Himalayan region, has resulted into coolness and comfortable weather, which is an additional benefit of the weather and climatic situation. The area has a decrease of monsoon rainfall by the end of September, and winter officially begins in mid-November. In the district of Uttar Dinajpur, the majority of the rainfall that falls between June and September ranges between 1101 and 3193 cm. (Figure 6a) and the temperature found ranging between 24°C - 26°C (Figure 6b). The northernmost part received the maximum rainfall because of closeness to the Himalayan Mountain belt. According to weather data, there is a positive correlation between rainfall and crop land suitability in the Uttar Dinajpur district, while a negative correlation was found between temperature and crop field suitability (Table 6).

LULC:

The LULC classification of Uttar Dinajpur district gives knowledge about the current quality and quantity of the land use practices (Bandyopadhyay *et al.*, 2009). LULC must be determined by considering how the earth's topography and biophysical cover are currently used (Pramanik, 2016; Kumar *et al.*, 2021). LULC analysis illustrates the geographical distribution and characteristics of different land types, including agricultural land, orchards, residential areas, forests, fallow land, grasslands, built-up areas, mixed vegetation, barren land, and water bodies. (Rabia *et al.*, 2013; Pramanik, 2016; Ozkan and Turan, 2020). In this study, entire Uttar Dinajpur district has been divided into five classes such as water bodies (4.07%), sandbars (0.22%), vegetation cover (6.56%), agricultural land (78.14%) and settlement area (11%) (Figure 5b). Hence it is clear that most of the land areas found under the agricultural use. Paddy, jute, legumes, and mustard are the primary crops grown in this region. The primary cash crops in the district are Jute and Tea. There is a high demand for the land needed to grow tea. In this MCDM-GIS based study, agricultural land use classes have a high value (i.e. $W = 10$) of weightage and followed by vegetation cover ($W = 8$). In recent years, there has been a tendency toward switching land usage from crop production to tea plantations (DCHB, 2011). Therefore, sufficient planning is necessary for the justified and sustainable use of Agrarian land, by which site suitability assessment for this area will be more beneficial for farmers and planners.

NDWI:

The spectral reflectance of land changes based on surface characteristics such as topsoil,

rocks, water sources, natural vegetation, built-up area, and so on (Hui *et al.*, 2008). Due to its high absorption capacity, water exhibits lower spectral reflectance compared to other surfaces (Zolekar *et al.*, 2015; Roy *et al.*, 2022). Consequently, in remote sensing images, wet soils tend to appear darker than dry soils (Zhang and Voss, 2006). Soil moisture content varies depending on factors such as soil thickness and texture (Zolekar and Bhagat, 2015). Moreover, the NDWI is considered an effective indicator of soil health and has a positive influence on agricultural productivity (Wang *et al.*, 2012). Here, NDWI values have been categorised into five distinct classes (Figure 7a). While a negative NDWI score in green denotes a comparatively dry location with lower the moisture content and a high NDWI value in yellow and red colour denotes greater moisture contents for plants growth.

Proximity to Road and River:

For the better management and development of agriculture, land accessibility is influenced by factors like roads and rivers (FAO, 2007). Because rivers offer water for irrigation, being close to one increases agriculture productivity (Mustafa *et al.*, 2011; Bhatia, 2014). Similarly,

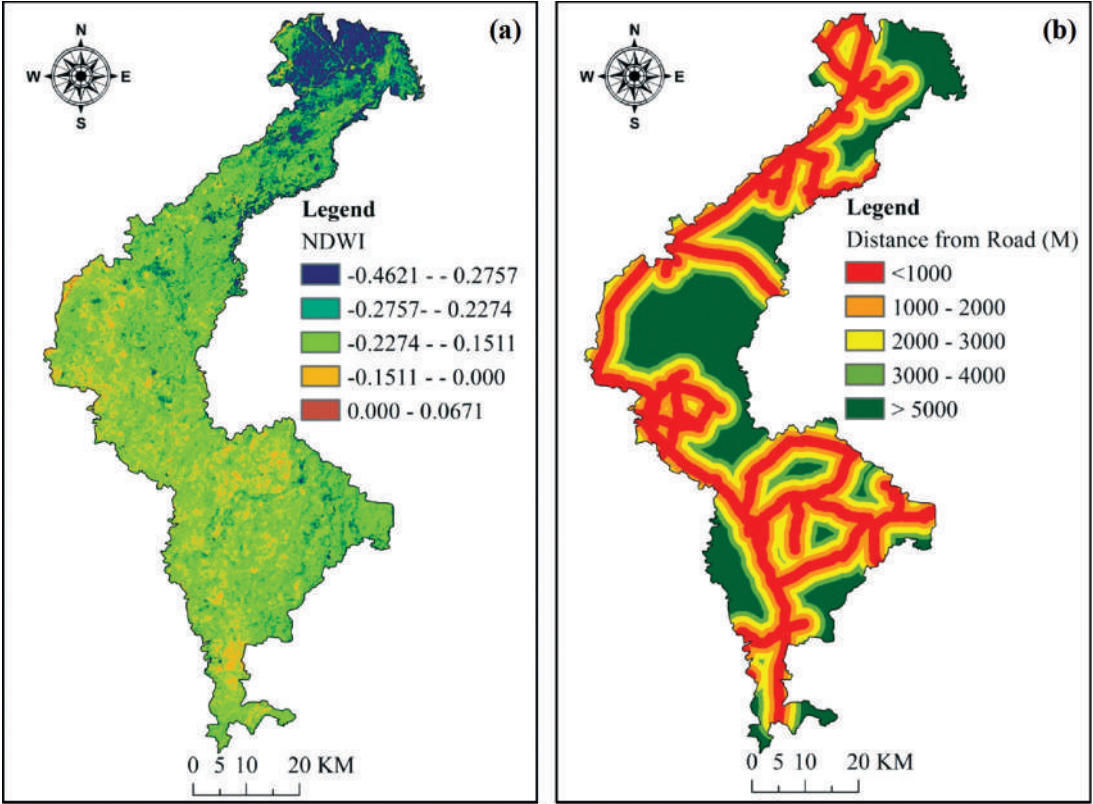


Figure 7. Potential agricultural land suitability indicators (a) NDWI (b) Proximity to road.

accessing the basic raw materials required for agricultural output is made easier by being near roadways (Pramanik, 2016). Additionally, the amount of land wetness decreases as the distance from rivers increase, and similarly growing distances from roadways and market indicates challenges of accessibility for farmers (Saha *et al.*, 2021). In this work, the buffer zonation map suggests that 1km to 2km distance from River, Road, and Market area is mostly suitable (Figure 7b and Figure 8a). Noteworthy, in case of proximity to road there is a negative relationship and on the other hand, same kind of relationship has been observed in proximity to river for the delineation of possible sites for land suitability to prosecute agricultural uses in this district of Uttar Dinajpur (Table 6).

Proximity to Market:

The rural marketing system is crucial for increasing output and consumption and boosting the economy faster. The most important agricultural market areas of Uttar Dinajpur district are Daspara hat, Goabari hat, Sonarpur hat, Kachakhati hat, Dhankoil hat, Debiganj hat, Panjipara hat, Sahapur hat, Chakulia hat, Kanki hat, Surjapur hat, Mohanbati hat, Bhatol hat, Panisala hat, Mahipur hat, Fatepur hat, and Rasakhowa hat etc. which boost the accessibilities of the

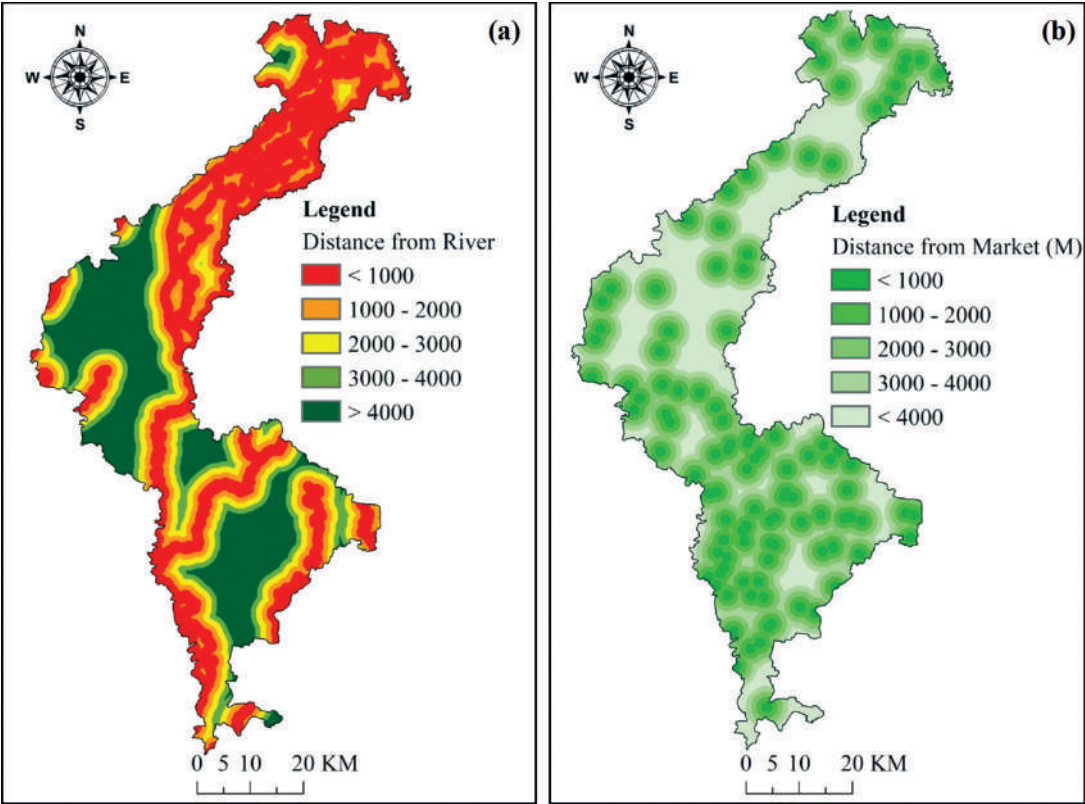


Figure 8. Potential agricultural land suitability indicators (a) Proximity to River (b) Proximity to market.

study area that enhance the suitability of land. From theoretical as well as practical point of view, proximity to markets and level of suitability of crop lands has an inverse relationship (Table 6) because distance is proportionately related with lower margin of production and it can be said to have high marketing value. Figure 8b shows the spatial scenario of local markets and linear distance from market centre.

Identification of agricultural land suitability classes:

It was found that the AHP with the integration of GIS is highly beneficial in determining the suitable places for agricultural production and this will be predicated on the combination of the twelve variables supporting the agriculture in the area (Kritikos and Davies, 2011). According to the assessment, around 1163.52 km² (43.57%) of land is highly suitable (S1), and 882.14 km² (33.04%) lands are moderately suitable (S2) (Table 8). These agriculturally productive areas (S1 and S2) contain flat plain along with gradual slope, optimum soil moisture content, loamy soil, ideal condition of temperature and rainfall incidences. Furthermore, these places have proximity to rivers and are close to transportation facilities, as well as nearness to the market which are economically significant (Girvan *et al.*, 2003). Subsequently 561.26 km² (21.02%) of land is marginally suitable (S3) just because of the presence of tea plantations in the northernmost part and poor irrigation facilities in the middle part of the study area. As a result, estimation was done that 63.35 km² (2.37%) is presently unsuitable (N1) for agricultural production, while 0.078 Km² (0.003%) is permanently unsuitable (N2) (Figure 9a & 9b). These sites are covered with forests, irregular landscape with comparatively small portion of high slope, constructional areas, and strong acidulated soils that affronts makechallengesforagriculture. Furthermore, the constraint map (Figure 9) shows that these locations are under canopy.As a result, in our current analysis, such vegetation limitations layers and preserved forest areas fall under the N1 and N2 zones (Table 7). These N1 and N2 sites, on the other hand, can be used for tourism and recreational activities (Akincietet *al.*, 2013).

Table 7. Details about the ALS class specific major characteristics

Land suitability classes	C. D. Block Name	Major Characteristics
Highly suitable (S1)	Raiganj, Itahar, Kaliyaganj, and Hemtabad	It consists a plain land with an average elevation of < 25m and very high amount organic carbon content (3–6.7%), suitable temperature (25°–26°C), sandy loam to loam soil which are more fertile for production of jute, wheat, rice, mustered etc. These areas are also very close to the source of water and irrigation, good transport facilities and also avail the market facilities which were more essential for buying and selling of the agricultural products.

Land suitability classes	C. D. Block Name	Major Characteristics
Moderate suitable (S2)	Islampur, Goalpokhar-1, Chopra, Karandighi, and Raiganj	These regions have smooth topography (25-50m), a medium to high incline, moderate soil wetness, coarse loam soil, an appropriate climatic condition, and being close to rivers, road and market being available and accessible. This region is also suitable for cultivation when managed properly.
Marginal suitable (S3)	Goalpokhar-2, Goalpokhar-1, Islampur, Chopra, and Karandighi	This region consists of Acidic soil, low soil humidity, gentle to steep slopes, flat to undulating topography, and closer to forest area which is moderately suited for cultivation with cost-effective management and fertilizers.
Currently nor suitable (N1)	Goalpokhar-2, Chopra, Karandighi Goalpokhar-1, and Islampur	Most of them include tea gardens, protected forest, constructed areas, and dense vegetation, as well as very toxic soils. These regions are not suitable for agricultural activity.
Permanently not suitable (N2)	Goalpokhar-2, Goalpokhar-1, Chopra, and Karandighi.	These areas have Unevenuplands with a sloping margins, tea gardens, bare rock, and a thick canopy of flora Therefore, these places can only be used for leisure and tourism-related activities.

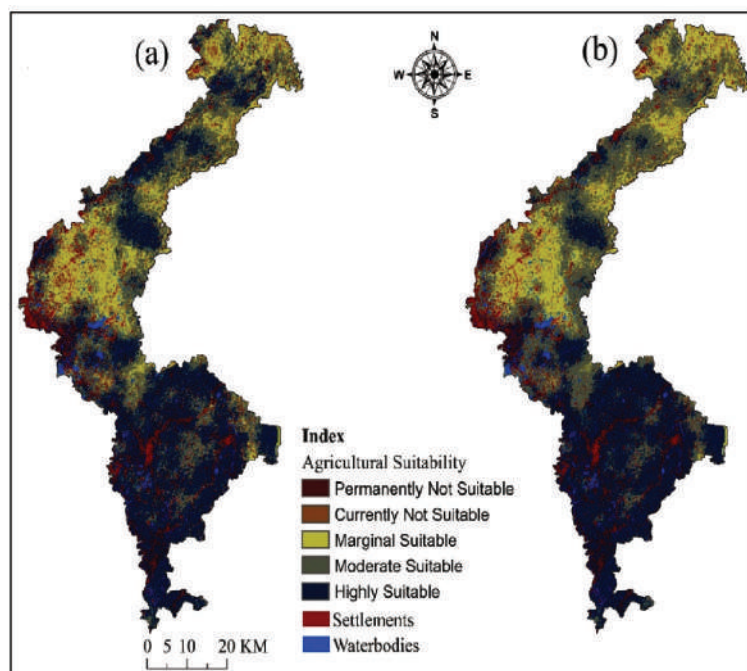


Figure 9. Spatial distribution map of agricultural suitability using (a) Fuzzy AHP (b) WS model.

Table 8. Statistics on ALS classes in Uttar Dinajpur district

Sl. No.	ALS Classes	Fuzzy AHP		Weighted Sum	
		Area (Km ²)	Area (%)	Area (Km ²)	Area (%)
1	Permanently Not Suitable	0.078	0.003	0.054	0.002
2	CurrentlyNot Suitable	63.574	2.363	22.158	0.824
3	Marginal Suitable	563.263	20.935	562.147	20.893
4	Moderate Suitable	890.196	33.084	1016.221	37.769
5	Highly Suitable	1173.523	43.616	1090.054	40.513
Total		2690.634	100.000	2690.634	100.000

The models generally indicate very low values for the permanently not suitable class across all blocks, with values ranging from 0.00 to 0.04 km² (Table 9). This suggests that the

Table 9. Block wise spatial distribution of different Agricultural suitability classes identified based on Fuzzy-AHP and WS model

Block Name	Model	Permanently not suitable (N2)	currently nor suitable (N1)	Marginal suitable (S3)	moderate suitable (S2)	Highly suitable (S1)	Total area in km2
Chopra	AHP Fuzzy	0.01	14.50	131.50	145.63	57.48	349.12
	WOS	0.01	8.29	149.05	164.00	27.71	349.06
Goalpokhor I	AHP Fuzzy	0.01	7.51	100.88	147.44	87.27	343.11
	WOS	0.00	8.11	86.83	182.77	65.44	343.15
Goalpokhar II	AHP Fuzzy	0.04	16.20	169.56	59.40	10.91	256.11
	WOS	0.02	7.73	170.93	71.13	6.31	256.12
Hemtabad	AHP Fuzzy	0.00	0.56	5.77	55.37	106.64	168.34
	WOS	0.00	1.00	5.66	36.55	125.21	168.42
Islampur	AHP Fuzzy	0.00	5.17	64.38	149.02	88.31	306.88
	WOS	0.00	2.02	91.59	151.66	61.66	306.93
Itahar	AHP Fuzzy	0.00	1.18	3.72	33.24	253.13	291.27
	WOS	0.00	1.00	10.39	30.16	249.77	291.32
Kaliyaganj	AHP Fuzzy	0.00	1.29	13.81	63.77	176.79	255.66
	WOS	0.00	0.00	2.53	54.76	198.39	255.68
Karandighi	AHP Fuzzy	0.01	7.82	54.05	130.36	97.19	289.43
	WOS	0.00	3.92	36.72	161.57	87.20	289.41
Raiganj	AHP Fuzzy	0.00	0.92	19.80	89.93	280.69	391.34
	WOS	0.00	3.00	8.28	88.57	291.51	391.36

*WOS - Weighted Overlay Sum

proportion of land facing permanent unsuitability for agriculture is minimal in these blocks. Both models show variations in the currently not suitable class. The Fuzzy-AHP model shows higher values in some blocks compared to the WOS model, indicating a larger area currently not suitable for agriculture. The WOS model tends to assign higher values for the marginal suitable class in most of the blocks, implying a larger extent of land that could potentially be improved for agriculture. The values for the moderate suitable class vary across blocks, with both models showing fluctuations. However, the AHP Fuzzy model assigns higher values in general, suggesting a larger area with moderate suitability. The highly suitable class is generally represented by smaller values compared to the other classes. However, the AHP Fuzzy model tends to assign higher values in some blocks, indicating a relatively larger extent of land considered highly suitable for agriculture.

The research employed two distinct MCDM models, Fuzzy AHP and the Weighted Sum (WS) method, to assess agricultural land suitability. A comparative analysis of these results provided crucial insights into their respective performances and practical implications for land-use planning. The validation results demonstrate that the Fuzzy AHP model exhibits superior performance and reliability, with an AUC value of 0.913, which is significantly higher than the 0.866 AUC value of the Weighted Sum model.

The block-wise analysis of the Fuzzy AHP and Weighted Sum models reveals significant discrepancies in their land classification, even though their overall total area values are very similar. For instance, in the Chopra block, the Fuzzy AHP model classifies a larger area as 'currently not suitable' (14.50 km²) and 'highly suitable' (57.48 km²) compared to the WS model (8.29 km² and 27.71 km² respectively), which conversely assigns a larger area to the 'marginal' and 'moderate' suitability classes. In Goalpokhor I, Fuzzy AHP identifies a larger area as 'highly suitable' (87.27 km²) than the WS model (65.44 km²), while the WS model assigns a significantly larger area to the 'moderate suitable' class (182.77 km²). The Fuzzy AHP model in Goalpokhar II classifies a considerably larger area as 'currently not suitable' (16.20 km²) compared to the WS model (7.73 km²), suggesting that it is more nuanced approach correctly identifies land with subtle constraints that the WS method might overlook minute details or simplified in approach. In Hemtabad and Raiganj, the WS model classifies a larger area as 'highly suitable' than the Fuzzy AHP model, whereas in Islampur, Fuzzy AHP attributes larger areas to both the 'currently not suitable' and 'highly suitable' classes compared to the WS model. In Itahar, Fuzzy AHP identifies a much larger area as 'highly suitable' (253.13 km²) while the WS model assigns a larger area to the 'marginal suitable' class, and in Kaliyaganj, the WS model classifies a significantly larger area as 'highly suitable' (198.39 km²) than Fuzzy AHP. Finally, in Karandighi, Fuzzy AHP identifies a larger area as 'currently not suitable' and a smaller area as 'moderate suitable' compared to the WS model. These block-level differences are critical for land-use planners, as relying on the less accurate WS model could lead to flawed policy decisions, such as misallocating resources to improve unsuitable land or failing to implement crucial environmental protection measures. Therefore, these findings strongly suggest that the more accurate and reliable output from the Fuzzy AHP model should be prioritized for effective and sustainable development within each specific block.

Validation of the model:

Validation is a crucial step in confirming the reliability and accuracy of an agricultural land suitability model (Zolekar and Bhagat, 2015). The validation of the study was conducted using a combination of methods, including a comparison with a prepared LULC map, verification against Google Earth imagery, and ground-level field visits. Google earth image is the most accurate method for validating the result of land suitability assessment on actual earth surface (Kumar and Ravikumar, 2018, Gradinaru *et al.*, 2018). The LULC map, created from Landsat 8 satellite imagery, provided a foundational dataset for the validation process, as it provides a snapshot of where agriculture is currently practiced or other kind of landuse whatever is the reality. The research further validated the model by producing a ROC curve and AUC value, based on a sample of 250 locations (50 sample sites from each class) over the study area

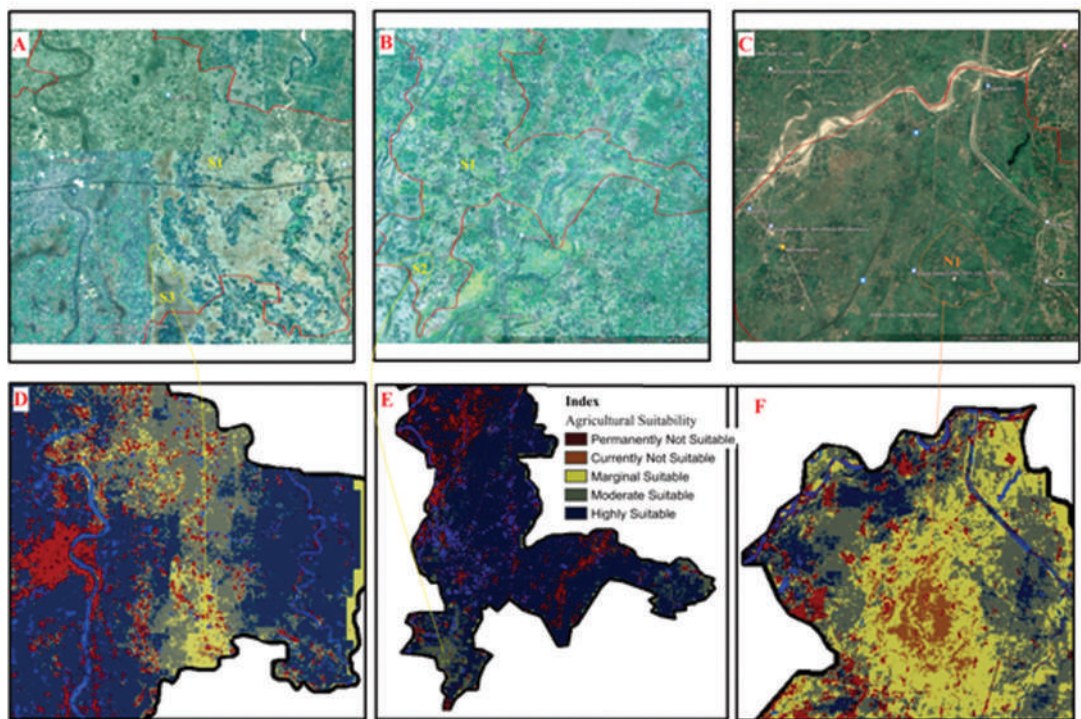


Figure 10. Ground verification of the model using Google Earth images (2023) and megascopic view of accepted ALS classes map, (A)Field comparison for identification of marginally suitable class (S3) being conformal in reality and verified by Google Earth image for the specific segment showing non-agricultural signatures which is close to marginally suitable class, (B) Similar sub-set shows highly suitable (S1) and moderately suitable class (S2) becoming perfectly conformal to the reality while ground-truthing through Google Earth images and necessary field investigation, Similar kind of ground-truthing showed currently not suitable class (N1) which is signifying presently as forest land and justified inference in reality, (D) output map of suitability classes showing justified delineation of classes by conformity with the reality for adjacent areas of Chopra block as case study-1, (E) Similar kind of execution alike sub-set D for adjacent areas of Itahar block as case study-2, and (F) Again similar kind of execution alike sub-set D and E for adjacent areas of Kaliyaganj block as case study-3

collected through the stratified random sampling. Here strata refer to the perceived output map classes (Figure9). Using the ArcSDM tool within a GIS environment, all necessary forms and procedures have been successfully completed. The agricultural suitability map, represented as a raster format, has been generated through a point-based inventory approach. This methodology facilitated the calculation of the ROC curve and AUC value, assessing the accuracy and performance of the map. The high AUC value of 0.913 (91.30%) for the Fuzzy AHP model confirms its strong predictive performance (a perfect AUC value is 1, indicating the maximum level of the accuracy. AUC values of 0.70 or higher are generally considered satisfactory). On validation of the selected sample points with their co-ordinate values through Google Earth platform we found conformal outcome with their original LULC character and the respective output class (Figure 9). Contextually, it is already furnished above with a high accuracy of >91% (Figure11). The ground-truthing component of the validation involved a direct comparison of the model's suitability maps with actual field conditions, visually represented in Figure 10.

Discussion:

Land suitability or assessment of the land is crucial for selecting the land use pattern and is advantageous of land use for future. So, the principal objective of this research was to encompass crucial factors, including soil parameters (i.e. soil pH, texture, moisture content, and organic carbon), climatic parameters (i.e. temperature and rainfall), topographic parameters (i.e. elevation and slope), LULC, as well as various accessibility parameters i.e. proximity to rivers, roads, and markets. MCDM approach is quite helpful since it gives a trustworthy result in terms of finding locations that are suitable for producing sustainable agriculture. The present study has also undergone through validation, enabling reliable application in the context of administration and planning.

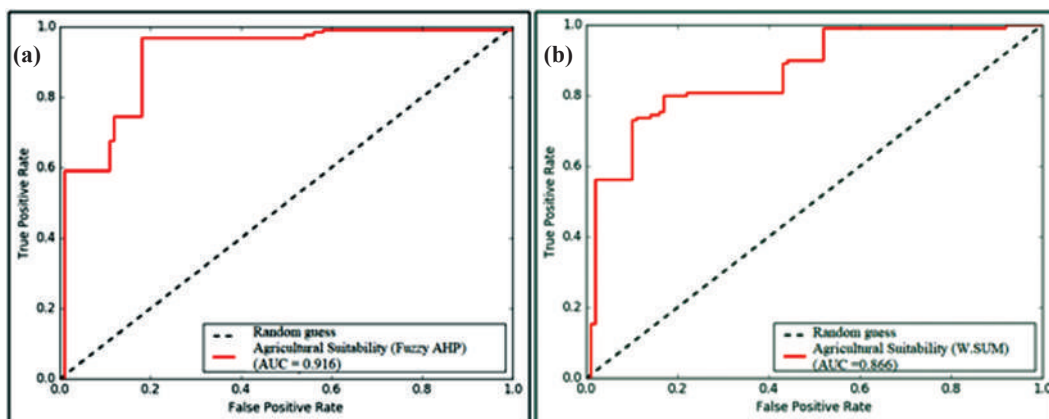


Figure 11. Validation graph of MCDM model based Agricultural Land Suitability map through ROC curve and AUC values (a) Fuzzy AHP = 91.60% (b) WOS= 86.60%). N = 250

The findings reveal that a substantial portion of the Uttar Dinajpur district is classified as highly or moderately suitable for agriculture, totalling over 76% of the area according to the Fuzzy AHP model. However, the LULC analysis indicates that 78.14% of the land is already under agricultural use, suggesting that a significant portion of current farming is conducted on land that is only marginally suitable. This disparity is a key indicator of unsustainable farming practices and helps explain the “declining trend in the use of land for crop production” noted in the present work. The suitability map can, therefore, be used to guide sustainable practices by identifying which areas have the greatest potential for productivity, and where soil health programs and fertility enhancement measures would be most effective.

Furthermore, the study sheds light on existing land-use conflicts. The analysis correctly identifies that the northern part of the district, which is home to expanding tea plantations, is topographically less suitable for traditional agriculture. This presents a complex trade-off between the economic benefits of tea production and the protection of arable land. The suitability map can serve as a crucial planning instrument to mediate these conflicts, ensuring that the most productive agricultural lands are protected from conversion for other uses.

The district’s vulnerability to climate-related hazards, such as annual flooding and drought, is well-documented through field investigations. The land suitability map, by identifying areas with optimal soil moisture and proximity to rivers, can inform the development of climate-resilient agricultural strategies. For example, areas classified as highly suitable with easy access to water can be prioritized for water-intensive crops, while marginally suitable land can be designated for the cultivation of more drought-resilient crops or for the application of agro-forestry systems, which can enhance soil health and buffer against climate shocks.

Hence the broader sustainability issues identified as outcome of this research work are (a) over prevalence of over cropping (b) cultivation without suitability judgement (c) rudimentary and older implementation of agricultural instrument (d) over dosing of chemical fertilization especially degrading the marginally suitable lands (Under judgement for agricultural transformation towards cash crops (tea and maize) for over dividends.

However, Uttar Dinajpur district is most suitable to the southern section due to its desirable soil characteristics and topographical features. However, the northern half and the middle part is primarily made up of undulating topographic features, numerous Tea plantations, protected forests; lack of infrastructural facilities; unplanned settlements hampered its suitability. However, there is still a maximum area in this northern region that falls within a zone that is only marginally suited, and with the appropriate technology and proper management strategy, it is possible to use these areas for efficient utilization. The study concluded that regions with favourable topography, sufficient soil moisture, optimum soil texture, or nearness to the rivers, roads and market still have a great impact on the suitability of a piece of land for agriculture. Similarly, the south-west monsoon climate also impacts the agriculture of this district. Most of the kharif crop mainly jute, paddy and Maize is totally dependent on monsoon and pump irrigation facilities. Paddy, wheat, jute, maize, mustard, pulses, and other crops make up the bulk of the district of Uttar Dinajpur; loamy and sandy loam soil is ideal for these crops (Photo plate 1).

Recommendations:

The findings of this research provide a clear foundation for developing targeted, site-specific policies for sustainable land management and agricultural planning in Uttar Dinajpur.

Soil Management Policies: Given that soil texture and pH are the most influential factors, policies should focus on providing technical and financial support for soil testing and amendments. The government should offer subsidies for farmers to apply lime to acidic soils, particularly in the marginally suitable northern areas. Furthermore, promoting the wise use of organic manures in conjunction with inorganic fertilizers is crucial for enhancing soil health and sustaining long-term yields, especially in the moderately and marginally suitable zones.

Land-Use Planning Policies: A strategic zoning plan should be implemented to protect the highly suitable agricultural lands (S1) from conversion to non-agricultural uses, such as residential settlements or tea plantations. The suitability map can guide planners to direct urban and industrial expansion toward areas classified as 'not suitable' for farming. Conversely, areas in the 'not suitable' classes that are not protected forests or tea gardens should be evaluated for alternative, non-agricultural uses like eco-tourism or recreational activities, as proposed by the study.

Environmental Protection and Climate Change Adaptation: To mitigate the impacts of flooding and drought, policies should promote the development of small-scale, community-based irrigation infrastructure in areas identified as moderately suitable (S2) but currently lacking water access. In marginally suitable areas (S3), agro-forestry or silvi-cultural systems should be encouraged to improve soil retention, enhance biodiversity, and provide alternative sources of income and food. The government should also invest in building necessary infrastructure, such as roads and rail lines, to improve market accessibility for farmers across all suitability zones.

Conclusion:

The research successfully used a GIS-based Multi-Criteria Decision-Making (MCDM) approach to identify the suitability of agricultural land in the Uttar Dinajpur district of West Bengal. Two methods were compared: Fuzzy AHP and the WS method. The study determined that Land Use/Land Cover (LULC), soil texture, and soil pH were the most significant factors in determining land suitability for agriculture in the region. The Fuzzy AHP model proved to be more accurate and reliable, with an AUC value of 0.913, compared to the Weighted Sum model's AUC of 0.866. This suggests that the Fuzzy AHP's nuanced approach is better for land-use planning in the district. The land suitability map generated by the Fuzzy AHP model found that the majority of the district's land is suitable for agriculture, with 43.616% classified as highly suitable, 33.084% as moderately suitable, and 20.935% as marginally suitable. The findings highlight a discrepancy between current widespread agricultural land use and the limited availability of highly suitable land, indicating that farming is often practiced on sub-optimal land.

The study provides a spatial framework that can inform the creation of site-specific policies to enhance soil management, mitigate land-use conflicts, and build resilience to

climate change. Despite the district possessing a considerable amount of land suitable for agriculture, unsustainable farming methods and population pressure have recently contributed to soil degradation and reduced fertility. The map shows how the land's innate potential to support agriculture is spatially represented. The district's main limitations include a dearth of agro-based enterprises, a scarcity of groundwater, and intense population pressure on the land. Therefore, we need to act right away to plan the optimal land usage for our future generations. To increase crop output, soil fertility, and sustain the ecological diversity of this area, agro forestry, high yielding variety seeds (HYV), and smart farming methods must be used. Therefore, using organic manures wisely in conjunction with inorganic fertilisers not only helps to produce sustainable yields but also preserves the soil's health without endangering future generations. Additionally, if there is a lack of suitability, other leisure or tourism activities ought to be promoted. The pastoral cropping systems can be used on land with a medium level of suitability. In the very low category of the land, the silvi-cultural system can be applied for better management. Last but not least, this research will aid in the development of related fields of study, as well as the better management of land usage by farmers and decision-makers. Overall, this comparison of agricultural suitability classes provides insights into the land suitability for agriculture in different blocks, helping in identifying areas with varying levels of suitability and supporting decision-making processes related to agricultural development and land-use planning. Governments should take the required steps to build the necessary infrastructure, such as roads or trains, to connect this area. So, the GIS-based Fuzzy AHP model successfully delineated agricultural land suitability in Uttar Dinajpur, providing a robust and reliable map for informed decision-making.

The research, however, has several limitations. The validation, while providing a high AUC value for the Fuzzy AHP model, lacks detailed information on the field sampling strategy, which could introduce a potential for bias. Additionally, the use of static climate data means the model does not fully account for the district's vulnerability to dynamic environmental changes. Based on these findings and limitations, future research should explore the following directions: Integrate dynamic climate models and scenario analysis to assess how land suitability might shift under different climate change projections. Conduct a more comprehensive socio-economic survey to better understand the human-centric factors that influence land-use decisions, such as market pressures and farmer knowledge systems. Compare the Fuzzy AHP model's performance with other data-driven machine learning models to further refine the predictive accuracy of the suitability map.

Overall, this research serves as a valuable resource for farmers and policymakers, offering a spatial framework for developing site-specific policies to enhance soil management, optimize land use, and protect the environment for long-term sustainability.

Acknowledgements:

The authors express sincere gratitude to the Department of Geography & Applied Geography at the University of North Bengal for providing them with the opportunity to carry out this research. Additionally, the authors would like to extend their appreciation to the FAO

Soil Portal, Bhuvan-NRSC, Geological Survey of India (GSI), and Indian Meteorological Department (IMD), USGS earth explorer, Google earth Pro as well as local farmers and government officials in the respective fields for providing the valuable data/information and share with us field experience without these the current research can't be possible.

Conflict of Interest: The authors affirm that they do not have any conflicts of interest yet to be disclosed.

References:

- Abdel Rahman, M. A., Natarajan, A., & Hegde, R. (2016). Assessment of land suitability and capability by integrating remote sensing and GIS for agriculture in Chamara Nagar district, Karnataka, India. *The Egyptian Journal of Remote Sensing and Space Science*, 19(1), 125-141. <https://doi.org/10.1016/j.ejrs.2016.02.001>
- Ahmadi Sani, N., Babaie Kafaky, S., Pukkala, T., & Mataji, A. (2016). Integrated use of GIS, remote sensing and multi-criteria decision analysis to assess ecological land suitability in multi-functional forestry. *Journal of forestry research*, 27, 1127-1135. <http://dx.doi.org/10.1007/s11676-016-0242-1>
- Ahmed, G. B., Shariff, A. R. M., Balasundram, S. K., & bin Abdullah, A. F. (2016). Agriculture land suitability analysis evaluation based multi criteria and GIS approach. In *IOP Conference Series: Earth and Environmental Science* (Vol. 37, No. 1, p. 012044). IOP Publishing. <https://doi.org/10.1088/1755-1315/37/1/012044>
- Akinci, H., Özalp, A. Y., & Turgut, B. (2013). Agricultural land use suitability analysis using GIS and AHP technique. *Computers and Electronics in Agriculture*, 97, 71–82. <https://doi.org/10.1016/j.compag.2013.07.006>
- Akpoti, K., Kabobah, A. T., & Zwart, S. J. (2019). Agricultural land suitability analysis: State-of-the-art and outlooks for integration of climate change analysis. *Agricultural systems*, 173, 172-208. <https://doi.org/10.1016/j.agsy.2019.02.013>
- Ananda, J., & Herath, G. (2009). A critical review of multi-criteria decision making methods with special reference to forest management and planning. *Ecological economics*, 68(10), 2535-2548. <https://doi.org/10.1016/j.ecolecon.2009.05.010>
- Anusha, B. N., Babu, K. R., Kumar, B. P., Sree, P. P., Veeraswamy, G., Swarnapriya, C., & Rajasekhar, M. (2023). Integrated studies for land suitability analysis towards sustainable agricultural development in semi-arid regions of AP, India. *Geosystems and Geoenvironment*, 2(2), 100131. <https://doi.org/10.1016/j.geogeo.2022.100131>
- Bandyopadhyay, S., Jaiswal, R. K., Hegde, V. S., & Jayaraman, V. (2009). Assessment of land suitability potentials for agriculture using a remote sensing and GIS based approach. *International Journal of Remote Sensing*, 30(4), 879-895. <https://doi.org/10.1080/01431160802395235>
- Barah, B. C. (2010). Hill agriculture: problems and prospects for mountain agriculture. *Indian Journal of Agricultural Economics*, 65(902-2016-67935).
- Bhagat, V. S. (2009). Use of Landsat ETM+ data for detection of potential areas for afforestation. *International Journal of Remote Sensing*, 30(10), 2607-2617. <https://doi.org/10.1080/01431160802552793>

- Bhagat, V. S. (2013). Use of remote sensing techniques for robust detection and estimations of soil organic carbon: A review. *Recent Patents on Space Technology*, 3(2), 83-102.<http://dx.doi.org/10.2174/18776116112029990001>
- Bhutia, S. (2014). Economic development and environmental issues in Darjeeling Himalaya of West Bengal, India: A theoretical perspective. *International Journal of Humanities and Social Science Invention*, 3(7), 42-47.
- Bin, Q., He-Jian, Z., Song-Lin, C., Römken, M. J. M., & Bi-Cheng, L. (2007). Land suitability assessment and land use change in Fujian Province, China. *Pedosphere*, 17(4), 493-504.[https://doi.org/10.1016/S1002-0160\(07\)60059-9](https://doi.org/10.1016/S1002-0160(07)60059-9)
- Bojorquez-Tapia, L. A., Diaz-Mondragon, S., & Ezcurra, E. (2001). GIS-based approach for participatory decision making and land suitability assessment. *International Journal of Geographical Information Science*, 15(2), 129-151.<https://doi.org/10.1080/13658810010005534>
- Bose, A., Mandal, G., & Chowdhury, I. R. (2020). A Study on Inter-Block Level Regional Disparity Analysis of Uttar Dinajpur District, West Bengal, India. *GEOGRAPHY IN THE 21ST CENTURY: EMERGING ISSUES AND THE WAY FORWARD*, 225.
- Bozdağ, A., Yavuz, F., & Günay, A. S. (2016). AHP and GIS based land suitability analysis for Cihanbeyli (Turkey) County. *Environmental Earth Sciences*, 75, 1-15.<https://doi.org/10.1007/s12665-016-5558-9>
- Cengiz, T., & Akbulak, C. (2009). Application of analytical hierarchy process and geographic information systems in land-use suitability evaluation: a case study of Dümrek village (Çanakkale, Turkey). *International Journal of Sustainable Development & World Ecology*, 16(4), 286-294.<https://doi.org/10.1080/13504500903106634>
- Dar, M. A., Wani, J. A., Raina, S. K., Bhat, M. Y., Malik, M. A., & Najar, G. R. (2012). Effect of altitude and depth on available nutrients in pear orchard soils of Kashmir. *Agropedology*, 22(2), 115-118.
- Das, M., Parveen, T., Ghosh, D., & Alam, J. (2021). Assessing groundwater status and human perception in drought-prone areas: a case of Bankura-I and Bankura-II blocks, West Bengal (India). *Environmental Earth Sciences*, 80(18), 636.<https://doi.org/10.1007/s12665-021-09909-8>
- DCHB. (2011). District Census Handbook, Uttar Dinajpur District. Retrieved from <https://censusindia.gov.in/nada/index.php/catalog/1334>
- Dengiz, O. (2013). Land suitability assessment for rice cultivation based on GIS modeling. *Turkish Journal of Agriculture and Forestry*, 37(3), 326-334.<https://doi.org/10.3906/tar-1206-51>
- District disaster management plan Uttar Dinajpur District, 2016-2017. <http://www.wbdmd.gov.in/writereaddata/uploaded/DP/UttarDinajpur.pdf>
- El Baroudy, A. A. (2016). Mapping and evaluating land suitability using a GIS-based model. *Catena*, 140, 96-104.<https://doi.org/10.1016/j.catena.2015.12.010>
- Ennaji, W., Barakat, A., El Baghdadi, M., Oumenskou, H., Aadraoui, M., Karroum, L. A., & Hilali, A. (2018). GIS-based multi-criteria land suitability analysis for sustainable agriculture in the northeast area of Tadla plain (Morocco). *Journal of Earth System Science*, 127, 1-14.<https://doi.org/10.1007/s12040-018-0980-x>

- FAO. (1976). A framework for land evaluation. Italy
- FAO. (2007). Land evaluation, towards a revised framework. Land and Water Discussion
- Feizizadeh, B., Roodposhti, M. S., Jankowski, P., & Blaschke, T. (2014). A GIS-based extended fuzzy multi-criteria evaluation for landslide susceptibility mapping. *Computers & geosciences*, 73, 208-221. <https://doi.org/10.1016/j.cageo.2014.08.001>
- Ghosh, M., & Ghosal, S. (2020). Determinants of household livelihood vulnerabilities to climate change in the Himalayan foothills of West Bengal, India. *International Journal of Disaster Risk Reduction*, 50, 101706. <https://doi.org/10.1016/j.ijdrr.2020.101706>
- Girvan, M. S., Bullimore, J., Pretty, J. N., Osborn, A. M., & Ball, A. S. (2003). Soil type is the primary determinant of the composition of the total and active bacterial communities in arable soils. *Applied and environmental microbiology*, 69(3), 1800-1809. <https://doi.org/10.1128/AEM.69.3.1800-1809.2003>
- Grădinaru, S. R., Triboi, R., Iojă, C. I., & Artmann, M. (2018). Contribution of agricultural activities to urban sustainability: Insights from pastoral practices in Bucharest and its peri-urban area. *Habitat International*, 82, 62-71. <https://doi.org/10.1016/j.habitatint.2018.09.005>
- Halder, J. C. (2013). Land suitability assessment for crop cultivation by using remote sensing and GIS. *Journal of geography and Geology*, 5(3), 65. <http://dx.doi.org/10.5539/jgg.v5n3p65>
- Hassan, I., Javed, M. A., Asif, M., Luqman, M., Ahmad, S. R., Ahmad, A., Akhtar, S... & Hussain, B. (2020). Weighted overlay based land suitability analysis of agriculture land in Azad Jammu and Kashmir using GIS and AHP. *Pakistan Journal of Agricultural Sciences*, 57(6). <https://doi.org/10.21162/PAKJAS/20.9507>
- Hemathilake, D. M. K. S., & Gunathilake, D. M. C. C. (2022). Agricultural productivity and food supply to meet increased demands. In *Future foods* (pp. 539-553). Academic Press. <https://doi.org/10.1016/B978-0-323-91001-9.00016-5>
- Iizumi, T., & Ramankutty, N. (2015). How do weather and climate influence cropping area and intensity. *Global food security*, 4, 46-50. <https://doi.org/10.1016/j.gfs.2014.11.003>
- IPCC Fifth assessment report climate change 2013. https://www.ipcc.ch/site/assets/uploads/2018/03/WG1AR5_SummaryVolume_FINAL.pdf
- Jafari, S., & Zaredar, N. (2010). Land suitability analysis using multi attributed decision making approach. *International journal of environmental science and development*, 1(5), 441.
- Jain, S. K., Singh, R. D., Jain, M. K., & Lohani, A. K. (2005). Delineation of flood-prone areas using remote sensing techniques. *Water resources management*, 19, 333-347. <http://dx.doi.org/10.1007/s11269-005-3281-5>
- Khan, M. A., Ahmad, R., & Khan, H. H. (2022). Multi-criteria land suitability analysis for agriculture using AHP and remote sensing data of northern region India. *Geographic Information Systems and Applications in Coastal Studies*. <https://doi.org/10.5772/intechopen.102432>
- Kilic, O. M., & Gunal, H. (2021). Spatial-temporal changes in rainfall erosivity in Turkey using CMIP5 global climate change scenario. *Arabian Journal of Geosciences*, 14(12), 1079. <http://dx.doi.org/10.1007/s12517-021-07184-2>

- Kılıc, O. M., Ersayın, K., Gunal, H., Khalofah, A., & Alsubeie, M. S. (2022). Combination of fuzzy-AHP and GIS techniques in land suitability assessment for wheat (*Triticum aestivum*) cultivation. *Saudi Journal of Biological Sciences*, 29(4), 2634-2644. <https://doi.org/10.1016/j.sjbs.2021.12.050>
- Kopittke, P. M., Menzies, N. W., Wang, P., McKenna, B. A., & Lombi, E. (2019). Soil and the intensification of agriculture for global food security. *Environment international*, 132, 105078. <https://doi.org/10.1016/j.envint.2019.105078>
- Koulouri, M., & Giourga, C. (2007). Land abandonment and slope gradient as key factors of soil erosion in Mediterranean terraced lands. *Catena*, 69(3), 274-281. <https://doi.org/10.1016/j.catena.2006.07.001>
- Kritikos TRH, Davies TRH (2011) GIS-based multi-criteria decision analysis for landslide susceptibility mapping at northern Evia, Greece. *Z DTSCH Ges Geowiss* 162(4):421–434. <https://doi.org/10.1127/1860-1804/2011/0162-0421>
- Kumar, A., & Ravikumar, A. S. (2018). Land capability and crop suitability using RS and GIS. *Int. J. Tech. Sci. Res. Eng.*, 1(2), 9-21.
- Kumar, A., Mishra, R. K., & Sarma, K. (2020). Mapping spatial distribution of traffic induced criteria pollutants and associated health risks using kriging interpolation tool in Delhi. *Journal of Transport & Health*, 18, 100879. <https://doi.org/10.1016/j.jth.2020.100879>
- Kumar, A., Pramanik, M., Chaudhary, S., & Negi, M. S. (2021). Land evaluation for sustainable development of Himalayan agriculture using RS-GIS in conjunction with analytic hierarchy process and frequency ratio. *Journal of the Saudi Society of Agricultural Sciences*, 20(1), 1-17. <https://doi.org/10.1016/j.jssas.2020.10.001>
- Ly, S., Charles, C., & Degré, A. (2013). Different methods for spatial interpolation of rainfall data for operational hydrology and hydrological modeling at watershed scale: a review. *Biotechnologie, agronomie, société et environnement*, 17(2), 392-406.
- Maddahi, Z., Jalalian, A., Zarkesh, M. K., & Honarjo, N. (2014). Land suitability analysis for rice cultivation using multi criteria evaluation approach and GIS. *European Journal of Experimental Biology*, 4(3), 639-648.
- Malczewski, J. (1999). *GIS and multicriteria decision analysis*. John Wiley and Sons, New York, NY.
- Mandal, P., Mandal, S., Halder, S., & Paul, S. (2021). Assessing and mapping cropland suitability applying geospatial and MIF techniques in the semiarid region with an integrated approach. *Arabian Journal of Geosciences*, 14(18), 1–19. <https://doi.org/10.1007/s12517-021-08171-3>
- Mateo, J. R. S. C. (2012). Weighted sum method and weighted product method. *Multi criteria analysis in the renewable energy industry*, 19-22. https://doi.org/10.1007/978-1-4471-2346-0_4
- Mojid, M., Mustafa, S., & Wyseure, G. (2010). Growth, yield and water use efficiency of wheat in silt loam-amended loamy sand. *Journal of the Bangladesh Agricultural University*, 7(2), 403410.
- Mustafa, A. A., Singh, M., Sahoo, R. N., Ahmed, N., Khanna, M., Sarangi, A., & Mishra, A. K. (2011). Land suitability analysis for different crops: a multi criteria decision making approach using remote sensing and GIS. *Researcher*, 3(12), 61-84.

- Orhan, D., İlhami, B., & Mahmut, Y. (2003). Geographic information systems and remotesensing based land evaluation of Beypazari area soils by ILSN model. *Turkish journal of agriculture and forestry*, 27, 145–153.
- Orhan, O. (2021). Land suitability determination for citrus cultivation using a GIS-based multi-criteria analysis in Mersin, Turkey. *Computers and Electronics in Agriculture*, 190, 106433. <https://doi.org/10.1016/j.compag.2021.106433>
- Otgonbayar, M., Atzberger, C., Chambers, J., Amarsaikhan, D., Böck, S., & Tsogtbayar, J. (2017). Land suitability evaluation for agricultural cropland in Mongolia using the spatial MCDM method and AHP based GIS. *Journal of Geoscience and Environment Protection*, 5(9), 238-263.
- Özkan, B., Dengiz, O., & Turan, İ. D. (2020). Site suitability analysis for potential agricultural land with spatial fuzzy multi-criteria decision analysis in regional scale under semi-arid terrestrial ecosystem. *Scientific reports*, 10(1), 22074. <https://doi.org/10.1038/s41598-020-79105-4>
- Park, S., Jeon, S., Kim, S., & Choi, C. (2011). Prediction and comparison of urban growth by land suitability index mapping using GIS and RS in South Korea. *Landscape and urban planning*, 99(2), 104-114. <https://doi.org/10.1016/j.landurbplan.2010.09.001>
- Planko, J., & Silvius, G. (2017). Compromising the ability of future generations to meet their own needs' (World Commission on Environment and Development 1987). This definition is widely used, and has often been interpreted as an appeal to only consume in such a way that we do not destroy too many resources, especially the. *Sustainability in Project Management*, 2.
- Pramanik, M. K. (2016). Site suitability analysis for agricultural land use of Darjeeling district using AHP and GIS techniques. *Modeling Earth Systems and Environment*, 2(2), 56. <https://doi.org/10.1007/s40808-016-0116-8>
- Rabia, A. H., & Terribile, F. (2013). Introducing a new parametric concept for land suitability assessment. *International Journal of Environmental Science and Development*, 4(1), 15. <http://dx.doi.org/10.7763/IJESD.2013.V4.295>
- Rahaman, S., Das, M., & Saha, S. (2022). Delineation of Groundwater Potential Zones Using Analytic Hierarchy Process (AHP) Technique in Balason River Basin of West Bengal, India, Riverine environment and its dynamics: Challenges, issues and sustainable managements, 1,
- Rhebergen, T., Fairhurst, T., Zingore, S., Fisher, M., Oberthür, T., & Whitbread, A. (2016). Climate, soil and land-use based land suitability evaluation for oil palm production in Ghana. *European Journal of Agronomy*, 81, 1-14. <https://doi.org/10.1016/j.eja.2016.08.004>
- Roy, S., Hazra, S., Chanda, A., & Das, S. (2022). Land suitability analysis using AHP-based multi-criteria decision model for sustainable agriculture in red and lateritic zones of West Bengal, India. *Journal of Earth System Science*, 131(4), 201. <https://doi.org/10.1007/s12040-022-01941-x>
- Roy, S., Singha, N., Bose, A., Basak, D., & Chowdhury, I. R. (2022). Multi-influencing factor (MIF) and RS-GIS-based determination of agriculture site suitability for achieving sustainable development of Sub-Himalayan region, India. *Environment, Development and Sustainability*, 1-33. <https://doi.org/10.1007/s10668-022-02360-0>
- Rudel, T. K., Schneider, L., Uriarte, M., Turner, B. L., DeFries, R., Lawrence, D., & Grau, R. (2009). Agricultural intensification and changes in cultivated areas, 1970–2005. *Proceedings of the National Academy of Sciences*, 106(49), 20675-20680. <https://doi.org/10.1073/pnas.0812540106>

- Saaty, T. L. (1980). *The Analytic Hierarchy Process: Planning, Priority Setting, Resource Allocation*. McGraw-Hill International, New York, NY, USA.
- Saaty, T. L. (1994). How to make a decision: the analytic hierarchy process? *Interfaces* 24:19–43
- Saha, S., Sarkar, D., Mondal, P., & Goswami, S. (2021). GIS and multi-criteria decision-making assessment of sites suitability for agriculture in an anabranching site of sooinriver, India. *Modeling Earth Systems and Environment*, 7, 571-588. <https://doi.org/10.1007/s40808-020-00936-1>
- Sarkar, G. (2021). *Changes in agricultural land use scenario in Uttar Dinajpur District, West Bengal* (Doctoral dissertation, University of North Bengal).
- Sengupta, S., Mohinuddin, S., Arif, M., Sengupta, B., & Zhang, W. (2022). Assessment of agricultural land suitability using GIS and fuzzy analytical hierarchy process approach in Ranchi District, India. *Geocarto International*, 37(26), 13337-13368. <https://doi.org/10.1080/10106049.2022.2076925>
- Shaw, S. K., Sravani, N., Sharma, A., & Anand, J. (2025). Assessment of probable zones of agricultural land suitability based on MCDM, probabilistic, and data-driven approach in Krishna District, India. *Environmental Monitoring and Assessment*, 197(3), 1-31.
- Slessarev, E. W., Lin, Y., Bingham, N. L., Johnson, J. E., Dai, Y., Schimel, J. P., & Chadwick, O. A. (2016). Water balance creates a threshold in soil pH at the global scale. *Nature*, 540(7634), 567-569. <https://doi.org/10.1038/nature20139>
- Taghizadeh-Mehrjardi, R., Nabiollahi, K., Rasoli, L., Kerry, R., & Scholten, T. (2020). Land suitability assessment and agricultural production sustainability using machine learning models. *Agronomy*, 10(4), 573. <https://doi.org/10.3390/agronomy10040573>
- Tashayo, B., Honarbakhsh, A., Azma, A., & Akbari, M. (2020). Combined fuzzy AHP–GIS for agricultural land suitability modeling for a watershed in southern Iran. *Environmental Management*, 66, 364-376. <https://doi.org/10.1007/s00267-020-01310-8>
- Tiwari, A., & Ajmera, S. (2020). Land suitability assessment for agriculture using analytical hierarchy process and weighted overlay analysis in ArcGIS ModelBuilder. In *Recent trends in civil engineering: Select proceedings of ICRTICE 2019* (pp. 735-762). Singapore: Springer Singapore. https://doi.org/10.1007/978-981-15-5195-6_56
- Tscharntke, T., Clough, Y., Wanger, T. C., Jackson, L., Motzke, I., Perfecto, I., & Whitbread, A. (2012). Global food security, biodiversity conservation and the future of agricultural intensification. *Biological conservation*, 151(1), 53-59. <https://doi.org/10.1016/j.biocon.2012.01.068>
- Ustaoglu, E., Sisman, S., & Aydinoglu, A. C. (2021). Determining agricultural suitable land in peri-urban geography using GIS and Multi Criteria Decision Analysis (MCDA) techniques. *Ecological Modelling*, 455, 109610. <https://doi.org/10.1016/j.ecolmodel.2021.109610>
- Wang, S., Fu, B. J., Gao, G. Y., Yao, X. L., & Zhou, J. (2012). Soil moisture and evapotranspiration of different land cover types in the Loess Plateau, China. *Hydrology and Earth System Sciences*, 16(8), 2883-2892. <https://doi.org/10.5194/hess-16-2883-2012>
- Yalew, S. G., Van Griensven, A., Mul, M. L., & van der Zaag, P. (2016). Land suitability analysis for agriculture in the Abbay basin using remote sensing, GIS and AHP techniques. *Modeling Earth Systems and Environment*, 2, 1-14. <https://doi.org/10.1007/s40808-016-0167-x>

- Yohannes, H., & Soromessa, T. (2018). Land suitability assessment for major crops by using GIS-based multi-criteria approach in AnditTid watershed, Ethiopia. *Cogent Food & Agriculture*, 4(1), 1470481. <https://doi.org/10.1080/23311932.2018.1470481>
- Zabihi, H., Ahmad, A., Vogeler, I., Said, M. N., Golmohammadi, M., Golein, B., & Nilashi, M. (2015). Land suitability procedure for sustainable citrus planning using the application of the analytical network process approach and GIS. *Computers and Electronics in Agriculture*, 117, 114-126. <https://doi.org/10.1016/j.compag.2015.07.014>
- Zadeh, L. A. (1965). Fuzzy sets. *Inform Control* 8:338–353.
- Zhang, H., & Voss, K. J. (2006). Bidirectional reflectance study on dry, wet, and submerged particulate layers: effects of pore liquid refractive index and translucent particle concentrations. *Applied optics*, 45(34), 8753-8763 <https://doi.org/10.1364/AO.45.008753>
- Zhang, X., Fang, C., Wang, Z., & Ma, H. (2013). Urban construction land suitability evaluation based on improved multi-criteria evaluation based on GIS (MCE-GIS): case of New Hefei City. *Chin Geogr Sci* 23:740–753.
- Zhang, Y. Y., Wu, W., & Liu, H. (2019). Factors affecting variations of soil pH in different horizons in hilly regions. *Plosone*, 14(6), e0218563. <https://doi.org/10.1371/journal.pone.0218563>
- Zolekar, R. B., & Bhagat, V. S. (2015). Multi-criteria land suitability analysis for agriculture in hilly zone: Remote sensing and GIS approach. *Computers and Electronics in Agriculture*, 118, 300-321. <https://doi.org/10.1016/j.compag.2015.09.016>



Assessment of Prevalence of Arsenicosis using TOPSIS Model in Malda District, West Bengal

Debapriya Poddar^{1*} and Sarbari Mukhopadhyay²

¹*Department of Geography and Applied Geography, University of North Bengal,
PO: North Bengal University, Dist: Darjeeling –734013, India*

²*Department of Geography, Maynaguri College, Maynaguri, Jalpaiguri –735224, India*

**Corresponding author: debapriyapoddar2011@gmail.com*

Abstract: The arsenic-contaminated ground water in Malda district is noxious to human health, as people have suffered from arsenicosis issues and numerous socioeconomic drawbacks. Though these difficulties are largely varied with education status and household income. The principal objective of this paper is to investigate the prevalence of inhabitants' knowledge, attitude, and practice about arsenicosis and to assess the relationship of such prevalence with education status and household income. TOPSIS model have applied to determine the level of prevalences. Altogether 19 questions of knowledge (10), attitudes (4), and practice (5) were enquired. TOPSIS results has exhibited the inhabitants have experienced very low (6.67%), low (28.00%), medium (28.33%), high (28.67%) and very high (8.33%) prevalence level. Paired t-test have measured the relationship of prevalence score with education status and household income. This study may assist the health personnel, policy makers, and Government to recognize the vulnerable inhabitants and to develop the healthier decisions regarding these issues.

Keywords: Prevalences, Arsenicosis, TOPSIS, Malda district

Introduction:

The accessibility of uncontaminated water is one of the key elements of any nation's Health and socio-economic development (Cvjetanovic, 1986; Nahar *et al.*, 2008; Das, 2013). Arsenic, a semi-metallic natural element is historically known as poison, arising different kind of diseases, affecting human being, though it is hazardous from long-term perspective. Actually, its toxicity starts from 2 to 20 years (Rana, 2013). The amalgamation of Arsenic in groundwater in Malda

district is the source of water pollution and expansively measured as environmental issue as the water source in Malda district is intensely reliant on groundwater (Madhuvan and Subramanian, 2006). South-western part of Malda district have contaminated with the hazardous level (0.5 mg/lit) of arsenic concentration in groundwater, diminishing its purity through some geogenic and anthropogenic actions. However, Arsenic (As), a toxic mineral, has heterogeneously concentrated in groundwater, extremely varied on spatial and regional scales. The arsenic-contaminated water is severely perilous and toxic to human health, as people have suffered from different health problems and face social and economic drawbacks (Parvez, 2006 and Sarkar, 2010). Such contamination has profoundly affected the individuals and spread through the community levels. The prevalence of different diseases or arsenicosis is firmly allied with age composition, sex composition, educational status, occupational structure, poverty level and economic status of the arsenicosis inhabitants as the socio-economic status and arsenic-related health hazards are strongly correlated. The TOPSIS model have applied to determine the prevalence of arsenicosis to study the level of such prevalence based on the respondents' perception. The level of prevalence of arsenicosis of each sample respondents has been calculated using TOPSIS model for combining all contradictory criteria. Generally household income and literacy rate differ significantly across the study area. The prevalence of arsenicosis have differed with such variation of literacy rate and different household incomes. However, limited research work has focused on prevalence of arsenicosis in India. Still, few research on this subject has done in the neighboring Bangladesh (Mahmood and Halder, 2011; Chaurasia et al. 2012). The School of Environmental Studies group, Jadavpur University (SOES), has also performed a comprehensive research work on 'As' contamination in W.B. Moreover, most of the research work have evaluated the status and sources of groundwater arsenic toxicity (Das *et al.*, 1996; Fazal, 2001; Singh, 2001; Rana, 2013; Bhardwaj *et al.*, 2019), the impact of arsenic contamination on human health only (Samaddar and Subba Rao, 2007; Haq *et al.*, 2012; Mahmood and Halder, 2011; Hoque, 2013; Das, 2013).

On the other hand, the research on emphasizing the socio-economic condition of the arsenicosis patients in West Bengal is inadequate (Mahmood and Halder, 2011; Das and Roy, 2013; Santra, 2017; Majumder and Bhunia, 2022). Although, Madhuvan and Subramanian, 2006; Purkait and Mukherjee, 2008; Panigrahi, 2016; Khanam *et al.*, 2021 have enlightens the scenario of arsenic contamination in Malda district. But the study of prevalence of arsenicosis in Malda district is not studied extensively previously. Hence, the current paper is to attempt to identify the prevalence of knowledge, attitudes and practices about arsenicosis as these are causes of the spread of arsenicosis in the arsenic hit areas of Malda district because there is a clear link between the knowledge, attitudes and practices about arsenicosis and arsenic exposure. Moreover, none of the research work have applied TOPSIS model to measure the prevalence level of knowledge, attitudes and practices about arsenicosis. Therefore, it is an urgent need for investigation and analysis on this crucial aspect. So, the principal objective of this paper is to study the prevalence of inhabitants' knowledge, attitude, and practice about arsenicosis issue using the TOPSIS model. It is necessary to take a holistic view of this issue and view it from a policy perspective.

2. Materials and methods:

2.1 Study area:

Malda (24°30'N to 25°32'N and 87°48'E to 88° 30'E) is an arsenic prone district of West Bengal covering an area of 3566.17 Km². It is demarcated by Jharkhand in the west, Bangladesh in the east and Murshidabad district in the southern segment of Malda. The district contains of two subdivisions i.e., Malda Sadar and Chanchal. On the other hand, Malda Sadar subdivision comprised of two municipality i.e., English Bazar and Old Malda municipality and 15 blocks. Seven blocks of them are arsenic contaminated (Figure 1). Generally, the district is characterized with low plain area slanting from north to southward direction. Alluvial soil is the most dominating soil of this district, originating from the rivers of Ganga, Kalindri, Tangon, Punarbhaba, and Mahananda. The maximum Arsenic concentration level in shallow tube wells in Malda district varies from 0.072 mg/l to 0.929 mg/l (Source: PHE, Malda, 2018).



Figure 1. Location of High and low 'As' concentrated blocks of Malda district

2.2 Data sources:

Principally primary data have used in present research work. The desired data have collected through the survey, conducting in the arsenic-contaminated regions in the study area depending on questionnaire method. Multi-stage random sampling method is performed to detect the study areas. At first, the arsenic contaminated blocks and villages have diagnosed based on the secondary sources. Secondly, sample villages have detected randomly with the help of random table. Next stage of sampling, arsenic-contaminated households was selected, and the expected sample was evaluated through the Cochran's method (Cochran, 1963) and lastly, 300 respondents have considered.

3. TOPSIS method:

The Technique for Order Preference by Similarity to an Ideal Solution (TOPSIS) has generally been applied to resolve multicriteria decision making (MCDM) problem (Balezantis et al. 2020). This technique is based on the Euclidean distance of decision-making alternatives (Khosravi *et al.*, 2019). The prime objective of this method is to find the best alternatives among many. The TOPSIS model determined the prevalence of arsenicosis on the basis of respondents' perception. To study the sample participant's knowledge, attitude and practices regarding arsenicosis issue, a total of 10, 4, and 5 criteria are measured, respectively. Correspondingly, awareness of respondents is also appraised and evaluated by six criteria. Then these criteria are categorized into two groups, beneficial and non-beneficial, and an equal weight (0.042) has been assigned to each criterion. The Euclidean distance from ideal best (S^+) and ideal worst (S^-) has been calculated for each criterion. Finally, the performance score (P_i) of the level of their prevalence about arsenicosis was calculated, where a lower value indicates poor condition and a higher value indicates the good prevalence of arsenicosis. The TOPSIS technique is used to find out the rank of the several discrete criteria. The TOPSIS technique is based on following steps.

The steps to implementation of the TOPSIS approach are as follows: Initially, the ratings of the criteria are assigned along with their alternatives. This method used vector data normalization V_{ij}^- , which is calculated as:

$$V_{ij} = \frac{V_{ij}}{\sqrt{\sum_{i=1}^n v_{ij}^2}}$$

Where V_{ij}^- is the vector normalization value of the i^{th} indicator of j^{th} attribute. Using TOPSIS method, the ideal best (x_j^+) and ideal worst value (x_j^-) are calculated using the following formulae:

$$x_j^+ = \{x_1^+, x_2^+, \dots, x_m^+\}$$

$$x_j^+ = \left\{ \left(\max \max x_{ij} \mid j \in \right), \min \min x_{ij} \mid j \in I^{ii} \right\}$$

$$x_j^- = \{x_1^-, x_2^-, \dots, x_m^-\}$$

$$x_j^- = \left\{ \left(\min x_{ij} \mid j \in I^i \right), \max \max x_{ij} \mid j \in I^{ii} \right\}$$

Where I^i is the beneficial criteria, I^{ii} is the non-beneficial criteria.

Then Euclidian distance S_i^+ between each criterion and ideal best (x_j^+) and Euclidean distance S_i^- between each criterion and ideal worst (x_j^-) are calculated as

$$S_i^+ = \sqrt{\sum_{j=1}^m (x_{ij} - x_j^+)^2}$$

$$S_i^- = \sqrt{\sum_{j=1}^m (x_{ij} - x_j^-)^2}$$

Finally, the performance Score (c_i) of the TOPSIS method is calculated using:

$$c_i = \frac{S_i^-}{S_i^+ + S_i^-}$$

The lowest score (c_i) represents the worst performance. The resulted TOPSIS value were categorized in to five classes as very low, low, medium, high, and very high prevalence.

Moreover, to assess the relationship of prevalence of arsenicosis with education status and household income paired t-test has been performed.

3 Prevalence of arsenicosis in the study area:

Scantiness of proper knowledge of arsenic toxicity may cause to several diseases and deaths (Hadi, 2003; Parvez, 2006). The attitudes and practices of individuals about arsenicosis issues have enhanced the hazardous condition of arsenic contamination. Proper knowledge, attitudes, and practice about arsenicosis have diminished the harshness of such disease and sustain the socio-economic condition of the victimized in the contaminated regions. Moreover, the awareness of arsenicosis is also vigorous for adopting some approaches that could possibly shrink the exposure to arsenic poisoning. Without proper knowledge of the adverse health effects of arsenic pollution and mitigation options, inhabitants will not be encouraged to maintain some intervention initiatives, organized by Government and non-Government organizations. Consequently, the individuals' attitudes and practices on arsenicosis have widely influenced the susceptibility of arsenicosis. Though the maximum percentage of the respondents know, arsenicosis is a curable, noncontagious disease and not ever influenced by heredity (Table 1). Moreover, about 65.00% of the respondents have an adequate knowledge regarding the persisting places of arsenic and the development process of arsenicosis ailments. Most of them (59.00%) have believed, victims should require proper medical care. On the other hand, though, 76.51% of respondents knew, water testing is only way to determine the contamination level of arsenic in tube well water but surprisingly only 30.67% of sample

respondents have identified their usable water is safe or not, undoubtedly representing their unawareness attitudes. At the same time, they have attained few miss-concept in some queries as approximately 44.33% respondents have still believed, arsenicosis is a contagious disease. Moreover, nearly 80% respondents do not have knowledge about the role of nutritious diet in preventing the arsenicosis disease, knowing only 17.67% of respondents.

Table 1. Prevalence of knowledge about arsenic contamination in the sample respondents in the study area

SI No.	Knowledge	Number of the respondents (n)	Prevalence (%)
1	Did not accept arsenicosis is curable	109	36.33
2	Did not trust arsenicosis is nothereditary origin	110	36.67
3	Knew the persisting place of arsenic	195	65.00
4	Knew the developmental process of arsenicosis	196	65.33
5	Did not accept arsenicosis is contiguous	167	55.67
6	Knew the preventive power of nutritious diet	53	17.67
7	Crucial to seek medical treatment if one needed	177	59.00
8	Knew usable water was safe	92	30.67
9	Knew, water testing determined the contamination level testing	215	76.51
10	Alternative source	227	75.67

Source: Household survey, 2019

Furthermore, about 91.33% respondents in Malda district have required substitute of non-polluted water to sink the adverse health effect of ‘As’ contaminated water. However, only 49.33% respondents decided to abandon the arsenic contaminated water source. (Table 2). At the same time, 50.67% arsenicosis sufferers have consumed arsenic contaminated water while knowing the severity of arsenicosis as they have attained don’t care attitude to arsenicosis issues. However, 60.67% of the study participants have favored to medical care after arising arsenicosis symptoms but in contrast, about 39.33% inhabitants have not still desired to any medical treatment. Moreover, only 47.33% respondents do not treat the arsenicosis patients as ostracized, but still more than 50% of the respondents are attaining few unexpected attitudes. In Bangladesh, arsenicosis patients are also the worst victims of ostracism (Rahaman *et al.*, 2018).

Table 2. Prevalence of attitudes about arsenic contamination in the sample respondents in the study area

SI No.	Attitude	Number of the respondents (n)	Prevalence (%)
1	Abandon the contaminated water source	148	49.33
2	Seek alternative source if contaminated	274	91.33
3	Would seek medical care when symptoms appeared	182	60.67
4	Should not ostracize arsenicosis patient	142	47.33

Source: Household survey, 2019

After arising the symptoms of arsenicosis ailments, about 76.67% respondents desired to examine their water sources while, remaining's are not concerned to investigate the arsenic contamination level in their water sources till now. So, huge number of sample respondents (57%) consumed 'As' contaminated water as they are extremely insensible about the hazardous impact of the consumption of arsenic-contaminated water. Furthermore, around 65% respondents have not participated in awareness raising programme and only 17.33% of respondents would attend the arsenic clinic if required as they are immensely uncaring about such vulnerable conditions. Though, 97.67% sample participants talked with the health workers during the home visit.

Table 3. Prevalence of practice about arsenic contamination in the sample respondents in the study area

SI No.	Practice	Number of the respondents (n)	Prevalence (%)
1	Agree to test water source	230	76.67
2	Used safe water	130	43.33
3	Interacted with awareness program	106	35.33
4	Agree to talk with health workers during the home visit	293	97.67
5	Would attend arsenic clinic, if required	52	17.33

Source: Household survey, 2019

3.1 Relationship between prevalence of knowledge, attitudes, and practice concerning arsenicosis issues with education status and income level:

Prevalence of knowledge, attitudes, and practice concerning arsenicosis issues is related with socio-economic condition of the respondents where, education status and income level have a

great impact on this. Henceforth, it is crucial to assess the education status and income level of the respondent. In the study area about 47.33% respondents have not achieved formal education. Only 10.33%, 9.33% and 10% of respondents have passed the upperprimary level, M.P and H.S standards respectively. Besides, very little proportion of the respondents have completed the graduation (17.67%) and post-graduation degrees (5.33%). Based on the study of the education level in Malda district, more vulnerable group of arsenicosis respondents are illiterate (Table 4).

Table 4. Education status of respondents in the study area

Educationstatus	Number of the respondents(n)	Percentage (%)
Illiterate	142	47.33
Upper primary	31	10.33
M.P	28	9.33
H. S	30	10.00
Graduate	53	17.67
Postgraduate	16	5.33

Source: Household survey, 2019

3.2 Respondents' income level:

The study of arsenicosis patients' income level is significant as prevalence of knowledge, attitudes, and practice level varied with it. Almost 31.65% of respondents have earned >Rs 6000 per month as they are unable to spend money for installation of arsenic-free water supply sources and also unable to purchase arsenic-free water daily. Unexpectedly, the respondents (30.94%) with monthly income of < Rs 25000 are also suffered from arsenicosis due to consumption of arsenic contaminated water for long period. However, some arsenicosis patients (37.41%) in Malda district, have earned about Rs 6000-25000 (Table 5) still they have compelled to use their tested arsenic-contaminated tube wells' water as the long distance of arsenic-free water supply source from their habitation, and also suffering from irregular supply of arsenic-free safe- water.

Table 5. Monthly income of sample respondents in the study area

Monthly income	Number of the respondents (n)	Percentage (%)
<6000	88	31.65
6000-25000	104	37.41
>25000	86	30.94

Source: Household survey, 2019

3.3 Assessment of prevalence of arsenicosis using TOPSIS method:

The prevalence level of arsenicosis of each sample respondents has been calculated using TOPSIS model for combining all contradictory criteria. The obtained TOPSIS results of prevalence level among the respondents are categorized into five classes, namely Very low (value <0.2), Low (value 0.2 - 0.3), Medium (value 0.3 - 0.4), High (value 0.4 - 0.5), and Very High (value >0.5) (Table 6).

3.3.1 Very high prevalence level of knowledge, attitudes, and practice concerning arsenicosis issues in the sample respondents:

Very high prevalence level has prevailed among 8.33% of respondents, attained a score of >0.50. Maximum respondents of this group are the inhabitant of Ratua-I block which contained relatively low arsenic concentration i.e., 0.497 mg/l and only one village of Haripur Gopi of Kahala Gram Panchayet is arsenic contaminated. So, the respondents of this block have been less vulnerable. Likewise, rarer respondents of this group live in Kaliachak-III block, though, it is highly arsenic contaminated (0.92 mg/l). Perhaps they have kept themselves from the use of such contaminated water based on their awareness level, perception level, literacy level as some of them have passed M.P standard or a few have acquired post-graduation degrees. Thus, they are not influenced by any local unscientific allegory about arsenicosis. Moreover, they are so cognizant, as they have permanently attained in all the Govt programs for obtaining knowledge about how to avoid these environmental issues. Besides, they have frequently purchased arsenic-free water for consuming purpose, since, they are able to keep themselves safe from arsenic contamination as all of them belonged to either the medium income group or wealthy groups having an income of Rs 15000 to Rs 150000 doing government service or business.

3.3.2 High prevalence level of knowledge, attitudes, and practice concerning arsenicosis issues in the sample respondents:

At the same time, about 28.67% respondents of Bangitola and Rathbari GP of Kaliachak-II block, Sahabajpur GP of Kaliachak-III block (0.92 mg/l), Amriti GP of English bazar block (0.61 mg/l), Silampur GP of Kaliachak-I block (0.81 mg/l), Mohongange of Ratua-I block (0.497 mg/l), Gobarjana GP of Ratua II blocks (0.07 mg/l) (0.1%) have experienced high

prevalence level. Except for Ratua-I and Ratua-II blocks, all the blocks are highly arsenic-contaminated. All the respondents with high prevalence level are literate, either they have acquired graduation or post-graduation degrees, since their awareness level is high and attained some explicit knowledge about the source, nature of Arsenic as well as complete information of these issues and all have practiced the normal behaviors with the arsenicosis patients. Moreover, maximum patient belonged to middle-income, higher middle-income, and wealthy group of poverty classes. Hence, they are able to buying arsenic-free water regularly for evading the harmful effect of arsenic-contaminated water. Amazingly, some illiterate participants from Ratua-I and Ratua -II blocks have experienced high prevalence level as they are motivated with prevailing surroundings and become aware of this matter. They also try to understand the actual source and nature of arsenicosis illnesses.

3.3.3 Medium prevalence level of knowledge, attitudes, and practice concerning arsenicosis issues in the sample respondents:

Moreover, medium prevalence level has observed among 28.33% of respondents, lived in Kaliachak-II are literate, passing upper primary, M.P or H.S. level as educated individuals can shirk the different superstitious believe regarding this issue and always attempted to explain all the matters rationally. Though, very small proportion of respondents of this group have no formal education. On the other hand, some respondents of this group are able to purchased arsenic free water on regular basis as they belonged to higher middle-income group but they still used the contaminated water as they are highly unaware and believed in some missed concepts about this issue, avoiding all the social problems associated with arsenicosis because, the severe result of Arsenic contamination has not appeared instantly; rather arisen after a long period. Similarly, some respondents from Enaetpur G.P and Manikchak G.P of Manikchak block, Silampur-2 G.P and Nawada Jadupur G.P from Kaliachak-I blocks have completed graduation or post-graduation degrees and belong to middle-income group. Based on their education status, their prevalence level should be high, but they are incredibly unaware and have not proper knowledge rather they are influencing by irrational views prevailed in their society. Some female populations from this block have same problem as they are poor and illiterate. On the other hand, most of the respondents of the medium prevalence level from Amriti G.P of English bazar have ignored all the arsenicosis issues due to lack of literacy and poor financial condition as they are achieving only upper primary level and several are illiterate belonging the poor and very poor income groups. However, only one respondent from the Ratua-II block has experienced the medium prevalence level, obtained graduation degree, and belonged to the middle-income group since, his prevalence level is not still high as he is not aware of and disregards this local problem.

3.3.4 Low prevalence level of knowledge, attitudes, and practice concerning arsenicosis issues in the sample respondents:

About 28.00% of respondents have attained low prevalence level, scoring 0.2 - 0.3. The participants of this group are the residents of Bangitola G.P, Rathbari G.P of Kaliachak-

II, Enaetpur G.P, and Manichak G.P of Manikchak, Kaliachak-III, English Bazar, and Kaliachak-I block. Maximum proportion of the respondents of this group lived in Kaliachak-III block. Few female populations were observed at Enaetpur G.P of Manickchak, English Bazar, and Kaliachak-I block. Though, individuals of this group lived at different blocks, but their education level and poverty level are almost same. All have belonged to very poor, poor, and lower- middle-income group. These poverty levels specified, respondents' financial condition is meager since they don't want to spend their incomes in purchasing arsenic-free water and health checking purposes. On the other hand, most of the respondents of this group are illiterate. Some of them have passed only the upper primary level. No respondents in this group lived in the Ratua-I and Ratua-II blocks.

3.3.5 Very low prevalence level of knowledge, attitudes, and practice concerning arsenicosis issues in the sample respondents:

Very low prevalence level has prevailed among 6.67% respondents obtaining a score of <0.2. Large number of participants from Rathbari GP of Kaliachak-II block have no formal education. Occupationally they are farmer, and daily laborers, since their poverty level is poor and very poor. Only one of them has passed M.P standards and one has H.S level, lived in higher middle-income group. Likewise, four respondents from Enaetpur G.P of Manikchak block have qualified graduation degrees and doing Govt service belong to higher middle-income group. However, their prevalence level is very low; as they motivated with their surroundings and wants to be rigid in their views. Moreover, few females from Kaliachak -II are unemployed and live in poor and very poor income group. But, three female respondents from Silampur-II G.P of Kaliachak-I block have passed M.P standard, but they belonged to very low prevalence level.

Table 6. Percentage of prevalence level among respondents using TOPSIS model

Performance score	Prevalence level	Frequency	Percentage (%)
<0.2	Very low	20	6.67
0.2 - 0.3	Low	84	28.00
0.3 - 0.4	Medium	85	28.33
0.4 -0.5	High	86	28.67
>0.5	Very high	25	8.33

4.The relationship of prevalence of arsenicosis with education status and monthly income:

Accordingly, the respondents with different prevalence (knowledge, attitudes, and practice concerning arsenicosis issues) level (Very low, Low, Medium, High and Very High) were

lived in different contaminated villages of different contaminated block in Malda district and such prevalence level is varied with education status and household monthly income. To assess the relationship between prevalence score and education status and between prevalence score and household income, paired t-test has been performed. In the first paired between performance score of prevalence and educational status, the 't'-statistic is -16.41 with degree of freedom of 299. The corresponding two-tailed p value is 0.00, which is less than 0.05. So, we can conclude that the mean difference of the prevalence of arsenicosis and education status is different from 0. On the other hand, second paired between the performance score of prevalence and household income, the corresponding t-statistic is -17.80, and the two-tailed p-value is 0.00. The mean paired difference is very high (Mean -20774) with very high variability (Std error mean. 1167). So, in the case of the second paired mean difference is also different from 0. Therefore, the prevalence of arsenicosis varies with educational status and monthly household income of respondents.

Table 7. Paired Sample Test

Paired	Mean	Std. Deviation	Std. Error Mean	t	Sig. (2 tailed)
Between Performance score and Education status	-6.16	6.51	0.38	-16.41	0.00
Between Performance score and Household income	-20774	20214	1167	-17.80	0.00

Conclusions:

Arsenicosis is discernibly influenced by education status and income status of the inhabitants. Prevalence of knowledge, attitude and practice regarding arsenicosis as well as arsenic contamination varied from one person to another person. Some of them have limited knowledge as arsenicosis is contagious, non-curable diseases and also a heriditical origin. Moreover, they have not specific knowledge concerning the persisting places of 'As' and the progressive procedure of arsenicosis ailments. Incredibly, very little proportion of the inhabitants have known the precautionary power of nutritious food on arsenicosis and avoided any medical treatment based on their ignorance attitudes against the environmental issues. Unpredictably, some of them are uninformed about their usable water is safe or not. While most of them have sought an alternative source of safe water, but only small proportion of respondents agreed to abandon the contaminated water source. Moreover, few hazardous people have still used the contaminated water after knowing the severe condition of arsenicosis and unexpectedly arsenicosis patients have treated as ostracized in modern-day. Besides, very little proportion have attained some awareness programs as they are highly conscious for disabling the vulnerability. Hence, the knowledge, attitudes, and practice on arsenicosis are diverse in nature, varying with education status and household monthly income of the population. However, all the respondents of very high, high, medium, low and very low prevalence level have lived in all the arsenic contaminated block in study area but such level differs from

one respondent to the other respondents, as their education level and monthly income level varies significantly. The respondents with very high prevalence level are exceedingly aware as they are highly literate and able to evade some superstitions regarding this issue and critic all the matters rationally. Moreover, they are able to purchased arsenic free water regularly as they belonged to higher-middle income group to higher income group. Due to the same reason (High literacy, middle to high income, high awareness level) 28.67% of respondents have obtained high prevalence level. Though sometimes literate people have attained medium prevalence level as they are highly unaware about arsenicosis; influenced by some irrational views prevailing in their surroundings. On the contradiction, in several times illiterate persons have experienced high prevalence level, influenced by their existing circumstances. Afterall, persons of medium to very low prevalence level are comforted with predominated irrational beliefs and some missed concepts about such environmental issues, since disregarding all the social and governmental initiatives against these difficulties and also incapable to maintain the needed steps for abolishing the arsenicosis problems. The poverty levels specify, the villager's financial ability to purchase arsenic-free water and continue the health checking procedure as it's beyond their economic capacity. Finally household income and literacy rate differ significantly across the study area and prevalence level varied from one person to another person.

References:

- Balezantis, T., Chen, X., Galnaityte, A., & Namiotko, V. (2020). Optimizing crop mix with respect to economic and environmental constraints: An integrated MCDM approach. *Science of The Total Environment*, 705, 135896.
- Bhardwaj, A., Rajput, R., & Misra, K. (2019). Status of arsenic remediation in India. In *Advances in water purification techniques* (pp. 219-258). Elsevier.
- Chaurasia, N., Mishra, A., & Pandey, S. K. (2012). Fingerprint of Arsenic contaminated water in India—A review. *J. Forensic Res*, 3(10). 51-67.
- Cvjetanovic, B. (1986). Health Effects and Impact of Water Supply and Sanitation, *World Health Statistics Quarterly*, 39(1), 105-117.
- Das, A. (2013). Socio-Economic and Gender aspects of Arsenicosis- A Case study in Rural West Bengal, *Journal of Humanities and Social Science*, 13(7), 74-83. Hadi, A., & Parveen, R. (2004). Arsenicosis in Bangladesh: prevalence and socioeconomic correlates. *Public Health*, 118(8), 559-564.
- Das, A., & Roy, J. (2013). Socio-economic fallout of arsenicosis in West Bengal: a case study in Murshidabad District. *J. Indian Soc. Agric. Stat*, 67, 267-78.
- Das, D., Samanta, G., Mandal, B. K., Chowdhury, T. R., Chanda, C. R., Chowdhury,
- Fazal, M. A., Kawachi, T., & Ichion, E. (2001). Extent and severity of groundwater arsenic contamination in Bangladesh. *Water International*, 26(3), 370-379.

- Haq, I., Hanif, W., Hasnain, G., & Durez, S. (2012). Socio-economic impacts on human life in Arsenic affected area of Basti Rasul Pur, Rahim Yar Khan, Pakistan. *Sustainable Agriculture Research*, 1(526-2016-37841).
- Hoque, S. R. (2013). A Study on Awareness about Arsenic Pollution in Rural West Bengal. *International Journal of Humanities and Social Science Invention*, 2, 43-46.
- Khanam, R., Hazra, G. C., Ghosh Bag, A., Kulsum, P. G. P. S., Chatterjee, N., & Shukla, A. K. (2021). Risk Assessment of Arsenic Toxicity Through Groundwater-Soil-Rice System in Malda District, Bengal Delta Basin, India. *Archives of environmental contamination and toxicology*, 81(3), 438-448.
- Khosravi, K., Shahabi, H., Pham, B. T., Adamowski, J., Shirzadi, A., Pradhan, B., ... & Prakash, I. (2019). A comparative assessment of flood susceptibility modelling using multi-criteria decision-making analysis and machine learning methods. *Journal of Hydrology*, 573, 311-323.
- Madhavan, N., & Subramanian, V. (2006). Factors affecting arsenic concentration in groundwater in West Bengal. *Environmental Chemistry Letters*, 4(2), 79-82.
- Mahmood, S. A. I., & Halder, A. K. (2011). The socio-economic impact of Arsenic poisoning in Bangladesh. *Journal of Toxicology and Environmental Health Sciences*, 3(3), 65-73.
- Mazumder, D. N. G., Ghosh, A., Majumdar, K. K., Ghosh, N., Saha, C., & Mazumder, N. (2008). Health and socio-economic effects of groundwater arsenic contamination in rural Bangladesh: new evidence from field surveys. *Journal of Environmental Health*, 70(9), 42-47.
- P. P., & Chakraborti, D. (1996). Arsenic in groundwater in six districts of West Bengal, India. *Environ Geochem* 18 (1), 5-15.
- Panigrahi, S. (2016). Groundwater Arsenic Contamination: A Study of Malda District of West Bengal, India. *Imperial Journal of Interdisciplinary Research*, 2(8), 742 -747.
- Parvez, F., Chen, Y., Argos, M., Hussain, A. I., Momotaj, H., Dhar, R., ... & Ahsan, H. (2006). Prevalence of arsenic exposure from drinking water and awareness of its health risks in a Bangladeshi population: results from a large population-based study. *Environmental health perspectives*, 114(3), 355-359.
- Purkait, B., & Mukherjee, A. (2008). Geostatistical analysis of arsenic concentration in the groundwater of Malda district of West Bengal, India. *Frontiers of Earth Science in China*, 2(3), 292-301.
- R. N. G. (2010). Arsenic contamination of groundwater and its health impact on the population of the district of Nadia, West Bengal, India. *Indian journal of community medicine: official publication of Indian Association of Preventive & Social Medicine*, 35(2), 331.
- Rahman, M. A., Rahman, A., Khan, M. Z. K., & Renzaho, A. M. (2018). Human health risks and socio-economic perspectives of arsenic exposure in Bangladesh: a scoping review. *Ecotoxicology and environmental safety*, 150, 335-343.

- Rana, M.J. (2013). Arsenic contamination of West Bengal, with reference to Malda district. *International Journal of Scientific Research*, 2 (2), 166-169.
- Samadder, S. R., & Subbarao, C. (2007). GIS approach of delineation and risk assessment of areas affected by arsenic pollution in drinking water. *Journal of Environmental Engineering*, 133(7), 742-749.
- Santra, B. K. (2017). Arsenic contamination of groundwater in West Bengal: awareness for health and social problems. *International Journal of Applied Science and Engineering*, 5(1), 43-46.
- Sarker, M. (2010). Determinants of arsenicosis patients' perception and social implications of arsenic poisoning through groundwater in Bangladesh. *International journal of environmental research and public health*, 7(10), 3644-3656.
- Sing, A.k. (2001). Arsenic Contamination in Groundwater of North-Eastern India. *International Water Resources Association*, 21(1), 50-58.



Rainfall Trend and its Variability Analysis of a Sub-tropical Rainfall River Basin

Asraful Alam¹, Md. Mofizul Hoque^{1*}, Jayanta Das¹, Aznarul Islam²

¹*Department of Geography, Rampurhat College, Rampurhat, Birbhum –731224*

²*Department of Geography, Aliah University, Kolkata –700014*

**Corresponding author: mofizul.10@gmail.com*

Abstract: Rainfall trends and variability analysis are very crucial from the perspective of climate change and sustainable water resources management. In the present study, they are analysed using Coefficient of Variation (CV), Rolling Standard Deviation (Rolling SD), Modified Mann-Kendall (MMK) test, Sen's Slope (SS), Pettitt's test and anomaly analysis based on district-wise annual rainfall data for 123 years from 1901 to 2023. The average annual rainfall varies from 1151.07 to 1584.13 mm, with a mean of 1318.27 mm. It is also found that the average annual rainfall is higher in the lower Damodar River Basin (DRB) than in the upper DRB. The CV indicates that the average annual rainfall variability is lower in the basin area. In addition, the rolling SD reveals that interannual rainfall variability has increased after the 1960s in the DRB. The MMK test and SS estimators reveal a negative trend in annual rainfall in the basin area, and a decreasing trend in the upper part of the basin. Pettitt's test indicates that the trend in annual rainfall in the upper part of the basin has shifted significantly after the 1990s, except in the Ramgarah, Giridih, and Dhanbad districts. The rainfall anomaly analysis shows that the negative anomaly trend has increased after 2000, indicating that the trend of drought-like situations has increased after 2000 in the basin area. The research work can be helpful for climate change adaptation and sustainable water management, effective agricultural planning, flood management and disaster risk reduction.

Keywords: Damodar River Basin; Modified Mann-Kendall; Rainfall anomaly analysis; Rainfall trend; Rolling SD; Sen's Slope

1. Introduction:

Rainfall is a crucial element of the climate that shapes the spatio-temporal pattern of water resources in an area or region (Kamble *et al.*, 2020). It is an important factor and active agent that shapes the Earth's surface. It influences agriculture and food security, hydrology and flood and drought risk, vegetation, soil erosion, and biodiversity (Saikh *et al.*, 2023). Rainfall is a critical water source for many uses, including agricultural, industrial, domestic and ecological water use (Fan *et al.*, 2025). However, uneven spatial and temporal distribution results in water shortages in some regions in some years (Kenabatho, 2025). Analysing rainfall trends and variability is vital in the context of climate change and sustainable water resources management (Ogunbode *et al.*, 2022). This analysis is a significant and effective tool for planning and water resources management in a region (Kumar *et al.*, 2023). Climate change is a global issue caused by several human activities (Comia *et al.*, 2025). It affects hydroclimatic variables such as precipitation, temperature, stream flow and extreme hydrometeorological events (Prakash and Chembolu, 2025). It raises the risk of water-related disasters (Chukwuma, 2025; Ishiwatari, 2025). It affects both human society and natural ecosystems. Rainfall pattern changes due to climate change and rising temperatures, which are also linked to it (Kumar *et al.*, 2023). Several studies have shown that precipitation patterns change over different time periods. Significant changes in rainfall patterns have amplified water pressure in many areas (Kenabatho, 2025). Thus, rainfall trend analysis is a significant step for addressing the climate change impact on water and food security and mitigating the impacts of climate change (Aditya *et al.*, 2021).

The tropical or sub-tropical regions are the most vulnerable due to climate change and the complex interaction among the oceans, land and atmosphere (Aditya *et al.*, 2021). India is affected and challenged by climate change, particularly its forests and agriculture (Kumar *et al.*, 2023). The Indian climate is mainly influenced by the south-west and north-east monsoonal regimes (Rao *et al.*, 2020). Droughts and floods are common phenomena in India (Subrahmanyam, 1988; Mujumdar *et al.*, 2020). The Damodar River Basin (DRB) lies in the eastern part of India, faces droughts and several devastating floods, and is influenced by the Indian monsoonal regimes (Bhattacharyya, 2011). Several devastating floods occurred in the basin area before the Damodar Valley Corporation (DVC). In this context, DVC plays a crucial role in controlling floods and mitigating the impacts of drought and floods in the basin area through sustainable water resource management by dams and barrages (Hoque *et al.*, 2022a). However, in recent decades, floods in the basin area have been a common issue due to the loss of water-holding capacity of DVC dams. Siltation in the reservoirs, climate change and anthropogenic activities are the major issues in the basin area. Moreover, stress on water resources (both surface and groundwater) increases due to over-exploitation for urban-industrial growth and agricultural expansion. Hence, rainfall trend analysis in the basin area is vital for mitigating the impacts of climate change and planning for sustainable water resources management. Therefore, the main purpose of the study is to analyse rainfall trends and variability using long-term rainfall data.

2. Database and methodology:

2.1 Study area:

The Damodar River Basin (DRB), is a sub-basin of the river Ganga lies in eastern India (Figure1a) (Hoque and Islam, 2024). It covers an area of 23,370.98 km² and extends from 84°30'E to 88°15'E and from 22°15' to 24°30'N in the Jharkhand and West Bengal states (Ghosh *et al.*, 2022). The basin experiences moist sub-humid climatic conditions (Hoque *et al.*, 2022b). The average annual rainfall is 1335 mm, and 82% falls during the monsoon period (June to September) (Ghosh *et al.*, 2016). The highest temperatures occur in May and June, when the maximum reaches 42°C in summer, while December and January are the coldest months, with a mean of 26°C. Mean relative humidity ranges from 40% in March, April and May to 80% from July to September (Chandra, 2003). The upper basin lies on the Chotanagpur plateau, while the lower basin lies on the Ganga-Damodar depositional plain, also known as the para deltaic surface (Islam *et al.*, 2023). The basin is home to numerous mineral resources, industries and mining activities, with a dense population (Hoque *et al.*, 2025). The basin has a population of 17.25 million, with a population density of 738 persons per Km² (Census, 2011).

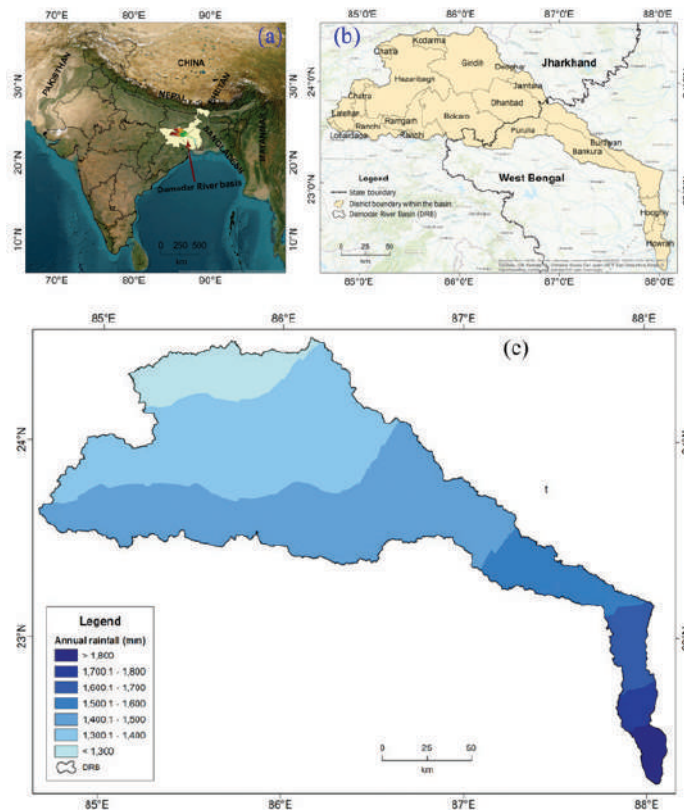


Figure 1. Location map of the study area, (a) DRB in the eastern part of India, (b) Districts in the DRB, and (c) Distribution of annual rainfall in the DRB during 2011-2020.

2.2 Data and Methodology:

A total of 123 years of rainfall data from 1901 to 2023 has been gathered for the present investigation. A district-wise annual rainfall data in the basin area is collected for this study. A total of 18 districts' rainfall data, i.e., 12 in Jharkhand and 6 in West Bengal, lie in the basin area, used for the present study. The detailed methodological procedure of the present study is shown in Figure 2.

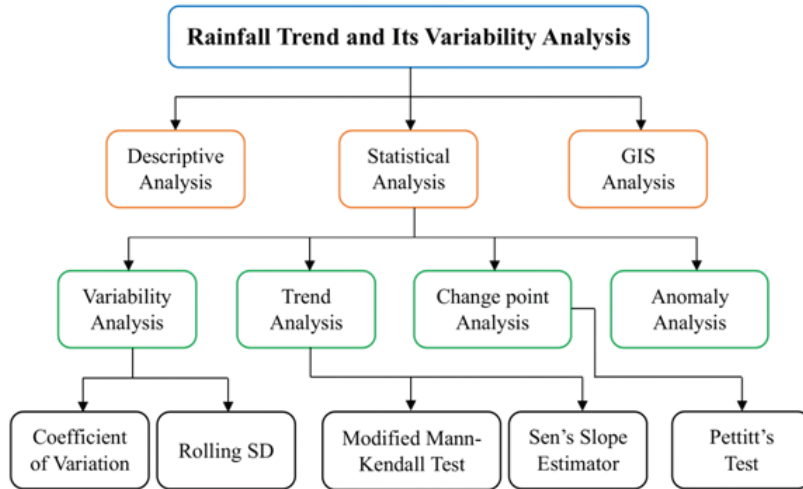


Figure 2. Methodological flow chart of the present investigation.

2.2.1 Variability test of rainfall:

2.2.1.1 Rolling Standard Deviation (Rolling SD);

A rolling standard deviation (rolling SD) is used to measure the volatility of a data set over a moving window of time. It recalculates the standard deviation for a given period instead of calculating a value for the entire data set as new data points arrive. It is computed using Eq. 1.

$$\sigma_{rolling} = \sqrt{\frac{\sum_{i=t-n+1}^t (x_i - \bar{x})^2}{n-1}} \quad (1)$$

Where n is the window length. x_i is each data point within the current window. \bar{x} is the simple moving average of the current window. t is the current time index.

2.2.2 Analysis of the trend:

2.2.2.1 Mann-Kendall (MK) Test:

The Mann–Kendall (MK) test is commonly used to evaluate trends in hydroclimatic studies (Das *et al.*, 2021). It is computed by using Eq. 2 (Mandal *et al.*, 2025).

$$\text{Var}(S) = \frac{n(n-1)(2n+5)}{18} \cdot \frac{n}{n_s^*} \quad (2)$$

2.2.2.2 Modified Mann-Kendall (MMK) Test:

It is a nonparametric technique for identifying trends in time-series data (Hamed and Rao, 1998). It replaces the standard MK test of variance (Var(S)) for autocorrelation, ensuring more accurate trend detection in time-series data (Ranjan *et al.*, 2023). It employs ± 1 continuity correction to reduce the effect of trend (Kumar *et al.*, 2023). It is computed by using Eqs. 3-4 (Mandal *et al.*, 2025).

$$\frac{n}{n_s^*} = \left[1 + \frac{2}{n(n-1)(n-2)} \times \sum_{i=1}^{n-1} (n-i)(n-i-1)(n-i-2)\rho_s(i) \right] \quad (3)$$

Where ρ_s is the rank autocorrelation function of the data. It is determined based on the autocorrelation between observation ranks.

$$\rho(i) = 2 \sin \left(\frac{\pi}{6} \rho_s(i) \right) \quad (4)$$

2.2.2.3 Sen's Slope (SS):

It is a nonparametric technique for estimating the slope of a trend in a time series of data pairs (Gupta and Verma, 2023). It estimates the median slope across all pairs of data points using simple linear regression. It is computed using Eq. 5.

$$Q_i = \frac{x_j - x_k}{j - k} \text{ for all } k < j \quad (5)$$

Where x_j and x_k are data values at times j and k .

Sen's slope estimator (Q). It is calculated using Eqs. 6 or 7.

$$\text{If } N \text{ is odd: } Q_{med} = \frac{Q_{N+1}}{2} \quad (6)$$

$$\text{If } N \text{ is even: } Q_{med} = \frac{1}{2} \left(\frac{Q_N}{2} + \frac{Q_{N+2}}{2} \right) \quad (7)$$

2.2.3 Analysis of the change point:

The Pettitt's test is a rank-based nonparametric arithmetic test used to identify change points existing in a data series (Conte *et al.*, 2019). It is broadly used in hydrological analysis and climate change (Mallakpour and Villarini, 2016). In the present study, it is used to detect a sudden change in the rainfall record. It is computed using Eq. 8 with the help of Eqs. 9 and 10.

$$V_k = 2 \sum_{i=0}^n m_i - k(n+1) \quad (8)$$

Where m_i denotes the rank of the i^{th} observation and k values from 1, 2, 3, ..., n .

$$K_n = \max |V_k| \quad (9)$$

A transition point occurs when V_k reaches a series maximum value K (Eq. 8). The statistical change point (SCP) test is then demarcated by solving Eq. 9.

$$K_{\alpha} = \left\{ -1n \alpha (n^3 + n^2 / 6) \right\}^{1/2} \quad (10)$$

Where n denotes the number of observations, and α denotes the significance level.

3. Results:

3.1 Rainfall characteristics:

In the basin area, the average annual rainfall ranges from 1151.07 to 1584.13 mm, with a mean of 1318.27 mm. The highest average annual rainfall (1584.13 mm) occurs in the Howrah district of West Bengal, while the lowest (1151.07 mm) occurs in the Chattra district of Jharkhand (Table 1). The minimum (MIN) average annual rainfall ranges from 486.40 to 1002.37 mm, with a mean of 735.51 mm. It is also low in the Chattra district and high in the Howrah district. The maximum (MAX) average annual rainfall varies from 1896.97 to 2308.22 mm, with a mean of 2117.67 mm. It is high in the Howrah district and low in the Latehar district (Figure 3). Moreover, the 25%, 50%, and 75% rainfall values are 946.46 to 1388.22 mm (mean 1147.79 mm), 1178.00 to 1548.67 mm (mean 1308.21 mm), and 1338.66 to 11756.38 mm (mean 1467.67 mm), respectively, across the basin. It is high in the Howrah district and low in the Chattra district for the 25%, 50% and 75% rainfall (Table 1). These results indicate that high rainfall occurs in the Howrah district, which lies in the lower basin area, and low rainfall occurs in the Chattra district, which lies in the upper basin area.

Table 1. District-wise descriptive statistics of rainfall (mm)

State	Districts in the basin	MIN	25%	50%	75%	MAX	Mean	SD	CV
West Bengal	Bankura	901.28	1275.03	1389.33	1563.06	2230.23	1422.45	234.06	16.45
	Burdwan	856.00	1259.21	1376.20	1533.59	2178.85	1410.21	223.45	15.85
	Hooghly	998.10	1312.16	1493.11	1660.14	2263.89	1501.81	262.11	17.45
	Howrah	1002.37	1388.22	1548.67	1756.38	2308.22	1584.13	279.36	17.63
	Purulia	798.00	1180.33	1297.97	1446.27	2108.10	1322.09	218.94	16.56
Jharkhand	Ranchi	791.00	1123.09	1259.24	1398.23	2017.21	1272.22	227.22	17.86
	Hazaribagh	681.80	1096.44	1270.97	1430.98	2105.55	1274.85	254.46	19.96
	Kodarma	559.30	1030.80	1227.51	1373.83	2034.02	1212.74	259.71	21.42
	Ramgarh	581.00	1128.16	1275.83	1436.98	2105.55	1284.29	255.92	19.93
	Chattra	486.40	946.46	1178.00	1338.66	1953.63	1151.07	290.70	25.25
	Jamtara	658.10	1162.39	1300.60	1473.62	2169.74	1325.99	252.14	19.02
	Deoghar	730.40	1097.92	1261.55	1435.72	2129.01	1276.09	264.13	20.70
	Giridih	597.40	1083.42	1247.61	1400.22	2112.61	1253.21	259.19	20.68
	Bokaro	706.40	1148.83	1311.46	1462.76	2202.88	1307.90	256.00	19.57
	Dhanbad	833.64	1185.45	1295.23	1461.88	2188.42	1328.81	225.89	17.00
	Lohardaga	731.40	1091.55	1275.41	1415.18	1993.62	1279.99	249.91	19.52
	Latehar	591.10	1002.93	1230.98	1362.84	1896.97	1202.78	261.69	21.76

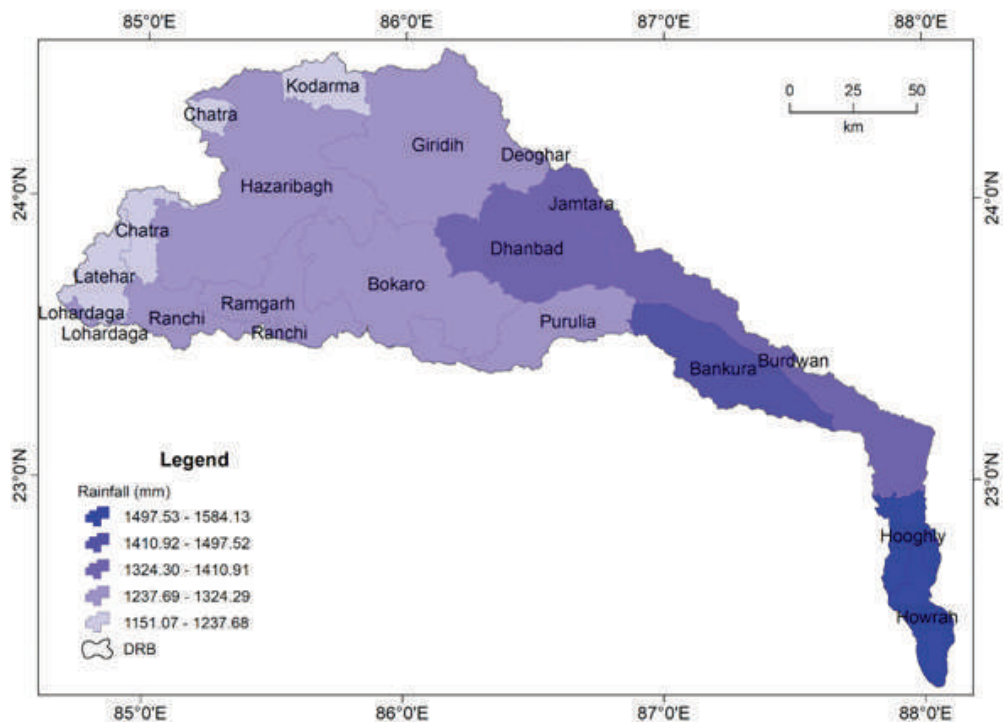


Figure 3. Distribution of average annual rainfall from 1901 to 2023.

3.2 Variability of rainfall pattern:

The variability of the rainfall pattern in the basin area has been analysed using the coefficient of variation (CV). In the study area, it ranges from 15.85 to 25.25%, with an average of 19.21% (Table 1). The rainfall variability is high at Chattra district and low at Burdwan based on the CV values. Moreover, it is classified as low ($CV < 20\%$), moderate ($20\% < CV < 30\%$), high ($CV > 30\%$), and very high ($CV > 40\%$) to identify the degree of variable climate fluctuations (Kumar *et al.*, 2023). A low rainfall variability is found for Bankura, Burdwan, Hooghly, Howrah, Purulia, Ranchi, Hazaribagh, Ramgarh, Jamtara, Bokaro, Dhanbad and Lohardaga districts. Whereas medium rainfall variability is found for Kodarama, Chattra, Deoghar, Giridih and Latehar districts in the basin area based on the categorical classification of CV. These results reveal that the average annual rainfall variability is less in the basin area.

Besides, rolling standard deviation (SD) has been used to measure the interannual variability in precipitation to account for year-to-year precipitation fluctuations. This method is essential to identify whether the intensity of the wet or dry period is increasing, decreasing or stable over a given time window. Higher variability is associated with greater irregularity of annual totals about the annual mean, which poses challenges for sectors dependent on water resources. From the 3-year rolling SD, it is observed that the variability of interannual

rainfall has increased in the basin area after the 1960s (Figure 4). Besides, high rainfall fluctuations are also observed between the 1960s and 2000s. These results also indicate that the fluctuations between wet and dry periods are increasing after the 1960s in the study area.

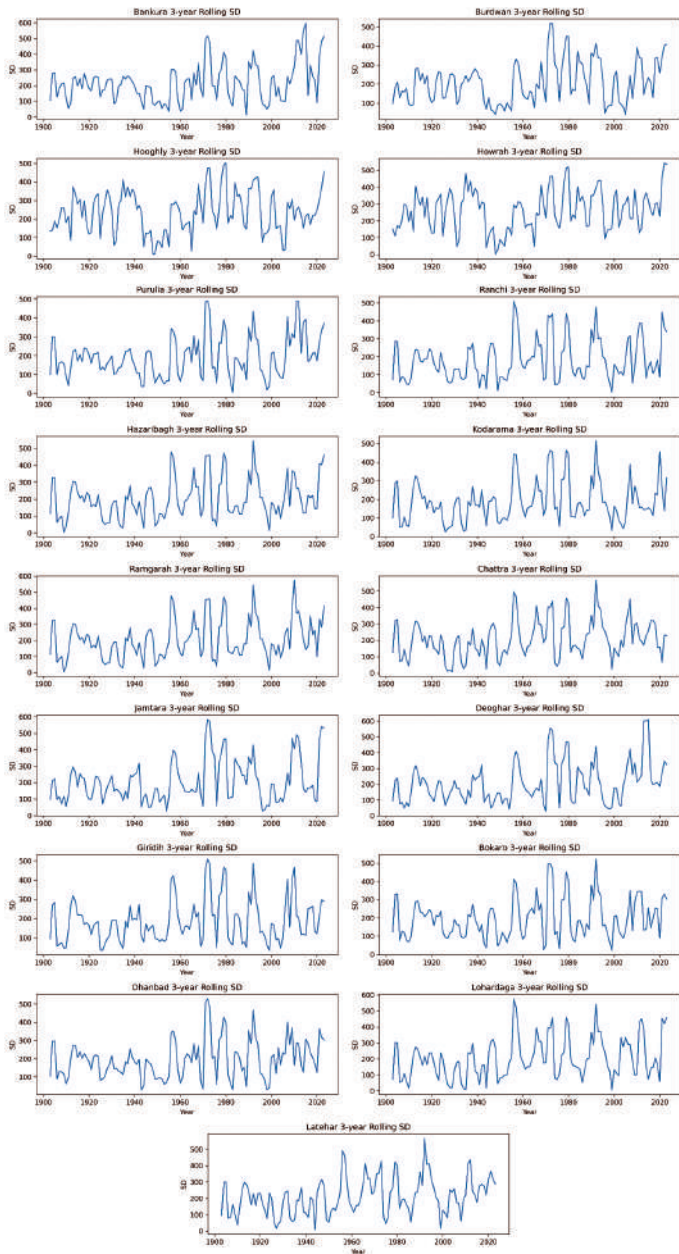


Figure 4. District-wise distribution and trend of the rolling SD.

3.3 Analysis of the rainfall trend:

In the present investigation, the annual rainfall trend has been analysed over 123 years from 1901 to 2023 using the Modified Mann-Kendall (MMK) test and Sen's Slope (SS) estimators. These methods have been applied to detect the magnitude and direction of the trend at a 5% significance level. In the study, no significant increasing or decreasing trend, i.e. no trend, is found for the districts of West Bengal state, which lie in the middle and lower basin area, whereas a significant decreasing trend at a 0.05% significance level is found for the districts of Jharkhand state, which lie in the upper part of the basin area (Figure 5 and Table 2). Only positive values of the MMK test (Z) and Sen's Slope (Q) with positive change are found for the Bankura and Howrah districts. The highest negative change (-36.308%) among the districts in the basin area is found for the Chattra district. Hence, these results reveal a negative trend in annual rainfall in the basin area, indicating a decline in the overall rainfall pattern, and a decreasing trend in the upper part of the basin, indicating a water shortage in the basin area.

Table 2. District-wise annual rainfall trend and percentage change (1901-2023)

State	Districts	mMK Test (Z)	Sen's Slope (Q) (mm/year)	P-value	Trend	Change (%)
West Bengal	Bankura	0.032	0.027	0.974	No trend	0.230
	Burdwan	-1.033	-0.517	0.302	No trend	-4.474
	Hooghly	-1.287	-1.099	0.198	No trend	-8.925
	Howrah	0.057	0.028	0.955	No trend	0.216
	Purulia	-1.200	-0.417	0.230	No trend	-3.845
Jharkhand	Ranchi	-3.497	-1.921	0.000	Decreasing	-18.423
	Hazaribagh	-3.419	-2.234	0.001	Decreasing	-21.381
	Kodarma	-3.376	-2.942	0.001	Decreasing	-29.599
	Ramgarh	-2.623	-1.692	0.009	Decreasing	-16.075
	Chattra	-4.092	-3.426	0.000	Decreasing	-36.308
	Jamtara	-3.488	-2.190	0.000	Decreasing	-20.152
	Deoghar	-5.241	-2.989	0.000	Decreasing	-28.576
	Giridih	-4.937	-3.283	0.000	Decreasing	-31.963
	Bokaro	-4.625	-2.578	0.000	Decreasing	-24.046
	Dhanbad	-2.825	-1.374	0.005	Decreasing	-12.616
	Lohardaga	-2.676	-1.714	0.007	Decreasing	-16.338
	Latehar	-2.706	-1.828	0.007	Decreasing	-18.541

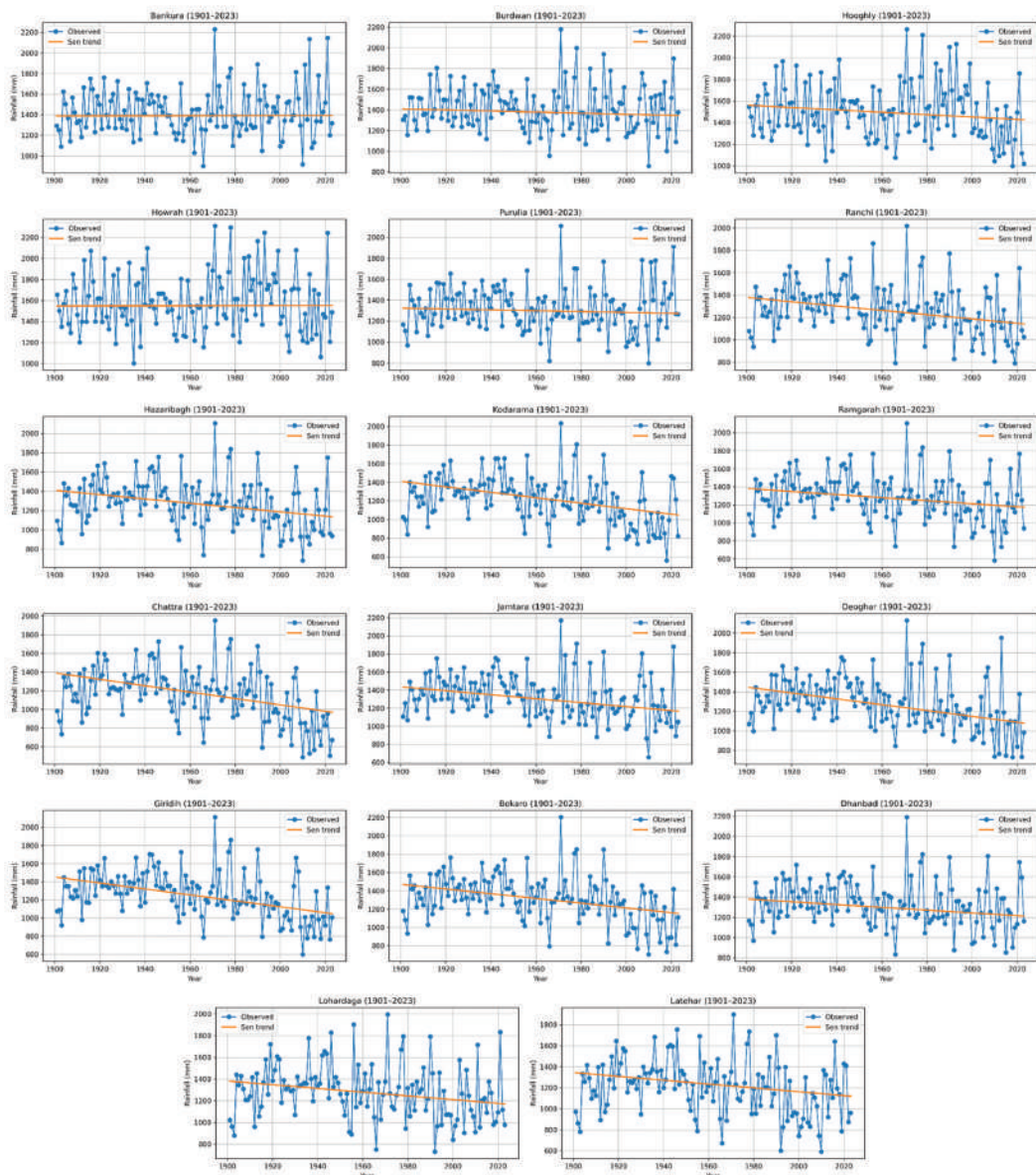


Figure 5. District-wise annual rainfall trend in the basin area (1990-2023).

3.4 Change point analysis:

A change point or a substantial shift in rainfall has been identified using Pettitt's test in the present research work. A significant change in the annual rainfall trend and the starting year of the movement has been detected in this investigation. The abrupt change in the annual

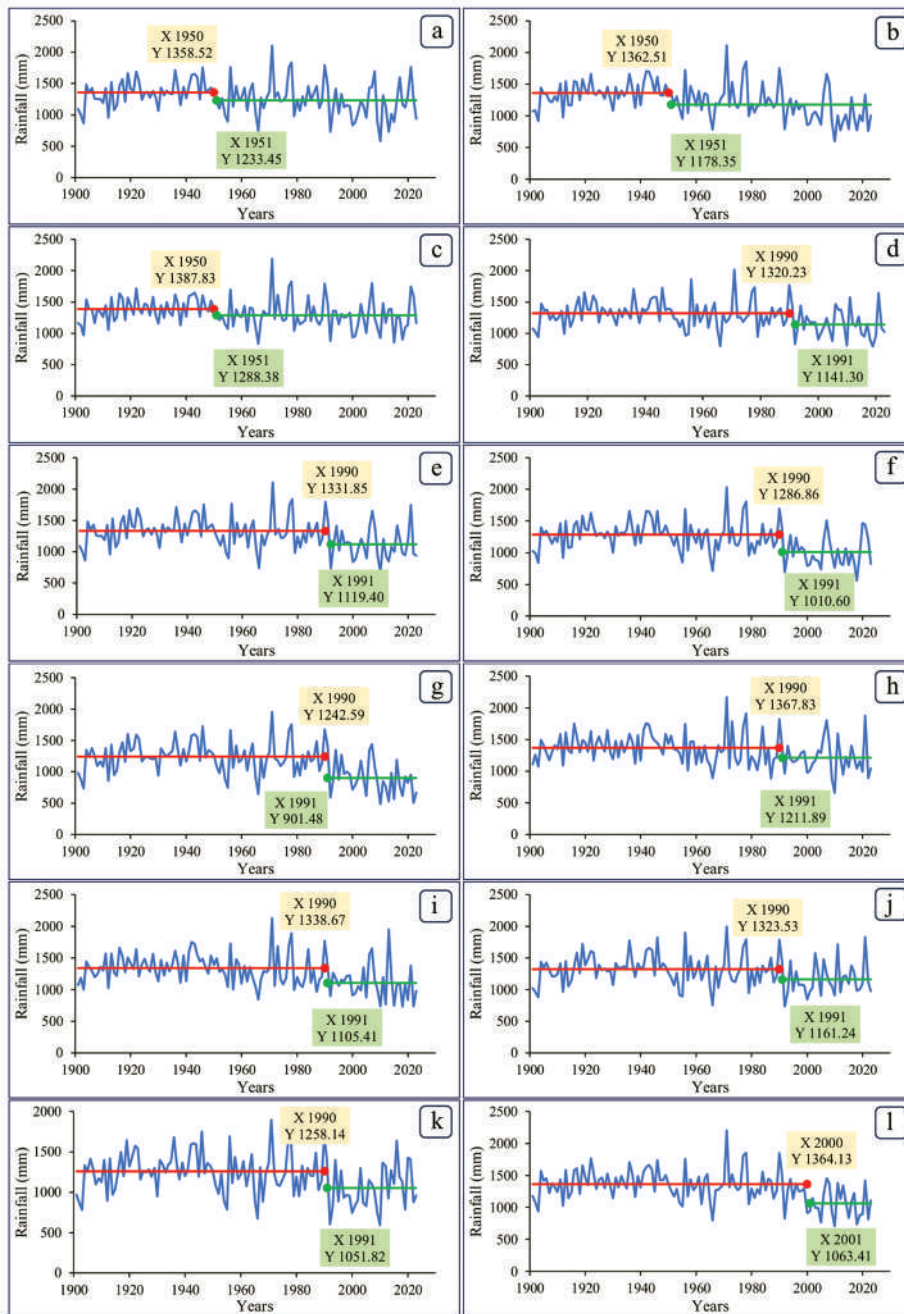


Figure 6. District-wise annual rainfall changes detection in the basin area using Pettitt's test, (a) Ramgarh, (b) Giridih, (c) Dhanbad, (d) Ranchi, (e) Hazaribagh, (f) Kodarma, (g) Chattra, (h) Jamtara, (i) Deoghar, (j) Lohardaga, (k) Latehar, and (l) Bokaro.

rainfall is observed only in the districts of Jharkhand state. The year 1950 is identified as a change point for the Ramgarah, Giridih, and Dhanbad districts (Figure 6a-c). However, the year 1990 is identified as a change point for the Ranchi, Hazaribagh, Kodarama, Chattra, Jamtara, Deoghar, Lohardaga, and Latehar districts (Figure 6d-k). By contrast, only the year 2000 is detected as a shift point for the Bokaro district in the study area (Figure 6l). These results indicate that the trend of the annual rainfall pattern in the upper part of the basin area is significantly shifted after the 1990s, except in the Ramgarah, Giridih, and Dhanbad districts.

A rainfall anomaly analysis is also performed to show the difference between observed rainfall and the long-term average at the same location and time. The positive anomaly (above normal) indicates more rain than usual. A high positive anomaly denotes heavy rainfall leading to flood risk and waterlogging. In contrast, a negative anomaly (below normal) indicates less rain than usual. A strong negative anomaly signifies drought conditions leading to water scarcity. Moreover, a zero or near-zero anomaly means rainfall close to normal, indicating typical seasonal behaviour. From this analysis, it is observed that the negative anomaly trend is increased after 2000 for Hooghly, Howrah, Ranchi, Hazaribagh, Kodarma, Ramgarh, Chattra, Jamtara, Deoghar, Gridih, Bokaro, Dhanbad, Lohardaga and Latehar districts in the basin. These results indicate that the trend of drought-like situations increases after 2000 in the basin area.

4. Discussion:

Analysis of rainfall trends and variability is particularly significant in the context of climate change and sustainable water resources management (Ogunbode *et al.*, 2022). As the DRB is influenced by the Indian monsoonal regimes, more than 75% of rainfall occurs during the monsoon (Hoque *et al.*, 2023; Selvaraj *et al.*, 2024). Rainfall is an unpredictable phenomenon (Selvaraj *et al.*, 2024). Thus, analysing rainfall trends and variability is vital for integrated water resource management (IWRM). It also provides information on spatio-temporal rainfall variability, trends and anomalies (Chisanga *et al.*, 2023). Hence, the annual rainfall trend and its variability in the subtropical river basin, the DRB, are assessed using district-wise annual rainfall data for 123 years from 1901 to 2023. The general rainfall characteristic in the basin area is that high rainfall occurs in the lower basin area, and low rainfall occurs in the upper basin area. The average annual rainfall variability is lower in the basin area. High rainfall fluctuation is detected between the 1960s and 2000s, and it has been rising since the 1960s in the study area. High interannual rainfall variability reduces crop yields and alters hydrological conditions in any area (Harp and Horton, 2023). This shifting of interannual rainfall impacts vegetation cover and soil erosion is associated with climate change-induced variations in rainfall patterns, especially increased inter-annual variability, changes in rainfall intensity and frequency (He *et al.*, 2024). It also impacts water quality in the basin area (Ezzati *et al.*, 2024). Besides, a negative trend in annual rainfall in the basin area and a decreasing trend in the upper part of the basin are observed in the study area. Our study findings are supported by the work of Praveen *et al.* (2020). The positive rainfall trend indicates that more rainfall may be received, while the negative trend in annual rainfall indicates a decrease in the overall

rainfall pattern (Kamble *et al.*, 2020). A decrease in annual rainfall can lead to water scarcity, which affects agricultural productivity and other water-based activities (Chakraborty *et al.*, 2025). The shift in the annual rainfall pattern in the upper part of the basin area is observed after the 1990s, except in the Ramgarh, Giridih, and Dhanbad districts. Praveen *et al.* (2020) found the change detection year after 1960 for most of the meteorological stations in India. Moreover, anomaly analysis of rainfall shows that the negative trend of rainfall anomalies has increased in most parts of the basin area after 2000, indicating that drought-like situations have increased after 2000 in the basin area. Our study findings are supported by Rao *et al.* (2023), who mentioned that the frequency of drought occurrence is three times, but the magnitude is lower in the last ten years.

Analysis of rainfall trends and variability is vital for assessing long-term climate change, estimating water resource accessibility and promoting agricultural planning. This analysis helps recognize drought, rainfall patterns and extreme flood events that cause flooding and soil and land erosion, aiding flood mitigation efforts, which are important for reducing disaster risk and infrastructure management. It is also helpful for dam-reservoir regulation in water resource management for various uses of water, such as irrigation, industry and domestic use, especially for demand and supply estimation. It is very helpful in informing policymakers about environmental sustainability and land use, particularly in regions that heavily depend on rain-fed agriculture. The major limitation of the study is the unavailability of daily and seasonal rainfall data at the district and basin levels, as well as the unavailability of daily, seasonal and annual temperature data for a long-term period at the district and basin levels. However, this study would be a valuable asset for policymakers and stakeholders to enhance climate resilience and sustainable water resource management at the district and basin levels.

5. Conclusions:

In the present investigation, the annual rainfall trend and its variability have been analysed in the subtropical river basin, the DRB, using district-wise annual rainfall data for 123 years from 1901 to 2023. The average annual rainfall varies from 1151.07 to 1584.13 mm, with a mean of 1318.27 mm. It is highest in the Howrah district, which lies in the lower DRB, and lowest in the Chattra district, which lies in the upper DRB. It is also observed that the average annual rainfall is higher in the lower DRB than in the upper DRB. From the rainfall variability analysis, it is found that the average annual rainfall variability is lower in the basin area based on the CV. In addition, it is also found that interannual rainfall variability has increased after the 1960s in the DRB as per the rolling SD. Moreover, from the annual rainfall trend analysis, a negative trend in annual rainfall in the basin area and a decreasing trend of annual rainfall in the upper part of the basin are observed. Besides, the trend in annual rainfall in the upper part of the basin has shifted significantly after the 1990s, except in the Ramgarh, Giridih, and Dhanbad districts, according to Pettitt's test. Furthermore, the precipitation anomaly analysis reveals that the trend of negative anomaly has increased after 2000, indicating that the basin area has experienced an increase in the trend of drought-like conditions after 2000. The study can be helpful for climate change adaptation and sustainable water management at the basin

or district level, as it helps to identify long-term changes, seasonal or annual fluctuations and flood or drought risks. It also helps in analysing rainfall patterns, which enables effective agricultural planning, flood management and disaster risk reduction.

References:

- Aditya, F., Gusmayanti, E., & Sudrajat, J. (2021). Rainfall trend analysis using Mann-Kendall and Sen's slope estimator test in West Kalimantan. In *IOP conference series: earth and environmental science* (Vol. 893, No. 1, p. 012006). IOP Publishing. DOI 10.1088/1755-1315/893/1/012006
- Bhattacharyya K (2011). The Lower Damodar River, India: understanding the human role in changing fluvial environment. Springer, New York. <https://doi.org/10.1007/978-94-007-0467-1>
- Census of India (2011). District Census Handbooks, Directorate of Census Operation. India. (Accessed 15 March 2019)
- Chakraborty, D., Roy, A., Singh, N. U., Saha, S., Das, S. K., Mridha, N.,... & Mishra, V. K. (2025). Assessing Climate Change Impact on Rainfall Patterns in Northeastern India and Its Consequences on Water Resources and Rainfed Agriculture. *Earth*, 6(1), 2. <https://doi.org/10.3390/earth6010002>
- Chandra, S. (2003). India: Flood management-Damodar river basin. *World Meteorological Organization and Associated Programme on Flood Management, Integrated flood Management-Case study*, 1-10.
- Chisanga, C. B., Nkonde, E., Phiri, E., Mubanga, K. H., & Lwando, C. (2023). Trend analysis of rainfall from 1981-2022 over Zambia. *Heliyon*, 9(11). <https://doi.org/10.1016/j.heliyon.2023.e22345>
- Chukwuma Sr, C. (2025). Invariance of Extreme Hydrologic Events and Climate Change in the Risk Reduction on Environment and Health. *Grn Int J Apl Med Sci*, 3(2), 92-102. DOI: 10.62046/gijams.2025.v03i02.011
- Comia, H. R., Kenée, F. B., Nelson, F. C., Americano, J. M., & Mucova, S. A. R. (2025). Trend analysis of rainfall and temperature in Metuge district, northern Mozambique. *Discover Atmosphere*, 3(1), 8. <https://doi.org/10.1007/s44292-025-00034-w>
- Conte, L. C., Bayer, D. M., & Bayer, F. M. (2019). Bootstrap Pettitt test for detecting change points in hydroclimatological data: Case study of Itaipu Hydroelectric Plant, Brazil. *Hydrological Sciences Journal*, 64(11), 1312-1326. <https://doi.org/10.1080/02626667.2019.1632461>
- Das, J., Mandal, T., Rahman, A. S., & Saha, P. (2021). Spatio-temporal characterization of rainfall in Bangladesh: an innovative trend and discrete wavelet transformation approaches: J. Das et al. *Theoretical and Applied Climatology*, 143(3), 1557-1579. <https://doi.org/10.1007/s00704-020-03508-6>
- Ezzati, G., Collins, A. L., Pulley, S., Galloway, J., Hawtree, D., & Mellander, P. (2024). Impacts of changing weather patterns on the dynamics of water pollutants in agricultural catchments: Insights from 11-year high temporal resolution data analysis. *Journal of Hydrology*, 644, 132122. <https://doi.org/10.1016/j.jhydrol.2024.132122>
- Fan, Y., Hou, Y., & Wang, S. (2025). Spatiotemporal evolution in water use structures of large-sized

irrigation district, China. *Stochastic Environmental Research and Risk Assessment*, 39(2), 479-491.

- Ghosh, S., Hoque, M. M., Saha, U. D., & Islam, A. (2022). Assessment of dam-induced changes in ecogeomorphological behaviour and fluvial functionality in the Damodar River, West Bengal, India. *AQUA—Water Infrastructure, Ecosystems and Society*, 71(6), 722-750. <https://doi.org/10.2166/aqua.2022.003>
- Gupta, L. K., & Verma, S. (2023). Rainfall and temperature trend analysis using mann-kendall and sen's slope estimator test in Kharun Watershed, Chhattisgarh, India. *Current Journal of Applied Science and Technology*, 42(23), 1-9. <https://doi.org/10.9734/cjast/2023/v42i234174>
- Hamed, K. H., & Rao, A. R. (1998). A modified Mann-Kendall trend test for autocorrelated data. *Journal of hydrology*, 204(1-4), 182-196. [https://doi.org/10.1016/S0022-1694\(97\)00125-X](https://doi.org/10.1016/S0022-1694(97)00125-X)
- Harp, R. D., & Horton, D. E. (2023). Observed changes in interannual precipitation variability in the United States. *Geophysical Research Letters*, 50(13), e2023GL104533. <https://doi.org/10.1029/2023GL104533>
- He, X., Miao, Z., Wang, Y., Yang, L., & Zhang, Z. (2024). Response of soil erosion to climate change and vegetation restoration in the Ganjiang River Basin, China. *Ecological Indicators*, 158, 111429. <https://doi.org/10.1016/j.ecolind.2023.111429>
- Hoque MM, Islam A, & Ghosh S (2022a). Environmental flow in the context of dams and development with special reference to the Damodar Valley Project, India: a review. *Sustain Water Resour Manag* 8(3):1–27. <https://doi.org/10.1007/s40899-022-00646-9>
- Hoque, M. M., & Islam, A. (2024). Spatio-temporal dynamics of ecological, bacteriological, and overall water quality of the Damodar River, India. *Environmental Science and Pollution Research*, 31(12), 18465-18484. <https://doi.org/10.1007/s11356-024-32185-5>
- Hoque, M. M., Islam, A., & Mahammad, S. (2022b). Assessing the surface and bottom river water quality for drinking purpose and human health risk analysis: a study of Damodar River, India. *Arabian Journal of Geosciences*, 15(23), 1734. <https://doi.org/10.1007/s12517-022-10987-6>
- Hoque, M. M., Islam, A., Islam, A. R. M. T., Pal, S. C., Mahammad, S., & Alam, E. (2023). Assessment of soil heavy metal pollution and associated ecological risk of agriculture dominated mid-channel bars in a subtropical river basin. *Scientific Reports*, 13(1), 11104. <https://doi.org/10.1038/s41598-023-38058-0>
- Hoque, M. M., Pal, S. C., Mandal, S., & Islam, A. (2025). Assessment of mollusc habitat suitability of an anthropogenically altered tropical river in India. *Environmental Monitoring and Assessment*, 197(10), 1140. <https://doi.org/10.1007/s10661-025-14593-3>
- Ishiwatari, M. (2025). Disaster risk reduction. In *Handbook of climate change mitigation and adaptation* (pp. 3679-3705). C. Cham: Springer Nature Switzerland. https://doi.org/10.1007/978-3-031-84483-6_147
- Islam, A., Sardar, N., Mohinuddin, S., Hoque, M. M., Sengupta, S., Das, B. C.,... & Sengupta, B. (2023). Quasi-equilibrium channel metamorphosis in planform of a subtropical river in India in post-dam period. *Catena*, 221, 106793. <https://doi.org/10.1016/j.catena.2022.106793>

- Kamble, K. M., Sthool, V. A., Upadhye, S. K., Jadhav, J. D., Bagade, S. V., & Giri, A. M. (2020). Trend Analysis of Rainfall and Rainy Days using Mann Kendall Method and Sen's Slope Estimator in Parola Tehsil of Jalgaon District of Maharashtra (India). *Int. J. Curr. Microbiol. App. Sci*, 9(12), 3038-3044. <https://doi.org/10.20546/ijcmas.2020.912.360>
- Kamble, K. M., Sthool, V. A., Upadhye, S. K., Jadhav, J. D., Bagade, S. V., & Giri, A. M. (2020). Trend Analysis of Rainfall and Rainy Days using Mann Kendall Method and Sen's Slope Estimator in Parola Tehsil of Jalgaon District of Maharashtra (India). *Int. J. Curr. Microbiol. App. Sci*, 9(12), 3038-3044. <https://doi.org/10.20546/ijcmas.2020.912.360>
- Kenabatho, P. K. (2025). Innovative trend analysis of long-term spatial-temporal rainfall patterns over Botswana: Implications for water resources management. *Journal of Hydrology: Regional Studies*, 58, 102217. <https://doi.org/10.1016/j.ejrh.2025.102217>
- Kumar, A., Kumar, S., Rautela, K. S., Shekhar, S., Ray, T., & Thangavel, M. (2023). Assessing seasonal variation and trends in rainfall patterns of Madhya Pradesh, Central India. *Journal of Water and Climate Change*, 14(10), 3692-3712. <https://doi.org/10.2166/wcc.2023.280>
- Mallakpour, I., & Villarini, G. (2016). A simulation study to examine the sensitivity of the Pettitt test to detect abrupt changes in mean. *Hydrological Sciences Journal*, 61(2), 245-254. <https://doi.org/10.1080/02626667.2015.1008482>
- Mandal, T., Das, J., Rahman, A. S., Saha, P., & Saha, S. (2025). Understanding the Teleconnections of ENSO and IOD with Rainfall Variation in India: T. Mandal et al. *Environmental Modeling & Assessment*, 1-31. <https://doi.org/10.1007/s10666-025-10065-7>
- Mujumdar, M., Bhaskar, P., Ramarao, M. V. S., Uppara, U., Goswami, M., Borgaonkar, H.,... & Niyogi, D. (2020). Droughts and floods. In *Assessment of climate change over the Indian region: a report of the Ministry of Earth Sciences (MoES), Government of India* (pp. 141-144). Singapore: Springer Singapore. https://doi.org/10.1007/978-981-15-4327-2_6
- Ogunbode, T. O., Esan, V. I., Samson, T. K., Oyelowo, O. J., & Asifat, J. T. (2022). Rainfall trend and its implications for sustainable crop production and Water resources Management: a Case Study of Iwo, Nigeria. *Journal of Applied Sciences and Environmental Management*, 26(8), 1415-1422. DOI:10.4314/jasem.v26i8.15
- Prakash, P., & Chembolu, V. (2025). An integrated assessment of hydro-meteorological extremes and water scarcity in a mountainous river catchment under climate change. *Hydrological Sciences Journal*, 70(15), 2825-2848. <https://doi.org/10.1080/02626667.2025.2566263>
- Praveen, B., Talukdar, S., Shahfahad, Mahato, S., Mondal, J., Sharma, P.,... & Rahman, A. (2020). Analyzing trend and forecasting of rainfall changes in India using non-parametrical and machine learning approaches. *Scientific reports*, 10(1), 10342. <https://doi.org/10.1038/s41598-020-67228-7>
- Ranjan, S., Singh, L., Bahuguna, A., & Rawat, A. (2023). Analysis of Trend Using Nonparametric Test for Rainfall and Rainy-Days in Jodhpur Zone of Rajasthan. *Indian Journal of Ecology*, 50(4), 1063-1068. DOI: <https://doi.org/10.55362/IJE/2023/4014>
- Rao, G., Sowjanya, A., Shekhar, D., Naik, B., & Kiran, B. V. S. (2023). Rainfall analysis over 31 years of Chintapalle, Visakhapatnam, high altitude and Tribal zone, Andhra Pradesh, India. *Mausam*, 74(3), 685-698.

- Rao, K. K., Kulkarni, A., Patwardhan, S., Kumar, B. V., & Kumar, T. V. (2020). Future changes in precipitation extremes during northeast monsoon over south peninsular India. *Theoretical and Applied Climatology*, 205-217. <https://doi.org/10.1007/s00704-020-03308-y>
- Saikh, N. I., Saha, S., Sarkar, D., & Mondal, P. (2023). Rainfall trend and variability analysis of the past 119 (1901-2019) years using statistical techniques: A case study of Kolkata, India. *Mausam*, 74(4), 1093-1112. <https://doi.org/10.54302/mausam.v74i4.5909>
- Selvaraj, B. R., Krishnasamy, S., & Dhason, J. M. I. (2024). Investigation of climate change by analysing the rainfall pattern in kuzhithuraiyar sub-basin of India using GIS-based spatial analysis. *Sustainable Chemistry for Climate Action*, 4, 100042. <https://doi.org/10.1016/j.scca.2024.100042>
- Subrahmanyam, V. P. (1988). Hazards of floods and droughts in India. In *Natural and Man-Made Hazards: Proceedings of the International Symposium held at Rimouski, Quebec, Canada, 3—9 August, 1986* (pp. 337-356). Dordrecht: Springer Netherlands. https://doi.org/10.1007/978-94-009-1433-9_24

Published by Prof. Prof. H. J. Syiemlieh, Editor, on behalf of the Geographical Society of North-Eastern Hill Region, Department of Geography, North-Eastern Hill University (NEHU), Shillong-793022 and Printed by Unique Phototype, 49 Guru Prosad Chowdhury Lane, Kolkata 700 006, India.